REGULATION OF HEPATIC INFLAMMATION AND THROMBOSIS DURING *SALMONELLA* INFECTIONS

by

JESSICA RUTH HITCHCOCK

A thesis submitted to the University of Birmingham for the degree of DOCTOR OF PHILOSOPHY

School of Immunity and Infection

College of Medicine and Dentistry

University of Birmingham

December 2013

ABSTRACT

Salmonella Typhimurium is one of the most common causes of bacteraemia in children in sub-Saharan Africa and is prevalent in HIV-infected individuals. However, symptoms of this systemic infection are unclear, and while fatalities are frequent, how infection kills is unknown. Here we use a mouse model of systemic (but resolving) infection to investigate physiological and immunological aspects of the host response to infection. The liver is colonised during systemic infection, and in the model used, bacterial numbers peak at day 7 and are largely resolved within a month. Inflammatory lesions, consisting of multiple leukocyte populations, develop within the liver. These persist and are more severe once bacterial clearance is established. Whilst lesions can develop in the absence of T and B cells, these cells contribute to the regulation of inflammatory foci. In the absence of interferon-γ, lesions do not develop and inflammation in the liver is largely absent.

In parallel, extensive platelet thrombosis occurs in the liver venous system and the shared kinetics with lesion formation suggest these phenotypes may be co-regulated. Here we describe how parenchymal and vascular inflammation are anchored by inflammatory up-regulation of podoplanin expression in the liver. Thrombosis is substantially abrogated in the absence of C-like lectin-type receptor-2 (CLEC-2) expression on platelets and we show that podoplanin (the physiological ligand for CLEC-2) expression on clodronate-sensitive myeloid populations is necessary for thrombus development. Therefore, the parallel association between inflammation and platelet activation could be the basis for developing novel treatments for systemic bacterial infections in humans.

ACKNOWLEDGEMENTS

I would like to thank everyone who has been involved in this fantastic project and who has helped me during the last four years, I have had a brilliant time. I would like to thank Adam for giving me the opportunity to have a go and for all his encouragement and ideas. I have had such an exciting project and I have thoroughly enjoyed my PhD, which has been hard work, but I have loved it. So thanks Adam for giving me this project. I would also like to thank David for his support and his genuine encouragement which has really kept me going! It is fantastic working with such a distinguished scientist and I am so grateful for all his input into my project. And I would like to thank Steve who has believed in me as a scientist and who has really challenged me but given me some great ideas too.

I especially want to thank everyone on the 4th floor who has made it so much fun! Thank you to Charlie and Spyda who have helped me out with all the long days; Charlie I am so grateful for all your liver mashing!! Thank you for all the encouraging songs (especially Laura and your beautiful voice)! And I am really grateful for all the actual practical help (Ewan, Yang, Adriana, Jenny, Sarah, Ruth). I would also like to thank Jenny, Colette, Razvan, John, Sian and Pete and all the others for your continued friendship and motivation throughout. You are all lovely. And I would like to thank everyone on the 1st floor (Kate, Leyre, Alex, Craig, Brenda and Alice) and in the liver labs and the QE (Guillaume, Saba, Amy) for letting me pester you and steal antibodies! Sarah, thanks for helping me print!

And thank you to all my family (mum, dad, Harry, Toby, Anthony, and especially William for being so supportive and patient. I have loved doing my PhD so thank you for believing in me. A special thank you to Harry for doing my page numbers! And thank you Granny for all your interest and your support and encouragement.

TABLE OF CONTENTS

LIST OF FIGURES

LIST OF TABLES

ABBREVIATIONS

ACK	Ammonium chloride potassium
ALP	Alkaline phosphatase
ALT	Alanine aminotransferase
AT	Antithrombin
AP	Alkaline-phosphatase
APC	Antigen presenting cell
APC	Allophycocyanin
APC-Cy7	Allophycocyanin-Cyanine-7
AST	Aspartate aminotransferase
B cell	Bone marrow-derived cell
BMSU	Biomedical services unit
Bt	Biotinylated
CD	Cluster of differentiation
CFU	Colony forming units
CLEC-2	C-type lectin-like receptor 2
Cre	Cre recombinase
CRP	C reactive protein
DAB	3, 3'-diaminobenzidine tetrahydrochloride
DC	Dendritic cell
DIC	Disseminated intravascular coagulation
EDTA	Ethylenediaminetetraacetic acid
FACS	Fluorescence activated cell sorting
Fc	Fragment constant
FCS	Foetal calf serum
Fig	Figure
FITC	Fluorescein Isothiocyanate
FS	Forward scatter
g	Gram
GGT	Gamma-glutamlytransferase
Gy	Grays
H and E	Haematoxylin and Eosin
HSEC	Hepatic sinusoidal endothelial cells
HRP	Horse-radish peroxidise
ICAM-1	Intercellular adhesion molecule-1
Ig	Immunoglobulin
IL	Interleukin
iNOS	Inducible nitric oxide synthase
IFN-γ	Interferon-gamma
Ig	Immunoglobulin
iNKT	Invariant natural killer T cell
i.p.	Intraperitoneal
i.v.	Intravenous
KO	Knock out
L	Litre
LB	Luria-Bertani

LPS	Lipopolysaccharide
MCH	Mean corpuscular haemoglobin
MCHC	Mean corpuscular haemoglobin concentration
MCV	Mean corpuscular volume
MFI	Median fluorescence intensity
MHC	Major histocompatibility complex
MLN	Mesenteric lymph nodes
MPV	Mean platelet volume
ND	None detected
NK	Natural killer
NKT	Natural killer T
NOD	Nucleotide binding and oligomerisation domain
NFκB	Nuclear factor kappa-light-chain-enhancer of activated B cells
NI	Non-infected
NLR	NOD-like receptor
NMS	Normal mouse serum
NTS	Non-typhoidal *Salmonellae*
OD	Optical density
PAMP	Pathogen associated molecular patterns
PBS	Phosphate buffered saline
PE	Phycoerythrin
PerCPcy5.5	Peridinin Chlorophyll Protein (Cyanin Dye)
PMPs	Platelet microbicidal proteins
PRR	Pattern recognition receptor
PARs	Protease activated receptors
PMN	Polymorphonuclear
PSGL-1	P-selectin glycoprotein ligand-1
PW	Pulse width
Rag	Recombination activating gene
RDW	Red cell distribution width
RES	Reticuloendothelial system
rpm	Revolutions per minute
ROS	Reactive oxygen species
Rpm	Rotations per minute
S. Enteritidi	*Salmonella enterica* serovar Enteritidis
S. Typhi	*Salmonella enterica* serovar Typhi
S. Typhimurium	*Salmonella enterica* serovar Typhimurium
STm	*Salmonella enterica* serovar Typhimurium
SS	Side scatter
SPI1	*Salmonella* pathogenicity island 1
SPI2	*Salmonella* pathogenicity island 2
TAFI	Thrombin-activated fibrinolysis inhibitor
T cell	Thymus-derived cell
Tbet	T-box expressed in T cells
TCR	T cell receptor
TF	Tissue factor
TFPI	Tissue factor pathway inhibitor

Th1	T helper 1
Th2	T helper 2
TLR	Toll-like receptor
TNF-α	Tumor necrosis factor-alpha
TNF-αR	Tumor necrosis factor-alpha receptor
Treg	Regulatory T cell
TUNEL	TdT-mediated dUTP-bitotin nick end labelling
VCAM-1	Vascular cell adhesion molecule-1
VWF	Von Willebrand factor
WT	Wild type

CHAPTER 1: INTRODUCTION

1.1 *Salmonellae* enterica

Salmonella enterica are intracellular Gram negative bacteria which cause a range of important diseases. *Salmonella enterica* serovar Typhi (*S*. Typhi) is a serovar specific to humans and higher primates and it causes typhoid fever. This disease places a large clinical burden on the developing world; data from the World Health Organisation reported in excess of 21 million illnesses and 200, 000 fatalities, caused by typhoid fever during the year 2000 (Crump et al., 2004). Non-typhoidal *Salmonellae* (NTS) including *Salmonella enterica* serovar Enteritidis (*S*. Enteritidis) and *Salmonella enterica* serovar Typhimurium (*S*. Typhimurium or STm) can be transmitted between animals and humans and are a major cause of food-related infections in developed countries and throughout the world (Hohmann, 2001).

1.1.1 Typhoid fever

Typhoid fever is a systemic infection which is endemic particularly in areas which lack clean available drinking water and suitable sewage-treatment systems (House et al., 2001). Studies on the prevalence of *S*. Typhi infections indicate that approximately half of culture-positive cases occur in children under 5 years old and the highest incidence of cases is found in children aged 2-3 years (Graham, 2002, Lepage et al., 1987, Sinha et al., 1999, Saha et al., 2001, Duggan and Beyer, 1975). Symptoms consist of fever approximately one week after initial infection, accompanied by enteritis and sometimes diarrhoea and bradycardia (Pramoolsinsap and Viranuvatti, 1998). Bacteraemia is low-level but enables bacterial dissemination and colonisation of organs including the spleen and liver (Santos et

al., 2001). Typhoid fever can result in organ damage and other complications including intestinal perforation, bleeding diathesis and encephalitis (van Basten and Stockenbrugger, 1994, Rao et al., 1978, Olubodun et al., 1994, Greig and Naidoo, 1981, Pramoolsinsap and Viranuvatti, 1998).

Typhoid fever can be treated with antibiotics and prognosis is usually good if diagnosed and treated quickly. However, prognosis is poorer in individuals with underlying conditions including anaemia or malaria, those with severe complications, and when antibiotic treatment is delayed (Pramoolsinsap and Viranuvatti, 1998). Choice of antibiotic depends on availability, however, resistance to the three first-line antibiotics (commonly used to treat typhoid fever) is a problem, especially in endemic areas (Mirza and Hart, 1993, Pramoolsinsap and Viranuvatti, 1998, Malik, 2002). In addition, typhoid fever can become persistent whereby bacteria can reside within infected individuals for many years (Gordon, 2008). These carriers of infection are vital for maintaining bacterial populations and act as reservoirs, occasionally releasing bacteria back into the environment in their stools. Carriers of *S*. Typhi include both typhoid patients and individuals who have never had clinical features of the disease (Monack et al., 2004b).

1.1.2 Non-typhoidal *Salmonellae* infections

In developed countries, NTS primarily causes gastroenteritis whereby ingestion of contaminated food leads to a local infection in the gastrointestinal tract and is associated with abdominal pain, vomiting and diarrhoea (Zhang et al., 2003). Infections are not associated with bacteraemia and are self-limiting, although they can become more severe in the immuno-compromised and the elderly (Hohmann, 2001, Levine et al., 1991). However, in developing countries including sub-Saharan Africa, NTS is a common cause of

systemic disease in children and HIV-infected individuals (Graham et al., 2000b, Gordon, 2008).

1.1.2.1 Systemic non-typhoidal *Salmonellae* infections in sub-Saharan Africa: prevalence and epidemiology

In tropical Africa, NTS is one of the most common causes of bacteraemia in children and is prevalent in HIV-infected individuals (Graham et al., 2000b, Graham et al., 2000c, Nesbitt and Mirza, 1989, Cheesbrough et al., 1997, Green and Cheesbrough, 1993, Mabey et al., 1987, Walsh et al., 2000, Lepage et al., 1987). In children, NTS bacteraemia is most prevalent between the ages of 6-24 months, with the highest incidence in those aged 10-14 months (Graham et al., 2000b, MacLennan et al., 2008). This may be partly explained by the increased incidence of intestinal infections at this age. Reduced integrity of the intestinal mucosa (a common feature of malnutrition) may make this age group more susceptible to invasive disease (Graham et al., 2000b, Berkowitz, 1992). Children aged 1-4 months are not particularly susceptible to NTS bacteraemia, which is associated with the presence of maternal antibody at this time (MacLennan et al., 2008).

In a study of inpatient children at the Queen Elizabeth Central Hospital, Blantyre, Malawi, 40% of blood culture isolates were NTS, and NTS bacteraemia was associated with a 24% case fatality rate (Walsh et al., 2000, Graham et al., 2000b). NTS also frequently causes pneumonia and bacterial meningitis in both neonates and in children over the age of 2 months. At the Queen Elizabeth Central Hospital, NTS meningitis has a case fatality rate of 57%, which has also been reported in other areas of tropical Africa (Molyneux et al., 1998, Graham et al., 2000b, Molyneux et al., 2000). NTS is frequently isolated from septic arthritis in children (Lavy et al., 1995, Molyneux and French, 1982). However, with the exception of

NTS meningitis and septic arthritis which are associated with recognisable symptoms, NTS bacteraemia can be difficult to identify (Graham et al., 2000b).

1.1.2.2 Clinical features of non-typhoidal *Salmonellae* bacteraemia

NTS bacteraemia can be difficult to recognise because there are often no major symptoms and it is frequently associated with underlying conditions which may have unrelated clinical features. Features of gastroenteritis such as vomiting and diarrhoea are usually absent. Generally, infected individuals are febrile, although if malnourished, which is common in infected children, fever can be less pronounced (Green and Cheesbrough, 1993). Symptoms associated with pneumonia (including tachypnea, dyspnea and cough) are frequently presented, and hepatosplenamegaly is often observed (Graham et al., 2000b).

Anaemia has been repeatedly observed in cases of NTS bacteraemia in African children, more so than with other Gram negative systemic bacterial infections (Graham et al., 2000b, Green and Cheesbrough, 1993). Associations between NTS bacteraemia and anaemia may be explained in part by the common co-incidence of NTS bacteraemia with malaria. The association between these infections was first reported in a study in Nigeria in 1975, and a link between the two has since been repeatedly confirmed (Duggan and Beyer, 1975, Mabey et al., 1987, Graham et al., 2000b). Both infections are more common in the rainy season and whilst NTS is repeatedly reported to affect the outcome of malaria, susceptibility to NTS bacteraemia is increased by malaria. For example, antibody responses are diminished and complement concentrations in the serum are reduced in patients with malaria (Greenwood et al., 1972, Greenwood et al., 1978). Malnutrition is also more prevalent during the rainy season in tropical Africa, which may increase susceptibility to NTS infection (Graham et al., 2000b).

It is likely that NTS comes from a variety of sources, including infected water and food, domestic animals, contact with infected humans, and the environment (Graham et al., 2000b). Nosocomial transmission is likely in many hospitals in developing countries. The diagnosis of NTS bacteraemia is often missed or delayed due to its elusive presentation and therefore inappropriate examination. Often blood is not cultured, both due to lack of facility but also if patients are admitted to clinic for additional reasons, including malaria and pneumonia. As with typhoid fever, NTS infections are currently treated with antibiotics, the choice depends both on treatment cost and the resistance of local bacterial strains (Kariuki et al., 2006, Graham et al., 2000b). Multidrug resistance is becoming a significant clinical problem in both S. Typhi and NTS infections; at present there are no vaccines for NTS bacteraemia (Gordon et al., 2008, MacLennan et al., 2008, Graham, 2002).

1.1.3 Animal models of *Salmonella* infections

Typhoid fever is specific to higher primates and humans, however, it can be modelled using STm infection of mice. This resembles human typhoid in terms of systemic bacterial distribution, bacterial growth kinetics and symptoms (including fever). This model has been established for a long time and has contributed to the development of vaccines against typhoid (Blanden et al., 1966, Harrison et al., 1997). However, the systemic NTS infections described in children and HIV-infected individuals in sub-Saharan Africa and other regions of the developing world have very similar features to typhoid with regard to the systemic nature of infection. Thus the murine STm infection model may also provide insights into human systemic NTS infection (in addition to typhoid)(Tsolis et al., 2011). Furthermore, STm is a natural rodent pathogen (Santos et al., 2001).

Different strains of mice show differing susceptibility to STm infection, and this is largely accounted for by the presence of the susceptibility gene *Ity*. This encodes Natural resistance-associated macrophage protein-1 (Nramp), a transmembrane divalent cation transporter, which is recruited into the cellular membrane of phagocytes in reticuloendothelial system (RES) organ macrophages when they undergo phagocytosis (Vidal et al., 1993, Jones and Falkow, 1996, Pie et al., 1997, Vidal et al., 1995). Therefore Nramp-susceptible strains of mice do not tolerate virulent intracellular bacterial infections due to an inability to regulate bacterial numbers within phagocytes. These mice die within a few days due to uncontrollable bacterial replication.

This system does not appropriately model the systemic NTS infections of humans in sub-Saharan Africa, where the bacteraemia is modest (Gondwe et al., 2010). However, by use of an attenuated strain of STm in an Nramp–susceptible strain of mouse, the systemic infection resembles elements of the infection in humans much more closely. STm virulence is associated with a variety of genes and a range of virulent and attenuated strains have been created for studying infections *in vivo* (Everest et al., 1997). In this study, we used an attenuated strain of STm whereby the a*roA* gene is mutated. This STm strain cannot synthesise aromatic amino acids, thus results in a slower bacterial doubling time (Monack et al., 2004b). Furthermore, by using a slower growing strain, infections persist for several weeks thus it is possible to follow the progression of the infection to resolution stage and investigate different stages of the immune response. In addition, there is an extensive range of genetically modified mice available on a C57BL/6 genetic background, which facilitates an indispensable mechanism for the investigation of the inflammatory immune response *in vivo*.

1.1.4 Pathogenesis of *Salmonella* Typhimurium infection

Salmonella Typhimurium (both in the West and in developing countries) is usually acquired orally. Following ingestion, STm crosses the epithelial barrier at the membranous epithelial (M) cells in the Peyer's patches (Carter and Collins, 1975). These M cells are specialised for uptake and transcytosis of gut antigens into phagocytic cells (Monack et al., 2004a). *Salmonella* Pathogenicity Island 1 (SPI1) genes are required to ensure epithelial crossing (Ohl and Miller, 2001). STm infects the phagocytes of the lamina propria and in non-systemic infections, the infection is self-limiting.

1.1.4.1 Pathogenesis of systemic *Salmonella* Typhimurium infection

In host-adapted systemic infection, such as NTS bacteraemia in humans in sub-Saharan Africa, or systemic STm infection in Nramp-susceptible mice, STm infects the lamina propria phagocytes as described above. However, STm then dissociates into the blood and lymphatics within infected phagocytes, and colonises organs of the RES, including the spleen and liver (Vazquez-Torres et al., 1999, Carter and Collins, 1974). This bacterial dissemination is illustrated in Figure 1.1. Additionally, STm can also disseminate from the gut into the blood via $CD18^{+}$ phagocytes without colonisation of the Peyer's patches. These two routes potentiate distinct immune responses. Whereas $CD18^{+}$-mediated *Salmonella* entry into the circulation stimulates systemic response, M cells induce a mucosal response (Vazquez-Torres et al., 1999).

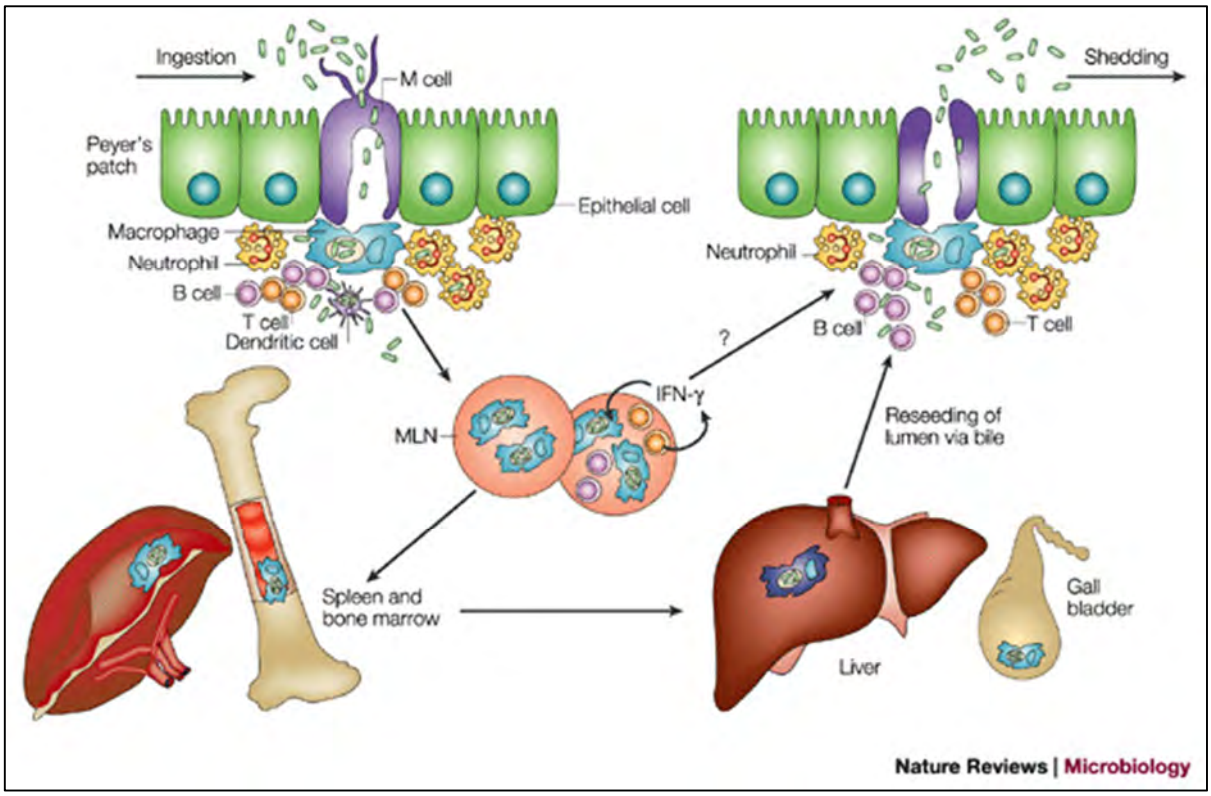

Figure 1.1 Dissemination of *Salmonella* from the gut.

When ingested, bacteria in the gut lumen invade M cells (specialised epithelial cells) within the Peyer's patches of the intestinal mucosa. Bacteria are taken up by macrophages and neutrophils in the lamina propria. During systemic infection, such as typhoid fever or systemic NTS infection, bacteria may be preferentially phagocytosed by dendritic cells and or macrophages which will disseminate via the bloodstream and lymphatics to secondary lymphoid tissues including the MLN. From here, they will be disseminated further, to the spleen, liver and other sites. Back on the lamina propria, the phagocytic cells secrete inflammatory cytokines which recruit T and B cells to the site. T cells can secrete inflammatory cytokines including IL12 (which stimulates IFNγ production), IFNγ (which is required for control of intracellular bacterial replication) and TNFα (which recruits additional innate cells). Bacteria can persist in these RES tissues and may reseed the intestinal mucosa via the MLN and bile ducts. Image taken from (Monack et al., 2004b).

During systemic infection, STm are predominantly located intracellularly within phagocytes, but are also observed extracellularly (Richter-Dahlfors et al., 1997, Conlan and North, 1992, Nnalue et al., 1992, Mastroeni et al., 1995, Hsu, 1989, Lin et al., 1987). However, intracellular survival within macrophages is necessary to avoid extracellular host

defence mechanisms and is required for bacterial virulence (Fields et al., 1986, Lindgren et al., 1996). Thus to survive within macrophages, bacteria must be resilient against complement killing and oxidative stress generated by macrophages. This is mediated by virulence genes known as *Salmonella* Pathogenicity Island 2 (SPI2) genes (Fields et al., 1986, Salcedo et al., 2001, Vazquez-Torres et al., 2000, Hensel, 2000).

1.1.5 Host immunity to *Salmonella* Typhimurium

During STm infection, effective control of bacterial growth requires both an innate and an adaptive cell-mediated host response. The innate system can control bacterial replication, however, an adaptive response is required to initiate bacterial clearance (Mastroeni et al., 1995, Richter-Dahlfors et al., 1997, Conlan and North, 1992).

1.1.5.1 Innate immune response to *Salmonella* Tyhphimurium

To ensure that an innate immune response is only initiated when the host may be in danger from an invading pathogen, and to prevent unwanted immune activation, the host must have a robust mechanism of pathogen detection. This is enabled by host pattern recognition receptors (PRRs), which recognise invaders by their surface expression of pathogen-specific molecules, known as pathogen associated molecular patterns (PAMPs) (Janeway and Medzhitov, 2002). Host cells do not express PAMPs, hence innate responses cannot be initiated following detection of host cells. Several different types of host PRRs can initiate differential immune responses. In the gut, Toll-like receptors (TLRs) and Nucleotide Binding and Oligomerisation Domain (NOD)-like receptors (NLRs) are important in PAMP recognition on invading pathogens, including *Salmonella* (Balaram et al., 2009).

When PRRs are activated by the relevant pathogenic stimuli, they signal via adaptor proteins in the cytoplasm (including myeloid differentiation factor 88 (Myd88)), which activate transcription factors (such as nuclear factor kappa-light-chain-enhancer of activated B cells (NFκB)) and ultimately induce transcription of inflammatory genes (Janeway and Medzhitov, 2002). These genes encode a multitude of inflammatory proteins, including pro-inflammatory cytokines such as tumor necrosis factor-α (TNFα), Interferon-γ (IFNγ), Interleukin (IL) -1, IL6, and IL8. Once translated into functional protein, pro-inflammatory cytokines bind their relevant receptors and often initiate cell proliferation, which drives an inflammatory response. Other inflammatory genes encode bactericidal proteins, nitric oxide synthase, cyclooxygenase-2 and pro-proliferation signalling molecules including mitogen-activated protein kinases (Balaram et al., 2009).

1.1.5.2 Innate cells

There are several different lineages of innate cells which express PRRs and are thus capable of detecting and responding to invading pathogens (Janeway and Medzhitov, 2002). These cells are collectively termed leukocytes and they are all derived from a common myeloid haematopoietic progenitor, as illustrated in Figure 1.2.

Innate cells include: dendritic cells (DCs) macrophages, neutrophils, eosinophils, basophils and natural killer (NK) cells. Although these cells are described under these labels there is a wide range of diversity in their expression of phenotypic markers, indicating that there are multiple sub-populations of these cells. The cell subsets investigated during this thesis are detailed further in the relevant results chapters. The induced inflammatory gene expression will differ in each cell type, enabling cell-type specific cytokine production, thus the inflammatory function of each cell type will vary accordingly. Some of the main

inflammatory functions of innate cells are outlined in Table 1.1. Importantly, the initiation of innate inflammation is a rapid process; these cells are constantly circulating the body and are fully equipped with the means to react quickly.

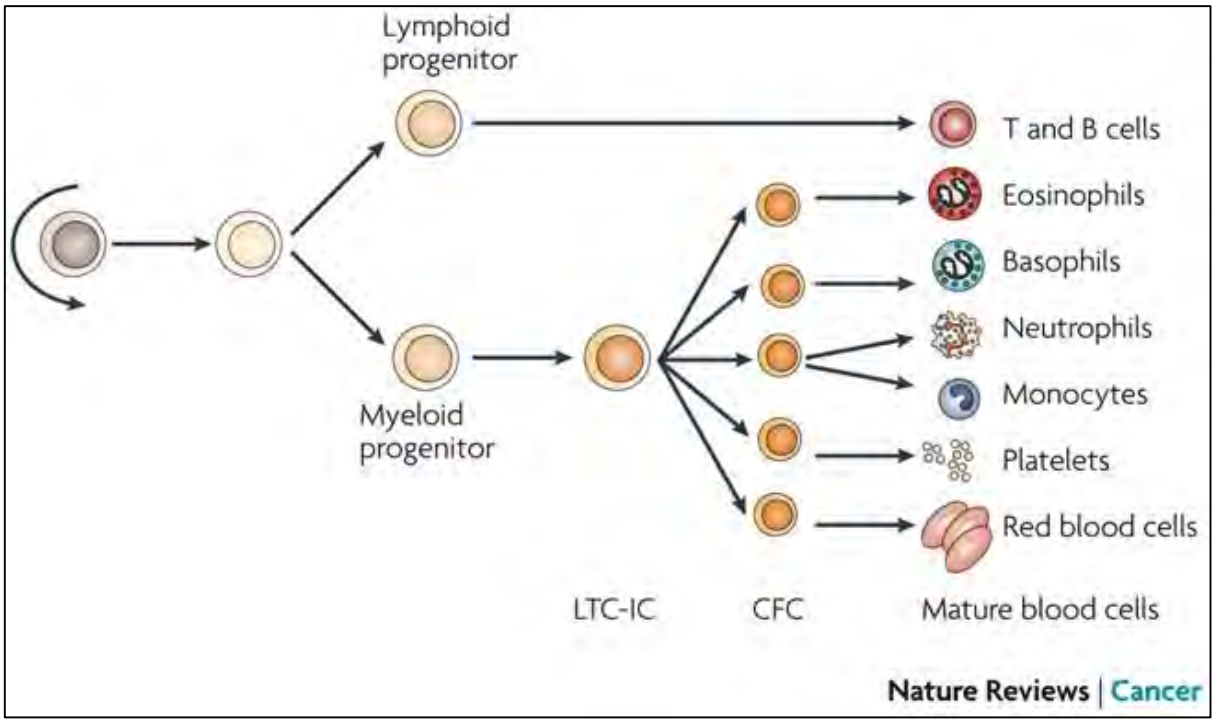

Figure 1.2 Haematopoiesis

Haematopoiesis is the hierarchical process in which new blood cells are generated. Multipotent haematopoietic stem cells (HSCs), (or SCID repopulating cells (SRCs)) are primitive cells which can give rise to all other progenitor cells, which then can reconstitute the repertoire of blood cells. HSCs (grey cell to left of Figure) give rise to lineage-restricted progenitors, which in turn, can proliferate or differentiate down either the lymphoid or myeloid lineages. Myeloid progenitor cells give rise to long-term colony-initiating cells (LTC-ICs) which give rise to colony-forming cells (CFCs), which give rise to myeloid-lineage cells. Mature blood cells cannot proliferate further. Image taken from (Corey et al., 2007).

Innate leukocyte	Important functions
Neutrophil	• Arrive first at the site of infection (Peveri et al., 1988). • Secrete chemokines to attract other innate cells. • Contain granules containing antibacterial proteins, and hydrolytic enzymes (Masson et al., 1969). • Phagocytose and kill intracellular bacteria by the respiratory burst (Segal, 2005). • Attracted by IL8
Macrophage	• Tissue resident phagocytes. • Phagocytose and kill intracellular bacteria by the generation of cytotoxic reactive oxygen species (ROS) (Umezawa et al., 1995).
Kupffer cell (liver resident macrophage)	• Can be both protective and destructive (Klein et al., 2007). • Produce pro-inflammatory cytokines including TNFα and IL6 which stimulates T cells (Tacke et al., 2009, Zimmermann et al., 2012). • Produce IL12 and IL18 which regulate NK cells (Hsu et al., 2007, Tacke et al., 2009). • Phagocytose bacteria and other infected host cells (Brown et al., 2010).
Dendritic cell (DC)	• Professional antigen presenting cells (APCs). Following antigen uptake and processing, DCs present antigen to lymphocytes in the context of major histocompatibility complex MHC (Banchereau and Steinman, 1998).

Table 1.1 Cells of the innate immune system

The cells of the innate system provide a rapid and robust defence against invading pathogens, including *Salmonella* (Janeway and Medzhitov, 2002). However, whilst this system can control pathogen invasion to some degree, in the case of STm infection, a cell-mediated response is required to establish bacterial clearance. Particularly in the case of STm, efficient bactericidal killing by macrophages requires T cell help, thus an adaptive response is necessary (Ramarathinam et al., 1993).

1.1.5.3 Innate versus adaptive immunity

Cells of the adaptive immune response, known as lymphocytes, of which there are two classes, are derived from a common lymphoid progenitor (Kondo et al., 1997). The two lineages of lymphocyte are called T and B lymphocytes, named after the primary lymphoid tissue in which they mature (the thymus and bone marrow, respectively). These cells differ fundamentally to those of the innate compartment in that they are antigen-specific. Thus during their generation, they are programmed to respond to a specific antigen in a process known as somatic recombination. On recognition of their specific antigen, these cells clonally proliferate, thus making copies of themselves which can also respond to the specific antigen which has been encountered. Whilst this enables a more directed immune strategy than the innate system, it takes a few days to develop, thus the innate response is vital during initial pathogen control, until the adaptive response is established.

1.1.5.4 Adaptive immunity to *Salmonella* Tyhphimurium

Although there are only two lineages of lymphocytes, these have been extensively compartmentalised into further sub-types based on surface expression of a multitude of markers (Jelley-Gibbs et al., 2008, Le Pottier et al., 2007). Subtypes of $CD4^+$ T lymphocytes are illustrated in a simplified form in Figure 1.3. These lymphocyte subpopulations have specific functions which have been described elsewhere (Mosmann et al., 1986, Mosmann and Coffman, 1989). $CD4^+$ T cells are particularly important in the primary response to STm because they promote the bactericidal effect of macrophages, they promote inflammation, and they mediate switched antibody production by B cells (Nauciel, 1990, Mittrucker et al., 1999, Monack et al., 2004b).

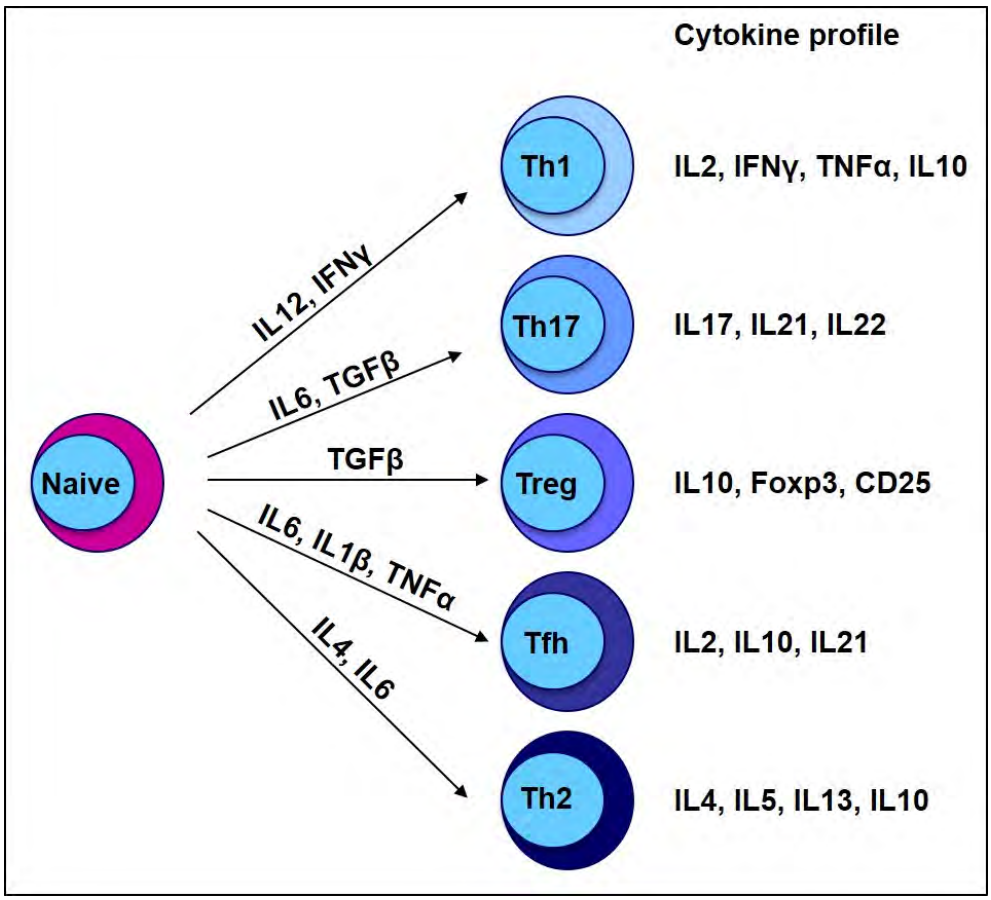

Figure 1.3 CD4$^+$ T cells differentiate down distinct lineages.

During CD4$^+$ T cell activation in the periphery, naïve CD4$^+$ T cells differentiate according to the local cytokine environment. T cells within each lineage have distinct functions, which are potentiated by their effector cytokine profiles. These lineages include Th1 cells, Th2 cells and regulatory T cells (discussed further here); and follicular T helper cells, and Th17 cells. Diagram adapted from (Jelley-Gibbs et al., 2008).

T cells become activated upon antigen presentation by innate antigen presenting cells such as DCs (Tacke et al., 2009, Winau et al., 2007). The direction of the response to Th1 or Th2 can depend on the antigen and the cytokine environment (Bobat et al., 2011, Serre et al., 2008, Balaram et al., 2009). STm induces a Th1 response and this response requires the transcription factor T-bet and is potentiated by pro-inflammatory Th1 cytokines IFN-γ, TNF-α, IL-2 and IL-12 (Pie et al., 1997, Ramarathinam et al., 1991). These cytokines repress Th2 signals including production of IL-4, thus maintaining a cell-mediated response (Balaram et

al., 2009). T cells are further stimulated to produce IFN-γ by DC and activated macrophage secretion of IL-12 (which additionally stimulates IFN-γ production by NK cells and NKT cells). Interferon-γ induces the bactericidal activity of macrophages and B cell Immunoglobulin (Ig) G2a production, thus is vital for defence against intracellular bacteria (Pie et al., 1996, Nauciel and Espinasse-Maes, 1992, Mastroeni et al., 1998, Kaufmann, 1993). The priming of Th1 responses in these models of infection is strongly dependent upon the collaboration of monocyte-derived and conventional DCs (Flores-Langarica et al., 2011).

To prevent overt immune activation, especially during inflammatory responses, regulatory T cells (Tregs) exert anti-inflammatory function including the release of anti-inflammatory cytokines such as IL10 (Chen et al., 2003). The transcription factor FoxP3 is associated with Tregs in mice. This is particularly important in persistent infections where the extent of macrophage activation can result in pathological damage to host tissues (Monack et al., 2004b). In addition to cell-mediated immunity, there are multiple other host strategies which contribute to immunity to STm. In particular, complement and antibody-mediated bacterial opsonisation, and humoral responses are essential, and these are discussed elsewhere (MacLennan et al., 2008, Mittrucker et al., 2000, Nakoneczna and Hsu, 1983, MacLennan et al., 2010).

1.2 Liver physiology

The liver is colonised during systemic *Salmonella* infection and in this study, we investigate the host inflammatory response in this effector site, therefore an understanding of liver anatomy is fundamental. The structure of the liver is highly dependent on the unique organisation of its vasculature, and this is detailed in Figure 1.4 (Thomson and Knolle, 2010).

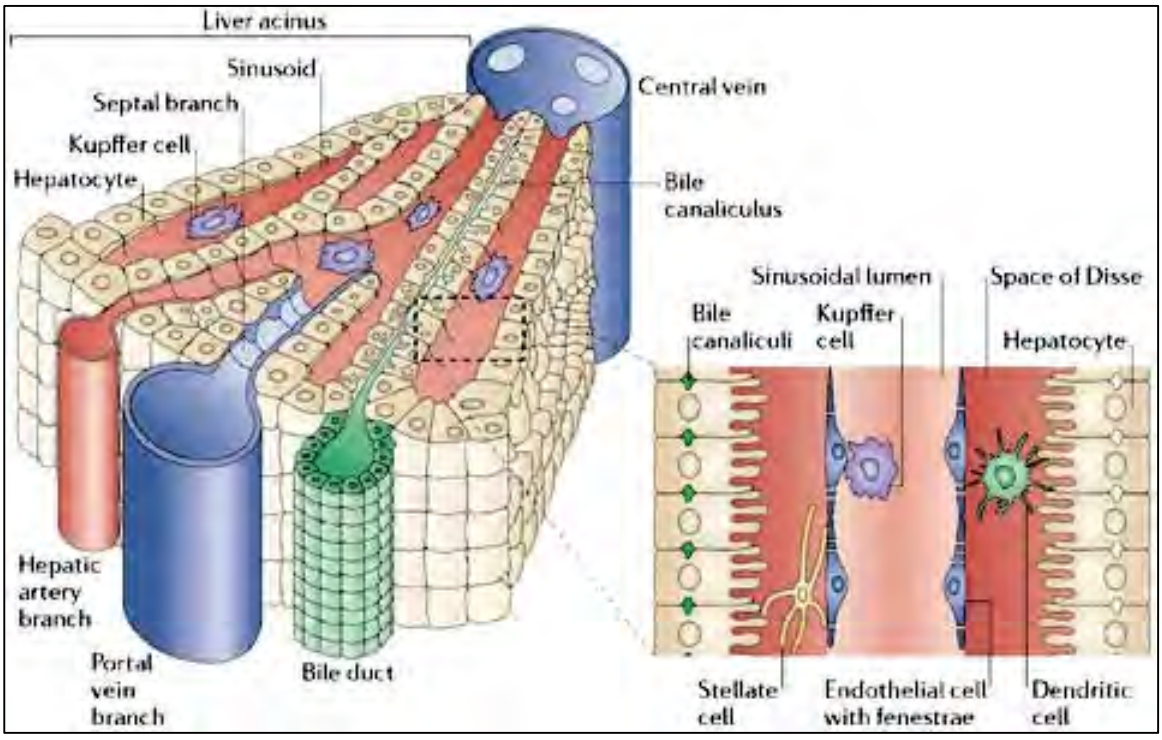

Figure 1.4 The acinus structure of the liver and its vasculature.

The portal vein (delivering blood from the gut) and the hepatic artery (delivering blood from the heart) meet in the intrahepatic portal tracts, and drain into the sinusoidal capillaries. Portal tracts also support bile ducts, which transport bile from the canaliculi (between adjacent plates of hepatocytes), to the extra-hepatic biliary system. Blood from the portal tract flows through the sinusoids, and is drained by the central vein. Inset: Sinusoids are lined by hepatic sinusoidal endothelial cells (HSEC) which are unique in that they lack basement membranes and tight junctions. HSEC are fenestrated and are organised into sieve plates. Kupffer cells, the liver resident macrophages, reside adjacent to sinusoidal endothelium. Below this is the space of Disse where stellate cells, hepatic fibroblasts, and extracellular matrix proteins are located. Image taken from (Adams and Eksteen, 2006).

1.2.1 Hepatic blood supply

The liver receives a dual blood supply whereby the hepatic portal vein carries blood from the gut and the hepatic artery supplies oxygenated blood from the heart (Crispe, 2003). On entering the liver, these vessels, together with the bile duct, branch into intrahepatic portal tracts, which are encased in connective tissue. The general architecture of the liver can be compartmentalised into multiple acini, which describes a small portion of hepatic tissue and the vasculature which serves it (Adams and Eksteen, 2006).

Blood enters the acinus at the portal tract where it flows into specialised capillaries called sinusoids. These provide a sponge-like environment where the separate blood supplies (oxygenated blood from the heart and nutrient/antigen-rich blood from the gut) mix before progressing through the acinus. Sinusoids run between chords of hepatocytes, (specialised parenchymal cells of the liver), to a central venule where blood is drained away towards the inferior vena cava. The sinusoids are lined with fenestrated sinusoidal endothelial cells which lack a basement membrane and tight junctions. This facilitates intimate contact between blood plasma (and its constituents) and hepatocytes. Blood flow through sinusoids is regulated by myofibroblast sphincters, and an oxygen gradient throughout each acinus (due to proximity to the portal tract) enables different acinus regions to maintain different hepatocyte functions. Consequently, some areas are more prone to hypoxic damage (Adams and Eksteen, 2006).

1.2.2 Cells of the liver

The parenchymal cells of the liver, hepatocytes, are polarised epithelial cells which run in parallel cords between the portal tract and central venule. These cords of hepatocytes are at least two cells thick, and running between adjacent hepatocytes is the bile canalliculus,

a small tributary of the bile duct branches in the portal tracts. Thus hepatocytes produce bile and secrete it (through the apical membrane) into these canalliculi, where it is drained towards the portal tracts, in the opposite direction to blood flow. The basolateral membrane of hepatocytes lies adjacent to the fenestrated endothelium of the sinusoids. The area between these cellular membranes, known as the space of Disse, is where stellate cells reside. Associated with the surface of sinusoidal endothelium are NK cells and Kupffer cells, liver-resident macrophages, which are important in pathogen defence. Kupffer cells express many innate recognition receptors which trigger phagocytosis, and can contribute to granuloma formation during infection (Beattie et al., 2010). Therefore, the liver is an important immunological organ, due to its capacity to detect both blood-borne and gut associated antigens (Liaskou et al., 2012).

1.2.2.1 Kupffer cells

Kupffer cells reside in the sinusoids, thus provide an extensive network of intravascular macrophages, strategically positioned for the detection of pathogens (Crispe, 2009, Bilzer et al., 2006, Zimmermann et al., 2012). Kupffer cell heterogeneity is reported in mice and humans with regard to expression of phenotypic markers, cellular function, and cellular origin (Kinoshita et al., 2010, Klein et al., 2007, Tacke et al., 2009). Two Kupffer cell populations have been defined in mice: a sessile, liver-resident population, and a more motile population, derived from bone-marrow precursors which are characterised by higher CD80 expression (Klein et al., 2007, Tacke et al., 2009).

1.2.3 Liver function

The liver plays a vital role in maintaining host homeostasis, particularly in digestion and metabolism (Protzer et al., 2012, Treyer and Musch, 2013). Hepatocytes regulate blood

glucose concentration by storing glucose as glycogen during hyperglycaemia and subsequently by elevating glucose concentrations by gluconeogenesis. Fatty acids are metabolised to triglycerides and ketones, and hepatocytes also produce cholesterol, plasma proteins, including albumin and clotting factors, and bile acid (Amitrano et al., 2002, Peck-Radosavljevic, 2007, Treyer and Musch, 2013). The liver is also vital in the elimination of toxic compounds, including ammonia, which is broken down to urea and released into sinusoidal blood for removal in the kidney, and other harmful substances including drugs and alcohol. These can be broken down and excreted via the urinary pathway, or conjugated to glutathione (for increased solubility), for excretion in bile.

1.2.4 The liver as an immunological organ

Due to its proximity to the gut, the liver is vital in immune surveillance (Gao et al., 2008). Gut-derived antigenic material is constantly delivered in the portal vein, and the liver must be permanently on guard (Zimmermann et al., 2012). Yet the constant exposure to foreign but safe antigens, such as food antigens, dictates the liver must also be highly tolerogenic (Tacke et al., 2009). A resting human liver contains at least 10^{10} lymphocytes, including T cells (predominantly primed memory cells), NK cells and NKT cells (Adams and Eksteen, 2006). Hepatic dendritic cells play a vital role in the maintenance of the tolerogenic state of the liver and features such as their enhanced phagocytic ability facilitates this function (Hsu et al., 2007). However, they play an equally vital role in immune induction, both in antigen presentation and in the activation of other immune cells via cytokine release (Hsu et al., 2007, Crispe, 2011). Multiple DC populations are found in the liver, located throughout the parenchyma and portal tracts (Adams and Eksteen, 2006, Jomantaite et al., 2004, Yoneyama and Ichida, 2005).

1.2.4.1 Inflammation in the liver

Entero-hepatic lymphocyte recirculation allows a constant monitoring of antigens in the gut and liver, enabling efficient recruitment of inflammatory cells when necessary (Grant et al., 2002, Seki et al., 2000). During inflammation, myeloid and plasmacytoid DCs enter the liver from the blood (Yoneyama and Ichida, 2005). On antigen encounter, myeloid DCs move through the space of Disse to the portal tracts where they enter lymph nodes, leaving the liver at the porta hepatis (Adams and Eksteen, 2006). Lymphocyte populations of the liver ($CD4^+$ and $CD8^+$ T cells, NK cells and NKT cells) can expand quickly. In addition, peripheral lymphocytes infiltrate from the portal vein or the hepatic artery and are captured by adhesion molecules expressed by hepatic sinusoidal endothelial cells (HSECs). Due to the low-shear flow of sinusoids, HSECs do not express selectins, which are classically required for tissue capture of lymphocytes. Instead, lymphocytes can directly interact with HSEC adhesion molecules (including Vascular Adhesion Protein-1, Vascular Cell Adhesion Molecule-1 and Intercellular Adhesion Molecule-1) via integrins (Lalor and Adams, 2002).

Chemokine expression differs at portal tracts and on sinusoidal endothelium. Some chemokines are constitutively expressed in portal areas, facilitating lymphocyte surveillance in addition to recruitment during inflammation. Fewer chemokines are expressed in parenchymal areas under normal conditions, however, infiltrates rely on chemokines to reach their target destination once inside the tissue (Lalor and Adams, 2002, Adams and Eksteen, 2006).

1.2.5 Detection of liver injury

Liver injury can manifest in multiple forms including: hepatitis (inflammation in the liver), cholestasis (disrupted bile flow), necrosis, pre-neoplastic/neoplastic injury, or reversible

pathologies such as steatosis. Other non-specific pathology can occur, particularly if the liver is not the primary site of pathology (Ramaiah, 2007). Biochemical analysis of the serum can indicate differential liver damage by the detection of different liver-specific components, including: leakage enzymes, cholestasis enzymes, and liver-synthesised products.

Hepatic leakage enzymes are located in the cytoplasm of hepatocytes and altered membrane permeability can result in their leakage through the basal-lateral membrane into the sinusoidal blood. Examples include: alanine aminotransferase (ALT) and aspartate aminotransferase (AST). For assessing hepatocyte injury, ALT is more informative as it is hepatocyte-specific and is found in both periportal and centrilobular cells (Amacher, 2002). Furthermore, ALT has a longer half-life (40-60 hours) than AST (12 hours), thus can provide a more sensitive measure of hepatocyte injury (Ramaiah, 2007). AST is additionally located in myocytes and erythrocytes, thus its presence in the serum can reflect muscle injury and hemolysis, respectively. Whilst ALT is a cytosolic protein, AST is both a cytosolic and a mitochondrial protein, thus more extensive hepatocyte injury is required to detect AST in the serum. Both the duration and extent of liver injury, and the rate of removal from serum affect measurement of these enzymes (Ramaiah, 2007, Solter, 2005).

Cholestasis (interrupted bile flow) is detected by increased hepatic production of cholestatic enzymes alkaline phosphatase (ALP) and gamma-glutamlytransferase (GGT). These are released into the canaliculi and blood following cholestasis, and in response to certain drugs (Ramaiah, 2007). Both enzymes are located in biliary epithelial cells; ALP is additionally found in the canaliculi of the intestinal mucosa, thus ALP concentrations can be altered by diet (Amacher, 2002). Total serum bilirubin is elevated in pre- and post-hepatic cholestasis when conjugated bilirubin leaks into the blood. However, total bilirubin

is also increased in the serum during hemolysis (pre-hepatic bilirubinemia) and when not properly secreted into canaliculli (post-hepatic bilirubinemia). Cholestasis-induction enzymes can usually be detected before increased serum bilirubin (Ramaiah, 2007).

The detection of liver-synthesised/metabolised products in the blood further assesses hepatobilliary function. Altered blood concentrations of coagulation proteins, albumin and ammonia can indicate liver injury, although, liver function must be severely disrupted to detect changes in the blood (Ramaiah, 2007). Measurement of bile acid (synthesised by hepatocytes) and bilirubin in the blood are used to assess hepatocyte uptake and detoxification, and are a specific indicator of liver injury (Ramaiah, 2007).

1.2.6 Liver pathology during systemic infection

Systemic infections are frequently associated with tissue pathology and this can occur in multiple tissues including the liver. In the liver, pathological lesions called granulomas can form. These are composed of specifically arranged infiltrated leukocytes and they can limit tissue damage from both the pathogen (by restricting dissemination) and the host inflammatory response (Saunders et al., 2004, Bokhari et al., 2008, Guilloteau et al., 1991). However, due to their disruption of liver architecture, lesions can cause irreparable damage to host tissue, and can be pathogenic (Herkel et al., 2005). Additionally, following infection resolution, the liver may undergo emergency tissue repair, thus leaving tissue further damaged by fibrosis (Wahl et al., 1986).

1.2.6.1 The impact of typhoid fever on the liver

Hepatitis is a common feature of typhoid fever (Pramoolsinsap and Viranuvatti, 1998). The impact of this can range from hepatomegaly and modest alterations in biochemical tests

to *Salmonella hepatitis*, characterised by acute pathology, abnormal liver function, and is frequently associated with jaundice (Serefhanoglu et al., 2003, Yildirim et al., 2010). *Salmonella* hepatitis occurs in all ages both in typhoid fever endemic and non-endemic areas, although incidence is highest in the East (reported in 4-8% of typhoid fever patients in India) (Pramoolsinsap and Viranuvatti, 1998). Severe *Salmonella* hepatitis occurs more frequently in patients with underlying infection, and those who are malnourished or anaemic (Khosla et al., 1988, Husain, 2011).

1.2.6.2 Pathology of *Salmonella* hepatitis

Salmonella hepatitis is characterised by hyperplasia of reticuloendothelial cells and development of granulomatous lesions known as *typhoid nodules* (Malik, 2002). These occur in both sinusoidal and portal areas and are formed by aggregation of Kupffer cells, macrophages and monocytes, and can be necrotic in the centre. Lymphoid cells are seen throughout the sinusoids (Ramachandran et al., 1974, Khosla et al., 1988, Pramoolsinsap and Viranuvatti, 1998). These lesions have been described in the liver during typhoid fever since 1860 (Mallory, 1898). In addition, cholestasis is associated with *Salmonella* hepatitis. This can be especially prominent during jaundice, which is likely to be caused by a combination of granulomatous pathology, (which may occur with portal phlebitis and cholangitis), and haemolysis (Pramoolsinsap and Viranuvatti, 1998, de Brito et al., 1977). Although biochemical tests can be severely altered during *Salmonella* hepatitis, this has not been directly linked with overt pathology (Huang et al., 2005). Increased serum concentrations of transaminase and bilirubin are common, whereas ALP and cholesterol may be mildly elevated (Pramoolsinsap and Viranuvatti, 1998). The disruption to liver function during *Salmonella* hepatitis has been associated with multiple organ injury and

disseminated intravascular coagulation (DIC) (Rao et al., 1978, Greig and Naidoo, 1981, Ozen et al., 1995, Huang et al., 2005).

1.2.6.3 Liver pathology during systemic NTS infections

There is little evidence of hepatic pathology and aberrant liver function in systemic NTS infections in humans. This may be due to the limited facilities available in endemic areas, in addition to illusive diagnosis of NTS infections. Considering the prevalence of hepatic complications in typhoid, and with bacterial colonisation of the liver apparent in murine studies, it is likely that hepatic complications in human systemic NTS infections may frequently pass by unreported.

1.2.6.4 Evidence in murine NTS infections

In murine models of NTS infections, hepatic pathology is similar to that seen in typhoid fever whereby histopathological lesions form in the liver, although the severity and kinetics vary with the infection conditions used (Nakoneczna and Hsu, 1980, Nakoneczna and Hsu, 1983, Conlan and North, 1992, Mastroeni et al., 1995, Umezawa et al., 1995, Everest et al., 1997, Richter-Dahlfors et al., 1997, Sheppard et al., 2003, Brown et al., 2006, Nix et al., 2007, Brown et al., 2010, Barreiros et al., 2000).

Briefly, a low dose (10^2 CFU) of virulent STm induces acute microscopic abscesses by day 4, which are initially composed of polymorphonuclear (PMN) leukocytes. By day 7, granulomas with necrotic centres are established with monocytes found at the periphery, which are resolved within 2 weeks and hepatic tissue is regenerated (Nakoneczna & Hsu, 1980). A higher dose (10^5 CFU) of virulent STm results in acute microscopic abscess formation by day 2, which cover 70% of the liver by day 4. Extensive necrosis is also

observed, and mice begin to die (Nakoneczna and Hsu, 1983). Thus STm virulence determines the kinetics of hepatic pathology, and this has been confirmed more recently (Richter-Dahlfors et al., 1997). Furthermore, control of bacterial growth during the first week of infection requires TNF-α and this has been additionally shown to be due to TNF-α-mediated macrophage recruitment in the formation of granulomas in the liver (Mastroeni et al., 1991, Mastroeni et al., 1995). Thus granuloma formation is a necessity for the host to control bacterial growth.

Additional studies have more recently described lesion formation in greater detail, including the presence of lymphocytes and the transient nature of PMN cells in these structures (using 3 x 10^3 CFU virulent STm) (Mastroeni et al., 1995). These studies report an absence of neutrophils in the liver during the first couple of days, but that these cells later occupy the central regions of foci, where necrosis is observed. Disintegrated neutrophils are later replaced by monocytes (Richter-Dahlfors et al., 1997). Incidentally, Kupffer cells have been described at the periphery of foci and in interstitial spaces, whilst infiltrating monocytes are observed within lesions in some studies (Richter-Dahlfors et al., 1997).

1.2.6.5 Inflammatory lesions disrupt parenchymal architecture

During infection, inflammation disrupts hepatic architecture as has been shown by fluorescent labelling of actin filaments, which enable visualisation of the hepatocyte plates, bile canaliculli, and sinusoids. Leukocyte infiltration disrupts hepatocyte plate architecture and this occurs prior to hepatomegaly. Additionally, visualisation of the junctions between hepatocytes (by cytokeratin Endo-A staining) further illustrates altered hepatocyte structure early post-infection (Richter-Dahlfors et al., 1997). Increased infection dose

results in a similar severity of altered hepatic morphology, but a faster progression of infection (Richter-Dahlfors et al., 1997).

1.2.6.6 Bacteria co-localise with macrophages in the liver

In the liver, STm has been visualised in multiple cell types including hepatocytes, Kupffer cells, neutrophils, although bacteria were not usually detected within PMN cells (due to their efficient killing of ingested bacteria). This study used a high dose (10^7 CFU) of virulent bacteria and infected hepatocytes were observed undergoing cell lysis and in contact with PMN leukocytes (Conlan and North, 1992). Growth of STm within hepatocytes and PMNs has been further demonstrated using both a lethal challenge dose (10^5 CFU virulent STm) and low bacterial dose in conjunction with neutralisation of TNF-α. Hepatocytes containing intracellular bacteria were severely damaged (Mastroeni et al., 1995). These studies both used un-physiological infection doses to enable bacterial visualisation *in vivo* (Hsu, 1989). Using a challenge dose which mimics natural systemic infection, STm are predominantly detected intracellularly within $CD18^+$ macrophages. These macrophages are largely located within lesions but can be seen in interstitial areas as infection progresses, however, STm always co-localises to leukocytes. Observation of bacterial cell division inside macrophages suggests this is the predominant site of proliferation (Richter-Dahlfors et al., 1997). Furthermore, a study into the dynamics of bacterial growth and foci development demonstrated that bacteria expand clonally within host cells and do not move between foci (Sheppard et al., 2003). Thus bacterial growth in the liver is due to increased infected cells, foci and increased infected cells per foci (Mastroeni and Sheppard, 2004, Richter-Dahlfors et al., 1997, Sheppard et al., 2003). The concept of a critical threshold in both

bacterial load of host cells and in foci size has been further addressed by stochastic modelling and histology (Mastroeni et al., 2009, Brown et al., 2006, Grant et al., 2009).

1.2.6.7. Infection, hepatic inflammation and haemostasis

Systemic bacterial infections, including those caused by NTS, can be associated with serious clinical complications including multiple organ failure (Karima et al., 1999, Graham et al., 2000b, Rajekar et al., 2008, Muyembe-Tamfum et al., 2009, de la Fuente-Aguado et al., 1999, Laing et al., 1995). These infections can additionally induce clinical complications of a haematological nature, including aberrant blood coagulation, as is seen with DIC (Wada et al., 2008). The severity of the haemostatic defect frequently correlates to outcome of infection (Yaguchi et al., 2004, Levi et al., 2000). Thus a complete understanding of how systemic infection affects both the host's immunological response and other physiological responses including inflammation and haemostasis are required to facilitate appropriate therapeutic control of these infections. The haemostatic system is described below.

1.3 Haemostasis

Blood flow is maintained by the haemostatic system, which tightly regulates the host mechanisms of response to vascular damage. This balanced system must be able to respond rapidly to blood vessel injury, but must be suitably regulated to prevent unnecessary activation, such as unwanted thrombosis. Components of the haemostatic system are: blood vessels, platelets, coagulation factors, coagulation inhibitors and fibrinolysis mediators (Hoffbrand et al. 2006). Haemostasis can become dysregulated during inflammation and this can result in a pro-coagulant environment and unwanted pathologies including DIC, and different mechanisms appear to regulate these events in the arterial and venous systems (Esmon, 2005, Engelmann and Massberg, 2013). In recent years, the extent to which coagulation and inflammation are closely regulated has become increasingly apparent. Here we summarise the general perception in the literature of the relationship between these physiological responses, and highlight important examples of this partnership during systemic infection.

1.3.1 Coagulation

Coagulation is the mechanism which gives rise to blood clotting. The coagulation system is composed of a tightly regulated cascade of coagulation factors which are located in the plasma (Engelmann and Massberg, 2013). Activation of this system results in the production of thrombin and conversion of fibrinogen to fibrin, which can form a haemostatic plug at the site of vessel injury by capturing platelets and other circulating cells (Furie and Furie, 2008). The cascade can be amplified at many levels, and is regulated by negative feedback, resulting in efficient and localised coagulation (Hoffbrand et al. 2006).

1.3.1.2 Endothelial cells in coagulation regulation

The vascular endothelium is responsible for maintaining sufficient blood supply to vital organs. Thus these cells are key to the regulation of coagulation and also of blood cell migration, expression and synthesis of adhesion molecules and chemokines, vasopermeability and vascular tonus (Keller et al., 2003, Esmon, 2005). Under normal conditions, endothelial cells express anticoagulant molecules including heparin sulphate, thrombomodulin and plasminogen activator. However, on endothelial activation, expression is switched to pro-coagulation molecules including tissue factor (TF) and Von Willebrand factor (VWF), but also cytokines, adhesion molecules and growth factors (Camerer et al., 1996, Keller et al., 2003). In addition, endothelial production of anticoagulant molecules including protein C and antithrombin (AT) can be reduced, and the endothelial involvement in the fibrinolytic system can be disrupted (Biemond et al., 1995, Keller et al., 2003, Levi et al., 1999).

Endothelial function can be impaired during activation and/or injury. For example, activated endothelial expression of adhesion molecules and the subsequent leukocyte recruitment can damage the endothelium, thus activating coagulation (Keller et al., 2003). A major role of the endothelium in maintaining haemostasis is the regulation of platelets. Platelets can bind to hepatic sinusoidal endothelial cells *in vitro* and this has been shown to increase leukocyte recruitment (Lalor et al., 2013). Endothelial cells prevent aggregation of activated platelets by the synthesis and secretion of nitric oxide and prostacyclin (Keller et al., 2003).

1.3.2 Platelets and platelet activation

Platelets are the second most abundant corpuscular constituents of blood and are small cells (1-3 μm diameter) produced by megakaryocytes in the bone marrow (Battinelli et al., 2007). In their resting form they are disc-shaped and upon activation they become spherical with pseudopodia (Yeaman, 2010). Platelets are a-nucleate but contain residual mRNA derived from their megakaryocyte parent cell, and important cellular components are stored within granules in the cytoplasm. These components include ADP and Ca^{2+}, in addition to proteins involved in haemostasis, such as VWF and fibrinogen, and microbicidal proteins are also stored in platelet granules (Fitzgerald et al., 2006a).

When vascular injury occurs in the arteriolar system, platelets are captured via binding of platelet membrane glycoproteins GP1bα and αIIbβ3 to VWF bound to exposed collagen (Hogan et al., 2002, Bergmeier et al., 2008). This interaction brings the platelet Ig receptor, GPVI, into the vicinity of collagen, resulting in platelet activation (Massberg et al., 2003). Platelet activation results in a conformational change in the platelet fibrinogen receptor GPIIb/IIIa, enabling its binding to immobilised fibrinogen and, among other ligands, soluble fibrinogen (Furie and Furie, 2005, Broze et al., 1988).

The presence of platelets at the site of injury is important in the provision of sufficient surface area of membrane phospholipid, which enables efficient activation of the coagulation cascade (Lentz, 2003). Rapid haemostatic plug formation is usually able to control bleeding temporarily and is regulated by endothelial cell-derived prostacyclin to prevent excessive platelet aggregation (Hoffbrand et al. 2006). However, fibrin cross-linking is required to stabilise the plug, which is especially important once platelet autolysis occurs (Hoffbrand et al. 2006).

1.3.2.1 Platelet activation through C-type lectin-like receptor 2

In addition to the GPVI-mediated platelet activation described above, platelets can become activated by other means. Interaction of platelet-expressed C-type lectin-like receptor 2 (CLEC-2) with its ligand podoplanin has been shown to activate platelets *in vitro* (Watson et al., 2010, Hughes et al., 2010b, Suzuki-Inoue et al., 2006). Podoplanin is a transmembrane glycoprotein (also referred to as gp38) found on multiple cell types, including stromal cells and inflammatory macrophages (Astarita et al., 2012). Its expression by lymphatic endothelial cells (LEC) (and not other blood endothelial cells) has enabled its use as a marker for lymphatic endothelium (Wetterwald et al., 1996). Podoplanin may contribute to the development of architecture in lymphoid organs such as the spleen and lymph nodes, and has an important role in orchestrating various aspects of inflammation in these sites (D. Withers, personal communication) (Astarita et al., 2012, Peters et al., 2011). However, podoplanin is the only reported physiological ligand for CLEC-2 and the relationship between podoplanin on LEC and platelet-expressed CLEC-2 is well defined and is necessary for the development of lymphatic vasculature (Suzuki-Inoue et al., 2010).

Expression of CLEC-2 is also detected on activated DCs although additional reports of expression on other cell types, including neutrophils, are now believed to be due to off-target effects of some antibodies (G. Desanti, manuscript in preparation) (Astarita et al., 2012, Kerrigan et al., 2009, Acton et al., 2012). Recently, there have been several reports of podoplanin-CLEC-2 interaction in various inflammatory scenarios. For example, CLEC-2 expressed by DCs can mediate DC motility within lymphoid tissues and can aid recruitment of these cells from the periphery, by interaction with podoplanin on LECs and fibroblastic reticular cells (FRCs) (Acton et al., 2012). Furthermore, the importance of CLEC-2 expression by platelets has been demonstrated in the maintenance of vascular integrity by

preventing haemorrhage during inflammation in lymph nodes and other sites (Boulaftali et al., 2013, Herzog et al., 2013). Accounts of podoplanin up-regulation during inflammation have also been reported on macrophages (Hou et al., 2010, Kerrigan et al., 2012). Thus podoplanin can have an impact on signalling in both inflammation and in platelet activation and so in theory, could link these two host responses. However, whilst platelets can be activated via CLEC-2 *in vitro*, as yet, there has been no evidence of inflammatory podoplanin expression and platelet activation via platelet-expressed CLEC-2 *in vivo*.

In mice, embryos which lack CLEC-2 generally do not survive, and this is possibly due to impaired lymphatic function as a consequence of blood-lymphatic mixing and a failure to inflate the lungs at term (Suzuki-Inoue et al., 2010, Finney et al., 2012). For this reason, the study of CLEC-2 in mice relies on the Cre lox system whereby CLEC-2 can be deleted on specific cells, for example, in PF4.Cre.CLEC-$2^{fl/fl}$ mice, CLEC-2 is deficient specifically on megakaryocytes and platelets (Finney et al., 2012, Tiedt et al., 2007). These mice have slightly reduced platelet numbers compared to WT mice, (due to mixing between blood and lymph), although this appears to be less severe than in the constitutive knockout which may explain the increased survival at term. Additionally, embryos which lack podoplanin frequently do not survive to adulthood, although this can be variable depending on the genetic background of mice used (Mahtab et al., 2008, Uhrin et al., 2010).

1.3.3 Thrombosis

Whilst haemostasis facilitates intravascular thrombus formation in response to vascular injury, this process can become pathological. Thrombosis, the formation of intravascular clot(s) which result in vessel occlusion, can initiate serious clinical events including myocardial infarction and stroke, which are the leading cause of death worldwide (Roger

et al., 2011). Thrombosis can occur in both veins and arteries although the pathological features in each are distinct (Engelmann and Massberg, 2013). However, both systems can enable activation of platelets and of the coagulation cascade.

Arterial thrombosis is frequently termed atherothrombosis due to its association with atherosclerotic plaque rupture. Typically, the endothelium becomes damaged during plaque rupture, and platelets are recruited to the exposed sub-endothelial molecules, for example by the platelet collagen receptor, GPVI (as in haemostasis) (Nieswandt et al., 2001). However, activated platelets recruit leukocytes (by chemokine release), and these can become associated with the growing thrombus (Furie and Furie, 2008). Additionally, platelets can form an adhesive bridge between the arterial vascular endothelium and circulating blood, which preferentially recruits monocytes to the endothelium (Kuckleburg et al., 2011). In contrast, venous thrombosis is often not associated with endothelial damage, however, endothelial cells can become activated, as in deep vein thrombosis (DVT) which promotes leukocyte recruitment, both indirectly and via expression of VWF (von Bruhl et al., 2012, Brill et al., 2011). The interactions between recruited leukocytes and platelets facilitate propagation of venous thrombosis, for example, by release of neutrophil extracellular traps (NETS) (von Bruhl et al., 2012).

1.3.4. Mouse models and haemostasis

The mouse is a powerful model for human coagulation disorders because there is a high degree of homology between many proteins of the coagulation system and their inhibitors (both physiological and pharmacological) between the species (Tsakiris et al., 1999, Hogan et al., 2002). However, some aspects of haemostasis differ in mice. For example, mice have a greater normal platelet count and a lower platelet volume than humans, and murine

platelets survive for approximately half the life span of human platelets (Corash et al., 1989, Tsakiris et al., 1999, Levin and Ebbe, 1994).

A significant difference between human and murine platelets is the presence of Fc gamma receptor IIa (FcγRIIa). This low affinity IgG receptor expressed by platelets (and multiple other cells) plays a key role in interactions between bacteria and platelets which can result in platelet aggregation (Kerrigan and Cox, 2010, Cohen-Solal et al., 2004, Tilley et al., 2013, Cox et al., 2011). Blocking signalling via FcγRIIa has been shown to prevent platelet aggregation in response to several bacteria, including *Staphylococcus* aureus, and thus is an important therapeutic target in infectious vascular pathologies, such as infective endocarditis (Fitzgerald et al., 2006b). However, the genetic equivalent of FcγRIIa is absent in mice, and so investigation of platelet-bacterial interactions via FcγRIIa must rely on transgenic mice (McKenzie et al., 1999).

1.3.5 The relationship between coagulation and inflammation

Inflammation and coagulation are two separate host responses which directly influence each other by cross-talk between the mediators of each system. Pro-inflammatory molecules can activate coagulation, block anticoagulation and fibrinolysis and alter platelet responses. For example, monocytes can release micro-particles which express intravascular tissue factor (TF), thereby facilitating activation of the coagulation cascade by interaction of TF with coagulation factor VIIa (Giesen et al., 1999). On the other hand, coagulation can promote an inflammatory environment by activating cells and by initiating release of inflammatory mediators, for example, from platelets (Esmon, 2005). Endothelial cells seem to be particularly important in this relationship because they produce many coagulation mediators, such as VWF (which influence inflammation), and are also very

responsive to inflammatory cytokines (which can initiate coagulation) (Brill et al., 2011, Keller et al., 2003).

1.3.6 Haemostasis and infection

Inflammatory activation of coagulation can be common during infection (Esmon, 2005, Levi and van der Poll, 2005, Cornet et al., 2007, Opal, 2003, Vervloet et al., 1998, Zeerleder et al., 2005). Coagulation activation during infection can be an important host response for the prevention of pathogen dissemination during systemic disease (Sun, 2006). For example, fibrin has long been associated with antimicrobial defence, both during coagulation and in extravascular regions such as the peritoneal cavity (Zinsser and Pryde, 1952, Degen et al., 2007). However, systemic bacterial infections can result in severe haemostatic complications including DIC (described below), immune thrombocytopenia purpura, infective endocarditis, stroke, and myocardial infarction (Elkind and Cole, 2006, Corrado et al., 2006, Franchini and Veneri, 2004). A feature which many of these conditions have in common is aberrant platelet function, and this may be pathogen induced (Fitzgerald et al., 2006a). The ability of pathogens to interfere with host coagulation to enhance dissemination and to overcome host immune surveillance mechanisms has also been reported (Degen et al., 2007, Valls Seron et al., 2010).

Despite the association between inflammation and coagulation, the relationship is not simple, especially during systemic infection. For example, sepsis, in which DIC is common, is characterised by both pro- and anti-inflammatory phases of host response (Lewis et al., 2012, Angus and van der Poll, 2013, van't Veer and van der Poll, 2008). Whilst platelet accumulation and increased aggregation have been shown in response to endotoxin in several animal models, in sepsis patients, reduced platelet aggregation is common. It is

believed that sepsis can promote platelet-release of vascular endothelial growth factor (VEGF), thus promoting vascular repair. Evidence suggests the content of platelet α-granules, including VEGF, may be altered at the megakaryocyte level during sepsis, possibly in response to inflammation (Yaguchi et al., 2004).

1.3.6.1 Disseminated intravascular coagulation

Disseminated intravascular coagulation is a syndrome which accompanies and often complicates another condition, such as bacterial septicaemia, haematological malignancy and trauma. DIC is characterised by consumption of coagulation factors and platelets and activation of the fibrinolytic system, which can be due to enhanced activation of coagulation or disrupted anticoagulation. However, the symptoms can be contradictory and so difficult to treat (Kitchens, 2009). These include microvascular thrombosis, and thrombo-embolic disease, however, thrombosis may be presented alongside excessive bleeding, which occurs due to depletion of coagulation proteins and platelets (Keller et al., 2003, Levi et al., 1999). The thrombi produced during DIC can be found in different organs, including the liver, and can promote multiple organ failure (Levi et al., 1999, Karima et al., 1999). The main strategy for treatment of DIC is resolution of the underlying disorder, although additional therapies, including anticoagulants may be used alongside to relieve symptoms (Levi et al., 1999).

1.3.7 The role of platelets in systemic infection

Bacteria can interact with platelets either directly or indirectly and this can promote platelet activation (Kerrigan and Cox, 2010, Petersen et al., 2010). Localised platelet activation can result in thrombus formation, whilst more systemic interactions can lead to activated platelet consumption and thrombocytopenia, and more severe complications

including DIC (Fitzgerald et al., 2006a). Platelet activation has been reported even when the bacteraemia is low level, and sometimes not detectable, but this may not necessarily be due to direct interactions between the bacteria and platelets (Franchini and Veneri, 2004). The literature suggests that platelet defects, either in platelet number or integrity, may correlate with infection severity, for example, low platelet counts can indicate poor outcome of infection (Yaguchi et al., 2004, Yeaman, 2010).

Platelets are believed to contribute to host defence against bacterial pathogens in a number of ways. Their expression of multiple innate receptors, including TLRs and complement receptors, enables recognition of microorganisms in the blood (Semple et al., 2011, Cox et al., 2011). There is growing evidence that platelets can directly interact with bacteria, thus are becoming recognised as important effector cells of the innate response and may also be vital in the initiation of effective adaptive responses (Kerrigan et al., 2002, Wong et al., 2013, Jenne et al., 2013, Cox et al., 2011, Engelmann and Massberg, 2013). An exciting example of the innate capacity of platelets is the 'touch-and-go' interaction between platelets and Kupffer cells in the liver (Wong et al., 2013). This brief interaction, facilitated by platelet expressed GPIb and VWF on Kupffer cells, results in sustained platelet adhesion via GPIIb/IIIa in the presence of bacteria, enabling platelets to surround bacteria at the Kupffer cell surface, and bacteria are subsequently destroyed. In addition, platelet cytoplamsic granules contain platelet microbicidal proteins (PMPs), including defensins, which are released during infection, and platelets can also release multiple cytokines which recruit leukocytes during infection (Yeaman, 2010, Fitzgerald et al., 2006a, Yeaman et al., 1998). Platelets can trigger NET production, and this has been shown to promote thrombosis (Clark et al., 2007, Brill et al., 2012, Fuchs et al., 2010).

1.3.7.1 Immunothrombosis

Immunothrombosis is a recently described process whereby during infection, coagulation is activated in host defence against the invading pathogen, and it is believed that this is distinct from haemostasis (Massberg et al., 2010, Engelmann and Massberg, 2013). Multiple strategies contribute to immumothrombosis, including monocyte and monocyte-derived microparticle TF delivery, NET formation, and direct anti-bacterial activity by platelets. Immunothrombosis contributes to innate host defence by retaining pathogens within fibrin structures and micro-thrombi, thus by restricting pathogen dissemination and preventing tissue invasion. Immune-mediated thrombi also concentrate host antimicrobial strategies and can promote recruitment of further host immune cells (Engelmann and Massberg, 2013).

1.3.7.2 Infection and vascular integrity

Whilst putative links between infection and cerebrovascular disease including stroke remain anecdotal, the association between infection and atherosclerosis has become more widely recognised in recent years (Elkind and Cole, 2006). Platelet contribution to vascular inflammation and the progression of atherosclerotic lesions has been demonstrated, and it is likely that infection may elevate vascular inflammation and platelet recruitment at all stages of pathogenesis (Fitzgerald et al., 2006a). Thus, evidence of infection-mediated inflammation leading to significant vascular pathology, particularly during chronic infection of *Helicobacter* pylori and *Chlamydia* pneumoniae, emphasises the urgency with which we require increased understanding of infectious inflammation and vascular disruption (Keller et al., 2003).

1.3.8 Haemostasis during *Salmonella* infection

Typhoid fever is frequently associated with anaemia, leukopenia, leukocytosis, eosinophilia, thrombocytopenia and bone marrow suppression (Yildirim et al., 2010, Malik, 2002, Butler et al., 1978, Serefhanoglu et al., 2003). Indeed, the onset of these haematological features contribute to the overall host response. For example, splenomegaly in conjunction with thrombocytopenia or leukopenia, is associated with a 2.5 fold increased risk of developing complications (Malik, 2002). Thrombocytopenia occurs in 25% of typhoid fever patients with *Salmonella* hepatitis (Pramoolsinsap and Viranuvatti, 1998). Its onset is a risk factor for multiple organ dysfunction syndrome (MODS); indeed, multiple organ failure has been associated with thrombocytopenia and thrombosis at autopsy (Nguyen et al., 2001). Thrombocytopenia-associated multiple organ failure (TAMOF), a syndrome associated with thrombosis in critically ill patients, has also been reported during *S*. Typhi infection (Nguyen and Carcillo, 2006, Yildirim et al., 2010).

Particularly in the pre-antibiotic era, thrombosis was ascribed to typhoid infections such as typhoid fever (Huckstep 1962). In addition, thrombosis of Peyer's patch capillaries leading to necrosis, haemorrhage and perforation of the intestine has been reported, as have myocarditis and DIC, although these are rare (Bitar and Tarpley, 1985, Santos et al., 2001, Malik, 2002). Additional haematological abnormalities during typhoid include arrested myeloid cell maturation in the bone marrow and reduced erythroblast and megakaryocyte numbers; increased histiocyte phagocytosis, and rapid onset of anaemia due to haemolysis, bone marrow suppression and occult bleeding (Malik, 2002). Indeed haemophagocytic syndromes in general play an important role in many infections, and this is particularly prevalent in typhoid (Janka, 2007, Fisman, 2000, Silva-Herzog and Detweiler, 2008, Silva-Herzog and Detweiler, 2010).

1.3.8.1 Haematological complications during NTS bacteraemia

One of the most frequent complications of NTS bacteraemia in children in tropical Africa is anaemia; 88% of children with NTS bacteraemia in Zaire also had anaemia (Graham et al., 2000b, Cheesbrough et al., 1997, Bronzan et al., 2007, Graham et al., 2000c, Lepage et al., 1987, Brent et al., 2006). However it is often not clear which is the underlying ailment: the bacteraemia or the anaemia. Additionally, NTS bacteraemia is frequently associated with either co-infection or recent infection by malaria, of which anaemia is an important feature (Bronzan et al., 2007, Berkley et al., 1999, Mackenzie et al., 2010). During malaria, peripheral red blood cells are diminished both by decreased erythropoiesis and by destruction (of both parasitised and non-parasitised cells) by macrophages in the spleen (Burgmann et al., 1996, Kurtzhals et al., 1997). The co-existence of NTS bacteraemia, anaemia and malaria are repeatedly reported to be caused by the disrupted immune response during co-infection (Mabey et al., 1987, Graham et al., 2000a). Malaria may reduce the capacity for macrophage bactericidal function, thus impairs the host response and increases host susceptibility to NTS (Graham et al., 2000a, Greenwood et al., 1978, Kaye et al., 1967, Warren and Weidanz, 1976). However, in some studies, increased bacterial growth may also be explained by increased iron availability during malarial haemolysis (Kaye and Hook, 1963).

With the exception of Sickle cell disease, the incidence of which is elevated in tropical Africa and poses a particular risk for bacterial sepsis, reports of additional haemostatic complications during systemic NTS infections are scarce and anecdotal (Ebong, 1986, Morpeth et al., 2009, Chang et al., 2003, Huang, 1996, Arora et al., 2011). For example, rare spontaneous bacterial peritonitis caused by NTS and *S*. Typhi have been occasionally reported in immune-suppressed patients, and mycotic aneurysm caused by NTS has also

been described (de la Fuente-Aguado et al., 1999, Laing et al., 1995, Rajekar et al., 2008, Muyembe-Tamfum et al., 2009). *Salmonella* meningitis has been associated with brain infarction and associated abscesses (Huang, 1996, Chang et al., 2003, Kim et al., 1999, Arentoft et al., 1993, van Sorge et al., 2011, Arii et al., 2001, Hanel et al., 2000). However, the pathogenesis of these and other haematological complications have not yet been explored in detail.

1.3.8.2 Haematological abnormalities in systemic NTS infection in mice

A recent study described altered blood homeostasis during systemic STm infection in mice (Brown et al., 2010). Thrombocytopenia is evident throughout infection and peaks in severity with bacterial load of tissues, splenomegaly and microcytic anaemia severity. Increased mean platelet volume and macro-platelets in blood film analysis suggested thrombopoiesis. Erythrocyte and reticulocyte microcytosis persists, yet increased reticulocyte counts suggest erythrocyte regeneration; polychromasia and erythrocytosis are observed. Erythrocyte anisocytosis occurs late, and fragmentation (schistocytes) of both mature and immature erythrocytes occurs at the peak of infection, but is absent later (Brown et al., 2010). Additionally, this study and others, have reported thrombosis during systemic NTS infection in mice, but these observations have been purely anecdotal (Brown et al., 2010, Mastroeni et al., 1995, Nakoneczna and Hsu, 1983, Roy et al., 2006, Wickham et al., 2007).

1.4 Rationale of study

1.4.1 The impact of *Salmonella* Typhimurium infection on the liver

In some areas of the developing world, a high proportion of NTS-infected children are reported to die within 24 hours of reaching clinic, yet how infection kills these children is unknown. Risk of severe disease and death is associated with bacteraemia, but frequently, unlike other systemic bacterial infections, no major symptoms are presented (Graham et al., 2000c). To determine how NTS bacteraemic children die, both immunological and physiological factors must be considered. A potential imbalance in homeostasis during infection may be linked to the cause of death.

To investigate the physiology of how the host responds to infection, we focussed on the liver. Aberrant hepatic pathology and function are common features of typhoid infections and NTS colonisation of the liver during murine infections is evident (Pramoolsinsap and Viranuvatti, 1998, Mastroeni et al., 1995). We hypothesised that liver disruption during infection may have significant physiological consequences, which may be a major contributing factor to the sudden deaths of young children in sub-Saharan Africa.

1.4.2 The impact of *Salmonella* Typhimurium infection on the circulatory system

Coagulation is an important host strategy for the prevention of bacterial dissemination, and co-regulation between inflammation and coagulation is evident in the literature. Haemostasis is a tightly regulated system, but imbalance during infection, such as that seen in DIC has been reported. However, with the exception of increased incidence of anaemia in regions where malaria is prevalent, there is very little evidence regarding haematological

abnormalities both in murine and human NTS infections. During our preliminary studies, an extensive thrombosis phenotype became apparent in the vasculature of the liver. Without knowing whether thrombosis is a protective host mechanism to infection, or an aberrant activation of coagulation, we wanted to investigate this phenotype further. We hypothesised that a coagulation disorder such as DIC could be the underlying cause of death in systemically NTS-infected African children.

1.4.3 Project aims

The aim of this project is to use a mouse model to investigate how NTS-infected children may die from infection. Future utilisation of these observations may be invaluable in the identification of novel therapeutic interventions to extend the time between presentation at clinic and host death. This may provide sufficient opportunity for the immune system or anti-microbial treatment to control infection.

To investigate how the liver and circulatory system contribute to the host response to infection, the following questions will be addressed:

- What events occur in the liver during infection?
- How is inflammation in the liver regulated?
- How does infection influence liver function?
- How is the circulatory system affected by infection?

Chapter 2: Materials and Methods

2.1 Materials

All reagents were purchased from Sigma-Aldrich (Poole, U.K.) unless otherwise stated. Details of all buffers used can be found at the end of this Chapter (section 2.10).

2.2 Mice

Six to eight week wild type (WT) C57BL/6J mice were obtained from HO Harlan OLAC Ltd. (Bicester, U.K.). All genetically modified mice used were bred from in-house colonies in the University of Birmingham Biomedical Services Unit (BMSU). The original sources of these mice are listed in Table 2.1. Aged (18 month old) WT mice were obtained from Charles River Laboratories. All animals were housed in the BMSU in conditions free from specific-pathogens. All experiments were performed in accordance with UK Home Office regulations and were ethically approved by the UK Ethics Committee.

Strain of mouse	**Phenotype**	**Source**
Rag $1^{-/-}$ (C57BL/6J)	Absence of T and B lymphocytes. Generated by disruption of Rag-1 gene and subsequent early inhibition of cell development	Professor Chris Buckley, University of Birmingham (Mombaerts et al., 1992b)
$IgH^{-/-}kappa^{-/-}$ (C57BL/6J)	Absence of B lymphocytes. Generated by breeding out the QM IgH transgene from QM mice (in which the other IgH locus is inactivated).	Dr Kai Toellner, University of Birmingham (Cascalho et al., 1996)
$TCR\beta\delta^{-/-}$ (C57BL/6J)	Absence of T lymphocytes (γδ and αβ).	Jackson Laboratory (Mombaerts et al., 1992a)

	Generated by targeted gene deletion of the TCR beta and delta genes	
T-bet$^{-/-}$ (C57BL/6J)	AbrogatedTh1 cell function and impaired IFNγ induction. Generated by disruption to T-bet gene by homologous recombination	Jackson Laboratory (Szabo et al., 2002)
B6.129S2-Cd8a^{tm1Mak}/J (CD8$^{-/-}$) (C57BL/6J)	Deficient in functional cytotoxic T-cells Deficient in CD8α protein production due to insertion of premature stop codon into the *Cd8a* gene.	Dr Nick Jones, University of Birmingham Jackson Laboratories (Fung-Leung et al., 1991)
Interferon-gamma$^{-/-}$ (C57BL/6J)	Deficient in IFNγ production due to insertion of premature stop codon into the *Ifng* gene.	Professor Richard Grencis, University of Manchester Jackson Laboratories (Dalton et al., 1993)
Interleukin (IL)-4$^{-/-}$ (BALB/c)	Generated by disruption to IL4 gene by homologous recombination	Professor Manfred Kopf, Basel Institute for Immunology, Switzerland
IL-4-Receptor alpha$^{-/-}$ (BALB/c)	Deficient in IL4-receptor alpha chain, therefore impaired IL4 and IL-13 signalling. Generated by Cre-mediated recombination of the IL4-receptor alpha allele through the cre/loxP system.	Professor James Alexander University of Strathclyde (Mohrs et al., 1999)
IL-6$^{-/-}$ (C57BL/6J)	Deficient in IL6 signalling Generated by disruption to IL6 gene by homologous recombination	Charles River Laboratories (Kopf et al., 1994)
IL-10$^{-/-}$ (C57BL/6J)	Deficient in IL-10 signalling. Generated by homologous recombination of IL-10 with a neomycin cassette. Mice develop chronic enterocolitis	Charles River Laboratories (Kuhn et al., 1993)

TNF-alpha Receptor$^{-/-}$ (C57BL/6J)	Mice fail to bind TNF Double mutant mice, defective in both*Tnfrsf1a* (p55) and *Tnfrsf1b* (p75) were generated by crossing single-mutant mice. Targeted disruption in both genes by insertion of neomycin resistance cassette.	Professor Richard Grencis, University of Manchester Jackson Laboratories (Peschon et al., 1998)
CD1d$^{-/-}$ (C57BL/6J)	Deficient in invariant NKT cells Targeted mutation into the *CD1d1* gene thus iNKT cells are not selected and subsequent early inhibition of cell development.	Dr Nick Jones, University of Birmingham Originally obtained from Luc van Kaer (Mendiratta et al., 1997)
Platelet factor 4. Cre.CLEC-2$^{fl/fl}$ (C57BL/6J)	CLEC-2 is deficient on platelets and megakaryocytes. Generated by Cre-mediated recombination of the CLEC-2 allele through the cre/loxP system (Tiedt et al., 2007).	Professor Steve Watson, University of Birmingham (Finney et al., 2012)

Table 2.1 Strains of genetically modified mice used.

2.2.1 Generation of irradiation bone marrow chimeric mice

Irradiation bone marrow chimeric mice were generated whereby IFNγ was absent in either haematopoietic cells, radiation-resistant cells, both cell types, or neither. All recipient mice were administered Baytril in their diet for two weeks prior to irradiation, according to BMSU protocol. WT and IFNγ$^{-/-}$ recipient mice were irradiated by 9 Grays (Gy) of γ-radiation over 2 doses of 450rads, 2 hours apart. These mice were reconstituted with either IFNγ-sufficient or IFNγ-deficient bone marrow (BM) from donor WT or IFNγ$^{-/-}$ mice respectively.

Donor mice were killed shortly before required and BM cells were isolated under sterile conditions. Cells were retrieved by flushing the femur and tibia in sterile RPMI (10 mL) through a 100 µm mesh. Cells were centrifuged (350 x g, for 8 minutes) and erythrocytes

were lysed for 1 minute using ACK Lysing buffer (Gibco, Paisley, UK). Cells were centrifuged (350 x g; 8 minutes), re-suspended in sterile RPMI and counted using a haemocytometer. Cells were washed twice in sterile PBS and were re-suspended at a density of 5 x 10^7/mL. Cells (200µL) were transferred i.v. into recipient mice (10^7 cells per mouse), one hour following the final irradiation dose. Four groups of donor – recipient mice were generated as described in Table 2.2. Mice were left to reconstitute for 10-12 weeks before infecting with STm as described in section 2.3.

Donor	Recipient
WT	WT
IFNγ$^{-/-}$	WT
WT	IFNγ$^{-/-}$
IFNγ$^{-/-}$	IFNγ$^{-/-}$

Table 2.2 Groups of donor and recipient mice used to generate bone marrow radiation chimeras

2.2.2 Generation of mixed irradiation bone marrow chimeric mice

A mixed bone marrow system was used to generate mice in which Tbet was absent specifically in T cells. These mice were kindly prepared by Dr Ruth Coughlan, University of Birmingham. The recipient mice were TCRβδ$^{-/-}$ mice (which lack total T cells). These mice were administered Baytril for 2 weeks prior to irradiation (8 Gy of γ-radiation over 2 doses of 450rads as described above).

Bone marrow was isolated from donor mice as described above. Donor mice were either TCRβδ$^{-/-}$, Tbet$^{-/-}$ or WT. Once prepared, cell suspensions from the donor mice were mixed whereby TCRβδ$^{-/-}$ cells were mixed with either WT or Tbet$^{-/-}$ cells at a ratio of 80:20. Therefore donor BM consisted of 80% TCRβδ$^{-/-}$ BM and 20% T-bet$^{-/-}$ BM or 80% TCRβδ$^{-/-}$

BM and 20% WT BM. In the generated mice, T cells lacked Tbet whereas the remainder of cells were Tbet sufficient. For those mice which received mixed WT instead of mixed Tbet$^{-/-}$ BM cells, all cells in the recipient mice were Tbet-sufficient. Donor cells (10^7 in 200 µL sterile PBS per mouse) were administered i.v. to irradiated recipients. Reconstitution was assessed at 6 weeks post cell transfer by flow cytometry of tail bleeds by Dr Ruth Coughlan. Mice were left to reconstitute for 10-12 weeks before infecting with STm as described below.

2.3 Infection of mice

2.3.1 Preparation of bacterial inoculum

All infections were with the attenuated *Salmonella enterica* serovar Typhimurium (STm) strain SL3261, originally obtained from Dr RA Kingsley (Wellcome Trust Sanger Institute, Cambridge) (Hoiseth and Stocker, 1981). STm were cultured overnight in 10 ml Luria-Bertani (LB) medium (Invitrogen, Paisley, UK) at 37^{o}C with aeration (180 revolution per minutes (rpm)). The overnight culture was diluted and incubated as described until bacteria reached late-log phase (optical density (OD) λ600 nm 0.8 – 1.0). Approximately 1 x 10^9 bacteria (1 ml culture) was harvested by centrifugation (6,000 x g for 5 minutes at 4^{o}C). Bacteria were washed twice in sterile Phosphate Buffered Saline (PBS) (at 6,000 x g for 5 minutes at 4^{o}C) and were then re-suspended in 1 ml sterile PBS. Bacteria were diluted to a final concentration of 2.5 x10^6 per ml.

2.3.2 Infection protocol

Mice were infected by intra-peritoneal (i.p.) injection (200 µl containing 5 x 10^5 bacteria). Occasionally, infections were performed by the intra-vascular (i.v.) route, and this is clearly stated in the appropriate results sections (see Section 5.2). Bacteria (200 µl inoculum containing 5 x 10^5 bacteria) were prepared and quantified as above. Infection doses were quantified using the Miles and Misra technique (Miles et al., 1938). Briefly, bacteria were serially diluted in sterile PBS and cultured overnight on agar plates at 37^{o}C.

2.3.3 Time-course of infection

Mice were infected as described above and were killed by a schedule 1 method at the required time post-infection, in accordance to Home Office Regulation. To establish the kinetics of infection in the liver, mice were infected on the same day and were killed at set time-points throughout infection, including days: 1, 2, 3, 5, 7, 14, 18, 21, 28, 35 and 50 post-infection. At least 3-4 mice were used at each time point. Genetically modified mice were used to elucidate the role of various cell types and molecular mediators in the host response to infection. These mice are detailed in Table 2.1. To compare the host response to infection in these mice with that in WT control mice, both WT and genetically modified mice were infected on the same day and were routinely killed at day 7 post-infection. This time-point was used for multiple studies because the pathological response in the liver of WT mice is fully established and well-characterised at this time.

2.3.4 Experiment end-point

At the time of sacrifice, blood was obtained by cardiac puncture which was performed under anaesthesia by insertion of a 25g x 5/8” gauge needle directly through the chest

cavity and into the heart. Approximately 1 mL blood was obtained from each animal. All needles and syringes used for obtaining blood were pre-coated in 5 mM Ethylenediaminetetraacetic acid (EDTA) to prevent coagulation. Tissues including the spleen, liver, kidney, lungs and brain were removed for further examination as described in the following sections.

2.4 Bacterial culture from infected tissues

The bacterial burden of the liver (and other tissues) was calculated to determine the extent of bacterial colonisation. Total mass of the liver was recorded and approximately 0.2g of each liver was disrupted through a 70 µm nylon-cell strainer (BD Biosciences) in 1 ml RPMI-1640 medium. Cell suspensions were serially diluted and plated onto LB agar plates. Plates were incubated overnight at 37^{o}C and bacterial colonies were counted the next day. Total colony forming units (CFU) per tissue were calculated using the mass of tissue cultured, the volume of culture, the dilution and volume of culture plated out. The equation is below.

$$\text{CFU} = \frac{\text{Liver mass}}{\text{Culture mass (0.2 g)}} \times \frac{\text{Volume cultured (1 mL)}}{\text{Volume plated (100 µL)}} \times \text{Dilution e.g. 100} \times \text{CFU counted}$$

To determine whether bacteria were evenly distributed throughout the liver, the entire tissue was divided into areas and the CFU per gram of liver was measured as described above. Liver areas are outlined below (Figure 2.1-2). Livers were divided into 4 lobes (A-D), the largest of which were further dissected into internal and peripheral regions. Liver

regions are detailed in Table 2.3. Bacteria were cultured uniformly from across the entire tissue (described in Chapter 3, Section 3.2), therefore in subsequent experiments, bacterial burden of the liver was measured using any 0.2 g of liver tissue located from any part of the liver.

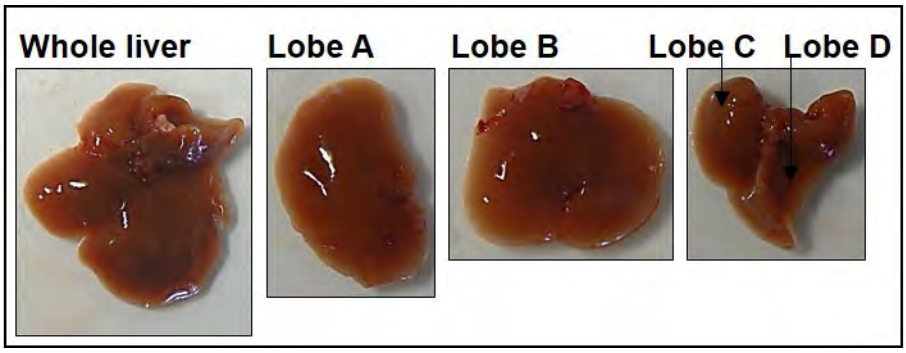

Figure 2.1 The liver and its constituent lobes (photographs not to scale)

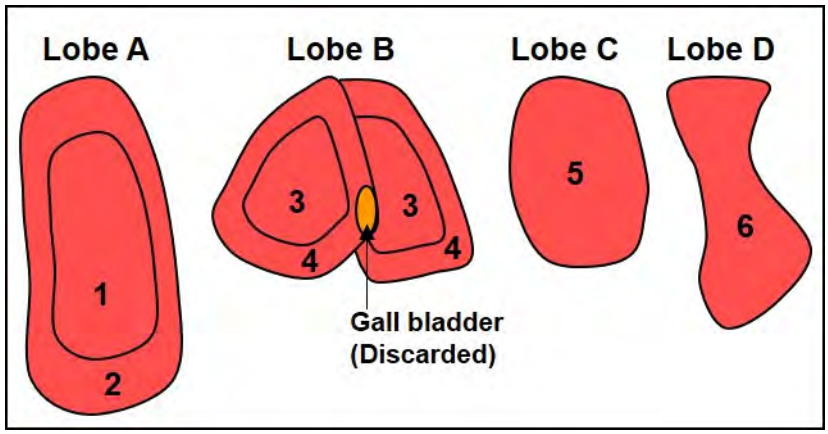

Figure 2.2 Regions of the liver.

The liver was divided into 6 regions to measure bacterial distribution throughout the liver. Lobes A-D match those in the photograph in Diagram 2.1. Lobes A and B were further dissected into peripheral and interior regions (Areas 1 and 2; 3 and 4). Diagram is not to scale.

Liver Area	Region
1	Interior of lobe A
2	Exterior of lobe A
3	Interior of lobe B
4	Exterior of lobe B
5	Lobe C
6	Lobe D

Table 2.3 Regions of the liver

2.5 Histology

2.5.1 Tissue preparation for histological examination

Once dissected, a portion of the liver to be examined histologically was separated from the rest of the tissue. This was then weighed and snap frozen immediately using liquid nitrogen. Rapid freezing was necessary to prevent unwanted post-mortem deterioration of the tissue. Liver tissue was stored at -80^{o}C until required. In addition, external pathology of the liver was assessed prior to freezing, and sometimes photographs were taken. However, tissues were frozen as soon as possible once excised. Occasionally, the spleen and lungs were also collected for histological examination. Spleens were frozen and were sectioned as described below (at a depth when the white pulp was clearly visible). Lungs were inflated with 4% Formaldehyde (Adams Healthcare Ltd, Leeds, UK) prior to removal and were kindly prepared, paraffin embedded and sectioned by Jean Shaw, Centre for Liver Research, University of Birmingham.

2.5.2 Sectioning liver tissue

All tissues were sectioned using a cryostat (Bright Instruments, Huntington, UK). Tissues were mounted using OCT TissueTek compound (Dako, Denmark) and serial 5-6 µm sections were taken onto micro slides (Surgipath). Slides were air dried for 1 hour before fixation in acetone at 4^{o}C for 20 minutes. Slides were air dried for 10 minutes, then stored in polythene bags at -20^{o}C.

To determine the distribution of pathology within the liver, initially each lobe of the liver was sectioned entirely. At depths of 100-150 µm, sections were stained using Tolluidine Blue (M. Khan) to monitor leukocyte infiltration. A few drops of Tolluidine Blue were applied to each section, prior to washing in water. This technique was later modified, so further livers were serially sectioned in two positions: near the top surface of the lobe and at the deepest region of the lobe, adjacent to the major vasculature (Figure 2.3).

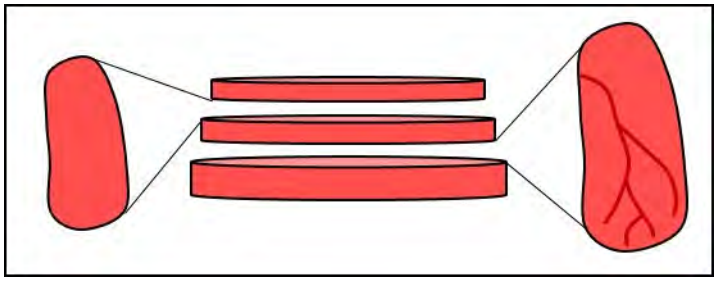

Figure 2.3 Sectioning liver tissue.
Liver lobes were serially sectioned in two positions: the top of the lobe (shown on the left) and the deepest region of the lobe, adjacent to the major vasculature (shown on the right).

At each position of each liver lobe, a section was stained using Tolluidine Blue as described above. The remaining slides were fixed and stored as described above. Pathology of the liver was very similar at both positions sectioned in all lobes and so subsequent tissues were only sectioned in one position: the middle of lobe A, adjacent to the major vasculature.

2.5.3 Haematoxylin and Eosin staining

Slides were removed from -20^{o}C storage and were thawed inside the sealed polythene bags prior to staining (to prevent condensation damage to tissues). Haematoxylin and eosin (H&E) staining was performed as described in Table 2.4 (all materials were purchased from Leica Microsystems, Peterborough, UK). Following staining, slides were mounted using DPX mountant.

Reagents	**Length of incubation (minutes)**
Water	2
Haematoxylin	4
Water	2
Acid alcohol	30 seconds
Water	2
Scott's tap water substitute	30 seconds
Water	2
Eosin	1
Water	2
Water	2
Alcohol	2
Alcohol	2
Alcohol	2
Alcohol	2
Clearene	2
Clearene	2
Clearene	1

Table 2.4 Reagents and incubation times of Haematoxylin and Eosin staining

2.5.4 Immunohistochemistry

Immunohistochemistry (IHC) was used to characterise the leukocyte infiltrate in the liver during infection. Slides were removed from -20^{o}C storage and were thawed inside sealed polythene bags as described above. Prior to staining, tissue sections were rehydrated in Tris buffer (pH 7.6), while primary antibody combinations were prepared. All antibodies used for IHC are detailed in Table 2.5. Antibodies were diluted in Tris buffer (pH 7.6) and 75 µl was added to each section. Slides were incubated at room temperature for 1 hour in a humidified chamber and were then washed twice in Tris buffer for 5 minutes. Secondary antibodies were adsorbed with normal mouse serum at 10% of the final volume for at least 30 minutes. Where hamster anti-mouse primary antibodies were used, goat anti-hamster IgG [heavy and light chains] (which had been commercially pre-adsorbed) was added to the secondary antibody solution prior to adding 75 µl to each section. Slides were incubated at room temperature in a humidified chamber for 45 minutes and were washed as above.

Secondary antibodies were linked to either biotin or horse-radish peroxidise (HRP). Alkaline-phosphatase (AP) complex (ABComplex, Vector Laboratories) was prepared by addition of avidin (solution A) and biotinylated AP (solution B) to Tris buffer (pH 7.6), both at a 1/100 dilution. The solution was incubated at room temperature for 30 minutes to enable formation of the AP complex. This was then added to each section and slides were incubated at room temperature in a humidified chamber for 40 minutes, then were washed as above.

Slides were developed using peroxidise (for HRP-linked antibodies) and AP (for biotin-linked antibodies) substrates. The peroxidise substrate, a 3, 3'-diaminobenzidine

tetrahydrochloride (DAB) tablet, was dissolved in 15 ml Tris buffer (pH 7.6) and was filtered. 50 µl hydrogen peroxide was added and substrate was added to the sections. Once developed to the required intensity, slides were washed as above. The AP substrates were prepared as follows: Levamisole (8 mg) was dissolved in 10 ml Tris buffer (pH 9.2). Napthol AS-MX phosphate (4 mg) was dissolved in 380 µl N,N-dimethyl-formide and was added to the centre of the Levamisole solution. Fast Blue BB salt (10 mg) was added and the solution was filtered and added to each section. Once developed, slides were washed in Tris buffer (pH 7.6) and then in dH_2O to stop any further reaction of the substrates. Slides were air dried and mounted using Glycerol.

2.5.4.1 Analysis of immunohistochemistry

Photographs of IHC-stained tissue sections were taken using a Leica CTR6000 microscope (Leica, Milton Keynes, UK) with Image J and QCapture software. Quantification of both H&E and immunohistochemistry stained slides was performed by point counting using a graticule. To measure the proportion of liver area occupied by inflammatory lesions, the number of grid intercepts on lesions was expressed as a proportion of the total number of intercepts over the area counted. A total of 60 grids was counted for each tissue, and were representative of the entire area. The number of cells per lesion was assessed for 30 lesions on each tissue section and these were representative of the entire section. The percentage of vessel occlusion was measured as a proportion of the number of grid intercepts on thrombi in the large vessels to the number of grid intercepts on the large vessels (where vessel area exceeded 150 intercepts). To standardise as far as possible, only the largest vessels (greater than 150 intercepts) were included, and livers were sectioned to approximately equivalent positions in each tissue.

Target	Species	Concentration	Working dilution	Source and clone
Anti-mouse CD3ε	Hamster	0.5 mg/mL	1/300	BD Pharmingen 145-2C11
Anti-mouse CD4	Rat	0.5 mg/mL	1/800	BD Pharmingen (L3T4) RM4-5
Anti-mouse CD8	Rat	1.0 mg/mL	1/800	AbD serotec YTS105.18
Anti-mouse FoxP3	Rat	0.5 mg/mL	1/50	eBiosciences FJK-16s
Anti-mouse F4/80	Rat	1.0 mg/mL	1/500	AbD serotec Cl:A3:1
Anti-mouse CD11c	Hamster	1.0 mg/mL	1/500	AbD serotec N418
Anti-mouse Ly6C-biotinylated	Rat	0.5 mg/mL	1:200	BD Biosciences AL-21
Anti-mouse Ly6G-biotinylated	Rat	0.5 mg/mL	1:200	eBioscience RB6-8C5
Anti-mouse podoplanin	Syrian hamster	0.5 mg/mL	1:200	eBioscience eBio8.1.1
Anti-mouse CD41	Rat	0.5 mg/mL	1:200	BD Pharmingen MWReg30
Anti-mouse Von Willebrand Factor	Rabbit	0.2 mg/mL	1:50	Santa Cruz Biotechnology H-300
Anti-mouse MHC II 1-A^b	Rat	0.5 mg/mL	1:200	BD Pharminghen M5/114.15.2
CD105	Rat	0.3 mg /mL	1:500	BD Biosciences MJ7/18
CD34	Rat	1 mg/mL	1:400	Serotec 1H6
Anti-rat IgG (heavy and light chains) Biotinylated	Rabbit	0.85mg/mL	1/600	DAKO Polylonal
Anti-sheep IgG (heavy and light chains) -HRP	Donkey	Discontinued	1/100	The Binding Site Polyclonal
Anti-sheep IgG (heavy and light chains) -HRP	Donkey	0.8 mg/mL	1:300	Jackson ImmunoResearch Polyclonal
Anti-hamster IgG (heavy and light chains)	Goat	1mg/ml	1/100	Southern Biotech Polyclonal

Table 2.5 Primary and secondary antibodies used in immunohistochemistry

2.5.5 Confocal microscopy

Confocal microscopy was used to further characterise inflammation in the liver during STm infection. Prior to staining slides were removed from -20^{o}C storage, thawed as described above and rehydrated in PBS for 5 minutes. Slides were blocked in 10% foetal calf serum (FCS) in PBS (100 µL per section) for 10 minutes. All subsequent staining steps were performed in 10% FCS in PBS and 100 µL antibody solution was added per section, and all antibodies used are detailed in Table 2.6. Primary antibodies were prepared at the appropriate concentrations and were added to each section. Slides were incubated in a moist chamber in the dark at room temperature for 1 hour. Slides were washed for 10 minutes in PBS prior to addition of appropriate secondary antibodies (and amplification steps). Slides were incubated for 45 minutes as above prior to washing for 10 minutes in PBS. If a third antibody was required, this was prepared as described in Table 2.6 and was added to each section. Slides were incubated for 45 minutes as above prior to washing for 10 minutes in PBS. All slides were incubated in Hoechst 33258 nuclear stain for 2 minutes, were washed in PBS and mounted using Prolong Gold Anti-fade Reagent (Invitrogen, Paisley, UK). Slides were stored in aluminium foil at -20^{o}C until required. A LSM510 microscope (Zeiss, Germany) was used to take images in conjunction with Zeiss LSM image software (Zeiss, Germany).

2.5.5.1 Confocal microscopy isotype controls

To ensure that the fluorescent levels of the LSM510 microscope were set accurately, each stain combination used was accompanied by a serial section control which was always stained alongside the sample of interest. All primary antibodies were omitted from this stain and 100 µL 10% FCS in PBS was added instead. All subsequent conjugated antibodies

were used as described above for the sample of interest. When acquiring images, all laser strengths were adjusted so that only minimal fluorescence was detected on isotype samples. This measure was taken to ensure the fluorescence detected was in conjunction with specific staining identified by the primary antibodies of interest, and that background fluorescence from the tissue was minimal. An example of an isotype control image is shown in Figure 3.7, Chapter 3, and this is representative of all isotype images used in this study (others have not been included).

Target	Species	Concentration	Working dilution	Source and clone
CD11b	Rat	1.0 mg/mL	1:400	AbD Serotec ICRF44
CD11c APC	Armenian Hamster	0.2 mg/mL	1:50	eBioscience N418
CD31 FITC	Rat	0.5 mg/mL	1:100	eBioscience 390
CD41 PE	Rat	0.2 mg/mL	1:100	eBioscience eBioMWReg30
CD41 (Purified)	Rat	0.2 mg/mL	1:200	eBioscience eBioMWReg30
CD45.2 FITC	Rat	0.5 mg/mL	1:400	eBioscience 104
CD248	Rabbit		1:400	A kind gift from Clare Isacke, Institute of Cancer Research
MHC II Biotinylated	Rat	0.5 mg/mL	1:100	eBioscience M5/114.15.2
Podoplanin Alexa Fluor 488	Syrian Hamster	0.5 mg/mL	1:200	eBioscience eBio8.1.1
Podoplanin (Purified)	Syrian Hamster	0.5 mg/mL	1:200	eBioscience eBio8.1.1
ICAM-1 FITC	Rat	0.5 mg/mL	1:100	eBioscience YN1/1.7.4
VCAM-1 eFluor 660	Rat	0.2 mg/mL	1:50	eBioscience 429
Von Willebrand Factor	Rabbit	0.2 mg/mL	1:50	Santa Cruz Biotechnology H-300

Hamster IgG (heavy and light chains) Biotinylated	Goat	0.5 mg/mL	1:100	Southern Biotech Polyclonal
FITC Alex Fluor 488	Rabbit	1.0 mg/mL	1:200	Invitrogen
Rat IgG (heavy and light chains) Cy3	Donkey	0.3 mg/ 400µL	1:200	Jackson ImmunoResearch
Rat IgG (heavy and light chains) FITC	Donkey	0.3 mg/ 250µL	1:100	Jackson ImmunoResearch
Armenian Hamster IgG (heavy and light chains) Alexa Fluor 647	Goat	0.5 mg/ 400µL	1:100	Jackson ImmunoResearch
Alexa Fluor 647 Streptavidin		1.0 mg/ 650µL	1:200	Jackson ImmunoResearch
Alexa Fluor 488 Streptavidin		2.0 mg/mL	1:100	Jackson ImmunoResearch
Cy3 Streptavidin		2.0 mg/mL	1:200	Jackson ImmunoResearch
Rabbit IgG (heavy and light chains) Cy3	Donkey	0.5 mg/ 400µL	1:200	Jackson ImmunoResearch
Rabbit IgG (heavy and light chains) FITC	Donkey	0.5 mg/ 400µL	1:100	Jackson ImmunoResearch
Rabbit IgG (heavy and light chains) Alexa Fluor 488	Donkey	0.5 mg/ 400µL	1:200	Jackson ImmunoResearch
Rabbit IgG (heavy and light chains) Alexa 647	Donkey	0.5 mg/ 400µL	1:300	Jackson ImmunoResearch

Table 2.6 Primary and secondary antibodies used by confocal microscopy

2.6 Flow cytometry

2.6.1 Isolation of single cell leukocyte suspensions from the liver

Leukocytes isolated from the livers of infected and non-infected mice were quantitatively characterised using a Fluorescent Activated Cell Sorter (FACS). On removal from mice, livers were kept on ice in 1 mL RPMI media supplemented with glutamine. The mass of the entire liver and of a portion used for flow cytometry (approximately 1.0 g) were recorded.

Splenocytes were used for single colour controls during FACS acquisition and were processed alongside cells isolated from the liver. However, steps 2.6.2 and 2.6.3 were not required. Instead, spleens were homogenised through a 70 µm nylon cell strainer (BD Biosciences) using normal media (RPMI + 2% FBS + 5 mM EDTA) and cells were harvested at 375 x g for 4 minutes at 4°C. Erythrocytes were lysed for 1 minute using Ammonium Chloride Potassium (ACK) Lysing buffer (Gibco, Paisley, UK). Splenocytes were then quantified as described in section 2.6.3.

2.6.2 Collagenase digestion

To ensure adequate isolation of all leukocyte subsets, livers were collagenase-digested and leukocytes were then enriched for using gradient centrifugation, as has been described elsewhere (Klein et al., 2007, Li et al., 2013, Sakai et al., 1978). Initially, livers were mechanically disrupted using dissection scissors in a 5 mL bijoux to ensure maximum and uniform surface area exposure. Collagenase D (Roche) was prepared at the appropriate dilution (approximately 1mg/mL) in sterile RPMI medium without FCS or EDTA. Enzyme solution (1mL) was added to each bijoux and livers were digested for 20 minutes at 37^{o}C with agitation (180 rpm). To stop collagenase activity, 0.5mM EDTA (approximately 200µL) was added to each tissue. Livers were homogenised through a 70 µm nylon cell strainer (BD Biosciences) using normal media (RPMI + 2% FBS + 5 mM EDTA) and were washed by centrifugation (375 x g, 4^{o}C for 5 minutes). Cells were re-suspended in 12 mL RPMI media (without FCS or EDTA) in preparation for gradient centrifugation.

2.6.3 Gradient centrifugation

Gradient centrifugation was used to ensure leukocytes were efficiently separated from other cellular contaminants including hepatocytes, erythrocytes and platelets, as has been

described elsewhere (Klein et al., 2007). The cell suspension from each tissue was first divided into two 6 mL samples (which we had identified as the optimum cell density when processing 1.0 g liver tissue). A Ficoll gradient was prepared at a 1:2 proportion of Ficoll-Paque PLUS (GE Healthcare) to cell suspension. Samples were centrifuged at 2000 rpm for 20 minutes at room temperature without brake, resulting in formation of a cell density gradient. The interface layer was collected as shown in Figure 2.4 and isolated cells were washed in RPMI (375 x g, 4^{o}C for 5 minutes). Cells were re-suspended in the desired volume of normal media (RPMI + 2% FBS + 5 mM EDTA) prior to quantification.

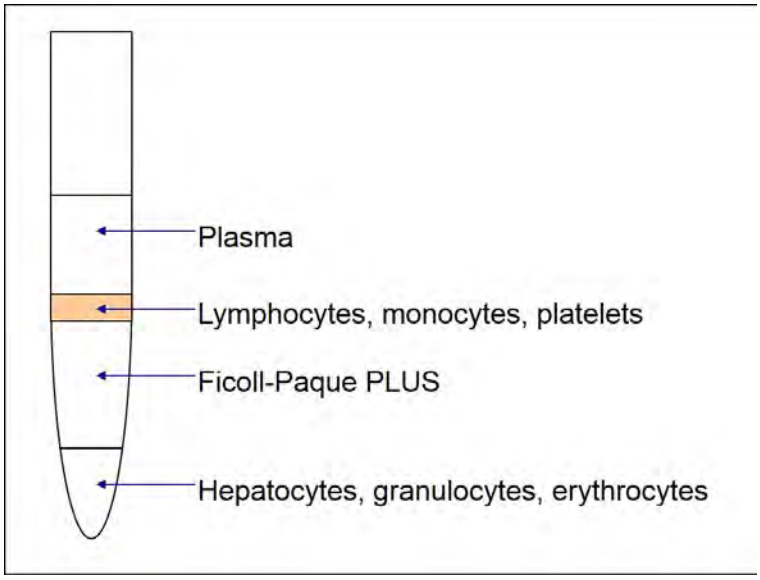

Figure 2.4 Isolation of the leukocyte fraction from Ficoll gradient. (Diagram adapted from Ficoll-Paque PLUS Instructions, GE Healthcare).

2.6.4 Cell quantification

Cell suspensions (10 µL each sample) were diluted in Trypan blue stain (1:10) and viable cells were quantified using a Haemocytometer grid. Cells were counted in two quadrats (4x4) at x10 magnification and the mean was used to calculate absolute number of cells as described by the equation below.

Cells per sample	=	Mean cell count	x	Dilution in Trypan blue (1:10)	x	Square factor (of haemocytometer) (10^4)	x	Volume (of cell suspension)

2.6.5 Extracellular staining

After determining cell numbers, samples were centrifuged (375 x g at 4°C for 5 minutes) and re-suspended in FACS buffer (PBS + 2% FBS + 5 mM EDTA + 0.1% Sodium Azide), at a cell density of approximately 5 x 10^6 /mL. Cells were plated in a 96 v-bottom well plate at 375 x g for 5 minutes at 4°C for FACS staining. Cell CD32/FcγIII and CD16/FcγII receptors were blocked prior to staining by incubating with anti-mouse CD16:CD32 for 20 minutes on ice. This and all other antibodies were prepared in FACS buffer and all dilutions are detailed in Table 2.7 below.

Cells were pelleted as described earlier and 50 µl of the appropriate antibody mix or compensation sample was added to each well. PBS (50 µl) was added to the unstained control. Cells were incubated on ice for 20 minutes in the dark. Cells were washed twice in FACS buffer (375 x g at 4°C for 5 minutes) and were re-suspended in 150 µl FACS buffer containing 0.1% Paraformaldehyde before storing at 4°C until acquisition. Cells were acquired using the CyAn FACS Analyser (Dako, Denmark) using Summit v4.3 software. Data were analysed using FlowJo software (Version 9.6.3(TreeStar)).

2.6.6 Intracellular staining

For measurement of all intracellular antigens by flow cytometry, the extracellular staining protocol outlined above was followed until the final fixation step (0.1% PFA).

Target	Species	Concentration	Working dilution	Source and clone
B220 PE Texas Red	Rat	0.2 mg/mL	1:500	BD Pharmingen RA3-6B2
B220 PerCP Cy5.5	Rat	0.2 mg/mL	1:300	BD Pharmingen RA3-6B2
CD3ε FITC	Armenian Hamster	0.5 mg/mL	1:100	eBioscience 145-2C11
CD3ε PE	Armenian Hamster	0.2 mg/mL	1:50	eBioscience 145-2C11
CD4 eFluor450	Rat	0.2 mg/mL	1:100	eBioscience RM4-5
CD8α APC	Rat	0.5 mg/mL	1:300	eBioscience 53-6.7
CD8α PerCP-Cy5.5	Rat	0.2 mg/mL	1:2000	eBioscience 53-6.7
CD11b APC	Rat	0.2 mg/mL	1:300	eBioscience M1/70
CD11b eFluor450	Rat	0.2 mg/mL	1:300	eBioscience M1/70
CD11c PE-Cy7	Armenian Hamster	0.2 mg/mL	1:200	BD Pharmingen HL3
CD16/32 (Purified)	Rat	0.5 mg/mL	1:100	BD Pharmingen 2.4G2
CD19 APC	Rat	0.2 mg/mL	1:200	BD Pharmingen ID3
CD19 APC-Cy7	Rat	0.2 mg/mL	1:200	BD Pharmingen ID3
CD44 PerCP-Cy5.5	Rat	0.2 mg/mL	1:200	eBioscience IM7
CD45 APC eFluor780	Rat	0.2 mg/mL	1:500	eBioscience 30-F11
CD62L PE	Rat	0.2 mg/mL	1:200	eBioscience MEL-14
CD138 APC	Rat	0.2 mg/mL	1:300	BD Pharmingen 281-2
F4/80 APC	Rat	0.2 mg/mL	1:200	eBioscience BM8
F4/80 FITC	Rat	0.5 mg/mL	1:100	eBioscience BM8

IgG2c PE	Rat	0.2 mg/mL		BD Biosciences A23-1
IgM PE	Rat	0.2 mg/mL		eBioscience 11/41
Ly6C PerCP-Cy5.5	Rat	0.2 mg/mL	1:500	eBioscience HK1.4
Ly6G PE	Rat	0.2 mg/mL	1:200	eBioscience RB6-8C5
MHC II (I-A/I-E) APC	Rat	0.2 mg/mL	1:500	eBioscience M5/114.15.2
NK1.1 FITC	Mouse	0.5 mg/mL	1:100	eBioscience PK136
Podoplanin PE	Syrian Hamster	0.2 mg/mL	1:100	eBioscience eBio8.1.1
IgG Isotype Control PE	Syrian Hamster	0.2 mg/mL	1:100	eBioscience

Table 2.7 Antibodies used for analysis by flow cytometry

2.6.6.1 Intracellular FoxP3 staining

For measurement of intracellular FoxP3 expression, isolated cells were permeabilised using the eBioscience kit, according to the manufacturer's instructions. Briefly, cells were fixed in 1X FoxP3 Fixation/Permeabilization Buffer (eBioscience) for 30 minutes at 4^{o}C, protected from light. After 30 minutes, 1X Permeabilization Buffer (eBioscience) was added before washing twice in 1X Permeabilization Buffer (375 x g at 4^{o}C for 5 minutes). Antibodies against intracellular target antigens (FoxP3) were diluted in 1X Permeabilization Buffer and cells were stained for 30 minutes at 4^{o}C, protected from light. Cells were then washed twice in 1x Permeabilization Buffer (375 x g at 4^{o}C for 5 minutes), and were re-suspended in FACS buffer and acquired using the CyAn FACS Analyser (Dako, Denmark), as described above.

2.6.6.2 Plasma cell intracellular staining

To investigate intracellular Ig in plasma cells, isolated cells were fixed in 1X Cytofix/Cytoperm (BD Biosciences), according to the manufacturer's instructions, for 20 minutes at 4^{o}C, protected from light. Antibodies against intracellular target antigens were diluted in permeabilisation buffer (diluted from 10X Permwash) (BD Biosciences). Cells were stained with the appropriate antibodies (or isotype controls) for 30 minutes at 4^{o}C, protected from light. Cells were washed in permeabilisation buffer and subsequently in FACS buffer (375 x g for 4 minutes at 4°C before re-suspension in FACS buffer and acquisition using the CyAn FACS Analyser (Dako, Denmark), as described above.

2.7 Clodronate treatment

For the depletion of Kupffer cells, mice were treated with clodronate-coated liposomes (Buiting and Van Rooijen, 1994, Van Rooijen, 1989). This procedure has been described elsewhere and is reported to deplete macrophages in the liver (Van Rooijen and Sanders, 1996, Wong et al., 2013). Briefly, mice were treated i.p with 200 µL clodronate suspension or PBS control liposomes 24 hours before STm infection (i.p.). The cell depletion was maintained by subsequent i.p. treatment of clodronate every 2-3 days. Mice were killed at 7 days post-infection and livers and blood were obtained (as described above) for further analysis.

2.8 Analysis of whole blood

The cellular components and other constituents of whole blood were quantified throughout infection at the time-points described in Section 2.3.3. Following cardiac

puncture (outlined in Section 2.3.4), blood was stored at room temperature and 100 µL from each sample was analysed using an automated ABX Pentra 60 Hematology Analyzer (Horiba ABX Diagnostics, France), according to the manufacturer's instructions. Each sample was analysed in triplicate and the mean for each parameter was calculated. The following parameters were measured: total white cell count, percentage of lymphocytes, monocytes, neutrophils, eosinophils and basophils, total red cell count, haemoglobin concentration, haematocrit, red cell distribution width, mean corpuscular volume, mean corpuscular haemoglobin, mean corpuscular haemoglobin concentration, platelet count and mean platelet volume. Blood plasma was separated from the remaining blood by centrifugation (6000 x g for 15 minutes). Plasma samples were stored at -20^{o}C until required for further analysis.

2.9 Biochemical liver function assays

To assess the extent of hepatocyte injury following infection, biochemical assays were performed on serum from infected mice in conjunction with the Biochemistry Department at Birmingham Women's Hospital. Peripheral blood was obtained from infected mice by cardiac puncture as described above and serum/plasma was frozen at -20^{o}C. The content of liver-specific enzymes and products was then quantified by automated equipment by Biochemistry Department technicians, according to the manufacturer's instructions. Concentrations of alanine transaminase, aspartate transaminase, alkaline phosphatase and total bilirubin were measured.

2.9 Statistical analysis

Differences between the medians of two groups was assessed using the two-tailed Mann-Whitney non-parametric sum of ranks test. The statistics programme in GraphPad Prism version 4.0 was used to calculate p values, which were interpreted as significant where $p \leq 0.05$. Consistency in results was ensured by performing the majority of experiments at least twice, and this is indicated in Figure legends. For analysis of statistical significance during a time-course of infection, each time-point was analysed compared to day 0 (non-infected mice) only. On histograms this is illustrated as in Figure 2.5 below. Additionally, statistical significance at the time of resolution was measured and this is indicated separately on the histogram. For example, differences between data recorded at day 14/21 and day 35 were analysed to determine statistical significance. If differences were not statistically significant, but were almost so, the p value is indicated on the figure.

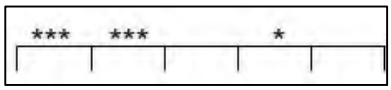

Figure 2.5 Example of statistical significance presentation during a time-course of infection. Each point was compared to day 0 values only.

2.10 Media and buffers

2.10.1 LB agar plates

LB medium (Invitrogen) 2.0% w/v and 2.0% w/v Bacteriological Agar (Melford Laboratories, Ipswich, UK) were dissolved in dH_2O and autoclaved at 121°C for 30 minutes. Plates were poured whilst agar was still molten and were dried at room temperature and stored at 4°C until required.

2.10.2 Buffers

Buffer	**Ingredients**	**Method**
Luria Bertani (L.B) Medium	LB medium (Invitrogen, Paisley, UK) 20% w/v	Dissolved in deionised water (dH_2O) and autoclaved at 121°C for 30 minutes. Media was used at room temperature.
Phosphate buffered saline (PBS) pH 7.4	8.0 g NaCl 0.2 g KCl 1.44 g Na_2HPO_4 0.24 g KH_2PO_4	Dissolved in 900 ml dH_2O and adjusted to pH 7.4, before finalising the volume (1 L). Autoclaved to sterilise.
Tris buffer pH 7.6	1.0 L of 200 mM Tris Base (6.057g Trizma base in 1L dH_20) 1.5 L of 154 mM NaCl (3.188g NaCl (Melford, Ipswich, UK) in 1L dH_20) 1.0 L of 0.1 N HCl (3.75ml 10.1M HCl (Fisher scientific, Loughborough UK)	Appropriate volumes of each buffer were added to prepare a final volume of 3.5L.
Tris buffer pH 9.2		Prepared as above (Tris Buffer pH 7.6) and HCl (1M) was added (dropwise) until pH 9.2 was reached, prior to making up to the desired volume with NaCl.

Table 2.8 Buffers

CHAPTER 3:

SALMONELLA TYPHIMURIUM INFECTION IN THE LIVER

3.1 Background

In sub-Saharan Africa, NTS-infected children frequently die within 24 hours of reaching clinic, yet how infection kills these children is unknown. Death is associated with bacteraemia, but frequently, unlike other systemic bacterial infections, no major symptoms are presented (Graham et al., 2000b). To determine how these individuals die from systemic NTS infection, both immunological and physiological factors must be addressed. During typhoid infections, the liver can be associated with both abnormal function and overt pathology (Pramoolsinsap and Viranuvatti, 1998). The liver is a vital organ and potential disruption during infection may have significant physiological consequences (Protzer et al., 2012, Crispe, 2003, Thomson and Knolle, 2010, Gao et al., 2008). Therefore, a thorough understanding of how the liver is affected by systemic NTS infections is required. It is well documented that during systemic *Salmonella* infections in mice, the liver becomes colonised by bacteria (Mastroeni et al., 1995). Therefore, to investigate how systemic *Salmonella* infections can affect the host physiologically, we examined the impact of infection on the liver.

Whilst bacterial colonisation of the liver during murine NTS infections is well known, the extent to which this relates to systemic infections in humans is less well understood. As outlined in Chapter 1 section 1.2.6.4, multiple studies have described the development of

histopathological lesions in the liver during systemic infection of mice (Nakoneczna and Hsu, 1980, Mastroeni et al., 1995, Everest et al., 1997). These studies have established a relationship between the kinetics of lesion development and the dose of bacterial inoculum used, and have identified several of the key cell types which contribute to these structures (Richter-Dahlfors et al., 1997, Sheppard et al., 2003, Grant et al., 2009). Furthermore, the dynamics of bacterial growth within host cells with particular reference to lesion size has also been well characterised, especially since the development of appropriate fluorescent-labelling techniques (Helaine et al., 2014). However, very few of these studies utilise physiologically relevant challenge doses and hence interpretation with regard to human infections must be undertaken with extreme caution. In addition, there is little evidence as to how inflammatory pathology in the liver may impact on liver function and therefore overall outcome of infection (Pramoolsinsap and Viranuvatti, 1998). Thus we were particularly keen to determine whether liver pathology may contribute more fundamentally to host susceptibility to systemic infection.

Here we use a systemic but resolving model of *Salmonella* Typhimurium (STm) infection in Nramp-susceptible mice, to study the liver during infection. The host response to this infection in secondary lymphoid tissues such as the spleen has been well characterised in the Cunningham lab (Cunningham et al., 2007). Briefly, bacterial replication during the first week of infection is controlled by the innate response. There is a high bacterial load in colonised sites which is, in effect, “capped” by innate cells. However, an adaptive response is required to clear bacteria from colonisation sites, and this is not established until around 18-21 days post-infection. Once this adaptive response can enforce bacterial clearance, bacterial numbers in colonised tissues resolve within about a month post-infection.

To determine if the kinetics of infection in the liver are similar to that seen in the spleen, we examined livers at various key time-points during infection, corresponding to different stages of the host immune response in the spleen. These included: day 7 (when peak bacterial load is limited by innate cells); day 21 (when the adaptive response is established and bacterial clearance has begun); day 28 (when bacterial clearance is well underway); and day 35 (when infection should be largely resolved). A later time-point of day 50-55 was used to identify any lasting effects of the infection in the liver. These key time-points have been used throughout this study to characterise how the infection is established and resolved in this effector site.

3.1.2 Aim of study

Here we show the kinetics of *Salmonella* colonisation in the liver and describe how the host responds to this systemic infection. The aims of this section were to:

- Describe hepatic colonisation of STm including bacterial distribution and kinetics of infection;
- Characterise inflammatory lesion development and resolution during the course of infection;
- Phenotype infiltrating leukocytes to identify which host immune cells contribute to this response.

RESULTS

3.2 The liver is colonised by *Salmonella* Typhimurium during systemic infection

WT mice were infected by intraperitoneal (i.p.) injection of 5 x 10^5 attenuated STm and at key time-points during infection, the liver bacterial burden was measured and the liver was examined for signs of pathology. Liver mass increases from day 3 post-infection and peaks at day 21 (Fig 3.1 A). After this time, hepatomegaly resolves, yet does not reach the original mass of non-infected mice by day 55. To check if this is an age-related phenotype (and if liver mass increases with age), aged mice (18 month old) were infected alongside 6-8 week WT C57BL/6J mice and hepatomegaly was measured during infection. Liver mass is equivalent in non-infected aged and non-aged mice, suggesting the observed hepatomegaly is infection-induced (Fig 3.1 B).

Viable bacteria can be cultured from the liver within 24 hours of infection (Fig 3.1 C). Bacterial burden in the liver peaks at day 7 post-infection and bacterial clearance is established by day 14, although bacterial numbers are not significantly cleared until day 21. Bacterial numbers are reduced over the following weeks, but can still be detected at 55 days. To ascertain the extent of bacterial colonisation in the liver relative to other colonised sites, the bacterial loads of the liver, spleen, brain, lungs, kidney and blood were measured at day 7 post-infection. At this peak time of bacterial burden in the liver, bacterial numbers are generally lower than those detected in the spleen but greater than other non-lymphoid organs (Fig 3.1 D).

Figure 3.1

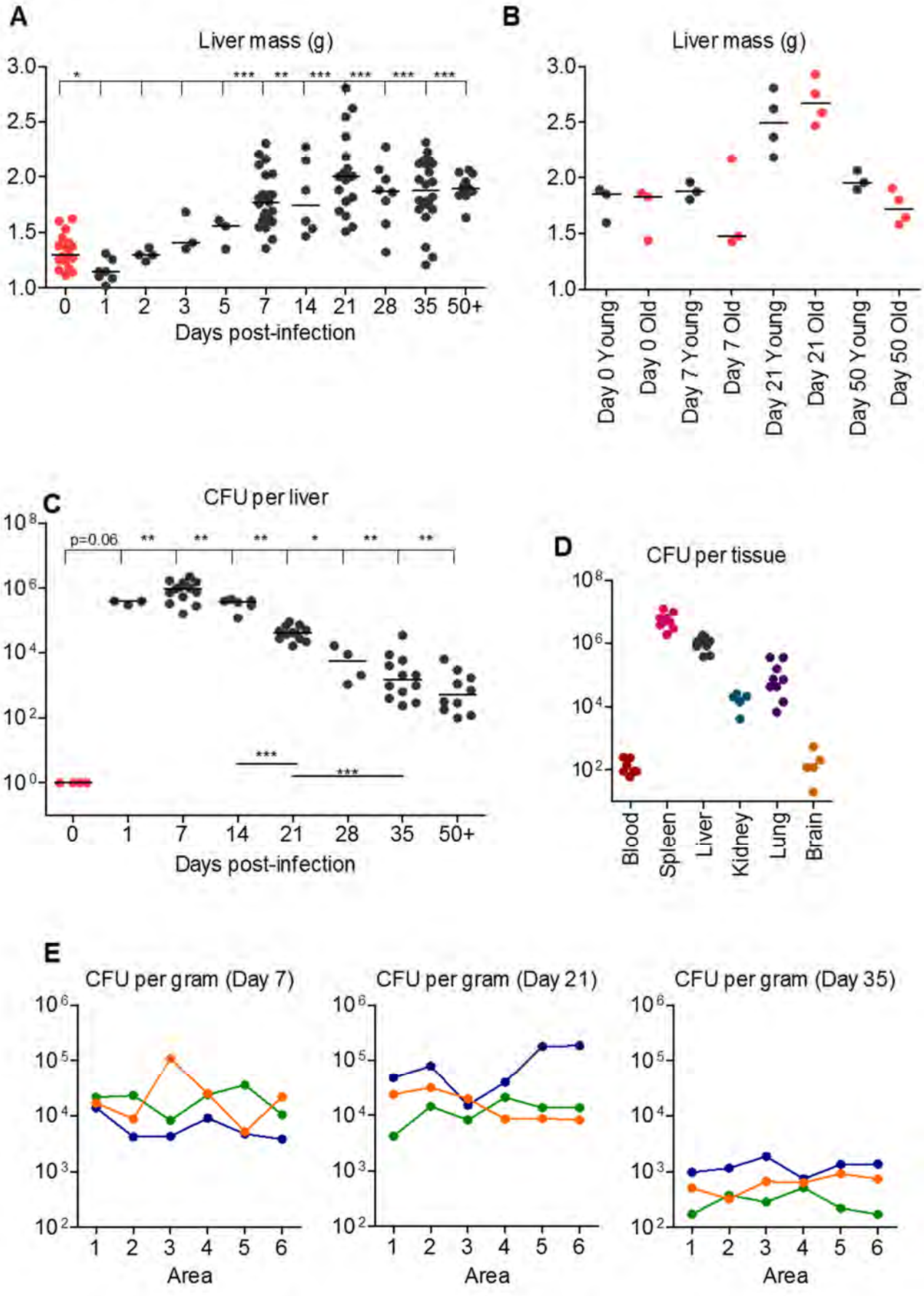
A
Liver mass (g)
3.0
2.5
2.0
1.5
1.0
0 1 2 3 5 7 14 21 28 35 50+
Days post-infection
B
Liver mass (g)
Day 0 Young
Day 0 Old
Day 7 Young
Day 7 Old
Day 21 Young
Day 21 Old
Day 50 Young
Day 50 Old
C
CFU per liver
p=0.06
0 1 7 14 21 28 35 50+
Days post-infection
D
CFU per tissue
Blood
Spleen
Liver
Kidney
Lung
Brain
E
CFU per gram (Day 7)
CFU per gram (Day 21)
CFU per gram (Day 35)
Area

Figure 3.1 During systemic infection, Salmonella colonises the liver and are distributed uniformly throughout the tissue.
WT mice were infected (i.p.) with 5 x 10^5 CFU attenuated *Salmonella* Typhimurium (STm). A) Liver mass was measured at the indicated time-points between days 1 and 50+ post-infection (50+ indicates between days 50 and 55; which varied in different experiments). Data are from multiple infection experiments with similar results. B) Young (6-8 weeks) and aged (18 months) WT mice were infected as described above. Liver mass was measured at days 0, 7, 21 and 50 post-infection. Data are taken from 1 experiment; n = 3 or 4. C) Bacterial colonisation was enumerated at the indicated time-points post-infection. Data are from the same mice as in A). D) WT mice were infected as described above and bacterial colonisation of the blood, spleen, liver, kidney, lungs and brain were enumerated at day 7 post-infection. Data are taken from 2 experiments with similar results, where n = >4 per tissue. E) WT mice were infected as described above and bacterial colonisation was measured in different regions of the liver throughout infection (expressed as CFU per gram liver tissue). Days 7, 21 and 35 are shown as representative time-points where each colour represents one mouse. The areas of the liver are described fully in Chapter 2, Section 2.4. Briefly, areas are as follows: 1) interior region of lobe A (largest lobe); 2) peripheral regions of lobe A; 3) interior regions of lobe B (attached to the gall bladder); 4) peripheral regions of lobe B; 5) lobe C; 6) lobe D. Data are taken from 1 experiment; n = 3. *p≤0.05 **p≤0.01 ***p≤0.001.

To assess whether bacterial distribution is even throughout the entire liver, bacterial numbers were additionally measured at different sites throughout the tissue, during the course of infection. Livers were divided into the four lobes, and both internal and peripheral areas of the two largest lobes were also examined. Days 7, 21 and 35 post-infection are shown as representative time points (Fig 3.1 E). Although there is some variation, bacterial colonisation is uniform across the entire tissue.

3.3 Liver pathology during infection

Having established that the liver is colonised throughout and that bacteria persist in this effector site even once they are completely cleared from lymphoid tissues such as the spleen, we wanted to determine to what extent infection causes liver pathology. The exterior surface of non-infected livers is smooth and shiny, with no blemishes or other distinctive features and livers are a reddish-pink colour (Fig 3.2 A). Within the first 48 hours of infection, some slight changes to this appearance are detected (data not shown), and these are apparent in all livers by day 7 post-infection (Fig 3.2 B). Pathological features include: loss of the smooth appearance; a tendency for peripheral regions of lobes to become bloodshot, and this can spread throughout the lobes; white/grey lesions of varying severity appear throughout the tissue (although these are more frequent on the smallest lobe). At day 21 post-infection, these features can be more severe (Fig 3.2 B). From day 28 onwards, lesions are largely absent but many livers remain bloodshot at the periphery and this can persist at day 50 (Fig 3.2 C-D).

Figure 3.2

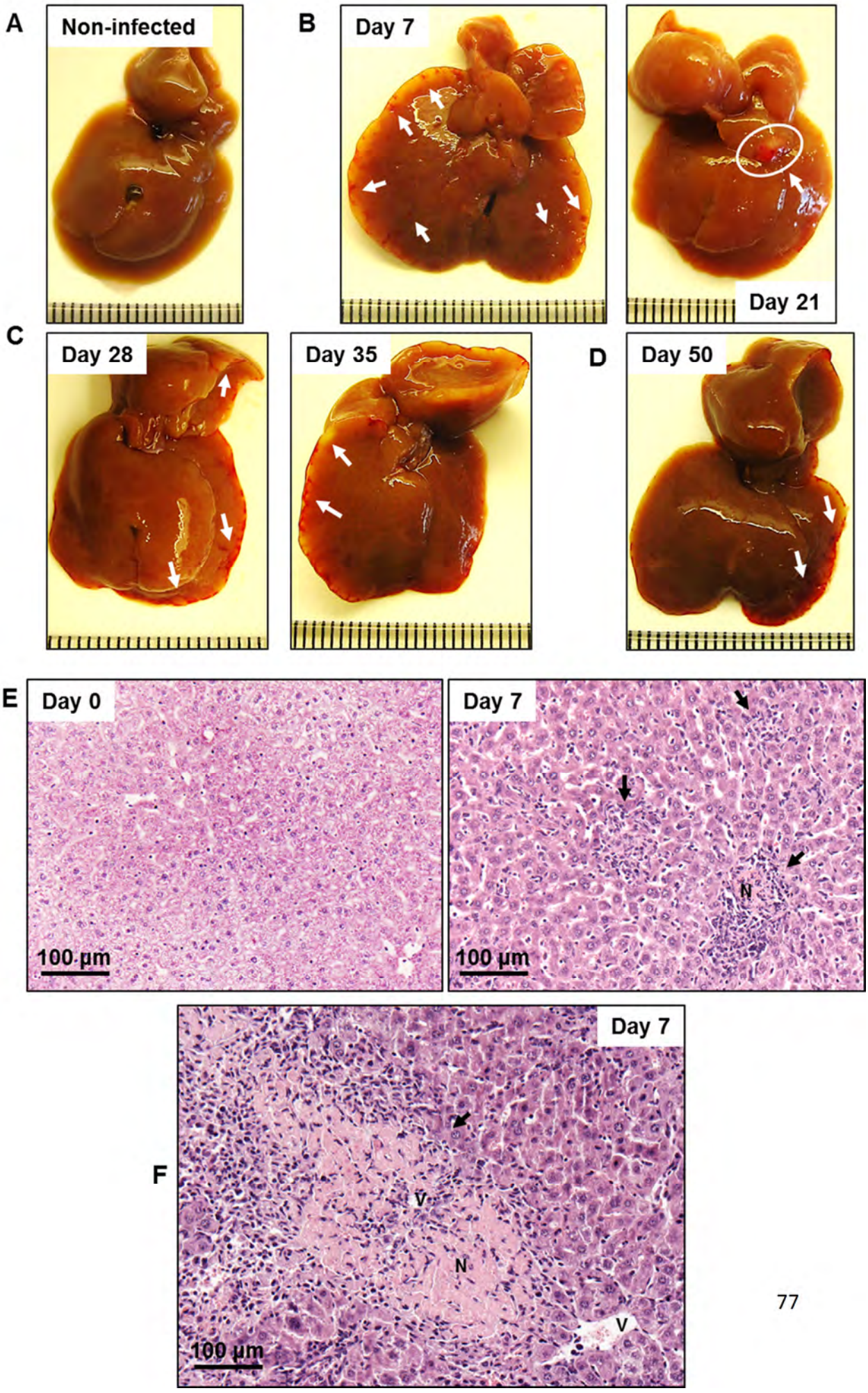
A
Non-infected
B
Day 7
Day 21
C
Day 28
Day 35
D
Day 50
E
Day 0
Day 7
N
100 µm
100 µm
F
Day 7
V
N
V
100 µm

Figure 3.2 The liver shows signs of pathology on the exterior surface and histologically, within the tissue

WT mice were infected (i.p.) with 5 x 10^5 CFU attenuated STm. Pathological features were examined on the surface of livers throughout infection. White arrows indicate pathological features, including white-coloured lesions and bloodshot tissue. A) Livers from non-infected mice do not show any signs of pathology. Distinct pathological features are apparent between B) days 7 and 21 (white circle indicates severe necrotic region); C) days 28 and 35 post-infection and D) day 50. Images are representative and are taken from one experiment where n = 4 at each time-point. E) WT mice were infected as described above and at days 0 and 7 post-infection, livers were removed and frozen tissue sections were stained using H&E. Black arrows indicate inflammatory lesions; N indicates necrosis; V indicates blood vessel. F) More extensive necrotic regions can be observed.

3.3.1 Hepatic lesions form rapidly after infection and peak between days 7 and 21 post-infection

Having identified pathological lesions on the liver surface, we were keen to determine how this pathology continues within the tissue and if it resembles that reported in other NTS infection models (Mastroeni et al., 1995, Richter-Dahlfors et al., 1997). We focussed on what cells and molecular mediators are in lesions with the view of investigating how hepatic pathology may affect liver architecture and the consequences this may have on liver function and infection outcome. Initially, we stained non- infected and infected livers with Haematoxylin and Eosin (H&E) to detect infiltrate in the parenchymal tissue during infection. Figure 3.2 E demonstrates the influx of cells into the liver at day 7 post-infection and the development of inflammatory lesions. These lesions can become necrotic in the centre, as shown in Figure 3.2 F. Interestingly, external lesions directly correspond to internal regions of hepatocyte necrosis (as illustrated by individually sectioning lesions visible on the liver surface and examining by H&E) (data not shown).

The proportion of the tissue area occupied by lesions was quantified by point counting of H&E stained sections. Non-infected livers contain rare infiltrated leukocytes which are sparsely distributed throughout the sinusoids and tend to gather in portal areas (Fig 3.3 A). Lesions are established by 2 days post-infection (data not shown), and are most pronounced at days 7 and 21 post-infection. Although there is an increased sinusoidal distribution of cells during infection, the majority of leukocytes localise to lesions, which are compact and can form proximal or distal to vessels. Leukocytes also associate with portal areas (as in non-infected mice).

Figure 3.3

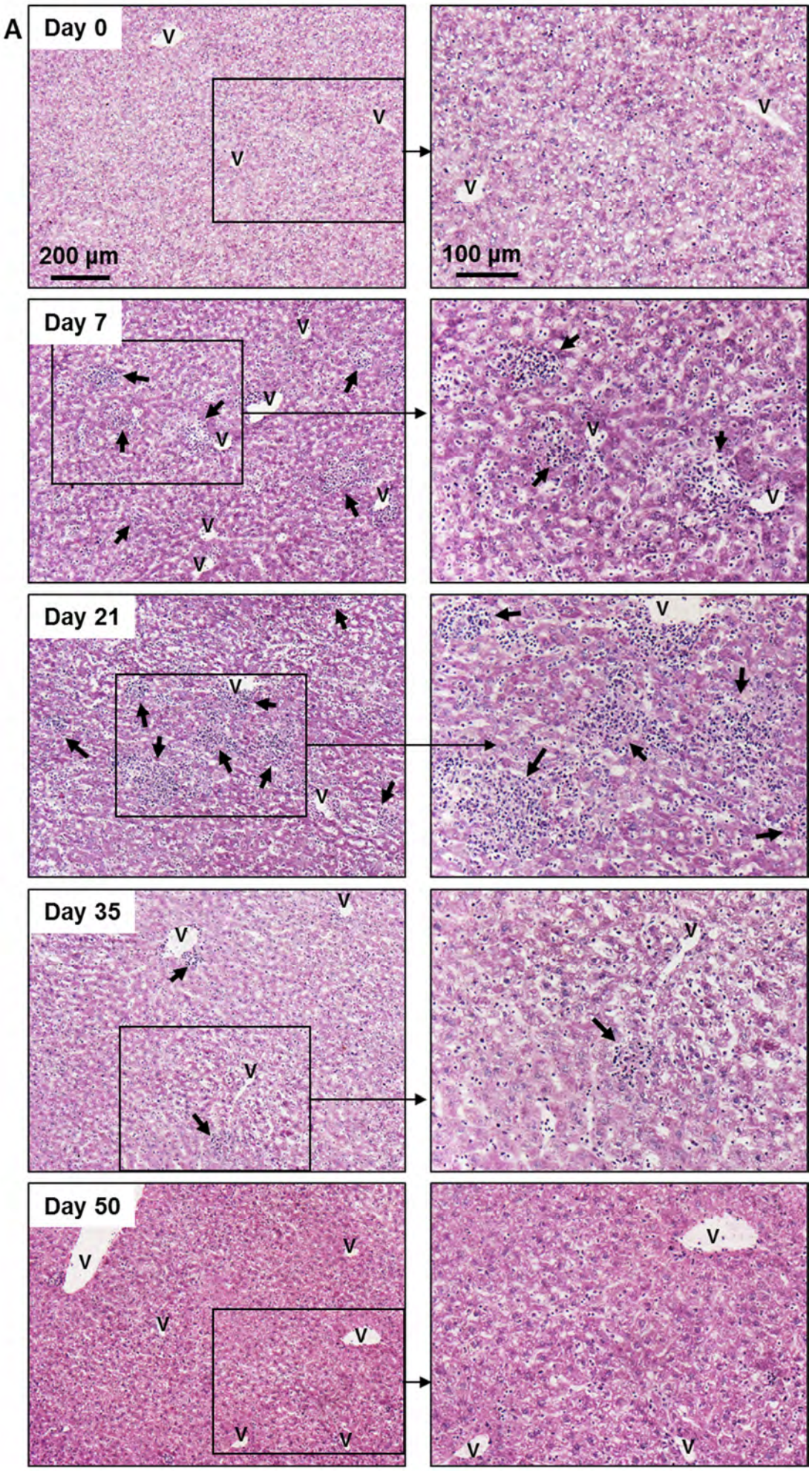

Figure 3.3 continued

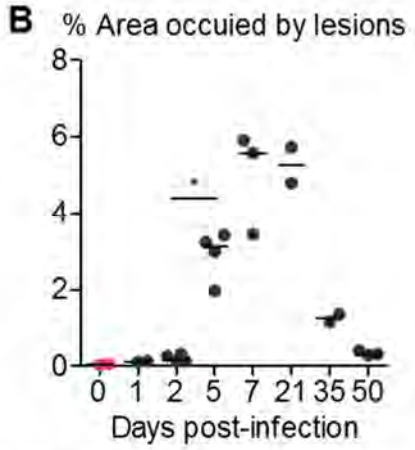

Figure 3.3 Inflammatory lesions form in the hepatic parenchyma during infection
WT mice were infected (i.p.) with 5 x 10^5 CFU attenuated STm. A) Livers were removed at various time-points post-infection and frozen tissue sections were stained using H&E. Representative images are shown of days 0, 7, 21, 35 and 50 post-infection, with the right-hand panel illustrating a higher magnification of an area within the left hand panel. Black arrows indicate inflammatory lesions; V indicates blood vessel. All images are taken from one experiment where n = 4 at each time-point. B) The percentage of total liver area which is occupied by inflammatory lesions was measured using point counting as described in section 2.5.4.1. Counting was performed across the entire tissue section at x 10 magnification. Mice in B) are the same as used in A). *p≤0.05 **p≤0.01 ***p≤0.001.

Pathology is most severe at day 21 and generally resolves by day 35 when the remaining foci are small and compact and there are fewer cells both in the sinusoids, and in portal areas (Fig 3.3 A and data not shown). After this time, although foci are largely absent, more cells associate with vessels than in non-infected mice. Images shown are representative of the entire liver; all lobes were analysed at 3 depths of sectioning and the phenotype is consistent throughout (data not shown).

3.3.2 Inflammatory lesions develop in the liver by both intraperitoneal and intravascular routes of infection

To assess whether development of inflammatory lesions in the liver is a consequence of infection and not an effect of infecting i.p., mice were infected by either i.p or intravascular (i.v.) injection and inflammation was examined. Hepatomegaly is equivalent in both infection routes at day 7, but greater at day 21 after i.v. infection, although this does not reach statistical significance (Fig 3.4 A). Bacterial loads and inflammatory lesion induction are equivalent at both time-points, irrespective of infection route (Fig 3.4 B-C and data not shown). Therefore both i.p. and i.v. infection results in similar systemic infection, as has been previously demonstrated in other murine *Salmonella* infections (Hsu, 1989).

3.3.3 Hepatic lesions contain heterogeneous populations of leukocytes

Immunohistochemistry (IHC) was used to identify what cells are present in inflammatory lesions. In non-infected mice, individual F4/80$^+$ Kupffer cells are found throughout the sinusoids and isolated CD3$^+$ T cells and CD11c$^+$ dendritic cells (DCs) are associated with portal areas (Fig 3.5 A).

Figure 3.4

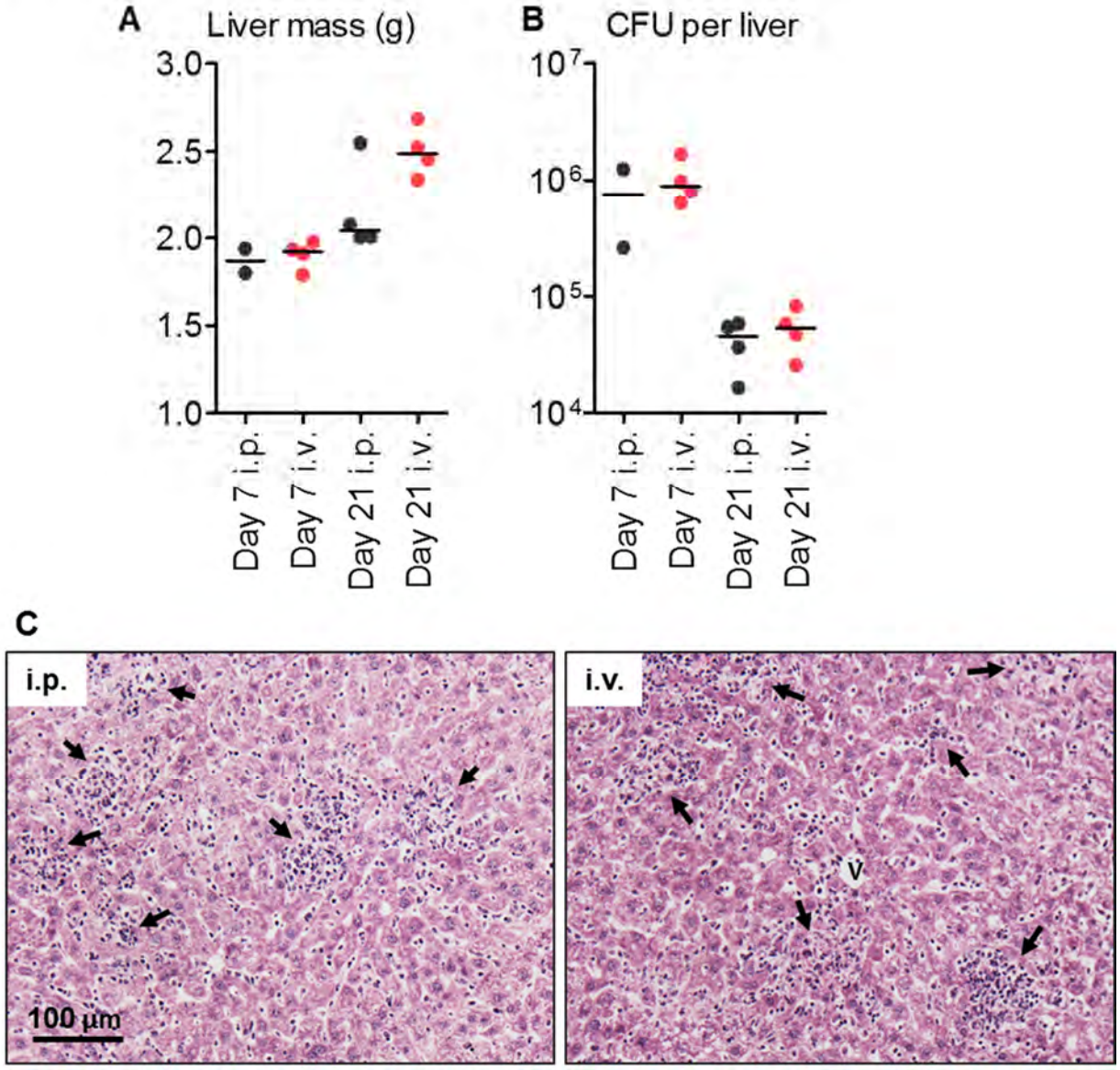

Figure 3.4 Bacterial colonisation of the liver occurs after both i.p. and i.v. infection
WT mice were infected either i.p. or i.v. with 5 x 10^5 CFU attenuated STm (using the same preparation of bacteria). A) Liver mass was measured at days 7 and 21 post-infection. B) Bacterial load of the liver was enumerated at days 7 and 21 post-infection. C) Livers were removed at day 7 and 21 post-infection and frozen tissue sections were stained using H&E (images from day 7 are shown). Black arrows indicate inflammatory lesions; V indicates blood vessel. All data are taken from 1 experiment where n = 2-4 (due to mis-injections in the day 7 i.p. group). All images are representative of all livers examined.

Figure 3.5

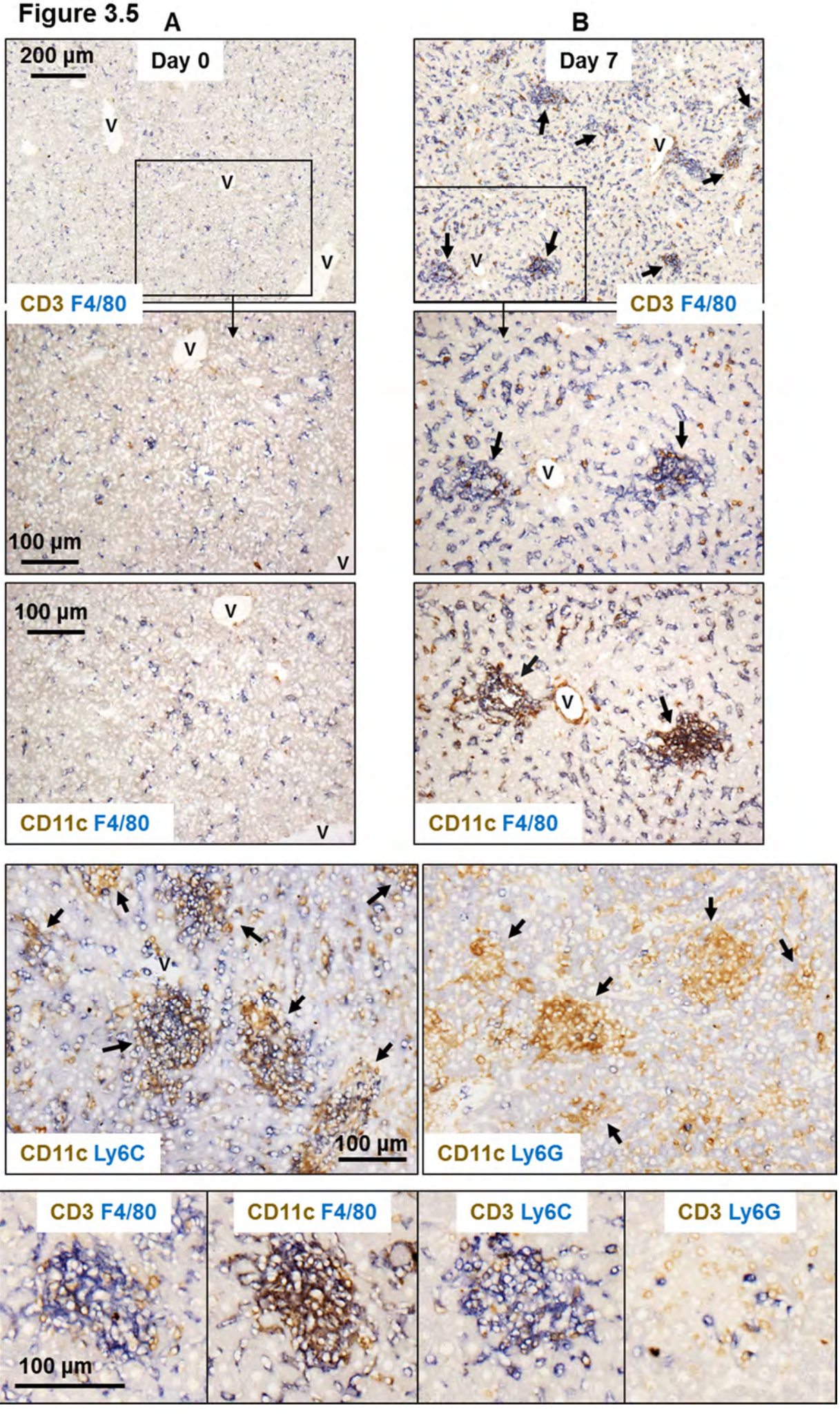
A
B
200 µm
Day 0
Day 7
V
CD3 F4/80
CD3 F4/80
100 µm
CD11c F4/80
CD11c F4/80
C
CD11c Ly6C
100 µm
CD11c Ly6G
D
CD3 F4/80
CD11c F4/80
CD3 Ly6C
CD3 Ly6G
100 µm

Figure 3.5 continued

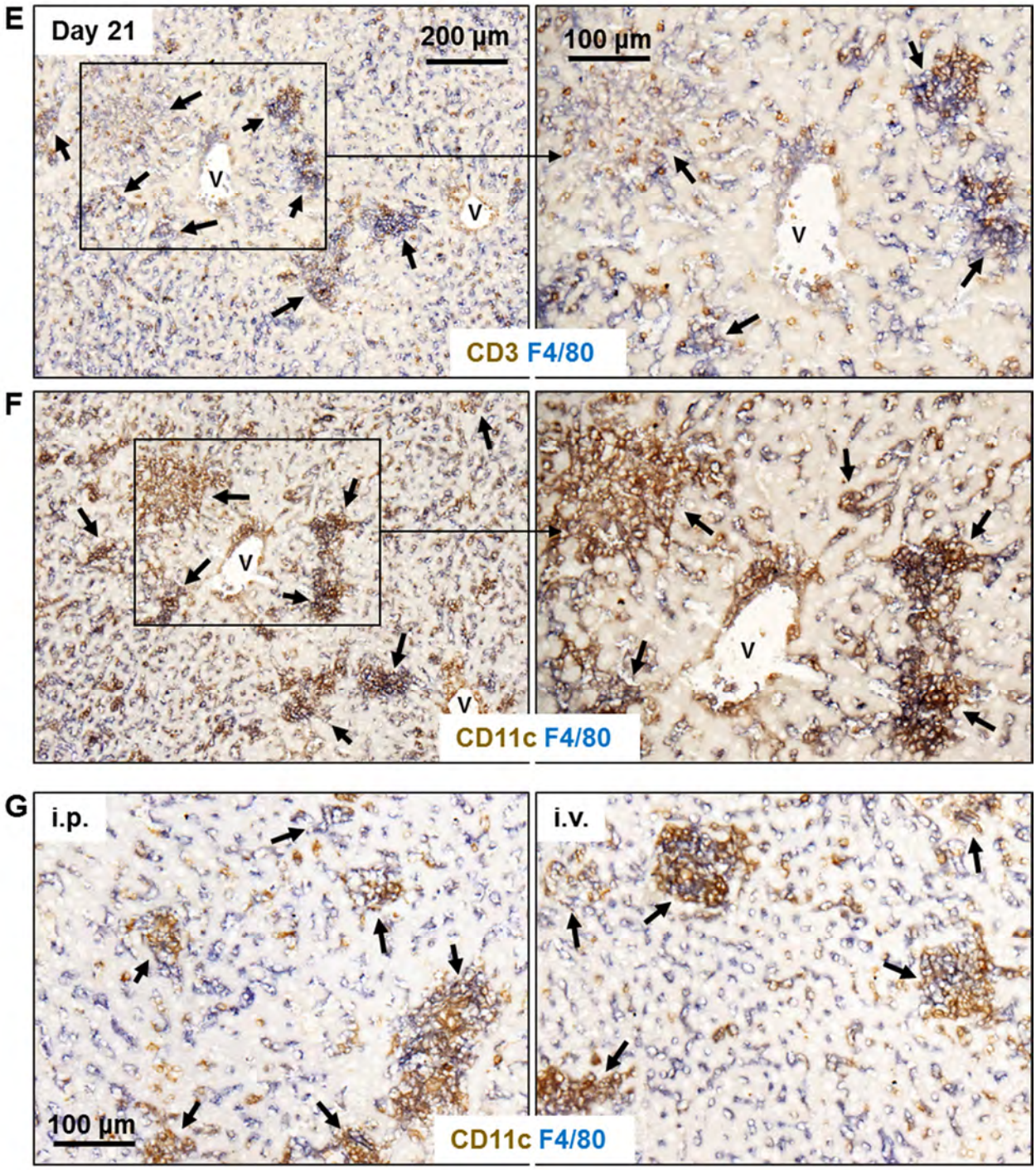

Figure 3.5 Identification of hepatic infiltrate by immunohistochemistry
WT mice were infected (i.p.) with 5 x 10^5 CFU attenuated STm and livers were removed at days 0 and 7 post-infection. Leukocyte infiltration was characterised on frozen tissue sections by immunohistochemistry (IHC). Black arrows indicate inflammatory lesions; V indicates blood vessel. A) Day 0 and B) Day 7-infected livers contain F4/80$^+$ cells (blue) and CD3$^+$ cells (brown) in the top 2 panels, and the boxed areas are magnified in the lower 4 panels. The bottom panels of A) and B) indicate F4/80$^+$ cells (blue) and CD11c$^+$ cells (brown). C) At day 7 post-infection, Ly6C$^+$ cells (blue) (left panel) and Ly6G$^+$ cells (blue) (right panel) are observed. CD11c$^+$ cells (brown) are also shown. D) IHC of serial sections of an inflammatory lesion indicate the multiple leukocytes present. Panel 1: blue F4/80$^+$ cells, brown CD3$^+$ cells; panel 2: blue F4/80$^+$ cells, brown CD11c$^+$ cells; panel 3: blue Ly6C$^+$ cells, brown CD3$^+$ cells; panel 4: blue Ly6G$^+$ cells, brown CD3$^+$ cells. E and F) Frozen liver serial sections from day 21-infected mice were examined by IHC. The right hand panel indicates a higher magnification of the boxed area in the left panel. E) CD3$^+$ cells (brown), F4/80$^+$ cells (blue). F) CD11c$^+$ cells (brown) F4/80$^+$ cells (blue). All images in A-F are representative from mice in 1 experiment (n=4) where all mice were infected on the same day. G) WT mice were infected either i.p. or i.v. with 5 x 10^5 CFU attenuated STm (using the same preparation of bacteria). CD11c$^+$ cells (brown) and F4/80$^+$ cells (blue) were identified by IHC (day 7 post-infection is shown).

At day 7 post-infection, lesions contain F4/80$^+$ cells, CD11c$^+$ cells, F4/80$^+$ CD11c$^+$ cells and cells positive for monocytic markers CD11b and Ly6C (Fig 3.5 B-C and data not shown). Neutrophils, identified by Ly6G$^+$ staining, can also be seen in lesions, although these are less common than other myeloid populations (Fig 3.5 C). T cells are frequently located at the periphery of lesions (Fig 3.5 B, discussed further below). We detect an increase in sinusoidally-distributed F4/80$^+$ cells which generally do not stain for CD11c (Fig 3.5 B). Therefore these cells are likely to be macrophages (including Kupffer cells) rather than F4/80-expressing DC subtypes (such as monocyte-derived DCs). Figure 3.5 D shows serially stained sections of a single inflammatory lesion.

At day 21 post-infection, lesions are similar and there is a higher density of cells in the sinusoids, mainly due to increased CD11c$^+$ and CD11c$^+$ F4/80$^+$ cells (Fig 3.5 E-F). Inflammatory lesions have a similar appearance by either the i.p. or i.v. route at both days 7 and 21 (Fig 3.5 G and data not shown).

3.3.4 Lesions contain CD4$^+$ and T regulatory cells at the periphery

As Th1 cells are required for STm infection control (Pie et al., 1997), we hypothesised that the majority of T cells present would be CD4$^+$ and so we stained sections for CD3, CD4, CD8 and FoxP3. In non-infected livers, T cells are rare and CD4$^+$ and CD8$^+$ T cells are found in similar proportions (Fig 3.6 A). At day 7 post-infection, T cells generally localise to the periphery of lesions and are mainly CD4$^+$. There are a greater proportion of CD8$^+$ T cells at day 21, although the majority are CD4$^+$, and there are more T cells in the sinusoids. There are fewer T cells by day 35 and these are concentrated in the remaining foci and both CD4$^+$ and CD8$^+$ cells are present (Fig 3.6 A).

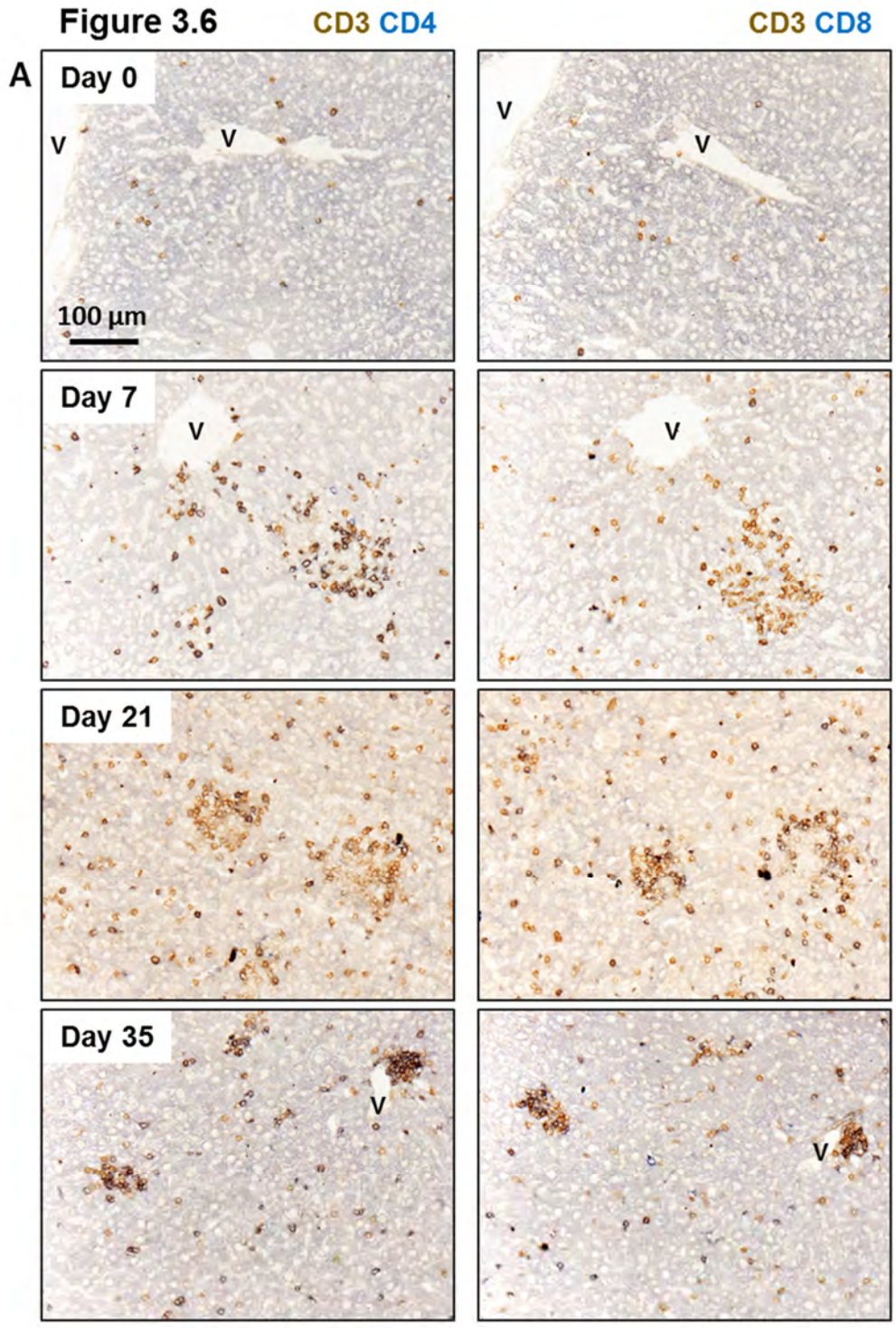

Figure 3.6 T cells in the liver during infection

WT mice were infected (i.p.) with 5 x 10^5 CFU attenuated STm and livers were removed at days 0, 7, 21 and 35 post-infection. A) T cells were identified by IHC using markers for CD3, CD4, and CD8. The left hand panel indicates $CD3^+$ $CD4^-$ cells (brown) and $CD3^+$ $CD4^+$ cells (black) at the indicated time-points. The right hand panel indicates $CD3^+$ $CD8^-$ cells (brown) and $CD3^+$ $CD8^+$ cells (black). Any blue cells indicate $CD4^+$ $CD3^-$ (left panel) and $CD8^+$ $CD3^-$ (right panel). Black arrows indicate inflammatory lesions; V indicates blood vessel. B) Regulatory T (Treg) cells were identified using markers for CD3 and FoxP3 where $CD3^+$ T cells are brown and Treg cells are positive for both CD3 (brown) and FoxP3 (blue/black). Black arrows indicate Treg cells. The right hand panel indicates higher magnification of the boxed area in the left panel. All images in A-B are representative from mice in 1 experiment (n=4) where all mice were infected on the same day. C) T cells which contributed to inflammatory lesions were quantified whereby 30 inflammatory lesions were counted per tissue section. Total $CD3^+$ cells and $FoxP3^+$ cells were counted. Data are from the same mice as in A and B.

Figure 3.6 continued CD3 FoxP3

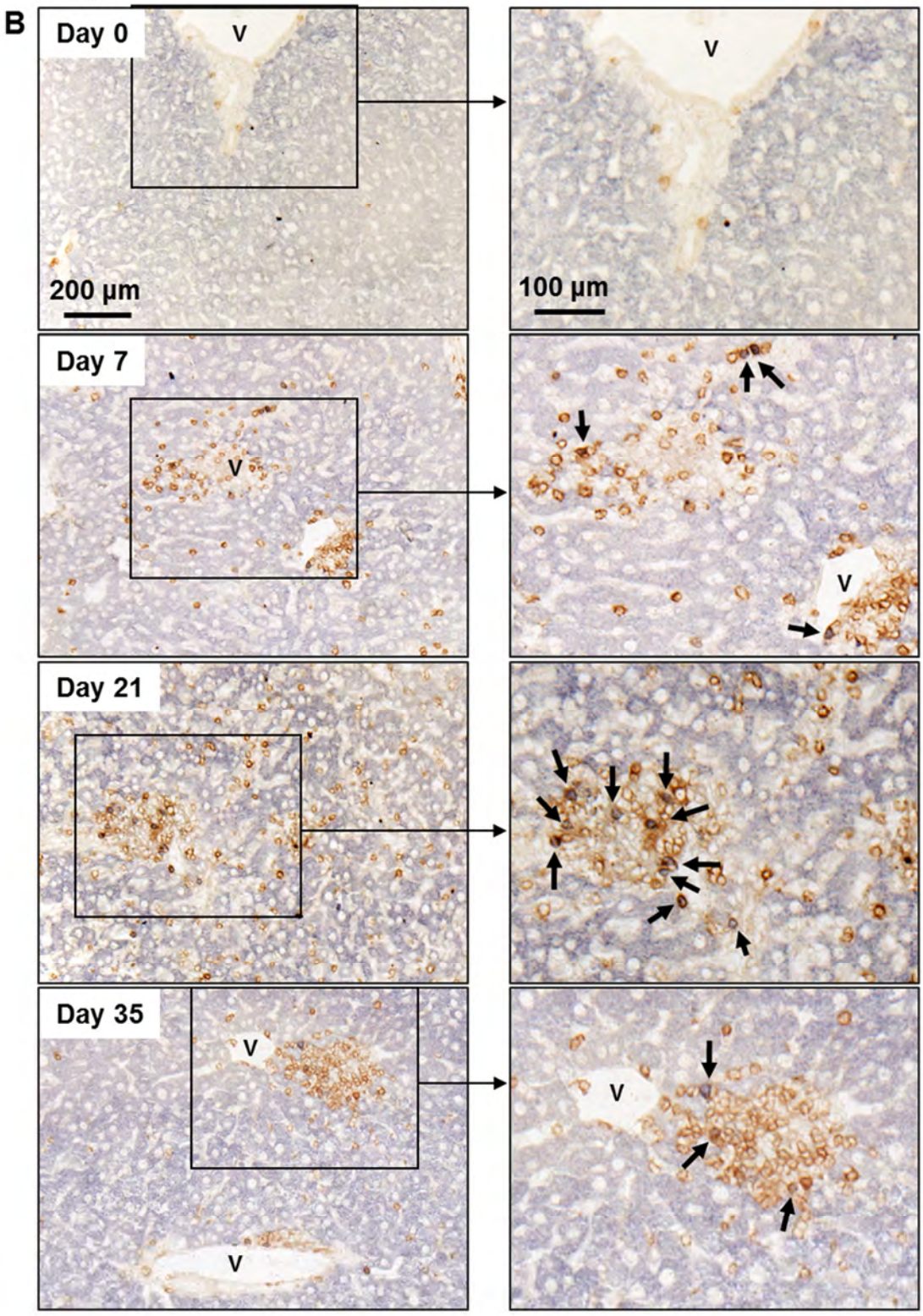

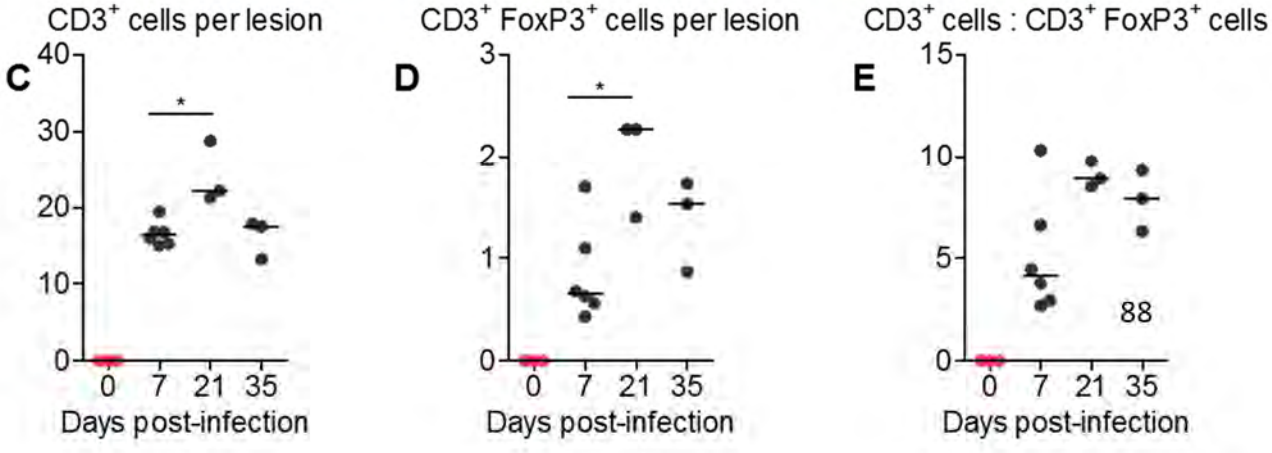

In non-infected livers, occasional FoxP3$^+$ regulatory T (Treg) cells are observed, but these are rare (Fig 3.6 B). Following infection, FoxP3$^+$ cells are observed both within lesions and adjacent to vessels (Fig 3.6 B and data not shown). The distribution of FoxP3$^+$ cells is similar at days 7 and 21, although there are more FoxP3$^+$ cells present at day 21. At day 35, some FoxP3$^+$ cells can be found in the remaining lesions, and fewer are observed beside vessels (Fig 3.6 B and data not shown). Quantification of IHC staining confirmed that the number of CD3$^+$ T cells per foci is greater at day 21 (Fig 3.6 C). The number of FoxP3$^+$ cells per lesion is also increased at day 21 and the ratio of CD3$^+$ FoxP3$^+$ cells to total CD3$^+$ cells is also elevated (Fig 3.6 D-E). Interestingly, there remains an elevated number of Treg cells per lesion at day 35 (Fig 3.6 D). In addition, considering lesions are generally smaller at this time-point than at day 7, a greater proportion of the total cells in a lesion are CD3$^+$ (because the number of CD3$^+$ cells per lesion is equivalent to that at day 7) (Fig 3.6 C and data not shown). This suggests lesions are made of a greater proportion of T cells relative to other populations at resolving stages of infection, and that Tregs make a prominent contribution to this. These data highlight the multitude of leukocyte populations present in lesions.

3.3.5 Podoplanin is expressed in inflammatory lesions

Having identified many of the leukocytes which contribute to inflammatory lesions, we wanted to identify other cell types associated with these structures, for which we used confocal microscopy. Infected livers were stained with CD45.2 to identify haematopoietic cells, in conjunction with podoplanin, a glycoprotein associated with inflammation (Farr et al., 1992). At day 7 post-infection, the majority of cells within inflammatory lesions are CD45.2$^+$, indicating they are haematopoietic (Fig 3.7 A). Podoplanin is also seen in lesions and co-localises with CD45.2$^+$ cells (magenta staining) (Fig 3.7 A).

Figure 3.7

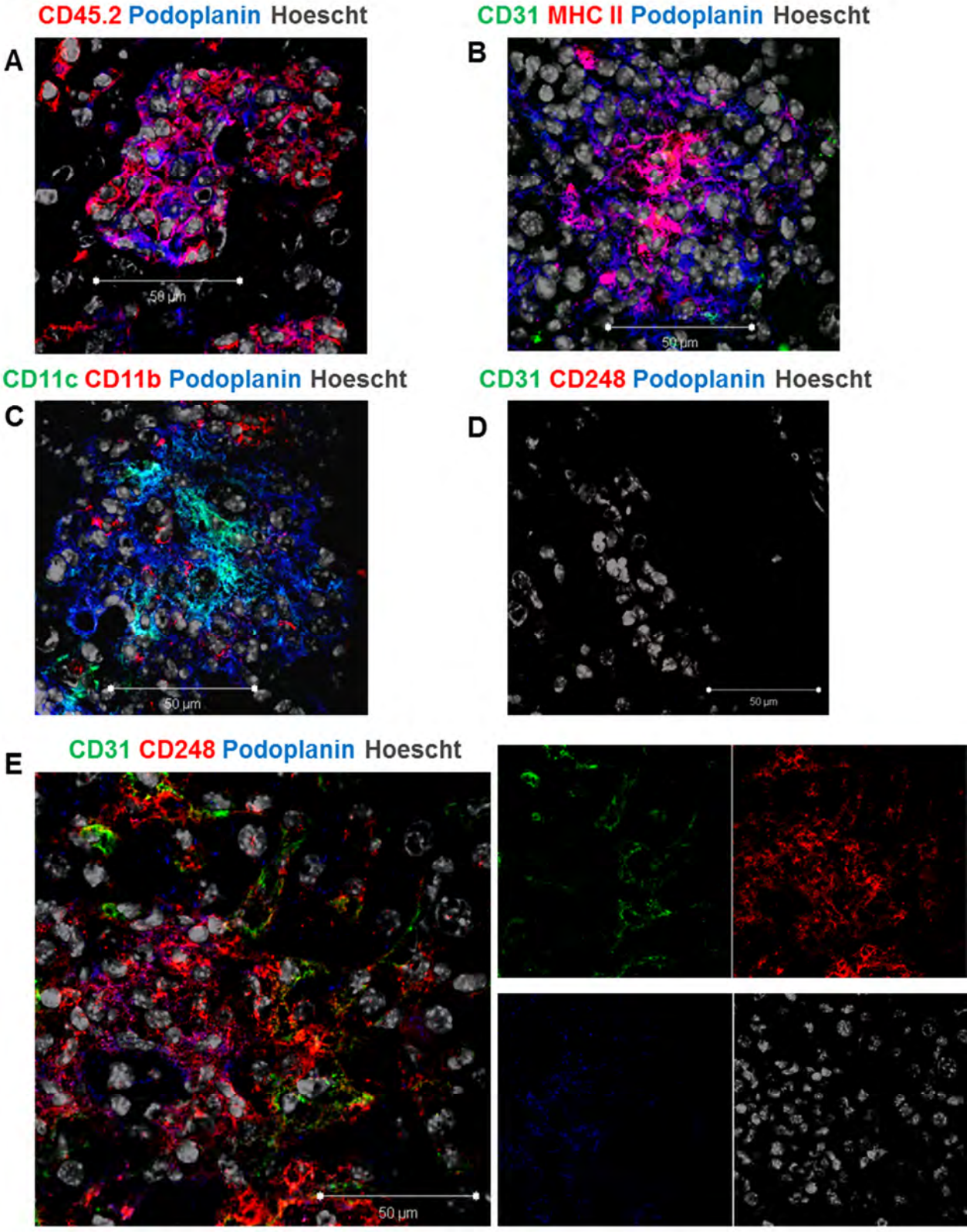

Figure 3.7 Confocal microscopy examination of inflammatory lesions
WT mice were infected (i.p.) with 5 x 10^5 CFU attenuated STm. At day 7 post-infection, livers were removed and frozen tissue sections were examined by confocal microscopy. All images are focussed on an inflammatory lesion (not serial sections) and are representative of all livers examined. A) Cells of haematopoietic lineage were identified using CD45.2 (red cells). Blue cells = podoplanin$^+$ cells; magenta cells CD45.2$^+$ podoplanin$^+$. B) Green cells = CD31$^+$; red cells = MHC II$^+$; blue cells = podoplanin$^+$; magenta cells = MHC II$^+$ podoplanin$^+$. C) Green cells = CD11c$^+$; red cells = CD11b$^+$; blue cells = podoplanin$^+$; cyan cells = CD11c$^+$ podoplanin$^+$; magenta = CD11b$^+$ podoplanin$^+$; white cells = CD11c$^+$ CD11b$^+$ podoplanin$^+$.D Isotype control image of E. E) Green cells = CD31$^+$; Red cells = CD248$^+$; Blue cells = podoplanin$^+$; Magenta cells = CD248$^+$ podoplanin$^+$; Yellow cells = CD31$^+$ CD248$^+$. The right-hand panel illustrates the single colour split of the main image.

Co-expression of podoplanin is also seen with MHC II (magenta staining), CD11c (cyan staining) and, to some extent CD11b (magenta staining), indicating that podoplanin can be expressed by myeloid cells, some potentially with antigen-presenting capabilities (Fig 3.7 B-C). Podoplanin was also stained in conjunction with CD31, an endothelial marker, also expressed on leukocytes, and CD248, expressed by fibroblasts and pericytes during liver fibrosis (Alridge, manuscript in preparation). The co-localisation of podoplanin with $CD248^{+}$ cells (magenta staining) together with the $podoplanin^{+}$ staining on $CD45.2^{-}$ cells in Figure 3.7 A, may indicate the presence of stromal populations in inflammatory lesions (Fig 3.7 D).

3.4 Leukocyte quantification and detailed phenotyping

Having identified some cells present within lesions, we wanted to assess these populations in more detail, for which we used flow cytometry. To ensure adequate isolation of leukocyte populations from the liver, both collagenase digestion and gradient centrifugation were used, as has been described elsewhere (Klein et al., 2007, Flores-Langarica et al., 2011, Cabrera et al., 2013, Crispe, 2001). Cells in the leukocyte fraction were isolated, quantified and total leukocyte cellularity of the liver was calculated. Cellularity in this leukocyte fraction (referred to for ease as leukocyte cellularity, although other $CD45^{-}$ cells are also retained here), increases very modestly within the first 24 hours but is increased by approximately 8-fold by day 3 (Fig 3.8 A). The highest cellularity is detected at days 14-21 and this is resolving by day 35.

To identify and quantify which cells contribute to this increased cellularity, leukocytes were stained with T cell, B cell, macrophage, neutrophil and DC markers and populations in the livers of non-infected mice were compared with those at day 7 post-infection.

Figure 3.8

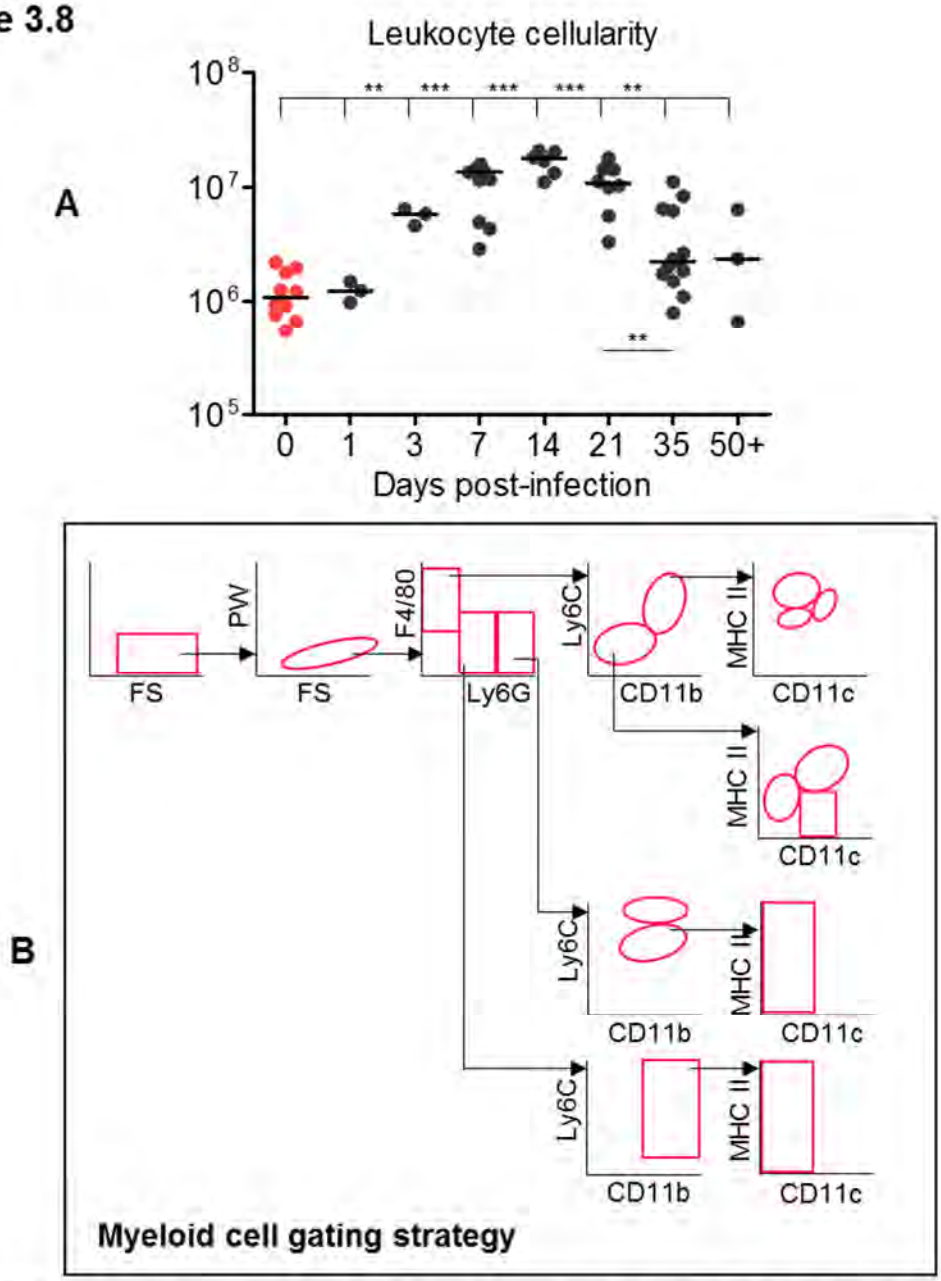

Figure 3.8 Absolute numbers of myeloid populations are elevated in the liver at day 7
WT mice were infected (i.p.) with 5 x 10^5 CFU attenuated STm. Leukocytes were isolated from the livers of non-infected and infected mice, by collagenase digestion and gradient centrifugation. A) The total number of leukocytes retrieved from the liver was calculated at the indicated time-points post-infection. Data are taken from 3 experiments with similar results. B) The gating strategy used to examine myeloid populations. F4/80^{hi} Ly6G^{lo} cells were separated according to Ly6C and CD11b expression where Kupffer cells = F4/80^{hi} Ly6G^{lo} CD11b^{lo} Ly6C^{lo} and monocytes = F4/80^{hi} Ly6G^{lo} CD11b^{hi} Ly6C^{hi}. Kupffer cells and monocytes were further examined based on expression of CD11c and MHC II. Neutrophil-type cells were classed as F4/80^{lo} Ly6G^{+} or F4/80^{lo} Ly6G^{hi}. Both subsets were further characterised by expression of CD11b, Ly6C and CD11c, MHC II as shown. C-M) WT mice were infected as described above and livers were examined from non-infected and day 7-infected mice. C) Representative FACS plots from non-infected (C) and day 7-infected (D) mice are shown. E) Absolute numbers of Kupffer cells and sub-populations of Kupffer cells were calculated. F) The percentages (out of total F4/80^{hi} Ly6G^{lo} cells) of Kupffer cells and the associated sub-populations. G) Absolute numbers of monocytes and sub-populations of monocytes. H) The percentages (out of total F4/80^{hi} Ly6G^{lo} cells) of monocytes and the associated sub-populations. I) The proportion of absolute numbers of Kupffer cells to absolute numbers of monocytes in the liver was calculated (y-axis indicates the ratio). J) Absolute numbers of Ly6G^{hi} cells and sub-populations of these cells. K) The percentages (out of total isolated leukocytes) of Ly6G^{hi} cells and the associated sub-populations. L) Absolute numbers of Ly6G^{+} cells and sub-populations of these cells. M) The percentages (out of total isolated leukocytes) of Ly6G^{+} cells and the associated sub-populations. Data in C-M are taken from 1 experiment where n = 3 (non-infected mice, and n = 7 day-7 infected mice). *p≤0.05 **p≤0.01 ***p≤0.001.

Figure 3.8 continued

C

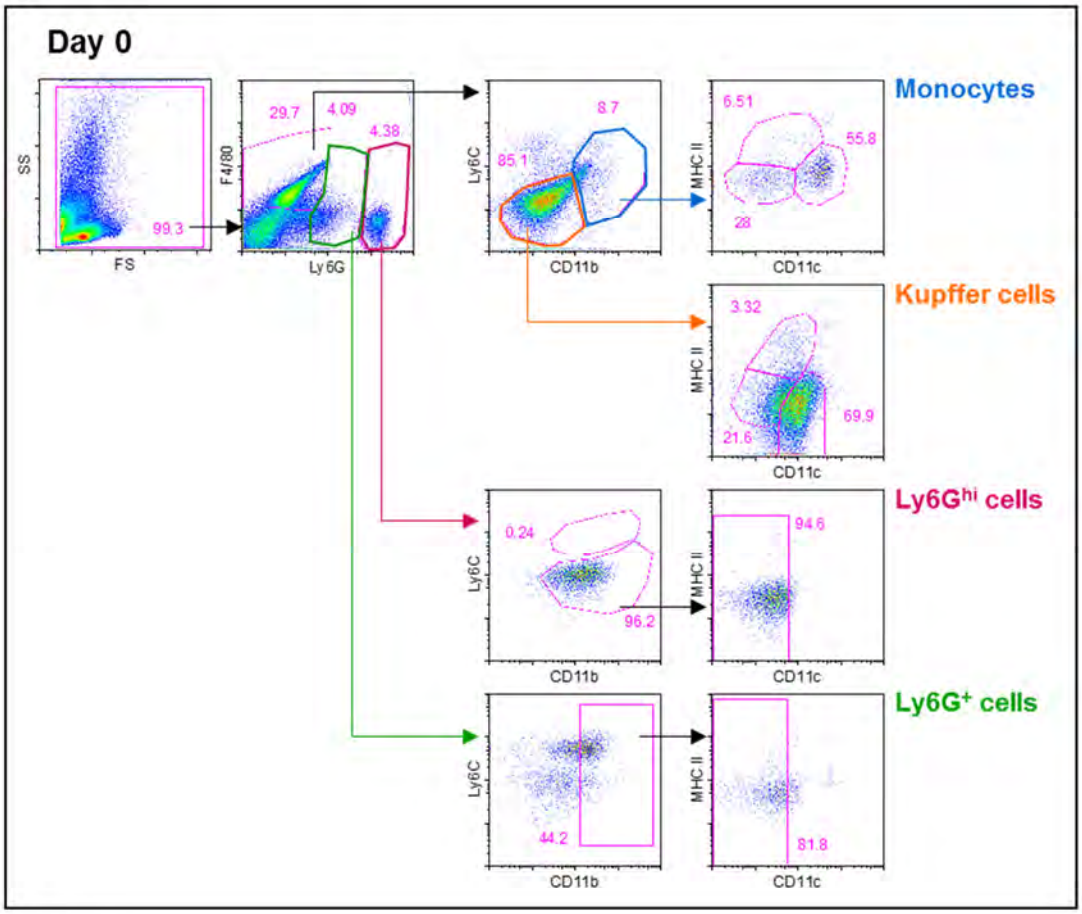

D

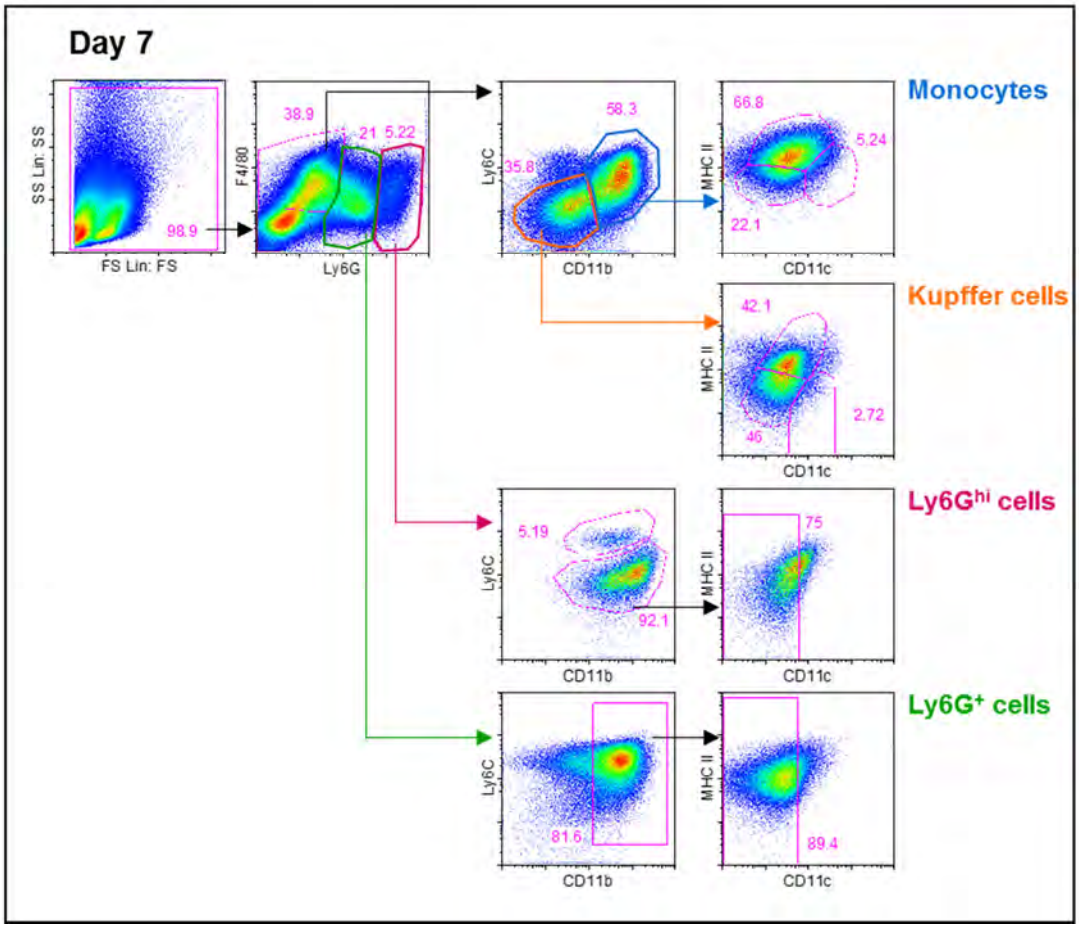

Figure 3.8 continued

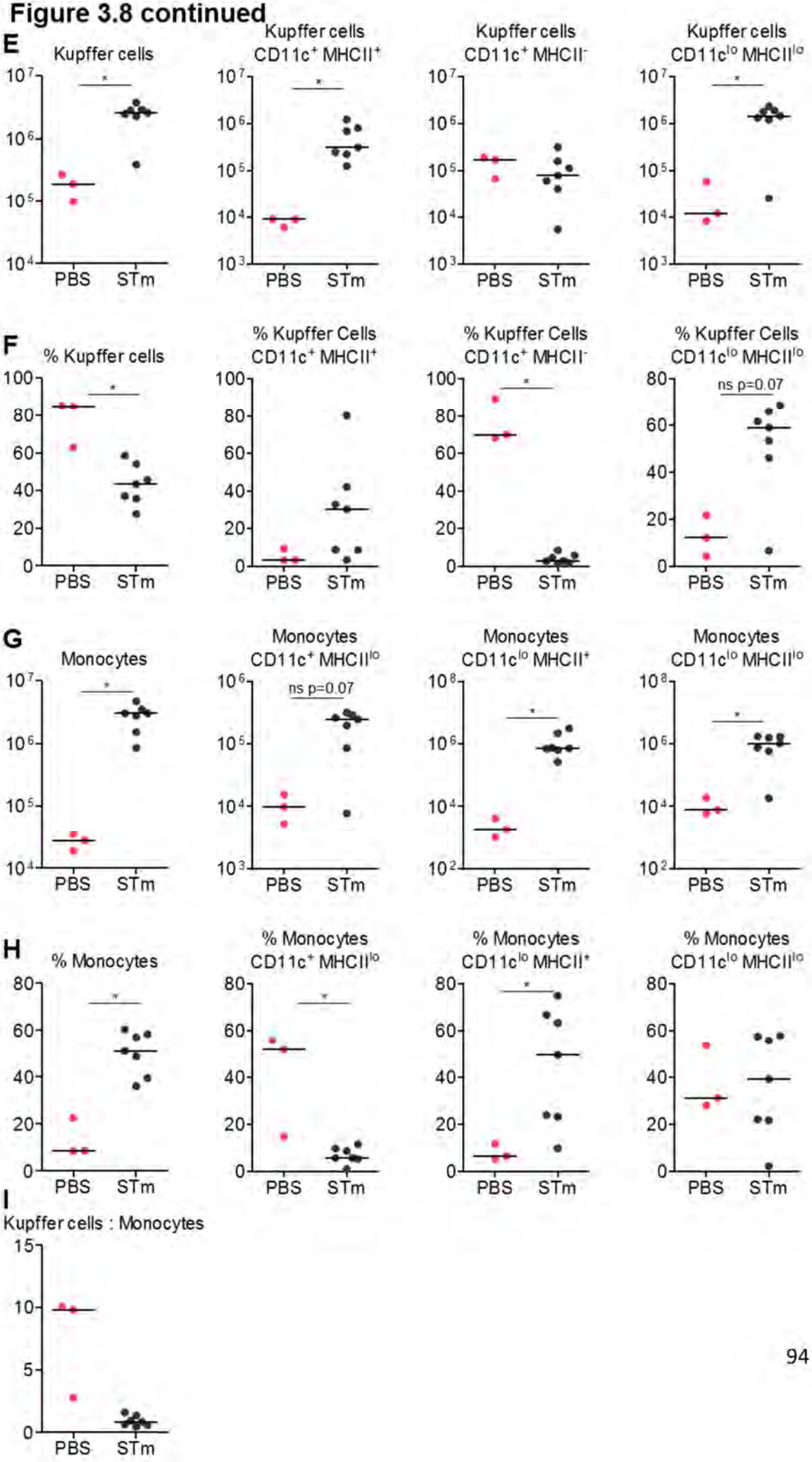

Figure 3.8 continued

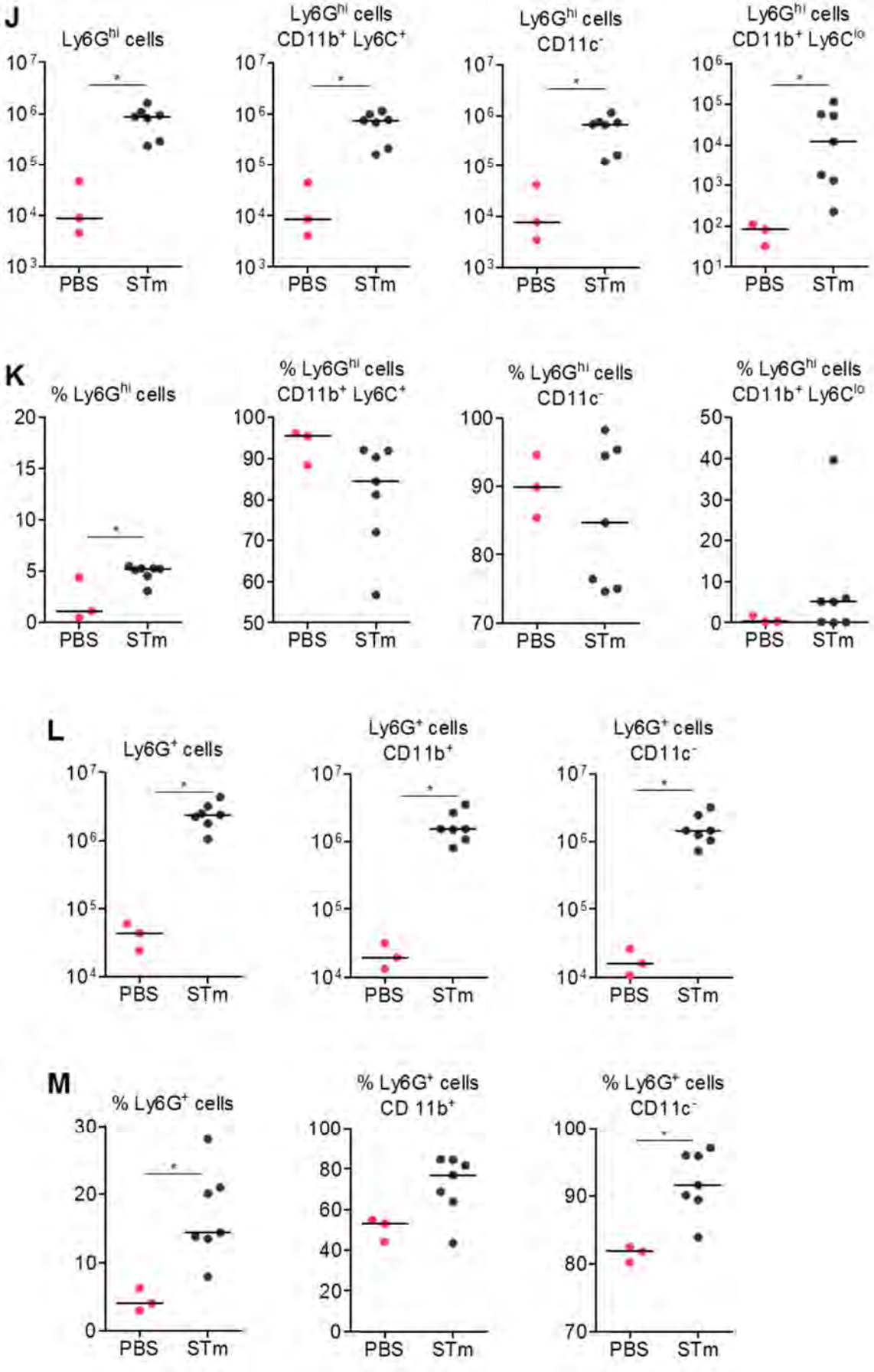

The gating strategy used to type myeloid cells in the liver is adapted from Frank Tacke et al. (Tacke et al., 2009)(F. Tacke, personal communication). In this way, Kupffer cells are F4/80^{+} Ly6G^{lo} CD11b^{lo} and Ly6C^{lo}, whereas monocytes are F4/80^{+} Ly6G^{lo} CD11b^{hi} Ly6C^{hi}. Both these populations can be further phenotyped by looking at expression of CD11c and MHC II. The gating strategies are illustrated and representative FACS plots are shown in Figure 3.8 B-D.

3.4.1 Kupffer cells are the dominant myeloid population in non-infected livers

In non-infected livers, approximately 85% of F4/80^{+} Ly6G^{lo} cells are Kupffer cells and monocytes make up the remaining 15% (Fig 3.8 C-F). Absolute numbers of both populations are relatively low and the ratio of absolute numbers of Kupffer cells to monocytes is greater than 1 (approximately 10 Kupffer cells to every monocyte) (Fig 3.8 E-I). In non-infected mice, most Kupffer cells are CD11c^{+} but do not express MHC II; around 5-10% Kupffer cells express high levels of MHC II and around 10% express low levels of MHC II (Fig 3.8 E-F). The majority of monocytes express CD11c to some extent, however, MHC II expression is low (Fig 3. 8 G-H).

3.4.2 Kupffer cells and monocytes are found at similar levels after infection

At day 7 post-infection, dramatically more monocytes are found in the liver, relative to non-infected mice (Fig 3.8 C-I). The proportion of Kupffer cells decreases from approximately 85% of F4/80^{+} Ly6G^{lo} cells to 40-50% at day 7, and the proportion of monocytes increases from 15% to 50-60% (Fig 3.8 F and H). This corresponds to an increase in absolute numbers of both cell types, with an approximate 10-fold increase in Kupffer cell numbers and a 100-fold increase in monocytes (Fig 3.8 E and G). After infection, the ratio of Kupffer cells to monocytes is around 1 (Fig 3.8 I). After infection, the proportion and

absolute number of CD11c^{lo} MHC II^{lo} Kupffer cells increases approximately 100-fold and the number of CD11c^{+} MHC II^{+} Kupffer cells increases approximately 20-fold (Fig 3.8 E-F). The number of CD11c^{+} MHC II^{-} cells remains similar to that seen in non-infected mice, however, as a percentage of total Kupffer cells, this population is severely reduced following infection, from a median of 70% of Kupffer cells to below 5% after infection (Fig 3.8 E-F). Absolute numbers of all monocyte subtypes increase following infection, however, the largest proportional difference is seen for CD11c^{lo} MHC II^{+} monocytes (Fig 3.8 G-H).

3.4.3 Ly6G^{+} populations increase post-infection

Neutrophil populations are also substantially augmented following infection. In non-infected livers, there are two main neutrophil populations, based on levels of Ly6G expression, of which the Ly6G^{+} population is more abundant than Ly6G^{hi} cells (Fig 3.8 C, J and L). In the Ly6G^{hi} population, approximately 90% of cells are CD11b^{+} Ly6C^{+} CD11c^{-} (Fig 3.8 K). Approximately half of the Ly6G^{+} population are CD11b^{+}, of which 80% are CD11c^{-} (Fig 3.8 M). After infection, both the proportions and absolute numbers of both the Ly6G^{hi} and Ly6G^{+} neutrophil populations increase (Fig 3.8 J-M). The number of Ly6G^{hi} cells increases 100-fold and Ly6G^{+} cell numbers increase approximately 70-fold (Fig 3.8 J and L). The phenotype of Ly6G^{hi} cells is not altered by infection; the proportion of cells expressing CD11b and Ly6C is similar to before infection, although this can be variable (Fig 3.8 K). However, there is a greater proportion and number of Ly6G^{+} cells expressing CD11b after infection (Fig 3.8 L-M).

3.4.4 Dendritic cell populations increase in the liver following infection

Whilst DCs are likely to contribute to some of the $CD11c^+$ gates discussed above, DC populations were examined separately using a gating strategy defined by Hsu et al. and illustrated in Figure 3.9 A (Hsu et al., 2007). Using this method, DCs are described as $CD11c^+$ $CD3^-$ $CD19^-$ and are classified into five sub-populations, which are shown in Table 3.1 below. Representative FACS plots are shown in Figure 3.9 B-C.

Dendritic cell subset	Phenotype
Natural Killer DC	$CD11b^{lo}$ $CD8\alpha^-$ $NK1.1^+$ $B220^+$
Myeloid DC	$CD11b^+$ $CD8\alpha^-$ $NK1.1^-$ $B220^-$
Lymphoid DC	$CD11b^-$ $CD8\alpha^+$ $NK1.1^-$ $B220^-$
Mixed Lymphoid/Myeloid DC	$CD11b^-$ $CD8\alpha^-$ $NK1.1^-$ $B220^-$
Plasmacytoid DC	$CD11b^-$ $CD8\alpha^-$ $NK1.1^-$ $B220^+$

Table 3.1 Classification of hepatic dendritic cells, adapted from (Hsu et al., 2007).

The absolute numbers of all DC subtypes increase following infection, however, the proportions of these populations vary considerably (Fig 3.9 D-F). The proportion of NK DCs increases from approximately 10% (of total $CD11b^{lo}$ $CD8\alpha^-$ DCs) in non-infected mice to 35% at day 7 (Fig 3.9 F). In contrast, myeloid DCs make up approximately 65% of total $CD11b^+$ $CD8\alpha^-$ DCs before infection, but this drops to less than 10% after infection (Fig 3.9 F). The proportions of lymphoid, mixed lymphoid/myeloid and plasmacytoid DCs all vary slightly with infection: the proportion of lymphoid DCs increases almost 2-fold; mixed lymphoid/myeloid DCs also become slightly more frequent, whereas plasmacytoid DC frequency decreases by approximately 10% (Fig 3.9 F).

Figure 3.9

A

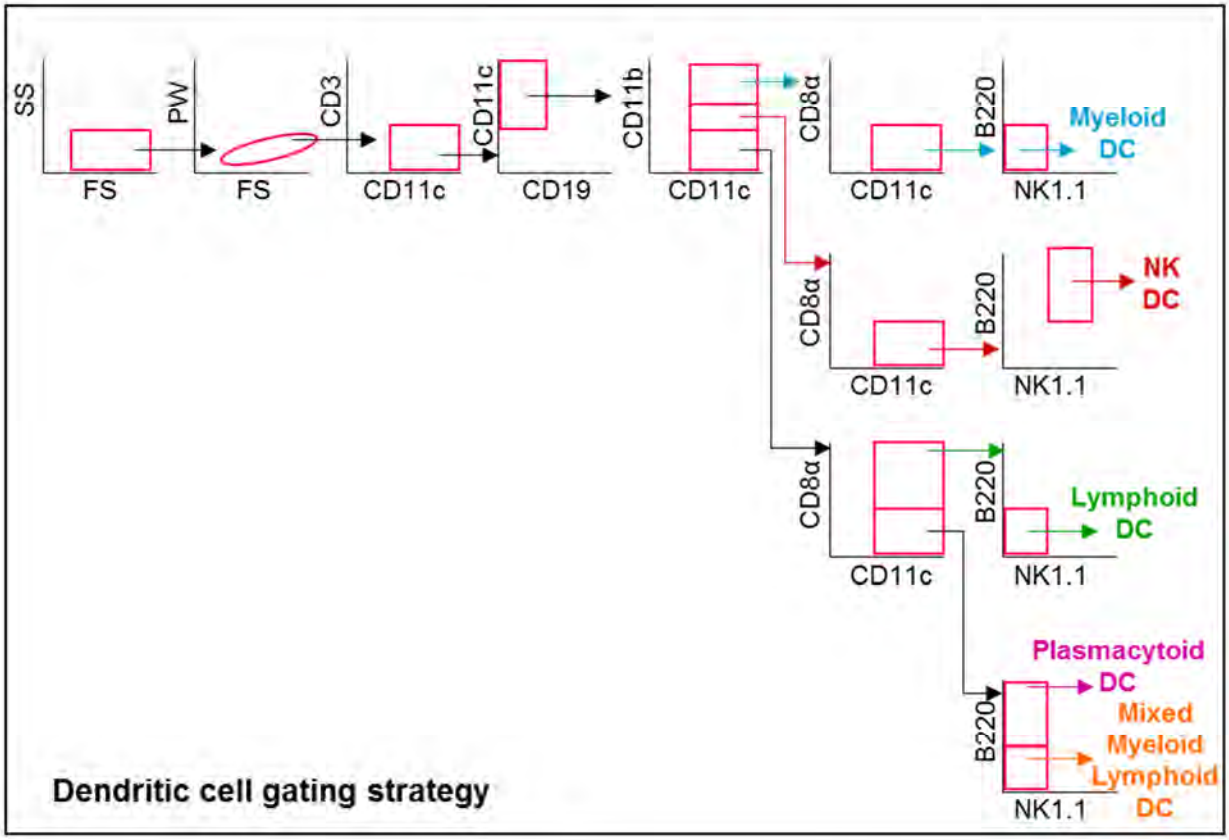

Figure 3.9 Absolute numbers of dendritic cell populations are elevated in the liver at day 7

WT mice were infected (i.p.) with 5 x 10^5 CFU attenuated STm. Leukocytes were isolated from non-infected and day-7 infected livers and dendritic cells (DCs) were analysed by FACS. A) The gating strategy used to examine DCs has been adapted from Hsu et al. 2007. B) Representative FACS plots from non-infected (B) and day 7-infected (C) mice are shown. D) Absolute numbers of $CD11c^+$ $CD3^-$ $CD19^-$ DCs are increased at day 7 relative to non-infected mice. E) Absolute numbers of DC subtypes (characterised as follows: NK DC = $CD11b^{lo}$ $CD8\alpha^-$ $NK1.1^+$ $B220^+$; Myeloid DC = $CD11b^+$ $CD8\alpha^-$ $NK1.1^-$ $B220^-$; Lymphoid DC = $CD11b^-$ $CD8\alpha^+$ $NK1.1^-$ $B220^-$; Mixed Myeloid/Lymphoid DC = $CD11b^-$ $CD8\alpha^-$ $NK1.1^-$ $B220^-$; and Plasmacytoid DC = $CD11b^-$ $CD8\alpha^-$ $NK1.1^-$ $B220^+$. F) The percentages of each DC subtype out of total $CD11c^+$ $CD3^-$ $CD19^-$ DCs was measured. Data are taken from 1 experiment where n = 3 (non-infected mice, and n = 7 day-7 infected mice). *p≤0.05 **p≤0.01 ***p≤0.001.

Figure 3.9 continued

B

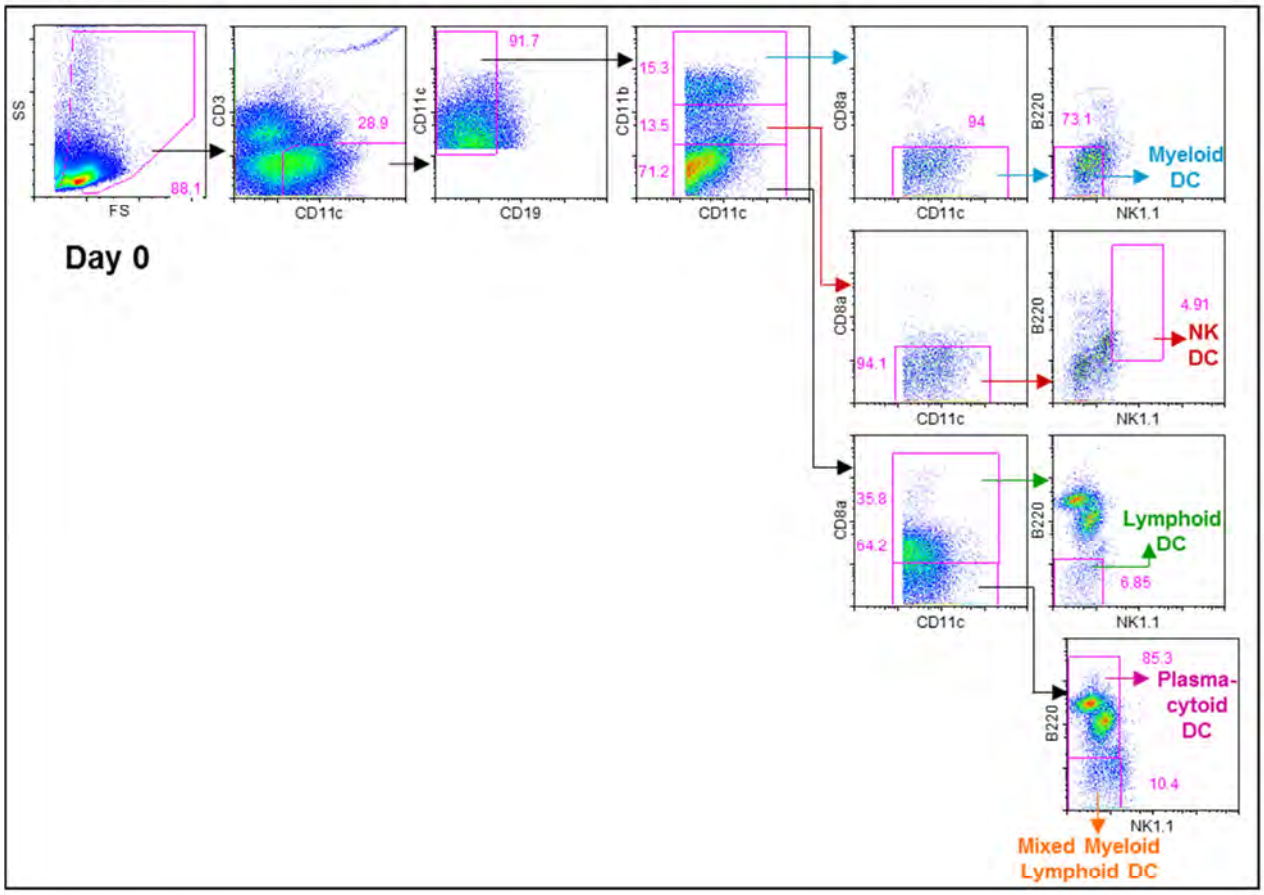

C

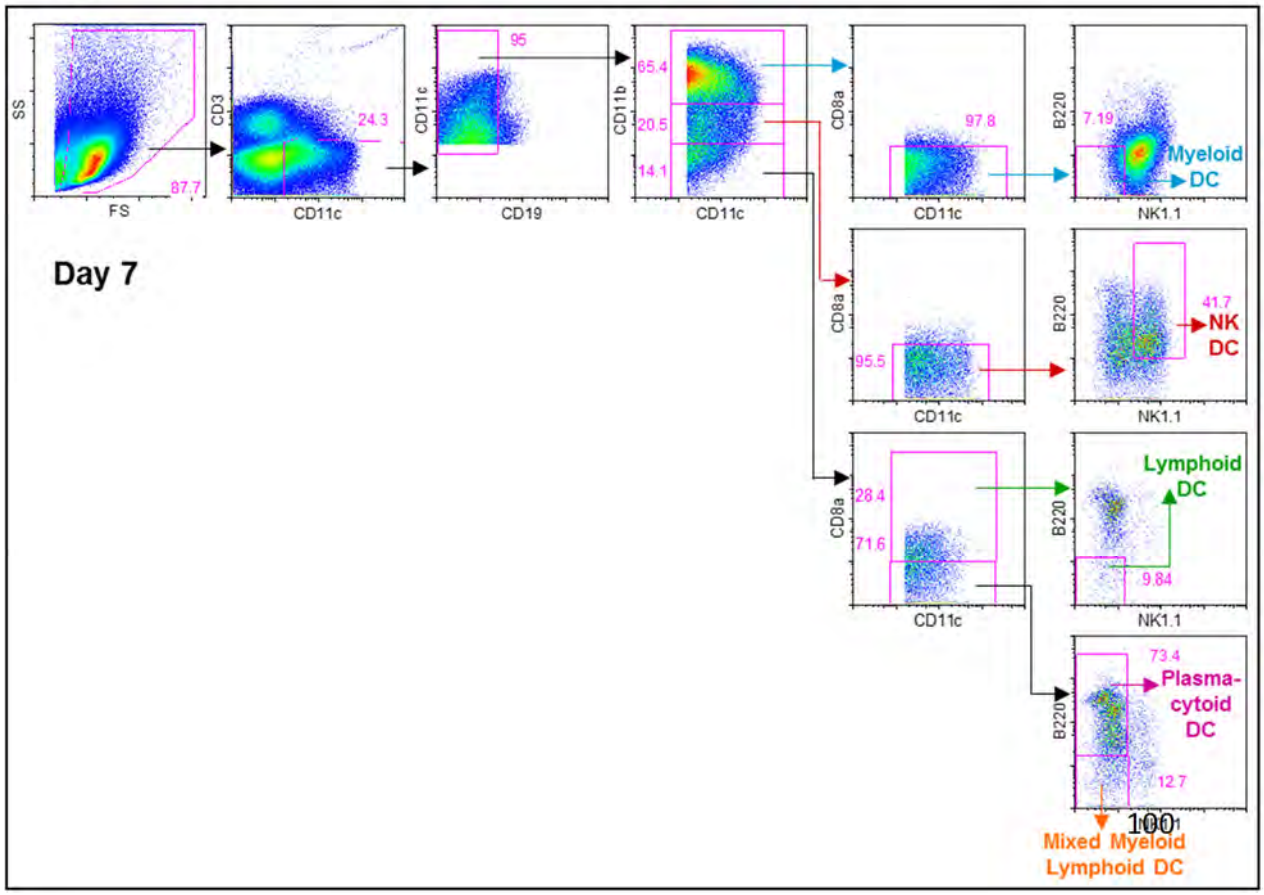

Figure 3.9 continued

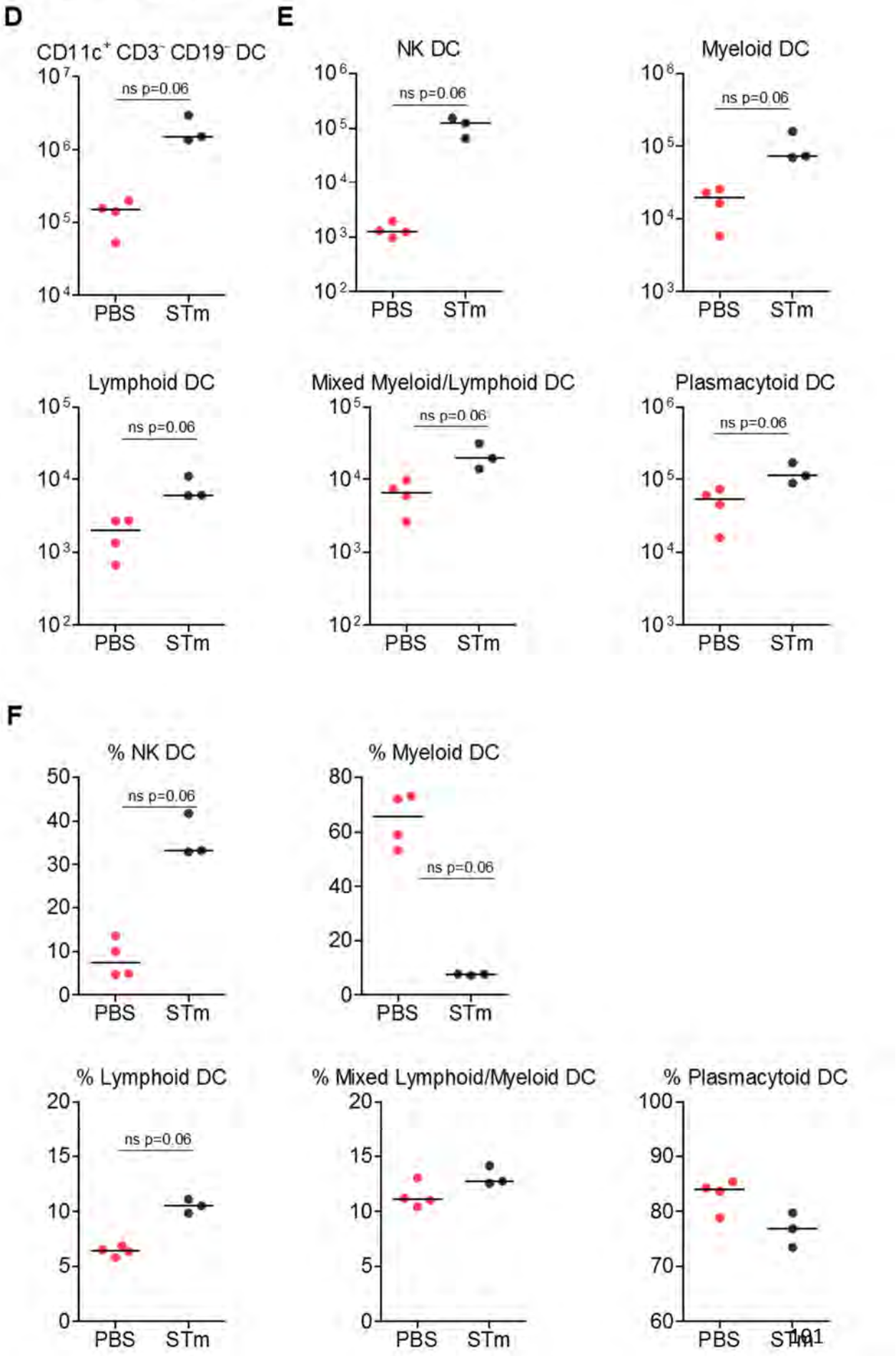

3.4.5 $CD3^+$ $CD4^+$ and $CD3^+$ $CD8^+$ T cells increase in the liver following infection

T lymphocytes were also phenotyped by flow cytometry and the activation status of T cells was examined using CD44 and CD62L expression (Ravindran and McSorley, 2005). The gating strategy used and representative FACS plots are shown in Figure 3.10 A-C. The absolute number of $CD4^+$ T cells is increased over 10-fold at day 7 post-infection, although the proportion of these cells out of total isolated leukocytes does not change significantly (Fig 3.10 D-E).

Absolute numbers of all $CD4^+$ T cell populations increase after infection; there is at least a 10-fold increase in numbers of both activated and central memory $CD4^+$ T cells (Fig 3.10 D). The proportion of activated $CD4^+$ T cells increases from approximately 70% in non-infected livers to around 90% after infection, and the proportion of naïve $CD4^+$ T cells is diminished, from approximately 20% to 5% (Fig 3.10 E).

All $CD8^+$ T cell populations examined also increase in absolute number after infection, with total $CD3^+$ $CD8^+$ cells increasing approximately 10-fold (Fig 3.10 F). However, as a proportion of total leukocytes, the frequency of $CD8^+$ T cells is reduced by about half, from 6% to 3% following infection (Fig 3.10 G). The proportion of activated $CD8^+$ T cells increases (from 25 to 65%) following infection whereas the frequency of naïve $CD8^+$ T cells decreases from around 50% to 10-20% (Fig 3.10 G).

Figure 3.10

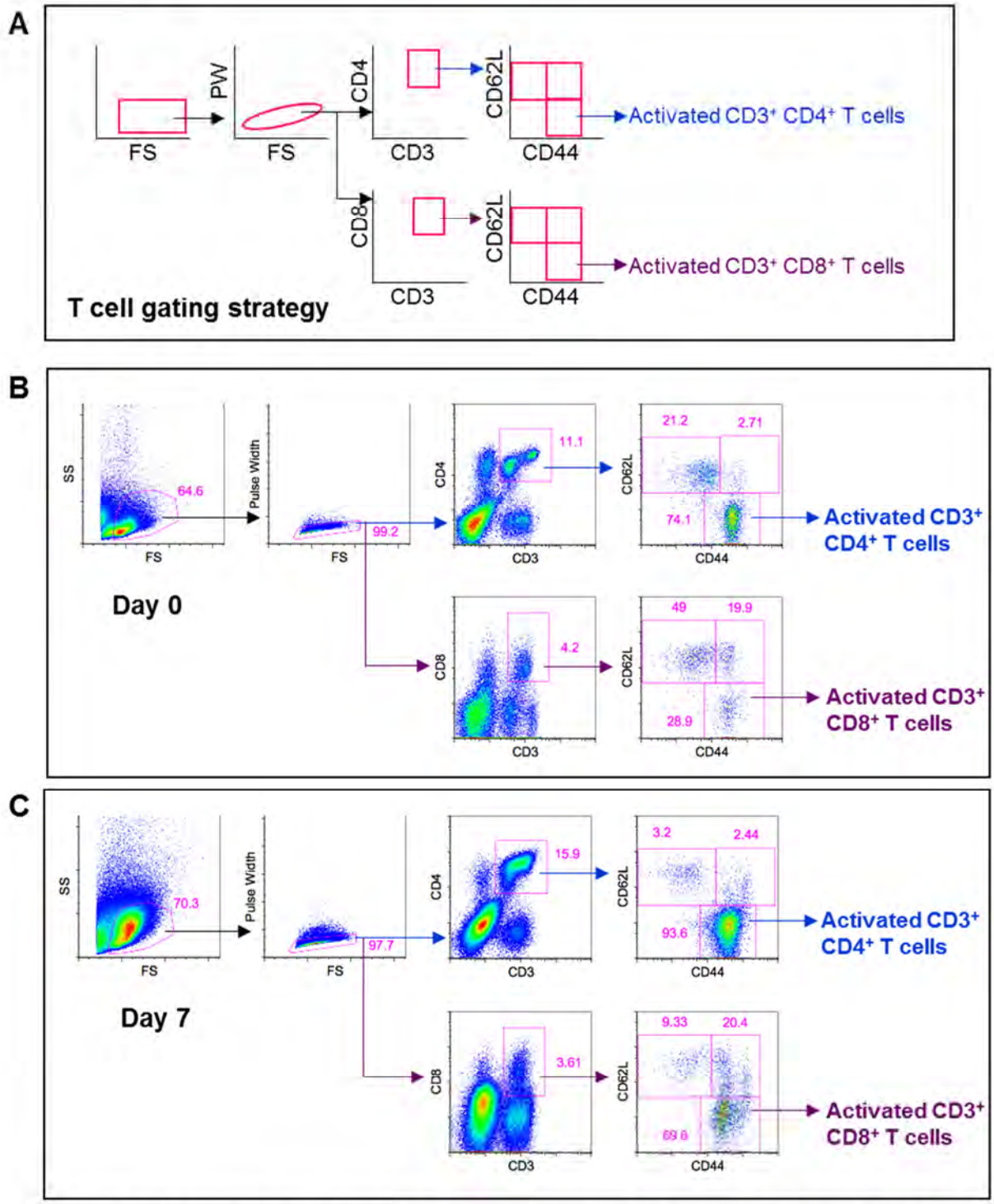

Figure 3.10 Absolute numbers of T cell populations are elevated in the liver at day 7
WT mice were infected (i.p.) with 5 x 10^5 CFU attenuated STm. Leukocytes were isolated from non-infected and day-7 infected livers and T cells were analysed by FACS. A) The gating strategy used to examine T cells is shown. $CD3^+$ $CD4^+$ and $CD3^+$ $CD8^+$ cells were examined for activation status, as identified by expression of CD62L and CD44. Activated T cells are described by $CD62L^{lo}$ $CD44^+$; whereas $CD62L^+$ $CD44^+$ cells are referred to as the central memory compartment; and $CD62L^+$ $CD44^-$ are naïve. B) Representative FACS plots from non-infected (B) and day 7-infected (C) mice are shown. D) Absolute numbers of total $CD3^+$ $CD4^+$ T cells and of activated, naïve and memory cells. E) The percentages of total $CD3^+$ $CD4^+$ T cells (out of total isolated lymphocyte-sized cells) and of activated, naïve and memory cells (presented as a proportion of total $CD3^+$ $CD4^+$ T cells). F) Absolute numbers of total $CD3^+$ $CD8^+$ T cells and of activated, naïve and memory cells. G) The percentages of total $CD3^+$ $CD8^+$ T cells (out of total isolated lymphocyte-sized cells) and of activated, naïve and memory cells (presented as a proportion of total $CD3^+$ $CD8^+$ T cells). Data are taken from 1 experiment where n = 3 (non-infected mice, and n = 7 day-7 infected mice). *p≤0.05 **p≤0.01 ***p≤0.001.

Figure 3.10 continued

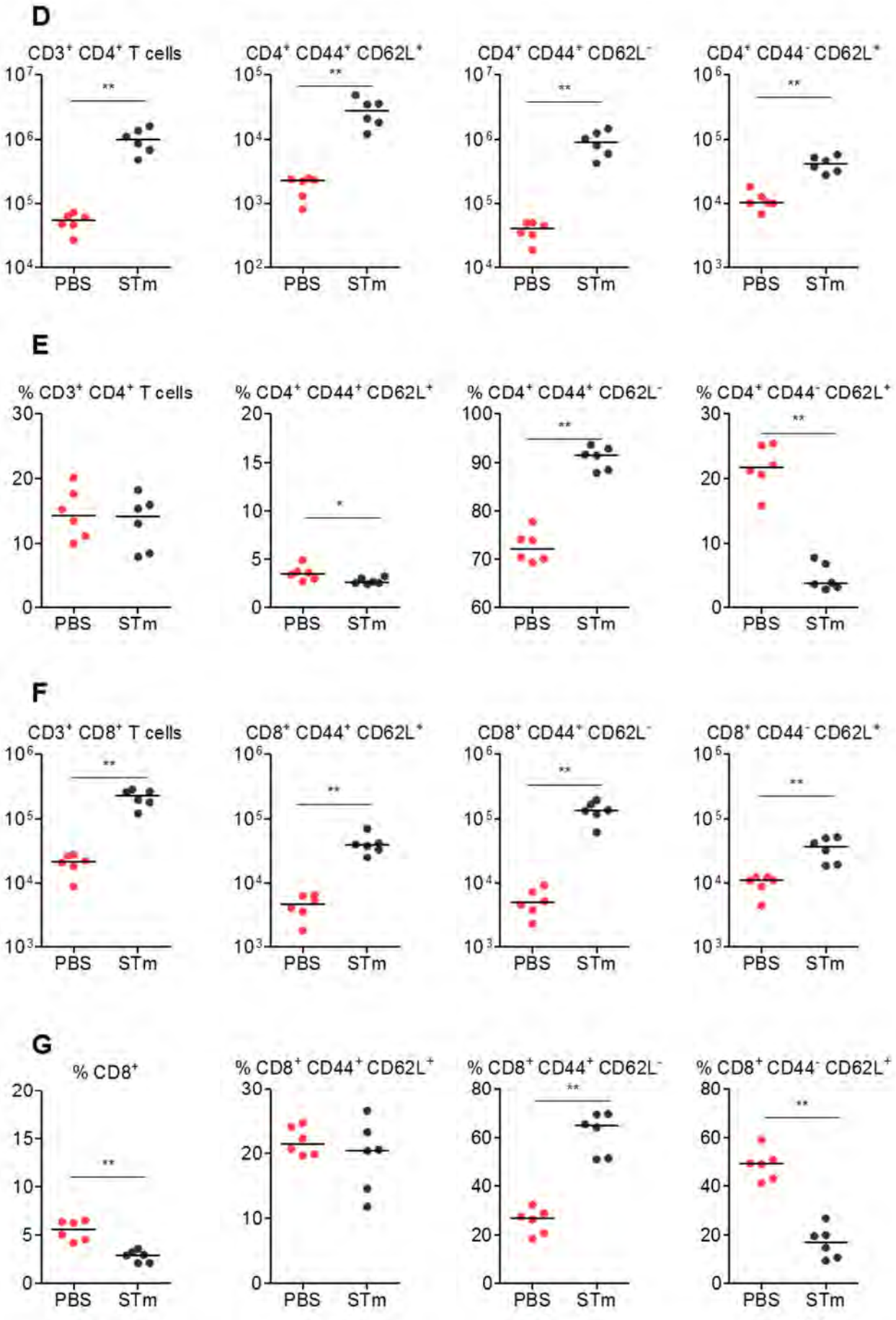

3.4.6 B lymphocytes increase in the liver following infection

Having been unable to detect B lymphocytes by histology in the liver due to interference caused by background reactivity of the tissue, these cells were examined in more detail by flow cytometry. B lymphocytes were gated on $B220^+$ $CD19^+$ cells and then examined for intracellular IgM and class-switched IgG2c, alongside plasma cell marker CD138 (Fig 3.11 A). Representative FACS plots are shown in Figure 3.11 B-C. The number of $B220^+$ $CD19^+$ cells increases post-infection (Fig 3.11 D). There are modest numbers of IgM^+ B cells in the livers of non-infected mice, and the majority of these are not plasma cells (Fig 3.11 F-G). After infection, there are increased IgM^+ cells, and the majority remain $CD138^-$. There are similar numbers of $IgG2c^+$ plasma cells to IgM^+ plasma cells in non-infected mice (approximately 5000 of each per liver) (Fig 3.11 F). However, there are approximately 10 fold more IgM^+ $CD138^-$ cells compared to $IgG2c^+$ $CD138^-$ cells following infection (Fig 3.11 F). There is an approximate 8-fold increase in $IgG2c^+$ plasma cells following infection, compared to a 2.5-fold increase in IgM^+ plasma cells (Fig 3.11 F).

3.5 Leukocyte quantification over the course of infection

These flow cytometry studies were performed on mice on the same day to enable direct comparison between non-infected and infected livers. Thus these data provide a useful quantitative measure of infiltration in the liver after infection, and this supports our histological observations. However, to provide a more complete understanding of the dynamics of leukocyte infiltration over the course of infection, leukocytes were isolated from livers at different time-points, and were analysed by flow cytometry.

Figure 3.11

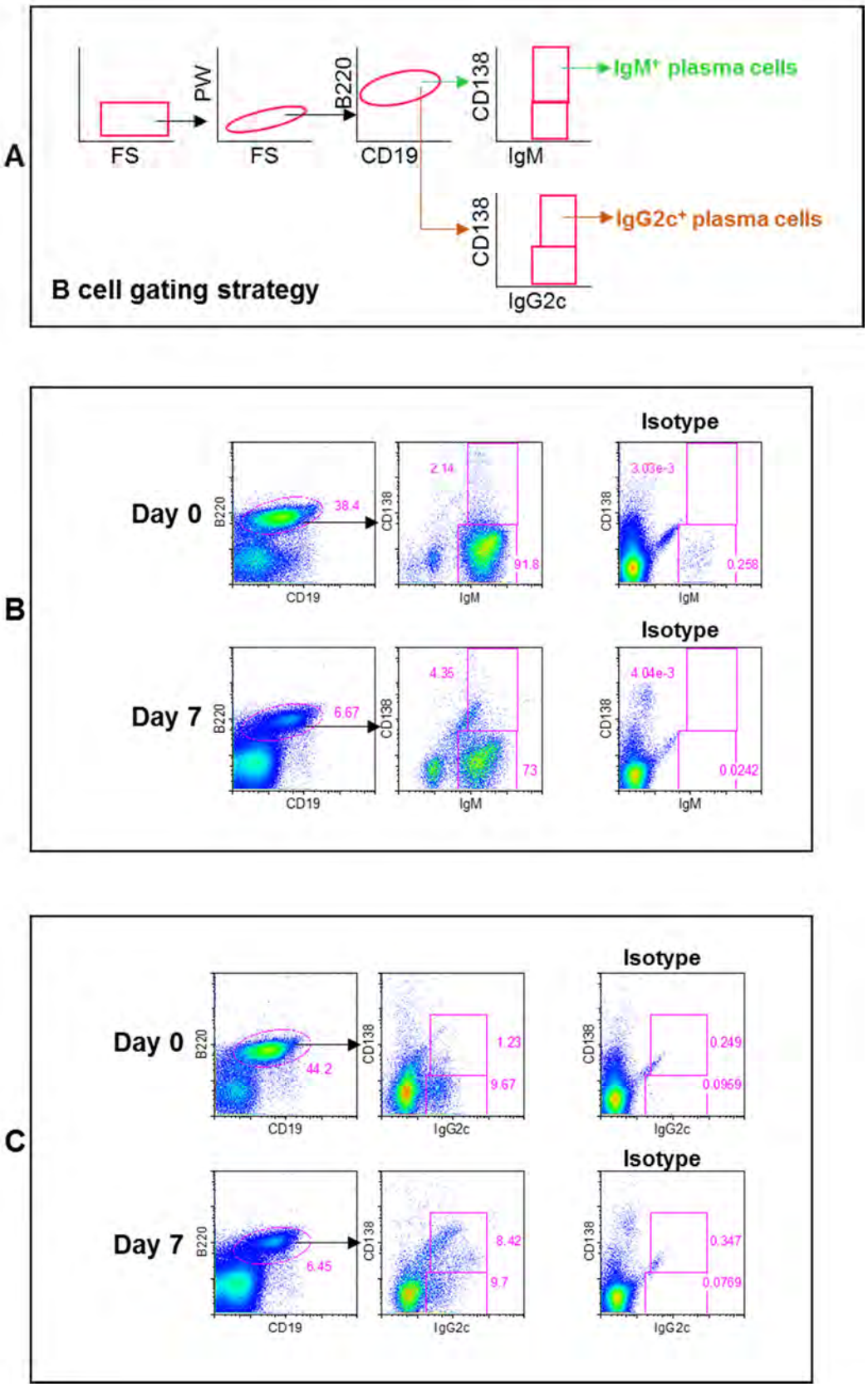
A
FS
PW
FS
B220
CD19
CD138
IgM
IgM+ plasma cells
CD138
IgG2c
IgG2c+ plasma cells
B cell gating strategy
B
Day 0
B220
CD19
38.4
CD138
IgM
2.14
91.8
Isotype
3.03e-3
0.258
Day 7
6.67
4.35
73
4.04e-3
0.0242
C
Day 0
44.2
1.23
9.67
IgG2c
0.249
0.0959
Day 7
6.45
8.42
9.7
0.347
0.0769

Figure 3.11 continued

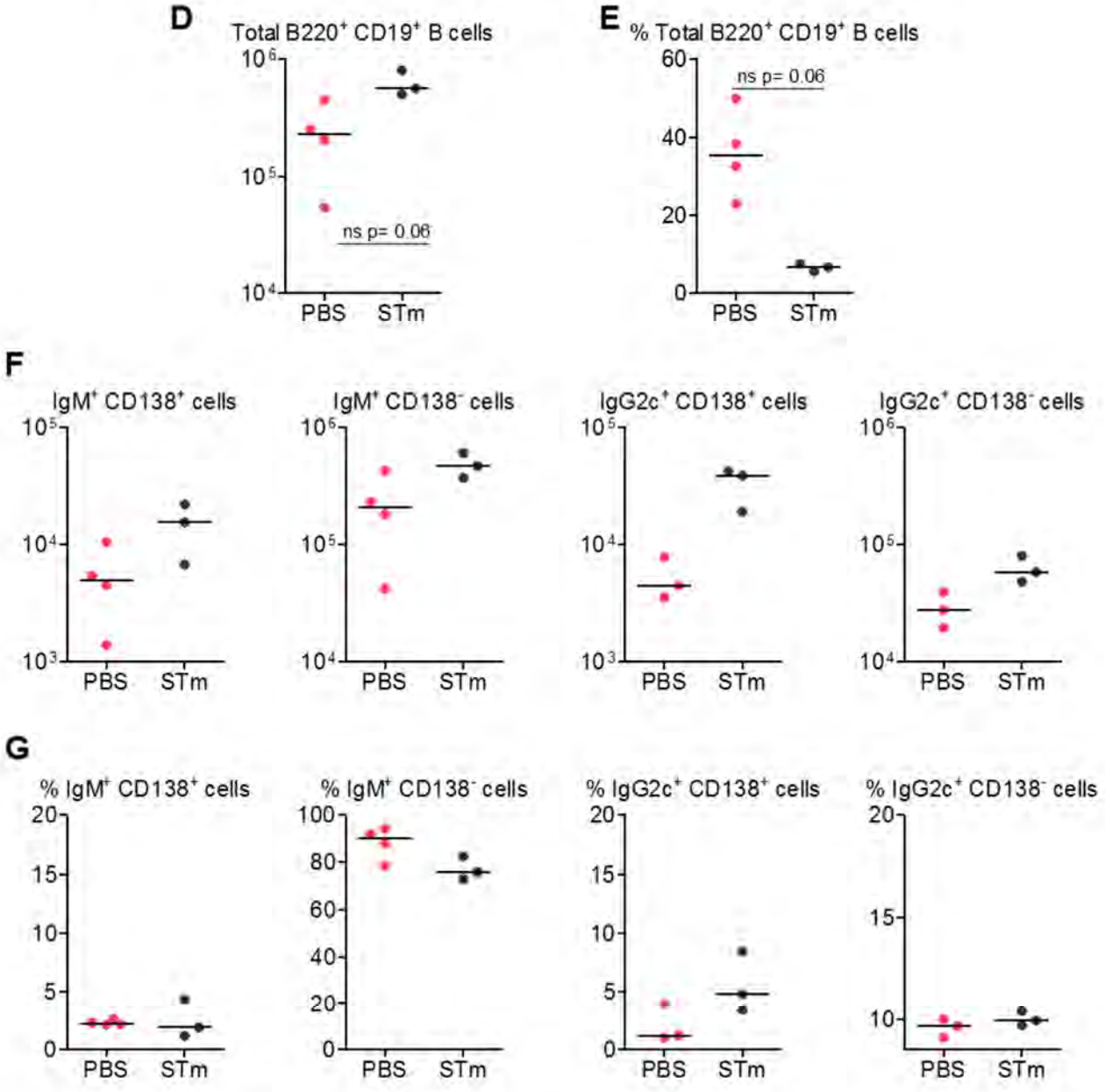

Figure 3.11 Absolute numbers of B cells are elevated in the liver at day 7
WT mice were infected (i.p.) with 5 x 10^5 CFU attenuated STm. Leukocytes were isolated from non-infected and day-7 infected livers and B cells were analysed by intracellular FACS staining. A) The gating strategy used to examine B cells is shown. B cells were defined by positive staining for extracellular markers B220 CD19. Plasma cells were identified by extracellular CD138 expression. Class-switching was measured by intracellular IgM or IgG2c staining. B) Representative FACS plots from non-infected and day 7-infected mice are shown for (B) IgM$^+$ and (C) IgG2c$^+$ cells. Appropriate isotype controls are provided. D) The absolute number of B220$^+$ CD19$^+$ B cells retrieved from the liver. E) The percentage of B220$^+$ CD19$^+$ B cells (out of total isolated lymphocyte-sized cells). F) Absolute numbers of B220$^+$ CD19$^+$ IgM$^+$ cells, and B220$^+$ CD19$^+$ IgG2c$^+$ cells (both plasma cells and non-plasma cells). G) The percentages of the cells described in F) (out of total B220$^+$ CD19$^+$ cells). Data are taken from 1 experiment where n = 3 (non-infected mice, and n = 7 day-7 infected mice). *p≤0.05 **p≤0.01 ***p≤0.001.

3.5.1 Myeloid cell numbers increase within 24 hours and peak at day 14

The gating strategy used to define myeloid cells and representative FACS plots illustrate how myeloid cell dynamics are altered during the first 35 days of infection (Fig 3.12 A-B). As discussed above, in a resting liver the myeloid cells are predominantly Kupffer cells, which constitute 80% of F4/80^{+} Ly6G^{lo} cells, and the ratio of Kupffer cells to monocytes is greater than 1 (Fig 3.12 C-E). Between 24 and 72 hours, the proportion of Kupffer cells begins to decline and the proportion of monocytes increases. This dynamic continues until day 14 when the ratio of Kupffer cells to monocytes is approximately 1, and the proportion of F4/80^{+} Ly6G^{lo} cells which are Kupffer cells is reduced to around 40-50%. At some point between days 14 and 35, this pattern begins to resolve; the proportion of Kupffer cells begins to increase and the proportion of monocytes falls (Fig 3.12 C-E).

When absolute numbers are considered, Kupffer cells are increased within 24 hours followed by a rapid increase in numbers between days 3 and 7 (Fig 3.12 C). Numbers of Kupffer cells continue to increase by day 14, and are resolving by day 35, but even at this time, there are approximately 8 times more Kupffer cells per liver than in a resting mouse. Monocytes increase steadily from within 24 hours until day 14; by day 3 numbers are increased 10-fold and they rise further to a maximum increase of 100-fold by day 14 (Fig 3.12 C). This is a greater fold increase than is seen in Kupffer cells, however by day 14, absolute numbers of both cell types are comparable. This is reflected in the ratio of Kupffer cells to monocytes which is approximately 1:1 at day 7 and is less than 1 at day 14 (Fig 3.12 D). By day 35, monocyte numbers are resolving, as is shown by absolute numbers, cell frequencies and Kupffer cell to monocyte ratio (Fig 3.12 C-E).

Figure 3.12

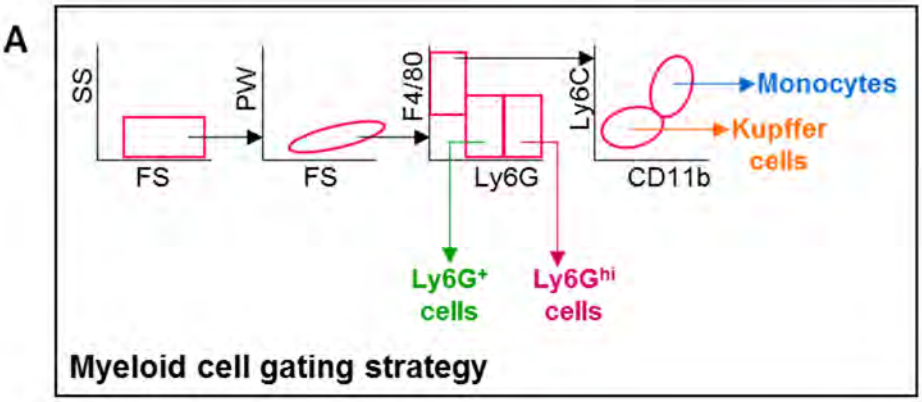
A
SS
FS
PW
FS
F4/80
Ly6G
Ly6C
CD11b
Monocytes
Kupffer cells
Ly6G+ cells
Ly6Ghi cells
Myeloid cell gating strategy

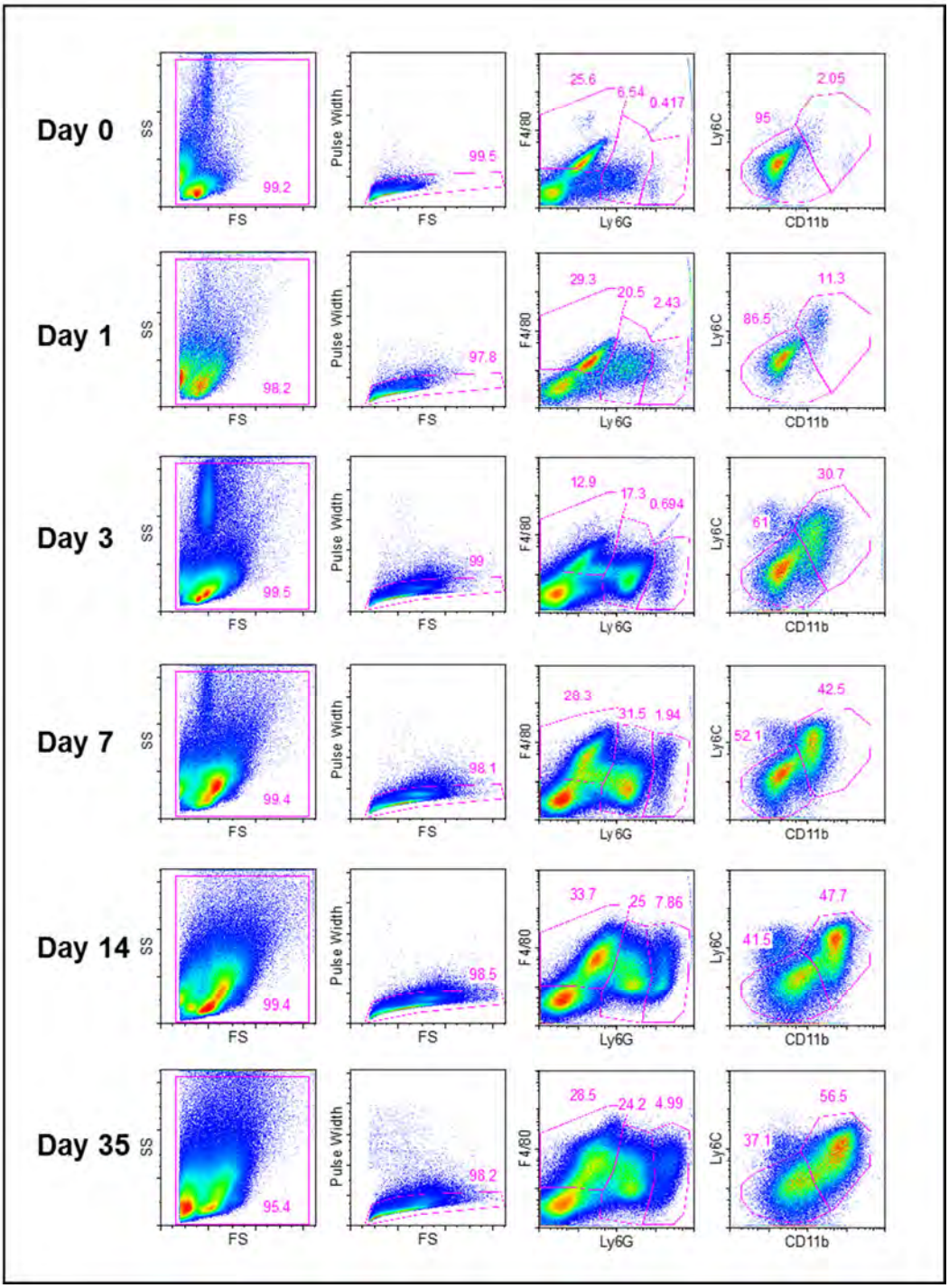
B
Day 0
Day 1
Day 3
Day 7
Day 14
Day 35
SS
FS
Pulse Width
F4/80
Ly6G
Ly6C
CD11b
99.2
99.5
25.6
6.54
0.417
95
2.05
98.2
97.8
29.3
20.5
2.43
86.5
11.3
99.5
99
12.9
17.3
0.694
61
30.7
99.4
98.1
28.3
31.5
1.94
52.1
42.5
99.4
98.5
33.7
25
7.86
41.5
47.7
95.4
98.2
28.5
24.2
4.99
37.1
56.5

Figure 3.12 continued

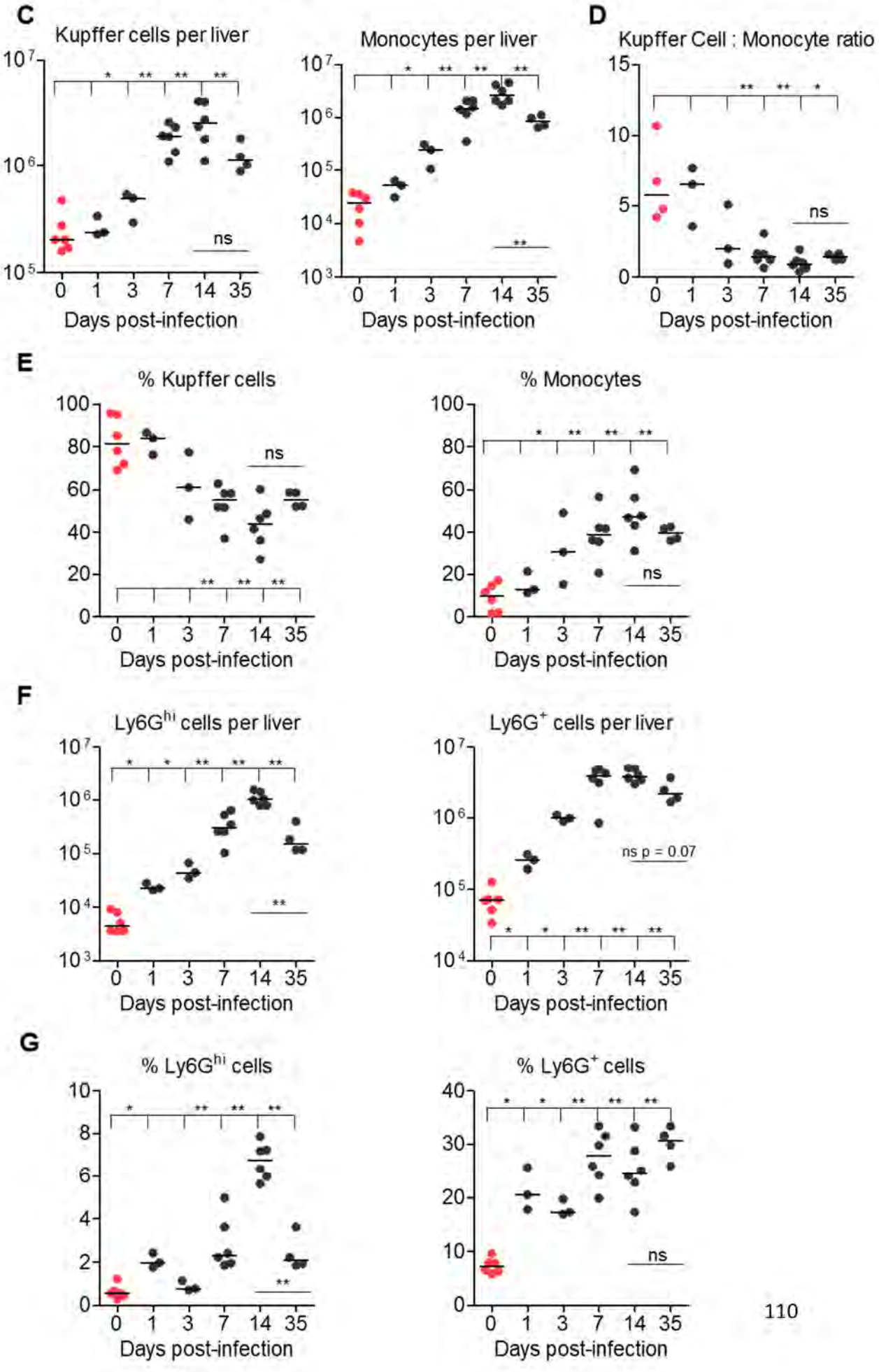

Figure 3.12 Myeloid cell numbers peak at days 7-14 post-infection
WT mice were infected (i.p.) with 5 x 10^5 CFU attenuated STm. Leukocytes were isolated from livers at days 0, 1, 3, 7, 14 and 35 post-infection and myeloid populations were examined by FACS. A) The gating strategy is indicated; cells were defined as follows: Kupffer cells = F4/80^{hi} Ly6G^{lo} CD11b^{lo} Ly6C^{lo} and monocytes = F4/80^{hi} Ly6G^{lo} CD11b^{hi} Ly6C^{hi}; neutrophil-type cells were classed as F4/80^{lo} Ly6G^{+} or F4/80^{lo} Ly6G^{hi}. B) Representative FACS plots are shown from mice at the time-points post-infection described above. C) Absolute numbers of Kupffer cells and monocytes retrieved from the liver at the indicated time-points post-infection. D) The ratio of absolute numbers of Kupffer cells to monocytes. E) The percentage of Kupffer cells and monocytes out of total F4/80^{hi} Ly6G^{lo} cells. F) Absolute numbers of Ly6G^{hi} and Ly6G^{+} cells retrieved from the liver at the indicated time-points post-infection. G) The percentage of the cells in F) (out of total leukocytes retrieved from the liver). Data are taken from 2 experiments where n = 3 at each time-point in each experiment *p≤0.05 **p≤0.01 ***p≤0.001.

Absolute numbers of Ly6G^{hi} and Ly6G^{+} populations increase by 24 hours (Fig 3.12 F). Both populations increase in number around 100-fold by day 7, however, whereas Ly6G^{hi} cell numbers continue to rise at day 14, Ly6G^{+} cell numbers are maintained and do not increase further. Cell numbers in both populations are resolving by day 35, although Ly6G^{hi} cells have resolved by a greater extent at this time. However, in terms of the percentage of total isolated leukocytes these populations have very different kinetics. Ly6G^{+} cells increase in frequency from 8 to 20% within 24 hours, then increase to around 25-30% by day 7 and this proportion is maintained at day 35 (Fig 3.12 G). In contrast, Ly6G^{hi} cells contribute less than 1% to the total isolated leukocytes in the liver of a non-infected mouse (Fig 3.12 G). These cells double in proportion to around 2% within 24 hours, then drop to almost resting proportions by day 3. By day 7, the frequency of these cells is again around 2% and this rises to around 7% at day 14. Although Ly6G^{hi} cells contribute less than 10% of total leukocytes in the liver, absolute numbers increase as leukocyte cellularity in the liver increases, thus these cells are likely to be important in the overall host response to infection.

3.5.2 Distribution of DC subsets is altered considerably during infection

Dendritic cells were not examined beyond day 14 in this study (because we were originally interested in their role during antigen presentation and initiation of immune responses), so we cannot comment on their contribution to, or kinetics during resolution. Representative FACS plots illustrate DC staining in Figure 3.13 A. Total dendritic cells (CD11c^{+} CD3^{-} CD19^{-}) are increased in the liver within 24 hours and are increased approximately 10-fold relative to resting numbers by day 3 (Fig 3.13 B).

Figure 3.13

Read this figure in landscape please

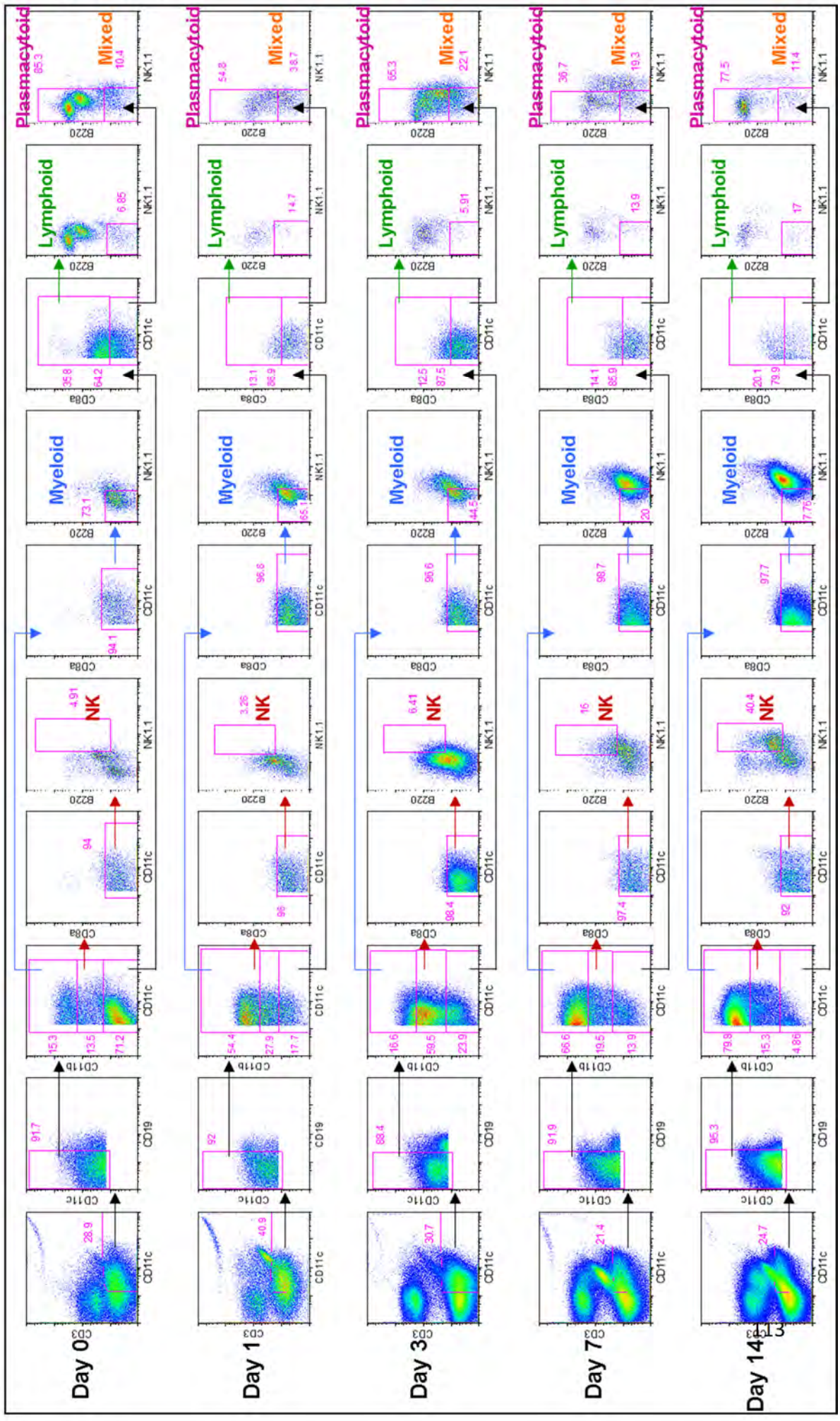

Figure 3.13 continued

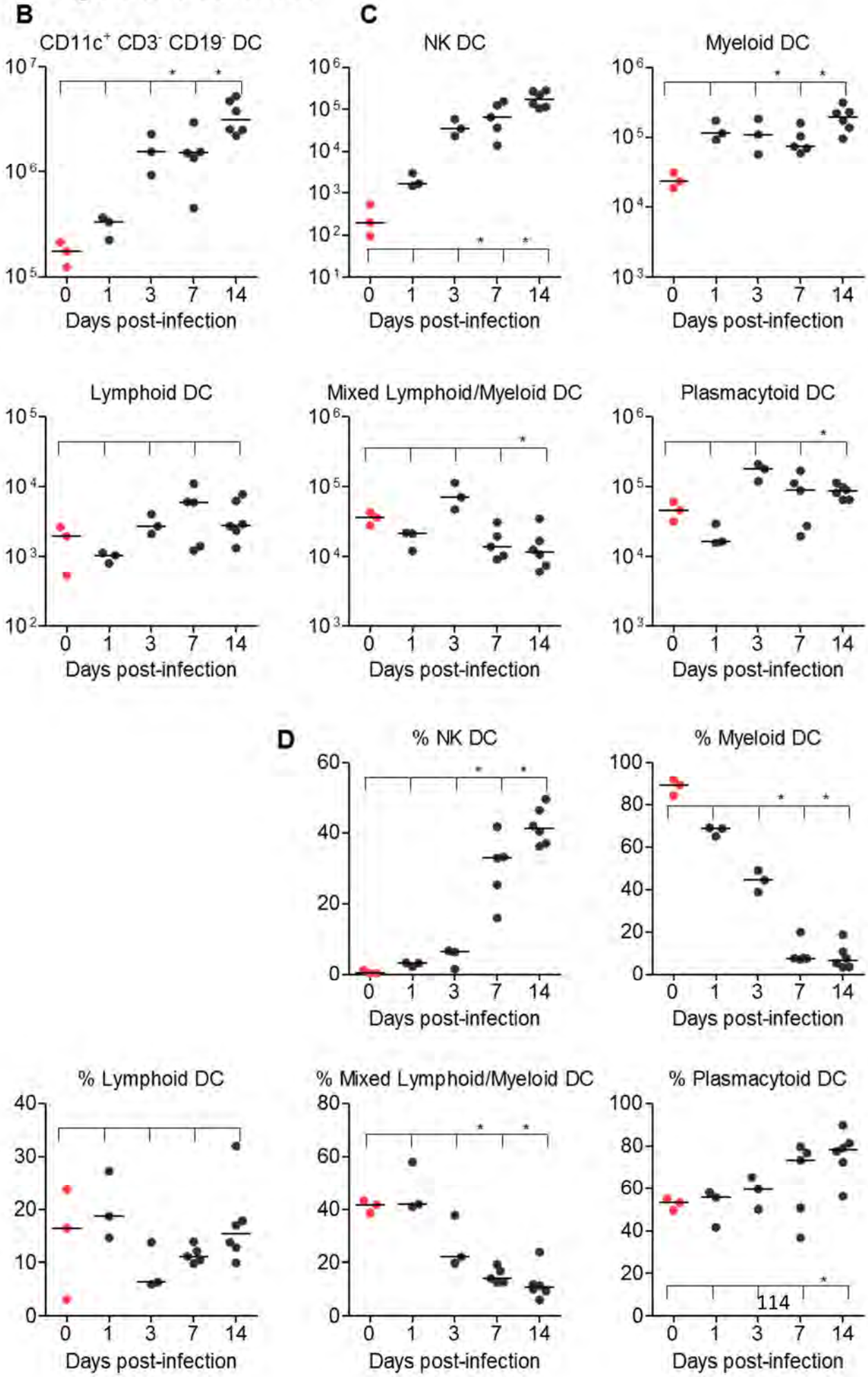

Figure 3.13 Dendritic cells accumulate in the liver during the first 2 weeks of infection
WT mice were infected (i.p.) with 5 x 10^5 CFU attenuated STm. Leukocytes were isolated from livers at days 0, 1, 3, 7 and 14 post-infection and DCs were examined by FACS. The gating strategy used is illustrated in Figure 3.9 where total $CD11c^+$ $CD3^-$ $CD19^-$ DCs are further phenotyped as follows: NK DC = $CD11b^{lo}$ $CD8\alpha^-$ $NK1.1^+$ $B220^+$; Myeloid DC = $CD11b^+$ $CD8\alpha^-$ $NK1.1^-$ $B220^-$; Lymphoid DC = $CD11b^-$ $CD8\alpha^+$ $NK1.1^-$ $B220^-$; Mixed Myeloid/Lymphoid DC = $CD11b^-$ $CD8\alpha^-$ $NK1.1^-$ $B220^-$; and Plasmacytoid DC = $CD11b^-$ $CD8\alpha^-$ $NK1.1^-$ $B220^+$. A) Representative FACS plots are shown from mice at the time-points post-infection described above. B) Absolute numbers of $CD11c^+$ $CD3^-$ $CD19^-$ DCs. C) Absolute numbers of DC subtypes: NK DCs, Myeloid DCs, Lymphoid DCs, Mixed Myeloid/Lymphoid DCs and Plasmacytoid DCs. D) The percentages of cells described in C) (as a percentage of total $CD11c^+$ $CD3^-$ $CD19^-$ DCs). Data are taken from 2 experiments where n = 3 at each time-point in each experiment *p≤0.05 **p≤0.01 ***p≤0.001.

These numbers are maintained and are further increased at day 14. The most pronounced increase in DC numbers in the liver occurs between 24 and 72 hours.

Further phenotyping identified that different populations of DCs have surprisingly different dynamics during the first 2 weeks of infection. Absolute numbers of NK DCs increase almost 1000-fold by day 14 and they also increase in proportion (of total $CD11c^+$ $CD3^-$ $CD19^-$ $CD11b^{lo}$ $CD8\alpha^-$ cells) (Fig 3.13 C-D). Myeloid DCs are increased by approximately 7-fold within 24 hours, and these numbers are maintained at day 14 (Fig 3.13 C). However, as a proportion (out of $CD11c^+$ $CD3^-$ $CD19^-$ $CD11b^+$ $CD8\alpha^-$ cells), myeloid DCs decrease steadily and severely from approximately 90% in non-infected mice to less than 10% by day 7 (Fig 3.13 D). Cell numbers in the remaining DCs subsets are all relatively stable over the time-course measured, however, the proportion of mixed lymphoid/myeloid DCs falls from day 3 onwards (Fig 3.13 C-D). The proportion of plasmacytoid DCs (out of $CD11c^+$ $CD3^-$ $CD19^-$ $CD11b^-$ $CD8\alpha^-$ cells) increases gradually from approximately 55% in resting mice to 80% at day 14 (Fig 3.13 D).

3.5.3 T cell subset numbers are altered during the time-course of infection

Representative FACS plots of T cells populations are shown in Figure 3.14 A. Resembling the pattern of cellularity, there is a small drop in $CD3^+$ $CD4^+$ T cells at day 1, but absolute numbers leap by day 3 and peak in numbers at day 14 (Fig 3.14 B). The proportion of total leukocytes which are $CD4^+$ T cells drops by 50% within 24 hours of infection, before reaching non-infected proportions by day 35 (Fig 3.14 B).

Figure 3.14

A

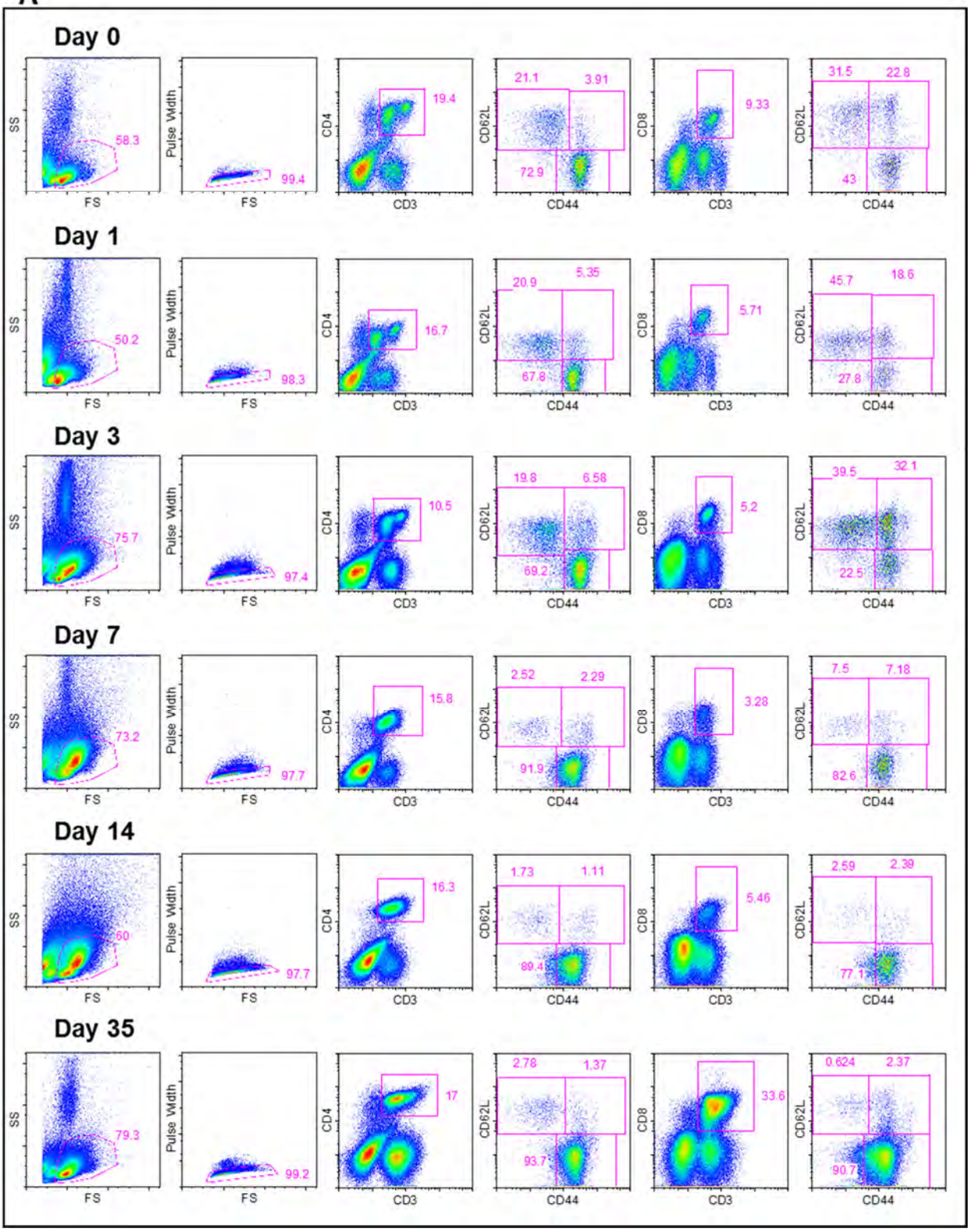
Day 0
SS
FS
58.3
Pulse Width
FS
99.4
CD4
CD3
19.4
CD62L
CD44
21.1
3.91
72.9
CD8
CD3
9.33
CD62L
CD44
31.5
22.8
43
Day 1
SS
FS
50.2
Pulse Width
FS
98.3
CD4
CD3
16.7
CD62L
CD44
20.9
5.35
67.8
CD8
CD3
5.71
CD62L
CD44
45.7
18.6
27.8
Day 3
SS
FS
75.7
Pulse Width
FS
97.4
CD4
CD3
10.5
CD62L
CD44
19.8
6.58
69.2
CD8
CD3
5.2
CD62L
CD44
39.5
32.1
22.5
Day 7
SS
FS
73.2
Pulse Width
FS
97.7
CD4
CD3
15.8
CD62L
CD44
2.52
2.29
91.9
CD8
CD3
3.28
CD62L
CD44
7.5
7.18
82.6
Day 14
SS
FS
60
Pulse Width
FS
97.7
CD4
CD3
16.3
CD62L
CD44
1.73
1.11
89.4
CD8
CD3
5.46
CD62L
CD44
2.59
2.39
77.1
Day 35
SS
FS
79.3
Pulse Width
FS
99.2
CD4
CD3
17
CD62L
CD44
2.78
1.37
93.7
CD8
CD3
33.6
CD62L
CD44
0.624
2.37
90.7

Figure 3.14 continued

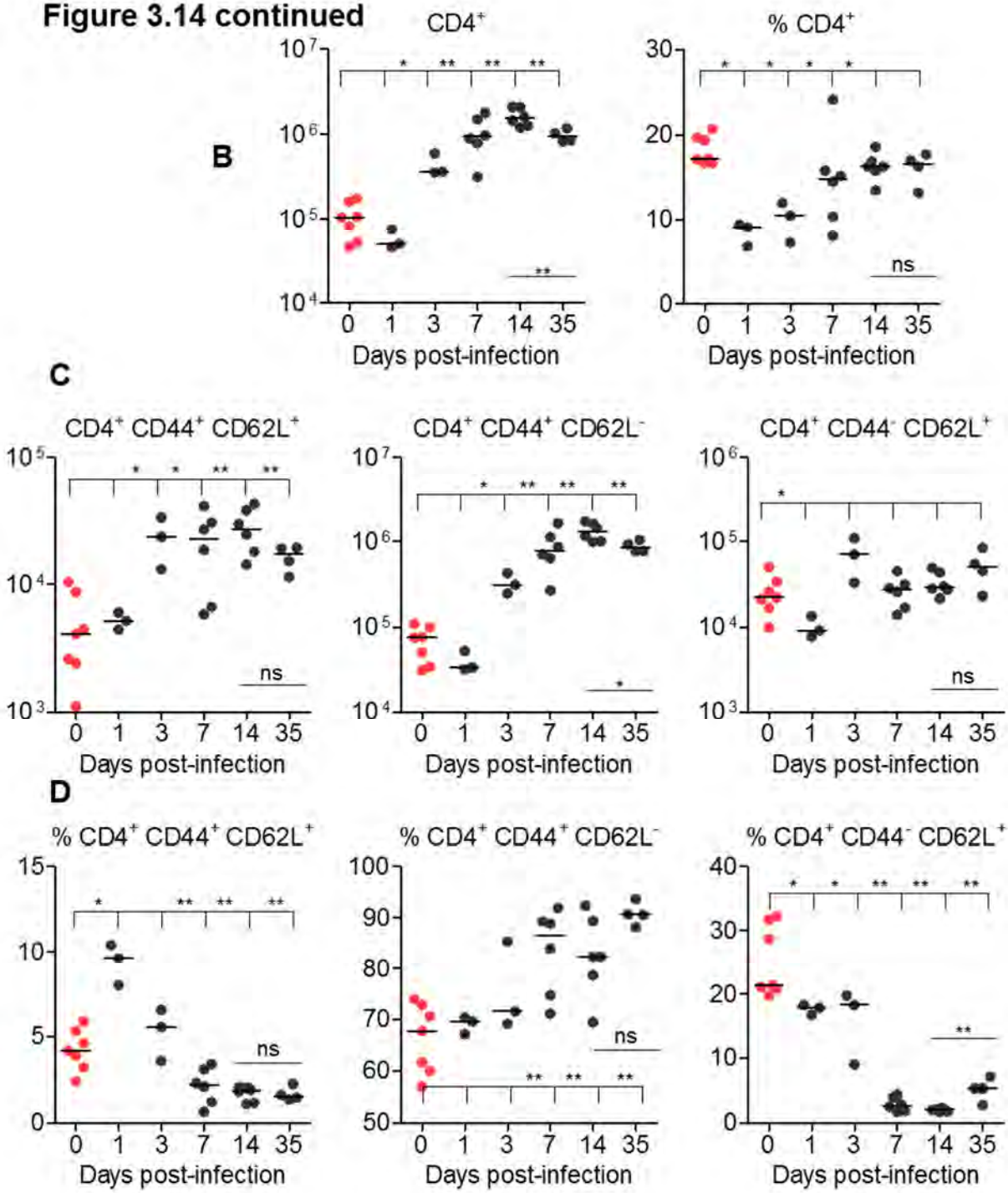

Figure 3.14 CD3+ CD4+ T cell numbers peak in the liver at day 7 post-infection whilst CD3+ CD8+ T cells become more abundant during resolution

WT mice were infected (i.p.) with 5 x 10^5 CFU attenuated STm. Leukocytes were isolated from livers at days 0, 1, 3, 7, 14 and 35 post-infection and T cells were quantified by FACS. The gating strategy used is illustrated in Figure 3.10. Activated T cells are described by CD62L^{lo} CD44+; CD62L+ CD44+ cells are referred to as the central memory compartment; CD62L+ CD44- are naïve. A) Representative FACS plots are shown from mice at the time-points post-infection described above. B) Absolute numbers of CD3+ CD4+ T cells retrieved from the liver are indicated throughout infection alongside the percentage of these cells (as a percentage of total lymphocyte-sized leukocytes isolated from the liver). C) Absolute numbers of CD3+ CD4+ central memory, activated and naïve T cells. D) Percentages of the cells described in C) (as a percentage of total CD3+ CD4+ cells). E) Absolute numbers of CD3+ CD8+ T cells retrieved from the liver are indicated throughout infection alongside the percentage of these cells (a percentage of total lymphocyte-sized leukocytes isolated from the liver). E) Absolute numbers of CD3+ CD8+ central memory, activated and naïve T cells. F) Percentages of the cells described in E) (as a percentage of total CD3+ CD8+ cells). Data are taken from 2 experiments where n = 3 at each time-point in each experiment *p≤0.05 **p≤0.01 ***p≤0.001.

Figure 3.14 continued

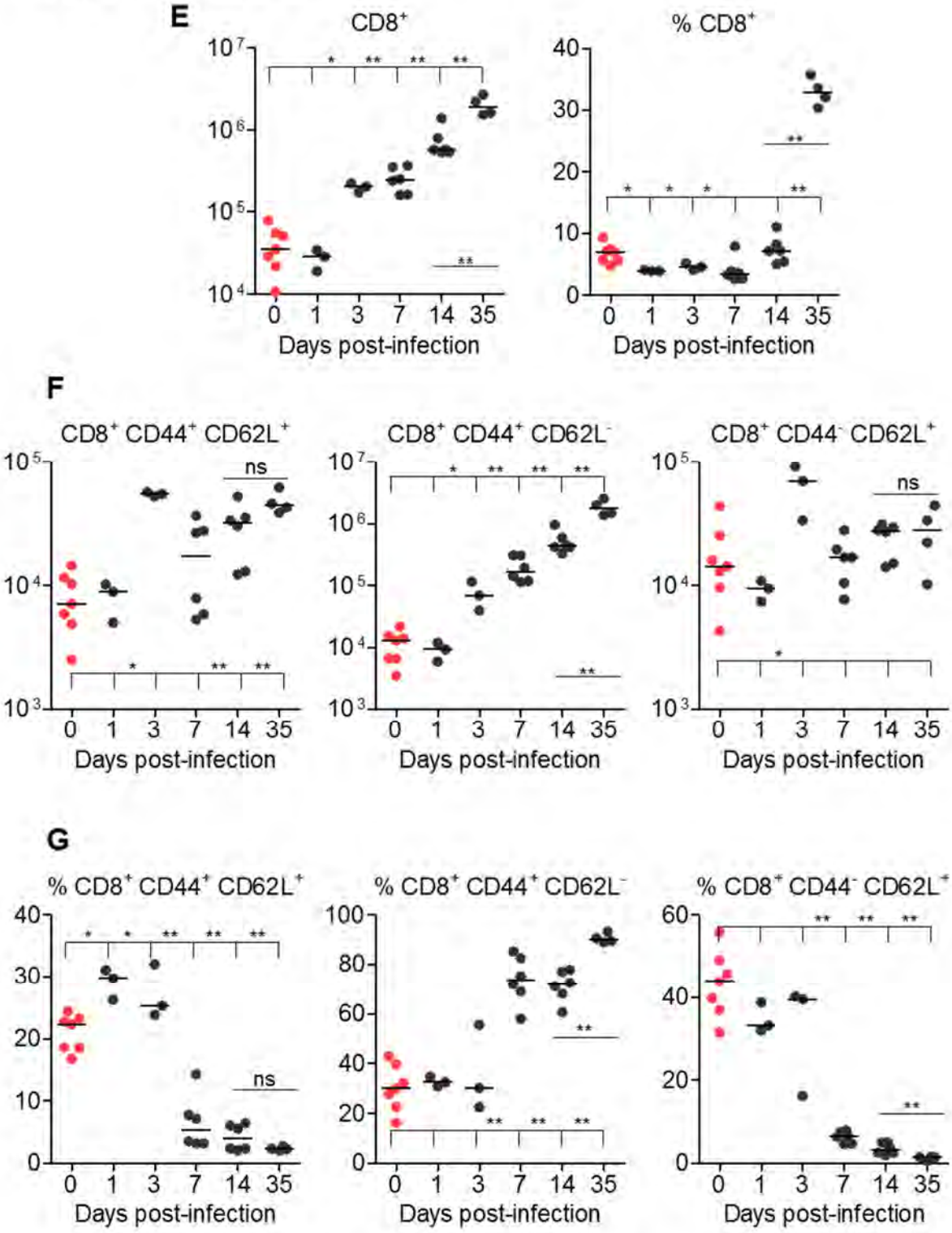

Most $CD4^+$ T cells are activated, with numbers almost 10-fold higher by day 3, although naïve and central memory cells are also increased at day 3 (Fig 3.14 C). The proportion of activated $CD4^+$ T cells increases steadily from approximately 70% in non-infected mice to 90% at day 35 (Fig 3.14 D). The proportion of naïve $CD4^+$ T cells is approximately 20-30% in non-infected mice and after day 3, becomes negligible, however, numbers remain constant throughout infection (Fig 3.14 C-D). Whereas the proportion of central memory $CD4^+$ T cells peaks at day 1, absolute numbers are elevated at day 3, and persist (Fig 3.14 C-D).

3.5.3.1 $CD8^+$ T cells are particularly abundant during the resolution stage

The dynamics of $CD3^+$ $CD8^+$ T cells is very different to that of $CD4^+$ T cells in the liver during infection. Numbers of $CD3^+$ $CD8^+$ T cells increase steadily from day 3 post-infection, however, $CD8^+$ T cells only peak in the liver at day 35, when they become the dominant T cell subset and numbers are almost 100-fold above those in non-infected mice (Fig 3.14 E). The proportion of these cells (out of total lymphocyte-sized cells) remains at approximately 5% until day 14, after which it increases to 35% by day 35 (Fig 3.14 E). In non-infected mice, the majority of $CD8^+$ T cells in the liver are naïve, but this drops shortly after infection from 40% in resting mice to less than 10% at day 7 (Fig 3.14 G). Absolute numbers of naïve $CD8^+$ T cells peak transiently at day 3 but are otherwise constant throughout infection (Fig 3.14 F). Approximately 30% of $CD8^+$ T cells are activated in non-infected mice, and this increases throughout infection to around 90% at day 35 (Fig 3.14 G). The absolute number of activated $CD8^+$ T cells drops very marginally in the first 24 hours, then rises constantly, reaching an over 100-fold increase at day 35, and there is no indication of resolution of these cell numbers (Fig 3.14 F). The proportion of effector memory $CD8^+$ T cells is elevated

early post-infection but falls after day 3, whilst absolute numbers are increased throughout infection (Fig 3.14 F-G).

3.6 Liver function alteration is limited during infection

Considering the extensive infiltration and pathology which develops in the liver and persists for several weeks during infection, we hypothesised that hepatocyte function may become disrupted. In particular, we suspected that infiltration and the localised necrotic regions (which can be extremely severe towards the periphery of lobes), may impair blood flow, affecting oxygen/nutrient supply to hepatocytes. To determine if liver function is maintained during infection, liver injury was measured by the detection of liver-specific enzymes and metabolites in the serum in the presence and absence of infection, as has been described elsewhere (Ramaiah, 2007). Normal serum concentrations of these components are listed in Table 3.2 (Mazzaccara et al., 2008).

Analyte	Male	Female
AST U/L	**75**	**91**
	55-91	51-122
ALT U/L	**61**	**55**
	46-70	42-73
ALP U/L	**84**	**145**
	67-128	103-217
Total bilirubin µmol/L	**7.2**	**7.9**
	5.1-11.9	3.4-14.3

Table 3.2. Serum biochemical analytes measured in C57BL/6J mice aged 4-8 months. Median is shown in bold; 2.5th-97.5th percentile intervals are indicated below. Table adapted from (Mazzaccara et al., 2008).

Alkaline phosphatase (ALP) concentration is greater than reference levels in non-infected mice, but falls significantly at day 7 post-infection, before steadily recovering (Fig 3.15 A). Serum concentrations of alanine transaminase (ALT) in non-infected mice are comparable to reference values and are elevated at day 7 and 21, but return to baseline as the infection resolves (Fig 3.15 B). The concentration of aspartate transaminase (AST) is greater than standard values at day 0, and is elevated at day 7 and, to a greater extent, at day 21 post-infection, but returns to normal as the infection resolves (Fig 3.15 C). The ratio of AST to ALT was calculated, however this remains fairly constant throughout infection (Fig 3.15 D). Similarly, the concentration of total bilirubin remains comparable to day 0 throughout infection (Fig 3.15 E).

These data suggest a limited injury to hepatocytes between days 7 and 21, corresponding to the peak in liver pathology. As pathology is resolved, concentrations of leakage enzymes return to normal, and cholestatic injury markers generally remain comparable to day 0 values throughout infection.

Figure 3.15

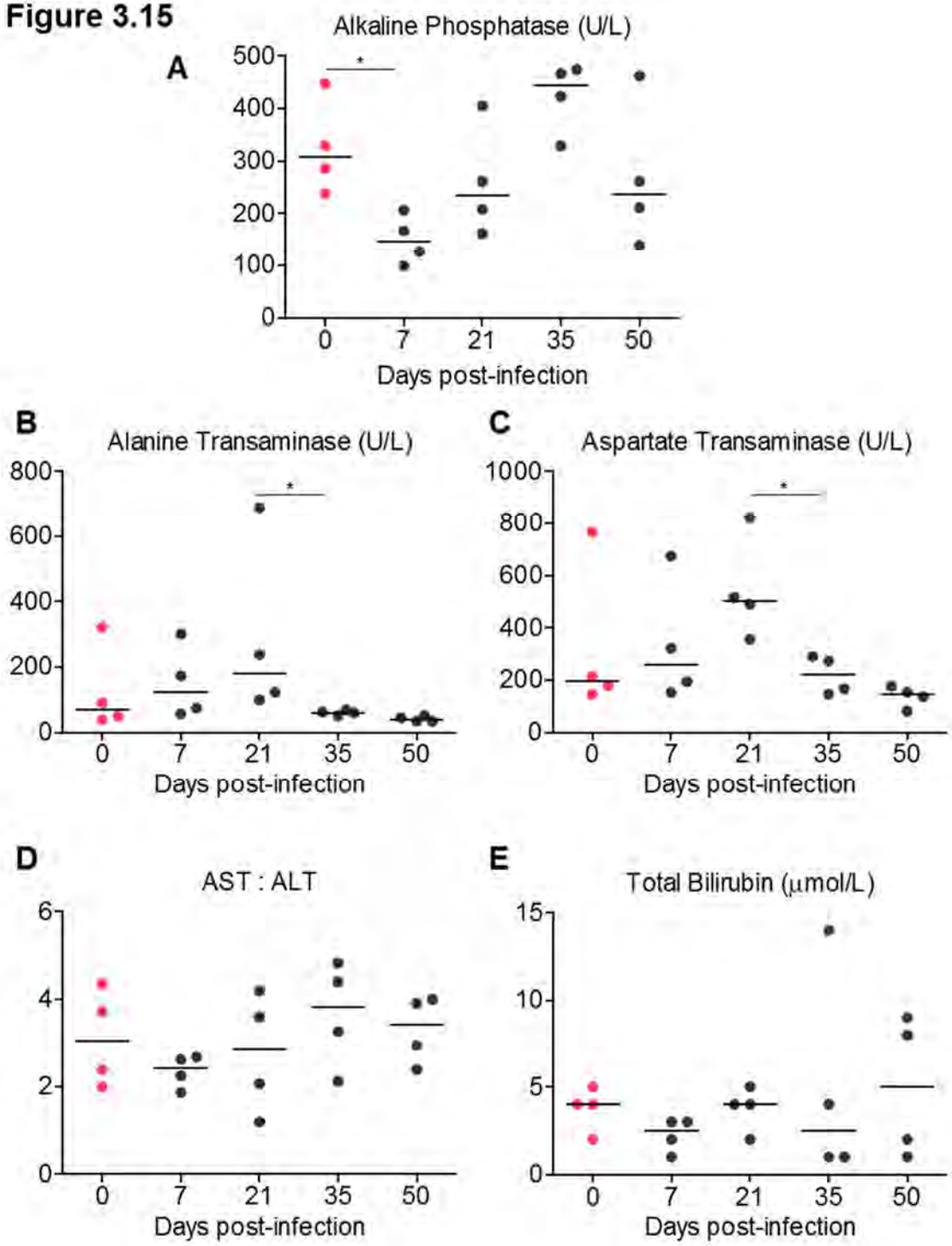

Figure 3.15 Biochemical assessment of liver injury during infection WT mice were infected (i.p.) with 5 x 10^5 CFU attenuated STm. The concentration of A) Alkaline phosphatase (ALP); B) Alanine transaminase (ALT); and C) Aspartate transaminase (AST) were measured in the serum from mice taken at days 0, 7, 21, 35 and 50 post-infection. D) The ratio of AST to ALT was calculated at each time-point described above. E) The concentration of total bilirubin was measured in the serum at the same time-points as described above. Data are taken from one experiment where n = 4 at each time-point. *p≤0.05 **p≤0.01 ***p≤0.001.

3.7 Discussion

Here we have described the kinetics of bacterial colonisation in the liver during our resolving systemic STm infection model. We have characterised the events which occur pathologically in the liver and have phenotyped and quantified leukocyte infiltration throughout infection.

3.7.1 *Salmonella* colonises the entire liver

Salmonella are detected in the liver within 24 hours of i.p. infection and the bacterial load peaks at day 7. In comparison to other peripheral sites, the bacterial burden of the liver, although lower than the spleen, is greater than the lungs and kidney. Importantly, bacteraemia is relatively low, and this reflects that measured in human systemic NTS infections in sub-Saharan Africa, thus highlights the relevance of our infection model (MacLennan et al., 2008).

By culturing distinct regions of the liver we identified that *Salmonella* are distributed throughout the entire tissue during the course of infection. This is an important observation because often certain regions of the liver can be more prone to pathology, both on the tissue surface and within. For example, lesions are frequently seen on the surface of smaller lobes, and necrotic tissue is more prominent towards the periphery of lobes, as identified by Haemotoxylin & Eosin staining (H&E) and by immunohistochemistry (IHC). Thus it is likely that the pathology we observe is immune mediated, and, although initiated by the presence of bacteria, not caused by the bacteria itself (for example by secreted bacterial toxins) (Nolan, 1981, Bilzer et al., 2006). Furthermore, this idea is supported by the relationship between the kinetics of bacterial load and pathology severity. Bacterial clearance is initiated by day 14 and is well established by day 21, as has

been shown previously in the spleen (Cunningham et al., 2007). However, we detect the most extensive infiltration and pathology in the parenchyma at around days 14-21, thus at a time when bacterial numbers are no longer at their peak. Therefore, it seems likely that the pathology we see in the liver is leukocyte- (as opposed to bacteria-) driven (Bilzer et al., 2006, Hsu, 1989).

3.7.2 Inflammatory lesions develop in the parenchyma of the liver

Others have previously described the formation of lesions in the liver during systemic *Salmonella* infection in mice (Richter-Dahlfors et al., 1997, Mastroeni et al., 1995, Nakoneczna and Hsu, 1980). These studies have detected bacteria within host cells which are localised to inflammatory lesions (Everest et al., 1997, Richter-Dahlfors et al., 1997). Thus although we do not measure bacterial concentration within lesions, it is likely that this is where bacteria reside in our infection model also.

We demonstrate the most abundant cells in lesions are F4/80$^+$, F4/80$^+$ CD11c$^+$, and Ly6C$^+$ myeloid populations. This is in general agreement with observations from other groups, taking into consideration differing kinetics of infections (Richter-Dahlfors et al., 1997). Based on our observations and flow cytometry data, we would conclude that inflammatory lesions are composed of both Kupffer cells and infiltrating monocyte populations, with a large increase in monocyte cell numbers post-infection. The F4/80$^+$ CD11c$^+$ staining of sinusoid localised cells would suggest that Kupffer cells maintain residence in this site during infection, as shown by others (Beattie et al., 2010). Previous studies have suggested that Kupffer cells do not overtly contribute to lesion composition, but we would argue that differing infection models using higher bacterial inoculums may account for this discrepancy (Richter-Dahlfors et al., 1997, Nnalue et al., 1992, Lin et al., 1987, Conlan and

North, 1992). Ly6C$^+$ cells are also found in sinusoids but these are generally CD11c$^-$. This indicates their monocyte phenotype as opposed to F4/80$^+$ DC populations including monocyte derived dendritic cells (MoDC)/inflammatory DCs (infDCs) (Segura and Amigorena, 2013, Flores-Langarica et al., 2011, Hespel and Moser, 2012, Tam et al., 2008). However, the F4/80$^+$ CD11c$^+$ cells in the sinusoids (generally referred to here as Kupffer cells) could also consist of MoDCs. Monocyte-derived DCs prime Th1 cells in this infection in the spleen, therefore they may also be important for antigen presentation in the liver (Flores-Langarica et al., 2011). To differentiate between Kupffer cells and MoDCs in the sinusoids, further characterisation by additional markers is required by confocal microscopy. However, the current literature regarding inflammatory DC populations in the liver (including MoDCs), especially in bacterial infections, reflects the importance of these populations and this must be addressed in the future (Segura and Amigorena, 2013, Schreiber et al., 2011).

Others have noted the abundance of polymorphonuclear (PMN) cells in inflammatory lesions following *Salmonella* infection (Nakoneczna and Hsu, 1980, Conlan, 1996). Although we do detect these cells in lesions (by both H&E and Ly6G$^+$ staining), we would suggest these cells are not particularly frequent relative to other myeloid populations. Neutrophils may be more prominent in lesion composition at earlier time-points (Richter-Dahlfors et al., 1997), however, it is important to note the differing infection models used by other groups (Mastroeni et al., 1995, Lin et al., 1987, Conlan and North, 1992, Hsu, 1989). Often, high bacterial inoculums are used which may stimulate very different responses in the host repertoire of leukocytes.

3.7.2.1 T cells are located at the periphery of inflammatory lesions

In non-infected livers, $CD3^+$ T cells are relatively rare and are located throughout the sinusoids, and are more commonly seen in portal regions. These cells are an even mix of $CD4^+$ and $CD8^+$ cells. Shortly after infection, the majority of T cells are $CD4^+$, which is expected considering the necessity for $CD4^+$ Th1 cells to mediate bacterial clearance (Ravindran et al., 2005).

After infection, T lymphocytes preferentially localise to the periphery of inflammatory lesions and there are greater numbers of $CD3^+$ T cells per lesion when pathology is most extensive. We hypothesised that T cells may play a role in the restriction of lesion growth in a similar manner to that seen by Tregs surrounding the islets of Langerhans cells in the pancreas during autoimmune inflammation, where these cells prevent islet infiltration (Sarween et al., 2004). Indeed we do detect some $FoxP3^+$ Treg cells in these regions. However, in WT mice, although the majority of $CD3^+$ cells are $CD4^+$, the frequency of Tregs is low. Thus it is likely that the majority of $CD3^+$ $CD4^+$ T cells found at the lesion periphery are of Th1 and other phenotypes (Ravindran and McSorley, 2005). Considering the localisation of bacteria in these lesions (reported by others (Richter-Dahlfors et al., 1997)) and the high density of myeloid populations in lesion (observed here), it is likely that these $CD4^+$ T cells may localise to these regions to interact with innate cells. A major function of activated Th1 cells is IFNγ production, and this will be discussed in the context of lesion development in the next chapter (Ramarathinam et al., 1993, Pie et al., 1997). In addition, the $CD8^+$ T cells detected in the liver following infection, are also likely to play an important role in the host response; this is also discussed in Chapter 4.

3.7.3 The majority of $CD4^+$ T cells are activated in the liver

Flow cytometry enabled more extensive phenotyping of both $CD4^+$ and $CD8^+$ T cells in the liver in the presence and absence of infection. In a resting mouse, the majority (70%) of $CD4^+$ T cells are effector ($CD44^+$ $CD62L^{lo}$), and most of the remaining $CD4^+$ T cells are naïve ($CD44^-$ $CD62L^+$). This has been described elsewhere (Mittrucker et al., 2002). The liver, due to its proximity to the gut and its extensive vascularisation, is constantly sampling the plethora of gut-derived antigens and is therefore an important effector tissue (Crispe, 2011). In conjunction with our histological data, the $CD4^+$ T cells detected at the lesion periphery must be generally activated, and are likely to be antigen specific (although we have not shown this) (Ravindran and McSorley, 2005).

3.7.3.1 The frequency of $CD8^+$ T cells is increased as infection resolves

By measuring proportions and numbers of leukocytes during the course of infection, we have identified that, in line with the general dynamics of infiltration in the liver, most populations tend to increase in number, then decline as inflammation is resolved. Considering the dominance of the Th1 response in the control of STm infection, we were surprised by the accumulation of $CD8^+$ T cells in the liver during the resolution stages. By histology, we have observed an even mix of $CD4^+$ and $CD8^+$ T cells in the absence of infection. During peak inflammation we detect a higher abundance of $CD4^+$ T cells, and as infection resolves, we detect a more balanced T cell population. However, quantification by flow has highlighted the prominence $CD3^+$ $CD8^+$ cells, particularly at later time-points.

$CD8^+$ T cells increase in absolute number fairly steadily from around day 3 post-infection. This is probably due to increased leukocyte cellularity in the liver during the course of infection, because the proportion of total lymphocytes which are $CD8^+$ remains constant

(at less than 10%) until at least day 7. From day 14, the proportion of $CD8^+$ T cells increases significantly, thus suggesting that these cells are important later during infection. Indeed the majority (90%) of these cells are activated at day 35, and histological data indicates their location both in lesions and in the sinusoids. Others have reported expansion of $CD8^+$ T cells during murine STm infection and have demonstrated the IFNγ-producing capabilities of these cells, following appropriate stimulation (Mittrucker et al., 2002). However, the mechanisms behind $CD8^+$ T cell contribution to *Salmonella* immunity are less well understood. The function of these cells is partly addressed using $CD8^{-/-}$ mice, and is detailed in Chapter 4.

3.7.4 Hepatocyte injury is detected but liver function is maintained as infiltration infiltration resolves

During typhoid fever, abnormal liver function has been reported by biochemical read-outs, although this has not been directly linked with overt pathology (Huang et al., 2005, Ramachandran et al., 1974). We detect heightened concentrations of hepatocyte leakage enzymes ALT and AST, at times when severe pathology is observed in the liver. Detection of these proteins in the blood can indicate membrane damage to hepatocytes, thus the term “hepatocyte leakage enzyme” (Ramaiah, 2007). Thus inflammation may induce some level of hepatocyte injury (Tacke et al., 2009, Zimmermann et al., 2012). The phenotype we observe resolves as infiltration is controlled thus there is no lasting evidence of hepatocyte injury. It should be noted that variability between mice at each time-point was quite high, making interpretation difficult, especially of cholestatic injury markers. In addition, ALT is not completely liver-specific, thus can be detected in the serum upon muscle cell damage and haemolysis (Ramaiah, 2007). AST is also present in erythrocytes and skeletal muscle,

thus its detection in serum doesn't necessarily indicate liver-specific injury (Ramaiah, 2007). Furthermore, anaemia and the associated haemolysis are strongly associated with systemic NTS infection (discussed further in Chapter 6) (Mabey et al., 1987). These phenotypes may contribute to elevated ALT and AST serum concentrations.

3.7.5 Parenchymal necrosis

We observed necrotic regions at the centre of inflammatory lesions, which we believe to be composed of necrotic hepatocytes due to the presence of remaining nuclei (S. Hubscher, personal communication). Necrotic sites can be extensive and, although distributed throughout the parenchyma, tend to be more common at the periphery of sections (although this has not been quantified). Necrotic regions are always surrounded by leukocytes, which are always absent from the necrotic centres of foci. Similar regions have been described elsewhere, both in association with typhoid fever and with systemic NTS infection (Richter-Dahlfors et al., 1997, Mallory, 1898) (Rubin & Weinstein, 1977). Others have eluded to restricted hepatocyte blood supply due to sinusoidal occlusion by infiltrating leukocytes as an explanation of this necrosis (Richter-Dahlfors et al., 1997, Mallory, 1898). In addition, STm is known to induce apoptosis of host cells during the infection process (Richter-Dahlfors et al., 1997). Thus we may be detecting both necrosis and apoptosis, and further investigation is required to differentiate between the two.

3.7.6 Summary

These data illustrate the extensive accumulation of both myeloid and lymphoid populations in the liver during infection. While it is likely that this is largely due to leukocyte infiltration, it is worth acknowledging the haematopoietic capabilities of the liver due to the presence of pluripotent stem cells in this site in adult mice (Taniguchi et al., 1996). Flow

cytometry in conjunction with histology provides substantial evidence as to which cells are in the liver, where they are distributed, and their dynamics during the course of infection. This provides useful information regarding which cells may be important in the driving of and the regulation of hepatic pathology. Some remaining questions particularly with regard to the role of particular cell types and signalling components, such as IFNγ, will be addressed in the next chapter.

CHAPTER 4:

THE REGULATION OF INFLAMMATION IN THE LIVER

4.1 Introduction

We showed in Chapter 3 the kinetics and constitution of inflammatory lesions in the liver during infection, with pathology peaking in severity when bacterial clearance is well established. This suggested that this pathology may be immune cell-mediated and driven by the pro-inflammatory environment rather than a direct response to the bacteria (Bilzer et al., 2006, Hsu, 1989). To further dissect the immunological response to infection in the liver we wanted to identify key cell types and molecular components which may be required for the development of inflammatory foci.

Previous studies have histologically identified multiple cell types which contribute to pathological lesions in the liver during murine systemic NTS infections (Nakoneczna and Hsu, 1980, Richter-Dahlfors et al., 1997, Mastroeni et al., 1995). In addition, some of the key cytokines involved in this pathology have been identified, although how these signalling components contribute to the process is less well understood (Mastroeni et al., 1995, Everest et al., 1997, Mastroeni et al., 1998). Furthermore, there is far less evidence describing to what extent individual inflammatory populations contribute functionally to the progression of lesion development beyond simple observation of the cells present. In Chapter 3, the leukocyte populations which accumulate in the liver during infection were rigorously phenotyped, therefore we have a clear understanding of which cells are present. In this Chapter, we sought to understand which of these cells and their associated

molecular products are required for lesion development. To our knowledge, this approach to understanding hepatic pathology during systemic NTS infection is novel.

To determine the contribution of individual cellular populations to the development of inflammatory lesions, mice which lacked specific immune cells or signalling mediators such as transcription factors and cytokines were infected and livers were examined at day 7 post-infection. Where possible, this analysis included both histological observation and flow cytometric analyses. The day 7 time-point was consistently used because inflammatory lesions are fully established in WT mice at this time and so it provides ample opportunity for comparison.

4.1.2 Aim of study

In this chapter we investigate how inflammatory lesions develop in the liver during infection. Here we:

- Identify immune cells or molecules which are required for the development of inflammatory lesions during infection (using genetically altered mice);
- Identify immune cells or molecules which regulate leukocyte accumulation in the liver during infection (using genetically altered mice);
- Determine whether the IFNγ necessary for inflammation is derived from a haematopoietic or non-haematopoietic source (by generating bone marrow radiation chimeric mice);
- Examine the role of Tbet in the relationship between $CD4^+$ Th1 cells and Treg cells during inflammation in the liver.

RESULTS

4.2 Inflammatory lesions develop in the liver in the absence of adaptive immune cells

To determine whether inflammatory lesions can develop in the absence of T and B cells, we used Rag-1-deficient mice. Livers from non-infected Rag-$1^{-/-}$ mice are similar to those from non-infected WT mice, albeit slightly larger, as shown by H&E staining and immunohistochemistry (IHC) (Fig 4.1 A-C).

Rag-1-deficient mice were infected alongside WT mice as described in Chapter 2 and livers were examined for pathology and leukocyte infiltration after 7 days. After infection, hepatomegaly in Rag-1-deficient mice is similar or less severe to that in WT mice, and the bacterial burden of the liver is slightly elevated (Fig 4.2 A-B). In the absence of B and T cells, livers tend to have a greater severity of pathology on the exterior of the tissue (Fig 4.2 C). Within the liver, inflammatory lesions still form in Rag-1 deficient mice, but are frequently smaller and more diffuse (Fig 4.2 D-E). Lesions contain single F4/80^{+}, CD$11c^{+}$, and double F4/80^{+} CD$11c^{+}$ cells as in WT mice, however, there are more cells in the sinusoids and in portal regions in Rag-1 deficient mice (Fig 4.2 E and data not shown).

Figure 4.1

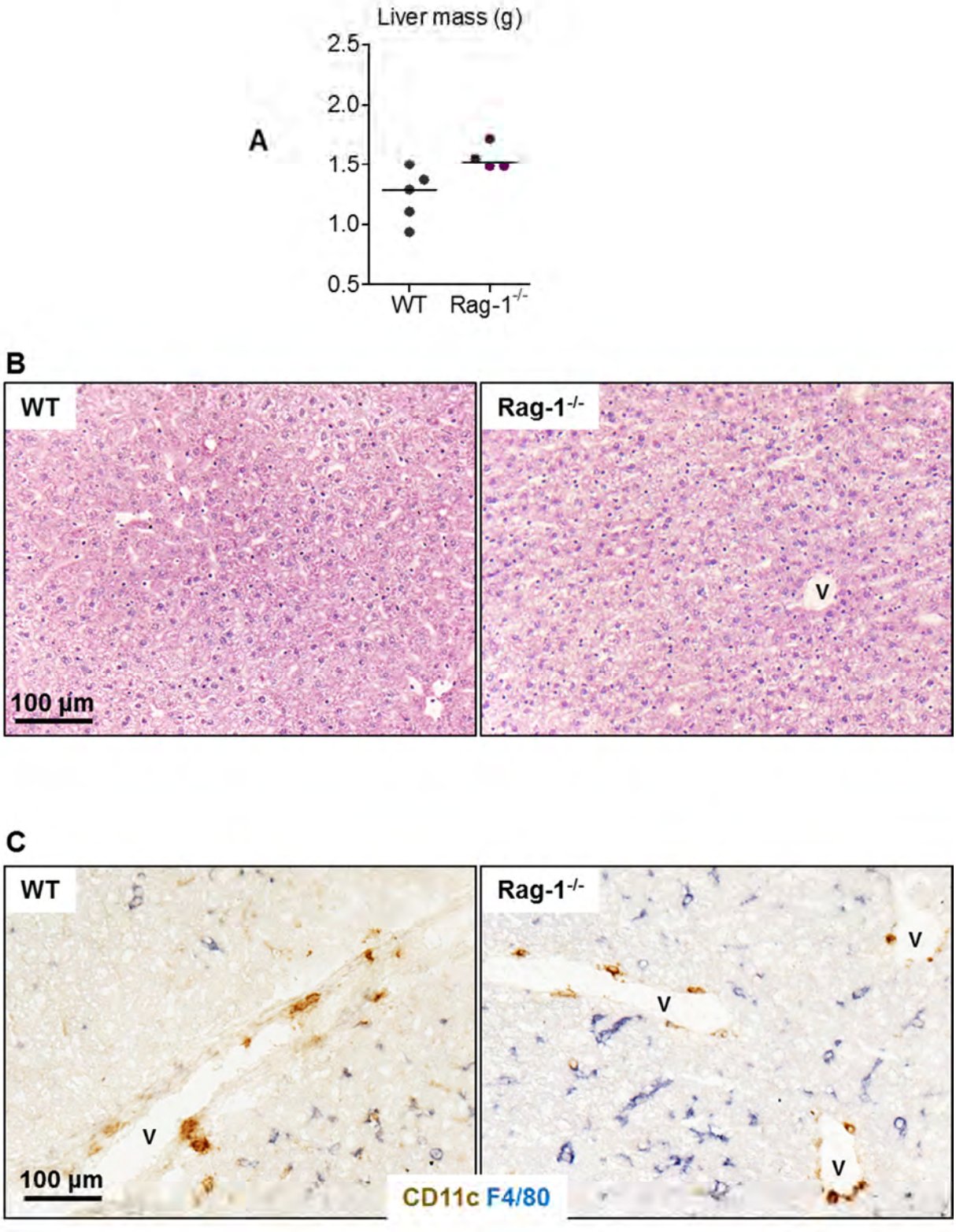

Figure 4.1 Livers from WT and Rag-1$^{-/-}$ mice are similar in the absence of infection
Livers were removed from non-infected WT and Rag-1$^{-/-}$ mice and A) liver mass was measured. Livers were examined histologically by C) H&E and D) IHC where F4/80^{+} cells = blue; CD11c^{+} cells = brown; double positive F4/80^{+} CD11c^{+} cells = black. V = vessel. Data are taken from one experiment where n = 4-5 in each mouse strain.

Figure 4.2

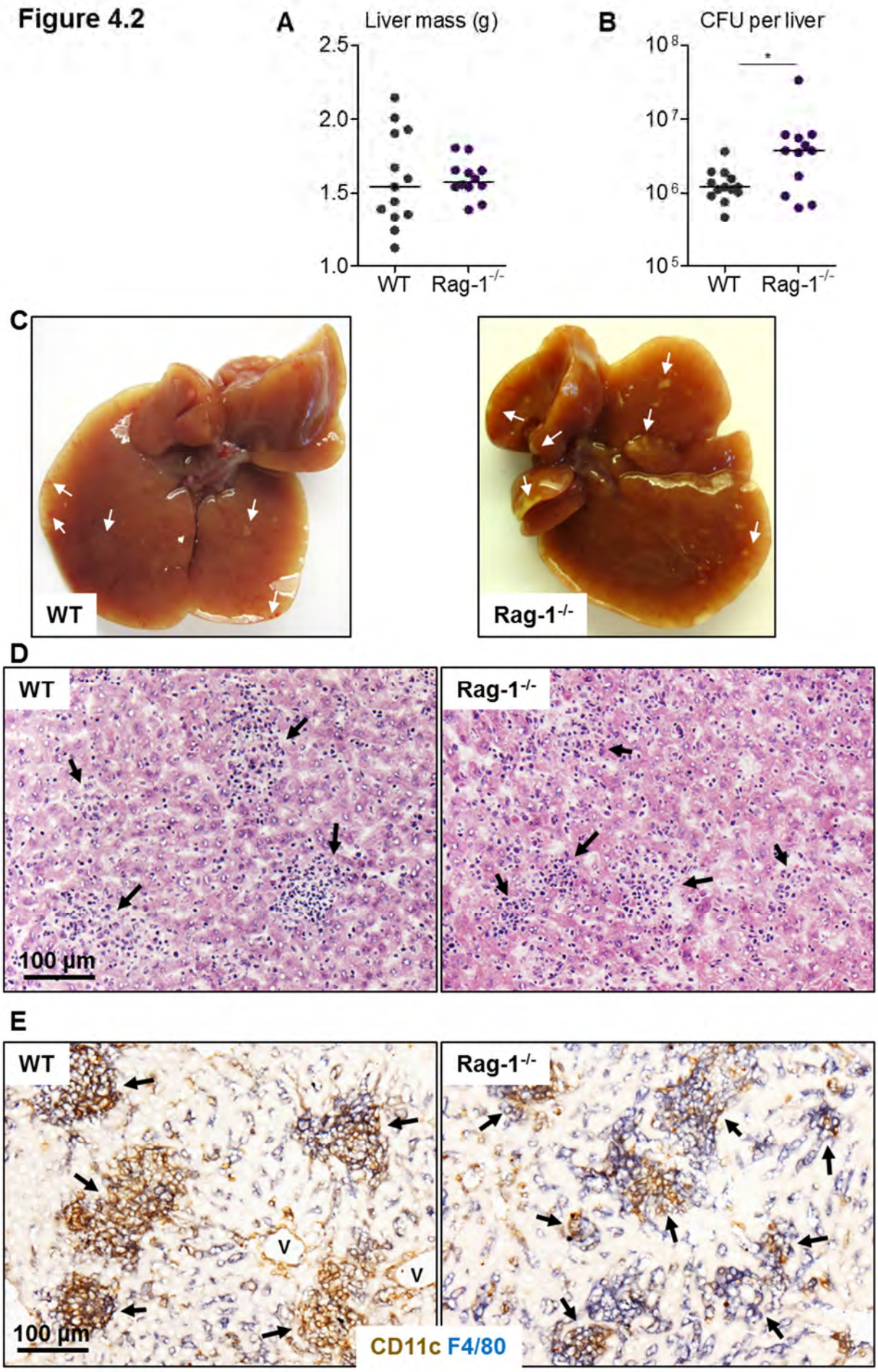
A
Liver mass (g)
2.5
2.0
1.5
1.0
WT
Rag-1-/-
B
CFU per liver
10^8
10^7
10^6
10^5
*
WT
Rag-1-/-
C
WT
Rag-1-/-
D
WT
Rag-1-/-
100 µm
E
WT
Rag-1-/-
V
V
100 µm
CD11c F4/80

Figure 4.2 continued

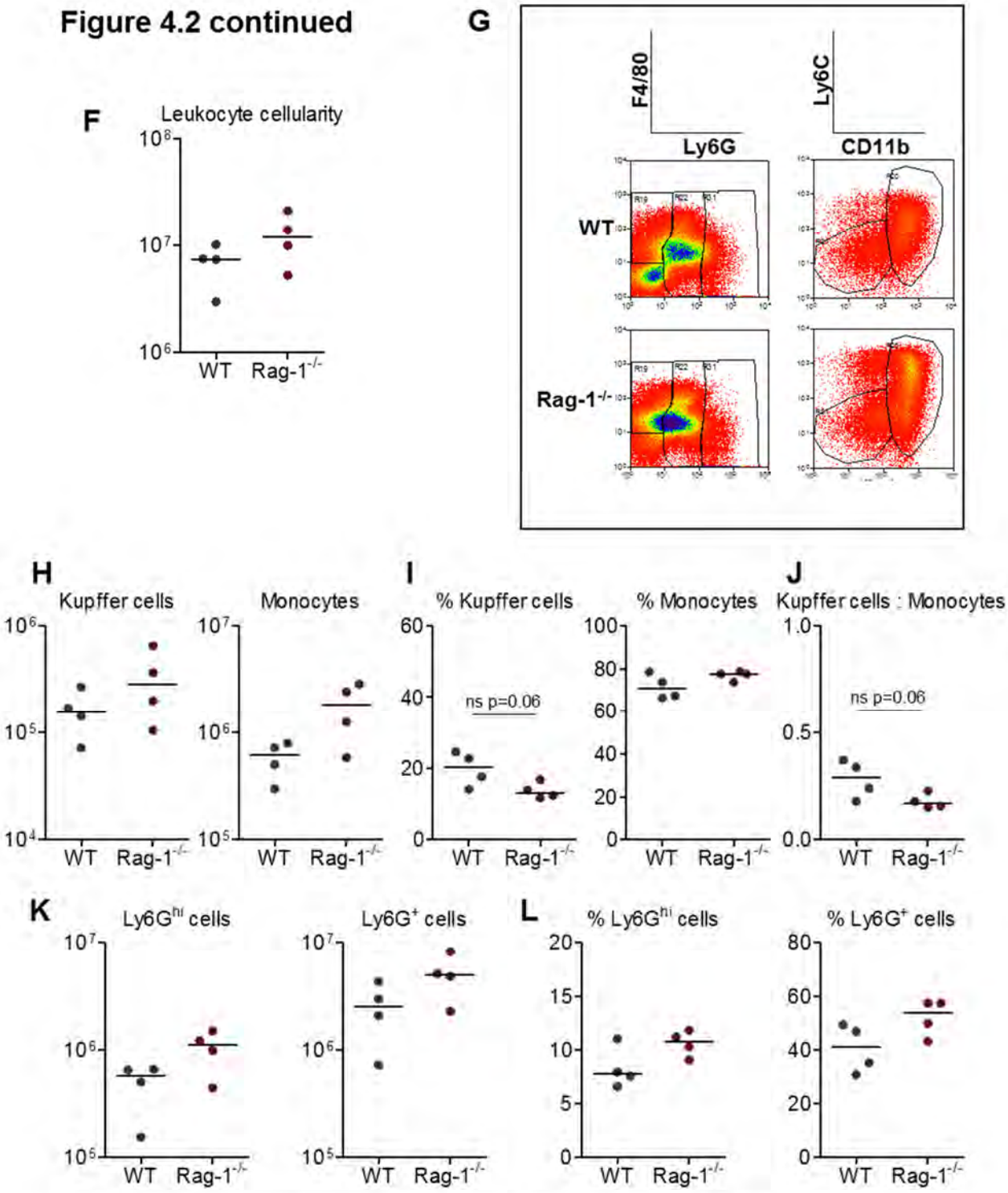

Figure 4.2 Inflammatory lesions develop in the absence of B and T cells

WT and Rag-1$^{-/-}$ mice were infected (i.p.) with 5 x 10^5 CFU attenuated STm for 7 days. Livers were removed and A) liver mass and B) bacterial burden of the liver were determined in each strain. C) Livers were examined for pathology on the exterior surface. White arrows indicate pathological features, including white-coloured lesions and bloodshot tissue. Development of inflammatory lesions and extent of hepatic leukocyte infiltration was assessed by D) H&E, and E) IHC where F4/80$^+$ cells = blue; CD11c$^+$ cells = brown; double positive F4/80$^+$ CD11c$^+$ cells = black. V = vessel; black arrows indicate inflammatory lesions. Leukocytes were isolated from the livers of these day 7-infected mice, by collagenase digestion and gradient centrifugation. F) The total number of leukocytes retrieved from the liver was calculated. G) Myeloid populations were analysed by FACS and representative FACS plots from WT and Rag-1$^{-/-}$ mice are shown. H) Absolute numbers and I) proportions (out of total F4/80^{hi} Ly6G^{lo} cells) for Kupffer cells and monocytes are shown, where Kupffer cells = F4/80^{hi} Ly6G^{lo} CD11b^{lo} Ly6C^{lo} and monocytes = F4/80^{hi} Ly6G^{lo} CD11b^{hi} Ly6C^{hi}. J) The proportion of absolute numbers of Kupffer cells to absolute numbers of monocytes in the liver was calculated. K) Absolute numbers and L) proportions (out of total isolated leukocytes) of Ly6G^{hi} cells and Ly6G$^+$ cells were determined. Data are taken from 1 experiment where n = 4 in each mouse strain. *p≤0.05 **p≤0.01 ***p≤0.001.

Flow cytometry was used to quantitatively assess the extent of leukocyte infiltration at day 7 post-infection in WT and Rag-1-deficient mice. Interestingly, total leukocyte cellularity of the liver is similar or elevated in the absence of lymphocytes (Fig 4.2 F). Representative FACS plots of myeloid staining are shown in Figure 4.2 G. Absolute numbers of Kupffer cells and monocytes are higher in Rag-1-deficient mice relative to WT, and a greater proportion of F4/80^{+} Ly6G^{lo} cells are monocytes (Fig 4.2 H-J). Absolute numbers and frequencies of Ly6G^{hi} and Ly6G^{+} cell populations are also higher in Rag-deficient mice (Fig 4.2 K-L). These data suggest that inflammation in the liver is not lymphocyte driven and lesion development does not require B or T cells. However, due to the more diffuse infiltration observed in the liver, either B or T cells or both cell types may be required for optimal inflammatory restriction.

4.3 Inflammatory lesions develop normally in the absence of B cells

To elucidate whether the importance of lymphocytes in hepatic immune regulation is B and/or T cell mediated, we examined inflammation in the livers of IgHκ$^{-/-}$ mice, which lack B cells specifically. In the absence of infection, livers from B cell-deficient mice resemble those from WT mice in size and histology (Fig 4.3 A and data not shown). Leukocytes isolated from IgHκ$^{-/-}$ and WT livers were examined by flow cytometry. In resting mice, the leukocyte cellularity is similar, as are the absolute numbers of all myeloid populations examined (despite variability between mice) (Fig 4.3 B-H). The proportions of Kupffer cells and monocytes are lower and higher respectively in mice lacking B cells, thus the ratio of Kupffer cells to monocytes is slightly less in these mice (Fig 4.3 E-F). Absolute numbers and frequencies of CD3^{+} CD4^{+} T cells are similar to WT (Fig 4.3 I-K).

Figure 4.3

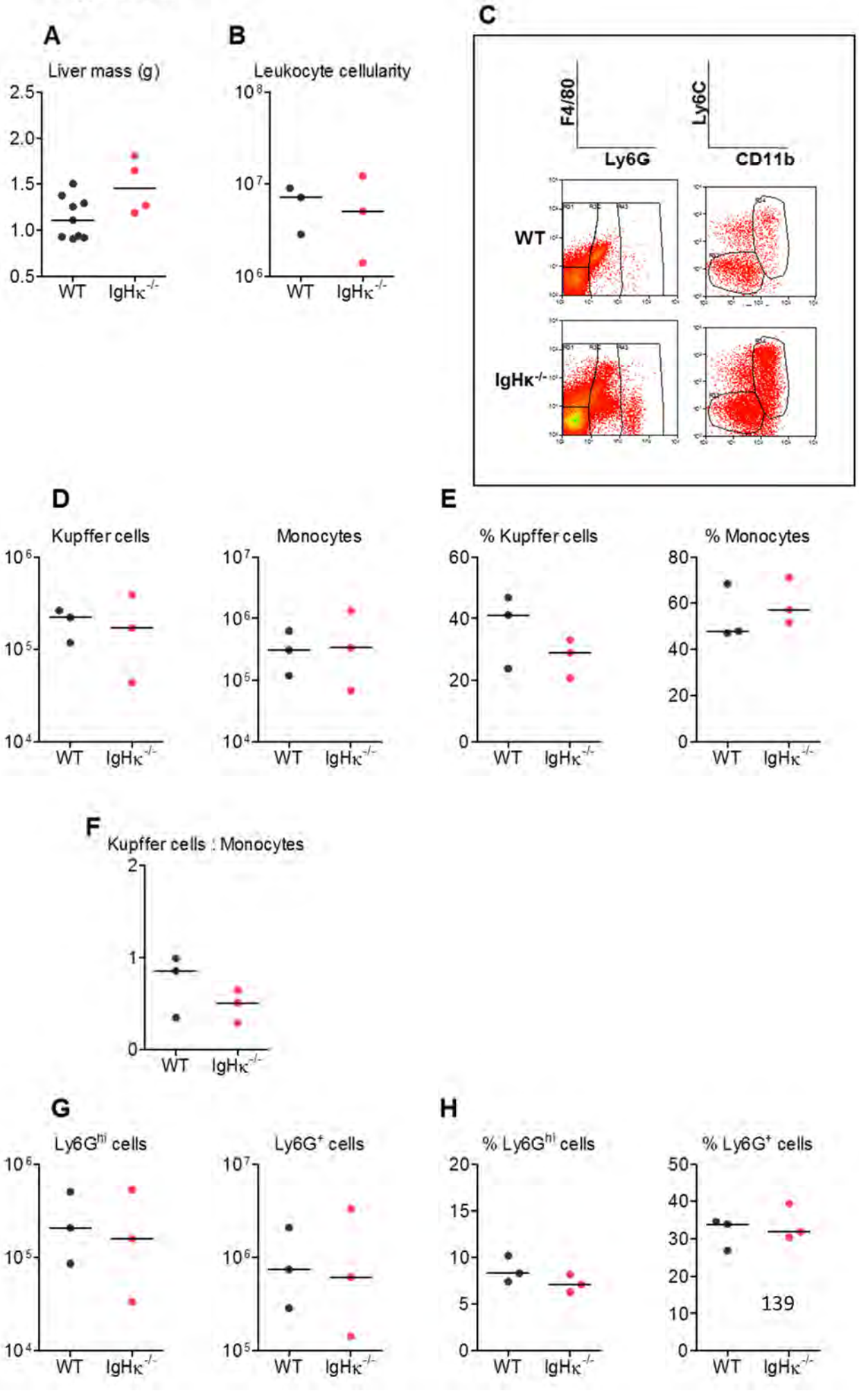
A
Liver mass (g)
2.5
2.0
1.5
1.0
0.5
WT
IgHκ-/-
B
Leukocyte cellularity
10^8
10^7
10^6
WT
IgHκ-/-
C
F4/80
Ly6G
Ly6C
CD11b
WT
IgHκ-/-
D
Kupffer cells
10^6
10^5
10^4
WT
IgHκ-/-
Monocytes
10^7
10^6
10^5
10^4
WT
IgHκ-/-
E
% Kupffer cells
60
40
20
0
WT
IgHκ-/-
% Monocytes
80
60
40
20
0
WT
IgHκ-/-
F
Kupffer cells : Monocytes
2
1
0
WT
IgHκ-/-
G
Ly6G^hi cells
10^6
10^5
10^4
WT
IgHκ-/-
Ly6G+ cells
10^7
10^6
10^5
WT
IgHκ-/-
H
% Ly6G^hi cells
20
15
10
5
0
WT
IgHκ-/-
% Ly6G+ cells
50
40
30
20
10
0
139
WT
IgHκ-/-

Figure 4.3 continued

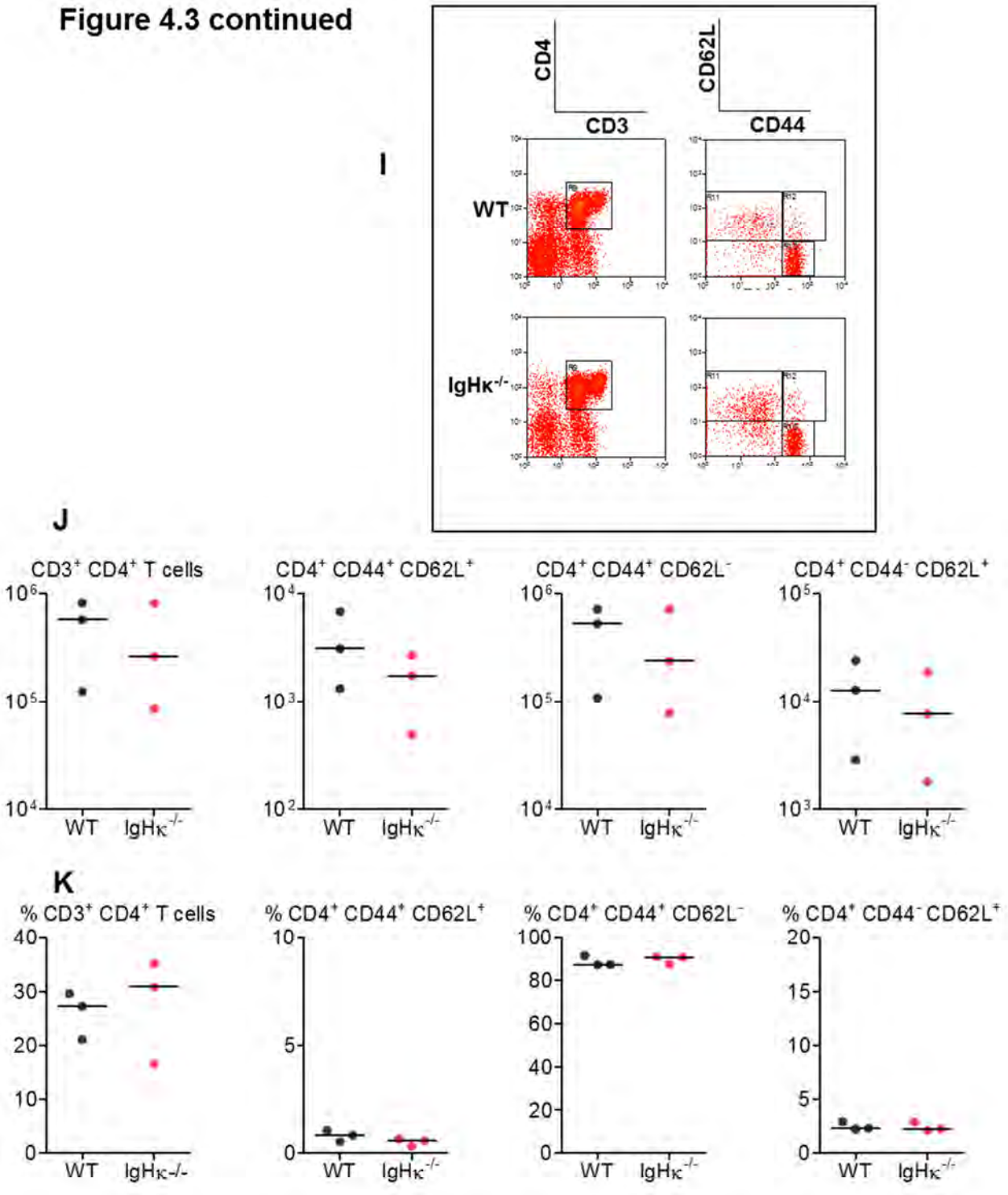

Figure 4.3 In the absence of infection, livers from WT and IgHκ$^{-/-}$ mice are similar
Livers were removed from non-infected WT and IgHκ $^{-/-}$ mice and A) liver mass was measured. Leukocytes were isolated from the livers of these non-infected mice, by collagenase digestion and gradient centrifugation. B) The total number of leukocytes retrieved from the liver was calculated. C) Myeloid populations were analysed by FACS and representative FACS plots from WT and IgHκ $^{-/-}$ mice are shown. D) Absolute numbers and E) proportions (out of total F4/80^{hi} Ly6G^{lo} cells) for Kupffer cells and monocytes are shown, where Kupffer cells = F4/80^{hi} Ly6G^{lo} CD11b^{lo} Ly6C^{lo} and monocytes = F4/80^{hi} Ly6G^{lo} CD11b^{hi} Ly6C^{hi}. F) The proportion of absolute numbers of Kupffer cells to absolute numbers of monocytes in the liver was calculated. G) Absolute numbers and H) proportions (out of total isolated leukocytes) of Ly6G^{hi} cells and Ly6G^{+} cells were determined. CD4^{+} T cells were examined by FACS for activation status, as identified by expression of CD62L and CD44. Activated effector T cells are described by CD62L^{lo} CD44^{+}; CD62L^{+} CD44^{+} cells are referred to as the central memory compartment; and CD62L^{+} CD44^{-} are naïve. I) Representative FACS plots from WT and IgHκ $^{-/-}$ mice are shown. J) Absolute numbers and K) proportions (out of total lymphocyte-sized cells isolated) are shown for the indicated CD4^{+} T cell subsets. Data are taken from 1 experiment where n = 3 in each mouse strain.

At day 7 post-infection, hepatomegaly and bacterial burden are similar in IgHκ$^{-/-}$ and WT mice, supporting previous studies which show B cells are not required for bacterial clearance at this time (Fig 4.4 A-B) (McSorley and Jenkins, 2000). However, IgHκ$^{-/-}$ mice tend to have more overt pathology on the tissue exterior than in WT mice, frequently with white lesions on the surface of the smaller hepatic lobes (Fig 4.4 C). However, inflammatory lesions in the liver resembled those of WT mice (Fig 4.4 D). Both F4/80^{+} cells and CD11c^{+} cells and F4/80^{+} CD11c^{+} cells are found in lesions and T cells are peripherally-located (Fig 4.4 E and data not shown). The frequency of cells in the sinusoids is similar to that in WT mice.

Leukocyte cellularity after infection is equivalent to WT in IgHκ$^{-/-}$ mice (Fig 4.4 F). The number of Kupffer cells is the same, although the proportion of total F4/80^{+} Ly6G^{lo} cells of this phenotype is lower in IgHκ$^{-/-}$ mice (Fig 4.4 G-J). Monocyte numbers are greater in the absence of B cells, and the proportion of these cells is increased 3-4 fold (Fig 4.4 G-J). However, both these phenotypes may be explained by the higher than usual ratio of Kupffer cells to monocytes in WT mice in this experiment. Number and frequency of Ly6G^{hi} cells are significantly increased in the absence of B cells, whereas Ly6G^{+} cells are more similar to WT (Fig 4.4 K-L).

Representative FACS plots of CD4^{+} T cell staining are shown in Figure 4.4 M. The proportion of total lymphocyte-sized cells which are CD4^{+} is significantly increased in the absence of B cells although the absolute number of these cells is similar to in WT mice (Fig 4.4 N-O). There is a greater number and frequency of naïve CD4^{+} T cells in the absence of B cells and the proportion of activated CD4^{+} T cells is significantly lower.

Figure 4.4

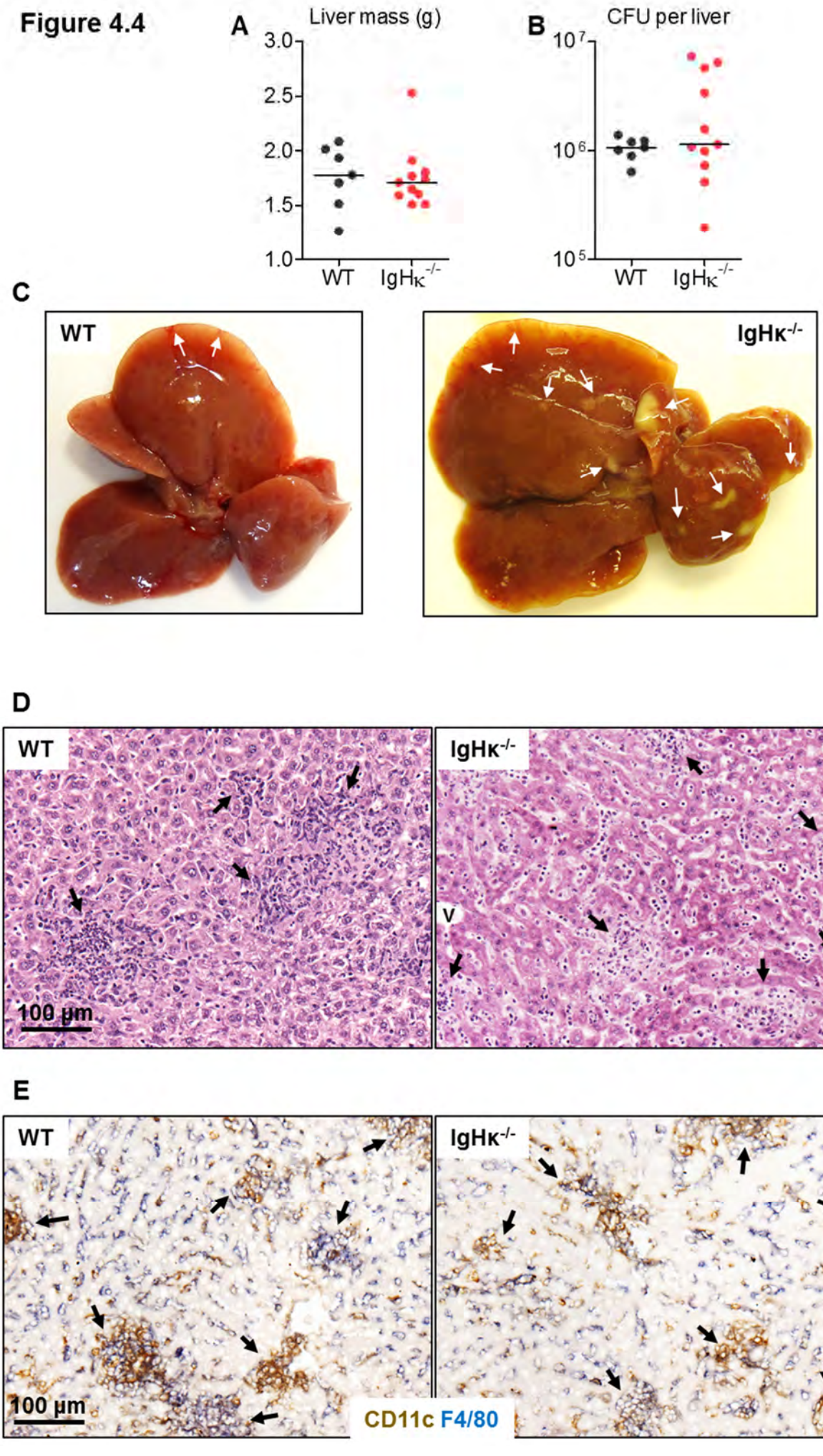
A
Liver mass (g)
3.0
2.5
2.0
1.5
1.0
WT
IgHκ-/-
B
CFU per liver
10^7
10^6
10^5
WT
IgHκ-/-
C
WT
IgHκ-/-
D
WT
IgHκ-/-
V
100 μm
E
WT
IgHκ-/-
100 μm
CD11c F4/80

Figure 4.4 continued

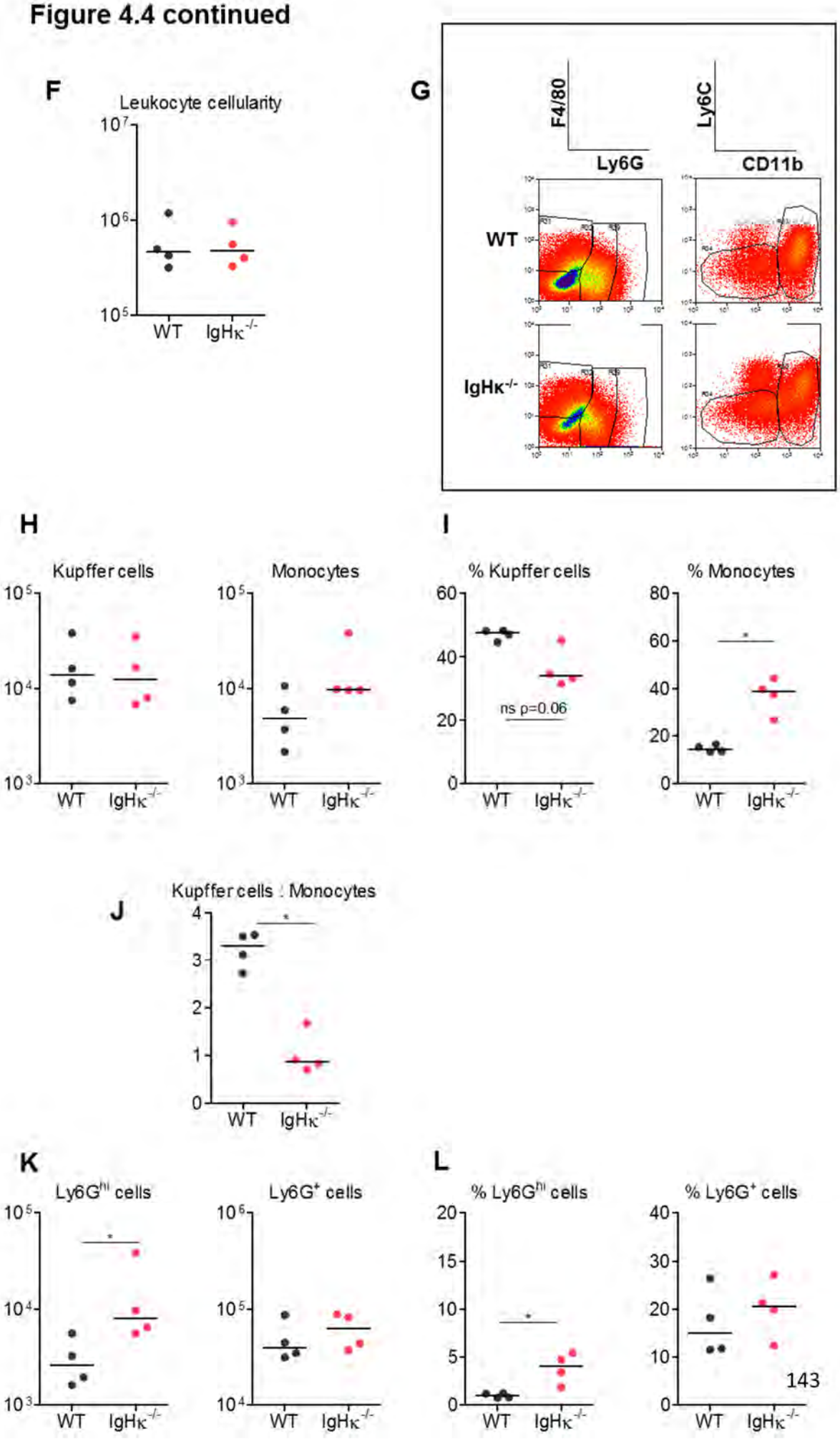

Figure 4.4 continued

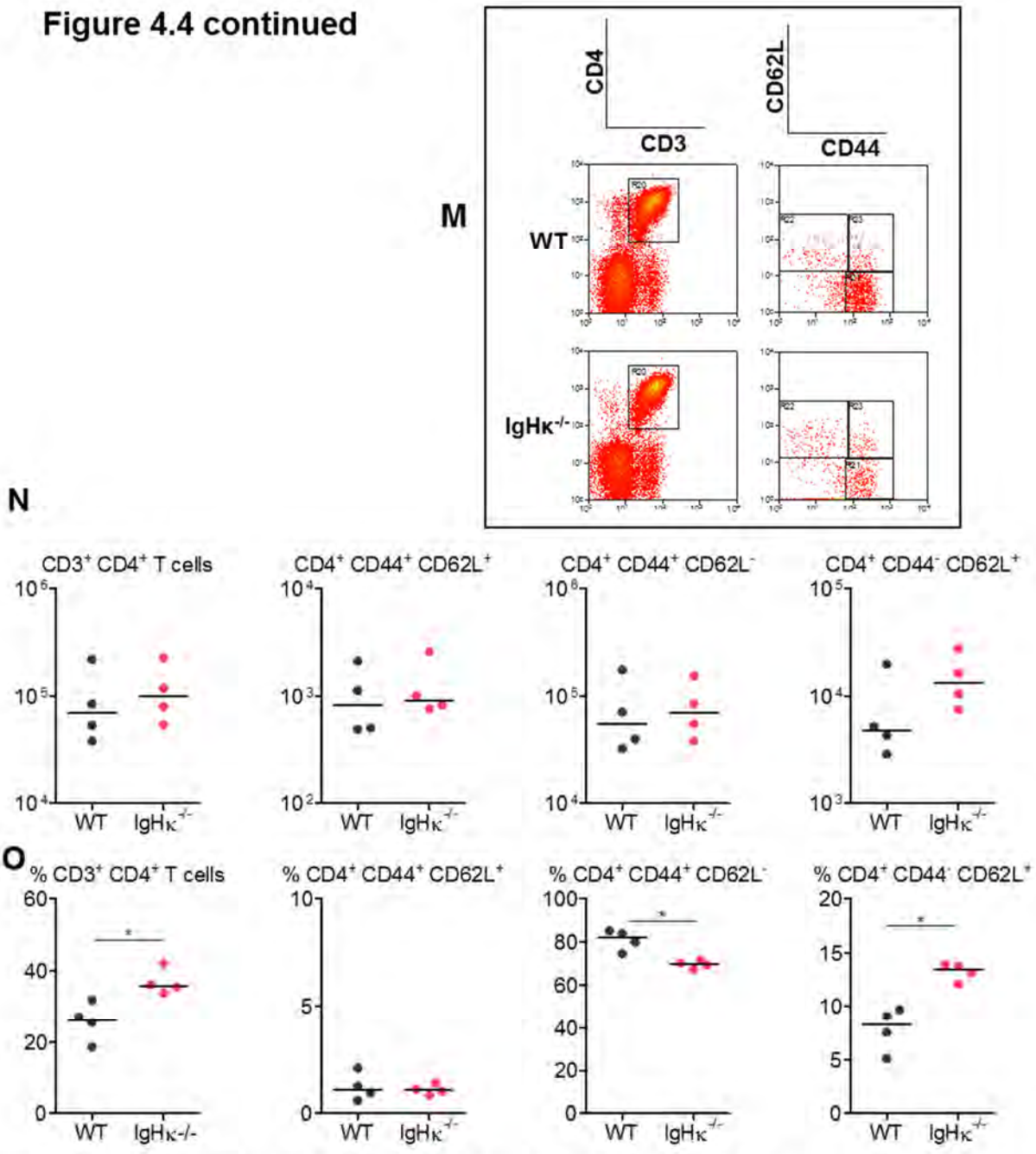

Figure 4.4 Inflammatory lesions develop in the liver in the absence of B cells

WT and IgHκ $^{-/-}$ mice were infected (i.p.) with 5 x 10^5 CFU attenuated STm for 7 days. Livers were removed and A) liver mass and B) bacterial burden of the liver were determined in each strain. C) Livers were examined for pathology on the exterior surface. White arrows indicate pathological features, including white-coloured lesions and bloodshot tissue. Development of inflammatory lesions and extent of hepatic leukocyte infiltration was assessed by D) H&E, and E) IHC where F4/80$^+$ cells = blue; CD11c$^+$ cells = brown; double positive F4/80$^+$ CD11c$^+$ cells = black. V = vessel; black arrows indicate inflammatory lesions. Leukocytes were isolated from the livers of these day 7-infected mice, by collagenase digestion and gradient centrifugation. F) The total number of cells retrieved from the liver in the leukocyte fraction of the gradient was calculated. G) Myeloid populations were analysed by FACS and representative FACS plots from WT and IgHκ $^{-/-}$ mice are shown. H) Absolute numbers and I) proportions (out of total F4/80^{hi} Ly6G^{lo} cells) for Kupffer cells and monocytes are shown, where Kupffer cells = F4/80^{hi} Ly6G^{lo} CD11b^{lo} Ly6C^{lo} and monocytes = F4/80^{hi} Ly6G^{lo} CD11b^{hi} Ly6C^{hi}. J) The proportion of absolute numbers of Kupffer cells to absolute numbers of monocytes in the liver was calculated. K) Absolute numbers and L) proportions (out of total isolated cells) of Ly6G^{hi} cells and Ly6G$^+$ cells were determined. CD4$^+$ T cells were examined by FACS for activation status, as identified by expression of CD62L and CD44. Activated effector T cells are described by CD62L^{lo} CD44$^+$; CD62L$^+$ CD44$^+$ cells are referred to as the central memory compartment; and CD62L$^+$ CD44$^-$ are naïve. M) Representative FACS plots from WT and IgHκ $^{-/-}$ mice are shown. N) Absolute numbers and O) proportions (out of total lymphocyte-sized cells isolated) are shown for the indicated CD4$^+$ T cell subsets. Data are taken from 1 experiment where n = 4 in each mouse strain. This experiment has been repeated and the data are representative of multiple experiments. *p≤0.05 **p≤0.01 ***p≤0.001.

These data highlight an inherent inflammatory phenotype in mice lacking B cells, whereby monocytes are increased in the liver. This phenotype is maintained following infection, and is accompanied by elevated numbers of naïve $CD4^+$ T cells.

4.4 T cells are dispensable for the development of inflammatory lesions but do contribute to hepatic inflammation

Having shown that B cells do not contribute to inflammatory lesion development, we were keen to determine whether T cells have a role in hepatic inflammation. To test this we infected WT and $TCR\beta\delta^{-/-}$ mice, whereby both αβ and γδ T cells are absent, and examined liver inflammation at day 7 post-infection. $TCR\beta\delta^{-/-}$ mice have slightly larger livers in the absence of infection than WT mice, but these are histologically similar (Fig 4.5 A and data not shown).

After infection, livers from T cell-deficient mice are significantly larger than those from WT mice, although they have similar bacterial burdens at this stage (Fig 4.5 B-C). The external appearance of T cell-deficient livers can be variable (data not shown). Inflammatory lesions are present in T cell-deficient mice but inflammation across the entire tissue appears more diffuse than in T cell-sufficient mice (Fig 4.5 D). Lesions consist of the same myeloid populations as are detected in WT mice (Fig 4.5 E).

Leukocyte cellularity is similar to WT livers after infection, despite the absence of T cells (Fig 4.5 F). Myeloid populations were examined by flow cytometry and representative FACS plots of cells are shown in Figure 4.5 G. In the absence of T cells, there is a more marked increase in absolute number and frequency of monocytes than in WT livers (Fig 4.5 H-J).

Figure 4.5

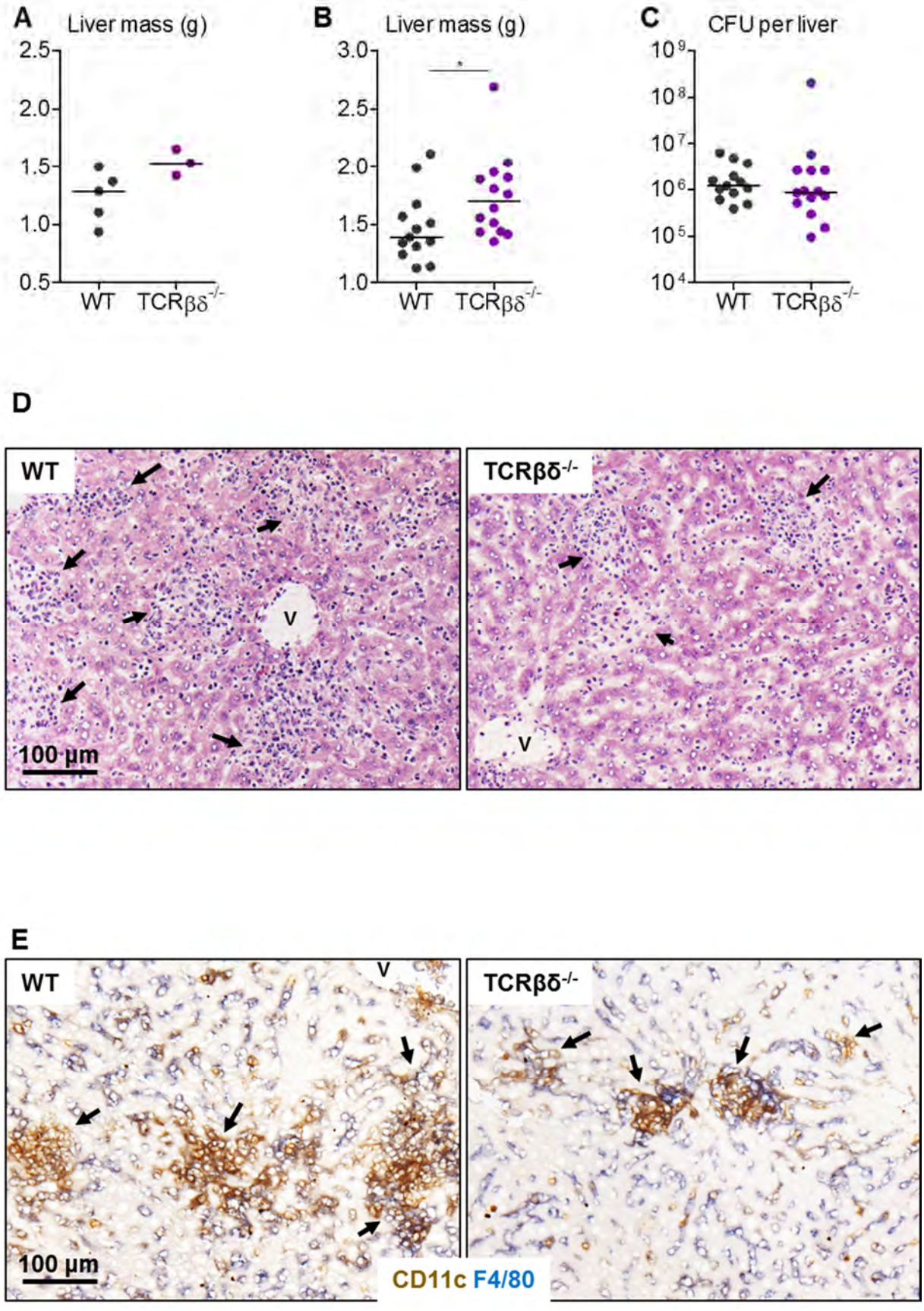
A
Liver mass (g)
2.5
2.0
1.5
1.0
0.5
WT
TCRβδ-/-
B
Liver mass (g)
3.0
2.5
2.0
1.5
1.0
*
WT
TCRβδ-/-
C
CFU per liver
10^9
10^8
10^7
10^6
10^5
10^4
WT
TCRβδ-/-
D
WT
V
100 µm
TCRβδ-/-
V
E
WT
V
100 µm
TCRβδ-/-
CD11c F4/80

Figure 4.5 continued

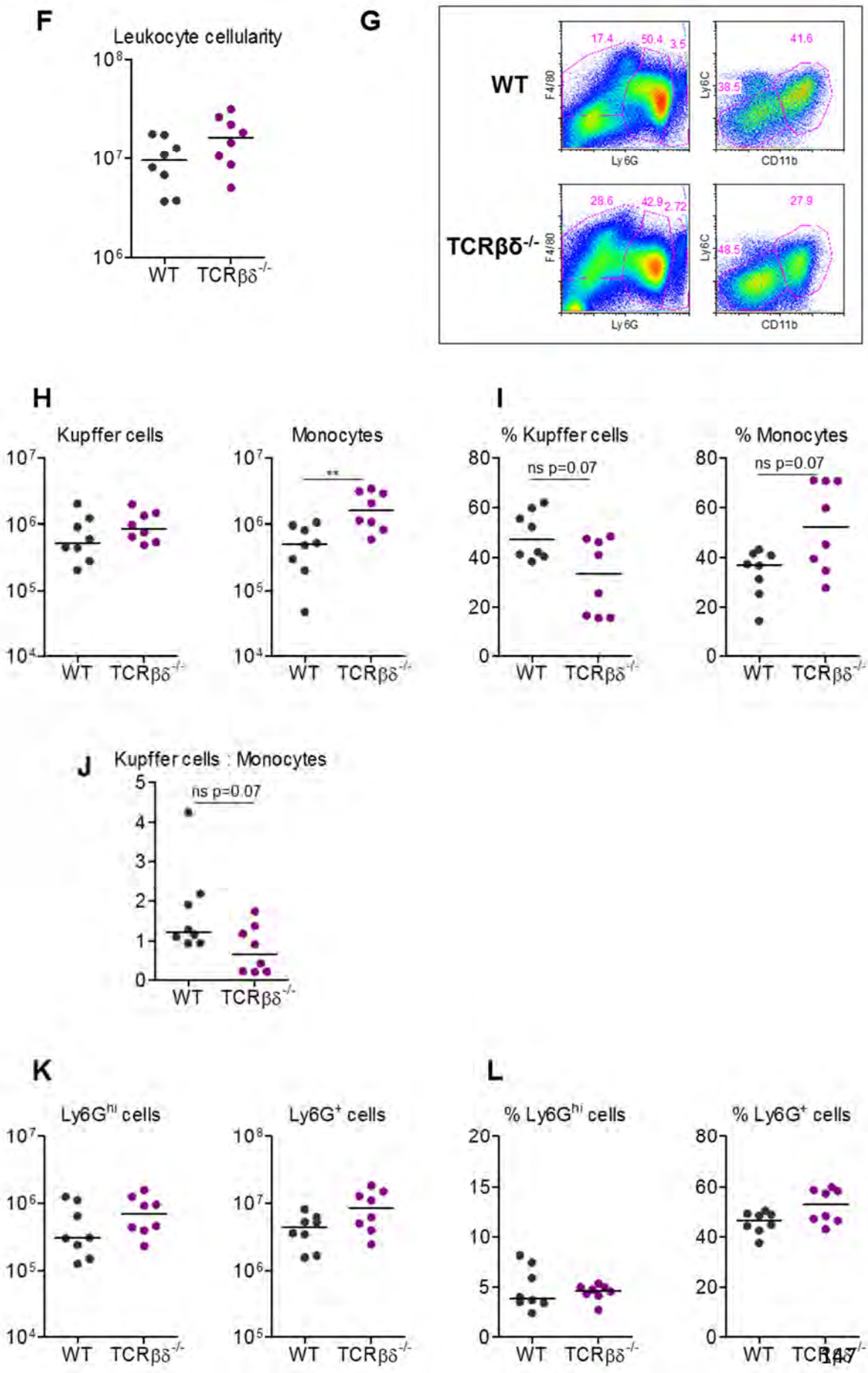

Figure 4.5 continued

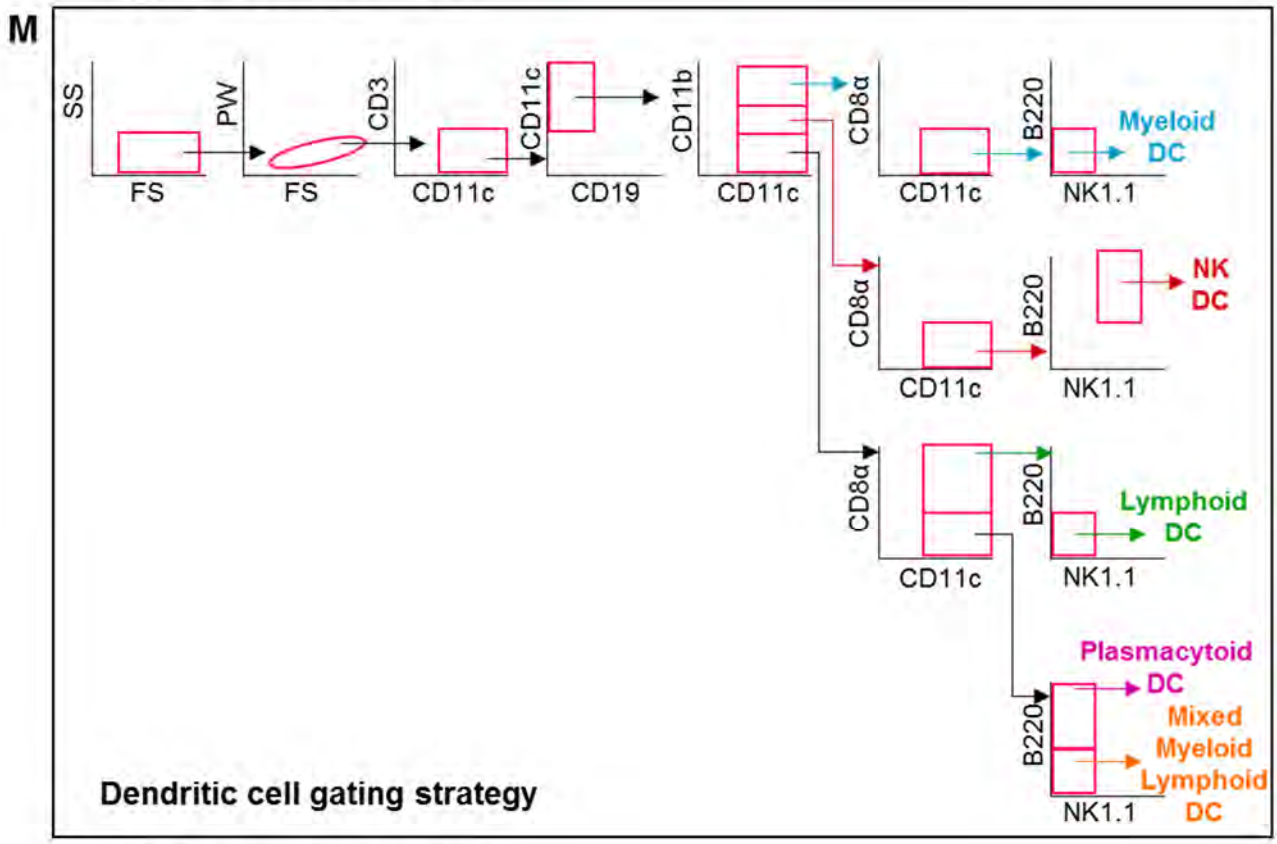

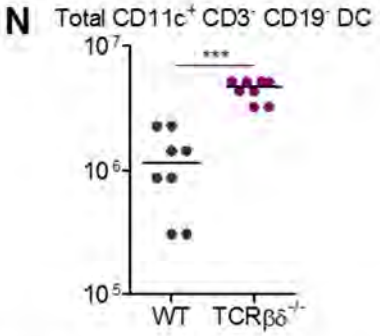

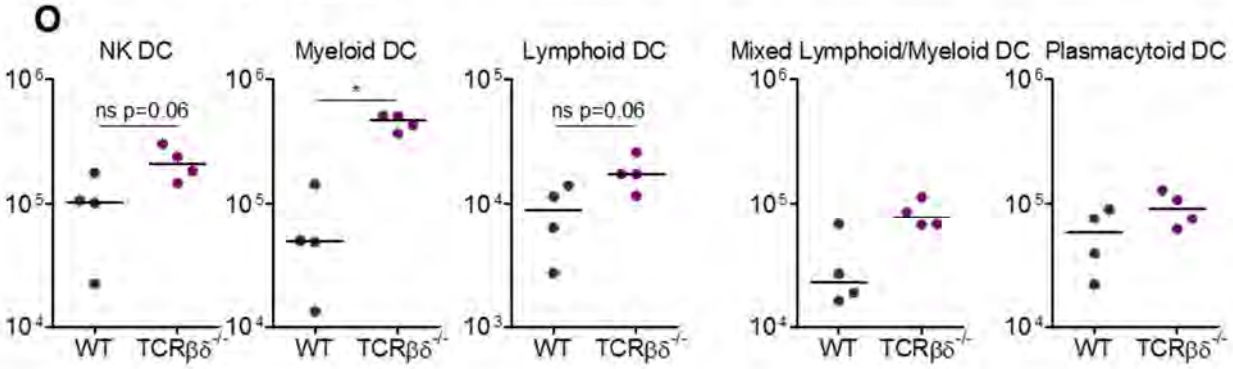

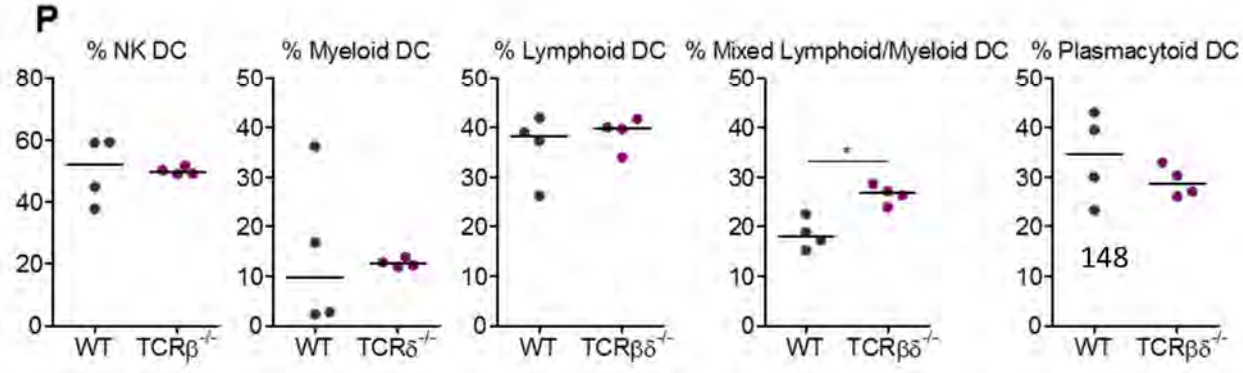

Figure 4.5 Inflammatory lesions develop in the liver in the absence of T cells
Livers were removed from non-infected WT and TCRβδ $^{-/-}$ mice and A) liver mass was measured. WT and TCRβδ $^{-/-}$ mice were infected (i.p.) with 5 x 10^5 CFU attenuated STm for 7 days. Livers were removed and B) liver mass (of infected mice) and C) bacterial burden of the liver were determined in each strain. Development of inflammatory lesions and extent of hepatic leukocyte infiltration was assessed by D) H&E, and E) IHC where F4/80$^+$ cells = blue; CD11c$^+$ cells = brown; double positive F4/80$^+$ CD11c$^+$ cells = black. V = vessel; black arrows indicate inflammatory lesions. Leukocytes were isolated from the livers of these day 7-infected mice, by collagenase digestion and gradient centrifugation. F) The total number of cells retrieved from the liver in the leukocyte fraction of the gradient was calculated. G) Myeloid populations were analysed by FACS and representative FACS plots from WT and TCRβδ $^{-/-}$ mice are shown. H) Absolute numbers and I) proportions (out of total F4/80^{hi} Ly6G^{lo} cells) for Kupffer cells and monocytes are shown, where Kupffer cells = F4/80^{hi} Ly6G^{lo} CD11b^{lo} Ly6C^{lo} and monocytes = F4/80^{hi} Ly6G^{lo} CD11b^{hi} Ly6C^{hi}. J) The proportion of absolute numbers of Kupffer cells to absolute numbers of monocytes in the liver was calculated. K) Absolute numbers and L) proportions (out of total isolated cells) of Ly6G^{hi} cells and Ly6G$^+$ cells were determined. Data are taken from 2 experiments where n = 3-4 in each mouse strain in each experiment. M) DC populations were gated as shown. Absolute numbers of N) total CD11c$^+$ CD3$^-$ CD19$^-$ DCs and O) DC subtypes are shown (characterised as follows: NK DC = CD11b^{lo} CD8α$^-$ NK1.1$^+$ B220$^+$; Myeloid DC = CD11b$^+$ CD8α$^-$ NK1.1$^-$ B220$^-$; Lymphoid DC = CD11b$^-$ CD8α$^+$ NK1.1$^-$ B220$^-$; Mixed Myeloid/Lymphoid DC = CD11b$^-$ CD8α$^-$ NK1.1$^-$ B220$^-$; and Plasmacytoid DC = CD11b$^-$ CD8α$^-$ NK1.1$^-$ B220$^+$. P) The percentages of each DC subtype out of total CD11c$^+$ CD3$^-$ CD19$^-$ DCs was measured. For DC analysis, total DCs were measured in two experiments (where n = 4 in each stain) and DC subset data is from one experiment (where n = 4 in each strain), which has not been repeated. *p≤0.05 **p≤0.01 ***p≤0.001.

Absolute numbers of Kupffer cells are similar to those in WT mice, although the proportion of F4/80^{+} Ly6G^{lo} cells which are Kupffer cells is reduced (Fig 4.5H-J). Proportions and numbers of all Ly6G^{+} populations are greater than those in WT, although not significantly (Fig 4.5 K-L). The gating strategy used to phenotype DC populations is shown in Figure 4.5 M. Total DCs (CD11c^{+} CD3^{-} CD19^{-}) are significantly heightened in the absence of T cells and this is seen in all five DC subclasses examined (Fig 4.5 N-P).

4.5 There are subtle integral abnormalities in leukocytes in Tbet-deficient livers

Having identified differences in the response in TCRβδ$^{-/-}$ mice, we wanted to examine whether a loss of specific T helper lineage-associated factors contributes to this. The importance of Th1 cells in the control of *Salmonella* infection in mice is known (Ravindran et al., 2005, Pie et al., 1997). Therefore Tbet$^{-/-}$ mice, which have a defective capacity to induce Th1 cells, were infected alongside WT mice, and livers were examined at day 7 post-infection.

Livers from non-infected Tbet-deficient mice are similar in mass, appearance and histology to WT (Fig 4.6 A and data not shown). To identify any integral anomalies in leukocyte composition in the absence of Tbet, livers were examined by flow cytometry. In the absence of infection, livers from both strains have a similar leukocyte cellularity (Fig 4.6 B). Representative FACS plots of myeloid cells are shown and absolute numbers of all populations examined are similar in the absence of Tbet (Fig 4.6 C-H). However, the relative proportions of Kupffer cells and monocytes are higher and lower, respectively, than in WT livers (Fig 4.6 C-H).

Figure 4.6

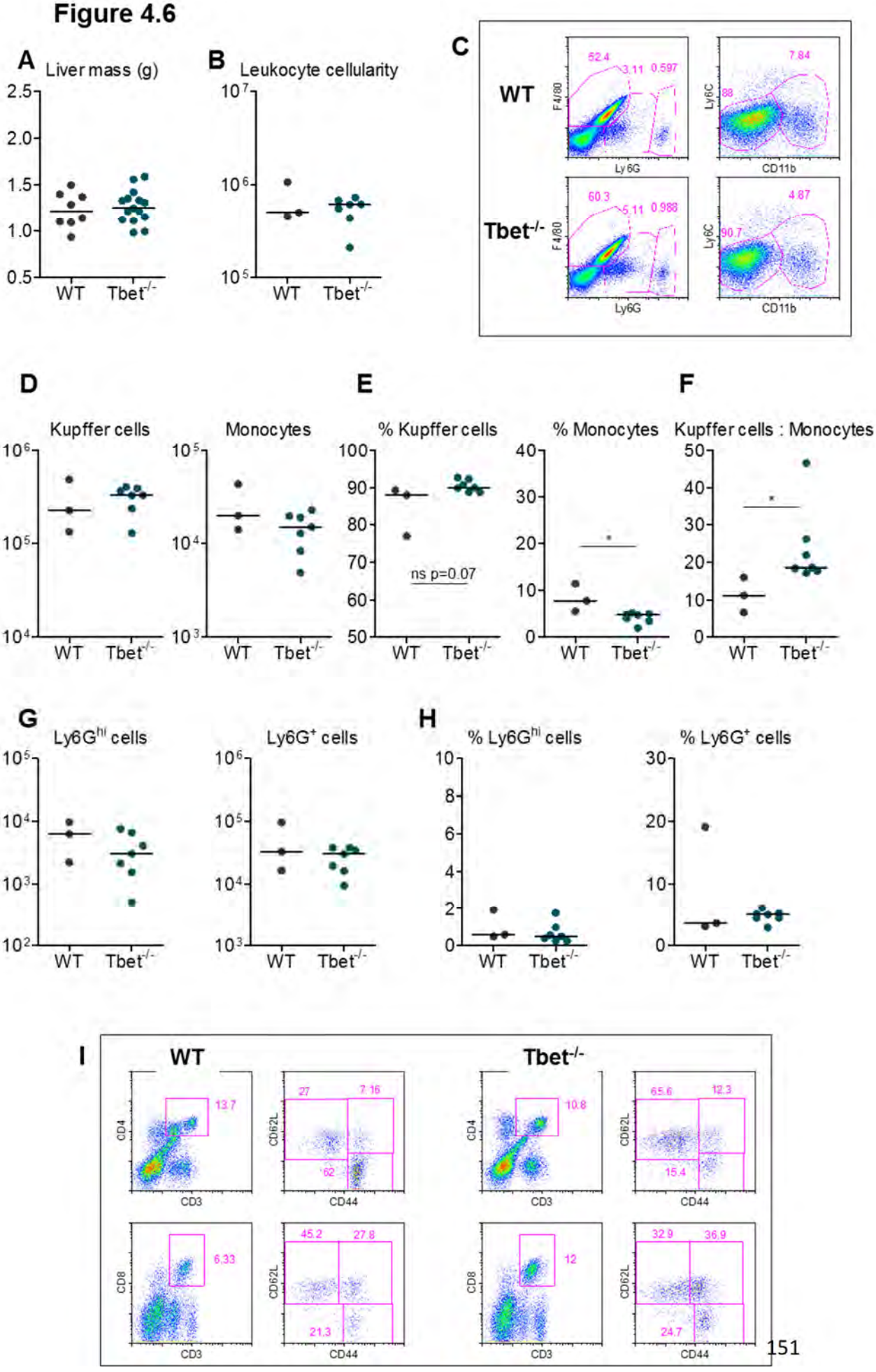
A
Liver mass (g)
2.5
2.0
1.5
1.0
0.5
WT
Tbet-/-
B
Leukocyte cellularity
10^7
10^6
10^5
WT
Tbet-/-
C
WT
Tbet-/-
F4/80
Ly6G
52.4
3.11
0.597
60.3
5.11
0.988
Ly6C
CD11b
88
7.84
90.7
4.87
D
Kupffer cells
Monocytes
E
% Kupffer cells
ns p=0.07
% Monocytes
F
Kupffer cells : Monocytes
G
Ly6G^hi cells
Ly6G+ cells
H
% Ly6G^hi cells
% Ly6G+ cells
I
WT
Tbet-/-
CD4
CD3
13.7
10.8
CD62L
CD44
27
7.16
62
65.6
12.3
15.4
CD8
6.33
12
45.2
27.8
21.3
32.9
36.9
24.7

Figure 4.6 continued

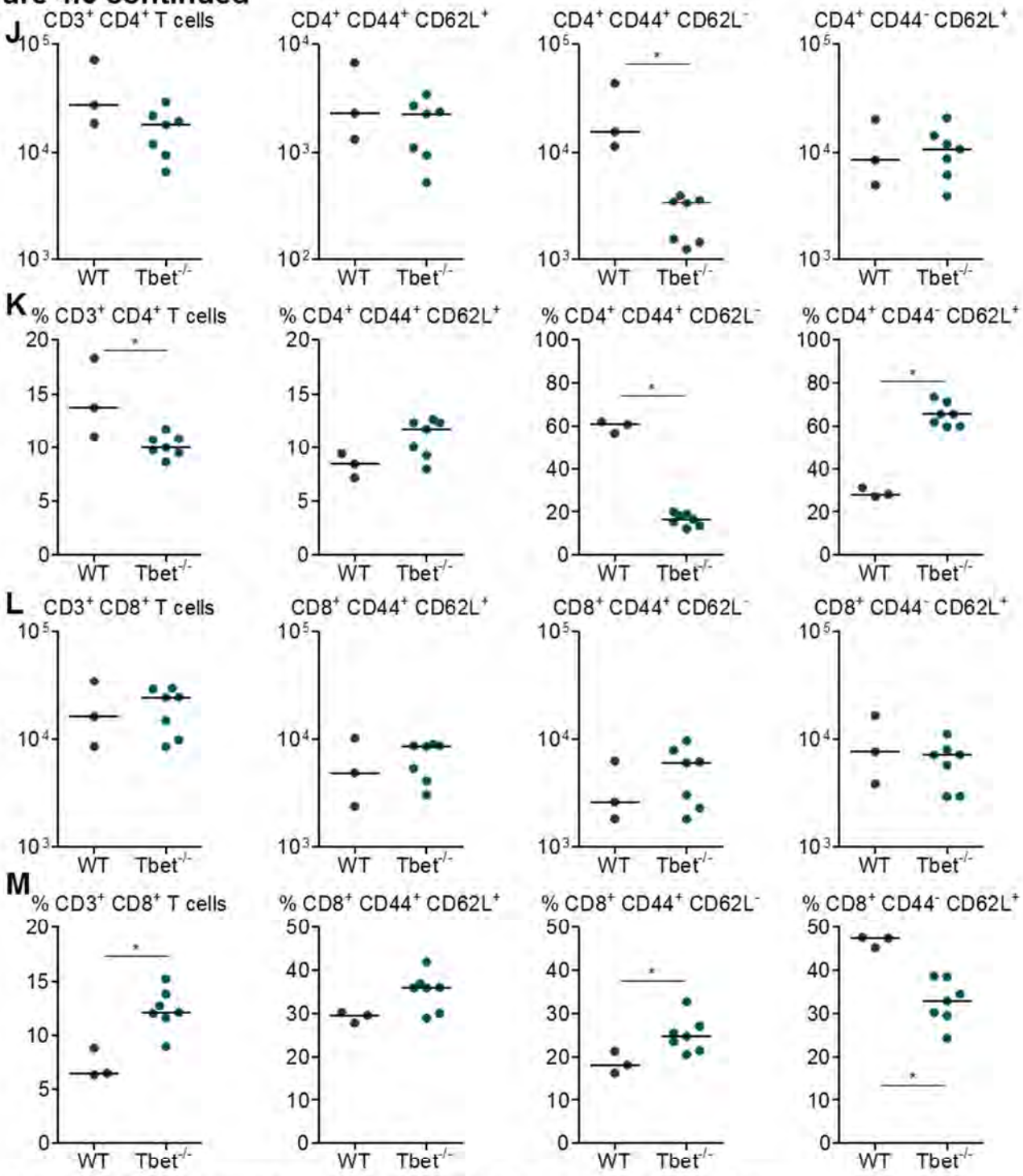

Figure 4.6 Tbet-deficient livers have subtle differences in T cell populations
Livers were removed from non-infected WT and Tbet $^{-/-}$ mice and A) liver mass was measured. Leukocytes were isolated from the livers of these non-infected mice, by collagenase digestion and gradient centrifugation. B) The total number of cells retrieved from the liver in the leukocyte fraction of the gradient was calculated. C) Myeloid populations were analysed by FACS and representative FACS plots from WT and Tbet $^{-/-}$ mice are shown. D) Absolute numbers and E) proportions (out of total F4/80^{hi} Ly6G^{lo} cells) for Kupffer cells and monocytes are shown, where Kupffer cells = F4/80^{hi} Ly6G^{lo} CD11b^{lo} Ly6C^{lo} and monocytes = F4/80^{hi} Ly6G^{lo} CD11b^{hi} Ly6C^{hi}. F) The proportion of absolute numbers of Kupffer cells to absolute numbers of monocytes in the liver was calculated. G) Absolute numbers and H) proportions (out of total isolated leukocytes) of Ly6G^{hi} cells and Ly6G^{+} cells were determined. T cells were examined by FACS for activation status, as identified by expression of CD62L and CD44. Activated effector T cells are described by CD62L^{lo} CD44^{+}; CD62L^{+} CD44^{+} cells are referred to as the central memory compartment; and CD62L^{+} CD44^{-} are naïve. I) Representative FACS plots from WT and Tbet $^{-/-}$ mice are shown. J) Absolute numbers and K) proportions (out of total lymphocyte-sized cells isolated) are shown for the indicated CD4^{+} T cell subsets, and in L) and M) for the indicated CD8^{+} T cell subsets. Data are taken from 1 experiment where n = 3 (in WT mice) and n = 7 (in Tbet $^{-/-}$ mice). *p≤0.05 **p≤0.01 ***p≤0.001.

There are subtle differences in the T cell populations of Tbet-deficient mice, and representative FACS plots are shown (Fig 4.6 I). Total $CD3^+$ $CD4^+$ T cell numbers are reduced and this is due to significantly reduced activated $CD4^+$ T cells (Fig 4.6 J). Whilst naïve $CD4^+$ T cell numbers are equivalent to WT, the proportion of these cells (out of total $CD3^+$ $CD4^+$ cells) is significantly higher (Fig 4.6 J-K). Numbers of $CD3^+$ $CD8^+$ T cells are similar to WT although a significantly greater proportion of leukocytes are $CD8^+$ in the absence of Tbet (Fig 4.6 L-M). There are also significantly greater proportions of activated and lower proportions of naïve $CD8^+$ T cells in Tbet-deficient mice (Fig 4.6 L-M).

4.5.1 Tbet is required for normal inflammatory lesion development in the liver

After infection, $Tbet^{-/-}$ mice have greater hepatomegaly that WT mice and bacterial numbers are significantly higher (Fig 4.7 A-B). Livers from these mice have similar signs of external pathology to WT livers (data not shown). Although inflammatory lesions develop in $Tbet^{-/-}$ mice, these are smaller and less frequent than in WT mice, and contain fewer T cells (Fig 4.7 C-E). There is a tendency for a higher sinusoidal distribution of $F4/80^+$, $CD11c^+$ and $F4/80^+$ $CD11c^+$ cells.

4.5.2 There is an enhanced regulatory environment in the absence of Tbet

Having identified a propensity for fewer $CD3^+$ T cells at the periphery of inflammatory lesions in the absence of Tbet, and considering the inability of $CD4^+$ cells to differentiate to Th1 cells in the absence of this transcription factor, we were interested in the phenotype of these peripheral $CD3^+$ cells. We hypothesised that there could be an increase in Treg cells in lesions in the absence of Tbet.

Figure 4.7

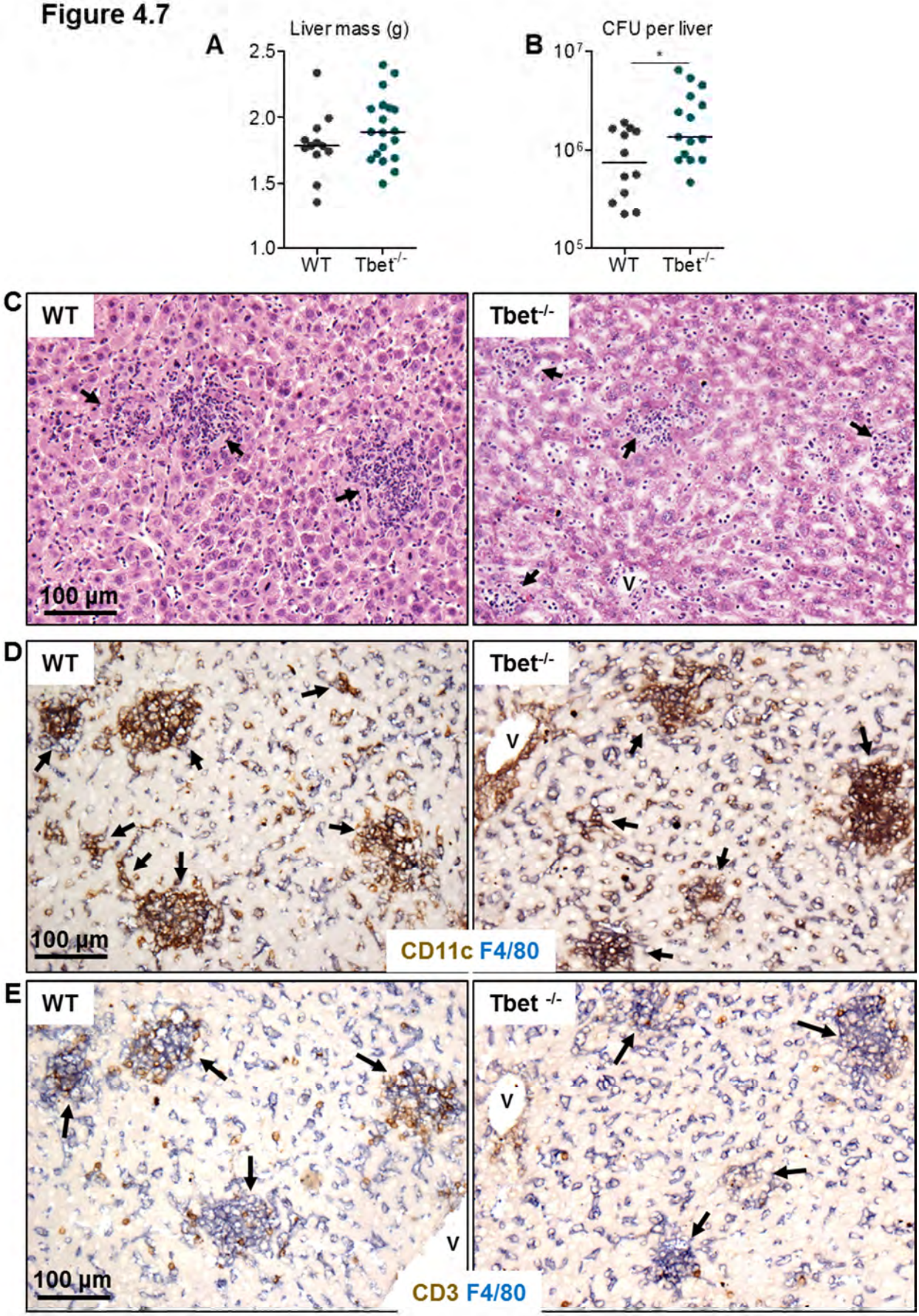

Figure 4.7 Tbet is required for normal inflammatory lesion development
WT and Tbet $^{-/-}$ mice were infected (i.p.) with 5 x 10^5 CFU attenuated STm for 7 days. Livers were removed and A) liver mass and B) bacterial burden of the liver were determined in each strain. Development of inflammatory lesions and extent of hepatic leukocyte infiltration was assessed by C) H&E, and serial sections were stained by IHC where D) F4/80$^+$ cells = blue; CD11c$^+$ cells = brown; double positive F4/80$^+$ CD11c$^+$ cells = black and E) F4/80$^+$ cells = blue; CD3$^+$ cells = brown. V = vessel; black arrows indicate inflammatory lesions. Data are taken from multiple experiments where n ≥ 4 in each strain of mice in each experiment. *p≤0.05 **p≤0.01 ***p≤0.001.

To test this, we infected Tbet-deficient mice and looked for FoxP3$^+$ T cells in the liver at day 7 post-infection by IHC. In the absence of Tbet there are more CD3$^+$ FoxP3$^+$ cells detected in the liver after infection relative to WT mice (Fig 4.8 A-B). These cells are concentrated at the periphery of inflammatory lesions and in vascular regions. Total CD3$^+$ cells and Tregs were quantified per lesion in WT and Tbet$^{-/-}$ mice. Tbet$^{-/-}$ mice have fewer CD3$^+$ cells per lesion, yet more CD3$^+$ FoxP3$^+$ cells per lesion, thus the ratio of CD3$^+$ FoxP3$^+$ cells to CD3$^+$ cells is far greater in Tbet$^{-/-}$ mice (Fig 4.8 C-E). These data suggest that the presence of Tbet promotes an inflammatory environment, thus reducing numbers of regulatory cells.

Despite an increased Treg presence in Tbet-deficient mice, hepatic infiltration is substantial, as is indicated by increased leukocyte cellularity in the liver (Fig 4.9 A). Representative FACS plots of myeloid populations are shown in the absence of Tbet (Fig 4.9 B). Numbers of all myeloid populations examined are elevated, and this is particularly marked in Ly6G^{hi} cells, the proportion of which doubles in the absence of Tbet (Fig 4.9 C-G). Representative T cell FACS plots are shown in Figure 4.9 H.

T cell numbers are equivalent to WT livers, although the percentage of total leukocytes which are CD3$^+$ CD4$^+$ cells are significantly lower, and of these cells, a significantly reduced proportion are activated (Fig 4.9 I-L). These data suggest in the absence of Th1 differentiation there is a general increase in myeloid cells matched by a diminution of non-FoxP3$^+$ T cells in lesions.

Figure 4.8

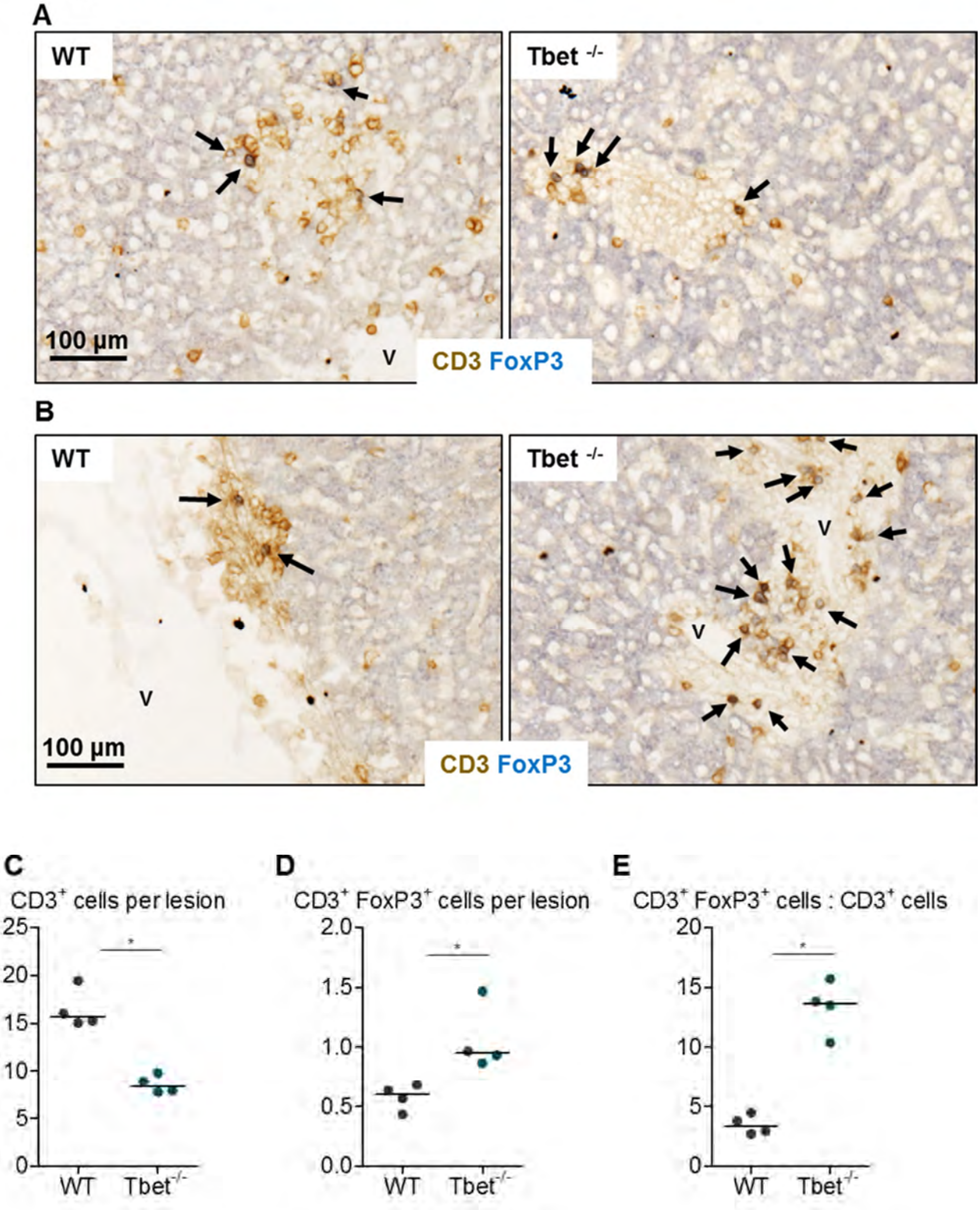

Figure 4.8 The environment is more regulatory in the absence of Tbet
WT and Tbet $^{-/-}$ mice were infected (i.p.) with 5 x 10^5 CFU attenuated STm for 7 days (as in Figure 4.7). Livers were removed and T cells were analysed by IHC in A) parenchymal areas and B) adjacent to vessels, where $CD3^+$ cells = brown and $CD3^+$ $FoxP3^+$ cells = black. Double positive $CD3^+$ $FoxP3^+$ cells are indicated with black arrows. T cells were quantified per lesion by measuring the mean of 30 in lesions distributed across the entire liver section. C) Mean number of $CD3^+$ cells per inflammatory lesion; D) mean number of $CD3^+$ $FoxP3^+$ cells per lesion; E) the proportion of $CD3^+$ cells to $CD3^+$ $FoxP3^+$ cells per lesion was calculated. Images are representative of all livers examined. Data are taken from multiple experiments where n ≥ 4 in each strain of mice in each experiment. *p≤0.05 **p≤0.01 ***p≤0.001.

Figure 4.9

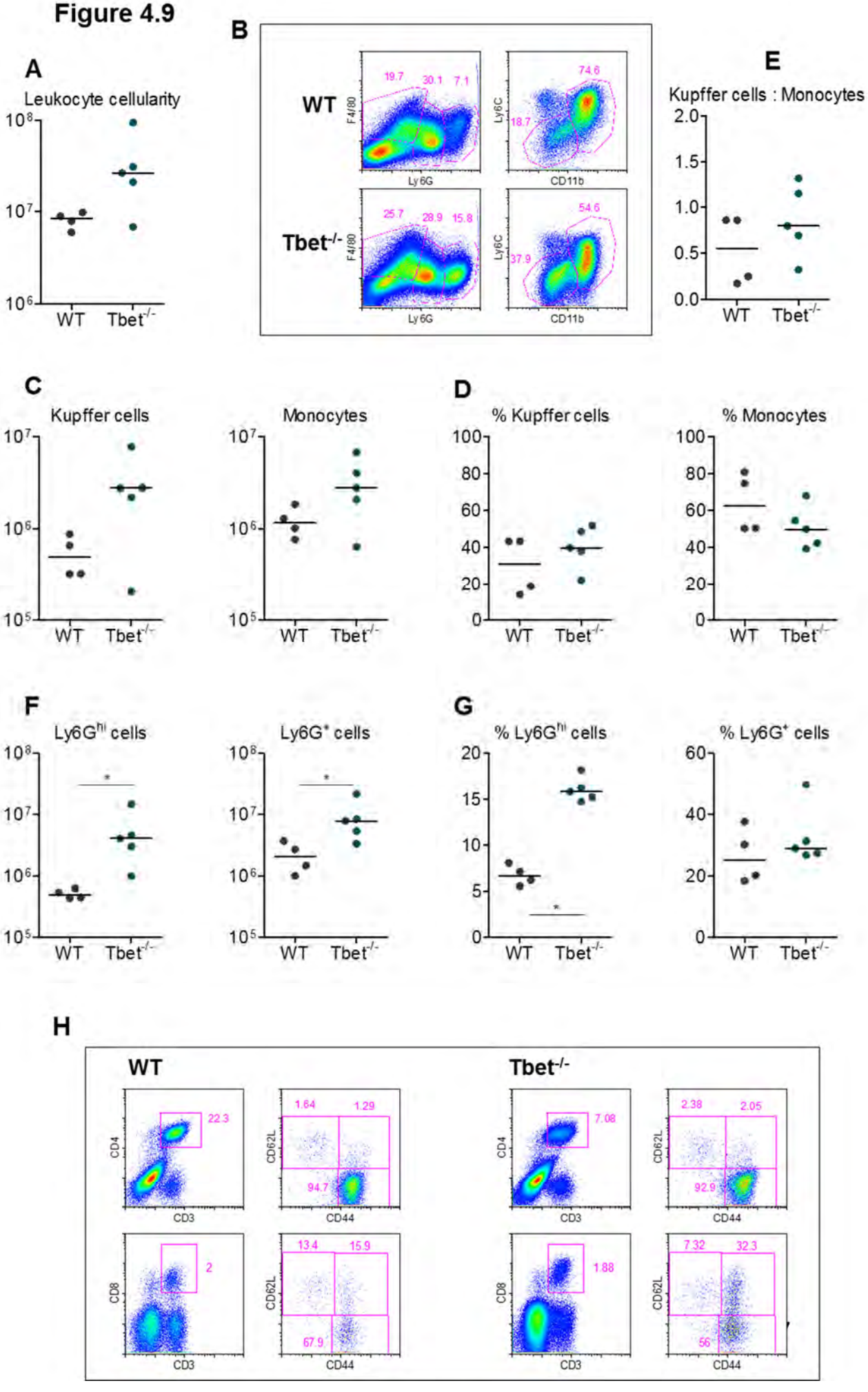
A
Leukocyte cellularity
WT
Tbet-/-
B
WT
Tbet-/-
F4/80
Ly6G
Ly6C
CD11b
19.7
30.1
7.1
74.6
18.7
25.7
28.9
15.8
54.6
37.9
E
Kupffer cells : Monocytes
C
Kupffer cells
Monocytes
D
% Kupffer cells
% Monocytes
F
Ly6Ghi cells
Ly6G+ cells
G
% Ly6Ghi cells
% Ly6G+ cells
H
WT
Tbet-/-
CD4
CD3
CD8
CD62L
CD44
22.3
1.64
1.29
94.7
2
13.4
15.9
67.9
7.08
2.38
2.05
92.9
1.88
7.32
32.3
56

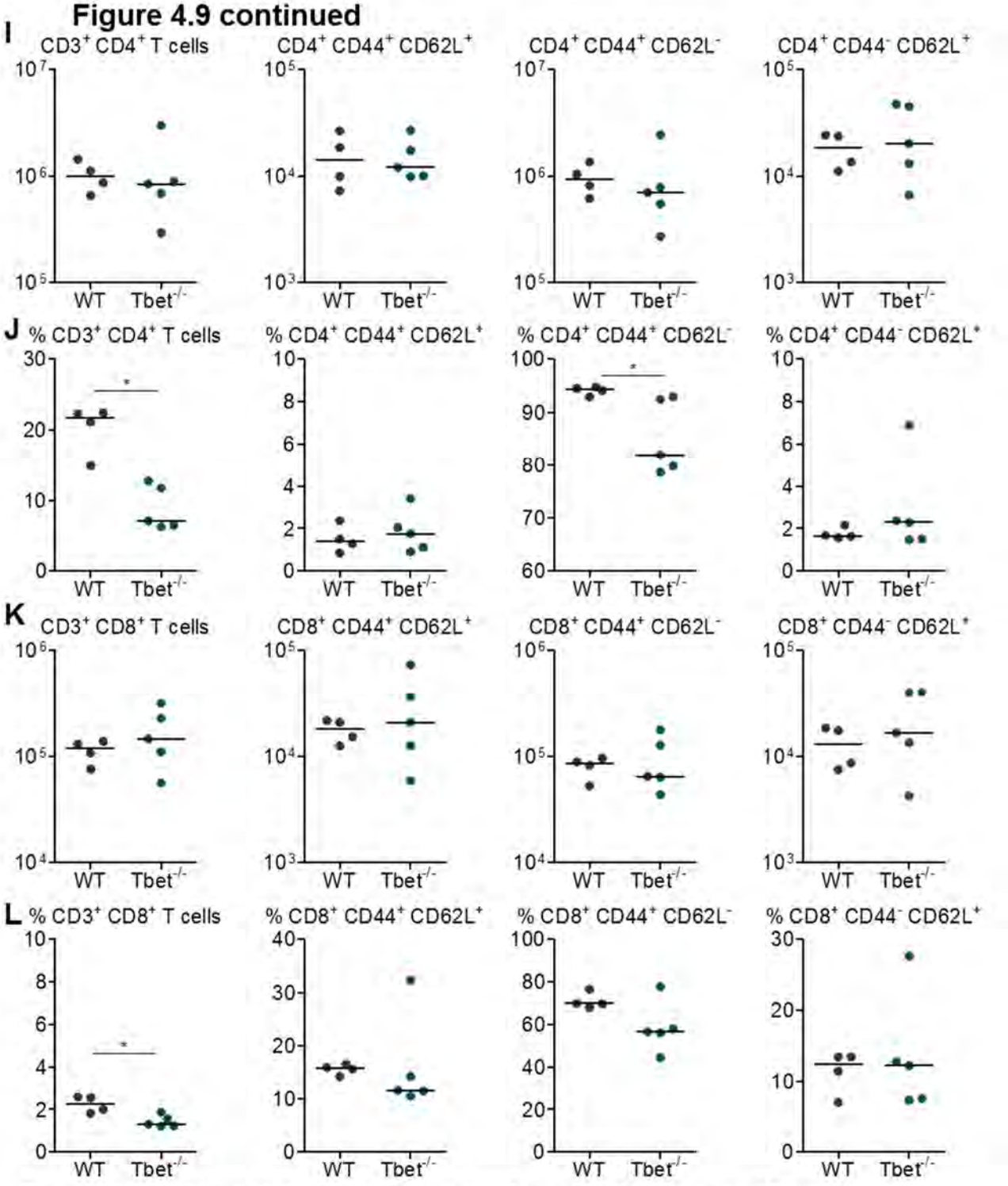

Figure 4.9 Myeloid populations in the liver are enhanced in the absence of Tbet

WT and Tbet $^{-/-}$ mice were infected (i.p.) with 5 x 10^5 CFU attenuated STm for 7 days (as in Figure 4.7). Livers were removed and leukocytes were isolated by collagenase digestion and gradient centrifugation. A) The total number of cells retrieved from the liver in the leukocyte fraction of the gradient was calculated. B) Myeloid populations were analysed by FACS and representative FACS plots from WT and Tbet $^{-/-}$ mice are shown. C) Absolute numbers and D) proportions (out of total F4/80^{hi} Ly6G^{lo} cells) for Kupffer cells and monocytes are shown, where Kupffer cells = F4/80^{hi} Ly6G^{lo} CD11b^{lo} Ly6C^{lo} and monocytes = F4/80^{hi} Ly6G^{lo} CD11b^{hi} Ly6C^{hi}. E) The proportion of absolute numbers of Kupffer cells to absolute numbers of monocytes in the liver was calculated. F) Absolute numbers and G) proportions (out of total isolated cells) of Ly6G^{hi} cells and Ly6G^{+} cells were determined. T cells were examined by FACS for activation status, as identified by expression of CD62L and CD44. Activated effector T cells = CD62L^{lo} CD44^{+}; central memory cells = CD62L^{+} CD44^{+}; and CD62L^{+} CD44^{-} = naïve. H) Representative FACS plots from WT and Tbet $^{-/-}$ mice are shown. I) Absolute numbers and J) proportions (out of total lymphocyte-sized cells isolated) are shown for the indicated CD4^{+} T cell subsets, and in K) and L) for the indicated CD8^{+} T cell subsets. Data are taken from one experiment where n = 4 (WT mice) and n = 5 (Tbet $^{-/-}$ mice), although the experiment has been repeated multiple times and these data are representative. *p≤0.05 **p≤0.01 ***p≤0.001.

4.5.3 Tbet expression in T cells drives an inflammatory phenotype

To test if these phenotypic observations are associated specifically with Tbet expression in T cells, we generated mixed bone marrow chimeras whereby total T cell-deficient mice were irradiated and then reconstituted with bone marrow harvested from either Tbet-sufficient or Tbet-deficient donor mice (Fig 4.10 A-B). Mice were infected as described above and livers were examined for inflammation at day 7 post-infection.

Although liver mass is similar, mice which lack Tbet in T cells have a higher bacterial load in the liver at day 7 post-infection, suggesting Tbet expression in T cells plays some role in facilitating bacterial clearance (Fig 4.10 C-D). We investigated the dynamics of $CD4^+$ T cell populations in these chimeric mice in more detail by flow cytometry, and representative FACS plots are shown (Fig 4.10 F). Despite equivalent leukocyte numbers being retrieved from livers of infected mice, there are approximately 6-fold fewer $CD3^+$ $CD4^+$ T cells in Tbet-deficient chimera livers (Fig 4.10 E-G). These cells also make up a significantly lower proportion of total lymphocytes isolated from the liver (Fig 4.10 H). In addition, number and proportion of activated $CD4^+$ T cells are significantly lower (Fig 4.10 G-H). These data indicate that Tbet in T cells is required for normal accumulation of $CD4^+$ T cells in the liver during infection.

Figure 4.10

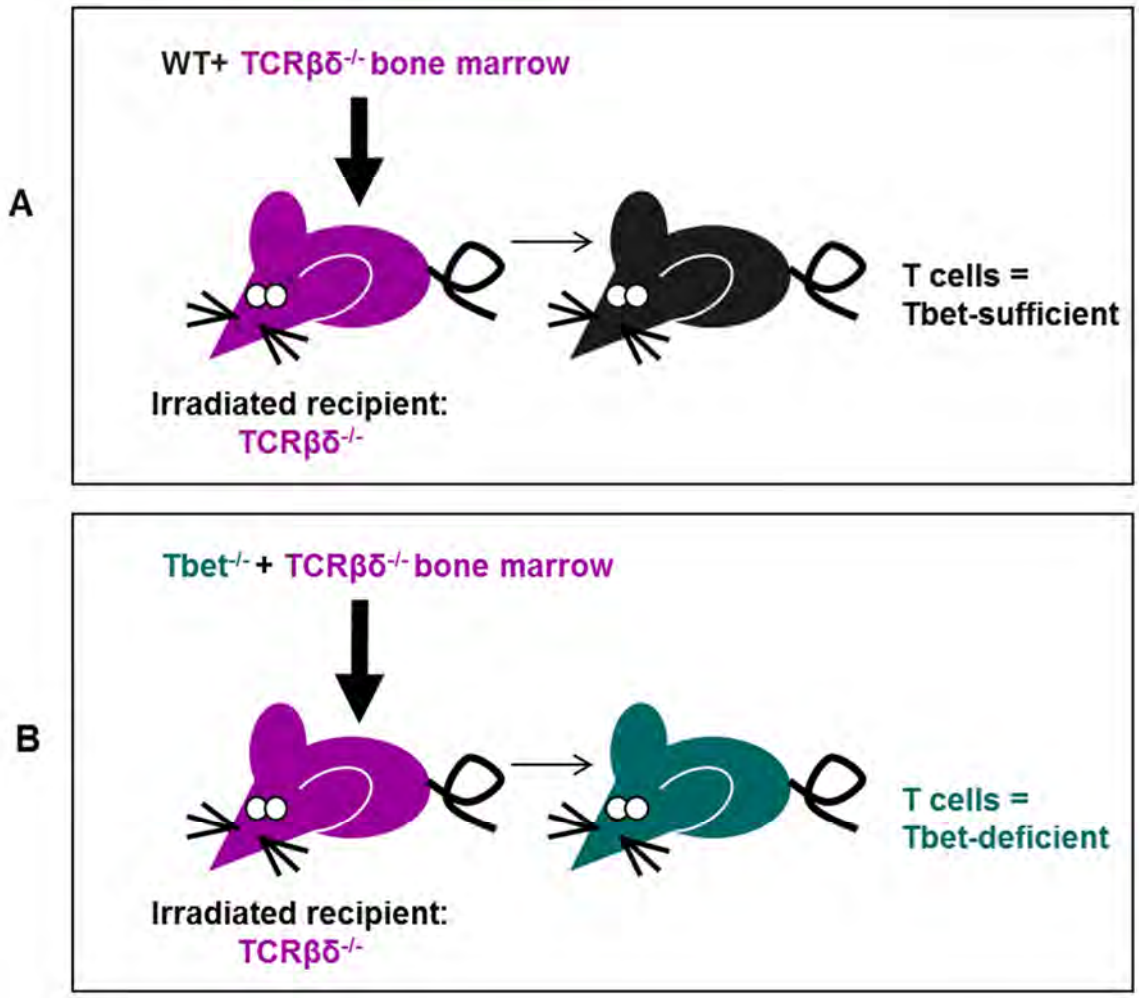

Figure 4.10 Tbet in T cells drives an inflammatory phenotype
Mixed bone marrow chimeras were generated whereby irradiated total T cell-deficient mice (TCRβδ $^{-/-}$) were reconstituted with TCRβδ $^{-/-}$ bone marrow cells (BM), supplemented with BM cells from either A) Tbet-sufficient (WT) or B) Tbet-deficient (Tbet $^{-/-}$) donor mice. Thus T cells in host mice were either Tbet-sufficient or Tbet-deficient. After reconstitution, both chimera groups were infected (i.p.) with 5 x 10^5 CFU attenuated STm for 7 days. Livers were removed and the C) liver mass and D) bacterial burden of the liver determined. Leukocytes were isolated by collagenase digestion and gradient centrifugation. E) The total number of cells retrieved from the liver in the leukocyte fraction of the gradient was calculated. $CD4^+$ T cells were examined by FACS for activation status, identified by CD62L expression, and for expression of FoxP3. F) Representative FACS plots are shown. G) Absolute numbers of $CD4^+$ T cells, activated $CD4^+$ T cells and $FoxP3^+$ $CD4^+$ T cells and H) the proportions of these populations (out of total lymphocyte-sized cells isolated) are shown. On each graph, WT TCRβδ $^{-/-}$ = irradiated TCRβδ $^{-/-}$ mice reconstituted with TCRβδ $^{-/-}$ and WT BM; Tbet$^{-/-}$ TCRβδ $^{-/-}$ = irradiated TCRβδ $^{-/-}$ mice reconstituted with TCRβδ $^{-/-}$ and Tbet$^{-/-}$ BM. Data are taken from one experiment where n = 4 per chimera group. *p≤0.05 **p≤0.01 ***p≤0.001.

Figure 4.10 continued

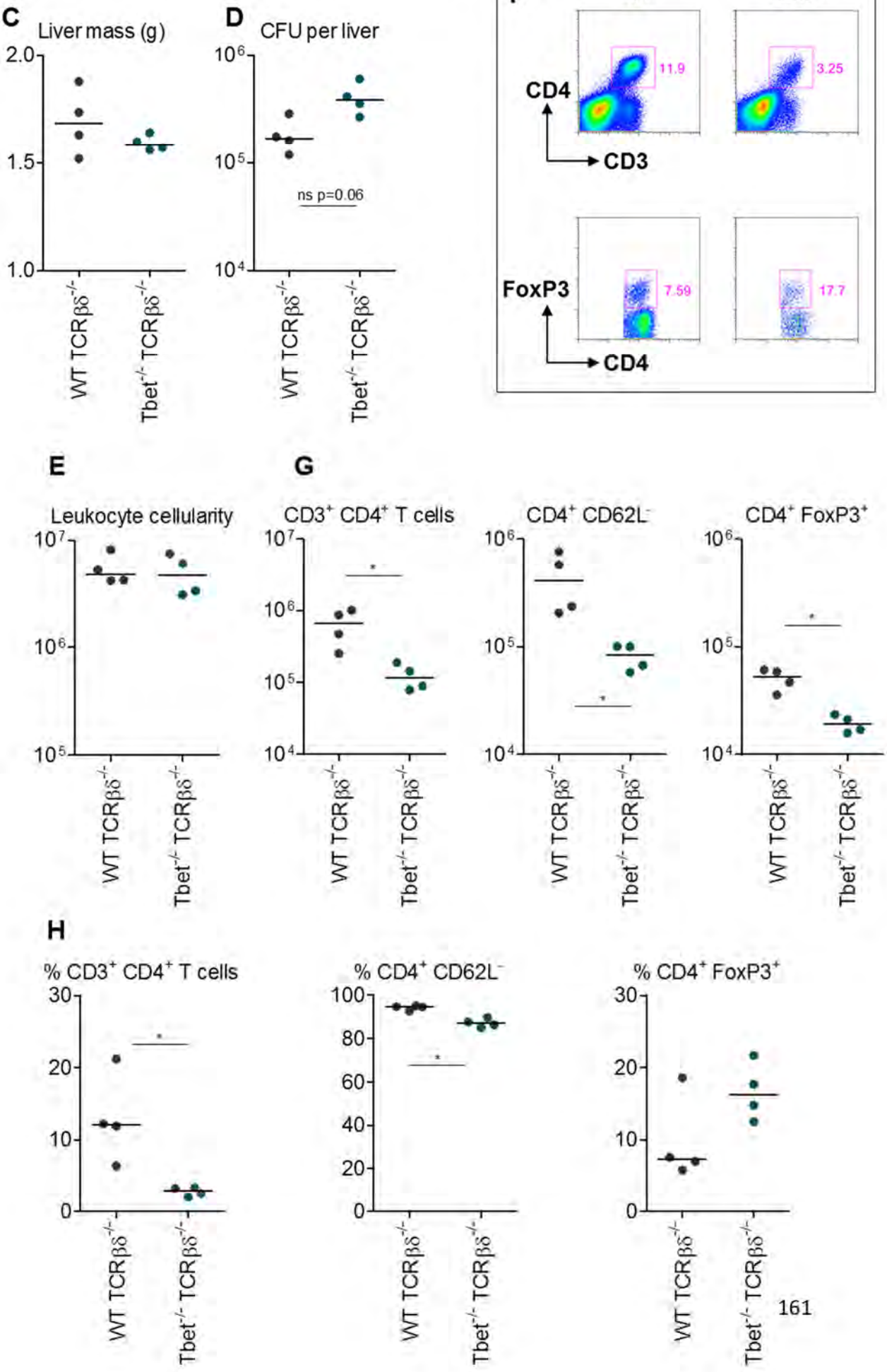

Considering that an absence of Tbet in $CD4^+$ T cells renders these cells unable to differentiate into cells of a Th1 phenotype, we were interested to see if the fate of T cells is altered in Tbet-deficient T cells. We hypothesised that $FoxP3^+$ T cell numbers may be altered in the absence of Tbet in T cells. Although absolute numbers of $CD4^+$ $FoxP3^+$ Tregs are lower in mice reconstituted with Tbet-deficient bone marrow, interestingly, the proportion of these cells is approximately doubled in these mice (Fig 4.10 G-H). Thus in the absence of Tbet in T cells, there is a heightened propensity for $CD4^+$ T cells to differentiate into a regulatory, FoxP3-expressing phenotype. These data suggest a role for T cell-expressed Tbet in driving a more pro-inflammatory (and less regulatory) environment.

4.6 Inflammation is abrogated in the absence of IFNγ

Interferon-γ is a Th1-associated cytokine, associated with macrophage activation during intracellular infections, and is important in the induction of inflammation in the liver following *Salmonella* infection (Kaufmann, 1993, Pie et al., 1997). To examine the role of IFNγ in our infection model, WT and IFNγ-deficient mice were infected as described above and liver inflammation was examined at day 7 post-infection.

Non-infected livers from IFNγ-deficient mice tend to be slightly smaller than those of age-matched WT mice, and this is far more apparent in spleen mass (Fig 4.11 A-B). Histologically, livers from both strains are similar (data not shown). Leukocyte cellularity is 2-3-fold lower in IFNγ-deficient mice relative to WT, and this correlates with diminished numbers of all myeloid populations examined (Fig 4.11 D-I). Representative FACS plots of myeloid and T cell staining are shown (Fig 4.11 D and J). Numbers of $CD3^+$ $CD4^+$ T cells are also lower in IFNγ-deficient mice relative to WT, and this is reflected in all sub-populations examined (Fig 4.11 K-L).

Figure 4.11

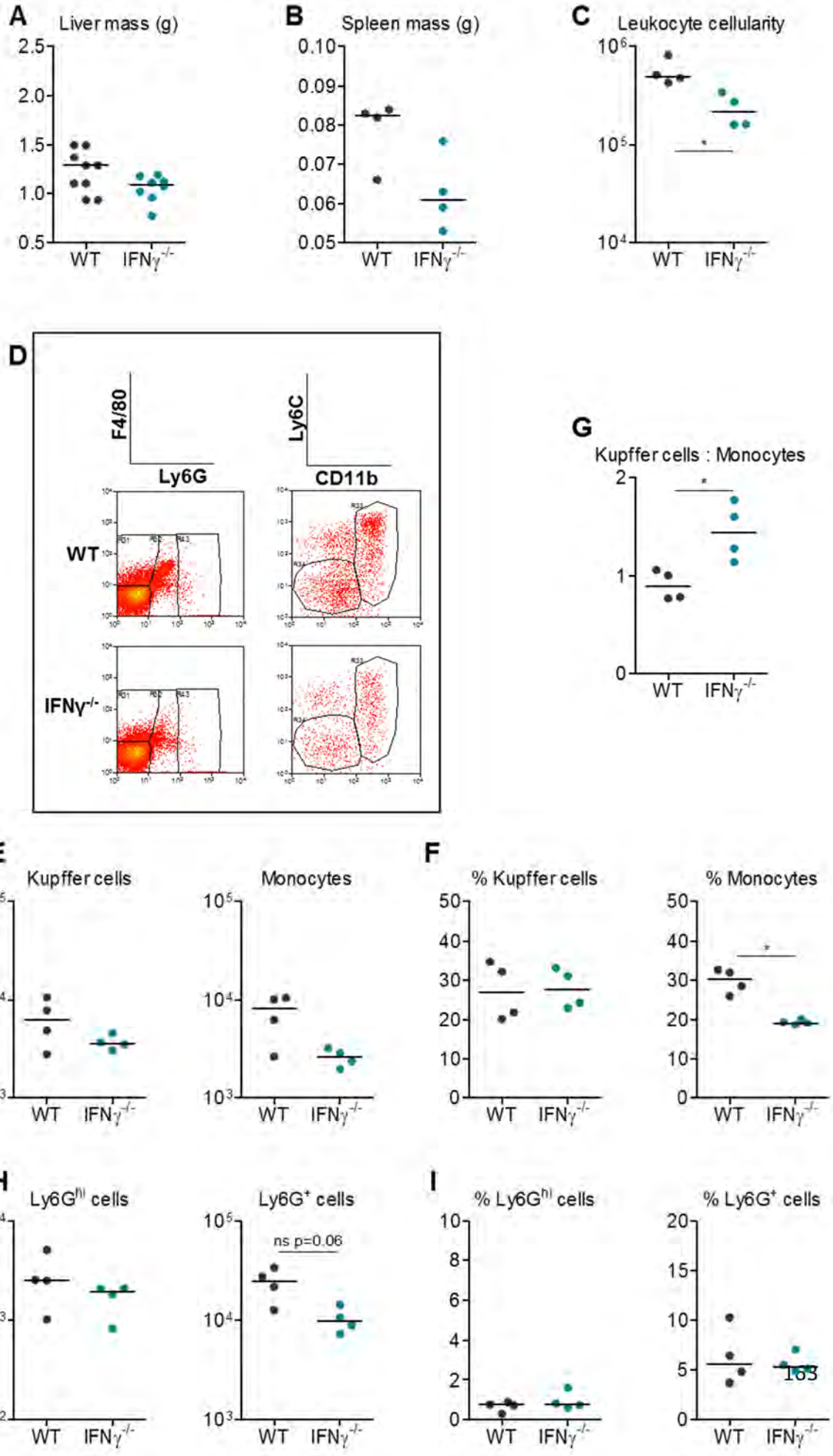
A
Liver mass (g)
2.5
2.0
1.5
1.0
0.5
WT
IFNγ-/-
B
Spleen mass (g)
0.10
0.09
0.08
0.07
0.06
0.05
WT
IFNγ-/-
C
Leukocyte cellularity
10^6
10^5
10^4
*
WT
IFNγ-/-
D
F4/80
Ly6G
Ly6C
CD11b
WT
IFNγ-/-
G
Kupffer cells : Monocytes
2
1
0
*
WT
IFNγ-/-
E
Kupffer cells
10^5
10^4
10^3
WT
IFNγ-/-
Monocytes
10^5
10^4
10^3
WT
IFNγ-/-
F
% Kupffer cells
50
40
30
20
10
0
WT
IFNγ-/-
% Monocytes
50
40
30
20
10
0
*
WT
IFNγ-/-
H
Ly6G^hi cells
10^4
10^3
10^2
WT
IFNγ-/-
Ly6G+ cells
10^5
10^4
10^3
ns p=0.06
WT
IFNγ-/-
I
% Ly6G^hi cells
10
8
6
4
2
0
WT
IFNγ-/-
% Ly6G+ cells
20
15
10
5
0
WT
IFNγ-/-

Figure 4.11 continued

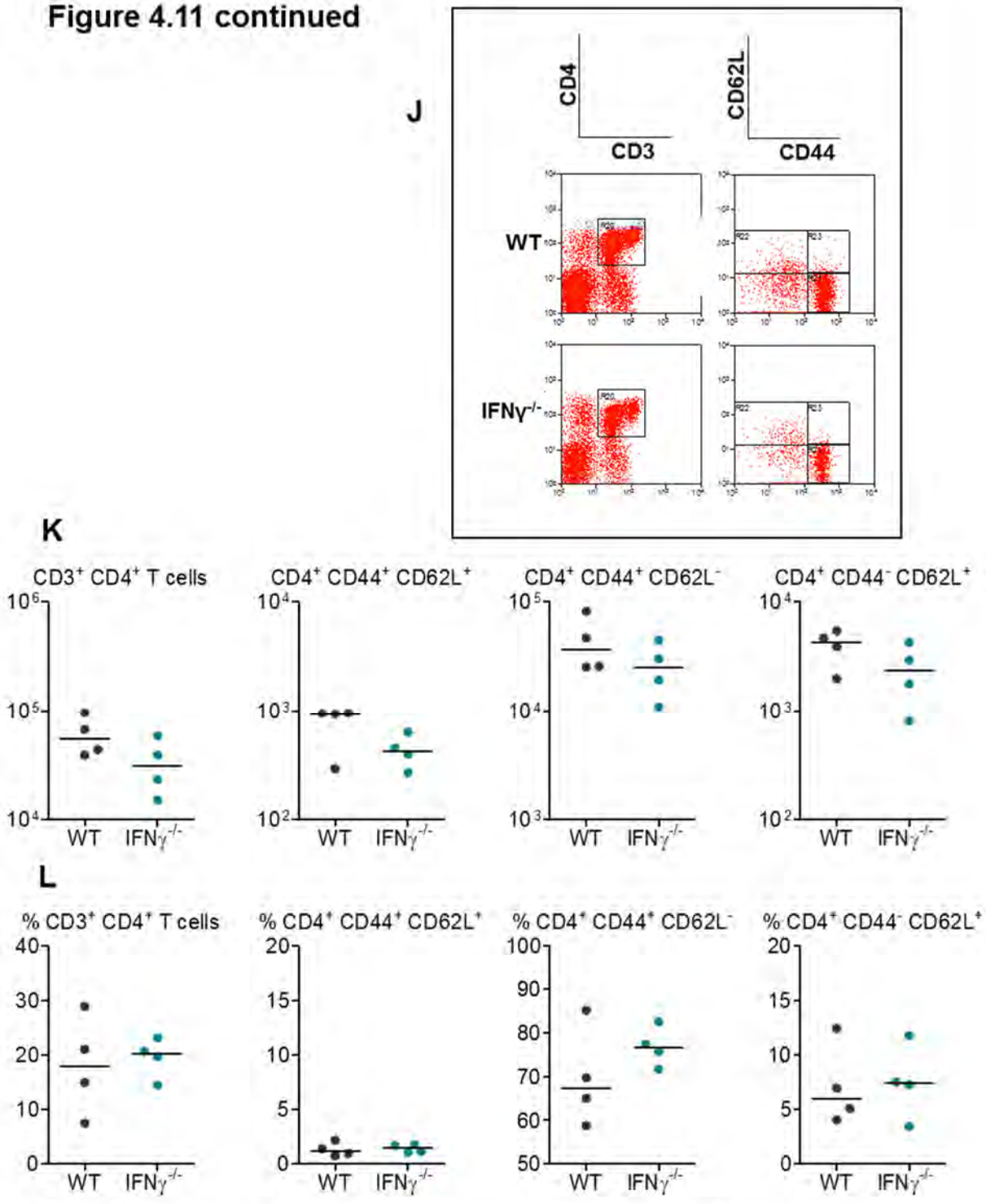

Figure 4.11 Leukocyte populations are dampened in interferon-γ-deficient mice
Livers and spleens were removed from non-infected WT and IFNγ $^{-/-}$ mice and A) liver and B) spleen mass were measured. Leukocytes were isolated from the livers by collagenase digestion and gradient centrifugation. C) The total number of cells retrieved from the liver in the leukocyte fraction of the gradient was calculated. D) Myeloid populations were analysed by FACS and representative FACS plots from WT and IFNγ $^{-/-}$ mice are shown. E) Absolute numbers and F) proportions (out of total F4/80^{hi} Ly6G^{lo} cells) for Kupffer cells and monocytes are shown, where Kupffer cells = F4/80^{hi} Ly6G^{lo} CD11b^{lo} Ly6C^{lo} and monocytes = F4/80^{hi} Ly6G^{lo} CD11b^{hi} Ly6C^{hi}. G) The proportion of absolute numbers of Kupffer cells to absolute numbers of monocytes in the liver was calculated. H) Absolute numbers and I) proportions (out of total isolated leukocytes) of Ly6G^{hi} cells and Ly6G^{+} cells were determined. CD4^{+} T cells were examined by FACS for activation status, as identified by expression of CD62L and CD44. Activated effector T cells = CD62L^{lo} CD44^{+}; central memory cells = CD62L^{+} CD44^{+}; and naïve cells = CD62L^{+} CD44^{-}. J) Representative FACS plots from WT and IFNγ $^{-/-}$ mice are shown. K) Absolute numbers and L) proportions (out of total lymphocyte-sized cells isolated) are shown for the indicated CD4^{+} T cell subsets. Data are taken from one experiment where n = 4 in each strain of mice. This experiment has been repeated multiple times and data are representative. *p≤0.05 **p≤0.01 ***p≤0.001.

At day 7 post-infection, whilst hepatomegaly is observed in IFNγ-deficient mice, it is generally not to the same extent as in WT (Fig 4.12 A). This contrast is far more apparent in splenomegaly, whereby spleen mass increases by a median 5-fold at day 7 in WT mice, and only by a median 2-3 fold in IFNγ-deficient mice (Fig 4.12 B). The median bacterial burden of the liver is 10-fold greater in mice lacking IFNγ, however, pathology is much lower (Fig 4.12 C-D). Livers from infected IFNγ$^{-/-}$ mice histologically resemble those from non-infected mice with occasional, sporadic inflammatory lesions. The absence of inflammatory F4/80^{+} and CD11c^{+} cells following infection is immediately apparent, as is the lack of T cells (Fig 4.12 D-E and data not shown).

Leukocyte cellularity of IFNγ$^{-/-}$ mice is lower than in WT mice following infection; absolute numbers of all myeloid populations examined are lower, although there is an increased proportion of monocytes (Fig 4.13 A-G). Similarly, numbers of CD3^{+} CD4^{+} and CD8^{+} T cell populations are lower in IFNγ$^{-/-}$ mice, however, there are greater proportions of naïve CD4^{+} and CD8^{+} T cells in the absence of IFNγ (Fig 4.13 H-L). These data support previous observations of deficient inflammation in the liver during bacterial infections/endotoxin treatment in the absence of IFNγ signalling (Hess et al., 1996, Toyonaga et al., 1994, Car et al., 1994).

Figure 4.12

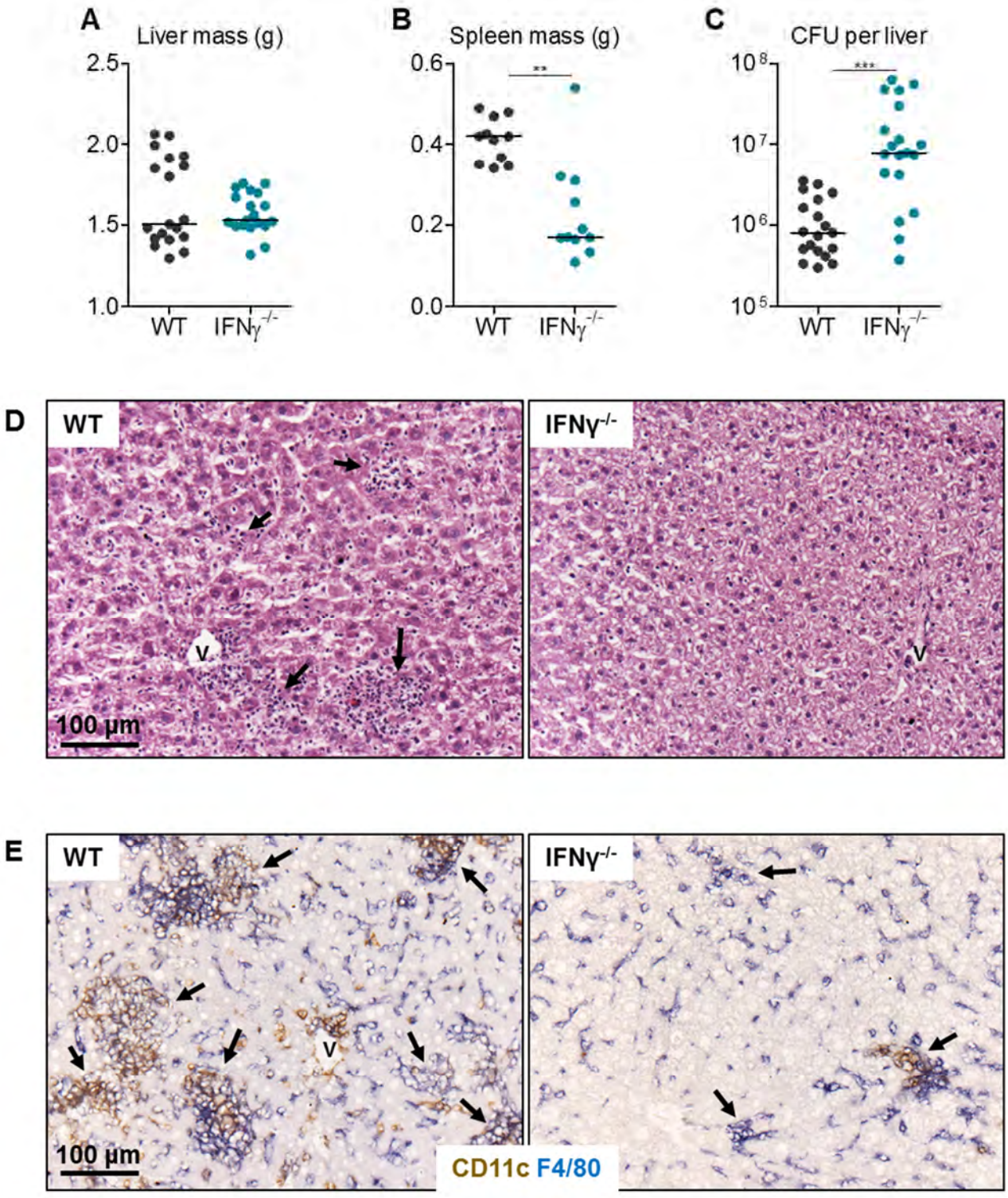

Figure 4.12 Hepatic pathology is severely diminished during infection in interferon-γ-deficient mice

WT and IFNγ $^{-/-}$ mice were infected (i.p.) with 5 x 10^5 CFU attenuated STm for 7 days. Livers and spleens were removed and A) liver mass, B) spleen mass and C) bacterial burden of the liver were determined in each strain of mice. Development of inflammatory lesions and extent of hepatic leukocyte infiltration was assessed by D) H&E and E) IHC where F4/80$^+$ cells = blue; CD11c$^+$ cells = brown; double positive F4/80$^+$ CD11c$^+$ cells = black. V = vessel; black arrows indicate inflammatory lesions. Data are taken from multiple experiments where n ≥ 4 in each strain of mice in each experiment. *p≤0.05 **p≤0.01 ***p≤0.001.

Figure 4.13

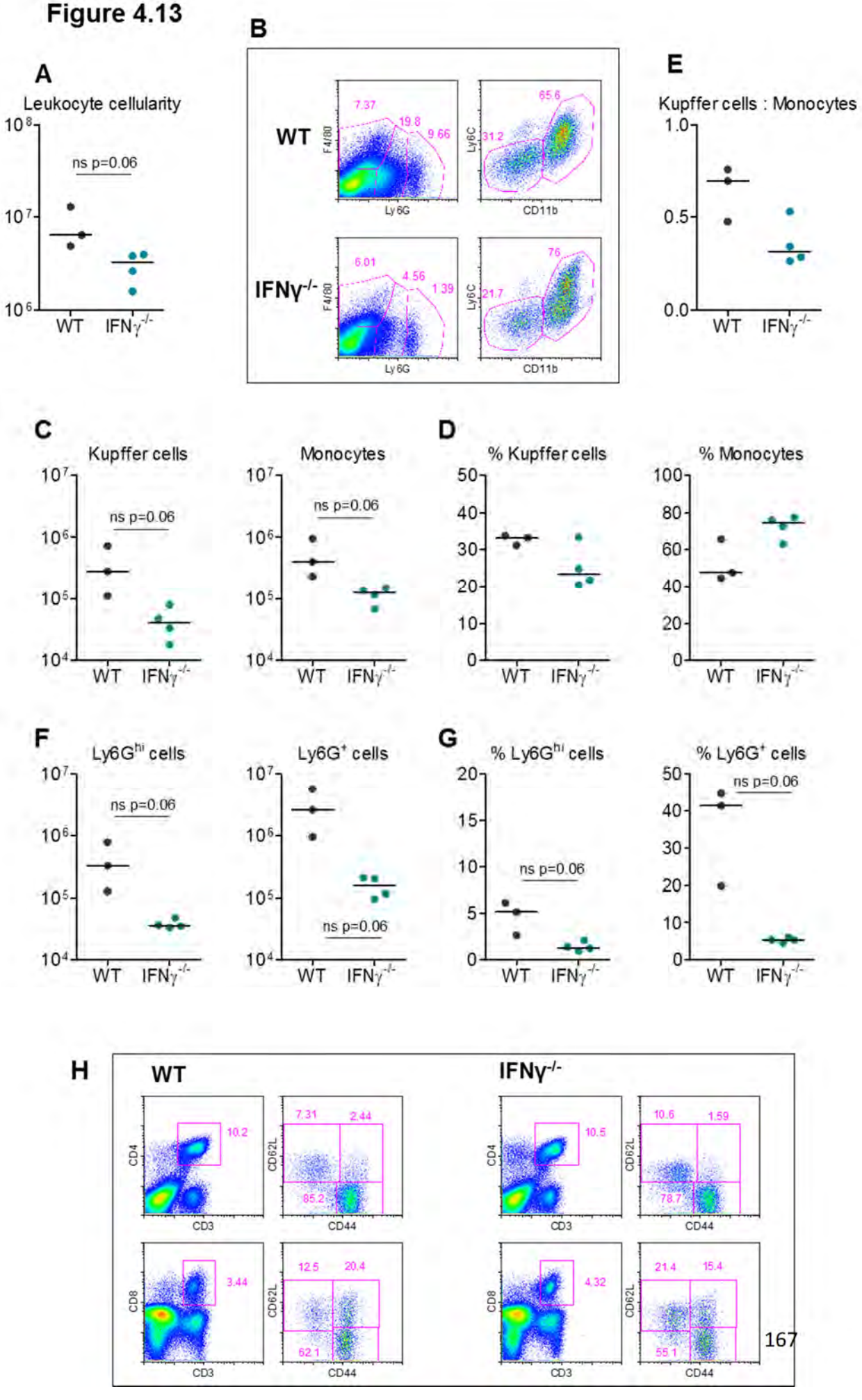
A
Leukocyte cellularity
ns p=0.06
WT
IFNγ-/-
B
WT
IFNγ-/-
F4/80
Ly6G
Ly6C
CD11b
7.37
19.8
9.66
65.6
31.2
6.01
4.56
1.39
76
21.7
E
Kupffer cells : Monocytes
C
Kupffer cells
Monocytes
D
% Kupffer cells
% Monocytes
F
Ly6Ghi cells
Ly6G+ cells
G
% Ly6Ghi cells
% Ly6G+ cells
H
WT
IFNγ-/-
CD4
CD3
CD62L
CD44
CD8
10.2
7.31
2.44
85.2
3.44
12.5
20.4
62.1
10.5
10.6
1.59
78.7
4.32
21.4
15.4
55.1

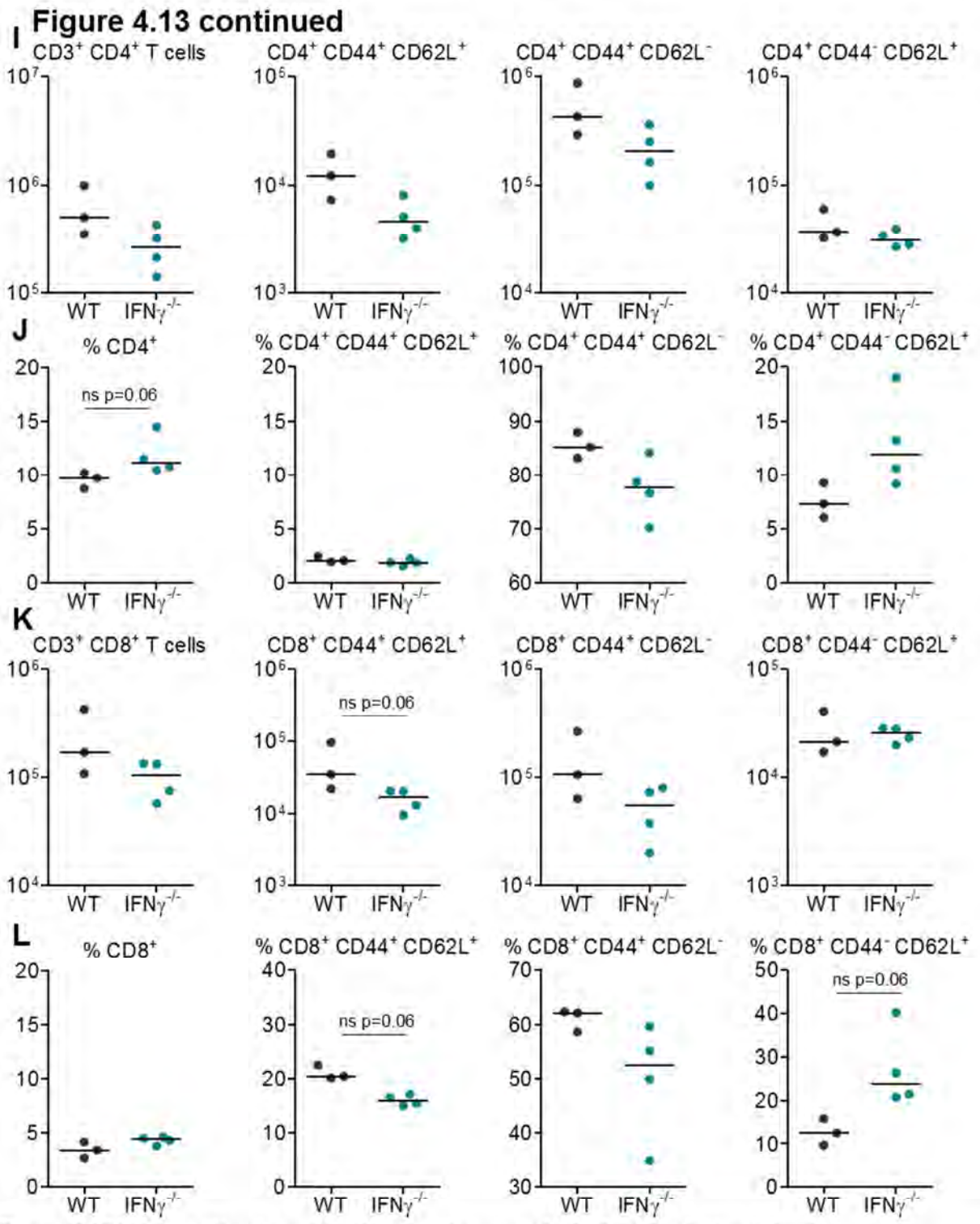

Figure 4.13 Inflammation is reduced in the absence of interferon-γ during infection
WT and IFNγ $^{-/-}$ mice were infected (i.p.) with 5 x 10^5 CFU attenuated STm for 7 days (as in Figure 4.12). Livers were removed and leukocytes were isolated by collagenase digestion and gradient centrifugation. A) The total number of cells retrieved from the liver in the leukocyte fraction of the gradient was calculated. B) Myeloid populations were analysed by FACS and representative FACS plots from WT and IFNγ $^{-/-}$ mice are shown. C) Absolute numbers and D) proportions (out of total F4/80^{hi} Ly6G^{lo} cells) for Kupffer cells and monocytes are shown, where Kupffer cells = F4/80^{hi} Ly6G^{lo} CD11b^{lo} Ly6C^{lo} and monocytes = F4/80^{hi} Ly6G^{lo} CD11b^{hi} Ly6C^{hi}. E) The proportion of absolute numbers of Kupffer cells to absolute numbers of monocytes in the liver was calculated. F) Absolute numbers and G) proportions (out of total isolated cells) of Ly6G^{hi} cells and Ly6G^{+} cells were determined. T cells were examined by FACS for activation status, as identified by expression of CD62L and CD44. Activated effector T cells = CD62L^{lo} CD44^{+}; central memory cells = CD62L^{+} CD44^{+}; and CD62L^{+} CD44^{-} = naïve. H) Representative FACS plots from WT and IFNγ $^{-/-}$ mice are shown. I) Absolute numbers and J) proportions (out of total lymphocyte-sized cells isolated) are shown for the indicated CD4^{+} T cell subsets, and in K) and L) for the indicated CD8^{+} T cell subsets. Data are taken from one experiment where n = 3 (WT mice) and n = 4 (IFNγ $^{-/-}$ mice), although the experiment has been repeated multiple times and these data are representative. *p≤0.05 **p≤0.01 ***p≤0.001.

4.6.1 IFNγ in haematopoietic cells is required for hepatic pathology

We next investigated the source of IFNγ necessary to drive inflammation in the liver during infection. To test this, we generated irradiation bone marrow chimeric mice whereby WT and IFNγ-deficient mice were irradiated and then reconstituted with either IFNγ-sufficient or IFNγ-deficient bone marrow cells from donor WT or IFNγ$^{-/-}$ mice. This enabled us to decipher whether the IFNγ necessary for inflammation and control of bacterial replication is derived from haematopoietic or non-haematopoietic populations. As control groups, we also generated chimeric mice whereby irradiated WT mice were reconstituted with WT donor bone marrow and irradiated IFNγ$^{-/-}$ mice were reconstituted with IFNγ$^{-/-}$ donor bone marrow (Fig 4.14 A-D). This enabled confirmation that any phenotypes were not simply effects of the procedure. Mice were infected as described and inflammation in the liver was examined at day 7 post-infection.

Liver mass in the WT to WT group is equivalent to that of normal WT (non-chimeric) mice at day 7, suggesting hepatomegaly occurs as normal in this group (in the absence of non-infected chimera controls, this provided a point of comparison) (Fig 4.15 A). Similarly, IFNγ$^{-/-}$ mice reconstituted with IFNγ$^{-/-}$ bone marrow, had smaller livers than the WT to WT group, as in straight non-chimeric IFNγ$^{-/-}$ mice. Hepatomegaly occurs in both the mixed bone marrow groups, suggesting IFNγ from either haematopoietic or non-haematopoietic cells can drive this phenotype, but that IFNγ is required.

Bacterial burden is similar in mice receiving WT bone marrow (despite hosts being IFNγ-sufficient or deficient), suggesting that IFNγ from haematopoietic cells is required for control of bacterial replication (Fig 4.15 B). Mice which lack all IFNγ have significantly higher bacterial loads than either of the WT donor cells groups.

Figure 4.14

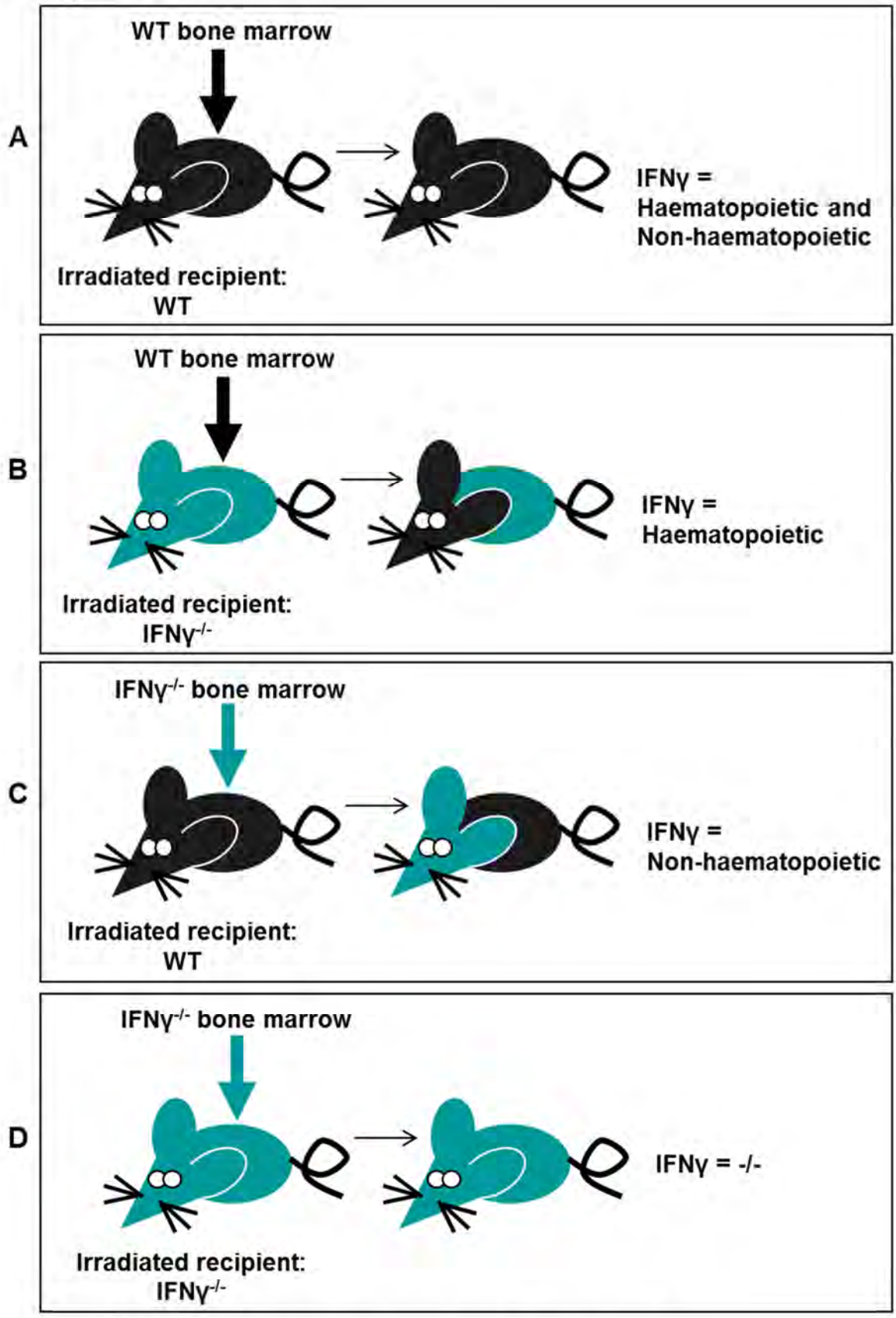

Figure 4.14 Generation of irradiation bone marrow chimera mice
Bone marrow (BM) chimeric mice were generated whereby irradiated WT and IFNγ$^{-/-}$ mice were reconstituted with either IFNγ-sufficient (WT) or IFNγ-deficient (IFNγ $^{-/-}$) BM cells from donor WT or IFNγ$^{-/-}$ mice. Four groups of mice were made whereby A) IFNγ was available from both haematopoietic and non-haematopoietic sources (WT to WT); B) IFNγ was available only from haematopoietic sources (WT to IFNγ$^{-/-}$); C) IFNγ was available only from non-haematopoietic sources (IFNγ$^{-/-}$ to WT); and D) mice were IFNγ-deficient. All mice were reconstituted for 10 weeks before infection (see Figure 4.15).

Figure 4.15

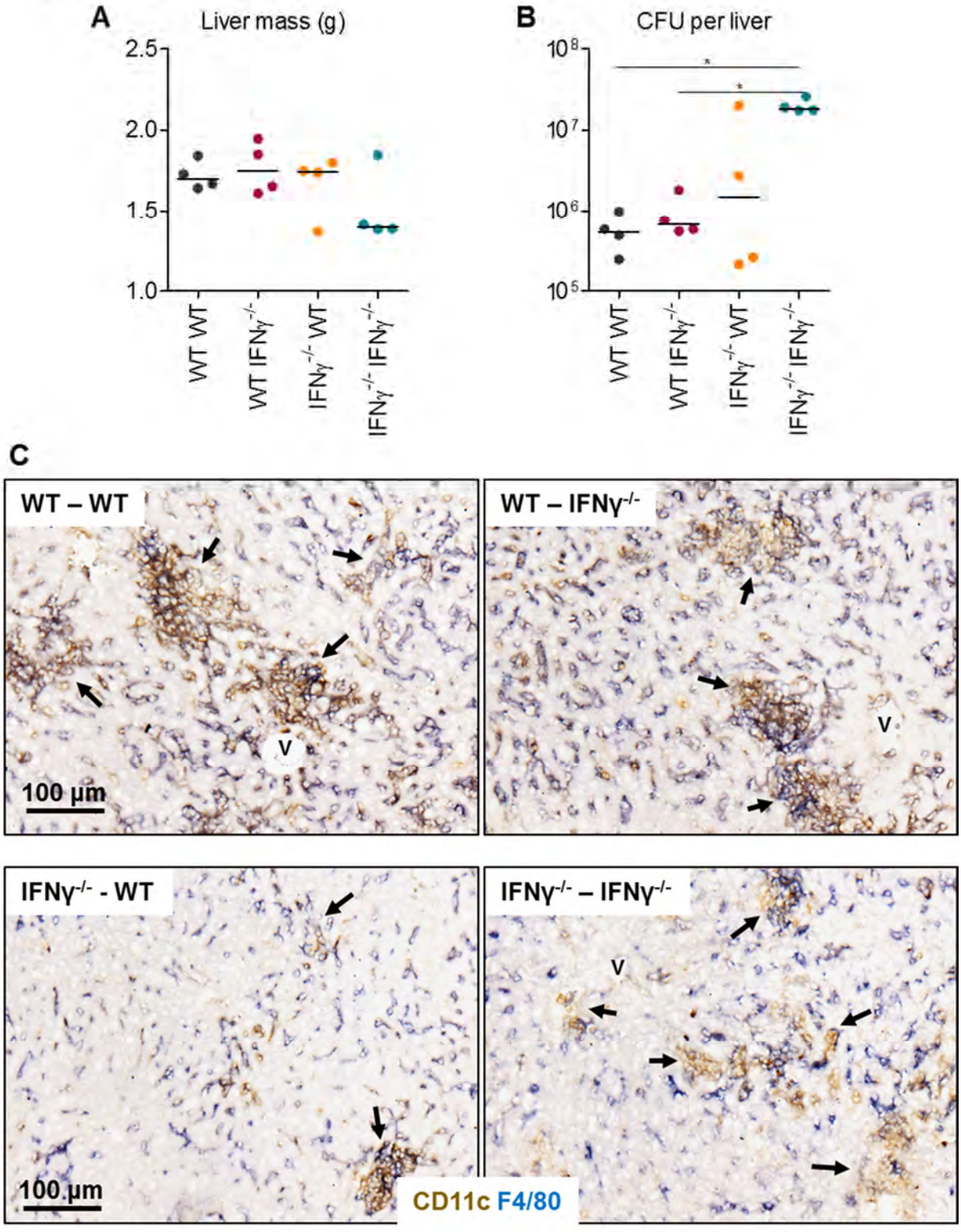

Figure 4.15 Interferon-γ from bone marrow-derived sources is required for inflammatory lesion formation

Irradiation bone marrow chimera mice were generated as described in Figure 4.14. All groups of mice were infected (i.p.) with 5 x 10^5 CFU attenuated STm for 7 days. Livers were removed and A) liver mass and B) bacterial burden of the liver were determined in each group. Groups are labelled as follows: the first strain describes the donor cells; the second describes the host: WT WT (WT BM cells into irradiated WT host); WT IFNγ$^{-/-}$ (WT BM cells into irradiated IFNγ$^{-/-}$ host); IFNγ$^{-/-}$ WT (IFNγ$^{-/-}$ BM cells into irradiated WT host); IFNγ$^{-/-}$ IFNγ$^{-/-}$ (IFNγ$^{-/-}$ BM cells into irradiated IFNγ$^{-/-}$ host). C) Development of inflammatory lesions and assessment of hepatic leukocyte infiltration was assessed by IHC where F4/80$^+$ cells = blue; CD11c$^+$ cells = brown; double positive F4/80$^+$ CD11c$^+$ cells = black. V = vessel; black arrows indicate inflammatory lesions. Data are taken from one experiment where n = 4 in each chimera group. *p≤0.05 **p≤0.01 ***p≤0.001.

When IFNγ is only available from non-haematopoietic sources, bacterial load is variable, suggesting that IFNγ from non-haematopoietic cells contributes to but cannot always control bacterial replication. In summary, hepatomegaly and bacterial burden are similar in mice which can produce IFNγ and this suggests that at this stage of the infection, there is some compensation for loss of IFNγ between different cellular sources.

This is also reflected by the extent of inflammation observed histologically. In the WT to WT group, inflammatory lesions form in the liver as they do in WT non-chimeric mice and show a similar cellular heterogeneity (Fig 4.15 C and data not shown). Inflammation and lesion development is seen to an equivalent extent in IFNγ-deficient mice which are reconstituted with WT bone marrow cells. However, mice which lack all IFNγ have reduced hepatic inflammation and lesion development. Lesions in these mice are less defined, although there is more inflammation than is seen in straight IFNγ$^{-/-}$ (non-chimeric) mice (as shown in Figure 4.12 E). This suggests that the chimera generation process intrinsically induces some degree of hepatic inflammation.

The significant finding is that when IFNγ is only available from non-haematopoietic sources (when irradiated WT mice are reconstituted with IFNγ$^{-/-}$ marrow cells), inflammation and lesion development is substantially diminished in the liver (Fig 4.15 C). There is a lack of sinusoidal F4/80^{+} cell accumulation and the few lesions which form are rare and are generally far smaller than those in IFNγ-sufficient mice. These data demonstrate that IFNγ from haematopoietic (bone marrow-derived) sources is required for hepatic inflammation and lesion development during infection.

4.6.2 IFNγ from haematopoietic sources drives Kupffer cell but not monocyte or or neutrophil accumulation in the liver

Leukocyte populations isolated from the liver were quantified in these chimeric mice, at day 7 post-infection by flow cytometry. Total cells retrieved during leukocyte isolation from livers is similar in all 4 groups of mice (Fig 4.16 A). Absolute number and proportion of Kupffer cells tends to be lower in mice reconstituted with bone marrow from IFNγ$^{-/-}$ mice (Fig 4.16 B-C). In contrast, absolute numbers of monocytes are similar in all groups of mice, and an increased proportion of F4/80^{+} Ly6G^{lo} cells are of monocyte phenotype in both groups of mice reconstituted with IFNγ-deficient bone marrow (Fig 4.16 C). This suggests that monocyte infiltration into the liver is not dependent on haematopoietic-derived IFNγ but that the accumulation of F4/80^{+} Kupffer cells is more haematopoietic-derived IFNγ-dependent. Thus Kupffer cell accumulation requires haematopoietic IFNγ to some extent.

This supports the histology whereby the majority of F4/80^{+} cells are single positive (they do not express CD11c) in mice reconstituted with IFNγ-deficient bone marrow (Fig 4.15 C). In contrast, many F4/80^{+} cells also express CD11c (black cells) in mice reconstituted with WT bone marrow, suggestive of Kupffer cell CD11c expression. Furthermore, the ratio of Kupffer cells to monocytes is generally higher in mice receiving WT bone marrow (Fig 4.16 D). This emphasises the more monocyte-dominant environment (reduced Kupffer cell accumulation) in the absence of haematopoietic-derived IFNγ.

Absolute numbers and proportions of Ly6G^{hi} cells are slightly elevated in all groups of chimeric mice relative to the WT to WT group (Fig 4.16 E). In contrast, the proportion (and to some extent) the absolute number of Ly6G^{+} cells is reduced in IFNγ-deficient recipient mice (Fig 4.16 E).

Figure 4.16

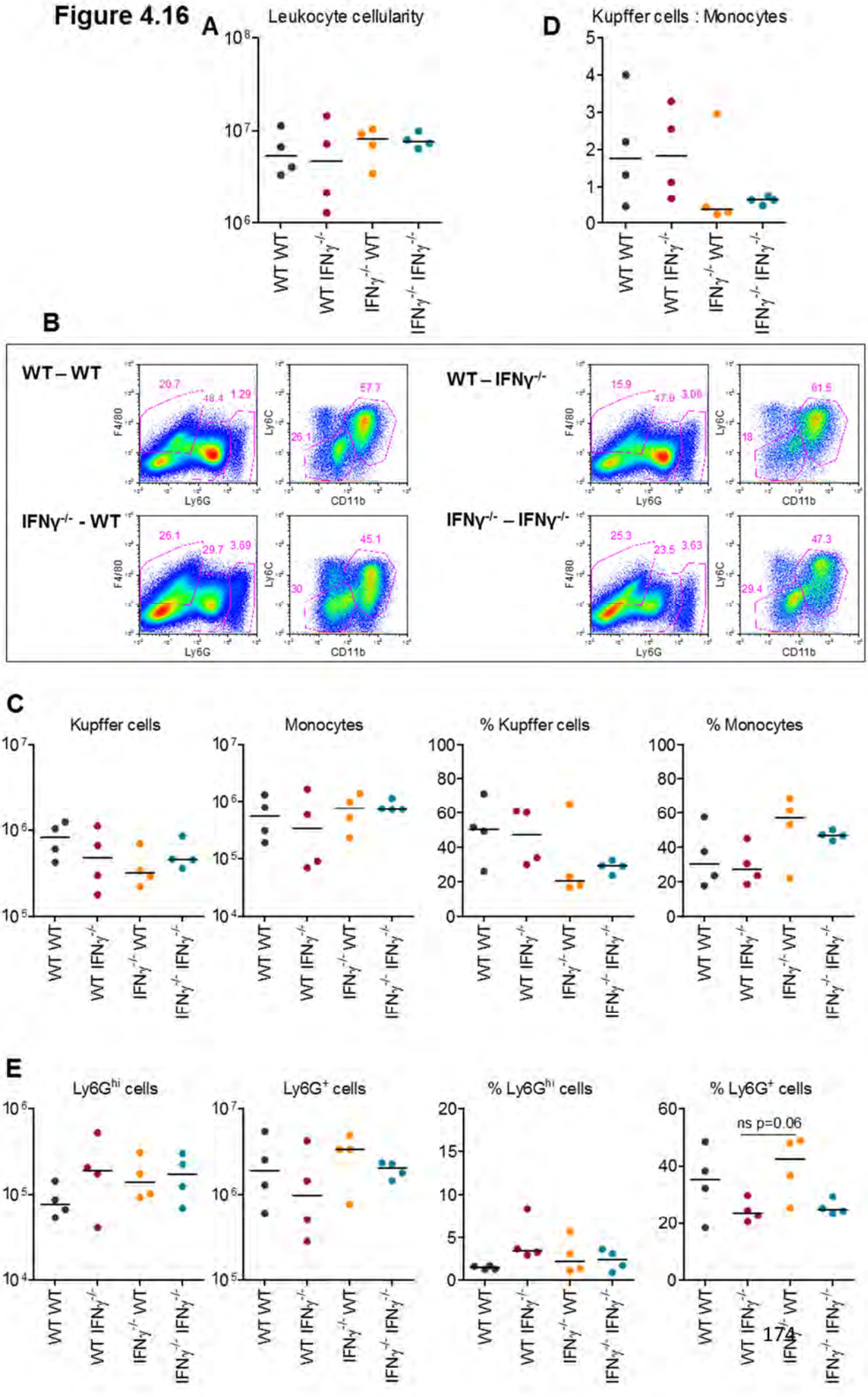
A
Leukocyte cellularity
D
Kupffer cells : Monocytes
WT WT
WT IFNγ-/-
IFNγ-/- WT
IFNγ-/- IFNγ-/-
B
WT – WT
WT – IFNγ-/-
IFNγ-/- - WT
IFNγ-/- – IFNγ-/-
F4/80
Ly6G
Ly6C
CD11b
C
Kupffer cells
Monocytes
% Kupffer cells
% Monocytes
E
Ly6Ghi cells
Ly6G+ cells
% Ly6Ghi cells
% Ly6G+ cells
ns p=0.06

Figure 4.16 Interferon-γ from bone marrow-derived sources drives Kupffer cell accumulation in the liver during infection

Irradiation bone marrow chimera mice were generated as described in Figure 4.14. Groups are labelled as follows: the first strain describes the donor cells; the second describes the host: WT WT (WT BM cells into irradiated WT host); WT IFNγ$^{-/-}$ (WT BM cells into irradiated IFNγ$^{-/-}$ host); IFNγ$^{-/-}$ WT (IFNγ$^{-/-}$ BM cells into irradiated WT host); IFNγ$^{-/-}$ IFNγ$^{-/-}$ (IFNγ$^{-/-}$ BM cells into irradiated IFNγ$^{-/-}$ host).

All groups of mice were infected (i.p.) with 5 x 10^5 CFU attenuated STm for 7 days. Livers were removed and leukocytes isolated by collagenase digestion and gradient centrifugation. A) Total cells retrieved from the liver in the leukocyte fraction of the gradient was calculated. B) Myeloid populations were analysed by FACS and representative FACS plots from each of the chimeric groups are shown. C) Absolute numbers and proportions (out of total F4/80^{hi} Ly6G^{lo} cells) for Kupffer cells and monocytes are shown, where Kupffer cells = F4/80^{hi} Ly6G^{lo} CD11b^{lo} Ly6C^{lo} and monocytes = F4/80^{hi} Ly6G^{lo} CD11b^{hi} Ly6C^{hi}. D) The proportion of absolute numbers of Kupffer cells to absolute numbers of monocytes in the liver was calculated. E) Absolute numbers and proportions (out of total isolated cells) of Ly6G^{hi} cells and Ly6G^{+} cells were determined. Data are taken from one experiment where n = 4 in each chimera group. *p≤0.05 **p≤0.01 ***p≤0.001.

This suggests that non-bone marrow-derived IFNγ is necessary to some extent for Ly6G$^+$ cell accumulation in the liver during infection, but that haematopoietic IFNγ can supplement this to some extent.

4.6.3 CD8$^+$ but not CD4$^+$ T cell dynamics are altered in the absence of haematopoietic IFNγ

Representative FACS plots of T cell populations are shown in Figure 4.17 A. Absolute numbers of CD3$^+$ CD4$^+$ T cells are similar in all groups, as are proportions of sub-populations of these cells (Fig 4.17 B-C). Whilst absolute numbers of CD3$^+$ CD8$^+$ T cells are similar in all groups, there are some small differences, particularly in proportions. Numbers and proportions of activated and naïve CD8$^+$ T cells are slightly reduced and slightly heightened respectively in groups with recipient IFNγ-deficient mice (Fig 4.17 D-E). The percentage of memory CD8$^+$ T cells is increased in all groups apart from the WT to WT group (Fig 4.17 E). These data suggest that CD4$^+$ T cell accumulation in the liver during infection is not IFNγ-dependent but that CD8$^+$ T cell sub-populations vary when IFNγ is available from different sources.

4.7 Inflammatory and anti-inflammatory cytokines

To examine the host response in the absence of other cytokines associated with inflammation, we infected mice deficient in TNFαR, IL6 or IL10 and assessed hepatic inflammation at day 7 post-infection.

Figure 4.17

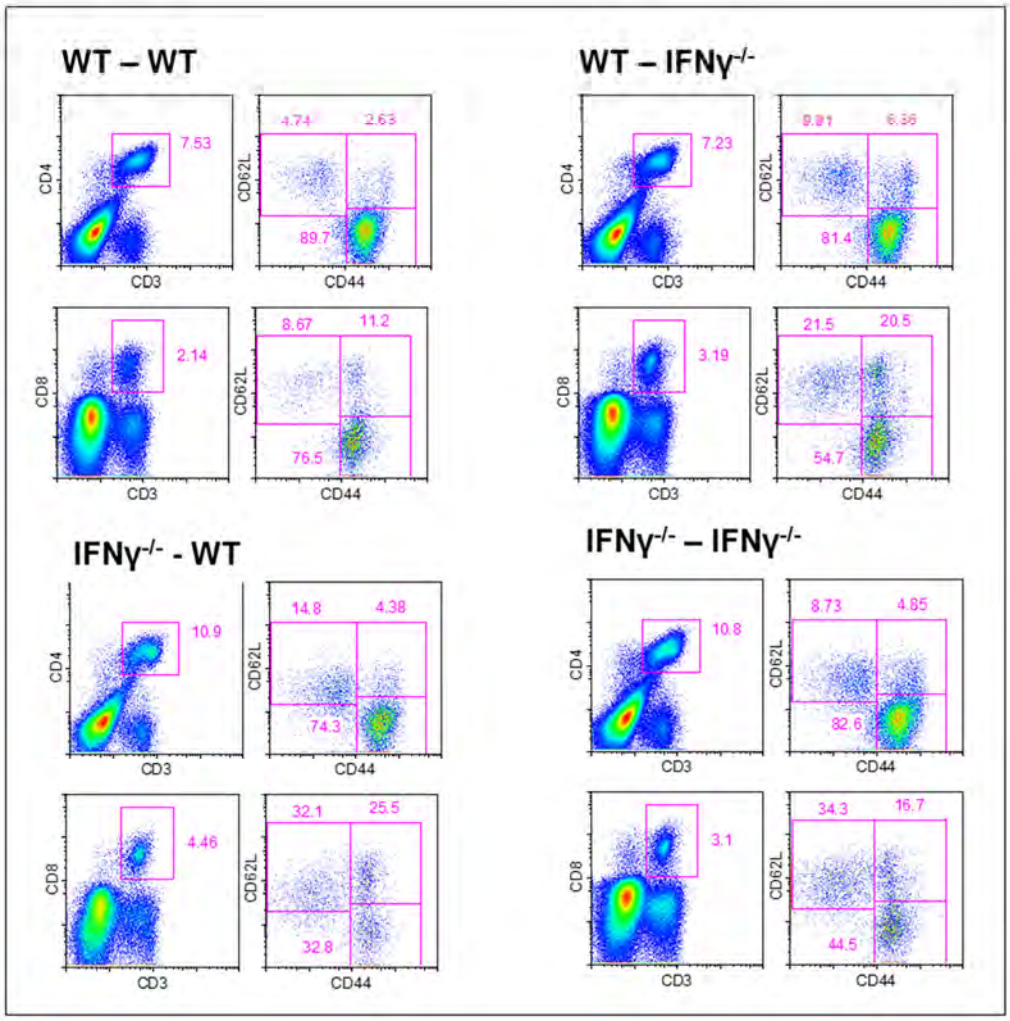

Figure 4.17 CD8⁺ T cell dynamics are altered during infection in the absence of haematopoietic interferon-γ

Irradiation bone marrow chimera mice were generated as described in Figure 4.14. Groups are labelled as follows: WT WT (WT BM cells into irradiated WT host); WT IFNγ$^{-/-}$ (WT BM cells into irradiated IFNγ$^{-/-}$ host); IFNγ$^{-/-}$ WT (IFNγ$^{-/-}$ BM cells into irradiated WT host); IFNγ$^{-/-}$ IFNγ$^{-/-}$ (IFNγ$^{-/-}$ BM cells into irradiated IFNγ$^{-/-}$ host).

All groups of mice were infected (i.p.) with 5 x 10^5 CFU attenuated STm for 7 days. Livers were removed and leukocytes isolated by collagenase digestion and gradient centrifugation. T cells were examined by FACS for activation status, as identified by expression of CD62L and CD44. Activated effector T cells = CD62L^{lo} CD44^{+}; central memory cells = CD62L^{+} CD44^{+}; and CD62L^{+} CD44^{-} = naïve. A) Representative FACS plots from each chimeric group are shown. B) Absolute numbers and C) proportions (out of total lymphocyte-sized cells isolated) are shown for the indicated CD4^{+} T cell subsets, and in D) and E) for the indicated CD8^{+} T cell subsets. Data are taken from one experiment where n = 4 in each chimera group. *p≤0.05 **p≤0.01 ***p≤0.001.

Figure 4.17 continued

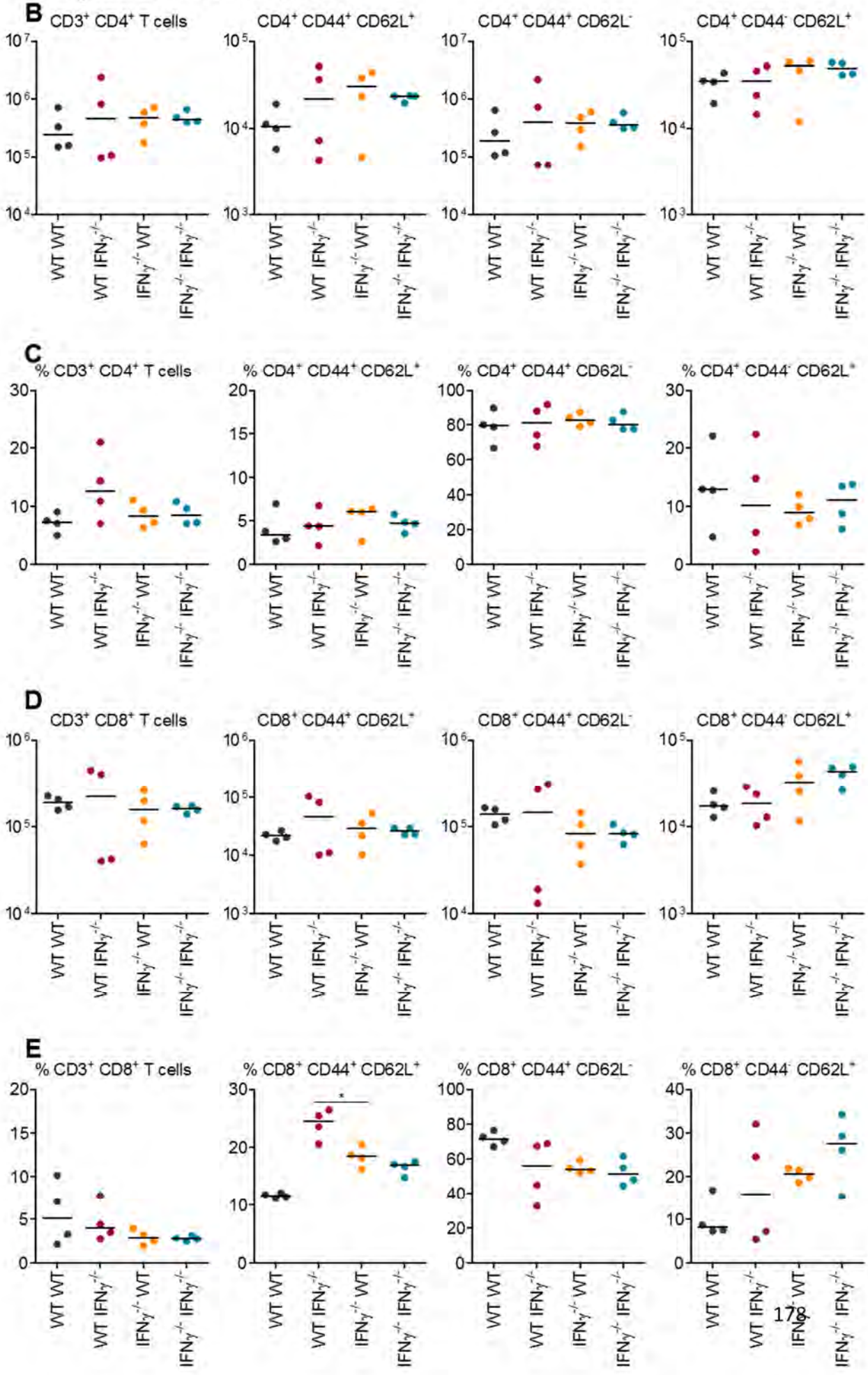

4.7.1 Inflammatory lesions develop in the liver in the absence of TNFαR signalling

signalling

In the absence of infection, liver mass is similar between WT and TNFαR$^{-/-}$ mice (Fig 4.18 A). For flow cytometric analysis, non-infected WT and TNFαR$^{-/-}$ livers were taken from mice on different days. Absolute numbers of myeloid cells and T cells are generally similar or lower than in WT, however, a lower proportion of cells are CD8^{+} and the distribution of CD8^{+} sub-populations is altered whereby there is a significantly lower percentage of central memory cells and a significantly higher percentage of naïve cells (Fig 4.18 B-K).

At day 7 post-infection, the mass and bacterial burden of TNFαR$^{-/-}$ livers are similar to WT (Fig 4.19 A-B). Inflammatory lesions are present in TNFαR$^{-/-}$ mice, indicating that signalling via this receptor is not required for lesion formation (Fig 4.19 C). However, fewer leukocytes are retrieved from livers of TNFαR$^{-/-}$ mice relative to WT (Fig 4.19 D). Absolute numbers and proportions of all myeloid populations are decreased, with the exception of an increased proportion of F4/80^{+} Ly6G^{lo} cells which are Kupffer cells (Fig 4.19 E-H). T cells are comparable in number and constituent to in WT livers (Fig 4.19 K-O). Whilst total CD11c^{+} cells are reduced in the absence of TNFαR, the dynamics of subsets are altered, whereby the proportion of myeloid and mixed myeloid/lymphoid DCs are greater than in WT (Fig 4.19 P-R). Thus whilst there are some alterations in leukocyte constituency, in particular the reduced accumulation of Kupffer cells, monocytes and DCs, loss of the inflammation-associated TNFαR molecule induces a distinct phenotype that differs to that associated with loss of IFNγ. Importantly, inflammatory lesions develop in the absence of TNFαR.

Figure 4.18

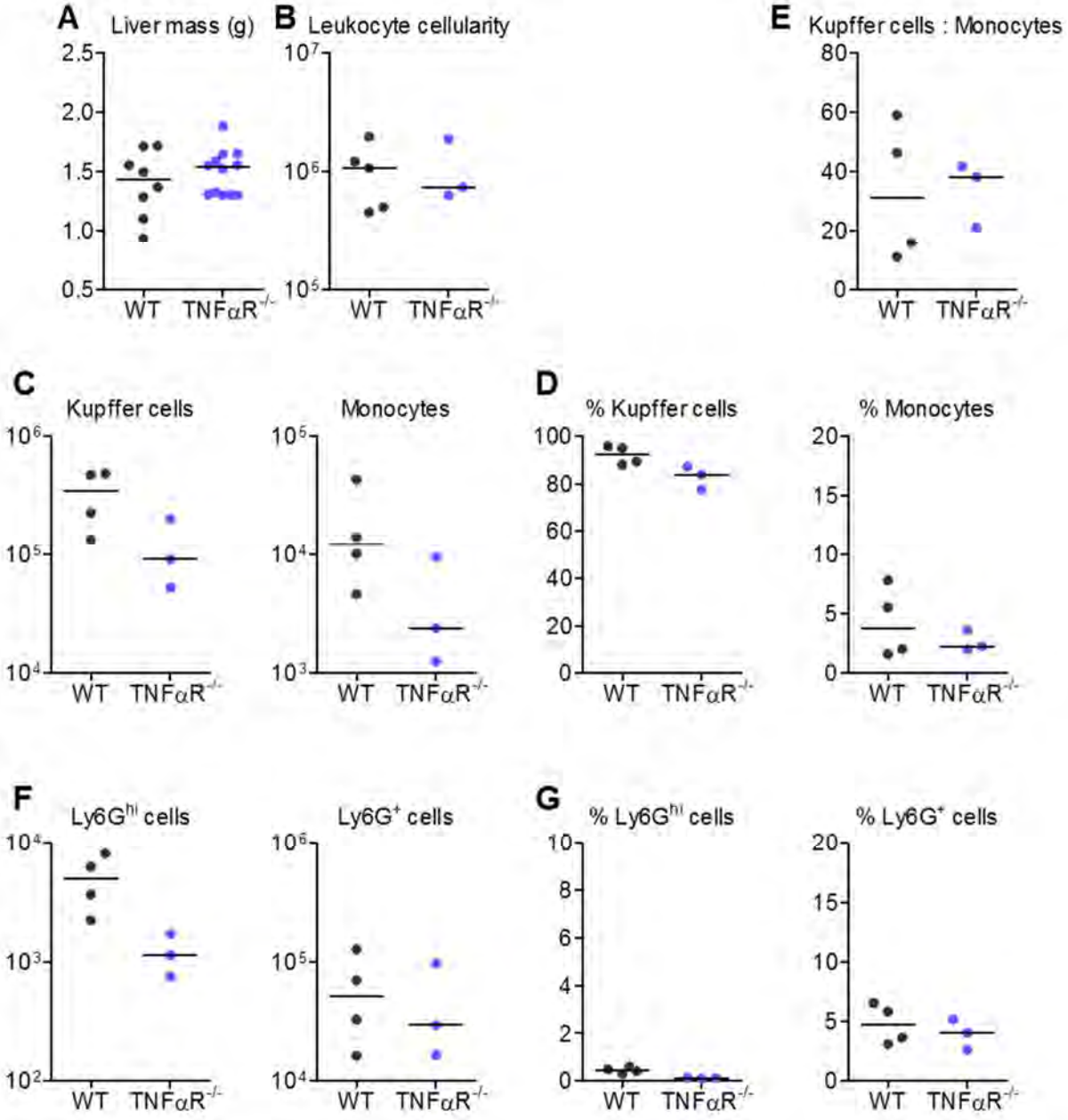

Figure 4.18 Leukocyte populations are subtly altered in the absence of tumor necrosis factor-α receptor

Livers were removed from non-infected WT and TNFαR $^{-/-}$ mice and A) liver mass was measured. Leukocytes were isolated from the livers by collagenase digestion and gradient centrifugation. B) The total number of cells retrieved from the liver in the leukocyte fraction of the gradient was calculated. Myeloid populations were analysed by FACS and C) absolute numbers and D) proportions (out of total F4/80^{hi} Ly6G^{lo} cells) for Kupffer cells and monocytes are shown, where Kupffer cells = F4/80^{hi} Ly6G^{lo} CD11b^{lo} Ly6C^{lo} and monocytes = F4/80^{hi} Ly6G^{lo} CD11b^{hi} Ly6C^{hi}. E) The proportion of absolute numbers of Kupffer cells to absolute numbers of monocytes in the liver was calculated. F) Absolute numbers and G) proportions (out of total isolated leukocytes) of Ly6G^{hi} cells and Ly6G^{+} cells were determined. T cells were examined by FACS for activation status whereby activated effector cells = CD62L^{lo} CD44^{+}; central memory cells = CD62L^{+} CD44^{+}; and naïve cells = CD62L^{+} CD44^{-}. H) Absolute numbers and I) proportions (out of total lymphocyte-sized cells isolated) are shown for the indicated CD4^{+} T cell subsets and in J) and K) for the indicated CD8^{+} T cell subsets. The data presented here were not acquired on the same day (WT mice were taken at a separate time to TNFαR $^{-/-}$ mice); this must be considered when drawing comparisons between the two mice strains. This experiment has not yet been repeated. *p≤0.05 **p≤0.01 ***p≤0.001.

Figure 4.18 continued

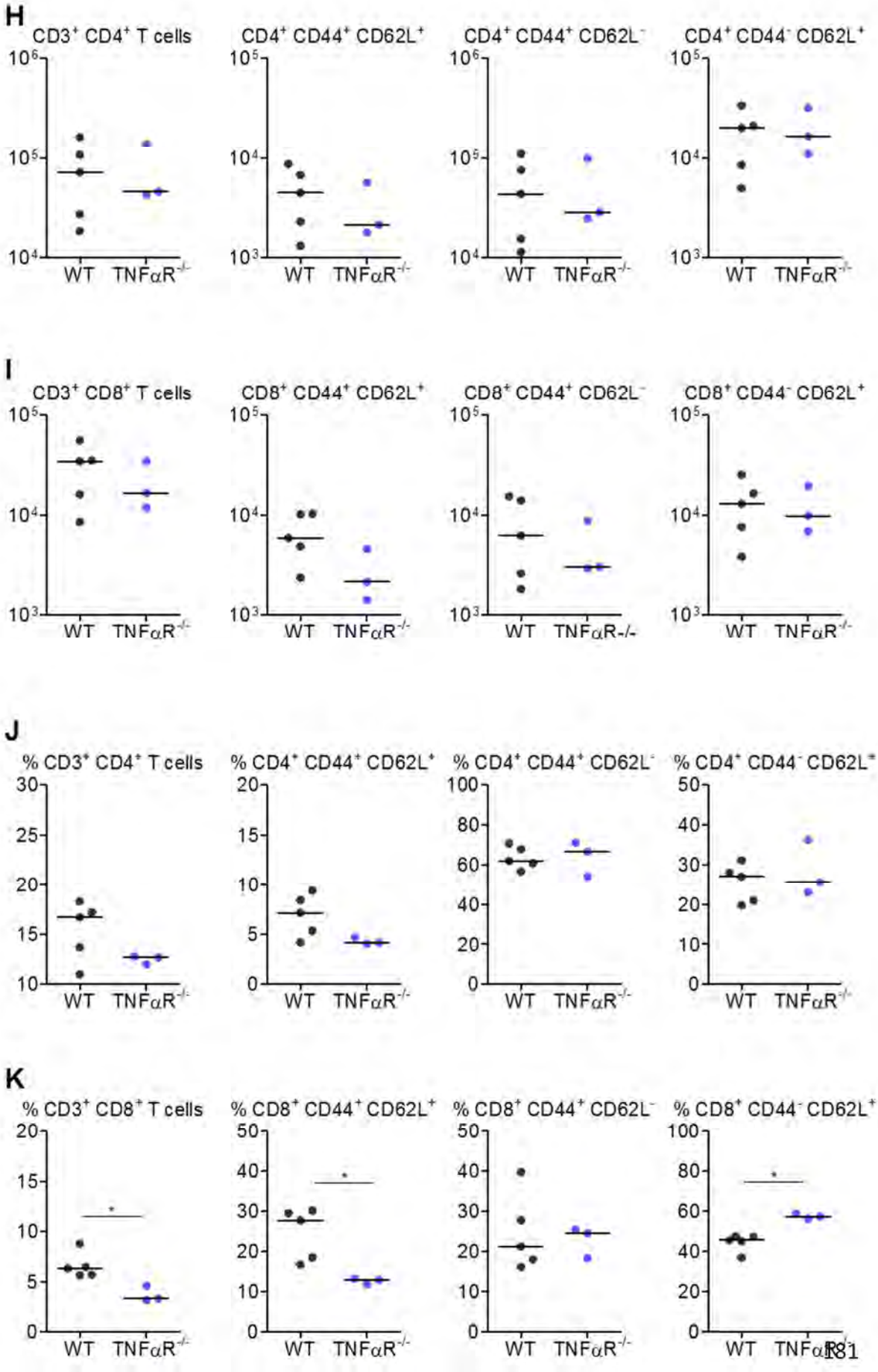

Figure 4.19

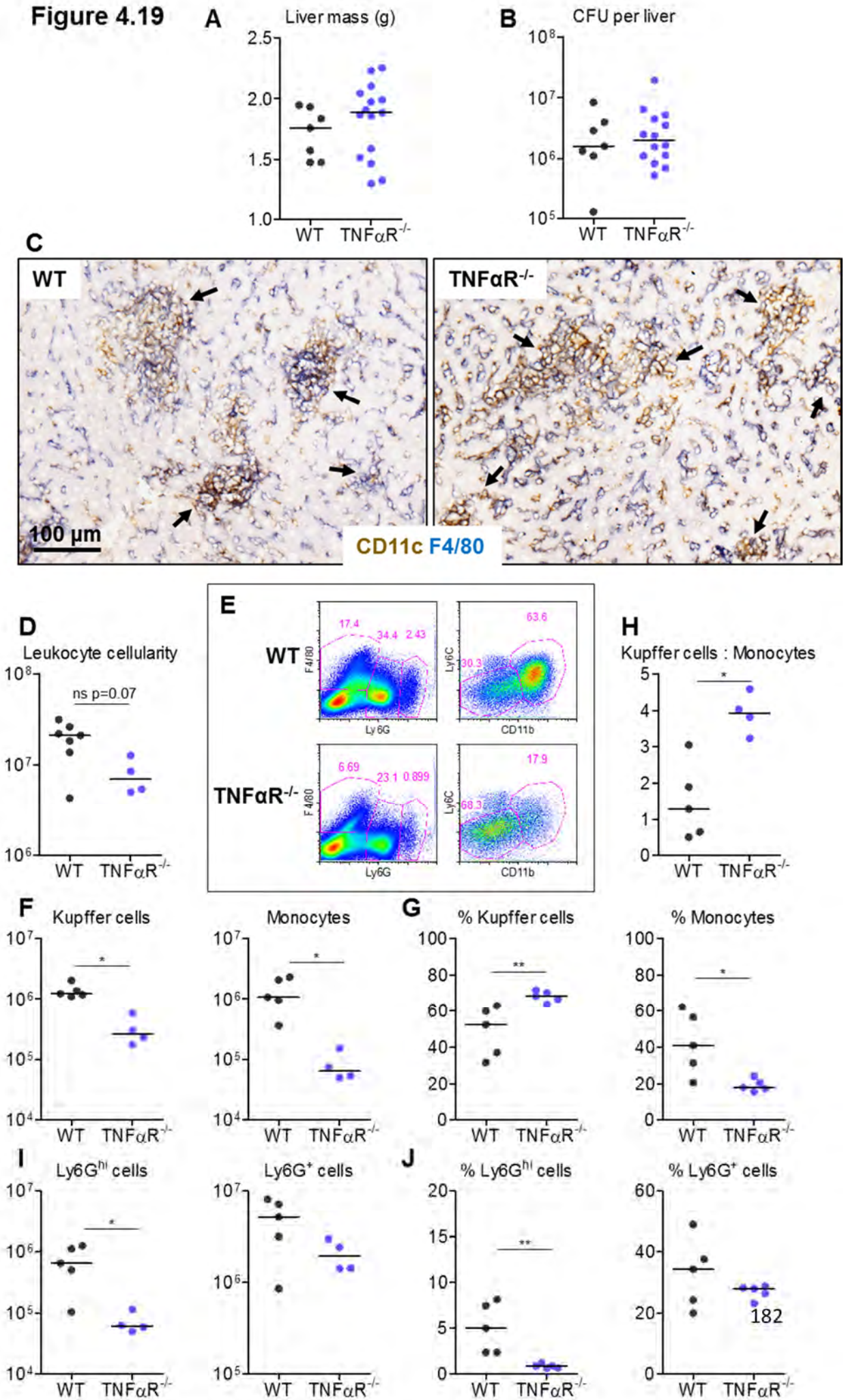
A
Liver mass (g)
2.5
2.0
1.5
1.0
WT
TNFαR-/-
B
CFU per liver
10^8
10^7
10^6
10^5
WT
TNFαR-/-
C
WT
TNFαR-/-
100 µm
CD11c F4/80
D
Leukocyte cellularity
ns p=0.07
10^8
10^7
10^6
WT
TNFαR-/-
E
WT
TNFαR-/-
F4/80
Ly6G
Ly6C
CD11b
17.4
34.4
2.43
63.6
30.3
6.69
23.1
0.899
17.9
68.3
H
Kupffer cells : Monocytes
5
4
3
2
1
0
*
WT
TNFαR-/-
F
Kupffer cells
Monocytes
10^7
10^6
10^5
10^4
*
WT
TNFαR-/-
G
% Kupffer cells
% Monocytes
100
80
60
40
20
0
**
*
WT
TNFαR-/-
I
Ly6G^hi cells
Ly6G+ cells
10^7
10^6
10^5
10^4
*
WT
TNFαR-/-
J
% Ly6G^hi cells
% Ly6G+ cells
20
15
10
5
0
60
40
20
0
**
182
WT
TNFαR-/-

Figure 4.19 continued

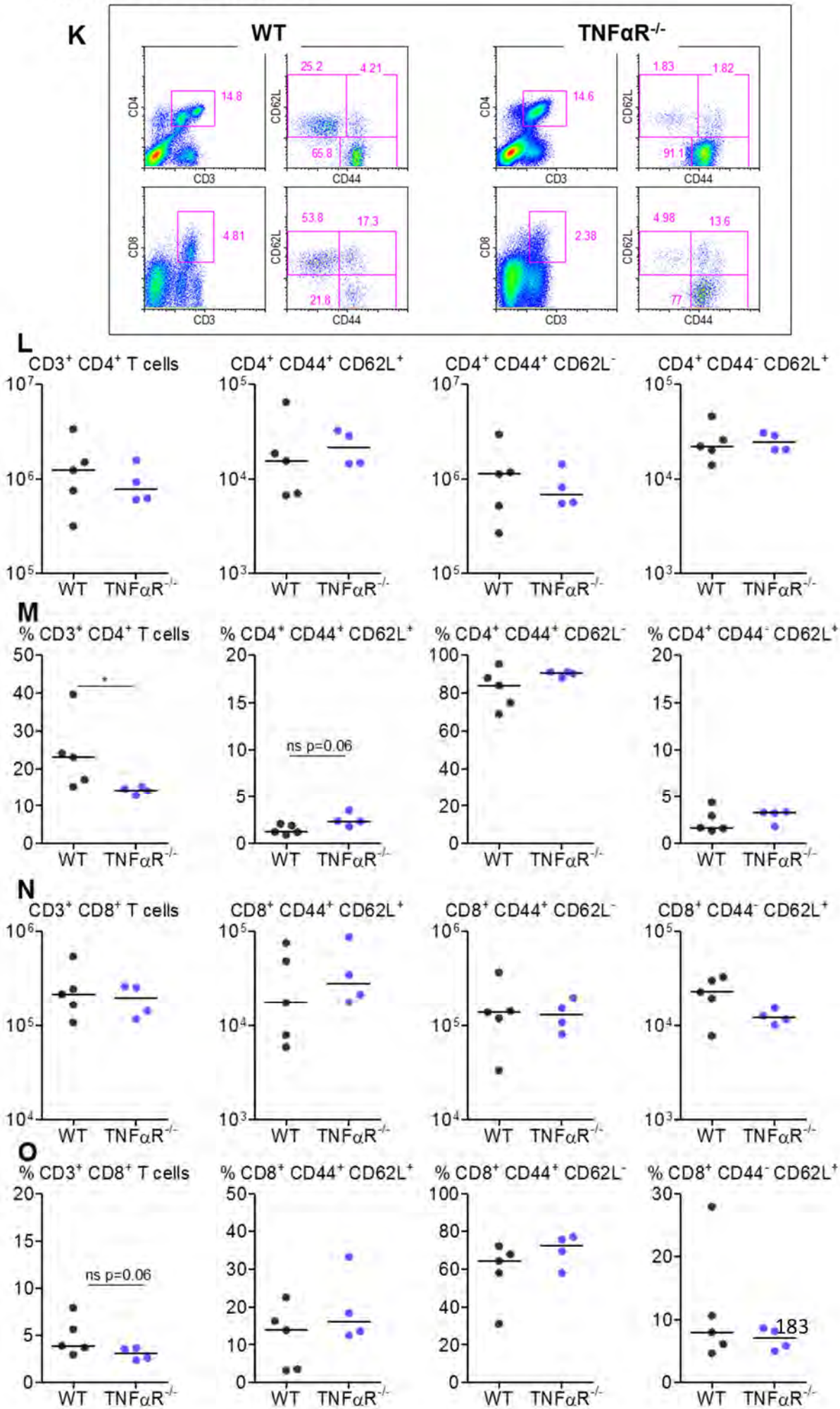

Figure 4.19 continued

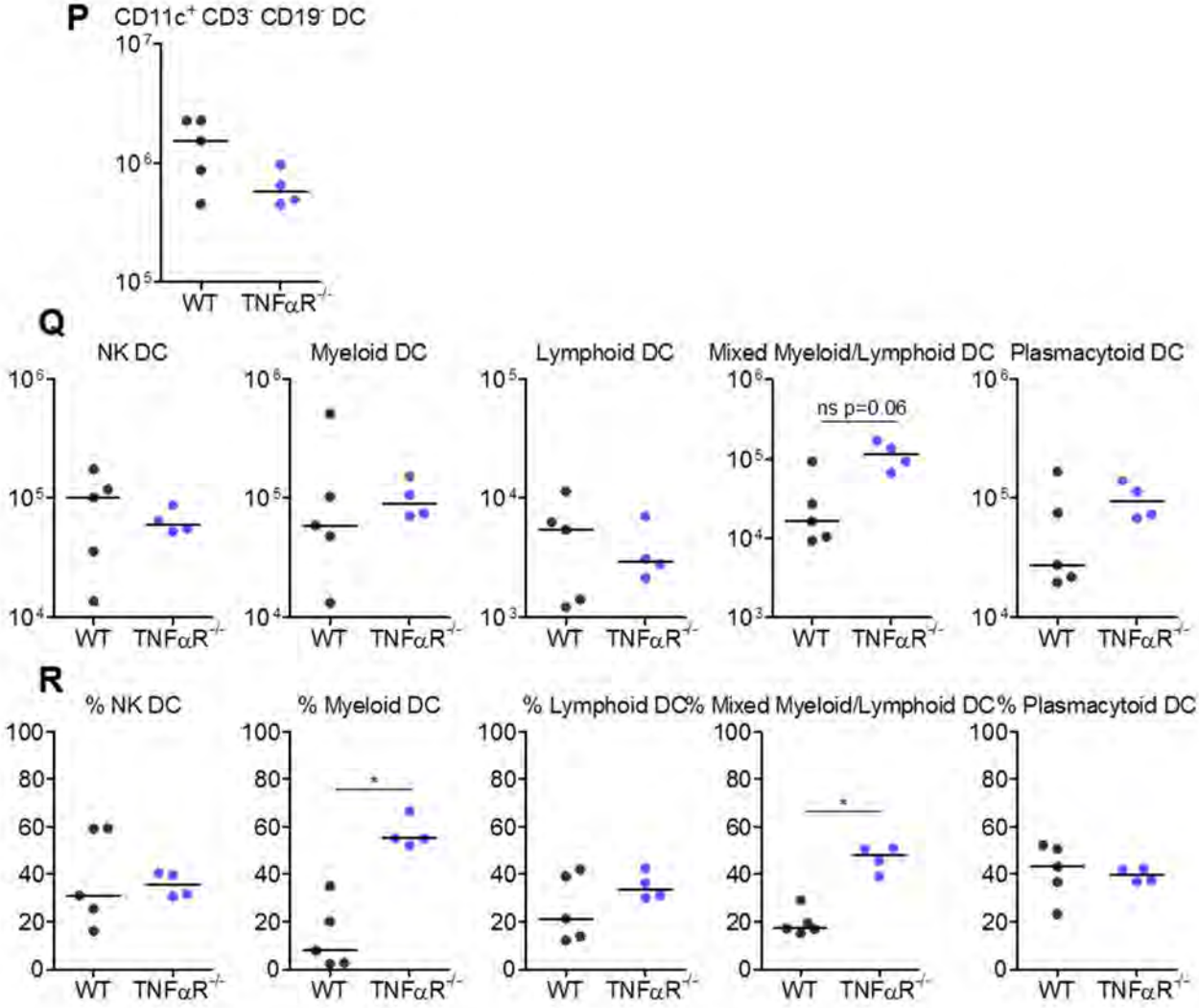

Figure 4.19 Inflammatory lesions develop in the absence of tumor necrosis factor-α receptor

WT and TNFαR $^{-/-}$ mice were infected (i.p.) with 5 x 10^5 CFU attenuated STm for 7 days. Livers were removed and A) liver mass and B) bacterial burden of the liver were determined in each strain of mice. Development of inflammatory lesions and extent of hepatic leukocyte infiltration was assessed by C) IHC where F4/80$^+$ cells = blue; CD11c$^+$ cells = brown; double positive F4/80$^+$ CD11c$^+$ cells = black. V = vessel; black arrows indicate inflammatory lesions. Images are representative and data shown are from multiple experiments where n ≥ 4 in each group.

Leukocytes were isolated by collagenase digestion and gradient centrifugation. D) Total cells retrieved from the liver in the leukocyte fraction of the gradient was calculated. E) Myeloid populations were analysed by FACS and representative FACS plots are shown. F) Absolute numbers and G) proportions (out of total F4/80^{hi} Ly6G^{lo} cells) for Kupffer cells and monocytes are shown, where Kupffer cells = F4/80^{hi} Ly6G^{lo} CD11b^{lo} Ly6C^{lo} and monocytes = F4/80^{hi} Ly6G^{lo} CD11b^{hi} Ly6C^{hi}. H) The proportion of absolute numbers of Kupffer cells to absolute numbers of monocytes in the liver was calculated. I) Absolute numbers and J) proportions (out of total isolated cells) of Ly6G^{hi} cells and Ly6G$^+$ cells were determined.

T cells were examined by FACS for activation status. Activated effector T cells = CD62L^{lo} CD44$^+$; central memory cells = CD62L$^+$ CD44$^+$; and naïve cells = CD62L$^+$ CD44$^-$. K) Representative FACS plots of T cell staining are shown. L) Absolute numbers and M) proportions (out of total lymphocyte-sized cells isolated) are shown for the indicated CD4$^+$ T cell subsets, and in N) and O) for the indicated CD8$^+$ T cell subsets.

DC populations were gated as shown in Figure 4.5. Absolute numbers of P) total CD11c$^+$ CD3$^-$ CD19$^-$ DCs and Q) DC subtypes are shown (characterised as follows: NK DC = CD11b^{lo} CD8α$^-$ NK1.1$^+$ B220$^+$; Myeloid DC = CD11b$^+$ CD8α$^-$ NK1.1$^-$ B220$^-$; Lymphoid DC = CD11b$^-$ CD8α$^+$ NK1.1$^-$ B220$^-$; Mixed Myeloid/Lymphoid DC = CD11b$^-$ CD8α$^-$ NK1.1$^-$ B220$^-$; and Plasmacytoid DC = CD11b$^-$ CD8α$^-$ NK1.1$^-$ B220$^+$. R) The percentages of each DC subtype out of total CD11c$^+$ CD3$^-$ CD19$^-$ DCs was measured. FACS data are taken from one experiment where n = 4-5 in each strain of mice. *p≤0.05 **p≤0.01 ***p≤0.001.

4.7.2 Inflammation is enhanced in the absence of IL10

In the absence of infection, IL10-deficient livers are of a similar mass and appearance to those of WT mice, and leukocyte distribution in the liver is similar (Fig 4.20 A and D, and data not shown). However, with the usual 5 x 10^5 dose of attenuated STm, $IL10^{-/-}$ mice show greater clinical signs after infection, so are typically infected with only one fifth of this (1 x 10^5 CFU). Mice were infected with this lower dose, and responses were assessed in the liver after 7 days.

Using this reduced inoculum, hepatomegaly can be less extensive in WT mice whereas, hepatomegaly in $IL10^{-/-}$ mice is substantial (Fig 4.20 B). Bacterial load of the liver is significantly lower in $IL10^{-/-}$ mice, despite these mice showing more clinical symptoms (lethargy, dishevelled fur, squinty). Inflammation in WT livers is less severe in response to the reduced bacterial infection dose, however, small foci do still form (Fig 4.20 E). Inflammatory lesions are more pronounced in $IL10^{-/-}$ livers. These data indicate that inflammation in the liver is enhanced in the absence of IL10, and that this is independent of bacterial load.

4.7.3 IL6 is not required for inflammatory lesion development in the liver

We assessed responses in the liver in mice lacking IL6 at day 7 post-infection. IL6-deficient mice have significantly larger livers than WT mice in the absence of infection, and this is visually apparent upon dissection (Fig 4.21 A). After infection, $IL6^{-/-}$ livers can reach up to 3g in mass; approximately 30% larger than WT infected livers, however, bacterial burden is similar to WT (Fig 4.21 B-C). Furthermore, inflammatory lesions develop normally and have a similar distribution of leukocyte infiltrate to that seen in WT mice (Fig 4.21 D).

Figure 4.20

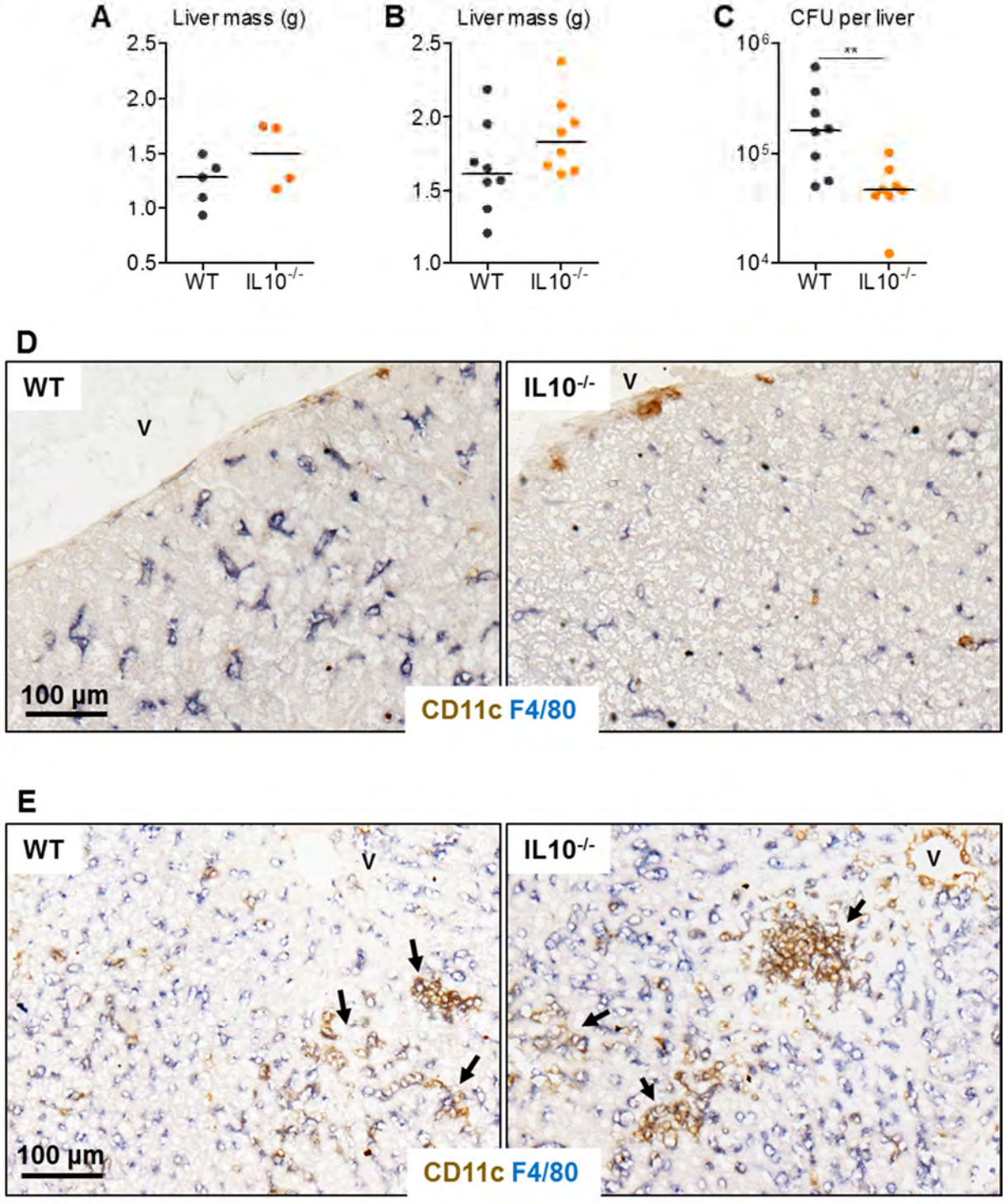

Figure 4.20 Inflammation in the liver is enhanced in the absence of interleukin 10
WT and IL10 $^{-/-}$ mice were infected (i.p.) with 5 x 10^5 CFU attenuated STm for 7 days. Livers were removed and liver mass in A) non-infected control mice and B) day 7-infected mice was measured and C) bacterial burden of the liver at day 7 was determined in each strain of mice. The extent of hepatic leukocyte infiltration was assessed by IHC in D) non-infected WT and IL10$^{-/-}$ mice and E) day 7-infected mice, where F4/80$^+$ cells = blue; CD11c$^+$ cells = brown; double positive F4/80$^+$ CD11c$^+$ cells = black. V = vessel; black arrows indicate inflammatory lesions. Images are representative and data shown are from multiple experiments where n ≥ 4 in each group. Non-infected IL10$^{-/-}$ mice have only been examined in one experiment. *p≤0.05 **p≤0.01 ***p≤0.001.

Figure 4.21

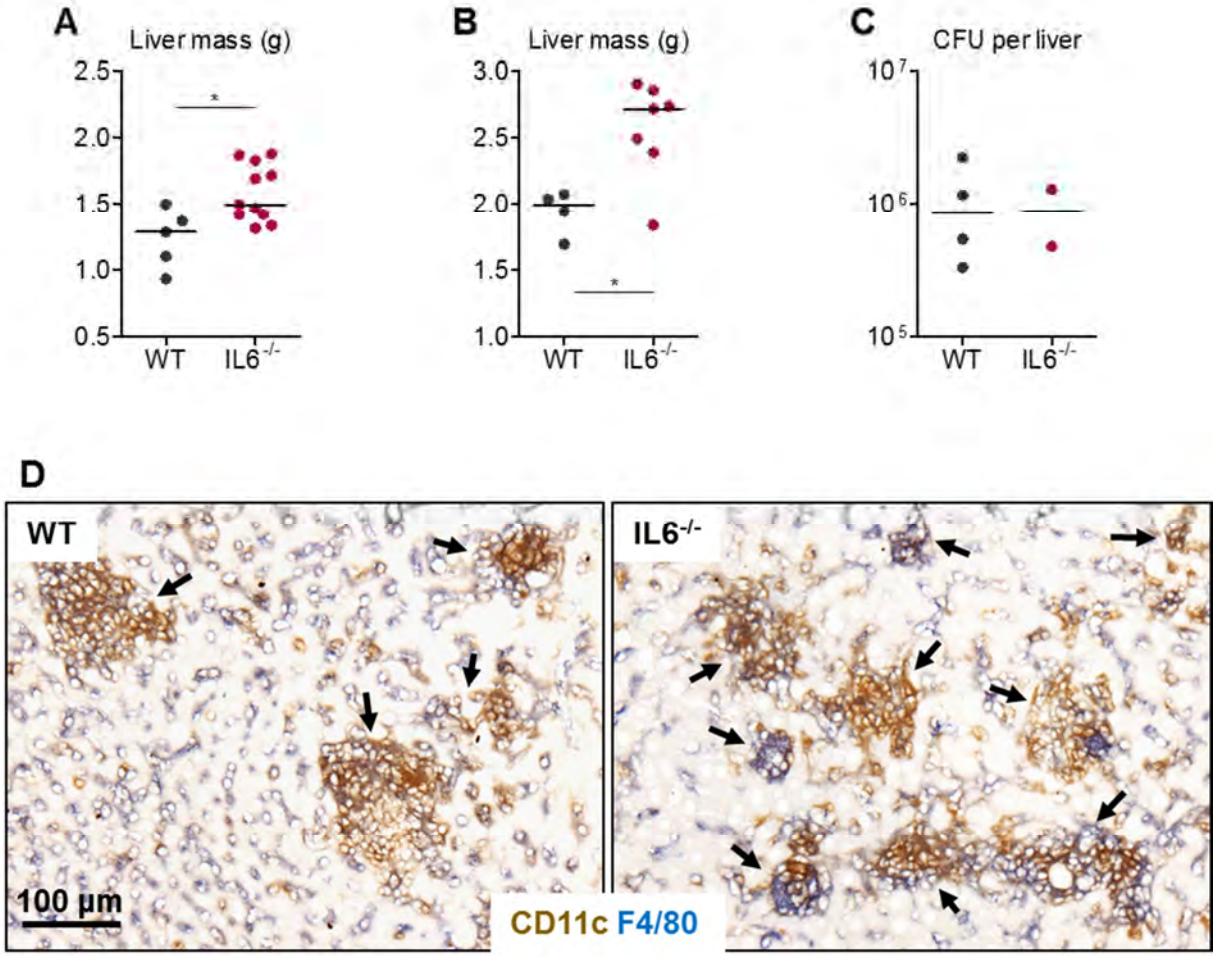

Figure 4.21 Inflammatory lesions develop in the absence of interleukin 6
WT and IL6 $^{-/-}$ mice were infected (i.p.) with 5 x 10^5 CFU attenuated STm for 7 days. Livers were removed and liver mass in A) non-infected control mice and B) day 7-infected mice was measured and C) bacterial burden of the liver at day 7 was determined in each strain of mice. D) The extent of hepatic leukocyte infiltration was assessed by IHC, where F4/80$^+$ cells = blue; CD11c$^+$ cells = brown; double positive F4/80$^+$ CD11c$^+$ cells = black. V = vessel; black arrows indicate inflammatory lesions. Images are representative and data shown are from multiple experiments where n ≥ 4 in each group, however, bacterial burden has only been examined in n = 2 IL6$^{-/-}$ mice and this has not yet been repeated. *p≤0.05 **p≤0.01 ***p≤0.001.

From these data we conclude that IL6 signalling is not necessary for inflammatory lesion development during infection.

4.8 Hepatic pathology is exacerbated in the absence of IL4

To investigate the role of other T cell subsets in the host response to infection, we infected mice deficient in IL4, IL4Rα, CD8 or CD1d and examined the livers after 7 days. Interleukin 4 is typically associated with Th2 responses and plays a role in controlling a number of processes such as Th2 differentiation, IgE switching, and in some inflammatory diseases such as asthma (Swain et al., 1990). Non-infected mice which lack IL4 resemble WT livers in both size and appearance (Fig 4.22 A and data not shown).

At day 7 post-infection, IL4-deficient livers are similar in size and bacterial burden to WT, yet show evidence of enhanced pathology (Fig 4.22 B-F). White lesions can be seen to a far greater extent than in WT mice, and these are particularly prominent at the periphery of lobes. In addition, there is a greater tendency for extensive necrotic regions, especially towards the edges of lobes in IL4-deficient livers (Fig 4.22 G). These are less common and far less extensive in WT livers. Inflammatory lesions develop in the livers of $IL4^{-/-}$ mice, but these tend to be smaller and more frequent than those seen in WT livers (Fig 4.22 H). These data suggest that IL4 may have a protective role during infection, thus minimising immune-mediated tissue damage.

Figure 4.22

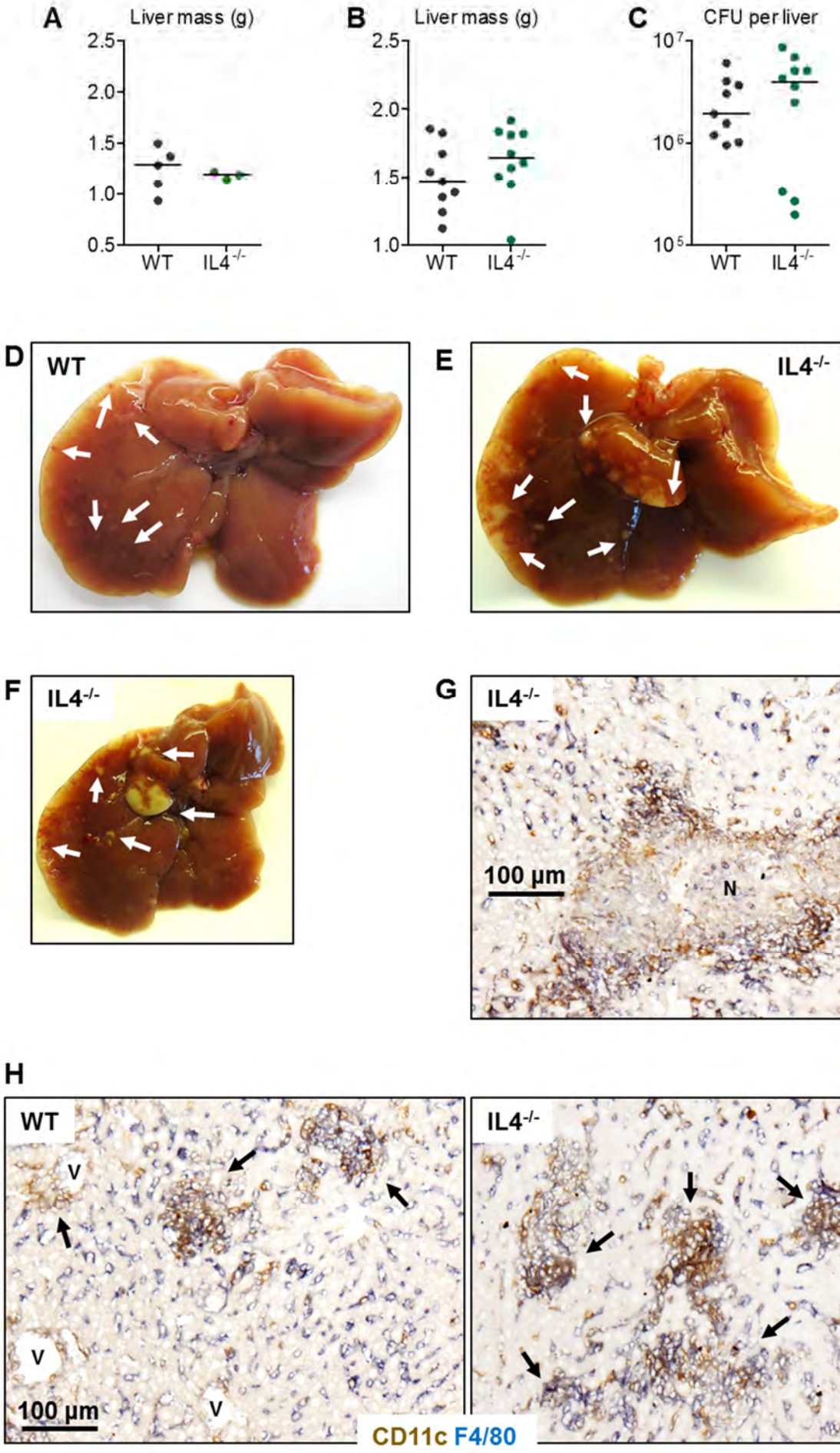
A
Liver mass (g)
2.5
2.0
1.5
1.0
0.5
WT
IL4-/-
B
Liver mass (g)
2.5
2.0
1.5
1.0
WT
IL4-/-
C
CFU per liver
10^7
10^6
10^5
WT
IL4-/-
D
WT
E
IL4-/-
F
IL4-/-
G
IL4-/-
100 µm
N
H
WT
V
V
V
100 µm
IL4-/-
CD11c F4/80

Figure 4.22 More severe pathology is observed in interleukin-4-deficient livers during infection

WT and IL4 $^{-/-}$ mice were infected (i.p.) with 5 x 10^5 CFU attenuated STm for 7 days. Livers were removed and liver mass in A) non-infected control mice and B) day 7-infected mice was measured. C) Bacterial burden of the liver at day 7 was determined in each strain of mice. D) WT and E-F) IL4$^{-/-}$ livers were examined for pathology on the exterior surface. White arrows indicate pathological features, including white-coloured lesions and bloodshot tissue. G) Necrosis was assessed within the tissue and H) the extent of hepatic leukocyte infiltration was assessed by IHC, where F4/80$^+$ cells = blue; CD11c$^+$ cells = brown; double positive F4/80$^+$ CD11c$^+$ cells = black. V = vessel; black arrows indicate inflammatory lesions. Images are representative and data shown are from multiple experiments where n ≥ 3 in each group. Livers from non-infected IL4$^{-/-}$ mice have only been examined once.

4.8.1 Inflammation in IL4Rα-deficient mice resembles WT

To determine whether this pathology is exacerbated by a loss of multiple Th2 cytokines, experiments were repeated in IL4Rα$^{-/-}$ mice, which are also deficient for IL13 signalling (Mohrs et al., 1999). Livers from non-infected IL4Rα$^{-/-}$ mice are a similar size and appearance to WT livers (Fig 4.23 A and data not shown). At day 7 post-infection, both mice have similar sized livers and bacterial burdens, however, the exterior pathology can be more severe in IL4Rα-deficient mice (although this is variable) (Fig 4.23 B-E). Despite this, inflammatory lesions develop similarly to those in WT mice (Fig 4.23 F). These data suggest that the enhanced pathology in IL4-deficient mice may be specific to IL4 as the phenotypes are not observed to the same extent in the absence of IL4Rα.

4.9 CD8 plays a role in accumulation of myeloid populations in the liver during infection

To investigate the role of CD8 in hepatic inflammation, mice lacking CD8 were infected and livers were examined at days 7 and 35 post-infection. In the absence of infection, liver mass and leukocyte cellularity are equivalent in CD8$^{-/-}$ and WT mice, and myeloid populations are similar (Fig 4.24 A-H). Absolute numbers of CD4^{+} T cells detected are similar to WT with the exception of fewer activated CD4^{+} T cells (Fig 4.24 I-J). However, proportions of CD4^{+} T cells are altered in the absence of CD8, whereby the proportion of activated T cells is lower and there are increased proportions of naïve and central memory cells (Fig 4.24 K).

Figure 4.23

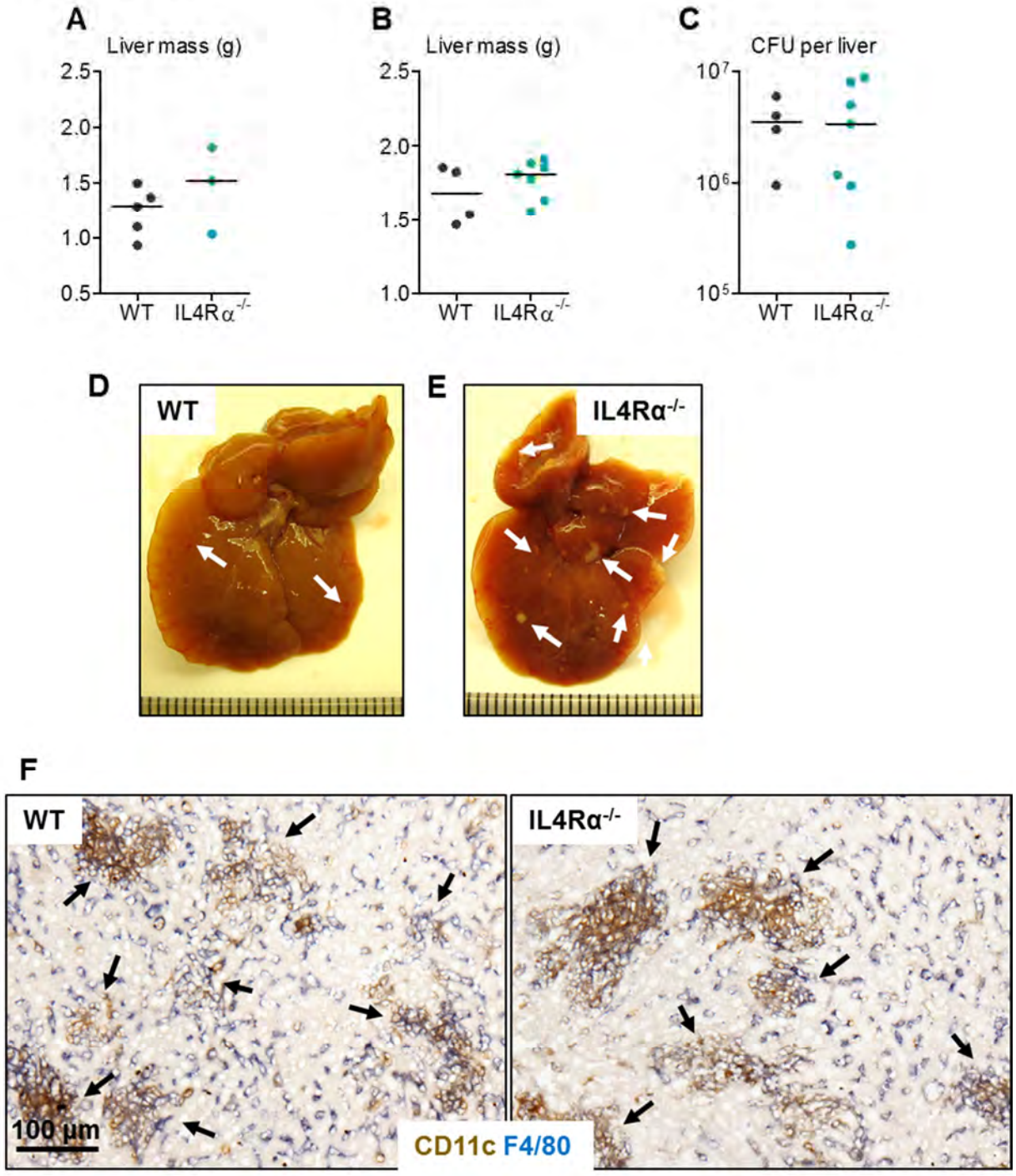

Figure 4.23 In the absence of interleukin-4 receptor-α, inflammation in the liver is similar to WT

WT and IL4Rα $^{-/-}$ mice were infected (i.p.) with 5 x 10^5 CFU attenuated STm for 7 days. Livers were removed and liver mass in A) non-infected control mice and B) day 7-infected mice was measured. C) Bacterial burden of the liver at day 7 was determined in each strain of mice. D) WT and E) IL4$^{-/-}$ livers were examined for pathology on the exterior surface. White arrows indicate pathological features, including white-coloured lesions and bloodshot tissue. F) The extent of hepatic leukocyte infiltration was assessed by IHC in WT and IL4Rα $^{-/-}$ livers, where F4/80$^+$ cells = blue; CD11c$^+$ cells = brown; double positive F4/80$^+$ CD11c$^+$ cells = black. V = vessel; black arrows indicate inflammatory lesions. Images are representative and data shown are from multiple experiments where n ≥ 3 in each group. Livers from non-infected IL4Rα$^{-/-}$ mice have only been examined once.

Figure 4.24

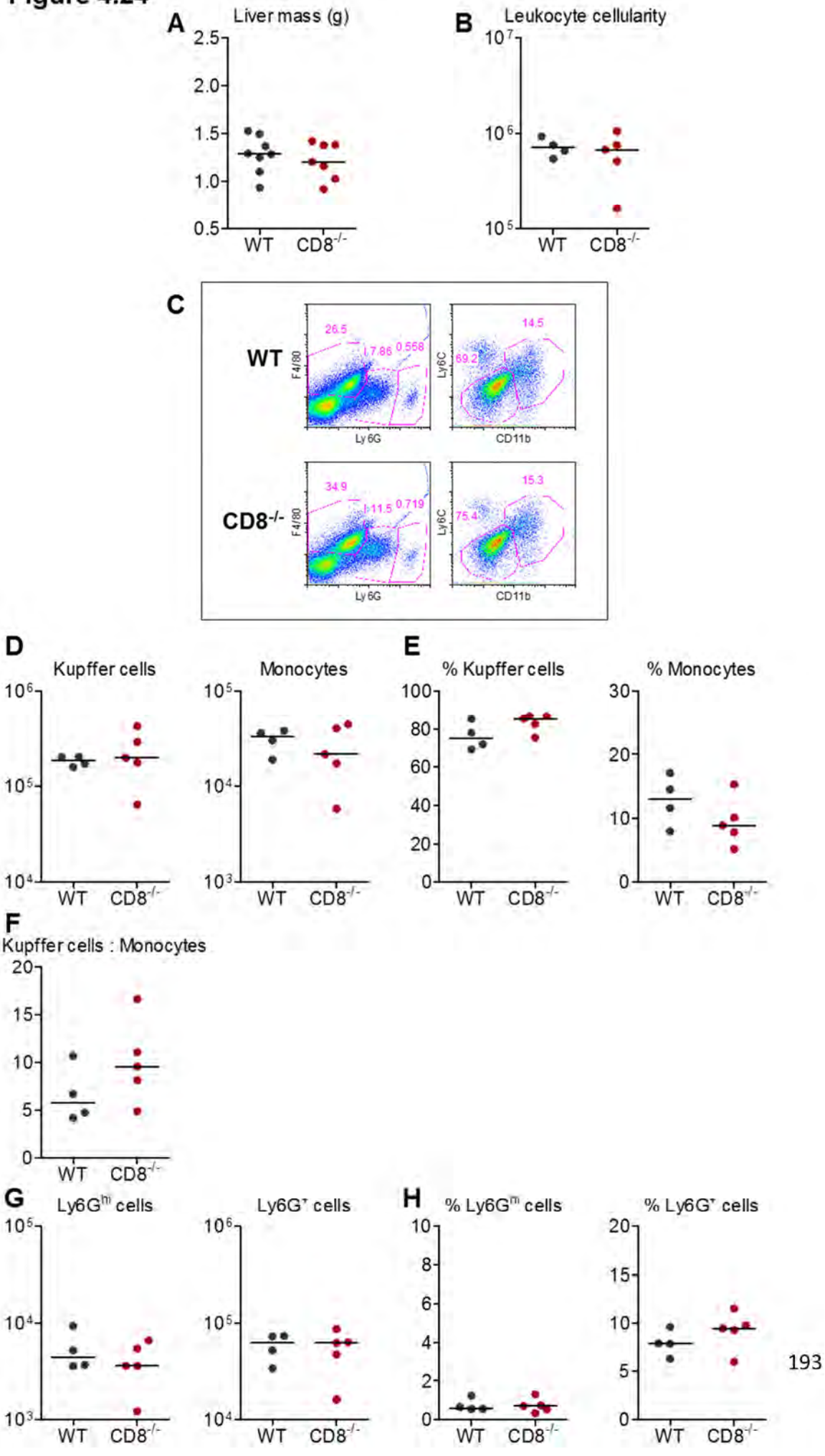
A
Liver mass (g)
2.5
2.0
1.5
1.0
0.5
WT
CD8-/-
B
Leukocyte cellularity
10^7
10^6
10^5
WT
CD8-/-
C
WT
CD8-/-
F4/80
Ly6G
Ly6C
CD11b
26.5
7.86
0.568
14.5
69.2
34.9
11.5
0.719
15.3
75.4
D
Kupffer cells
Monocytes
E
% Kupffer cells
% Monocytes
F
Kupffer cells : Monocytes
G
Ly6G^hi cells
Ly6G^+ cells
H
% Ly6G^hi cells
% Ly6G^+ cells

Figure 4.24 continued

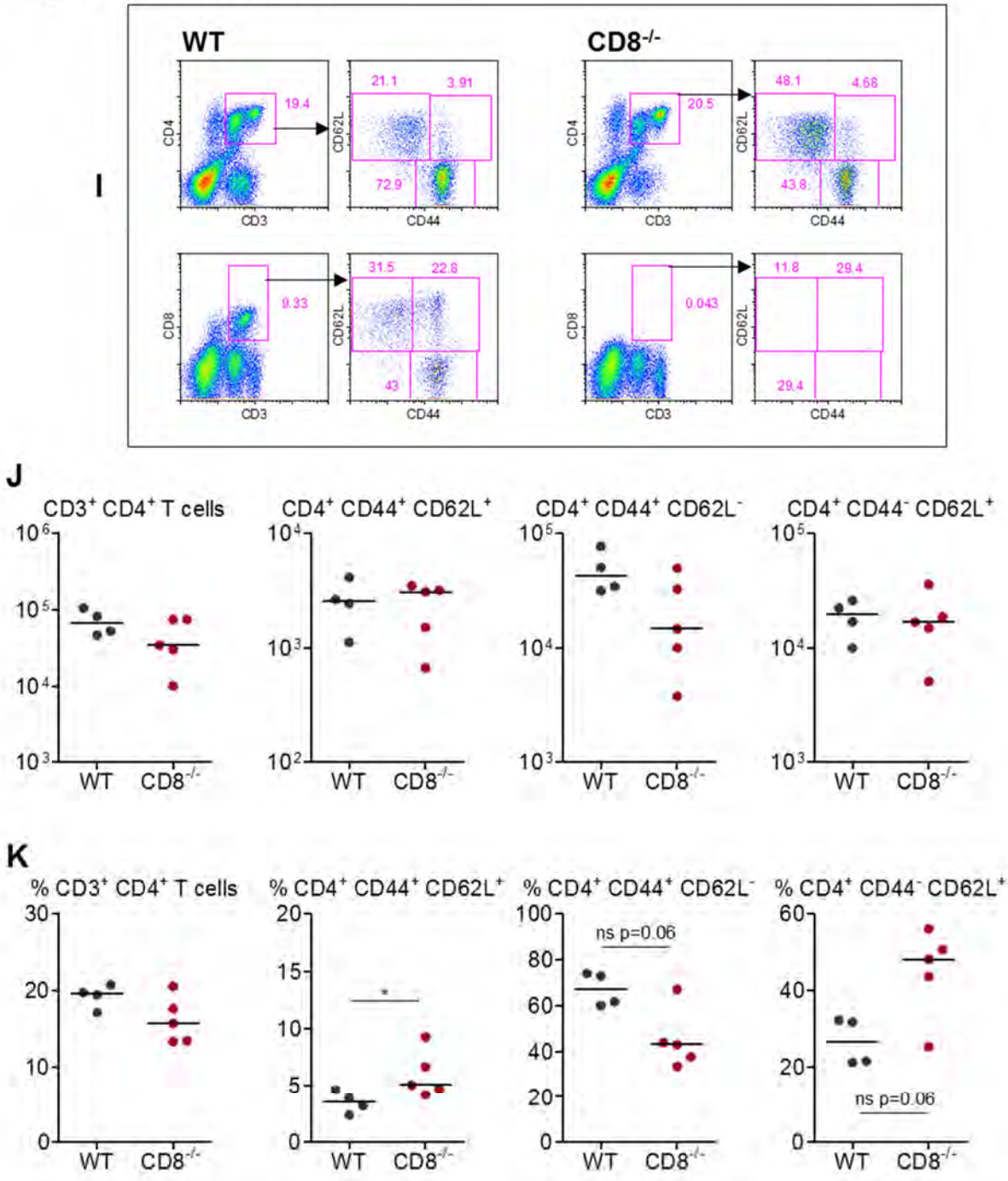

Figure 4.24 Livers from non-infected CD8$^{-/-}$ mice are similar to WT
Livers were removed from non-infected WT and CD8$^{-/-}$ mice and A) liver mass was measured. Leukocytes were isolated from the livers by collagenase digestion and gradient centrifugation and B) cells retrieved from the liver in the leukocyte fraction of the gradient were quantified. C) Myeloid populations were analysed by FACS and representative FACS plots illustrate the staining. D) Absolute numbers and E) proportions (out of total F4/80^{hi} Ly6G^{lo} cells) for Kupffer cells and monocytes are shown, where Kupffer cells = F4/80^{hi} Ly6G^{lo} CD11b^{lo} Ly6C^{lo} and monocytes = F4/80^{hi} Ly6G^{lo} CD11b^{hi} Ly6C^{hi}. F) The proportion of absolute numbers of Kupffer cells to absolute numbers of monocytes in the liver was calculated. G) Absolute numbers and H) proportions (out of total isolated leukocytes) of Ly6G^{hi} cells and Ly6G^{+} cells were determined. T cells were examined by FACS for activation status whereby activated effector cells = CD62L^{lo} CD44^{+}; central memory cells = CD62L^{+} CD44^{+}; and naïve cells = CD62L^{+} CD44^{-}. I) Representative plots are shown to illustrate T cell staining. J) Absolute numbers and K) proportions (out of total lymphocyte-sized cells isolated) are shown for the indicated CD4^{+} T cell subsets. Data shown are from one experiment where n = 4 in each group. Non-infected livers from CD8$^{-/-}$ mice have only been examined once. *p≤0.05 **p≤0.01 ***p≤0.001.

Liver mass in $CD8^{-/-}$ mice is slightly increased at day 7 and decreased at day 35, relative to WT, although this is not statistically significant (Fig 4.25 A). The bacterial burden is similar to that of WT livers at day 7 post-infection, but is approximately 2-fold higher in $CD8^{-/-}$ mice at day 35, suggesting CD8 plays some role in bacterial clearance at later stages of infection (Fig 4.25 B). Absolute numbers of leukocytes isolated from livers are similar in each strain at both time-points (Fig 4.25 C). Numbers of all myeloid subsets are not more than 2-fold different to WT mice at either time-point, however, the proportion of $F4/80^{+}$ $Ly6G^{lo}$ cells which are Kupffer cells is lower at both time-points and the proportion of monocytes is increased, relative to WT (Fig 4.25 D-I). The ratio of Kupffer cells to monocytes is lower in $CD8^{-/-}$ mice at both time-points, although this does not reach statistical significance (Fig 4.25 G).

Absolute numbers of all $CD4^{+}$ T cell subsets are higher at day 7 in CD8-deficient mice, although are all proportionally similar to WT (Fig 4.25 J-L). At day 35, all $CD4^{+}$ T cell numbers and proportions are comparable to WT (Fig 4.25 J-L). These data indicate that CD8 plays a role in myeloid cell accumulation in the liver during infection, however, whether this is due to CD8 expression by T cells or other cell types is unknown.

4.10 Invariant natural killer T cells coordinate myeloid and lymphoid inflammation, and are important in inflammation resolution

Invariant natural killer T (iNKT) cells are prominent in the liver and so we were keen to explore what role they play in hepatic inflammation during infection (Seki et al., 2000). To test this, we infected mice lacking CD1d, the atypical MHC molecule required for iNKT cell activation (Emoto and Emoto, 2009).

Figure 4.25

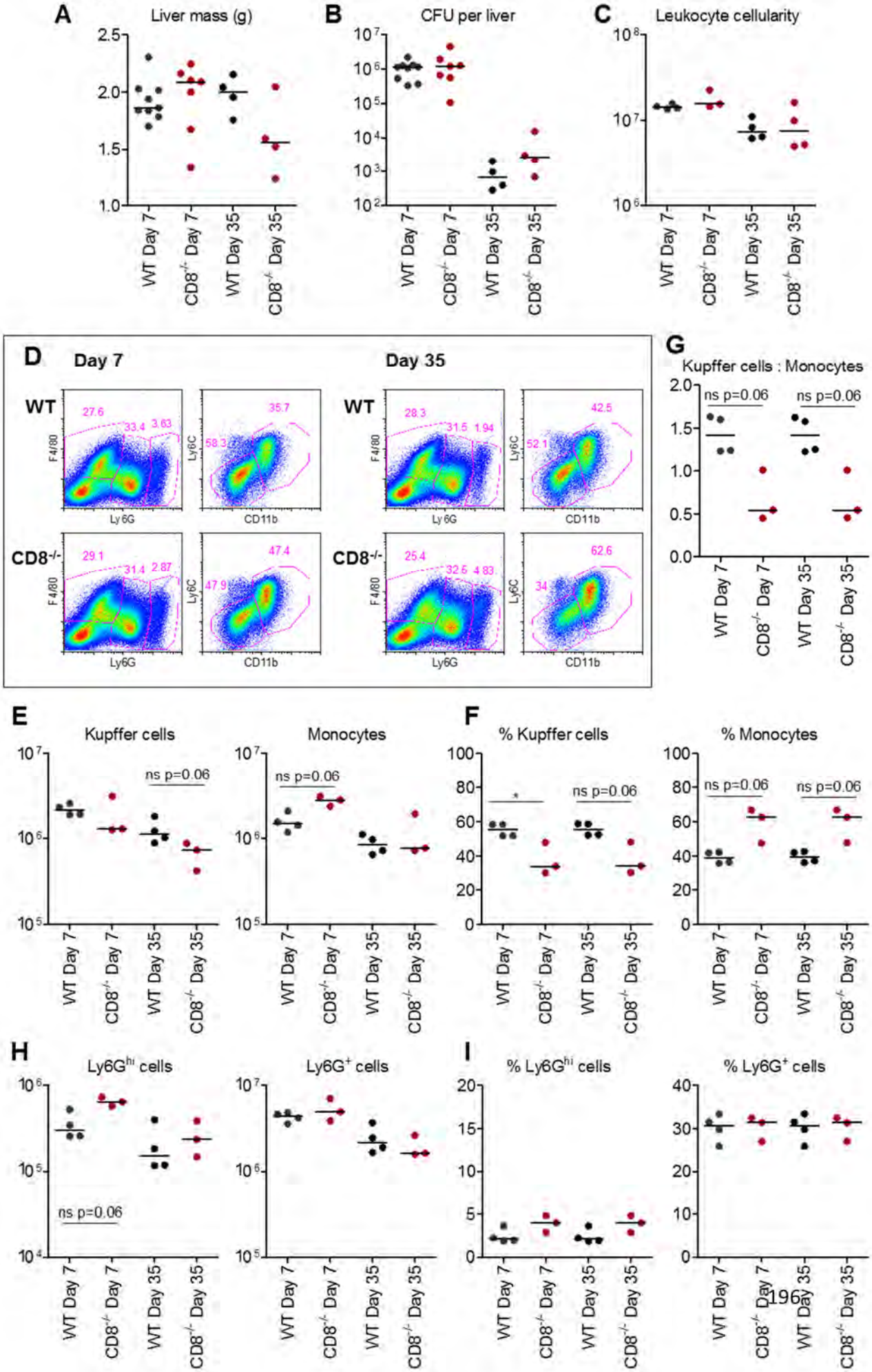
A
Liver mass (g)
B
CFU per liver
C
Leukocyte cellularity
WT Day 7
CD8-/- Day 7
WT Day 35
CD8-/- Day 35
D
Day 7
Day 35
WT
CD8-/-
F4/80
Ly6G
Ly6C
CD11b
27.6
33.4
3.63
35.7
58.3
28.3
31.5
1.94
42.5
52.1
29.1
31.4
2.87
47.4
47.9
25.4
32.5
4.83
62.6
34
G
Kupffer cells : Monocytes
ns p=0.06
E
Kupffer cells
Monocytes
F
% Kupffer cells
% Monocytes
*
H
Ly6Ghi cells
Ly6G+ cells
I
% Ly6Ghi cells
% Ly6G+ cells

Figure 4.25 continued

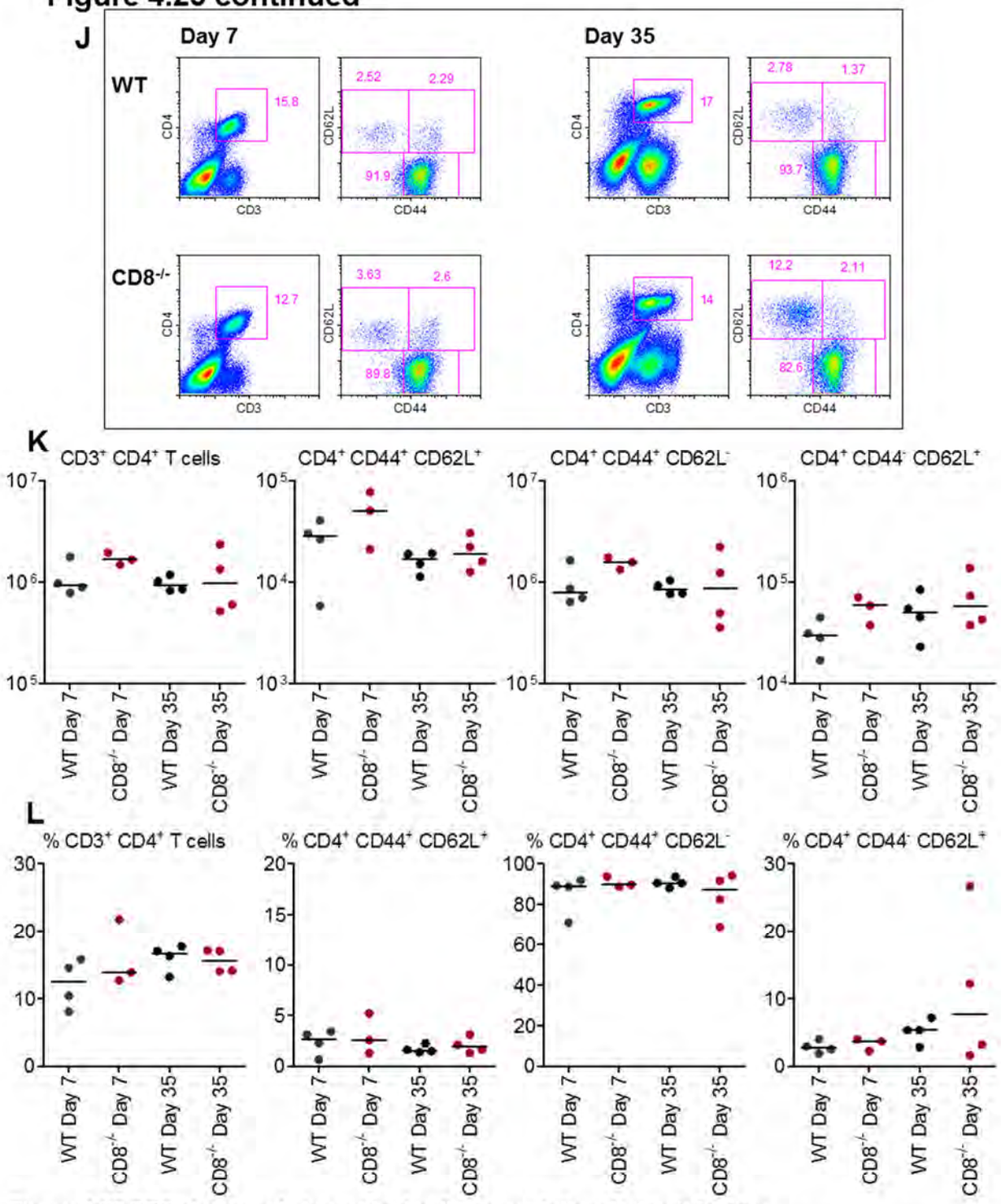

Figure 4.25 CD8 plays a role in myeloid cell accumulation during infection
WT and CD8$^{-/-}$ mice were infected (i.p.) with 5 x 10^5 CFU attenuated STm. Livers were removed at days 7 and 35 post-infection and A) liver mass and B) bacterial burden of the liver were determined. Leukocytes were isolated by collagenase digestion and gradient centrifugation. C) Total cells retrieved from the liver in the leukocyte fraction of the gradient were quantified. D) Myeloid populations were analysed by FACS and representative plots are shown at day 7 and 35 post-infection. E) Absolute numbers and F) proportions (out of total F4/80^{hi} Ly6G^{lo} cells) for Kupffer cells and monocytes are shown, where Kupffer cells = F4/80^{hi} Ly6G^{lo} CD11b^{lo} Ly6C^{lo} and monocytes = F4/80^{hi} Ly6G^{lo} CD11b^{hi} Ly6C^{hi}. G) The proportion of absolute numbers of Kupffer cells to absolute numbers of monocytes in the liver was calculated. H) Absolute numbers and I) proportions (out of total isolated cells) of Ly6G^{hi} cells and Ly6G^{+} cells were determined. T cells were examined by FACS for activation status. Activated effector T cells = CD62L^{lo} CD44^{+}; central memory cells = CD62L^{+} CD44^{+}; and naïve cells = CD62L^{+} CD44^{-}. J) Representative FACS plots of T cell staining are shown at days 7 and 35 post-infection. K) Absolute numbers and L) proportions (out of total lymphocyte-sized cells isolated) are shown for the indicated CD4^{+} T cell subsets. Data shown are from one experiment where n = 3-4 in each group. This experiment has been performed once. *p≤0.05 **p≤0.01 ***p≤0.001.

In the absence of CD1d, iNKT cells cannot undergo selection in the thymus, so their development is blocked (Mendiratta et al., 1997). Inflammation was examined in the liver at days 7 and 35 post-infection.

In the absence of infection, liver mass, leukocyte cellularity and myeloid cell numbers and proportions, are all similar or slightly lower in $CD1d^{-/-}$ livers (Fig 4.26 A-H). Numbers and proportions of total $CD4^+$ T cells are significantly lower in $CD1d^{-/-}$ livers, which is due to significantly fewer activated and naive $CD4^+$ T cells (Fig 4.26 I-K). However, the proportions of naïve and central memory $CD4^+$ T cells are significantly increased relative to WT mice (Fig 4.26 K). In contrast, total $CD8^+$ T cell numbers are similar to WT, but this disguises a significantly increased number and proportion of effector $CD8^+$ T cells and diminution in naïve $CD8^+$ T cells (Fig 4.26 L-M).

After infection, liver mass is equivalent in WT and CD1d-deficient mice at both day 7 and 35 (Fig 4.27 A). Although the bacterial load is equivalent in both groups at day 7, $CD1d^{-/-}$ mice have 50-100 fold more bacteria per liver than WT mice at day 35, indicating a role for iNKT cells in bacterial clearance (Fig 4.27 B). However, at day 7, inflammatory lesions develop normally in livers of CD1d-deficient mice (Fig 4.27 C-D). Despite this, fewer leukocytes are retrieved from the livers of $CD1d^{-/-}$ mice at day 7, and there are lower absolute numbers of all myeloid populations examined (Fig 4.27 E-K). In contrast, leukocyte numbers, in particular myeloid numbers, are elevated at day 35 relative to WT, and the ratio of Kupffer cells to monocytes does not resolve (Fig 4.27 E-K). These observations probably reflect continued infection at this later time-point.

Figure 4.26

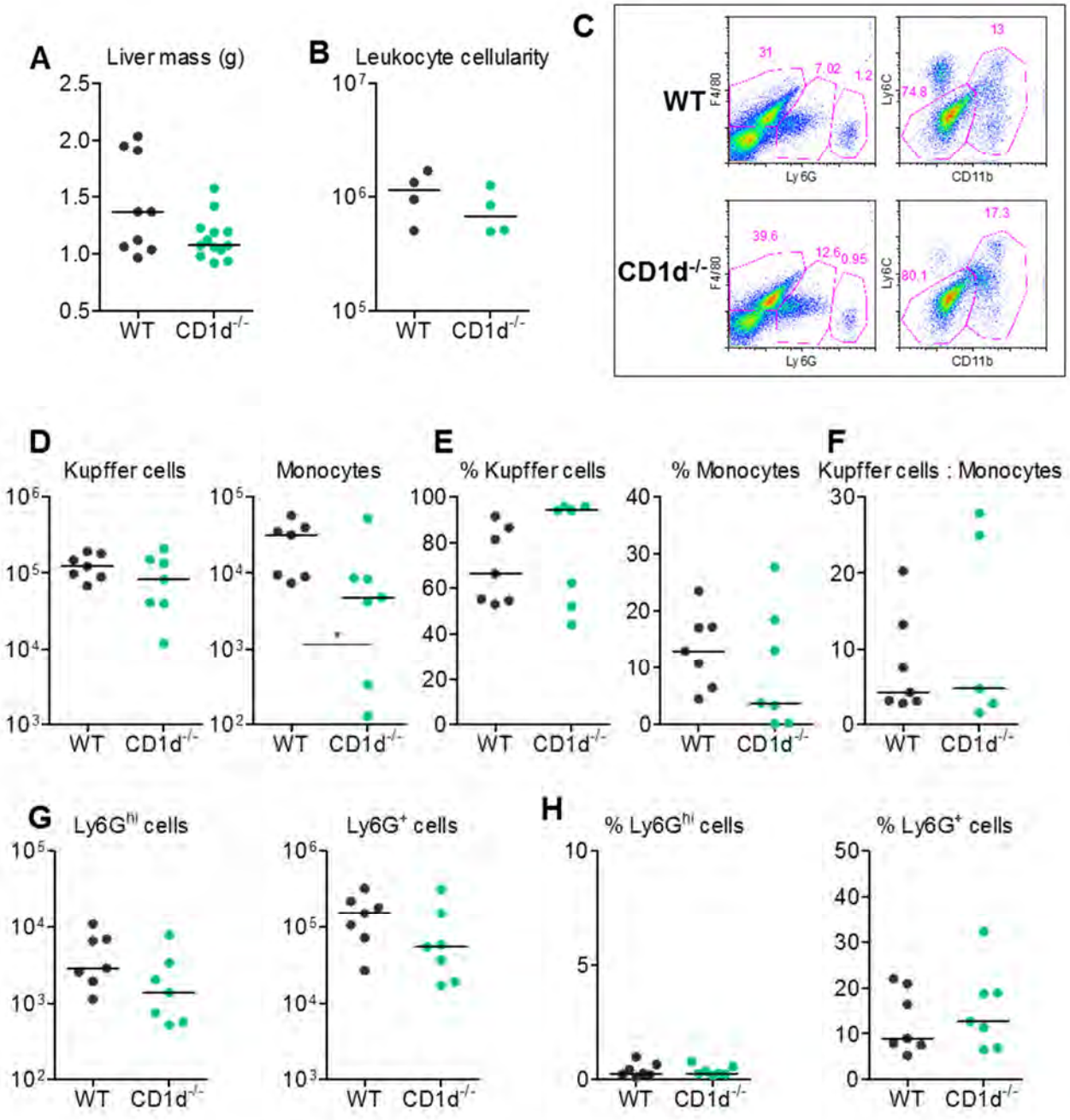

Figure 4.26 T cell populations are subtly altered in the absence of CD1d
Livers were removed from non-infected WT and CD1d $^{-/-}$ mice and A) liver mass was measured. Leukocytes were isolated from the livers by collagenase digestion and gradient centrifugation and B) cells retrieved from the liver in the leukocyte fraction of the gradient were quantified. C) Myeloid populations were analysed by FACS and representative FACS plots illustrate this staining. D) Absolute numbers and E) proportions (out of total F4/80^{hi} Ly6G^{lo} cells) for Kupffer cells and monocytes are shown, where Kupffer cells = F4/80^{hi} Ly6G^{lo} CD11b^{lo} Ly6C^{lo} and monocytes = F4/80^{hi} Ly6G^{lo} CD11b^{hi} Ly6C^{hi}. F) The proportion of absolute numbers of Kupffer cells to absolute numbers of monocytes in the liver was calculated. G) Absolute numbers and H) proportions (out of total isolated cells in the leukocyte fraction) of Ly6G^{hi} cells and Ly6G^{+} cells were determined. T cells were examined by FACS for activation status whereby activated effector cells = CD62L^{lo} CD44^{+}; central memory cells = CD62L^{+} CD44^{+}; and naïve cells = CD62L^{+} CD44^{-}. I) Representative plots are shown to illustrate T cell staining. J) Absolute numbers and K) proportions (out of total lymphocyte-sized cells isolated) are shown for the indicated CD4^{+} T cell subsets, and in L) and M) for the indicated CD8^{+} T cell subsets. Data shown are from one experiment where n = 4 in each group. Non-infected livers from CD1d$^{-/-}$ mice have only been examined once. *p≤0.05 **p≤0.01 ***p≤0.001.

Figure 4.26 continued

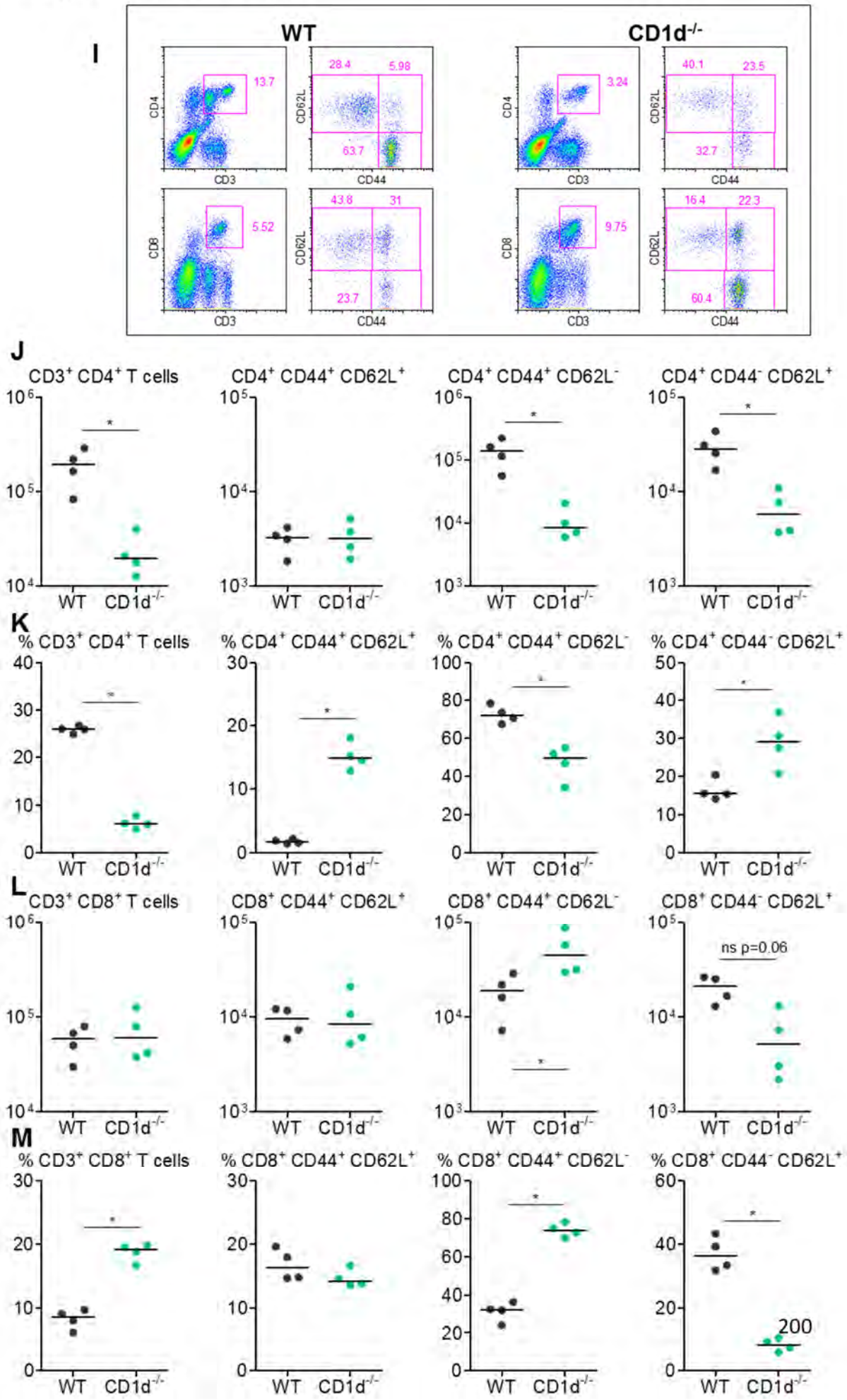

Figure 4.27

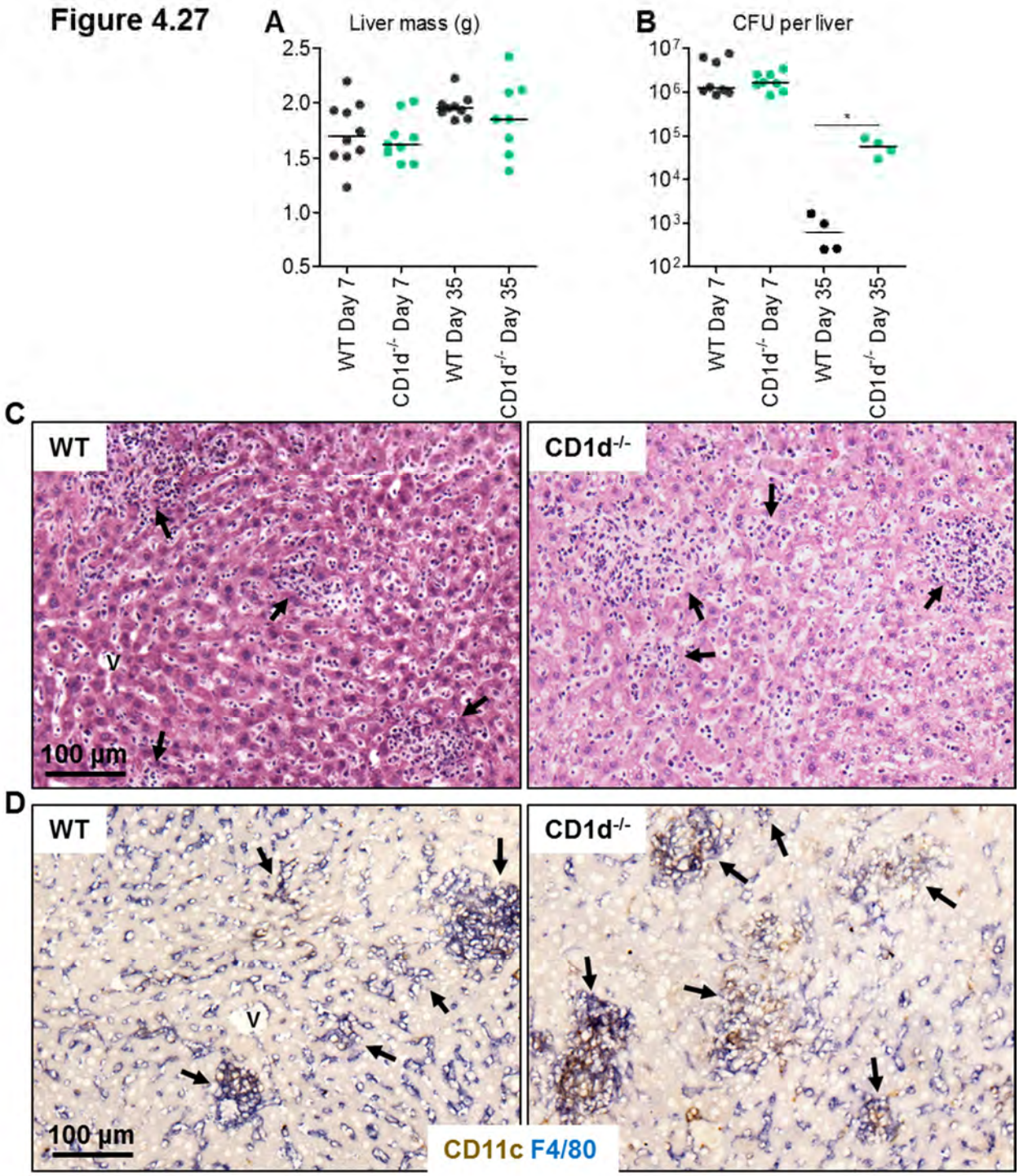

Figure 4.27 Mice deficient in CD1d have defective bacterial clearance at day 35 post-infection
WT and CD1d$^{-/-}$ mice were infected (i.p.) with 5 x 10^5 CFU attenuated STm. Livers were removed at days 7 and 35 post-infection and A) liver mass and B) bacterial burden of the liver were determined. The development of inflammatory lesions and extent of leukocyte infiltration were assessed at day 7 post-infection by C) H&E and D) IHC, where F4/80$^+$ cells = blue; CD11c$^+$ cells = brown; double positive F4/80$^+$ CD11c$^+$ cells = black. V = vessel; black arrows indicate inflammatory lesions. Images are representative and data shown are from multiple experiments where n ≥ 3 in each group.
See next page: Leukocytes were isolated by collagenase digestion and gradient centrifugation. E) Total cells retrieved from the liver in the leukocyte fraction of the gradient were quantified. F) Myeloid populations were analysed by FACS and representative plots are shown at day 7 and 35 post-infection. E) Absolute numbers and F) proportions (out of total F4/80^{hi} Ly6G^{lo} cells) for Kupffer cells and monocytes are shown, where Kupffer cells = F4/80^{hi} Ly6G^{lo} CD11b^{lo} Ly6C^{lo} and monocytes = F4/80^{hi} Ly6G^{lo} CD11b^{hi} Ly6C^{hi}. G) The proportion of absolute numbers of Kupffer cells to absolute numbers of monocytes in the liver was calculated. H) Absolute numbers and I) proportions (out of total isolated cells) of Ly6G^{hi} cells and Ly6G$^+$ cells were determined. Data shown from day 7 are from multiple experiments where n ≥ 3 in each group. Data shown from day 35 are from one experiment where n = 4-5 per group. This experiment has been performed several times, and data shown are representative. *p≤0.05 **p≤0.01 ***p≤0.001.

Figure 4.27 continued

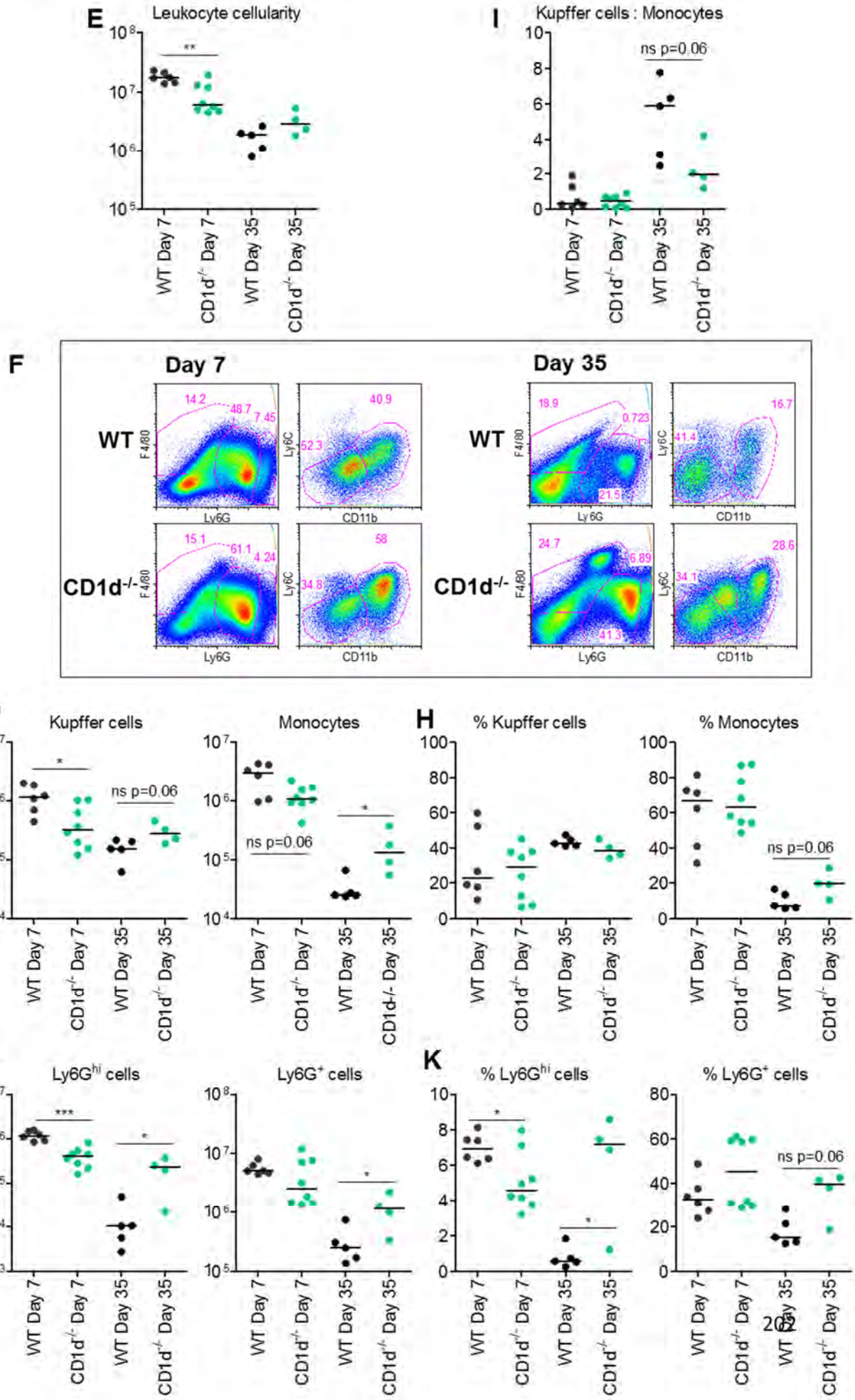

There are fewer $CD3^+$ $CD4^+$ T cells detected at day 7 in $CD1d^{-/-}$ mice and this is most pronounced in the 10-fold lower number of activated cells (though is apparent in all sub populations) (Fig 4.28 A-B). The proportion of total leukocytes which are $CD3^+$ $CD4^+$ is significantly reduced in $CD1d^{-/-}$ mice at day 7, yet percentages of sub-populations are generally comparable to WT (Fig 4.28 C). At day 35, $CD4^+$ T cell numbers are similar to WT mice with the exception of lower naïve cells in $CD1d^{-/-}$ mice. In contrast, numbers of $CD8^+$ T cells more resemble those seen in WT, with the exception of fewer naïve cells in $CD1d^{-/-}$ mice at both time-points (Fig 4.28 D-E). $CD8^+$ T cell proportions vary relative to WT mice, especially at day 7 when there is a greater percentage of central memory and lower percentages of activated and naïve $CD8^+$ T cells (Fig 4.28 F). These data highlight an altered T cell environment in the liver during infection in mice lacking CD1d whereby $CD4^+$ T cell numbers are generally diminished.

Figure 4.28

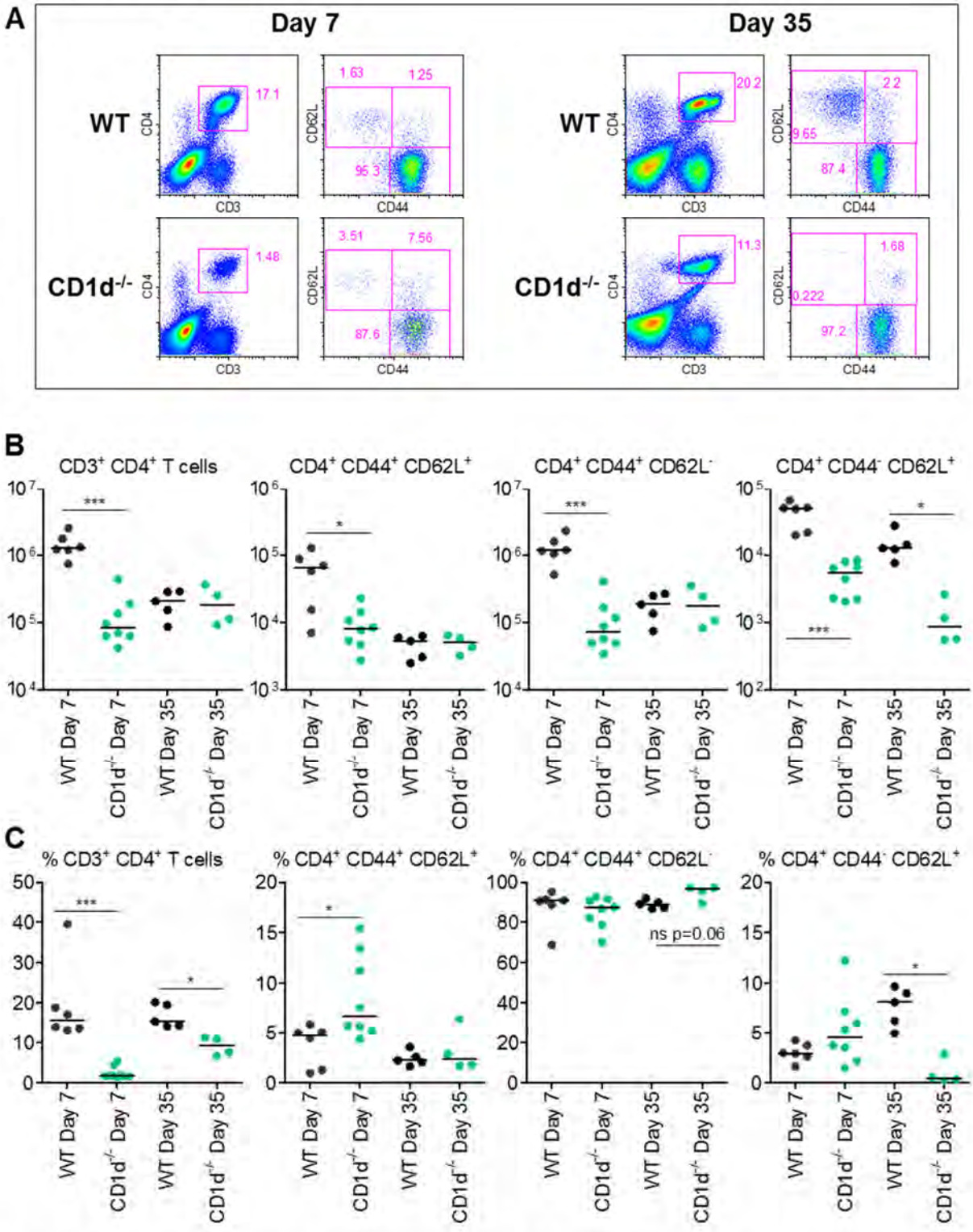

Figure 4.28 T cell populations in the liver are altered in CD1d-deficient mice
(Continued from 4.27). WT and CD1d$^{-/-}$ mice were infected (i.p.) with STm (as described in Figure 4.27). Livers were removed at days 7 and 35 post-infection, leukocytes were isolated and T cells were examined by FACS for activation status. Activated effector T cells = CD62L^{lo} CD44^{+}; central memory cells = CD62L^{+} CD44^{+}; and naïve cells = CD62L^{+} CD44^{-}. A) Representative FACS plots of CD4^{+} T cell staining are shown at days 7 and 35 post-infection. B) Absolute numbers and C) proportions (out of total lymphocyte-sized cells isolated) are shown for the indicated CD4^{+} T cell subsets. See next page: D) Representative FACS plots of CD8^{+} T cell staining are shown at days 7 and 35 post-infection. E) Absolute numbers and F) proportions are shown for the indicated CD8^{+} T cell subsets. Data shown from day 7 are from multiple experiments where n ≥ 3 in each group. Data shown from day 35 are from one experiment where n = 4-5 per group. This experiment has been performed several times, and data shown are representative. *p≤0.05 **p≤0.01 ***p≤0.001.

Figure 4.28 continued

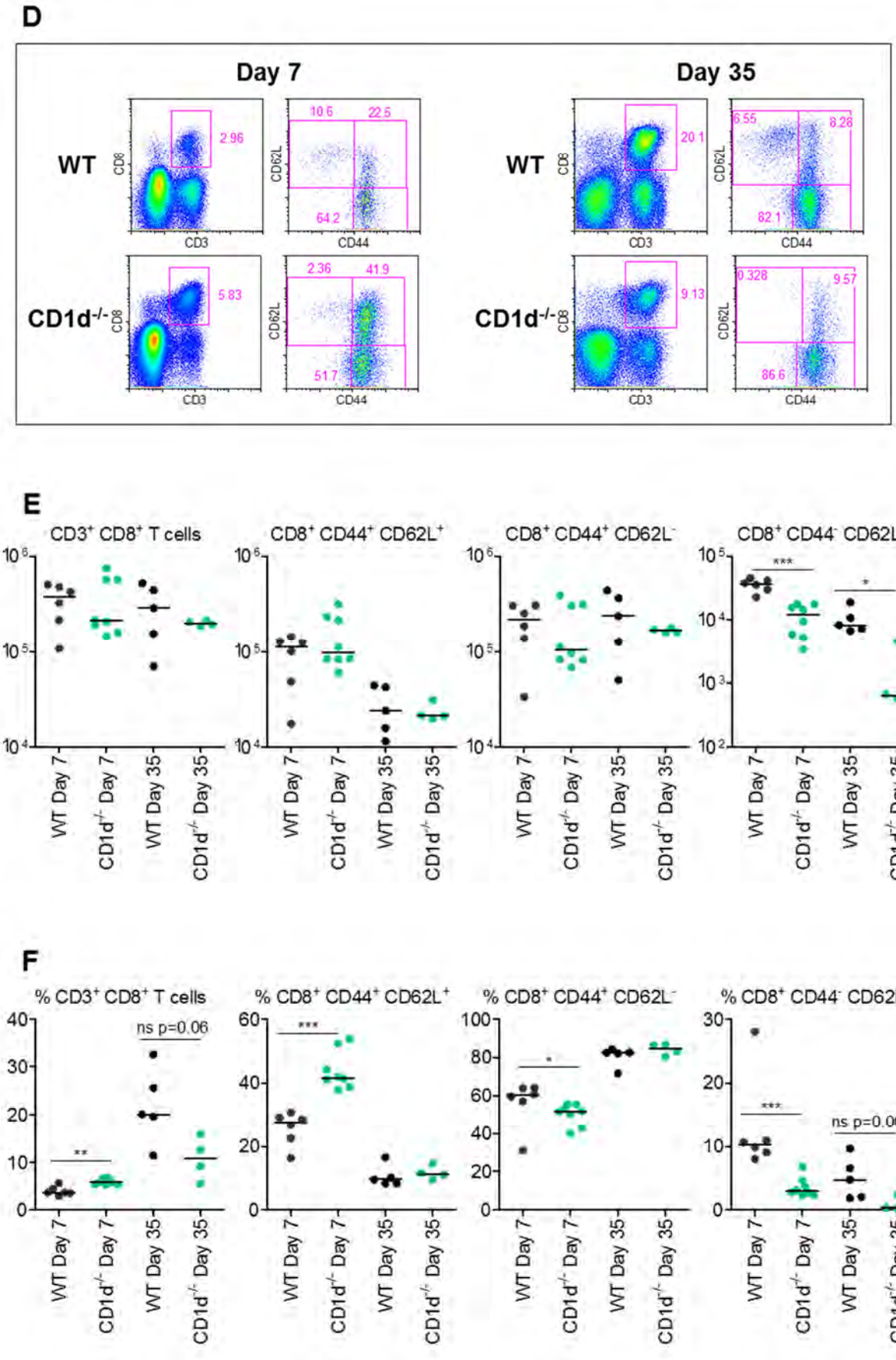

4.11 Discussion

In this chapter we have demonstrated that adaptive cells, although not required for the development of inflammatory lesions, play an important role in their persistence and in the regulation of inflammatory dynamics in the liver. Of particular interest we have identified that Th1 cells drive leukocyte infiltration in the liver during infection and that in the absence of Tbet, the environment is more regulatory. This phenotype is even more pronounced when Tbet is absent specifically from T cells, thus reinforcing the role of Th1 cells in inflammation. In the absence of IFNγ in haematopoietic cells there is a lack of inflammation in the liver during STm infection.

4.11.1 Inflammatory lesions develop in the absence of adaptive immune cells

In mice which lack B and T lymphocytes, inflammatory lesions are observed normally at day 7 post-infection. There can be a more diffuse sinusoidal distribution of parenchymal infiltrate, and lesions can be slightly less defined, but they do form. In the absence of B cells specifically, lesion development is identical to that in WT mice, indicating that B cells are not required to any extent in the formation of inflammatory lesions. When T cells specifically are absent, lesions are present, but as in Rag-1-deficient mice, they can be slightly more diffuse. Therefore, T cells may play some role in the organisation and persistence of lesions once they are formed, but neither B nor T cells are required for initial lesion development. Despite the absence of the entire T cell compartment in TCRβδ$^{-/-}$mice, leukocyte cellularity increases. This is apparent for all myeloid populations measured and may suggest that T cells play a role in regulating innate leukocyte infiltration in the liver.

4.11.2 Tbet is required for normal inflammation in the liver

To elucidate which T cell subset(s) contribute to inflammatory lesion growth, we used genetically altered mice which lacked molecules associated with Th1 and Th2 responses. Lesions form normally in the absence of aspects of Th2 cell signalling (in IL4-deficient mice), and NKT cells (in CD1d-deficient mice). Lesions have not yet been examined histologically in the absence of $CD8^+$ T cells. However, in the absence of Th1 cells (in Tbet-deficient mice), although lesions can form, they are smaller and occur less frequently than in WT mice. This phenotype is more severe than in the absence of total T cells and implicates a role of Th1 cells in lesion maintenance.

4.11.3 Th1 cells drive inflammation in the liver

Tbet is the transcription factor required for $CD4^+$ T cells to differentiate into Th1 cells (Szabo et al., 2000). However, Tbet is not solely expressed in $CD4^+$ T cells, and various roles in other leukocyte populations have been described. For example, Tbet in B cells is important for the production of IgG2a class-switched antibodies, and Tbet expression is required in DCs and $CD8^+$ T cells for the normal function of these cells during immune responses (Mohr et al., 2010, Lugo-Villarino et al., 2003, Sullivan et al., 2003). Whilst Tbet-deficient mice therefore lack Th1 cells, this transcription factor is universally absent, thus the phenotypes we observe may be due to the role of Tbet in other populations.

To address this, we generated mixed bone marrow irradiation chimera mice whereby specifically T cells lacked Tbet. These chimeras demonstrate similar phenotypes to those in mice which are universally deficient in Tbet. Despite this important observation, we cannot comment as to the importance of Tbet expression in $CD8^+$ T cells in our system. In mice lacking CD8 expression we observe substantial differences to WT mice in leukocyte

populations in the liver at the resolution stages of infection. However, as yet we have no evidence that this is due to CD8 expression in T cells, although both histological and flow data illustrate the prominence of $CD8^+$ T cells at later stages of infection. Even if these phenotypes are caused by $CD8^+$ T cells (and not expression of CD8 in other cell types such as DCs), as yet we do not have any data regarding $CD8^+$ T cells in the Tbet/TCRβδ chimeras. Hence we do not know whether Tbet expression in $CD8^+$ T cells plays any role in the function of these cells during inflammation in this system (Sullivan et al., 2003).

4.11.4 In the absence of Tbet there is a more regulatory environment

We demonstrate that in the absence of Tbet, there are fewer $CD3^+$ cells in each inflammatory lesion, and we would expect this to be due to a lack of Th1 cells in these mice. However, there is an increased presence of $FoxP3^+$ regulatory T cells (Tregs) in lesions relative to in Tbet-sufficient mice. In addition, there are less leukocytes observed within the sinusoids in Tbet-deficient mice. These observations suggest that in the absence of Tbet, Tregs may, in some capacity, prevent extensive infiltration which is usually driven by Th1 cells. Whether, in the absence of Th1 cells, Tregs are less “held back” due to the less inflammatory environment, so can accumulate in the liver more readily, or in the absence of Tbet, there is a more fundamental phenotype with regard to $CD4^+$ T cell fate, is not yet known. It should be noted, however, that Tbet expression can be induced in Tregs in an IFNγ-mediated manner, and that this enables their migration into the vicinity of Th1 cells, thus facilitating their efficient regulation of effector cells (Koch et al., 2009).

Regulatory T cells either develop in the thymus from immature $CD4^+$ cells, or peripheral mature but naïve $CD4^+$ T cells can differentiate down a regulatory route outside the thymus (Sakaguchi, 2004, Fehervari and Sakaguchi, 2004). In the absence of Tbet expression at the

developmental stage in the thymus, potentially a greater proportion of $CD4^+$ T cells may develop down the regulatory $FoxP3^+$ lineage in the thymus. Therefore this may explain increased numbers of Tregs in the liver. Alternatively, more peripheral $CD4^+$ T cells may be induced to become regulatory in the absence of pro-inflammatory Th1 cells (in Tbet-deficient mice). However, because $FoxP3^+$ cells in the liver are rare in the absence of infection, we would expect peripheral induction of Treg differentiation to require an inflammatory stimulus (which may be absent in Th1-deficient mice). This is beyond the scope of this study but provides an interesting observation for future investigation. Finally, the increased proportion of $CD4^+$ $FoxP3^+$ cells detected by flow in the mixed bone marrow chimera mice, which lack Tbet specifically in T cells, further emphasises the inflammatory nature of $Tbet^+$ T cells (Ravindran et al., 2005).

4.11.5 IFNγ is required for inflammatory lesion development

The major role of Th1 cells in control of intracellular bacterial infections such as STm is in IFNγ production (Ravindran et al., 2005). Interferon-γ is required to induce efficient phagocytosis by macrophages and hence is vital in effective bacterial clearance (Mastroeni, 2002). Indeed we and others have demonstrated elevated bacterial loads (in a range of bacterial infections) in the absence of IFNγ (Hess et al., 1996, Nauciel and Espinasse-Maes, 1992, Yamamoto et al., 2001, Kupz et al., 2013, Cooper et al., 1993, Mastroeni et al., 1992). Here we demonstrate, in the absence of IFNγ, inflammatory lesions do not develop and leukocyte infiltration is abrogated.

4.11.6 A haematopoietic IFNγ source is required for bacterial clearance and hepatic inflammatory organisation

Considering the similarities between the phenotypes of mice lacking Tbet and mice lacking IFNγ (whereby bacterial load is elevated and inflammation diminished, but to a greater extent in IFNγ-deficient mice), we wanted to further investigate the relationship between hepatic inflammation, bacterial load and IFNγ availability. For this we generated radiation bone marrow chimera mice. These mice clearly demonstrate that IFNγ from a radiation-sensitive (thus probably haematopoietic) source is required for both bacterial clearance and organisation of leukocyte infiltration into inflammatory lesions in the liver. Furthermore, we have recently repeated this experiment including an additional day 21 time-point and early indications suggest that these phenotypes are exacerbated at this time in mice which lack haematopoietic IFNγ (data not shown). However, to fully establish whether it is IFNγ produced by T cells, we will need to generate mixed bone marrow chimeras using IFNγ-deficient and TCRβδ-deficient mice.

4.11.7 Haematopoietic and non-haematopoietic IFNγ have different effects on innate infiltration in the liver

Flow cytometry highlighted differences in leukocytes isolated from the liver depending on the available source of IFNγ. Absolute numbers and proportions of Kupffer cells were reduced at day 7 in mice which had either IFNγ from non-BM sources, or were completely IFNγ-deficient. Whereas mice which had non-BM-derived IFNγ had higher absolute numbers and proportions of $Ly6G^{+}$ and $Ly6G^{hi}$ cells relative to mice with BM-derived IFNγ. These data suggest that non-haematopoietic IFNγ plays a role in the accumulation of neutrophils in the liver during inflammation, whilst Kupffer cell expansion is dependent (to

some extent) on haematopoietic IFNγ. As mentioned above, bacterial loads are greater in mice which lack total IFNγ and are generally elevated in mice whereby IFNγ is derived from non-BM sources. These are the same groups of mice with lower-than-WT numbers of Kupffer cells. These data could be interpreted as IFNγ from BM cells is required for both Kupffer cell expansion and bacterial clearance, which would suggest that in the liver it is Kupffer cells which are responsible for bacterial phagocytosis. One could hypothesise that this BM source of IFNγ is Th1 cells, although this is speculative as multiple bone-marrow derived cells produce this cytokine (Ravindran et al., 2005, Seki et al., 1998). Finally, $CD4^+$ T cells do not require any IFNγ source for accumulation in the liver, whereas $CD8^+$ T cell numbers and proportions are dampened when IFNγ is lacking from any compartment (BM, non-BM or both).

4.11.8 Signalling through TNFα is not required for inflammatory lesion development

To determine whether the lack of inflammatory lesion development in the absence of IFNγ is due to pro-inflammatory signals in general, we used TNFαR-deficient mice. In these mice, inflammatory lesions develop as normal at day 7, demonstrating that TNFαR signalling is not required. Indeed bacterial load is equivalent to WT in these mice at day 7, thus at this time, TNFαR plays no role in innate control of bacterial replication. These data reflect that the phenotype seen in IFNγ-deficient mice may be specific to that cytokine.

Despite TNFαR not being required for lesion development, there are pronounced differences in leukocyte populations in the liver in the absence of this receptor. Absolute numbers of all myeloid populations examined are reduced and the ratio of Kupffer cells to monocytes is greater than 1 (as it is in non-infected mice). This reflects a more Kupffer cell-

dominated environment, highlighting defects in monocyte accumulation in the liver in the absence of TNFαR signalling. This would suggest that in these mice, although lesions develop, they may be composed more of Kupffer cells and less of monocytes ($Ly6C^{hi}$ cells) and neutrophils ($Ly6G^{+}$). It is likely these lesions remain functional as bacterial loads are not affected. Despite the altered proportions of myeloid cells, however, absolute numbers of Kupffer cells are also reduced relative to WT. This may implicate defects in Kupffer cell proliferation or in differentiation of circulating monocytes into tissue resident macrophages in the absence of TNFαR (Seki et al., 2000). Numbers and relative proportions of both $CD4^{+}$ and $CD8^{+}$ T cell subsets are unaffected by lack of TNFαR.

4.11.9 Inflammation resolution: the roles of $CD8^{+}$ T cells and iNKT cells

As eluded to above, we detect substantial differences in leukocyte accumulation in the liver during resolution of infection in mice which lack either CD8 or CD1d.

4.11.9.1 $CD8^{+}$ T cells in monocyte dispersal

In Chapter 3, we demonstrated how $CD8^{+}$ T cell numbers peak during infection resolution. We also showed that in WT mice hepatomegaly does not fully resolve within 50 days of infection. Here we show that in $CD8^{-/-}$ mice, hepatomegaly is reduced to a greater extent than in WT mice at day 35 post-infection, suggesting a putative link between numbers of $CD8^{+}$ T cells and liver mass during infection resolution. The increase in $CD8^{+}$ T cell numbers and proportions which we detect in WT mice at day 35 would suggest these cells have a function at this time. Whilst there are no significant alterations to $CD4^{+}$ T cell populations in the absence of CD8, the proportion of monocytes in the liver at day 35 remains elevated. This, in addition to the accumulation of $CD8^{+}$ T cells in the liver at this time, may suggest $CD8^{+}$ T cells play a role in resolution of infiltrating $Ly6C^{hi}$ monocytes. An important point in

this context is that although we have examined the activation status of T cells, we have not investigated their cytokine profiles. This is an important future step.

Bacteria, although cleared by day 35 in the absence of CD8, generally persist to a greater extent than in WT mice. Recently, CD8 has been shown to play a role in antibody class switching, thus the defective bacterial clearance we detect in the liver may be accounted for by diminished antibody responses (Faustini, manuscript in preparation). However, whether these effects are due to T cell expression of CD8 or expression by other cells including DCs are not yet known (Hsu et al., 2007).

4.11.10 Invariant NKT cells are required for bacterial clearance

Mice lacking iNKT cells have an impairment in their ability to clear bacteria from the liver. As bacterial loads are similar to WT mice at day 7, this suggests that CD1d is important in the resolution of infection. However, leukocyte cellularity is reduced at day 7 and elevated at day 35 relative to WT, suggesting both reduced initial accumulation of infiltrate, and defective inflammatory resolution. Hence iNKT cells are important in both the onset and resolution of inflammation in the liver.

Inflammatory lesions develop normally in CD1d-deficient mice by day 7 post-infection, and livers from these mice have an equivalent bacterial load to WT at this time. Yet despite the elevation in myeloid cells at day 35, bacteria are not cleared, although burdens are lower than day 7. The ratio of Kupffer cells to monocytes does not resolve as it does in WT mice, reflecting a greater proportion of monocytes; numbers of $Ly6G^{+}$ and $Ly6G^{hi}$ cells are also increased. Invariant NKT cells are an important source of IFNγ, although it is suggested they are not as potent IFNγ producers as NK cells (Emoto and Emoto, 2009, Seki et al., 1998). However, these data may potentially indicate that in the absence of iNKT cells, there is

reduced IFNγ production (by haematopoietic cells) and that this may prevent adequate accumulation of Kupffer cells (as shown by the IFNγ chimera data) and hence bacterial clearance is impaired. The enhanced presence of monocytes and Ly6G-expressing cells may not contribute to bacterial clearance to the extent that Kupffer cells may do, (as suggested in the IFNγ chimera experiment where higher bacterial loads corresponded with lower proportions of Kupffer cells). These findings potentially contribute to the IFNγ chimera data discussed above and it will be interesting if the haematopoietic IFNγ source is both T and non-T cell-dependent (Seki et al., 2000).

In addition, there are 10-fold fewer activated $CD4^+$ T cells at day 7 in $CD1d^{-/-}$ mice, again, suggesting a relationship between iNKT cells and $CD4^+$ T cell accumulation in the liver during infection. This defect is also apparent in non-infected mice, yet numbers of activated $CD8^+$ T cells are higher in non-infected $CD1d^{-/-}$ mice. Furthermore, numbers of $CD8^+$ T cells are maintained at day 35 as they are in WT mice, indicating that during resolution, the absence of iNKT cells bears no effect on $CD8^+$ T cells.

4.12 Conclusion

Here we have demonstrated the necessity for IFNγ in hepatic inflammation during *Salmonella* infection and have identified that a haematopoietic source of this cytokine is required for lesion development. Whilst adaptive cells are not required for the initial development of inflammatory foci in the liver during infection, these cells play a significant role in the regulation of inflammation in the liver. We have begun to explore the balance between inflammation and inflammatory regulation in the liver, which is facilitated by expression of Tbet in T cells. These observations contribute to our understanding of inflammation in parenchymal liver tissue and have highlighted several avenues of study

which may influence how inflammation is perceived with regard to therapeutic intervention. In addition to parenchymal inflammation in this murine model, we, and others, detect severe vascular occlusion in the blood vessels during infection. This is descried fully in the next chapter.

CHAPTER 5:

THE REGULATION OF HEPATIC THROMBOSIS AFTER SYSTEMIC *SALMONELLA* INFECTION

5.1 Introduction

The direct and indirect contributions of platelets to immune responses are becoming increasingly well recognised. There are multiple reports of platelets assisting other innate players and this has been described fully in section 1.3.7, Chapter 1. Infection is a wonderfully appropriate platform to further investigate the role of platelets in immune regulation because it provides an insight into the physiological consequences of this interaction. And this is becoming increasingly recognised, as the therapeutic control of bacterial infection begins to reach beyond ever-problematic obstacles (such as antibacterial resistance) to other physiological effects of infection, including multiple organ failure and, as we describe here, thrombosis. Indeed, the recent introduction of the term *Immunothrombosis* emphasises the importance of this emerging field (Engelmann and Massberg, 2013). Here we have studied how thrombus development is regulated during *Salmonella* infection. Thrombosis is a well described feature of typhoid, but the mechanisms behind it remain relatively unexplored.

5.1.1 Thrombosis and *Salmonella* infections

In the context of murine NTS infections, there are occasional reports of thrombosis during infection, and these are generally in reference to colonised RES organs including the spleen and liver (Roy et al., 2006, Nakoneczna and Hsu, 1983, Mastroeni et al., 1995, Brown et al.,

2010). Additionally, DIC-like phenotypes have been reported in some studies (Brown et al., 2010). These observations are brief and descriptive, without offering insight as to how or why thrombosis occurs. In human NTS infections, haemostatic abnormalities of any description are little more than anecdotal. There is, however, more evidence of thrombosis in human *S*. Typhi infections (Malik, 2002, Serefhanoglu et al., 2003, Yildirim et al., 2010, Butler et al., 1978, Nguyen et al., 2001). Furthermore, especially before the advent of antibacterial therapeutics, thrombosis was ascribed to typhoid fever and multiple additional bleeding complications were also commonly associated with this disease (Huckstep 1962). Incidentally, these bleeding abnormalities have been linked to cause if death in infected individuals (Huckstep 1962). Thus, thrombosis during *Salmonella* infections in humans is well documented, yet has received little attention. In this Chapter, we will describe this thrombosis phenotype and investigate the mechanism of platelet activation.

5.1.2 Aim of study

We were keen to explore the thrombosis phenotype which occurs in the hepatic vasculature during systemic *Salmonella* infection. We were particularly interested in the potential co-regulation between inflammation within the liver and in the vascular system, and in the relationship between inflammation and platelet activation. Thus the aims of this section were to:

- Characterise the thrombosis phenotype over the course of infection;
- Identify which host immune cells contribute to this response;
- Determine the mechanism of thrombosis;
- Understand the relationship between thrombosis and tissue inflammation.

5.2 Thrombi develop in the hepatic venous system during systemic *Salmonella* infection

Alongside the development of inflammatory foci in the liver, thrombosis is observed in the hepatic vasculature within 5 days of intraperitoneal (i.p.) *Salmonella* infection. This can be very extensive, completely occluding the vessel lumen in places (Fig 5.1 A-D). These thrombi develop specifically in the veins of the liver, (identified by thin vascular walls), and in particular thrombi are found in the portal vein, identified histologically by proximity to the hepatic artery, bile ducts and lymphatic vessels, all of which contribute to the portal tract (Fig 5.1 E). Thrombi are not detected in arteries and arterioles in the liver. To confirm that thrombosis is not a phenotype specific to the i.p. infection route, intravenous infections were also performed and the extent of thrombosis measured at day 7 and 21 post-infection. Thrombosis occurs to a similar extent as for i.p. injection (Fig 5.1 F-G). We do not detect vascular occlusion in the spleen, kidney, lung, brain and thymus (Fig 5.1 H-I and not shown). Therefore, in this model of infection, thrombosis appears to be a liver-specific host response to *Salmonella* infection, occurring primarily in the portal vein.

5.2.1 Thrombi develop with parallel kinetics to hepatic inflammatory lesions

To understand how thrombosis contributes to the host response to infection, thrombi development over the time-course of infection was characterised by histology. Thrombi appear around day 5 post-infection and peak in severity at day 21 and are largely resolved by day 35 (Fig 5.2 A-B and data not shown).

Figure 5.1

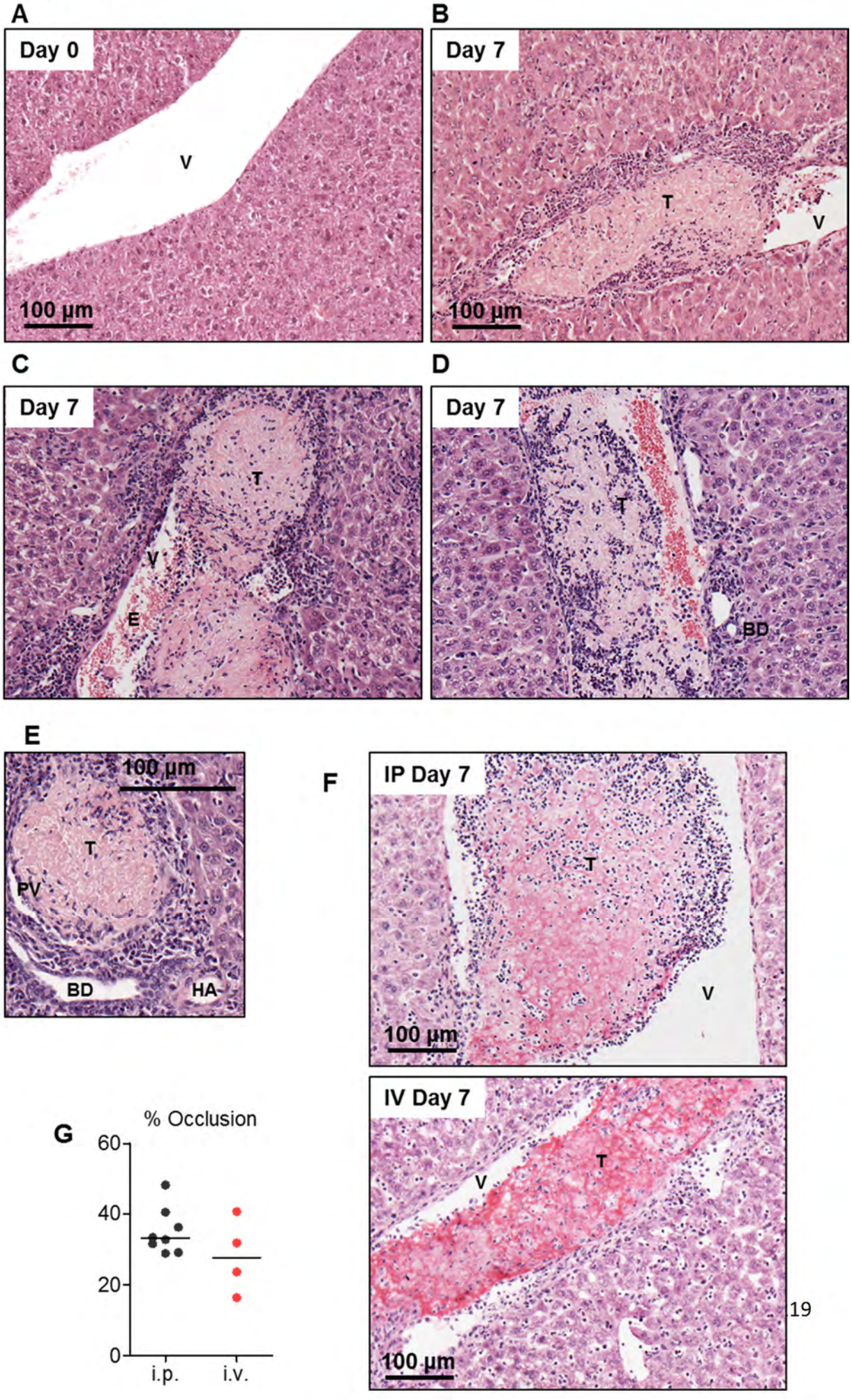
A
Day 0
V
100 µm
B
Day 7
T
V
100 µm
C
Day 7
T
V
E
D
Day 7
T
BD
E
100 µm
T
PV
BD
HA
F
IP Day 7
T
V
100 µm
IV Day 7
T
V
100 µm
G
% Occlusion
60
40
20
0
i.p.
i.v.

Figure 5.1 continued

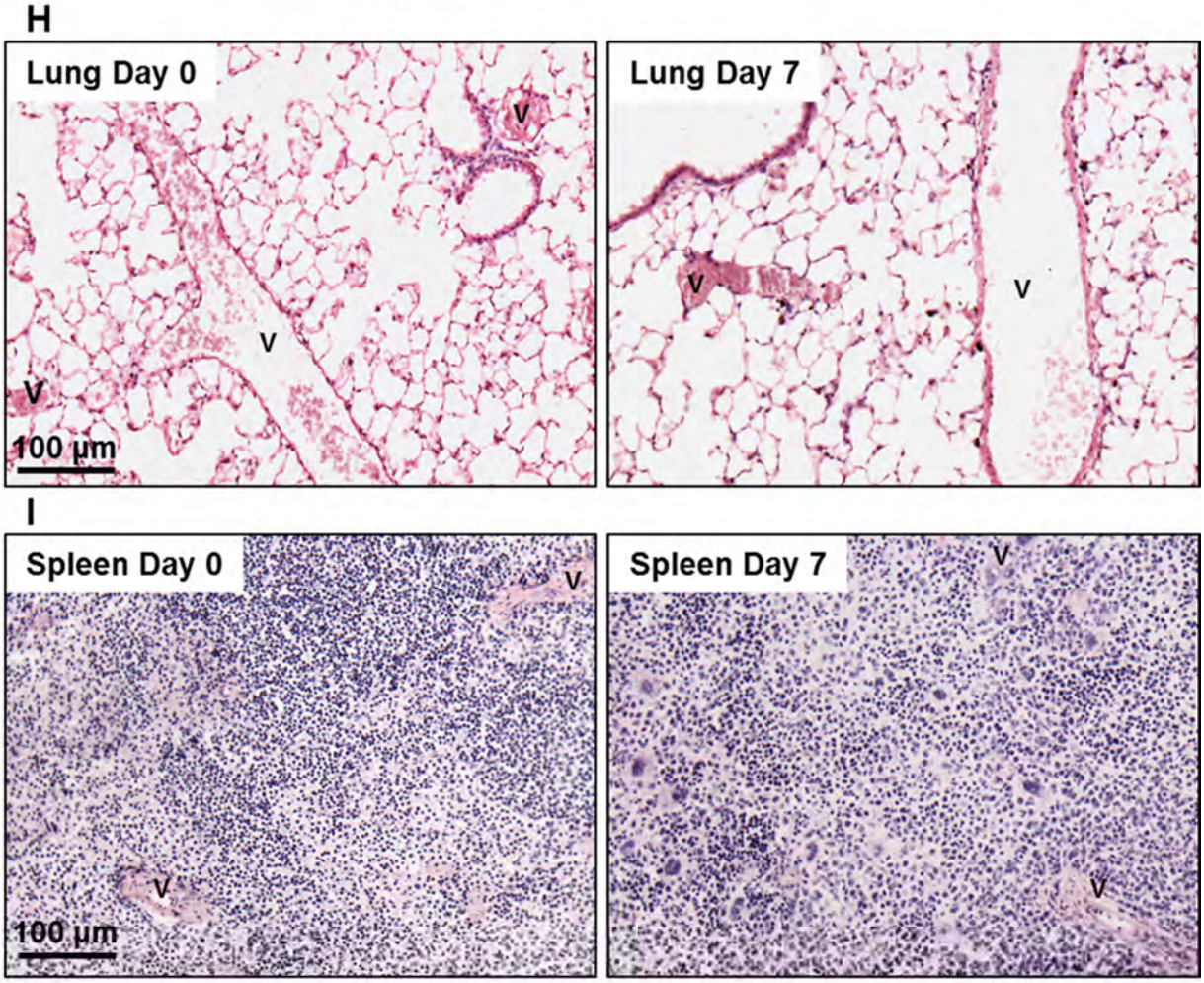

Figure 5.1 Thrombi develop in veins in the liver during Salmonella infection
WT mice were infected (i.p.) with 5 x 10^5 CFU attenuated STm. Livers were removed at days 0 and 7 post-infection and frozen tissue sections were examined by H&E. A) The vasculature is intact in livers from non-infected mice; V = vessel. B-D) At day 7 post-infection, thrombi are observed in the liver vasculature; V = vessel; T = thrombus; E = erythrocytes; BD = bile duct. E) Thrombi are detected primarily in the portal vein (PV), identified by proximity to hepatic artery (HA) and bile ducts (BD). Images are representative of all livers studied; thrombi are observed in all WT mice at day 7 post-infection. Images are taken from different mice in different experiments. F) WT mice were infected i.p. or i.v. with 5 x 10^5 CFU attenuated STm (using the same preparation of bacteria) for 7 days. Frozen tissue sections were examined by H&E (V = vessel; T = thrombus) and G) the percentage of vessel occlusion was quantified by point counting of all large vessels per tissue section (detailed in section 2.5.4.1). Counts are expressed as a percentage. Images are representative and are taken from one experiment where n = 4. H-I) WT mice were infected (i.p.) as described above and the lungs (H) and spleen (I) were examined at days 0 and 7 post-infection. Spleens were frozen before sectioning, whereas lungs were preserved in Formaldehyde and were paraffin-embedded. All tissues were examined by H&E for thrombus formation (V = vessel). Images are representative of 2 separate experiments, where n = 4 in each.

Figure 5.2

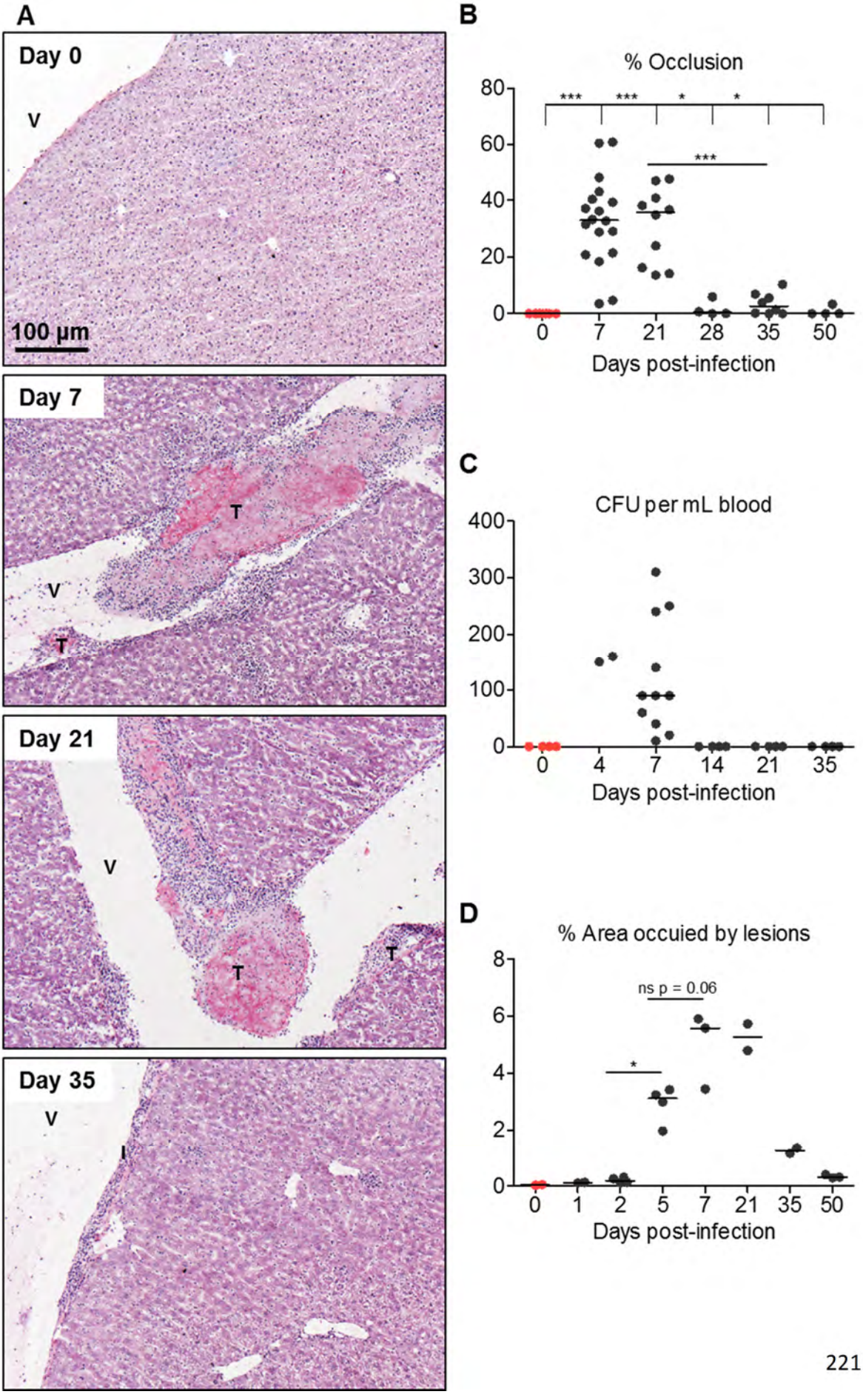
A
Day 0
V
100 µm
Day 7
T
V
T
Day 21
V
T
T
Day 35
V
B
% Occlusion
80
60
40
20
0
***
***
*
*
***
0
7
21
28
35
50
Days post-infection
C
CFU per mL blood
400
300
200
100
0
0
4
7
14
21
35
Days post-infection
D
% Area occuied by lesions
8
6
4
2
0
ns p = 0.06
*
0
1
2
5
7
21
35
50
Days post-infection

Figure 5.2 Thrombosis is most severe between days 7 and 21 post-infection
WT mice were infected (i.p.) with 5 x 10^5 CFU attenuated STm. A) At key time-points post-infection (days 0, 7, 21, 28, 35 and 50) livers were removed and thrombus formation was examined on frozen tissue sections by H&E. V = vessel; T = thrombus; I infiltrate. All images are representative and are taken from the same experiment where n = 4 at each time-point. B) The extent of thrombosis was quantified by point counting the percentage of occlusion of all large vessels per tissue section (detailed in section 2.5.4.1). Counts are expressed as a percentage. Data are taken from multiple experiments with similar results, where n > 4 at each time-point. C) WT mice were infected (i.p.) as described and bacteraemia was calculated in the blood at the indicated time-points post-infection. Data are taken from one experiment experiments where n > 2 at each time-point (with the exception of day 7 post-infection; data are taken from multiple experiments). D) Figure repeated from section 3.3B. The percentage area of liver tissue sections was quantified by point-counting at the indicated time-points post-infection. *p≤0.05 **p≤0.01 ***p≤0.001. I) The proportion of Kupffer cells to monocytes during infection. J)

Whilst infection is required for thrombus development, it is not related to bacteraemia directly as the severity of bacteraemia peaks around day 7 post-infection, and bacteria cannot be detected in the blood beyond day 14 (Fig 5.2 C). Thus the severity of thrombosis peaks at day 21 when viable bacteria are no longer found in the blood. This suggests that thrombus development and indeed maintenance of thrombus severity is determined by the host response to infection, or bacteria in tissues, rather than purely relating to the presence of bacteria in the blood. Intriguingly and suggestively, the kinetics of thrombus development and resolution more closely parallel those of inflammatory foci in the liver, rather than those of bacterial colonisation of the liver (Fig 5.2 D). We therefore hypothesised that both these features of the host response to infection share elements of co-regulation.

All quantification of thrombosis severity in this study is presented as a percentage of vessel occlusion. For this measure to be comparable, it is assumed that total vessel area is equivalent both in the presence and absence of infection, and in all mouse strains used, (see below). Due to the substantial hepatomegaly after infection, it is likely that the proportion of tissue occupied by vessel may differ. To standardise as far as possible, generally thrombi have been quantified in an equivalent large portion of the portal vein in each tissue, although this is an approximation to be aware of.

5.2.3 Thrombi are composed of platelets and are surrounded by a leukocyte cuff

The composition of thrombi was investigated to identify which host cells may play a role in thrombus formation. Since thrombi are well established within one week of infection, livers from infected mice were examined at 7 days post-infection. The white appearance of

thrombi suggested a high platelet content, which was confirmed by staining for the platelet-specific integrin subunit αIIb (CD41) (Fig 5.3 A). Furthermore, thrombi are Von Willebrand factor (VWF)-positive as shown by magenta dual $CD41^+$ VWF^+ cells in Figure 5.3 B-D. This further supports the platelet composition of thrombi, as activated platelets bind to VWF (Lenting et al., 2012). In addition, $CD31^+$ vascular endothelial cells also express VWF during infection, shown by cyan staining (Figure 5.3 B-C).

We hypothesised that thrombi form in situ in the liver (rather than forming in other sites) for the following two reasons. Firstly: thrombi consistently appear to be closely associated with the host vessel wall and are rarely seen free in the vessels. This association predominantly occurs at sites of leukocyte accumulation (Fig 5.3 E). Secondly, thrombi are surrounded by a heterogeneous cuff of leukocytes (Fig 5.3 F-H). These cells were identified by immunohistochemistry (IHC) as being variably positive for F4/80, CD11c, CD3, and Ly6C. These leukocytes are found around the surface of thrombi, whilst $Ly6G^+$ cells, when found, are consistently located within the bulk of the thrombus.

Seeing as we detect endothelial expression of VWF during infection, we looked for further evidence of endothelial activation during infection to decipher whether this surface may provide platelet-activating stimuli. Endothelial up-regulation of V-CAM-1, ICAM-1, CD105 and Ly6C were identified at day 7 post-infection by IHC (data not shown). However, we do not detect MHC II expression by $CD31^+$ endothelial cells following infection, which can be a useful marker of endothelial activation (data not shown) (Puntener et al., 2012). These data suggest there are selective changes in the endothelial phenotype after *Salmonella* infection.

Figure 5.3

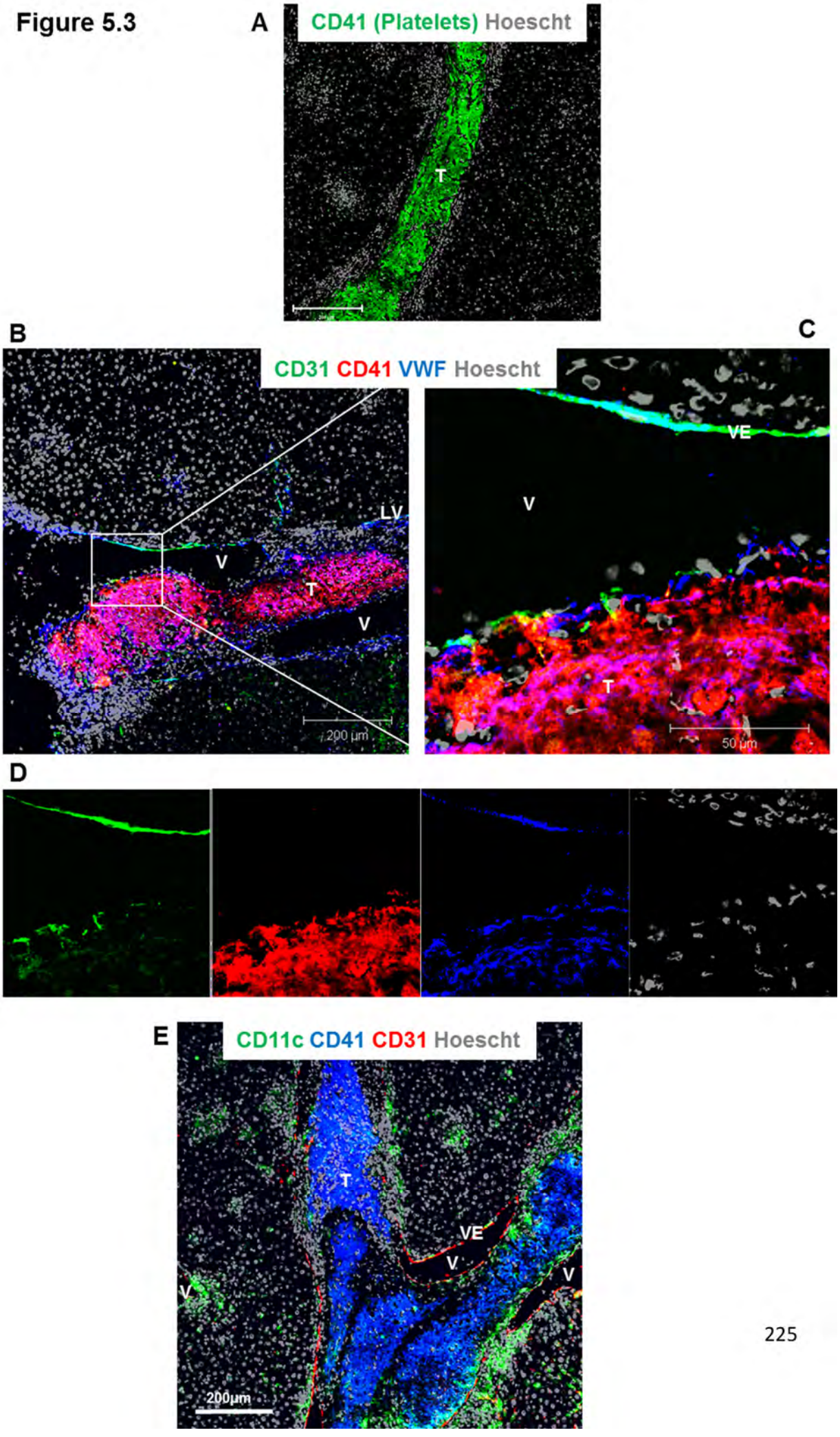
A
CD41 (Platelets) Hoescht
T
B
CD31 CD41 VWF Hoescht
LV
V
T
V
200 µm
C
VE
V
T
50 µm
D
E
CD11c CD41 CD31 Hoescht
T
VE
V
V
V
200µm

Figure 5.3 continued

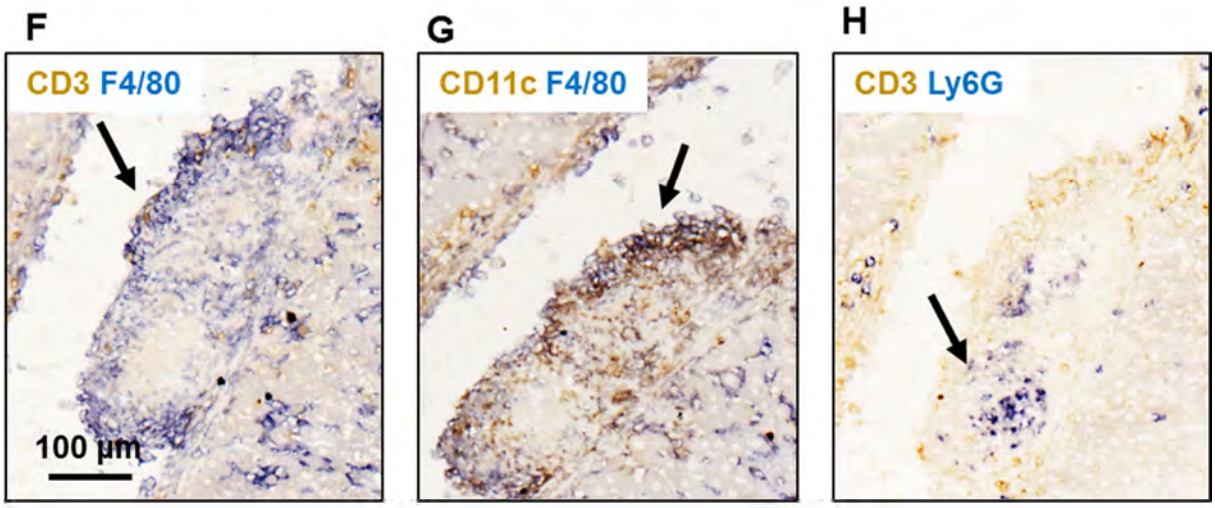

Figure 5.3 Thrombi are composed of CD41⁺ platelets and have a leukocyte cuff
WT mice were infected (i.p.) with 5 x 10^5 CFU attenuated STm for 7 days. Livers were frozen and sectioned for histological examination. A) Thrombi are composed of CD41⁺ platelets (green). B-D) Platelets in thrombi co-localise with Von Willebrand Factor (VWF), shown by magenta staining of red CD41⁺ cells and blue VWF⁺ cells. CD31-expressing vascular endothelial cells (green) express VWF (cyan staining); yellow staining shows CD31⁺ CD41⁺ cells. The boxed area in B) is magnified in C) and single colours are shown in D). E) Platelet thrombi associate with CD31⁺ vascular endothelium at sites of leukocyte infiltration (illustrated by CD11c⁺ cells). CD31⁺ cells = red; CD41⁺ cells = blue; CD11c⁺ cells = green. V = vessel; T = thrombus; LV = lymphatic vessel. VE = vascular endothelium. F-H) Serial sections were stained by IHC to identify leukocytes in contact with platelet thrombi. F) CD3⁺ cells (brown) and F4/80⁺ cells (blue); G) CD11c⁺ cells (brown) and F4/80⁺ cells (blue); H) CD3⁺ cells (brown) and Ly6G⁺ cells (blue). All images are representative and are taken from different experiments where n = 4. Confocal images are co-stained with nuclear dye Hoescht.

5.3 Thrombosis in the liver is paralleled by a severe thrombocytopenia

Considering platelets are the main constituent of the thrombi seen in the liver during infection, we hypothesised that these cells could play a vital role in the systemic response to infection. To measure how platelet numbers are altered by *Salmonella* infection, platelets in the blood of infected mice were quantified throughout the time-course of infection. Reference values for platelet numbers from the literature are indicated in Table 5.1 below. Blood obtained from non-infected mice were in accordance with reference values.

Parameter	Male	Female
Platelets (per mm^3)	7.54×10^5	7.57×10^5

Table 5.1. Median platelet counts of C57BL/6J mice aged 3-7 months. Table adapted from (Mazzaccara et al., 2008).

Severe thrombocytopenia is observed in the blood by day 7 post-infection, and this persists at day 21 (Fig 5.4 A). Platelet numbers begin to resolve by day 28 and are normal by day 50. Within this time frame, the mean platelet volume (MPV) shows some limited inverse correlation with platelet numbers, with an elevated MPV observed at both day 7 and 21 (Fig 5.4 B). Mean platelet volume is normal by day 50. Both increased MPV and reduced platelet counts occur in parallel with severity of thrombosis in the liver. In addition, increased megakaryocytes are observed in the spleen at day 7 post-infection (Fig 5.4 C-D).

Figure 5.4

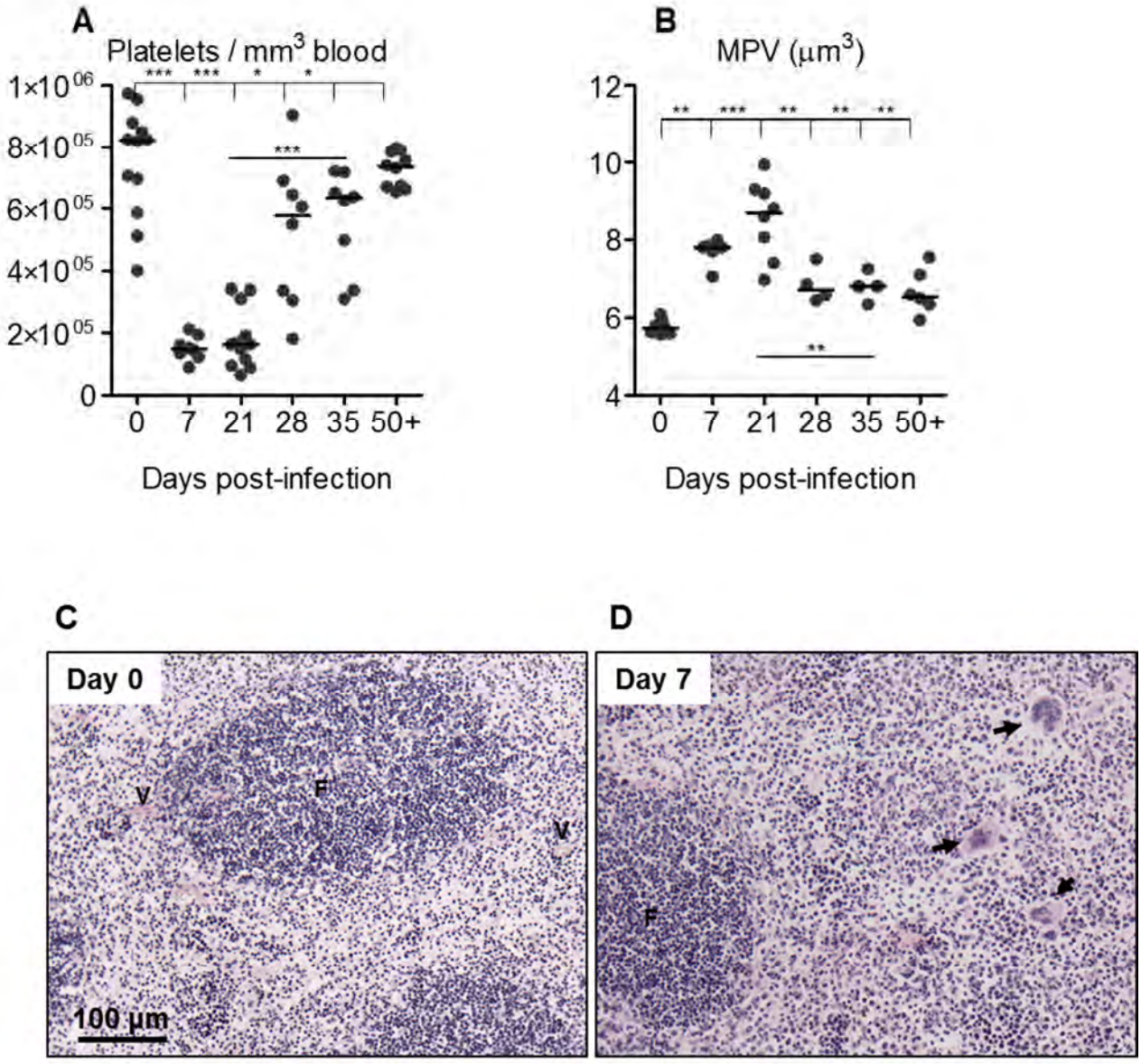

Figure 5.4 Thrombocytopenia is pronounced during infection in addition to increased platelet volume

WT mice were infected (i.p.) with 5 x 10^5 CFU attenuated STm. A) At the indicated time-points post-infection, mice were killed and platelet numbers and B) mean platelet volume were measured in the blood. Data are taken from multiple experiments showing similar results, where n > 3 at each time-point in each infection. C) WT mice were infected as described and megakaryocytes were detected in the spleen by H&E staining of frozen spleen sections at days 0 and 7 post-infection. Images are representative of one experiment where n = 4 at each time-point. V = vessel; F = follicle; black arrows indicate megakaryocytes. *p≤0.05 **p≤0.01 ***p≤0.001.

5.4 Development of thrombosis occurs independently of the adaptive immune response

To investigate how the host immune response may contribute to thrombosis (and whether thrombosis is regulated in a similar manner to foci formation), we wanted to know if thrombi develop in mice which lack key components of the host's repertoire of immune cells or molecules. Importantly, thrombi are not detected in non-infected mice of any strain used in this study (data not shown). Whilst platelet numbers and MPV in non-infected mice are similar across all strains used, there are subtle variations in some strains: in particular Rag-1$^{-/-}$, IgHκ$^{-/-}$, TNFαR$^{-/-}$ and IL10$^{-/-}$ mice have modest elevations in platelet numbers (Fig 5.5 A-B).

To determine which host cells are important in thrombosis, mice which lacked B lymphocytes, T lymphocytes or both B and T lymphocytes were infected and thrombus formation in the liver was quantified after 7 days. Generally, thrombi develop normally in the absence of total lymphocytes (Fig 5.6 A-C), and of B cells (Fig 5.7 A-C), or T cells (Fig 5.8 A-C), although this can be variable. However, the presence of thrombi in these mice indicate that the initiation of thrombosis does not require the adaptive immune response. This parallels the observation that inflammatory lesions also develop in the absence of B cells and T cells (described in Chapter 4). In addition, the thrombocytopenia and MPV in these mice after infection, whilst variable, is comparable to that seen in infected WT mice; (in exception, Rag-1$^{-/-}$ mice have less severe thrombocytopenia than WT mice) (Fig 5.6 to 5.8 D-E).

Figure 5.5

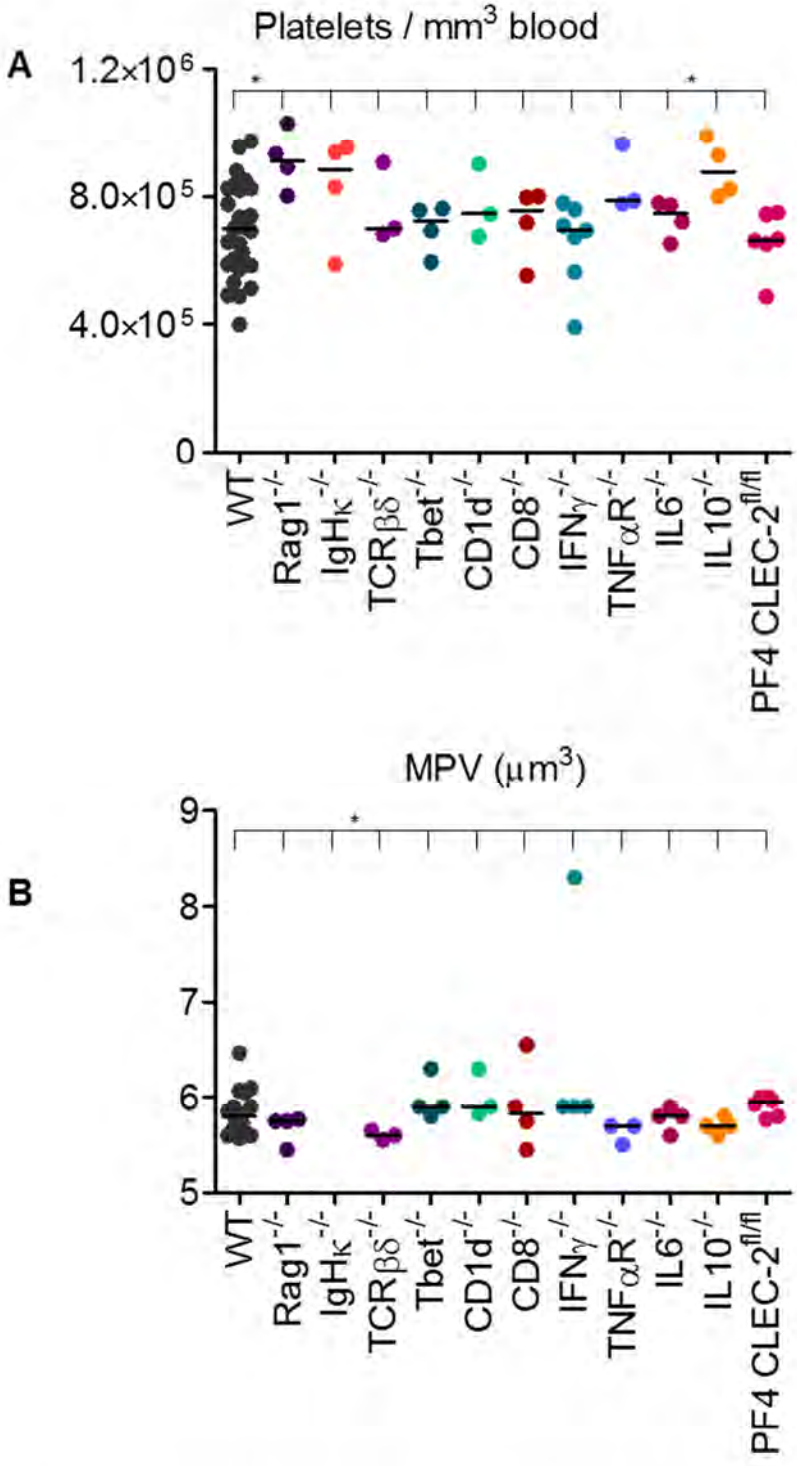

Figure 5.5 Platelet numbers and mean platelet volume are similar in all strains of mice examined

Non-infected, resting WT and genetically modified mice were killed and blood was obtained for measurement of A) platelet numbers and B) mean platelet volume. Data are taken from different experiments on different days where n > 3 for each strain of mice. Details of mice strains can be found in Chapter 2 section 2.2. *p≤0.05 **p≤0.01 ***p≤0.001.

Figure 5.6

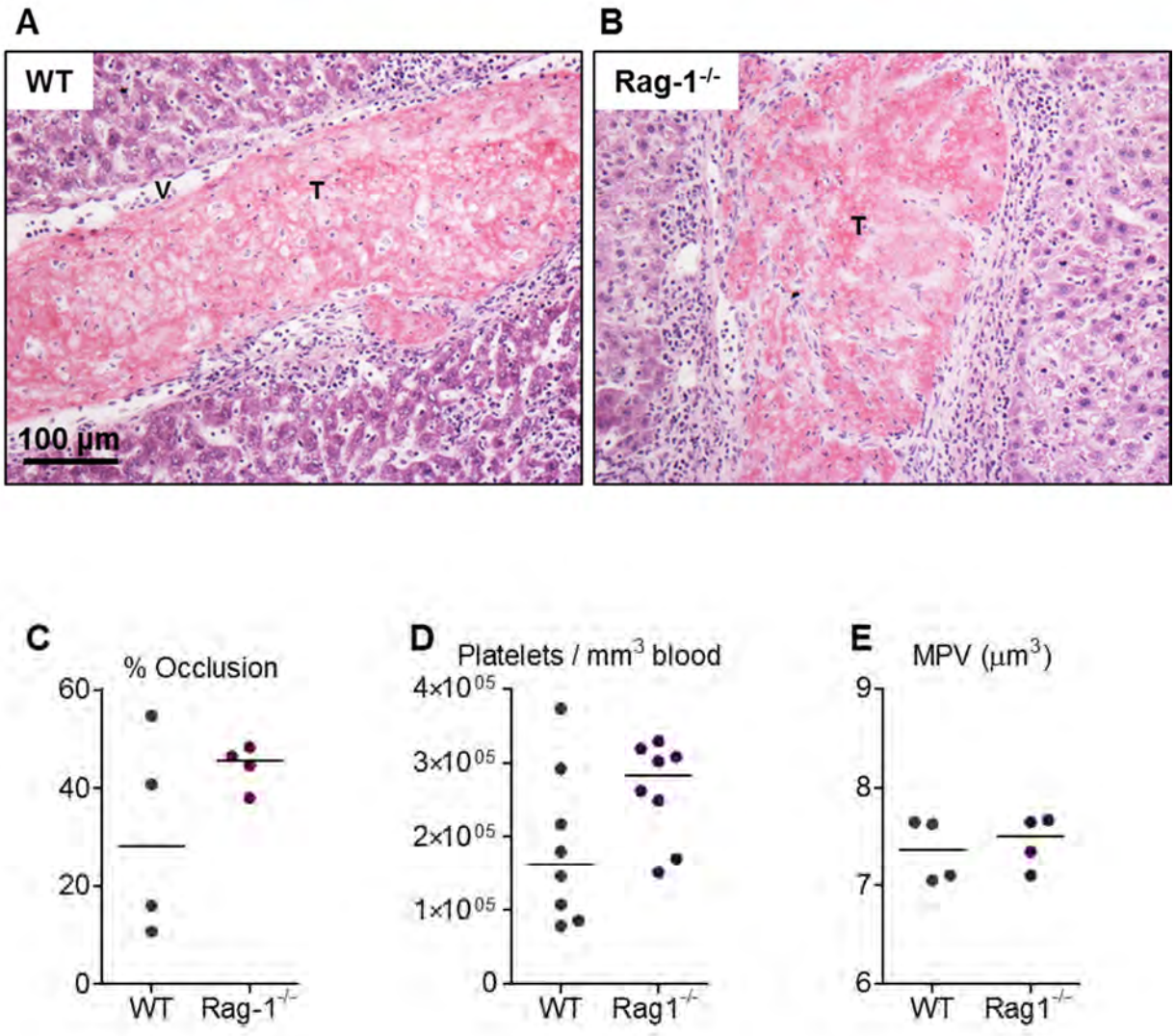

Figure 5.6 Thrombi develop in the liver in the absence of B and T cells
WT and Rag-1$^{-/-}$ mice were infected (i.p.) with 5 x 10^5 CFU attenuated STm. At day 7 post-infection, livers from A) WT and B) Rag-1$^{-/-}$ mice were examined for thrombosis by H&E of frozen tissue sections. Images are representative of multiple experiments, each with n = 4 per mouse strain. V = vessel; T = thrombus. C) The extent of thrombosis was quantified by point counting the percentage of occlusion of all large vessels per tissue section (detailed in section 2.5.4.1), and counts are expressed as a percentage. Data are taken from one experiment, where n = 4 in each mouse strain. WT and Rag-1$^{-/-}$ mice were infected as in A and B) and blood was obtained from day 7-infected mice for assessment of D) platelet numbers and E) mean platelet volume. Data are from the mice detailed in A and B above (with the exception of mean platelet volume data which was only available for one experiment).

Figure 5.7

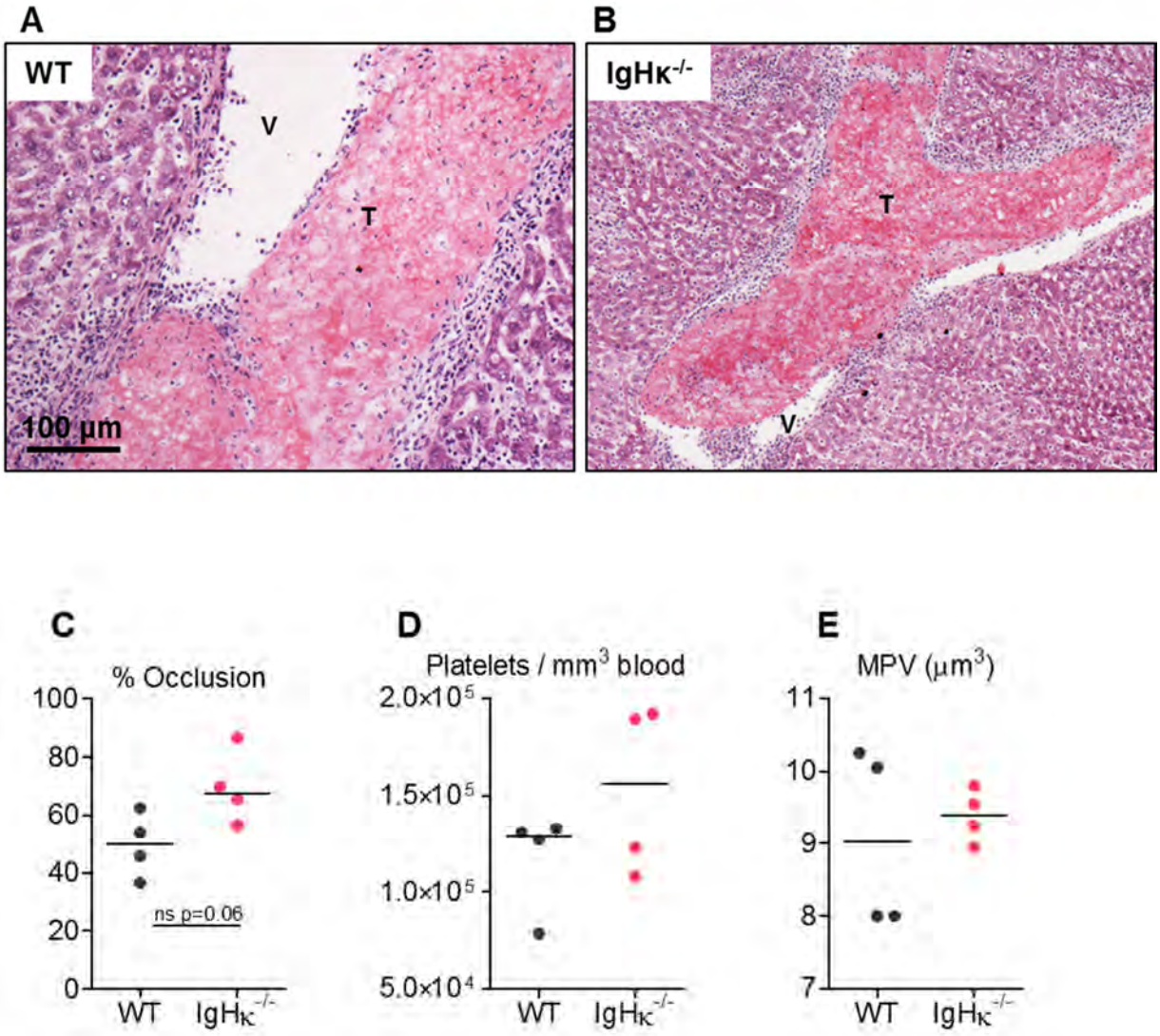

Figure 5.7 Thrombi develop in the liver in the absence of B cells
WT and IgH$^{-/-}$κ$^{-/-}$ (IgHκ$^{-/-}$) mice were infected (i.p.) with 5 x 10^5 CFU attenuated STm. At day 7 post-infection, livers from A) WT and B) IgHκ $^{-/-}$ mice were examined for thrombosis by H&E of frozen tissue sections. Images are representative of one experiment where n = 4 per mouse strain. V = vessel; T = thrombus. C) The extent of thrombosis was quantified by point counting the percentage of occlusion of all large vessels per tissue section (detailed in section 2.5.4.1), and counts are expressed as a percentage. Data are taken from one experiment, where n = 4 in each mouse strain. WT and IgHκ $^{-/-}$ mice were infected as in A and B) and blood was obtained from day 7-infected mice for assessment of D) platelet numbers and E) mean platelet volume. Data are from the mice detailed in A and B above. *p≤0.05 **p≤0.01 ***p≤0.001.

Figure 5.8

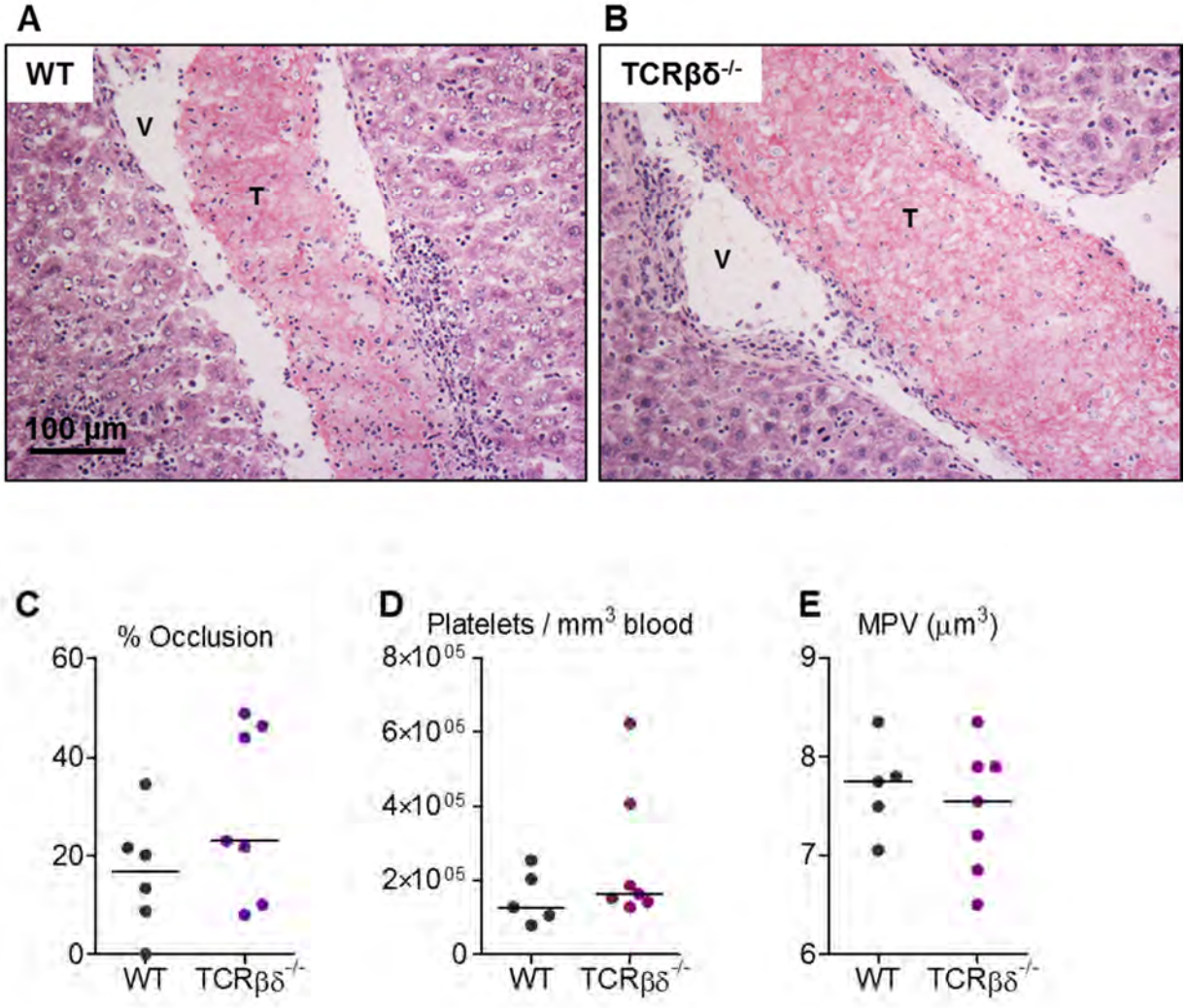

Figure 5.8 Thrombi develop in the liver in the absence of T cells
WT and TCRβδ$^{-/-}$ mice were infected (i.p.) with 5 x 10^5 CFU attenuated STm. At day 7 post-infection, livers from A) WT and B) TCRβδ$^{-/-}$ mice were examined for thrombosis by H&E of frozen tissue sections. Images are representative of multiple experiments where n = 3 per mouse strain in each experiment. V = vessel; T = thrombus. C) The extent of thrombosis was quantified by point counting the percentage of occlusion of all large vessels per tissue section (detailed in section 2.5.4.1), and counts are expressed as a percentage. Data are taken from the mice detailed in A and B above. WT and TCRβδ$^{-/-}$ mice were infected as in A and B) and blood was obtained from day 7-infected mice for assessment of D) platelet numbers and E) mean platelet volume. Data are from the mice detailed in A and B above.

5.5 Thrombosis is augmented in the absence of Tbet, but not IL4

Although inflammatory foci develop normally in the absence of lymphocytes, as described in Chapter 4, we found that loss of Tbet, (the transcription factor required for $CD4^+$ Th1 cell differentiation), resulted in reduced parenchymal pathology (Fig 4.7). Lesion formation is reduced in Tbet-deficient mice at day 7 post-infection, and there is reduced leukocyte infiltration into sinusoids. At day 18, there is still an inability to form discrete lesions, but there is an abundance of sinusoidal infiltration and parenchymal pathology is, thus, extremely severe (data not shown). The inability of these mice to clear infection may also contribute to these differences at day 18 (data not shown).

To determine the importance of Tbet in thrombus development, Tbet-deficient mice were infected and the extent of thrombosis measured 7 days post-infection. Unexpectedly, in the absence of Tbet, the severity of thrombosis is significantly augmented; the proportion of vascular occlusion is approximately doubled in these mice (Fig 5.9 A-C). This phenotype is further exacerbated at day 18 (data not shown), when thrombosis is associated with severe infiltration of vascular regions, correlating with the extensive parenchymal pathology observed at this time. Although thrombosis in Tbet-deficient mice is more severe than that observed in WT mice, the extent of thrombocytopenia is similar between these two strains (Fig 5.9 D). However, MPV is further increased in Tbet-deficient mice relative to WT, which is suggestive of a more severe platelet phenotype in the absence of Tbet (Fig 5.9 E).

Figure 5.9

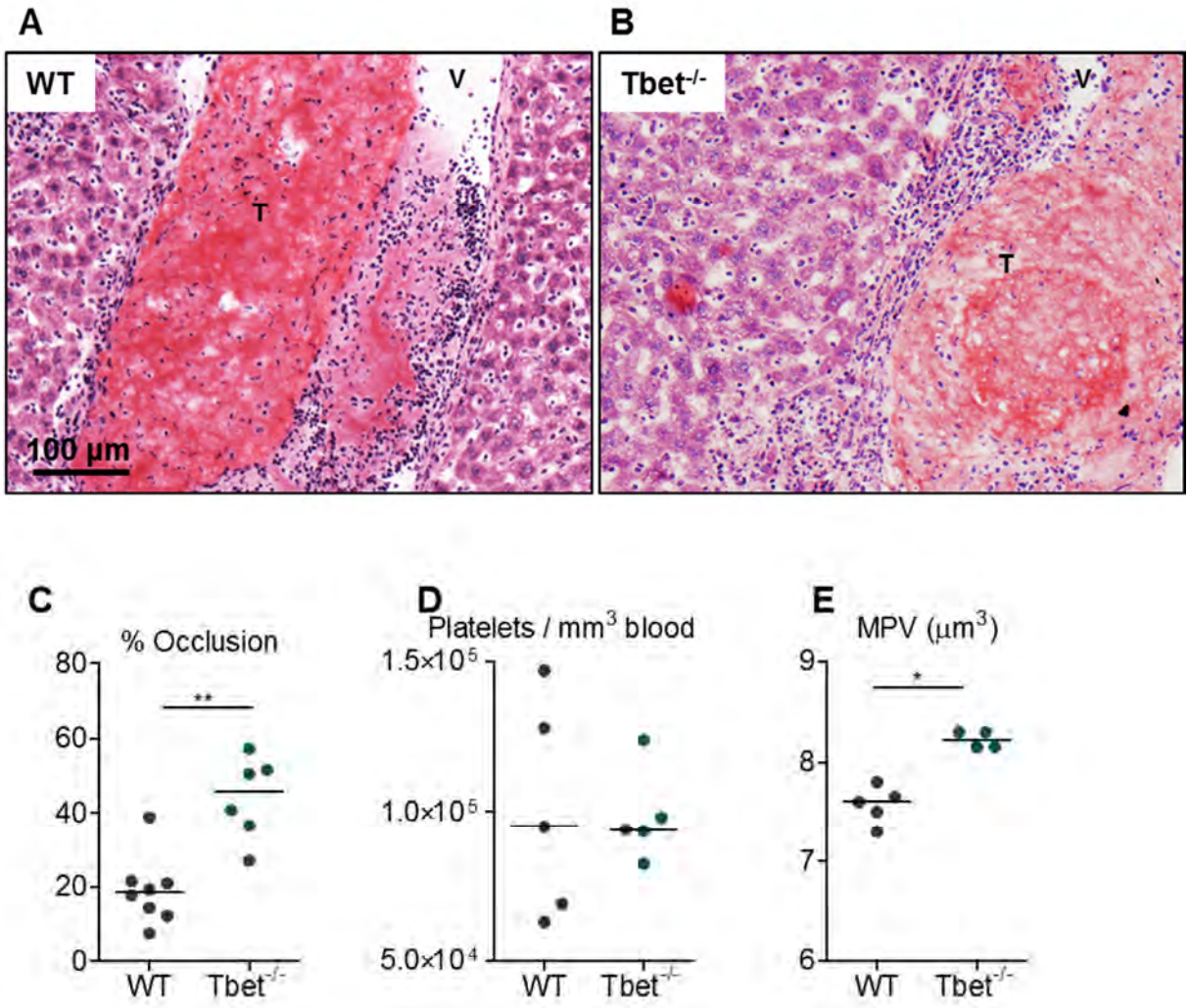

Figure 5.9 Thrombosis is more extensive in the absence of Tbet
WT and Tbet$^{-/-}$ mice were infected (i.p.) with 5 x 10^5 CFU attenuated STm. At day 7 post-infection, livers from A) WT and B) Tbet$^{-/-}$ mice were examined for thrombosis by H&E of frozen tissue sections. Images are representative of multiple experiments where n > 3 per mouse strain in each experiment. V = vessel; T = thrombus. C) The extent of thrombosis was quantified by point counting the percentage of occlusion of all large vessels per tissue section (detailed in section 2.5.4.1), and counts are expressed as a percentage. Data are taken from the mice detailed in A and B above. WT and Tbet$^{-/-}$ mice were infected as in A and B) and blood was obtained from day 7-infected mice for assessment of D) platelet numbers and E) mean platelet volume. Data are from one experiment where n = 5 per mouse strain. *p≤0.05 **p≤0.01 ***p≤0.001.

In contrast, preliminary studies indicate that thrombus development may be dampened by the absence of IL4, yet is unaltered by the absence of IL4Rα (Fig 5.10 A-D). However, both these mice strains have modestly reduced thrombocytopenia and less elevation in MPV, relative to WT mice (Fig 5.10 E-F). The contrast in thrombosis phenotype between these two strains suggested a role for IL-13 in thrombosis regulation, because IL-13 and IL4 both signal via IL4-Rα (Mohrs et al., 1999). To test this, we infected IL13-deficient mice and examined thrombosis at day 7 post-infection. Thrombosis is of a similar severity to that seen in WT mice (data not shown), suggesting the reduced thrombosis seen in $IL4^{-/-}$ mice is specific to that cytokine. To determine the role of iNKT cells in thrombosis development, we infected mice lacking CD1d. Whilst thrombosis and extent of thrombocytopenia are similar to WT in these mice, MPV is significantly greater than in WT mice (Fig 5.11 A-D).

Taken together, these data indicate that both inflammatory lesions and thrombosis develop independently of adaptive immune cells. However, there are circumstances in which Tbet can restrict host-mediated tissue pathology and thrombosis. Therefore, although adaptive immune cells are not required for the development of thrombosis, it is likely that the adaptive immune response may have an important role in the regulation of this phenotype.

Figure 5.10

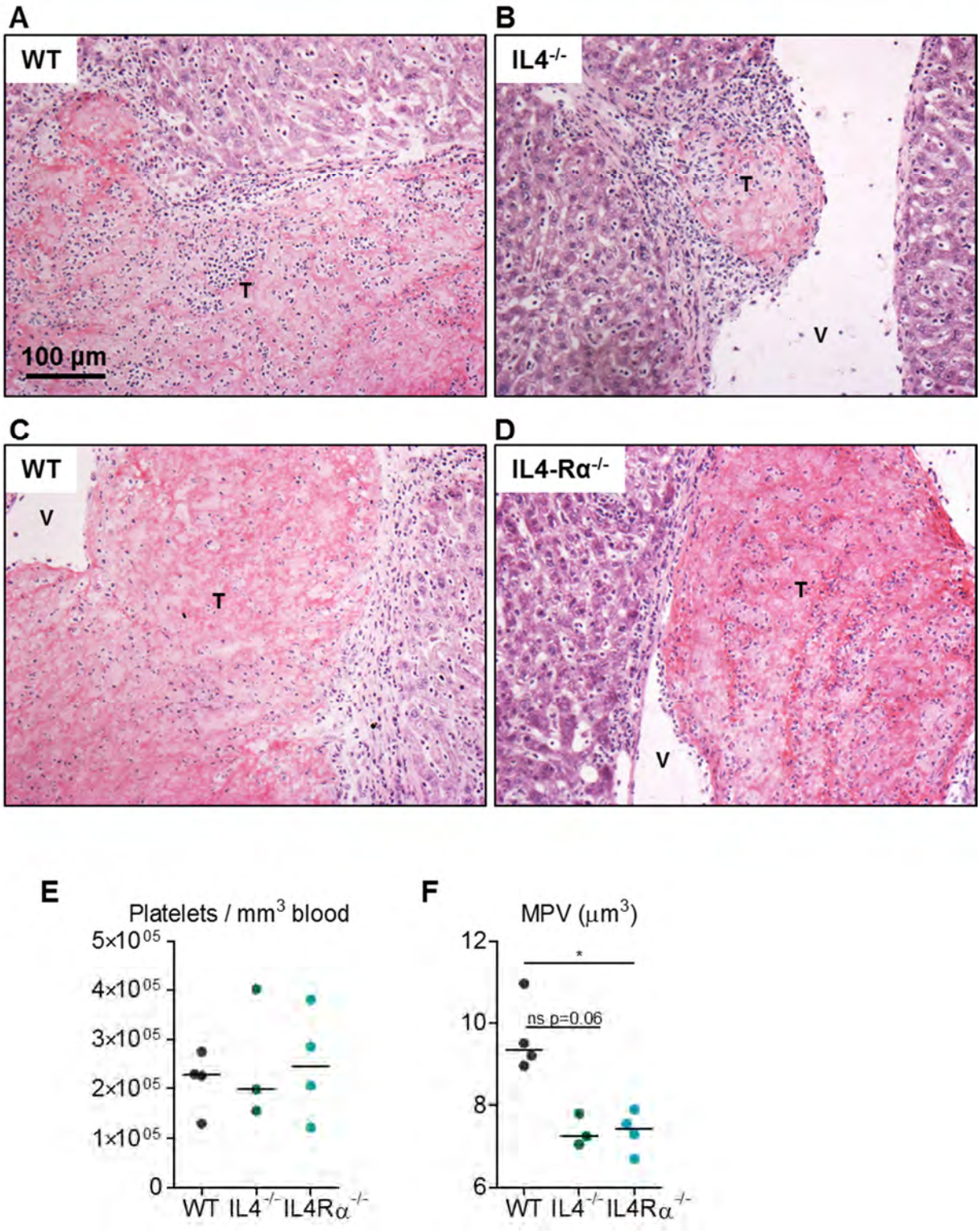

Figure 5.10 The severity of thrombosis is dampened in mice lacking IL4 but not IL4Rα
WT, IL4$^{-/-}$ and IL4Rα$^{-/-}$ mice were infected (i.p.) with 5 x 10^5 CFU attenuated STm. At day 7 post-infection, livers were examined for thrombosis by H&E of frozen tissue sections. A) WT and B) IL4$^{-/-}$ mice and C) WT (the same as in A) and D) IL4Rα$^{-/-}$ mice. Images are representative and are from one experiment where n = 4 per mouse strain. V = vessel; T = thrombus. Blood was obtained from the day 7-infected mice (described above) for assessment of E) platelet numbers and F) mean platelet volume. Data are taken from the mice detailed above. *p≤0.05 **p≤0.01 ***p≤0.001.

Figure 5.11

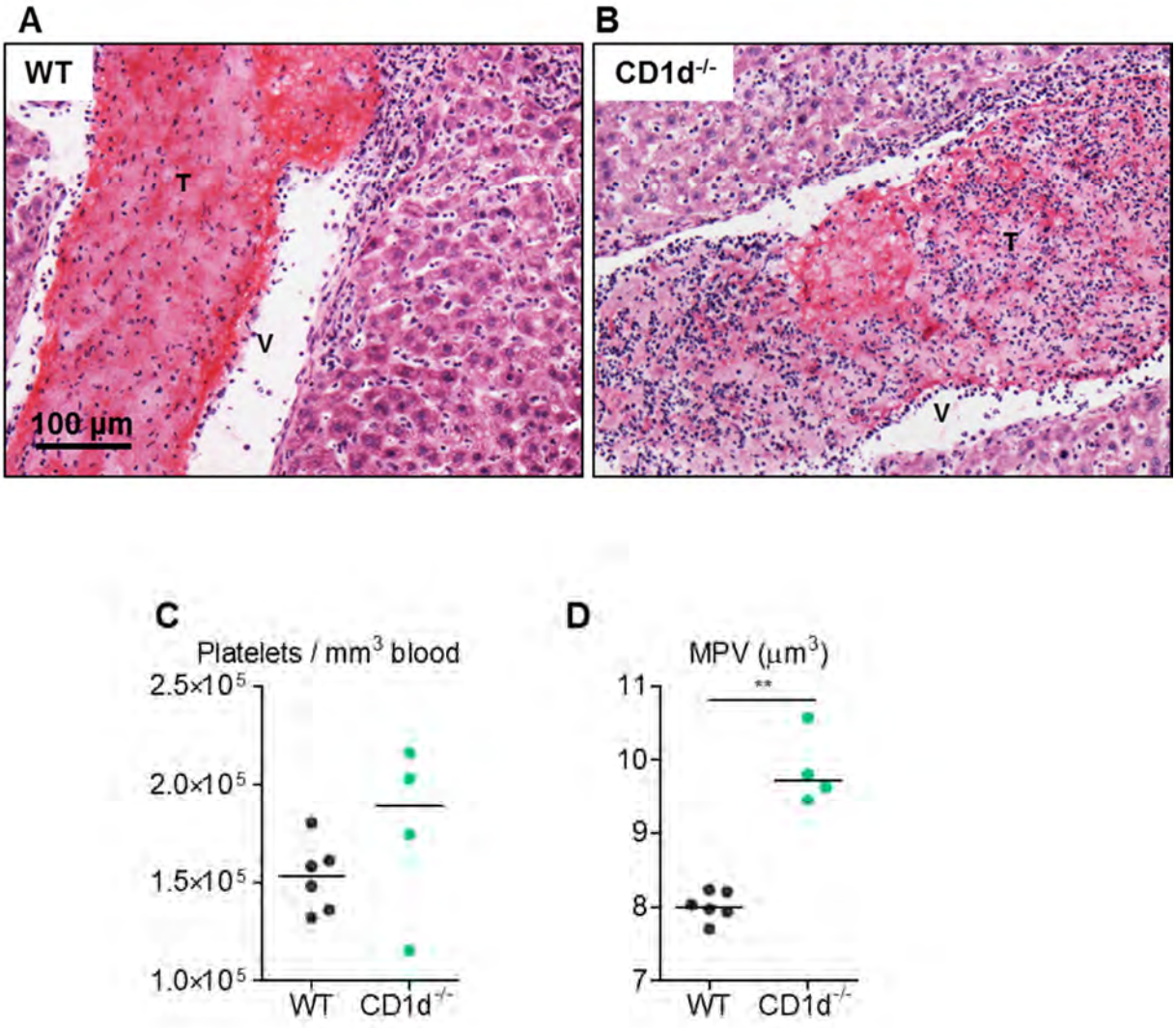

Figure 5.11 Thrombosis severity is similar to WT in the absence of CD1d
WT and CD1d$^{-/-}$ mice were infected (i.p.) with 5 x 10^5 CFU attenuated STm. At day 7 post-infection, livers of A) WT and B) CD1d$^{-/-}$ mice were examined for thrombosis by H&E of frozen tissue sections. Images are representative and are from one experiment where n = 5-6 per mouse strain. V = vessel; T = thrombus. Blood was obtained from the day 7-infected mice (described above) for assessment of C) platelet numbers and D) mean platelet volume. Data are taken from the mice detailed above. *p≤0.05 **p≤0.01 ***p≤0.001.

5.6 Thrombosis is driven by pro-inflammatory cytokine-mediated inflammation

Seeing as thrombosis occurs in the absence of the adaptive immune response, we wanted to determine to what extent the process is regulated by innate mechanisms. One major feature of the innate immune response is inflammation and so we hypothesised that inflammation may be mediating thrombosis during infection. We used mice lacking IFNγ to test this because we were aware that these mice lack leukocyte infiltration in the liver following *Salmonella* infection, despite a similar or enhanced bacterial burden to that seen in WT mice (Kupz et al., 2013, Nauciel and Espinasse-Maes, 1992, VanCott et al., 1998). Indeed, an absence of inflammatory lesion development is observed in IFNγ-deficient mice in our NTS infection model (Fig 4.12). In the absence of IFNγ, thrombosis is abolished (Fig 5.12 A-C). This demonstrates that thrombus development is dependent on IFNγ-mediated inflammation, and, as in inflammatory foci development, is not dependent purely on bacterial burden. Furthermore, these mice have a significantly less severe thrombocytopenia than WT mice and MPV is unchanged after infection (Fig 5.12 D-E).

To test whether this lack of thrombosis in the absence of inflammation was specifically due to the absence of IFNγ, or was related to inflammatory signals per se, thrombus development in mice lacking TNFαR was examined. It was demonstrated in Chapter 4 that although a lack of IFNγ is associated with a lack of inflammation in the liver, inflammatory foci formation is not affected by loss of TNFαR signalling (Fig 4.19). In contrast, thrombosis is significantly abrogated on day 7 in the absence of TNFαR, despite these mice developing inflammatory foci (Fig 5.13 A-C).

Figure 5.12

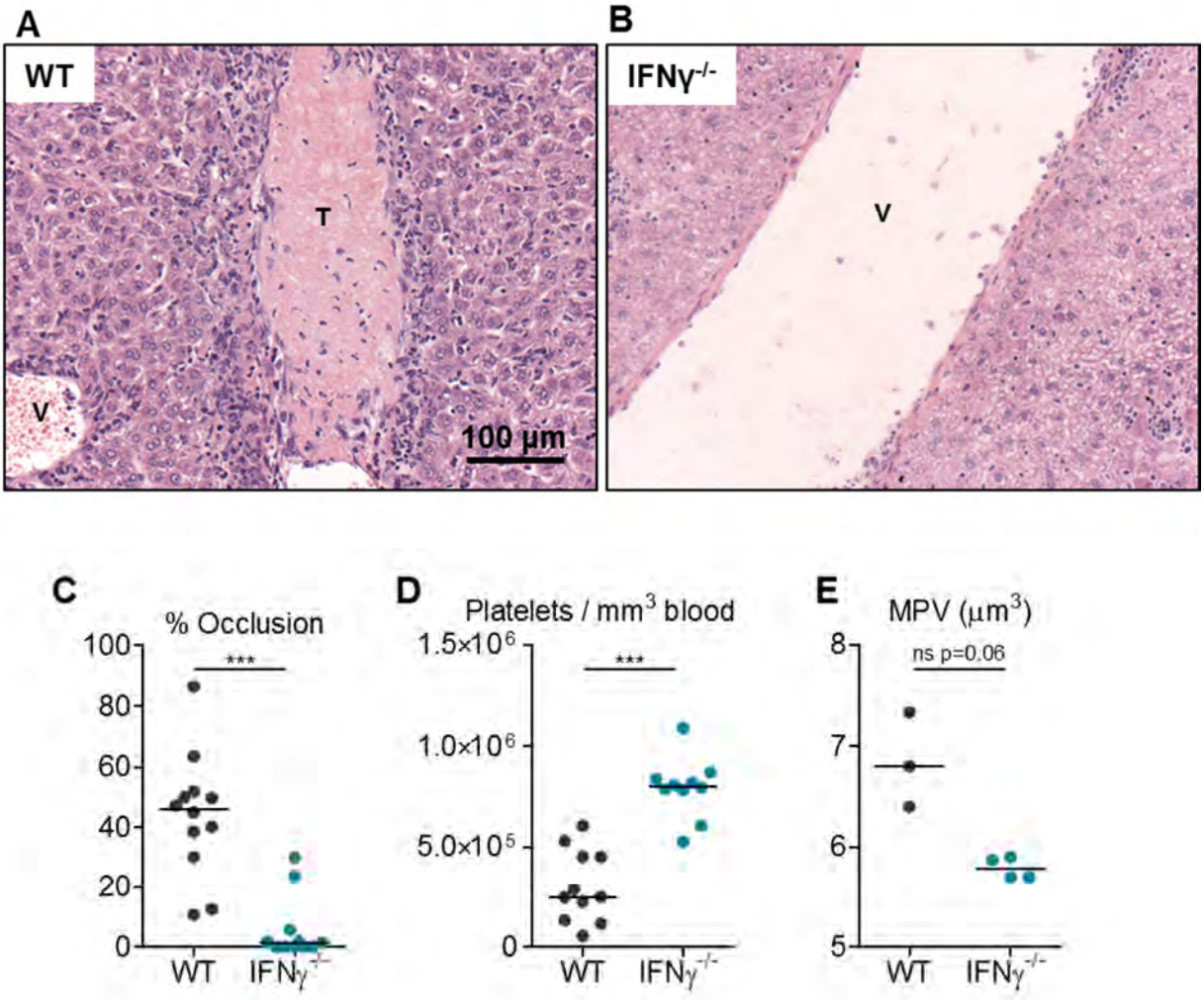

Figure 5.12 Thrombosis in the liver is abolished in the absence of interferon-γ
WT and IFNγ$^{-/-}$ mice were infected (i.p.) with 5 x 10^5 CFU attenuated STm. At day 7 post-infection, livers from A) WT and B) IFNγ$^{-/-}$ mice were examined for thrombosis by H&E of frozen tissue sections. Images are representative of multiple experiments where n ≥ 3 per mouse strain in each experiment. V = vessel; T = thrombus. C) The extent of thrombosis was quantified by point counting the percentage of occlusion of all large vessels per tissue section (detailed in section 2.5.4.1), and counts are expressed as a percentage. Data are taken from multiple experiments where n ≥ 3 per mouse strain in each experiment. WT and IFNγ$^{-/-}$ mice were infected as described above and blood was obtained from day 7-infected mice for assessment of D) platelet numbers and E) mean platelet volume. Data are taken from multiple experiments where n ≥ 3 per mouse strain in each experiment (Data for mean platelet volume are taken from one experiment where n = 4 per mouse strain). *p≤0.05 **p≤0.01 ***p≤0.001.

Figure 5.13

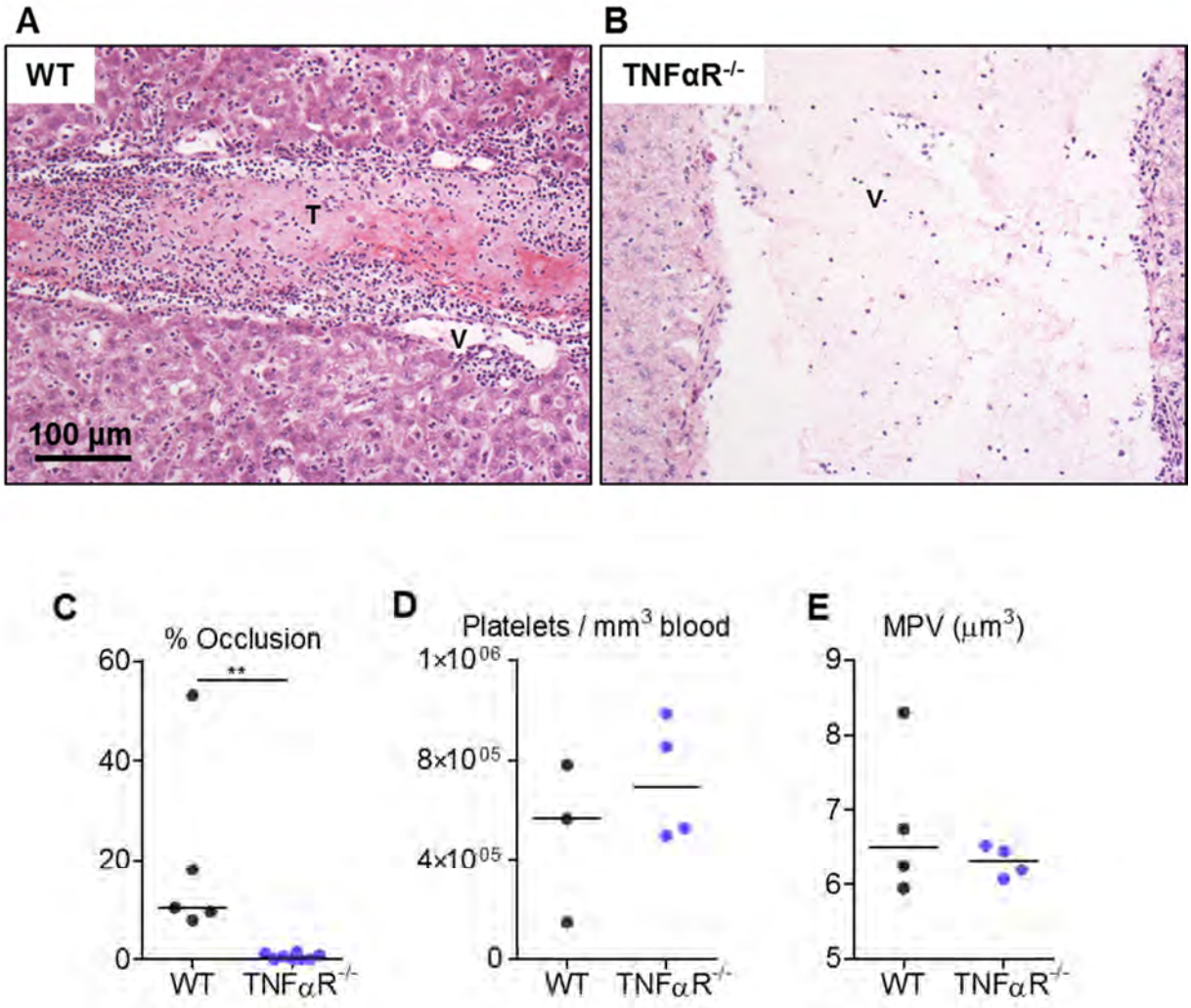

Figure 5.13 Thrombosis in the liver is abolished in the absence of tumor necrosis factor-α Receptor

WT and TNFαR$^{-/-}$ mice were infected (i.p.) with 5 x 10^5 CFU attenuated STm. At day 7 post-infection, livers from A) WT and B) TNFαR$^{-/-}$ mice were examined for thrombosis by H&E of frozen tissue sections. Images are representative of multiple experiments where n ≥ 3 per mouse strain in each experiment. V = vessel; T = thrombus. C) The extent of thrombosis was quantified by point counting the percentage of occlusion of all large vessels per tissue section (detailed in section 2.5.4.1), and counts are expressed as a percentage. Data are taken from multiple experiments where n ≥ 3 per mouse strain in each experiment. WT and TNFαR$^{-/-}$ mice were infected as described above and blood was obtained from day 7-infected mice for assessment of D) platelet numbers and E) mean platelet volume. Data are taken from one experiment where n = 4 per mouse strain. *p≤0.05 **p≤0.01 ***p≤0.001.

Furthermore, mice deficient in TNFαR have less severe thrombocytopenia and less augmented MPV compared to WT mice (although the MPV measured in WT controls is particularly low in this experiment) (Fig 5.13 D-E).

Considering the inflammatory component of thrombosis, we hypothesised that in the absence of molecules associated with supressing inflammation, thrombosis may be enhanced. To test this, IL10 deficient mice were infected and thrombosis was measured after 7 days. As IL10-deficient mice are more sensitive to infection, a reduced bacterial dose was used and so thrombi development in WT mice was less severe. Thrombosis is significantly exacerbated in the absence of IL10 (Fig 5.14 A-C). Furthermore, thrombocytopenia is more pronounced and MPV is elevated further compared to WT mice (Fig 5.14 D-E). This further supports the relationship between inflammation and thrombosis.

However, it is important to note that cytokines associated with inflammation may not always contribute to thrombosis. For example, there is a similar level of thrombosis in IL6-deficient mice relative to WT (Fig 5.15 A-C). Furthermore, thrombocytopenia is significantly more severe in IL6-deficient mice, showing that thrombosis is not the sole cause of the thrombocytopenia (Fig 5.15 C-D). Mean platelet volume in IL6-deficient mice is similar to that measured in WT mice (Fig 5.15 E). Overall, these data support an established relationship between thrombosis in the liver and platelet numbers in the blood, however, reduced circulating platelets during infection is not entirely explained by thrombus development.

Figure 5.14

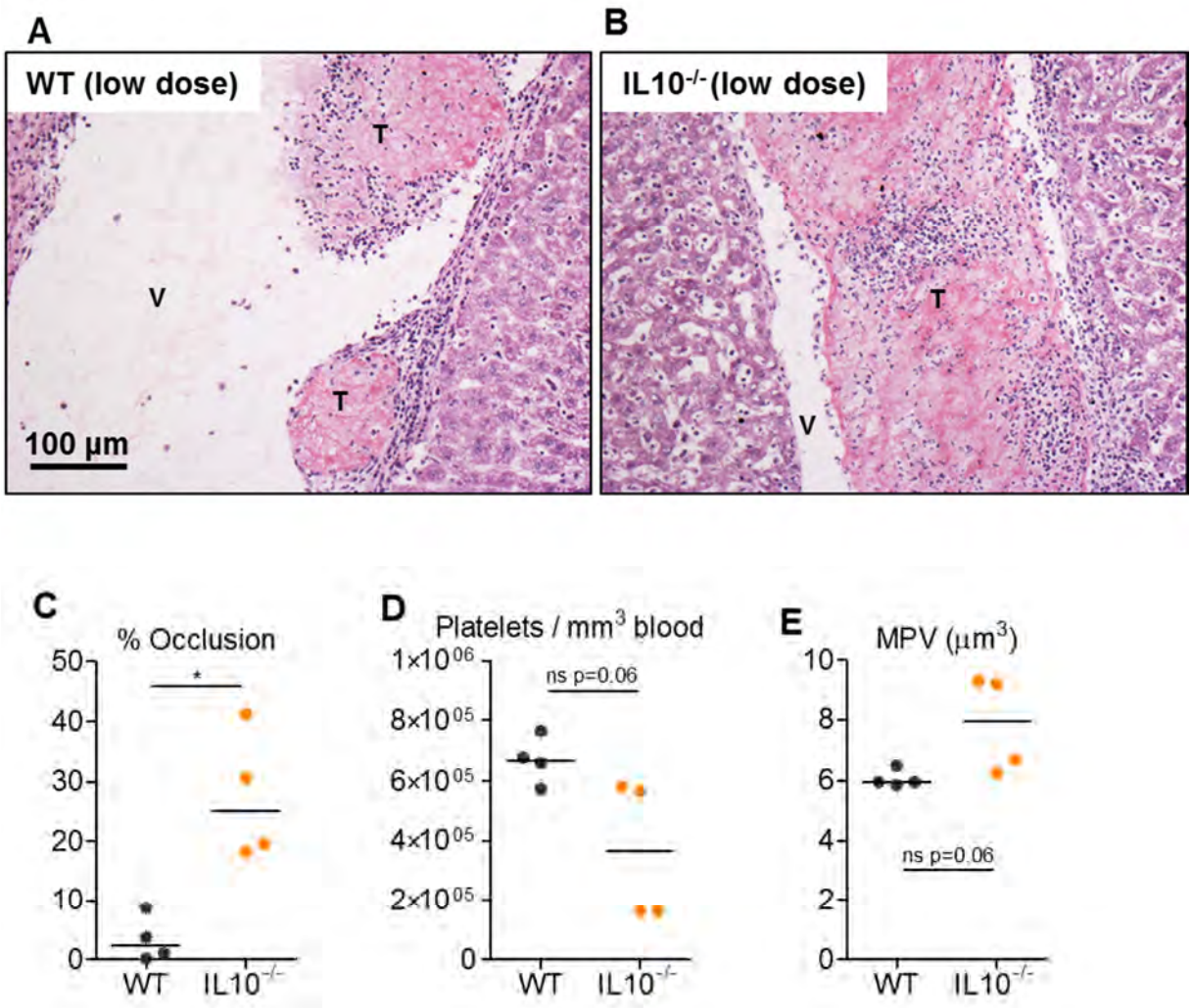

Figure 5.14 Hepatic thrombosis of mice lacking interleukin-10 is more severe than in WT mice

WT and IL10$^{-/-}$ mice were infected (i.p.) with (a lower than usual dose of) 10^5 CFU attenuated STm. At day 7 post-infection, livers from A) WT and B) IL10$^{-/-}$ mice were examined for thrombosis by H&E of frozen tissue sections. Images are representative of multiple experiments where n > 3 per mouse strain in each experiment. V = vessel; T = thrombus. C) The extent of thrombosis was quantified by point counting the percentage of occlusion of all large vessels per tissue section (detailed in section 2.5.4.1), and counts are expressed as a percentage. Data are taken from one experiment where n = 4 per mouse strain in each experiment. WT and IL10$^{-/-}$ mice were infected as described above and blood was obtained from day 7-infected mice for assessment of D) platelet numbers and E) mean platelet volume. Data are taken from one experiment where n = 4 per mouse strain. *p≤0.05 **p≤0.01 ***p≤0.001.

Figure 5.15

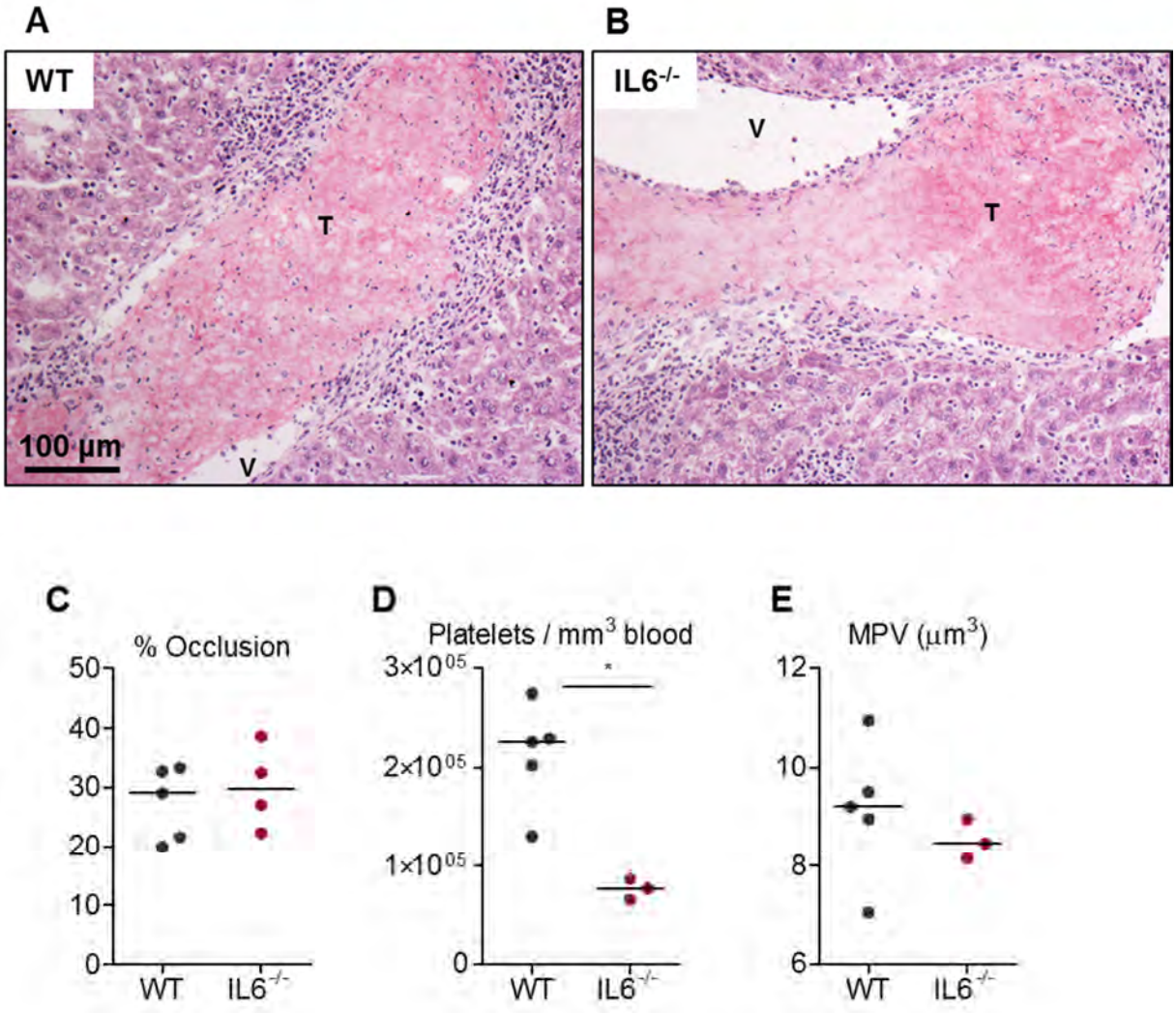

Figure 5.15 Thrombosis severity is similar to or greater than WT in the absence of IL6
WT and IL6$^{-/-}$ mice were infected (i.p.) with 5 x 10^5 CFU attenuated STm. At day 7 post-infection, livers from A) WT and B) IL6$^{-/-}$ mice were examined for thrombosis by H&E of frozen tissue sections. Images are representative of and are from one experiment where n > 3 per mouse strain. V = vessel; T = thrombus. C) The extent of thrombosis was quantified by point counting the percentage of occlusion of all large vessels per tissue section (detailed in section 2.5.4.1), and counts are expressed as a percentage. Data are taken from one experiment where n > 3 per mouse strain. WT and IL6$^{-/-}$ mice were infected as described above and blood was obtained from day 7-infected mice for assessment of D) platelet numbers and E) mean platelet volume. Data are taken from one experiment where n > 3 per mouse strain. *p≤0.05 **p≤0.01 ***p≤0.001.

5.7 Podoplanin expression is increased in the liver during infection

We wanted to investigate how IFNγ-mediated inflammation could result in thrombus formation so we began to consider potential signalling components which could be involved in both inflammation and in platelet activation. One such potential molecule which could link these two physiological processes is podoplanin which is up-regulated on macrophages and Th17 cells in inflammation and activates platelets through CLEC-2 (Astarita et al., 2012, Hou et al., 2010). So we looked for podoplanin expression in the liver in the presence and absence of infection.

In non-infected livers, podoplanin expression is restricted to lymphatic endothelium associated with portal regions (Fig 5.16 A). Following infection, there is increased podoplanin expression in the liver. This is predominantly found in the inflammatory foci and associated with host vascular endothelium, particularly in regions adjacent to thrombi (Fig 5.16 B). Podoplanin expression is also detected within the sinusoids in both non-infected and infected mice by IHC, and this occurs in conjunction with F4/80^{+} staining, suggestive of podoplanin expression by Kupffer cells (Fig 5.16 C-D). So we hypothesised that increased podoplanin expression in the liver may be conducive to thrombosis development via platelet activation mediated by CLEC-2.

Figure 5.16

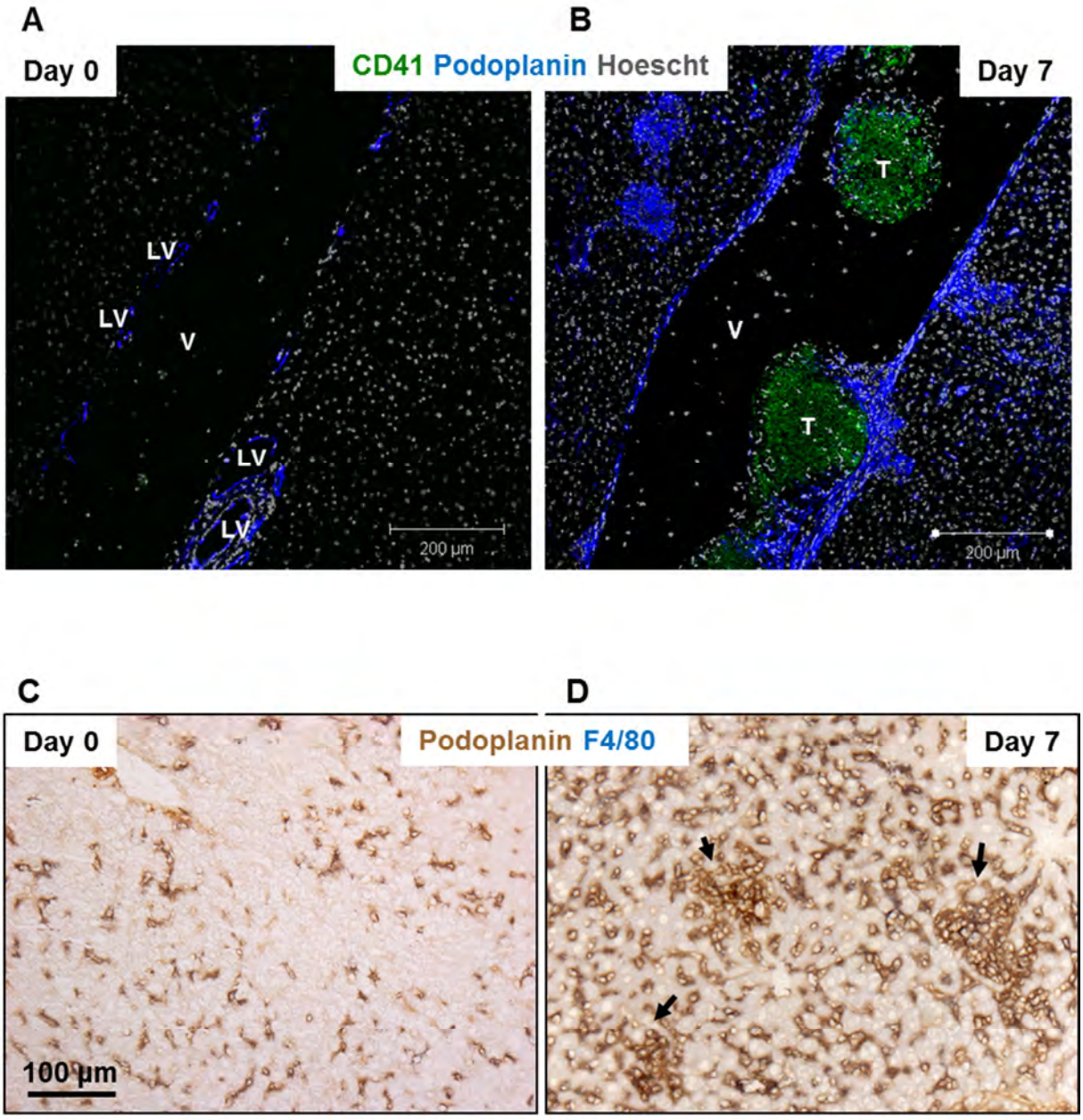

Figure 5.16 Podoplanin expression is increased in the liver after infection
WT mice were infected (i.p.) with 5 x 10^5 CFU attenuated STm for 7 days. Podoplanin expression was assessed on frozen tissue sections from the livers of A) non-infected and B) day 7-infected mice by confocal microscopy. CD41 (platelets) = green; podoplanin = blue. Images are co-stained with nuclear dye Hoescht = grey. V = vessel; T = thrombus; LV = lymphatic vessel. Images are representative from multiple experiments, where n = 4 at each time-point. C) WT mice were infected as described above and podoplanin expression was assessed by IHC in C) non-infected and D) day 7-infected livers. Podoplanin = brown; F4/80 = blue; (double positive staining = black). Black arrows indicate inflammatory lesions. Images are representative from multiple experiments, where n = 4 at each time-point.

5.8 Platelet activation via CLEC-2 is required for thrombus development

To test the involvement of platelet activation through CLEC-2, we used PF4.Cre.CLEC-$2^{fl/fl}$ mice, whereby CLEC-2 is selectively deleted in cells that express platelet factor 4; primarily megakaryocytes and platelets, as shown below. These mice were infected and the extent of thrombosis was measured after 7 days.

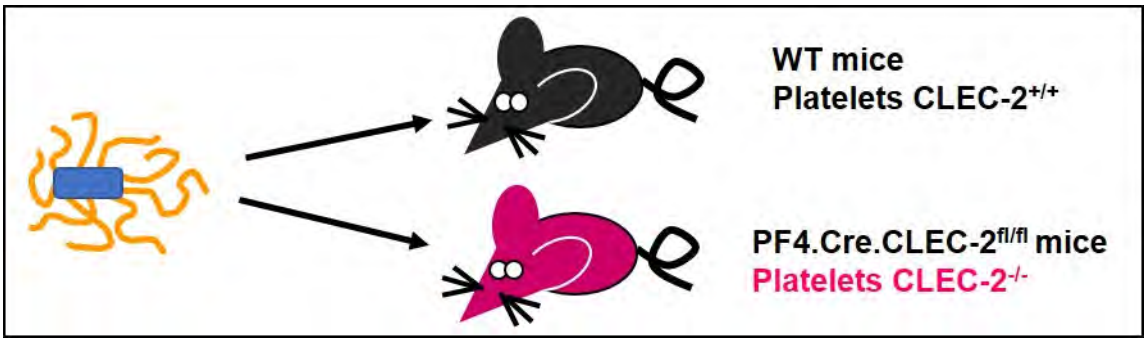

Diagram 5.1 *Salmonella* infection of PF4.Cre.CLEC-$2^{fl/fl}$ mice. Platelet expression of CLEC-2 is indicated on the right.

In these mice, thrombus development is nearly or totally abrogated, indicating that CLEC-2 expression on platelets is required for thrombus development (Fig 5.17 A-C). However, despite the diminished thrombosis in these PF4.Cre.CLEC-$2^{fl/fl}$ mice, a severe thrombocytopenia and elevated MPV is still observed (Fig 5.17 D-E).

We were keen to examine the extent of inflammation in these PF4.Cre.CLEC-$2^{fl/fl}$ mice, to ascertain whether, in the absence of CLEC-2 on platelets, there was any feedback on inflammation, particularly on podoplanin expression. By histology, cellular infiltration is very similar to that seen in WT mice, despite less extensive hepatomegaly in these mice (Fig 5.17 F-H). Bacterial loads in the liver are comparable to in WT mice (Fig 5.17 I).

Figure 5.17

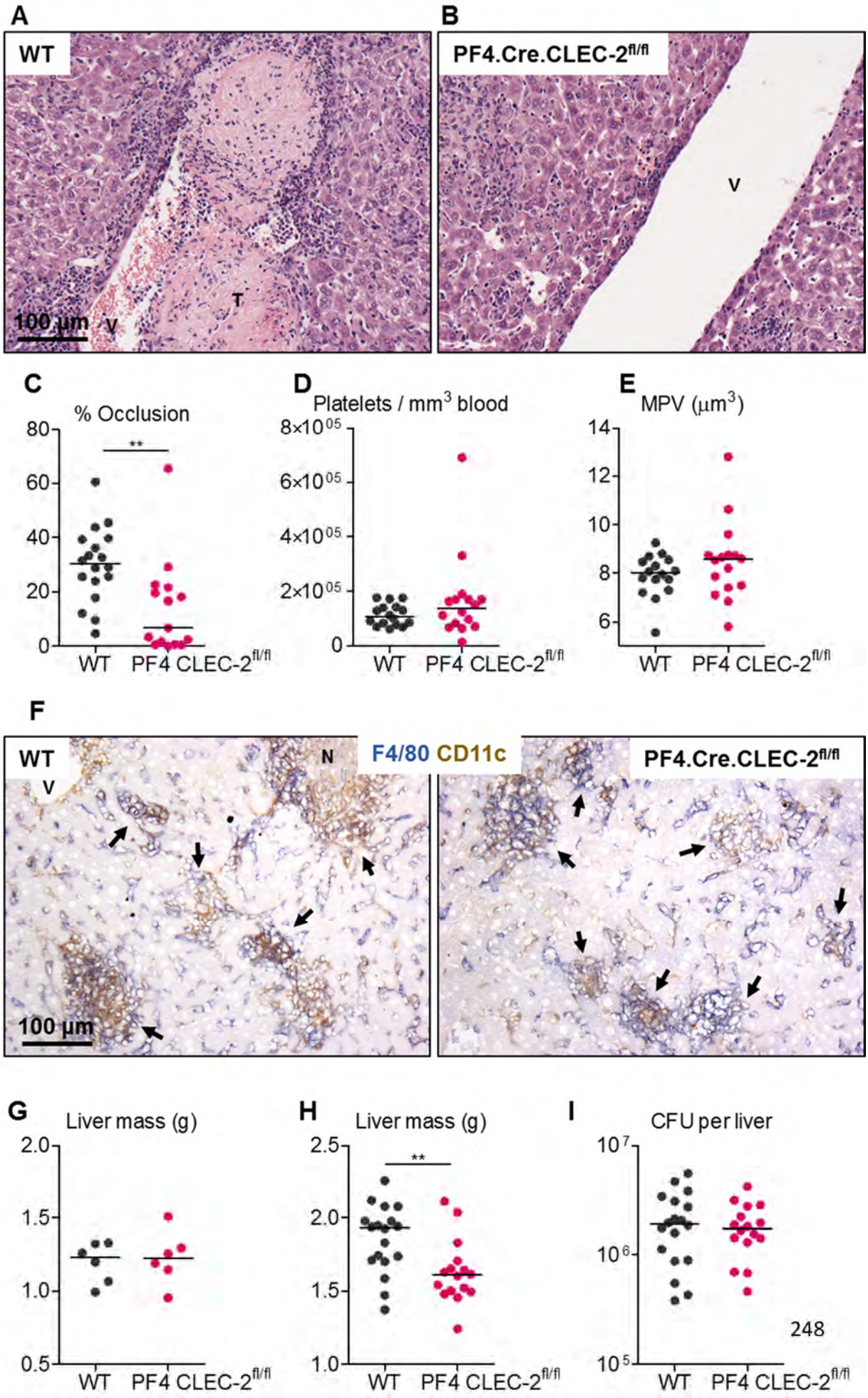
A
WT
T
V
100 µm
B
PF4.Cre.CLEC-2fl/fl
V
C
% Occlusion
**
80
60
40
20
0
WT
PF4 CLEC-2fl/fl
D
Platelets / mm3 blood
8×10 05
6×10 05
4×10 05
2×10 05
0
WT
PF4 CLEC-2fl/fl
E
MPV (µm3)
14
12
10
8
6
WT
PF4 CLEC-2fl/fl
F
WT
V
N
F4/80 CD11c
PF4.Cre.CLEC-2fl/fl
100 µm
G
Liver mass (g)
2.0
1.5
1.0
0.5
WT
PF4 CLEC-2fl/fl
H
Liver mass (g)
**
2.5
2.0
1.5
1.0
WT
PF4 CLEC-2fl/fl
I
CFU per liver
10 7
10 6
10 5
248
WT
PF4 CLEC-2fl/fl

Figure 5.17 Expression of CLEC-2 on platelets is required for thrombosis development
WT and PF4.Cre.CLEC-$2^{fl/fl}$ mice (whereby CLEC-2 expression is absent in platelets and megakaryocytes) were infected (i.p.) with 5 x 10^5 CFU attenuated STm. At day 7 post-infection, livers from A) WT and B) PF4.Cre.CLEC-$2^{fl/fl}$ mice were examined for thrombosis by H&E of frozen tissue sections. Images are representative of multiple experiments where n = 3-4 per mouse strain in each experiment. V = vessel; T = thrombus. C) The extent of thrombosis was quantified by point counting the percentage of occlusion of all large vessels per tissue section (detailed in section 2.5.4.1), and counts are expressed as a percentage. Data are taken from multiple experiments where n = 4 per mouse strain in each experiment. WT and PF4.Cre.CLEC-$2^{fl/fl}$ mice were infected as described above and blood was obtained from day 7-infected mice for assessment of D) platelet numbers and E) mean platelet volume. Data are taken from multiple experiments where n = 3-4 per mouse strain in each experiment. F) WT and PF4.Cre.CLEC-$2^{fl/fl}$ mice were infected as described above and inflammatory lesion development was assessed at day 7 post-infection on frozen liver sections by IHC. F4/80 = blue; CD11c = brown; double positive cells = black. V = vessel; N = necrosis; black arrows indicate inflammatory lesions. Images are representative from multiple experiments, where n = 3-4 at each time-point. Liver mass from G) non-infected and H) day 7-infected WT and PF4.Cre.CLEC-$2^{fl/fl}$ mice are taken from mice infected as in A and B above. I) The bacterial burden in the liver of these mice was calculated at day 7 post-infection (from mice infected as in A and B above). On histograms, PF4.Cre.CLEC-$2^{fl/fl}$ mice are written PF4 CLEC-$2^{fl/fl}$. *$p \leq 0.05$ **$p \leq 0.01$ ***$p \leq 0.001$.

Flow cytometry was used to quantify leukocyte infiltration. Representative FACS plots indicate the gating strategies used to analyse myeloid infiltrate, DCs and T cells in WT and PF4.Cre.CLEC-2$^{fl/fl}$ mice (Fig 5.18 A-F). Absolute numbers of Kupffer cells, monocytes, Ly6G^{+} and Ly6G^{hi} cells are equivalent in WT and PF4.Cre.CLEC-2$^{fl/fl}$ mice at day 7 post-infection (Fig 5.19 A-D). Total DC numbers are also equivalent to WT, as are NK DCs, myeloid DCs, plasmacytoid DCs and mixed myeloid/lymphoid DCs. There are reduced lymphoid DCs in PF4.Cre.CLEC-2$^{fl/fl}$ mice after infection (Fig 5.19 E-J). There are also reduced CD4^{+} T cells, especially activated cells, however, numbers of CD8^{+} T cells are similar to those seen in WT mice (Fig 5.19 K-N). Importantly, a similar increase in podoplanin expression is seen in PF4.Cre.CLEC-2$^{fl/fl}$ and WT mice after infection by IHC (Fig 5.20 A-C). Therefore, these data indicate that platelet activation occurs through CLEC-2 and occurs in conjunction with elevated podoplanin expression during inflammation.

5.8.1 CLEC-2 and increased podoplanin expression are conducive, but not sufficient for thrombosis development

We have demonstrated that CLEC-2 expression on platelets is required for platelet activation and thrombus development during *Salmonella* infection, as is increased podoplanin expression. To confirm that podoplanin up-regulation is a consequence of inflammation, we examined podoplanin expression in IFNγ$^{-/-}$ mice, which lack inflammation during infection. Podoplanin expression is not increased at day 7 in IFNγ$^{-/-}$ mice, which illustrates the inflammatory-association of podoplanin up-regulation during infection (Fig 5.21 A-B). However, thrombosis is also absent in TNFαR-deficient mice, despite normal foci formation in the parenchymal tissue.

Figure 5.18

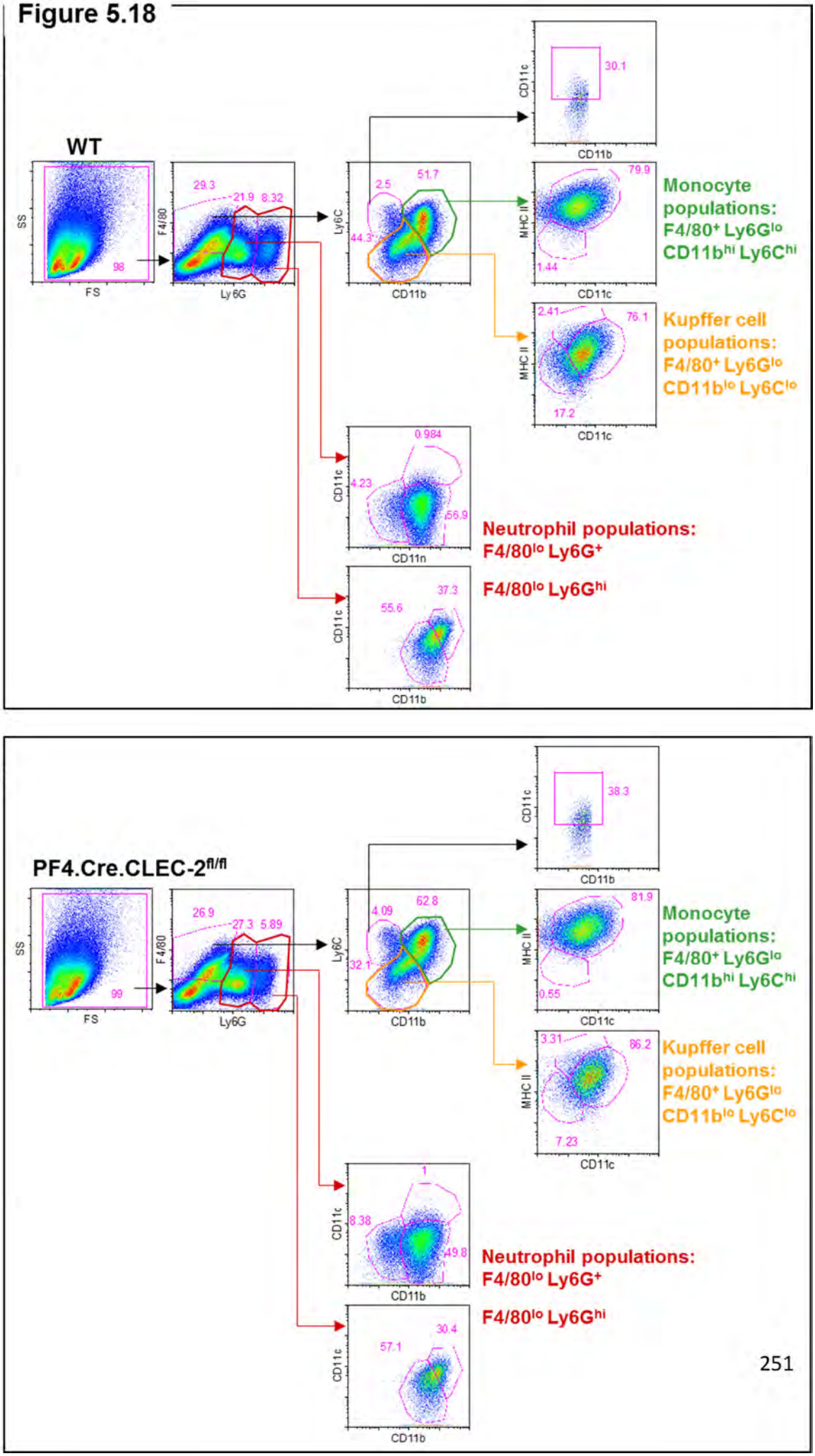
A
WT
SS
FS
98
F4/80
Ly6G
29.3
21.9
8.32
Ly6C
CD11b
2.5
51.7
44.3
CD11c
30.1
MHC II
79.9
1.44
Monocyte populations:
F4/80+ Ly6Glo
CD11bhi Ly6Chi
2.41
76.1
17.2
Kupffer cell populations:
F4/80+ Ly6Glo
CD11blo Ly6Clo
CD11n
0.984
4.23
56.9
Neutrophil populations:
F4/80lo Ly6G+
37.3
55.6
F4/80lo Ly6Ghi
B
PF4.Cre.CLEC-2fl/fl
99
26.9
27.3
5.89
4.09
62.8
32.1
38.3
81.9
0.55
3.31
86.2
7.23
1
8.38
49.8
30.4
57.1

Figure 5.18 continued

C

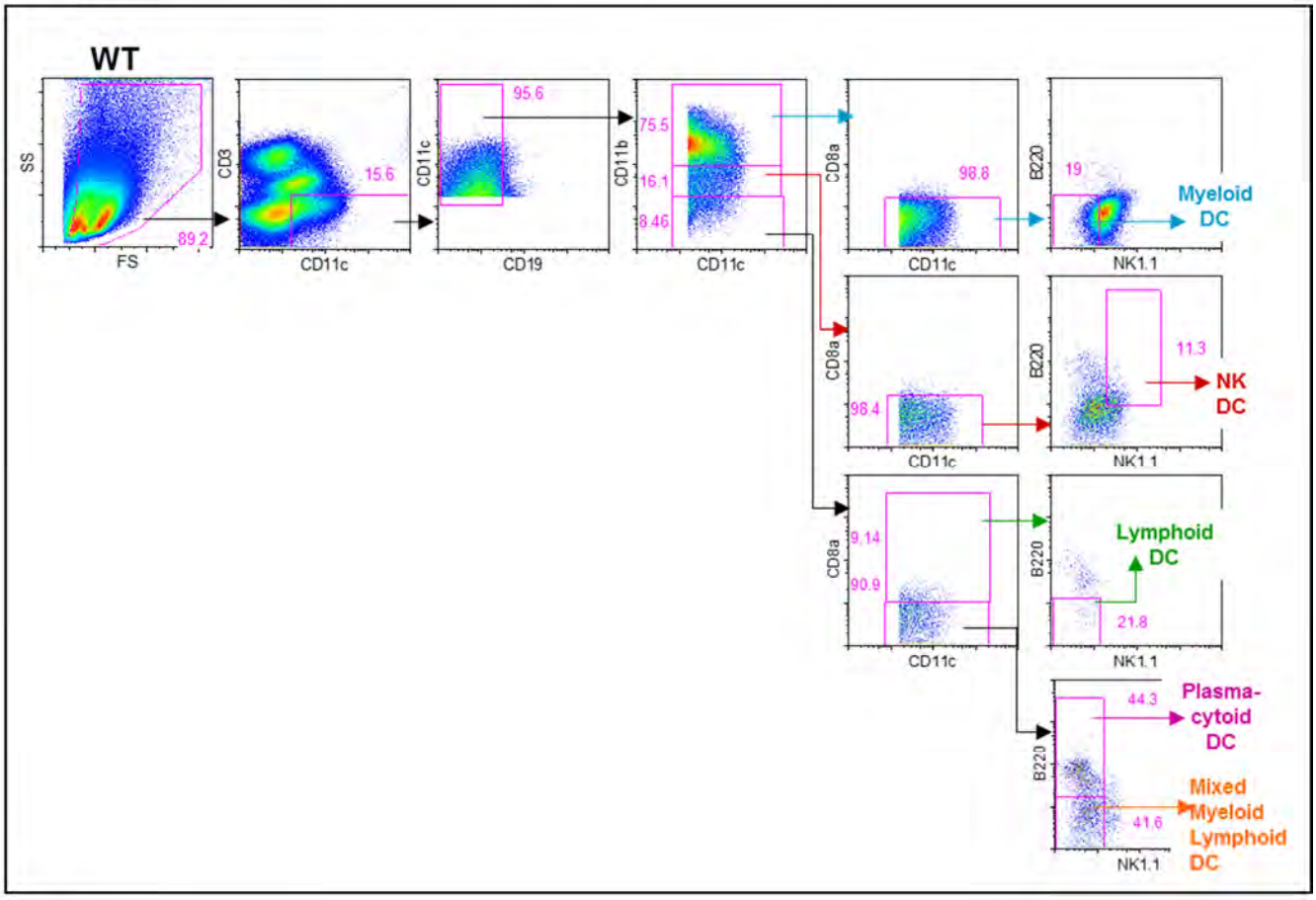

D

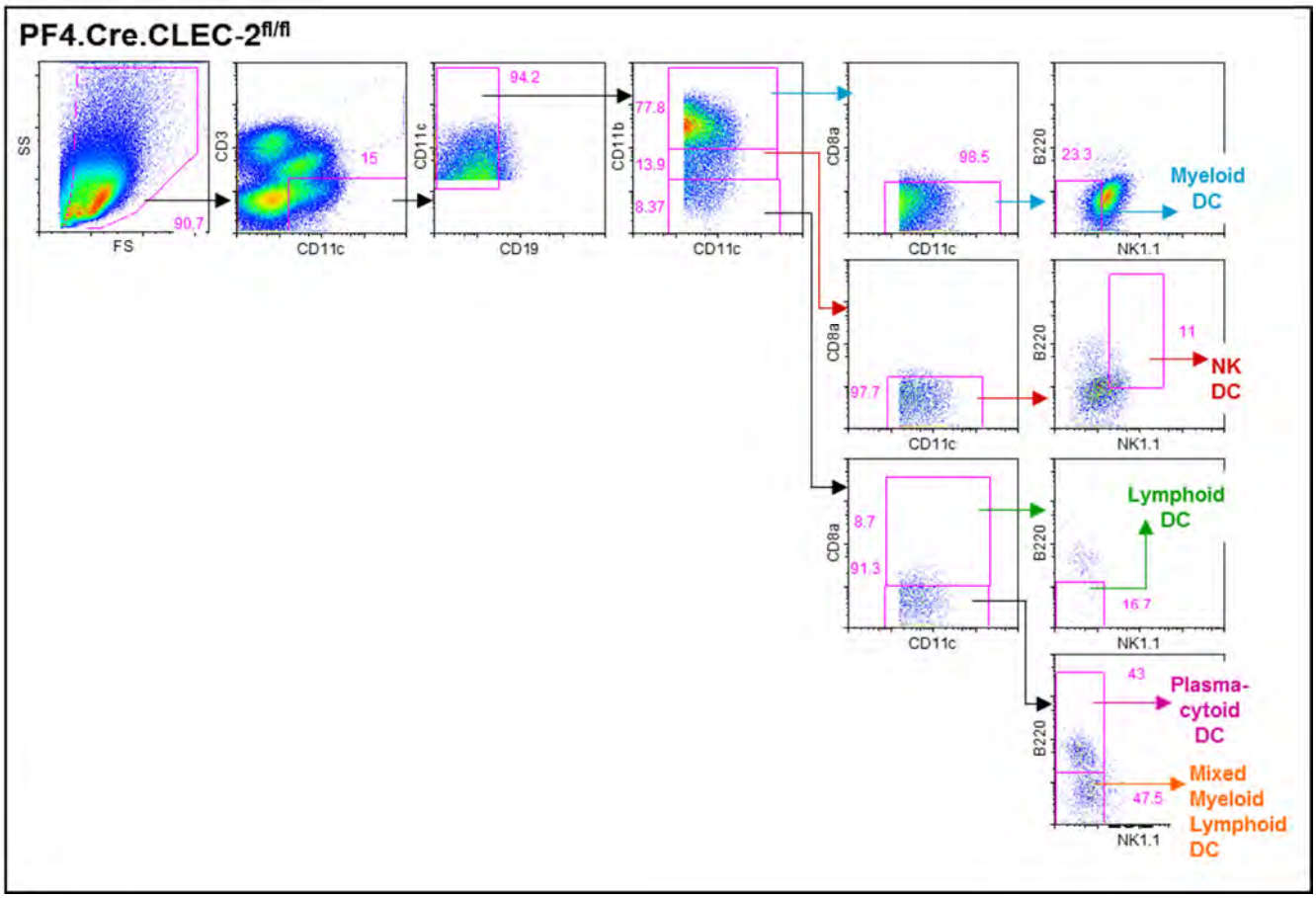

Figure 5.18 continued

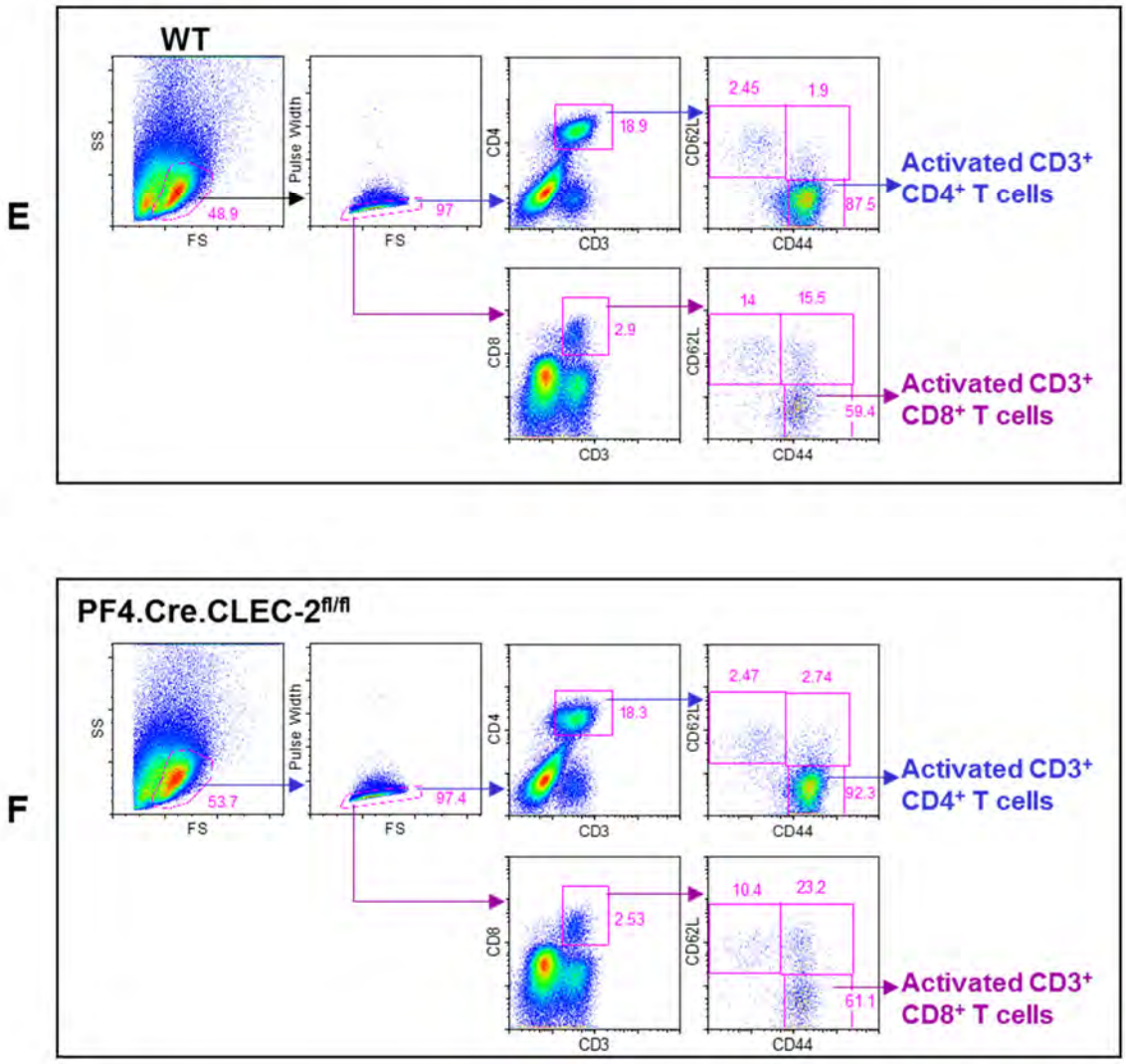

Figure 5.18 Gating strategy and FACS plots for quantification of hepatic infiltrate
WT and PF4.Cre.CLEC-2$^{fl/fl}$ mice (whereby CLEC-2 expression is absent in platelets and megakaryocytes) were infected (i.p.) with 5 x 10^5 CFU attenuated STm. Leukocyte infiltrate in the liver was quantitatively assessed by FACS. The gating strategy and representative FACS plots for myeloid populations in A) WT and B) PF4.Cre.CLEC-2$^{fl/fl}$ mice is shown on the 1st page; for DC populations in C) WT and D) PF4.Cre.CLEC-2$^{fl/fl}$ mice is shown on the 2nd page; and for T cell populations in E) WT and F) PF4.Cre.CLEC-2$^{fl/fl}$ mice is shown above. FACS plots are representative from one experiment, where n = 9 in WT mice and n = 5 in PF4.Cre.CLEC-2$^{fl/fl}$ mice.

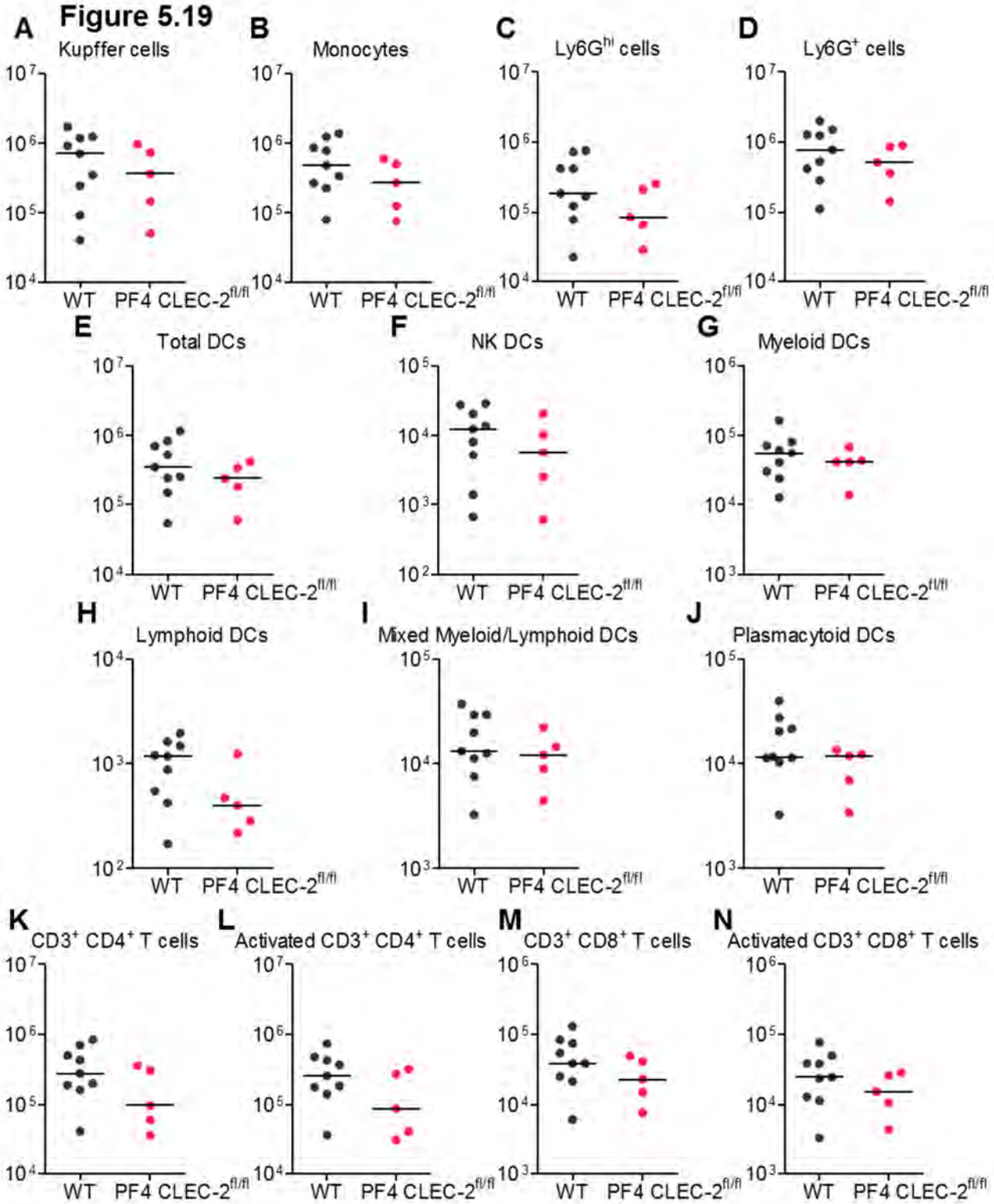

Figure 5.19 Hepatic infiltrate is comparable to WT in mice lacking CLEC-2 on platelets
WT and PF4.Cre.CLEC-2$^{fl/fl}$ mice were infected (i.p.) with 5 x 10^5 CFU attenuated STm. Leukocyte infiltrate in the liver was quantitatively assessed by FACS in non-infected and day 7-infected mice. The gating strategies and representative FACS plots can be seen in Figure 5.18. Absolute numbers of the indicated cell populations are shown, whereby cells are phenotyped as follows:
A) Kupffer cells (F4/80$^+$ Ly6G^{lo} CD11b^{lo} Ly6C^{lo}); B) monocytes (F4/80$^+$ Ly6G^{lo} CD11b^{hi} Ly6C^{hi}); C) Ly6G^{hi} cells (F4/80^{lo} Ly6G^{hi}); D) Ly6G$^+$ cells (F4/80^{lo} Ly6G$^+$); E) total DCs (CD11c$^+$ CD3$^-$ CD19$^-$); F) NK DCs (CD11c$^+$ CD3$^-$ CD19$^-$ CD11b^{lo} CD8α$^-$ NK1.1$^+$ B220$^+$); G) myeloid DCs (CD11c$^+$ CD3$^-$ CD19$^-$ CD11b$^+$ CD8α$^-$ NK1.1$^-$ B220$^-$); H) lymphoid DCs (CD11c$^+$ CD3$^-$ CD19$^-$ CD11b$^-$ CD8α$^+$ NK1.1$^-$ B220$^-$); I) mixed myeloid/lymphoid DCs (CD11c$^+$ CD3$^-$ CD19$^-$ CD11b$^-$ CD8α$^-$ NK1.1$^-$ B220$^-$); J) plasmacytoid DCs (CD11c$^+$ CD3$^-$ CD19$^-$ CD11b$^-$ CD8α$^-$ NK1.1$^-$ B220$^+$); K) total CD3$^+$ CD4$^+$ T cells; L) activated CD3$^+$ CD4$^+$ T cells (CD62L^{lo} CD44$^+$) ; M) total CD3$^+$ CD8$^+$ T cells; and N) activated CD3$^+$ CD8$^+$ T cells (CD62L^{lo} CD44$^+$) . Data are taken from one from one experiment, where n = 9 in WT mice and n = 5 in PF4.Cre.CLEC-2$^{fl/fl}$ mice. On histograms, PF4.Cre.CLEC-2$^{fl/fl}$ mice are written PF4 CLEC-2$^{fl/fl}$.

Figure 5.20

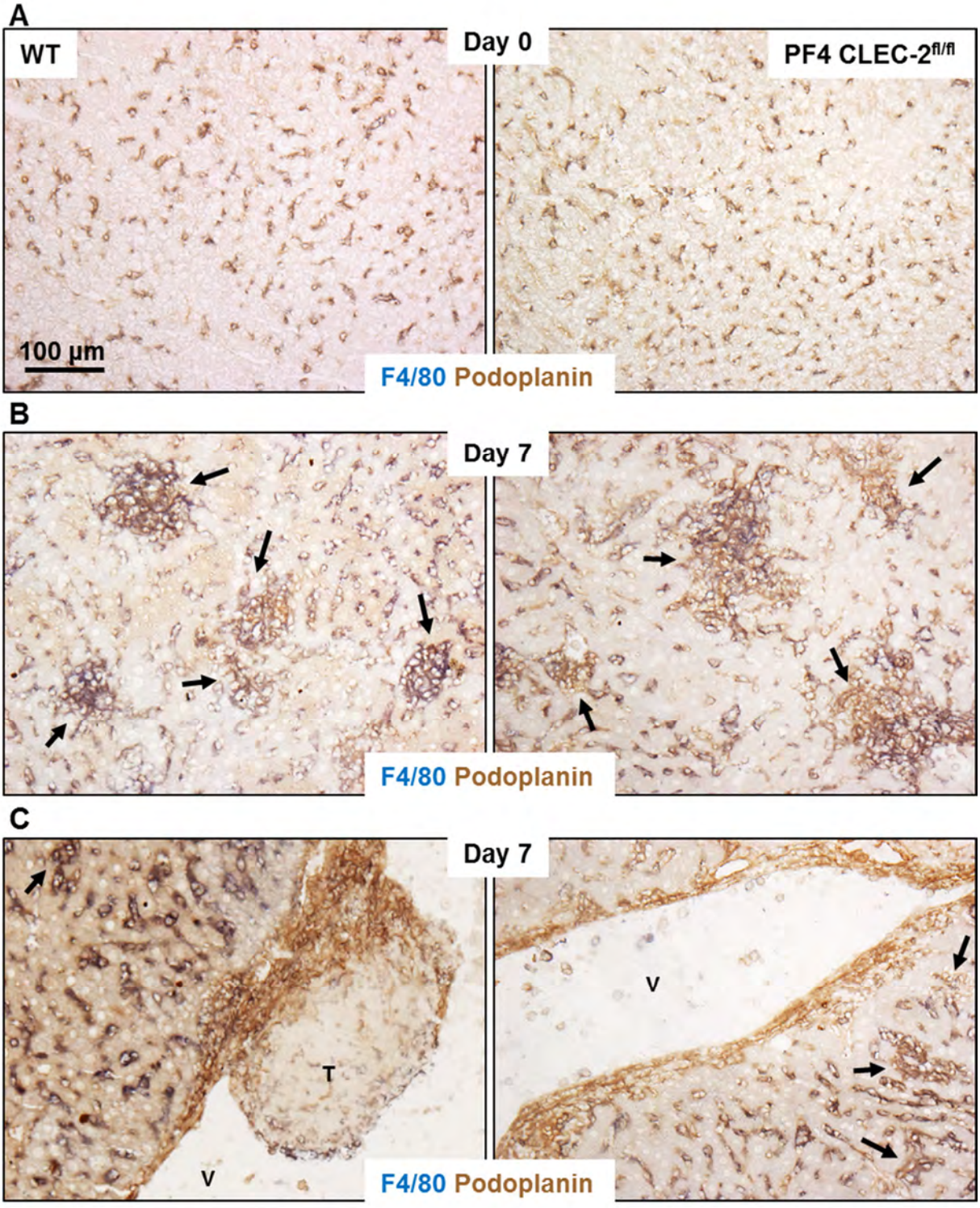

Figure 5.20 Podoplanin expression is comparable in WT and PF4.Cre.CLEC-2$^{fl/fl}$ mice
WT and PF4.Cre.CLEC-2$^{fl/fl}$ mice were infected (i.p.) with 5 x 10^5 CFU attenuated STm. Podoplanin expression was assessed on frozen tissue sections from the livers of A) non-infected WT and PF4.Cre.CLEC-2$^{fl/fl}$ mice and B) day 7-infected mice WT and PF4.Cre.CLEC-2$^{fl/fl}$ mice by IHC. Podoplanin = brown; F4/80 = blue; (double positive staining = black). Black arrows indicate inflammatory lesions. Podoplanin expression was assessed both in parenchymal areas (A-B) and C) adjacent to vessels in WT and PF4.Cre.CLEC-2$^{fl/fl}$ mice. V = vessel; T = thrombus. Images are representative of multiple experiments, where n = 4 at each time-point.

Figure 5.21

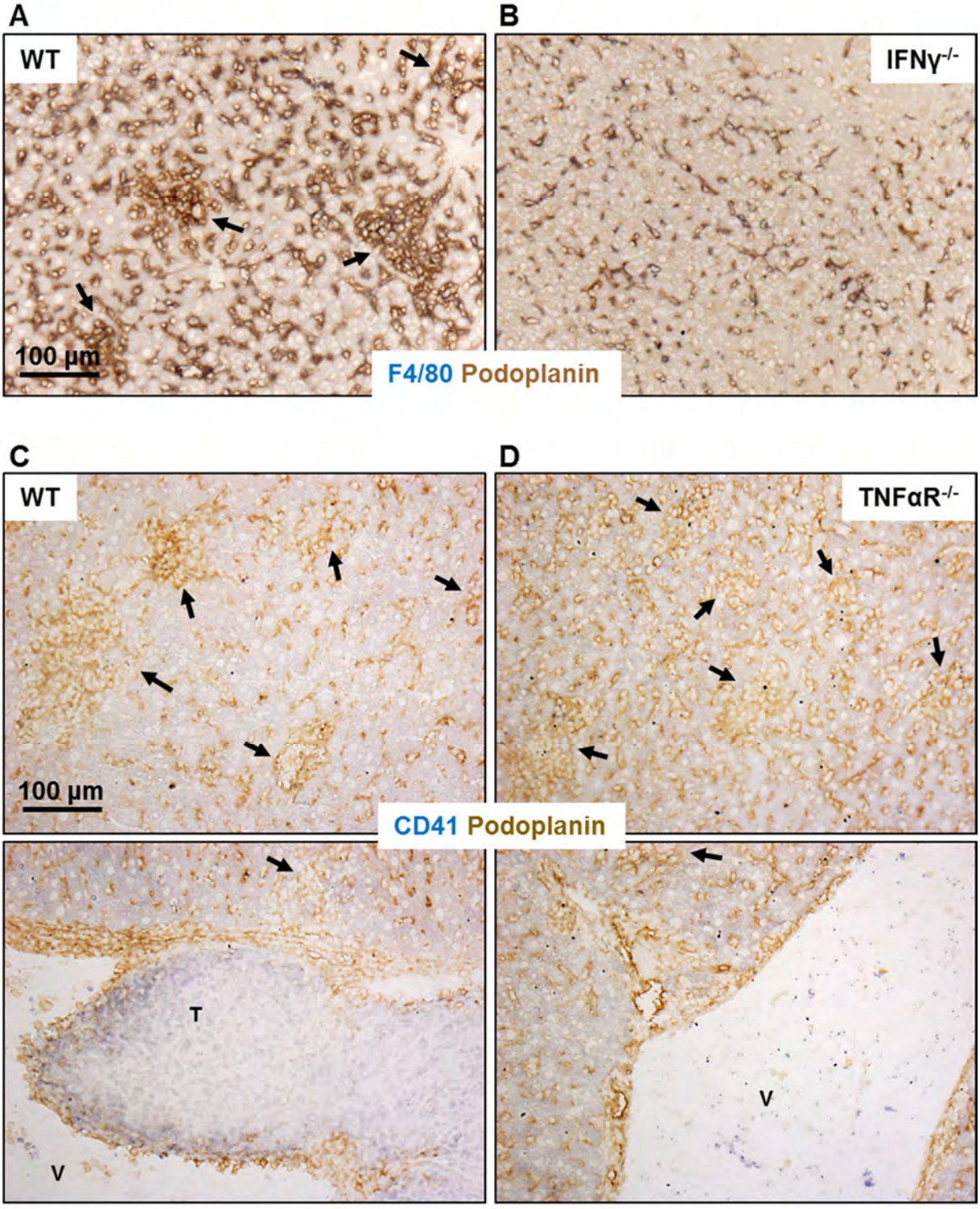

Figure 5.21 Podoplanin expression is not up-regulated in interferon-γ-deficient mice, but is in the absence of tumor necrosis factor-α-Receptor signalling

WT, IFNγ$^{-/-}$ and TNFα-R$^{-/-}$ mice were infected (i.p.) with 5 x 10^5 CFU attenuated STm for 7 days. Podoplanin expression was assessed in frozen tissue sections from the livers of A) WT and B) IFNγ$^{-/-}$ mice in parenchymal areas at day 7 post infection by IHC. Podoplanin = brown; F4/80 = blue; (double positive staining = black). Black arrows indicate inflammatory lesions. Images are representative of multiple experiments, where n = 4 in each strain of mice. Podoplanin expression was further assessed in C) WT and D) TNFαR$^{-/-}$ mice in both parenchymal areas (middle panels) and vascular areas (lower panels) at day 7 post infection by IHC. Podoplanin = brown; CD41 (platelets) = blue. V = vessel; T = thrombus; black arrows indicate inflammatory lesions. Images are representative of multiple experiments, where n = 4 in each strain of mice.

Thus we looked for podoplanin expression in TNFαR-deficient mice following infection, hypothesising that they would lack podoplanin up-regulation. However, despite a lack of thrombus development, podoplanin expression appears similar to that seen in infected WT mice (Fig 5.21 C-D). Therefore, expression of podoplanin in the liver is not sufficient for thrombus development and a TNFαR-mediated signal is also required.

5.9 Podoplanin is expressed on multiple cells adjacent to vessels

Elucidating which cells are expressing podoplanin was addressed initially by confocal microscopy. As stated above, podoplanin expression in the liver of non-infected mice is predominantly restricted to lymphatic endothelial cells, although it is also found on some $F4/80^+$ cells (Fig 5.16). During infection, podoplanin is expressed by both $CD45^+$ and $CD45^-$ populations, reflecting its co-localisation with both haematopoietic and non-haematopoietic populations (Fig 5.22 B). We do not detect podoplanin expression on $CD31^+$ vascular endothelial cells at any point before, or during infection (Fig 5.22 A and C). Initially we focussed on podoplanin expression on $CD45^+$ cells because we observed $podoplanin^+$ $F4/80^+$ cells in the livers of both non-infected and infected mice, suggesting that macrophage populations may express podoplanin. Moreover, others have reported increased podoplanin expression by macrophages during inflammation both *in vitro* and *in vivo* (the spleen) (Hou et al., 2010, Kerrigan et al., 2012). We particularly focused on periportal areas adjacent to thrombi.

Figure 5.22

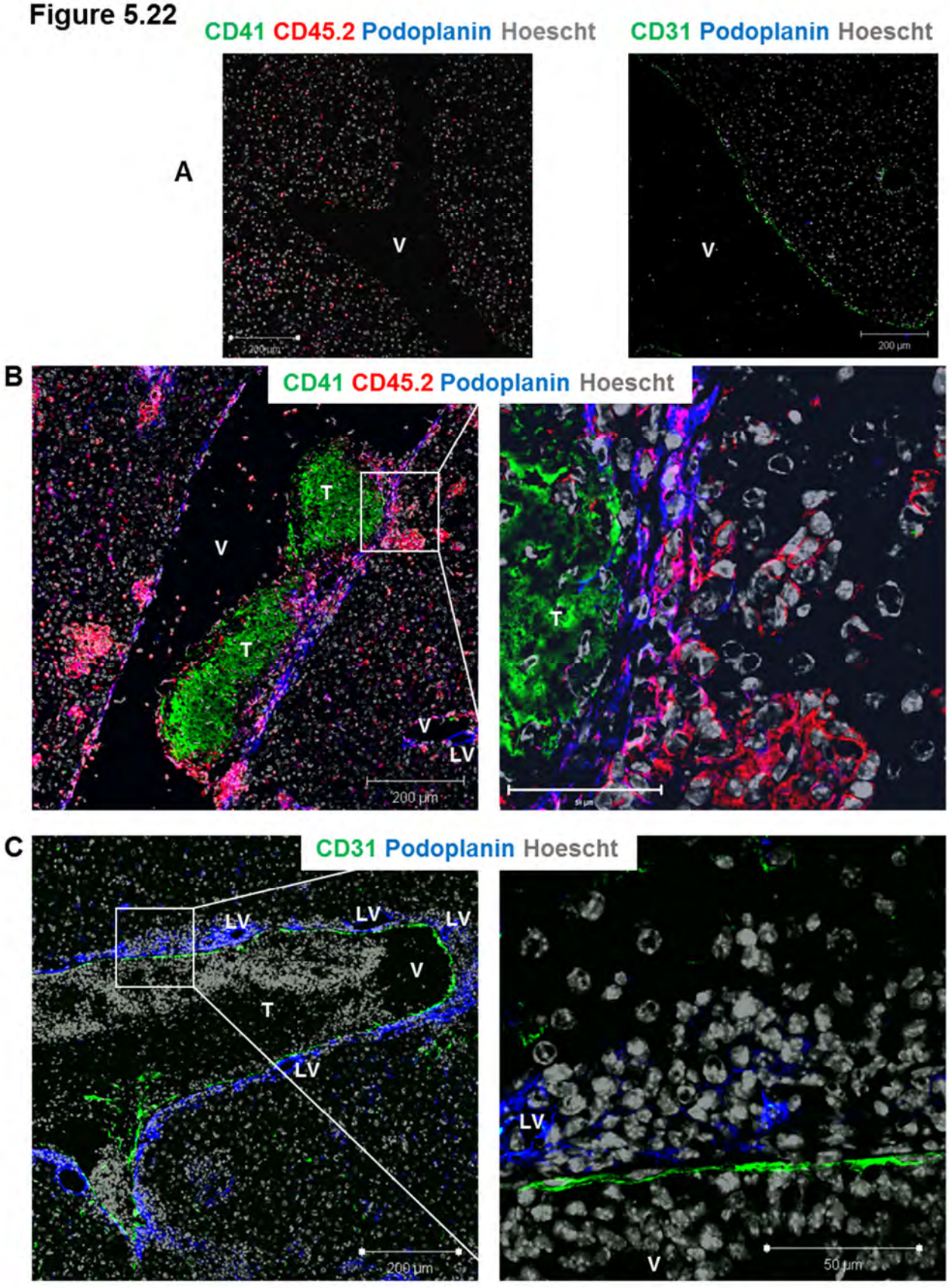

Figure 5.22 Podoplanin is expressed by haematopoietic and non-haematopoietic cells but not by CD31⁺ vascular endothelium

WT mice were infected (i.p.) with 5 x 10^5 CFU attenuated STm for 7 days. Podoplanin expression was assessed on frozen tissue sections from the livers of A) non-infected and B) and C) day 7-infected mice by confocal microscopy. In A) (left panel) and B) (both panels), CD41⁺ cells (platelets) = green; CD45.2⁺ cells = red; podoplanin⁺ cells = blue; CD45.2⁺ podoplanin⁺ cells = magenta. In C) (both panels), CD31⁺ cells = green; podoplanin⁺ cells = blue. In B) and C), the panel on the right is a high magnification enlargement of the boxed area in the left panel. All images are co-stained with nuclear dye Hoescht = grey. V = vessel; T = thrombus; LV = lymphatic vessel. Images are representative from multiple experiments, where n = 4 at each time-point.

Macrophage expression of podoplanin was examined by confocal microscopy. In the absence of infection, isolated F4/80$^+$ cells are detected in the sinusoids, some CD11c$^+$ cells are seen in portal regions and podoplanin is generally restricted to lymphatic endothelium (Fig 5.23 A and C). At day 7, F4/80$^+$ cells are abundant near to the vessels and many of these express CD11c (Fig 5.23 B and D). Podoplanin expression by F4/80$^+$ CD11c$^+$ cells appears white. Some CD11c$^+$ cells express podoplanin but not F4/80 and some CD11c$^+$ cells express neither podoplanin nor F4/80. Single positive podoplanin-stained cells indicate either lymphatic vessels or podoplanin expression by non F4/80 or CD11c expressing cells.

There are few CD11b$^+$ cells in non-infected livers and these accumulate near vessels, and co-staining with CD11c is rare (Fig 5.24 A and C). At day 7, CD11b$^+$ cells are increased in periportal areas, and some of these cells express podoplanin (Fig 5.24 B and D). There are also white cells, indicating podoplanin expression by CD11c$^+$ CD11b$^+$ cells. However, the majority of podoplanin expression is found on CD11c$^+$ cells and on CD11c$^-$ CD11b$^-$ cells. CD11b$^+$ podoplanin$^-$ cells are also common, suggesting podoplanin is not expressed by cells expressing high levels of CD11b (monocyte populations). These data suggest podoplanin is expressed predominantly by F4/80$^+$ CD11c$^+$ and F4/80$^+$ CD11c$^-$ cells and to some extent by CD11b$^+$ cells, although CD11b expression is relatively low on podoplanin$^+$ cells.

Figure 5.23

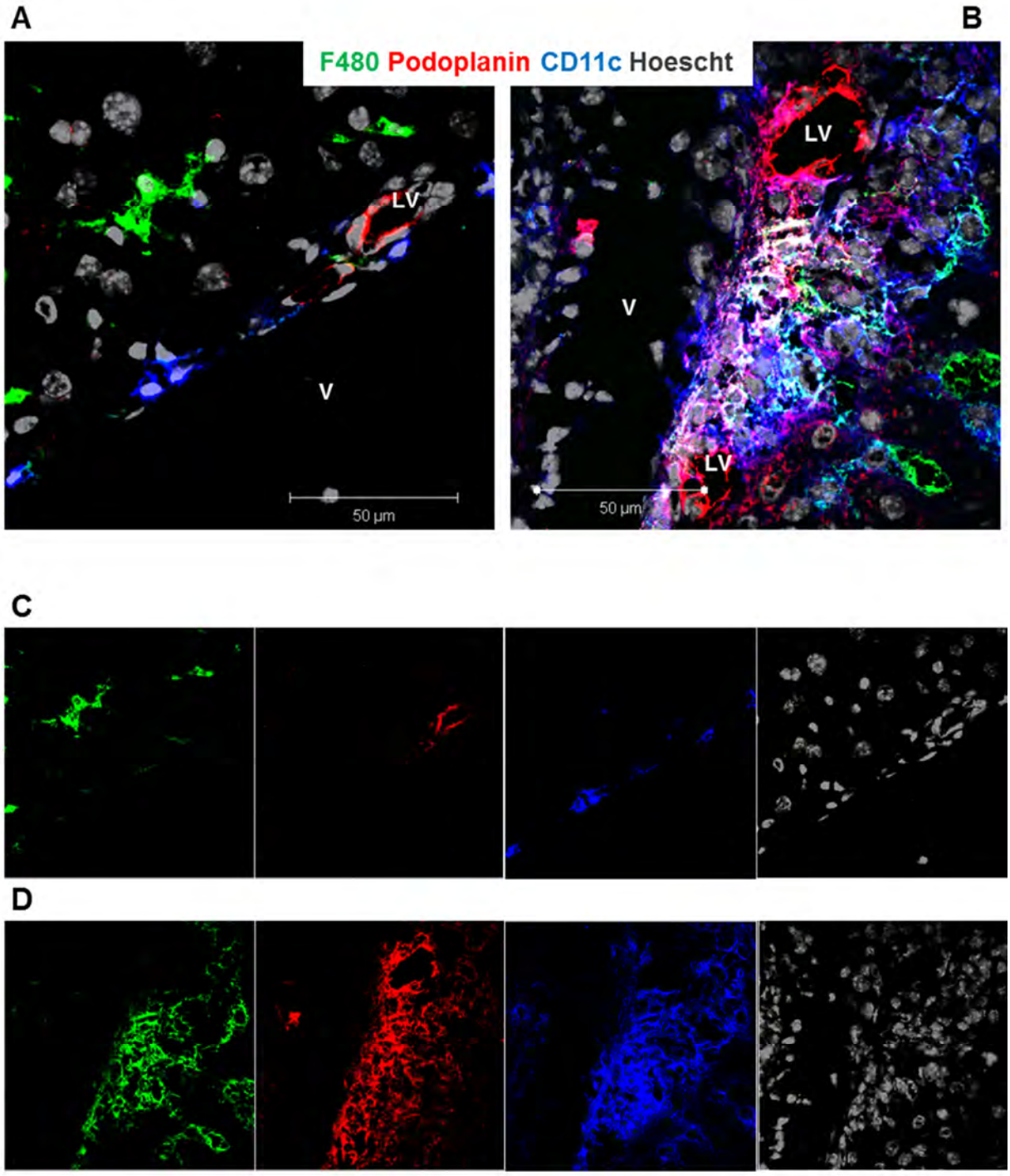

Figure 5.23 Haematopoietic podoplanin expression at vessels is predominantly by CD11c⁺ F4/80⁺ cells after infection

WT mice were infected (i.p.) with 5 x 10^5 CFU attenuated STm for 7 days. Podoplanin expression was assessed on frozen tissue sections from the livers of A) non-infected and B) day 7-infected mice by confocal microscopy. In both images, F4/80⁺ cells = green; podoplanin⁺ cells = red; CD11c⁺ cells = blue; F4/80⁺ CD11c⁺ cells = cyan; F4/80⁺ podoplanin⁺ cells = yellow; CD11c⁺ podoplanin⁺ cells = magenta; CD11c⁺ F4/80⁺ podoplanin⁺ cells = white. Both images are co-stained with nuclear dye Hoescht = grey. V = vessel; LV = lymphatic vessel. Individual colours are shown in C) for the image from the non-infected liver; and D) for the image from the day 7-infected liver. Both images are representative of multiple experiments, where n = 4 at each time-point.

Figure 5.24

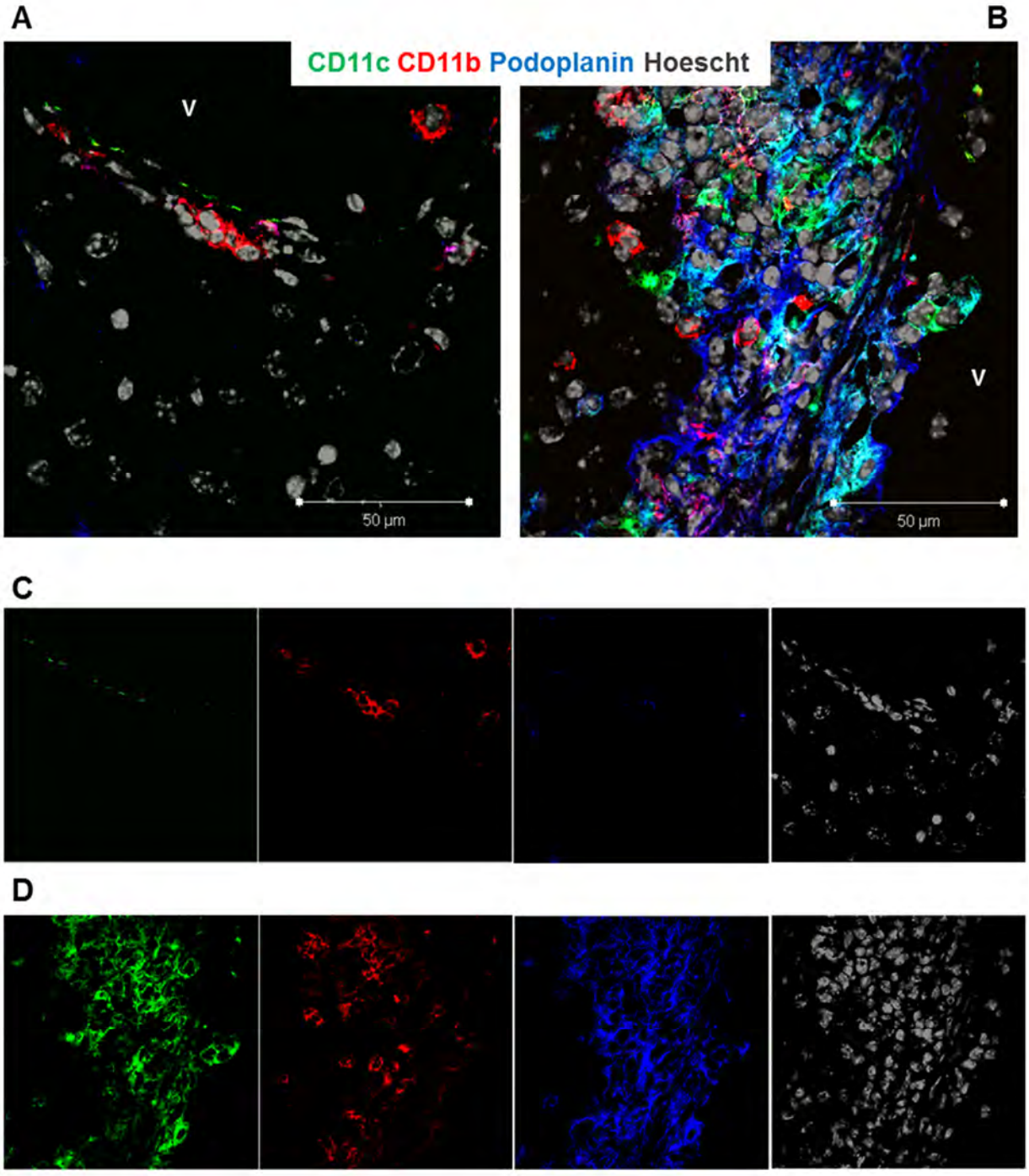

Figure 5.24 Podoplanin is expressed by CD11c⁺ cells and to a lesser extent, CD11b⁺ cells near vessels after infection

WT mice were infected (i.p.) with 5 x 10^5 CFU attenuated STm for 7 days. Podoplanin expression was assessed on frozen tissue sections from the livers of A) non-infected and B) day 7-infected mice by confocal microscopy. In both images, CD11c⁺ cells = green; CD11b⁺ cells = red; podoplanin⁺ cells = blue; CD11c⁺ CD11b⁺ cells = yellow; CD11c⁺ podoplanin⁺ cells = cyan; CD11b⁺ podoplanin⁺ cells = magenta; CD11c⁺ CD11b⁺ podoplanin⁺ cells = white. Both images are co-stained with nuclear dye Hoescht = grey. V = vessel. Individual colours are shown in C) for the image from the non-infected liver; and D) for the image from the day 7-infected liver. Both images are representative of multiple experiments, where n = 4 at each time-point.

5.9.1 Podoplanin expression on non-haematopoietic cells during infection

Having shown that podoplanin is expressed by both $CD45^+$ and $CD45^-$ populations at day 7 post-infection we were keen to characterise non-haematopoietic distribution of podoplanin expression in the liver using confocal microscopy. As illustrated above, $podoplanin^+$ $CD45^-$ cells are mostly located adjacent to the vasculature, especially in portal regions where thrombi are found, and can be seen in inflammatory lesions (Fig 5.22 B). The following markers were used to further characterise these cells: ICAM-1, VCAM-1, CD248 and CD31.

In non-infected livers, podoplanin expression is not detected on $ICAM\text{-}1^+$ cells, and there is very little VCAM-1 staining present (Fig 5.25 A-C). At day 7 post-infection, there is extensive up-regulation of ICAM-1 expression throughout the parenchyma, including in portal regions (Fig 5.25 D-F). Expression of VCAM-1 is also increased following infection, and many $VCAM\text{-}1^+$ cells are also $ICAM\text{-}1^+$. Podoplanin co-localises with $ICAM\text{-}1^+$ cells, $VCAM\text{-}1^+$ cells and $ICAM\text{-}1^+$ $VCAM\text{-}1^+$ cells and is also found on $ICAM\text{-}1^-$ $VCAM\text{-}1^-$ cells, in addition to its expression by lymphatic endothelial cells. There are very few $podoplanin^+$ cells which do not express ICAM-1 or VCAM-1 in areas adjacent to the portal vein, and there are $ICAM\text{-}1^+$ and $VCAM\text{-}1^+$ cells in this area which do not express podoplanin. As a point of reference, expression of these markers was also examined in the spleen at day 7 post-infection. As in the liver, there is much overlap in ICAM-1 and VCAM-1 staining and the abundance of white cells reflects podoplanin expression by cells expressing both ICAM-1 and VCAM-1 (Fig 5.26 A-E).

Figure 5.25

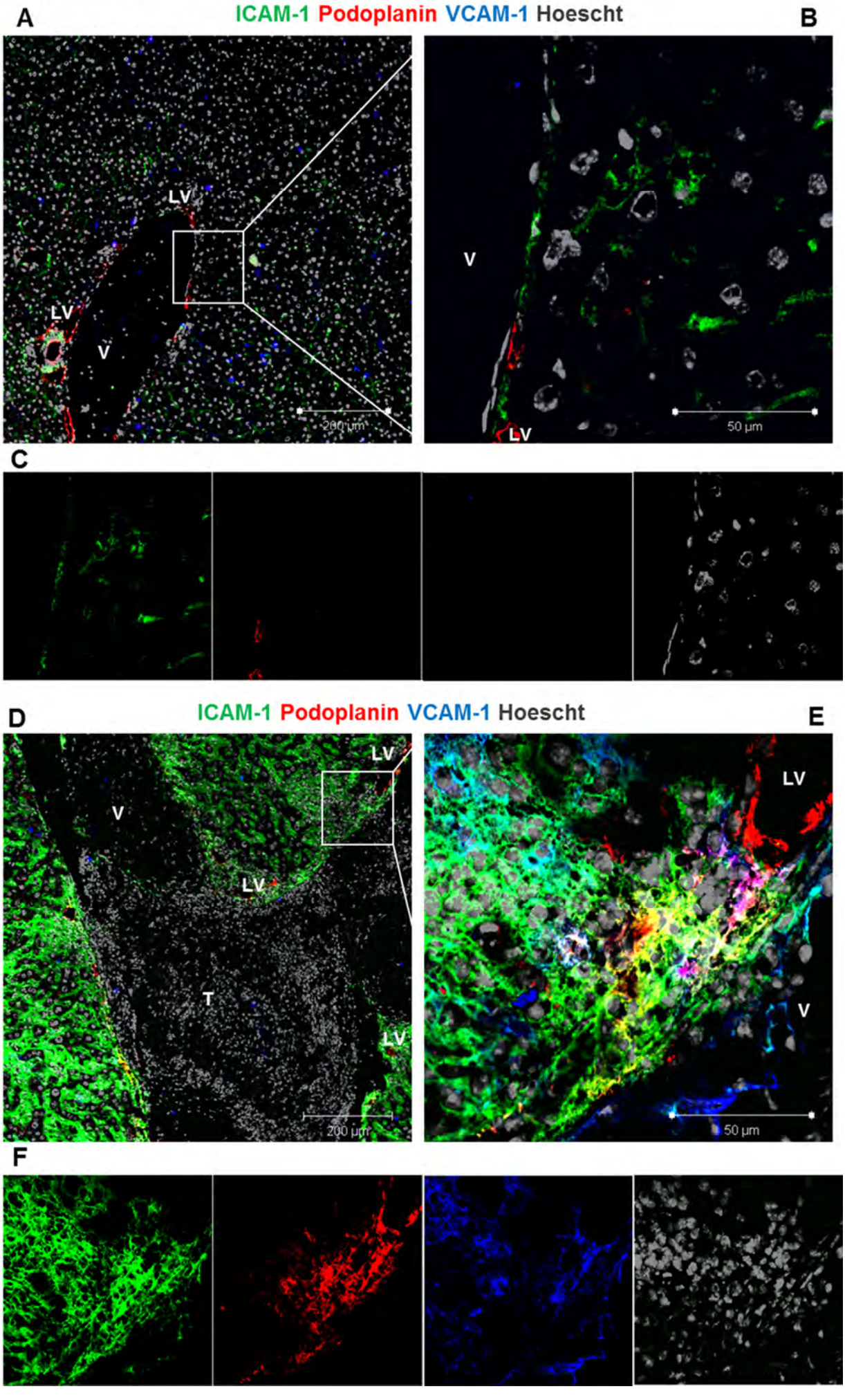
A
ICAM-1 Podoplanin VCAM-1 Hoescht
B
LV
LV
V
200 µm
V
LV
50 µm
C
D
ICAM-1 Podoplanin VCAM-1 Hoescht
E
LV
V
LV
T
LV
200 µm
LV
V
50 µm
F

Figure 5.25 Podoplanin is expressed by ICAM-1$^+$ and VCAM-1$^+$ cells in the liver during infection

WT mice were infected (i.p.) with 5 x 10^5 CFU attenuated STm for 7 days. Podoplanin expression was assessed on frozen tissue sections from the livers of A-C) non-infected and D-F) day 7-infected mice by confocal microscopy. In all images, ICAM-1$^+$ cells = green; podoplanin$^+$ cells = red; VCAM-1$^+$ cells = blue; ICAM-1$^+$ VCAM-1$^+$ cells = cyan; ICAM-1$^+$ podoplanin$^+$ cells = yellow; VCAM-1$^+$ podoplanin$^+$ cells = magenta; and ICAM-1$^+$ VCAM-1$^+$ podoplanin$^+$ cells = white. All images are co-stained with nuclear dye Hoescht = grey. V = vessel; T = thrombus; LV = lymphatic vessel. B) A high magnification enlargement of the boxed area in A) and the individual colours are shown in C). E) A high magnification enlargement of the boxed area in D) and the individual colours are shown in F). Both images are representative of multiple experiments, where n = 4 at each time-point.

Figure 5.26 Podoplanin is expressed by ICAM-1$^+$ and VCAM-1$^+$ cells in the spleen during infection

WT mice were infected (i.p.) with 5 x 10^5 CFU attenuated STm for 7 days. Podoplanin expression was assessed on frozen tissue sections from the spleens of day 7-infected mice by confocal microscopy. In all images, ICAM-1$^+$ cells = green; podoplanin$^+$ cells = red; VCAM-1$^+$ cells = blue; ICAM-1$^+$ VCAM-1$^+$ cells = cyan; ICAM-1$^+$ podoplanin$^+$ cells = yellow; VCAM-1$^+$ podoplanin$^+$ cells = magenta; and ICAM-1$^+$ VCAM-1$^+$ podoplanin$^+$ cells = white. All images are co-stained with nuclear dye Hoescht = grey. V = vessel. A) Low magnification image of spleen tissue. B) A high magnification enlargement of the left-hand boxed area in A) and the individual colours are shown in C). D) A high magnification enlargement of the right-hand boxed area in A) and the individual colours are shown in E). Both images are representative of one experiment, where n = 4 at each time-point.

Figure 5.26

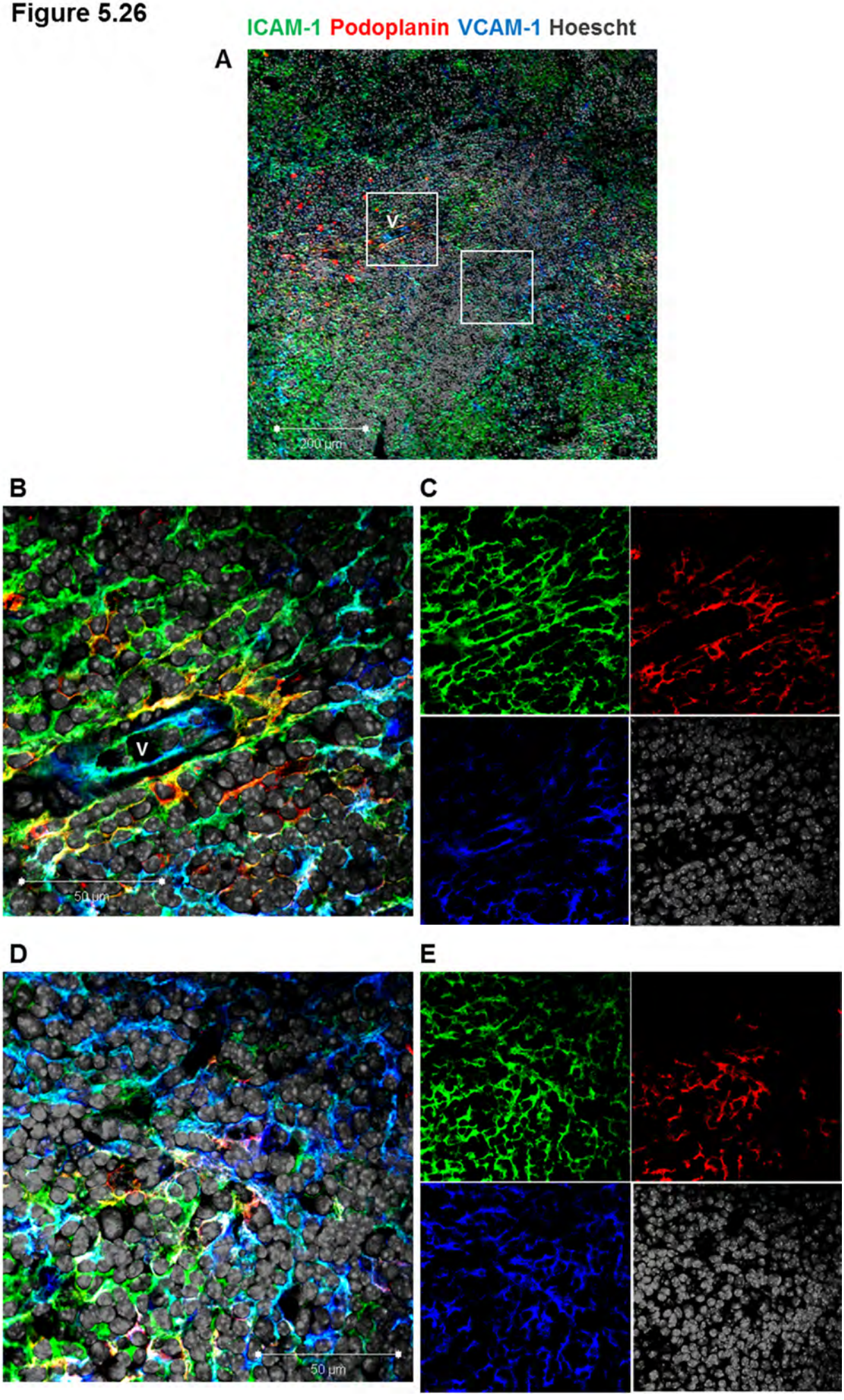

Endosialin, or CD248, is a stromal cell marker expressed on fibroblasts and pericytes (Lax et al., 2007). These cells are located under the vascular endothelium, (where podoplanin$^+$ cells are detected following infection), so we hypothesised that CD248$^+$ cells may express podoplanin. In non-infected livers, CD31$^+$ vascular endothelial cells line the vessels and CD248$^+$ cells lie adjacent to this on the tissue side (Fig 5.27 A-C). Expression of CD31 can be detected on sinusoidal endothelium and expression of CD248 can be seen in similar areas. Podoplanin expression is restricted to lymphatic endothelium and is also detected on isolated cells in the parenchyma (likely to be F4/80$^+$ cells) (Fig 5.27 A-C).

At day 7 post-infection, CD31 expression is found at the vasculature/parenchyma boundary, as in non-infected mice (Fig 5.27 D-F). Expression of CD248 is increased upon infection and is located both adjacent to CD31$^+$ vascular endothelium and additionally is detected in the parenchyma, where it appears at the edges of sinusoids and in inflammatory lesions. Podoplanin co-localises with CD248 staining to some extent, however, there are also both single positive blue and red cells present. Taken together, these data suggest non-haematopoietic populations contribute to podoplanin expression in the liver during infection.

5.9.2 Podoplanin is expressed by CD45$^+$ and CD45$^-$ cells during infection

Having shown where podoplanin is up-regulated in the liver during infection, flow cytometry was used to identify to what extent it is expressed by different populations. To enable direct comparison and to assess small changes in podoplanin expression, FACS analysis was performed on non-infected and day 7-infected livers on the same day. Initially, cells were classified by CD45 expression and podoplanin expression was measured in both groups.

Figure 5.27

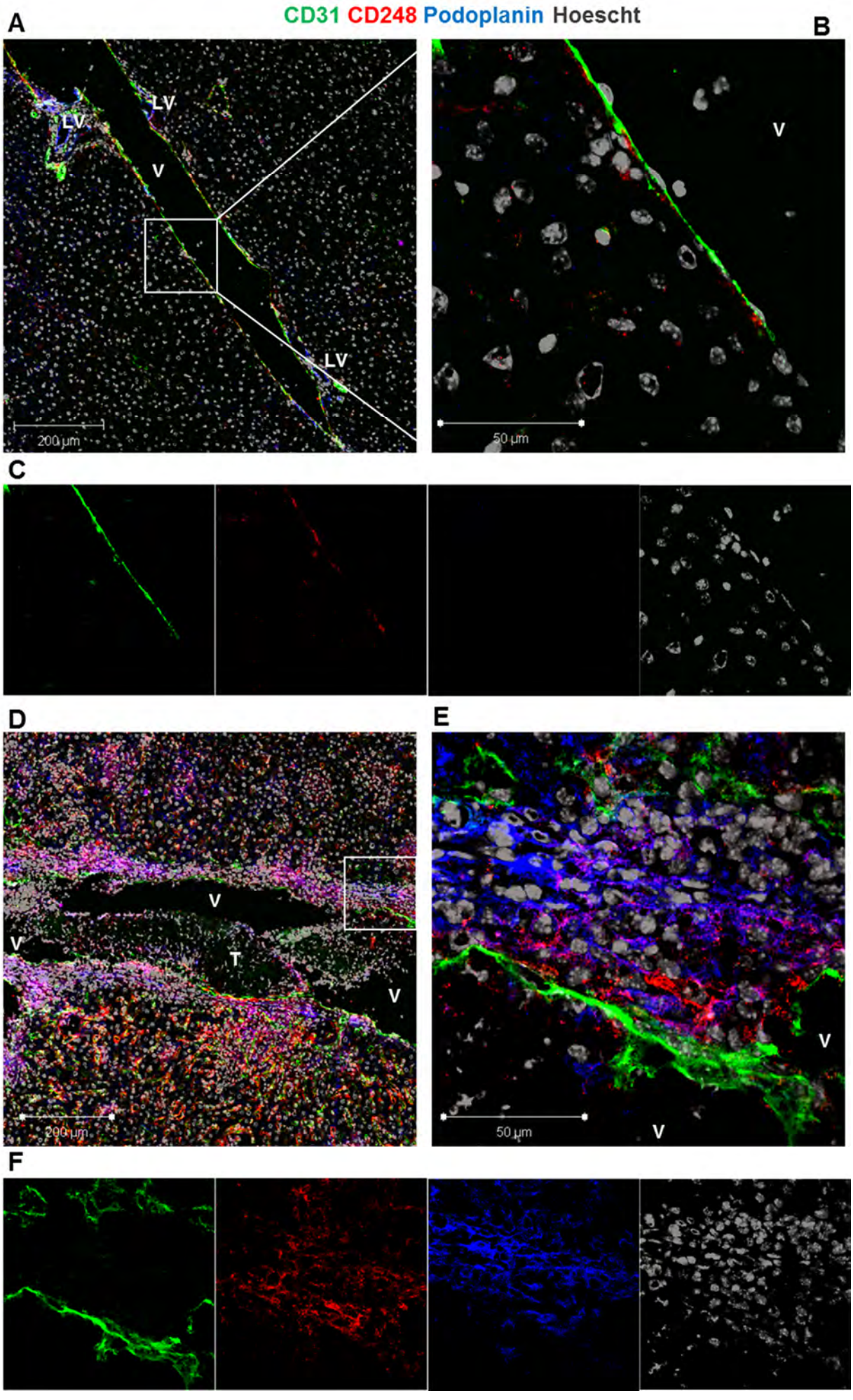
A
CD31 CD248 Podoplanin Hoescht
B
LV
LV
V
LV
200 µm
V
50 µm
C
D
V
V
T
V
200 µm
E
V
50 µm
V
F

Figure 5.27 Podoplanin is co-expressed by CD248$^+$ cells in the liver during infection
WT mice were infected (i.p.) with 5 x 10^5 CFU attenuated STm for 7 days. Podoplanin expression was assessed on frozen tissue sections from the livers of A-C) non-infected and D-F) day 7-infected mice by confocal microscopy. In all images, CD31$^+$ cells = green; CD248$^+$ cells = red; podoplanin$^+$ cells = blue; CD31$^+$ podoplanin$^+$ cells = cyan; CD31$^+$ CD248$^+$ cells = yellow; podoplanin$^+$ CD248$^+$ cells = magenta; and CD31$^+$ podoplanin$^+$ CD248$^+$ cells = white. All images are co-stained with nuclear dye Hoescht = grey. V = vessel; T = thrombus; LV = lymphatic vessel. B) A high magnification enlargement of the boxed area in A) and the individual colours are shown in C). E) A high magnification enlargement of the boxed area in D) and the individual colours are shown in F). Both images are representative of multiple experiments, where n = 4 at each time-point.

However, the collagenase-digestion and gradient centrifugation during the processing of tissues enriches for leukocytes, thus the retrieved $CD45^-$ cells represent only a fraction of the true $CD45^-$ content of the liver.

5.9.2.1 Podoplanin expression by $CD45^-$ cells

The gating strategy and representative FACS plots are shown in Figure 5.28 A-C. Numbers of $CD45^+$ cells and $CD45^-$ cells significantly increase at day 7 post-infection (Fig 5.28 D-E). There is an approximate 50-fold increase in $CD45^-$ cells at day 7, and the number of podoplanin$^+$ $CD45^-$ cells increases approximately 20-fold (Fig 5.28 E-F). The percentage of podoplanin$^+$ $CD45^-$ cells decreases after infection, which supports the modest increase in podoplanin$^+$ $CD45^-$ cells seen relative to the total increase in $CD45^-$ cell numbers (Fig 5.28 E-G). To ensure that flow analysis was as inclusive as possible of $CD45^-$ cells (which are often difficult to isolate from tissues), the "heavy" fraction of the Ficoll gradient was also assessed for podoplanin expression. It is this fraction where hepatocytes end up following gradient centrifugation so other $CD45^-$ cells may also be retained here. It proved particularly difficult to quantify cells in this fraction so all analysis focusses on proportions rather than absolute numbers.

Despite leukocyte enrichment, it is inevitable that some leukocytes will be retained in further layers of the gradient. The proportion of $CD45^+$ cells detected in the non-leukocyte fraction significantly increases following infection, and median fluorescent intensity (MFI) of podoplanin is slightly elevated on total $CD45^+$ cells (Fig 5.29 A-C). The proportion of $CD45^-$ cells decreases after infection, and although the percentage of these cells expressing podoplanin increases, podoplanin MFI is reduced in $CD45^-$ cells following infection (Fig 5.29 C-F).

Figure 5.28

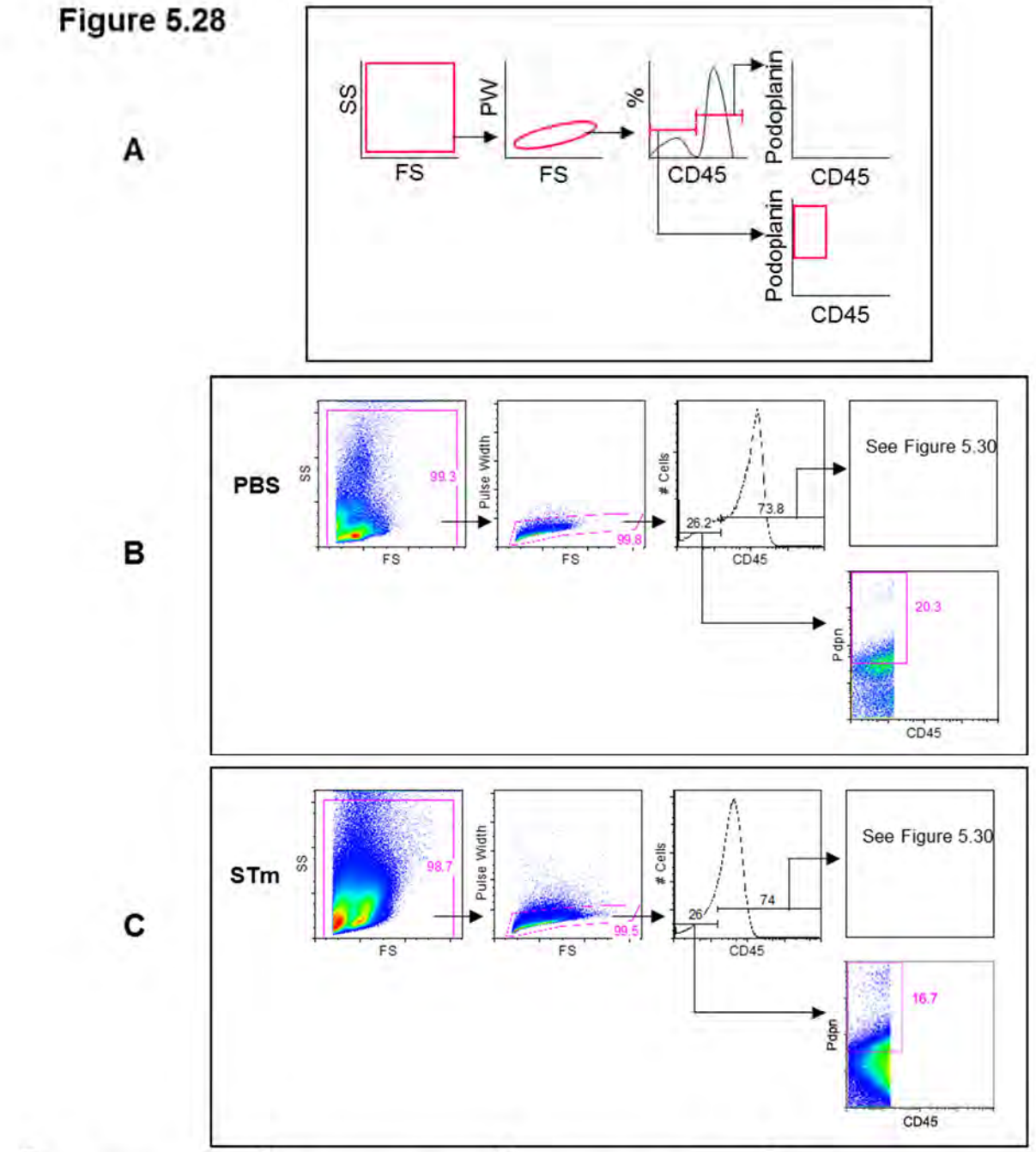

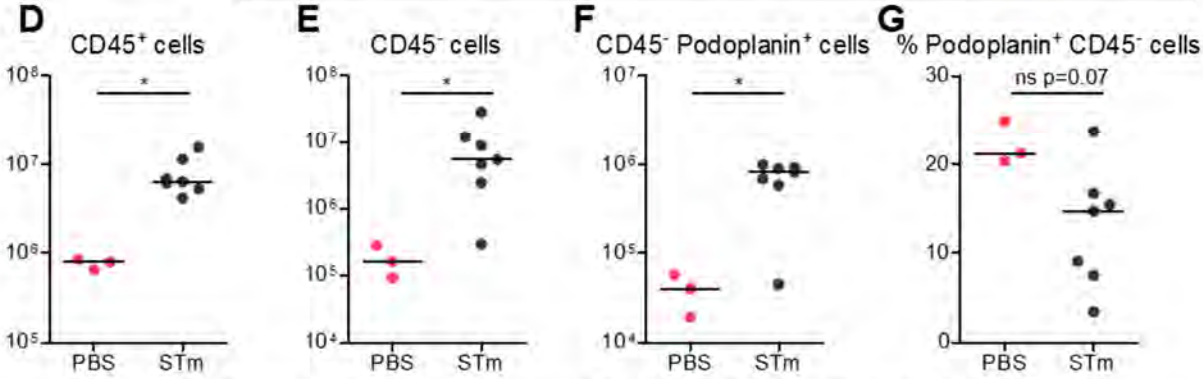

Figure 5.28 Podoplanin is expressed on CD45⁺ and CD45⁻ cells in the liver
WT mice were infected (i.p.) with 5 x 10^5 CFU attenuated STm or PBS for 7 days. Leukocytes were extracted fro the liver by collagenase digestion and gradient centrifugation, and cells retrieved in the leukocyte fraction were examined by FACS for podoplanin expression at day 7 post-infection. A) The gating strategy used is outlined. Representative FACS plots of B) PBS-infected and C) day 7 STm-infected mice are shown. Absolute numbers of D) CD45⁺ cells and E) CD45⁻ cells and F) CD45⁻ podoplanin⁺ cells. G) The percentage of CD45⁻ cells which express podoplanin. Data are taken from one experiment where n = 3 (PBS) and n = 7 (STm-infected). The experiment presented has been repeated multiple times and results shown are representative. *p≤0.05 **p≤0.01 ***p≤0.001.

Figure 5.29

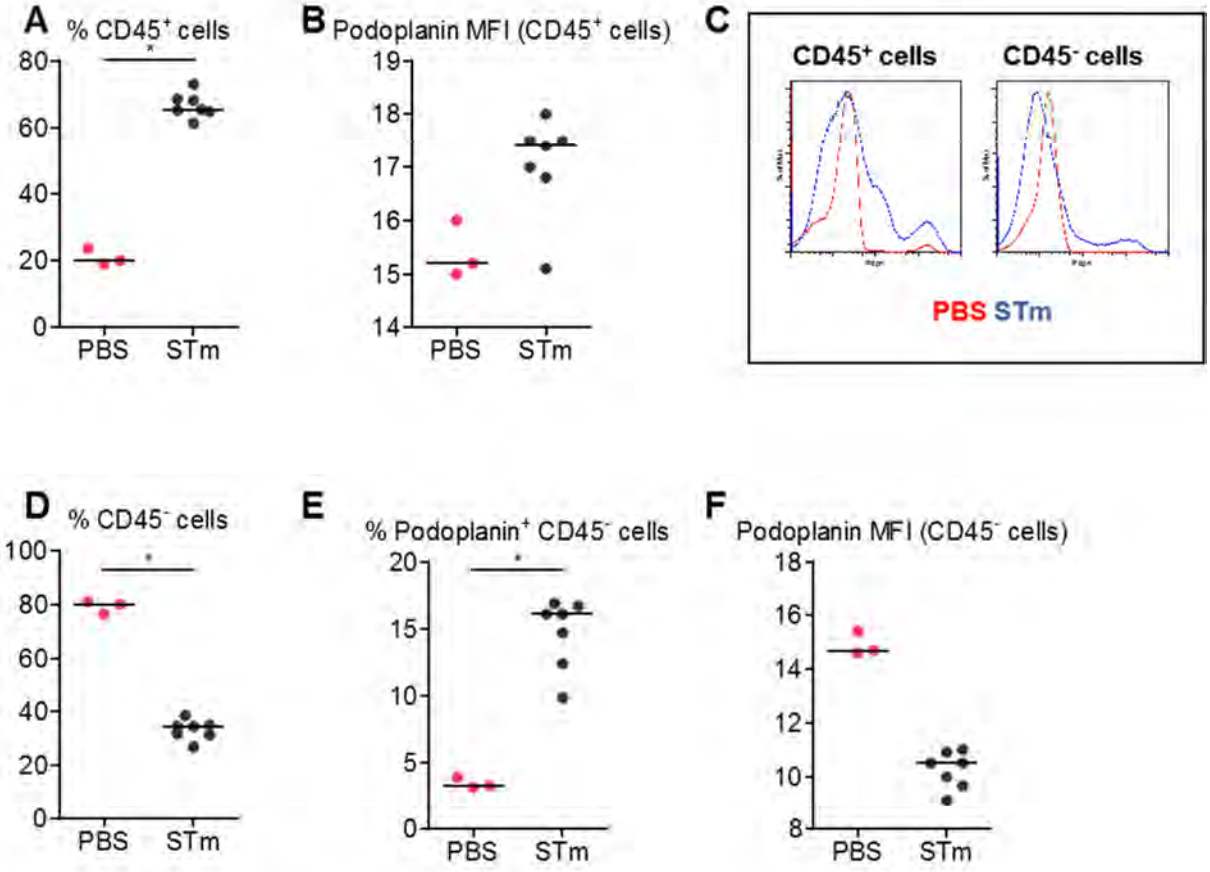

Figure 5.29 Podoplanin is expressed on CD45⁺ and CD45⁻ cells retrieved from the non-leukocyte fraction of the Ficoll gradient

WT mice were infected (i.p.) with 5 x 10^5 CFU attenuated STm or PBS for 7 days. Leukocytes were extracted from the liver by collagenase digestion and gradient centrifugation, and cells retained in the non-leukocyte fraction were examined by FACS for podoplanin expression at day 7 post-infection. The gating strategy is outlined in Figure 5.26 above. A) Proportion of cells which are CD45⁺. B) Relative median fluorescent intensity of podoplanin expressed by CD45⁺ cells. C) Histogram showing podoplanin expression in PBS-infected mice (red) and STm-infected mice (blue) in CD45⁺ and CD45⁻ cells retrieved from the non-leukocyte fraction of the Ficoll gradient. D) Proportion of cells which are CD45⁻. E) Proportion of CD45⁻ cells which express podoplanin. F) Relative median fluorescent intensity of podoplanin expressed by CD45⁻ cells. Data are taken from one experiment where n = 3 (PBS) and n = 7 (STm-infected). The experiment presented has been repeated multiple times and results shown are representative. *p≤0.05 **p≤0.01 ***p≤0.001.

In these studies, the MFI in an indicated population is inclusive of all events acquired, therefore, can seem lower than expected (particularly in comparison to levels detected histologically). Despite this, comparison of relative MFI between populations derived from the same sample can be extremely useful. However, in the non-leukocyte fraction of the Ficoll gradient, the majority of cells will be hepatocytes, thus will negatively skew interpretation of $CD45^-$ podoplanin expression.

5.9.2.2 $CD45^+$ podoplanin-expressing cells are primarily $CD11c^+$ $F4/80^+$

Initial screening of different $CD45^+$ cells revealed that podoplanin expression is not detected above isotype levels on $CD3^+$ cells or $CD31^+$ cells, but is detected on $F4/80^+$ cells, MHC II^+ cells and to a lesser extent on $CD11c^+$ cells (data not shown). Therefore, to further phenotype $CD45^+$ cells based on podoplanin expression, cells were initially separated into three populations by their expression of CD11c and F4/80, as illustrated in Figure 5.30 A-B.

The absolute number of podoplanin-expressing cells increases in all three populations, however, the dynamics of this differ between populations (Fig 5.30 C-E). There is a 5-10-fold increase in the number of $CD11c^+$ $F4/80^-$ $podoplanin^+$ cells after infection, however, the proportion of $CD11c^+$ $F4/80^-$ cells which express podoplanin is slight; approximately 3% $CD11c^+$ $F4/80^-$ cells express podoplanin in non-infected livers, and this increases to 6% by day 7 (Fig 5.30 C and F). In the $CD11c^-$ $F4/80^+$ population, $podoplanin^+$ cells are extremely rare in non-infected livers, yet increase by approximately 100-fold after infection (Fig 5.30 D). The percentage of $CD11c^-$ $F4/80^+$ cells expressing podoplanin increases from 1% to approximately 20% after infection (Fig 5.30 G). In contrast to both these populations, there is a substantial frequency and number of $CD11c^+$ $F4/80^+$ $podoplanin^+$ cells in non-infected livers, the number of which increases 20-fold after infection (Fig 5.30 E and H).

Figure 5.30

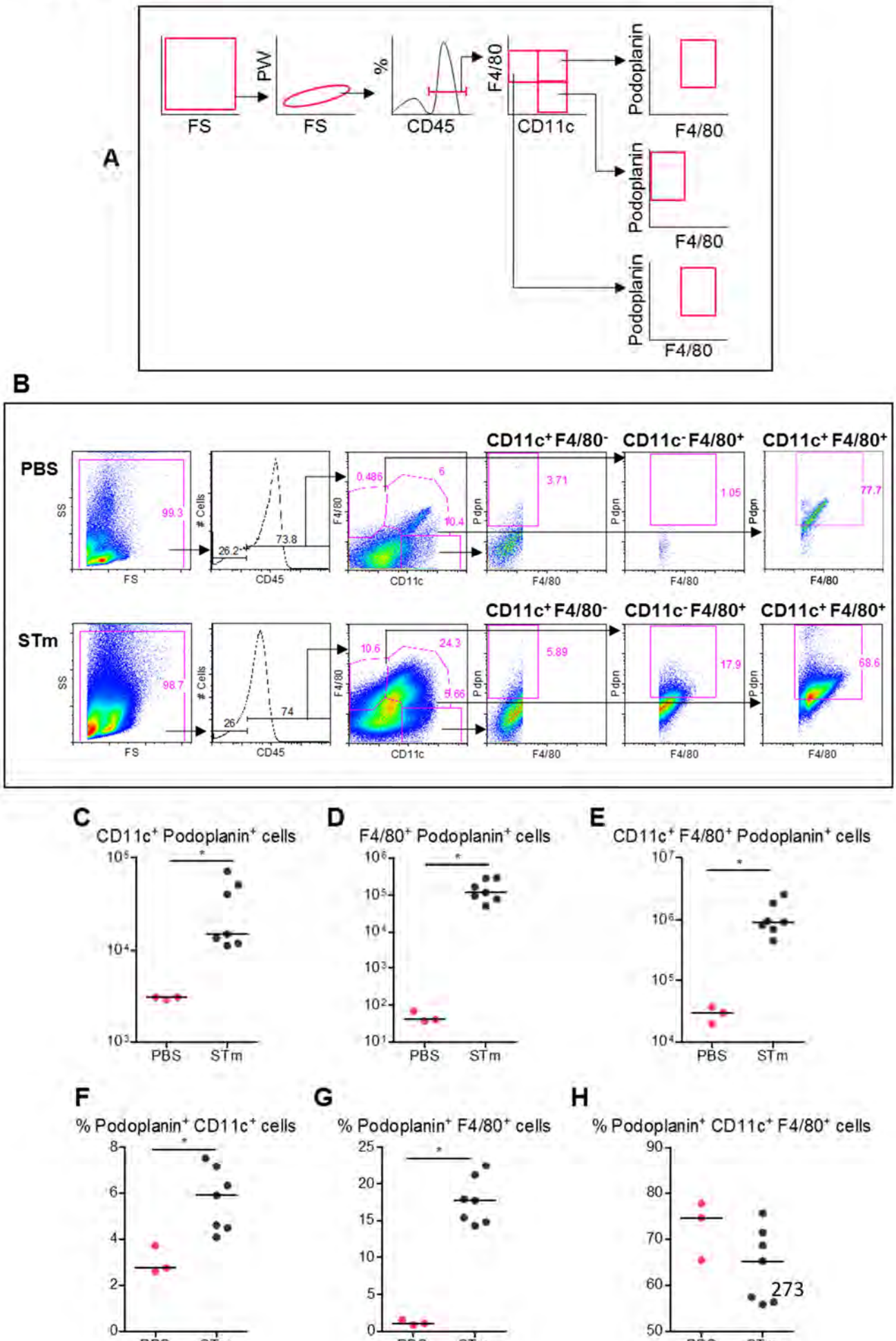
A
FS
PW
FS
%
CD45
F4/80
CD11c
Podoplanin
F4/80
Podoplanin
F4/80
Podoplanin
F4/80
B
PBS
STm
CD11c+ F4/80-
CD11c- F4/80+
CD11c+ F4/80+
SS
FS
Cells
CD45
F4/80
CD11c
Pdpn
F4/80
99.3
26.2
73.8
0.486
6
10.4
3.71
1.05
77.7
98.7
26
74
10.6
24.3
5.66
5.89
17.9
68.6
C
CD11c+ Podoplanin+ cells
D
F4/80+ Podoplanin+ cells
E
CD11c+ F4/80+ Podoplanin+ cells
PBS
STm
F
% Podoplanin+ CD11c+ cells
G
% Podoplanin+ F4/80+ cells
H
% Podoplanin+ CD11c+ F4/80+ cells
273

Figure 5.30 Podoplanin is largely expressed on CD11c$^+$ F4/80$^+$ cells and expression is induced on F4/80$^+$ cells after infection

WT mice were infected (i.p.) with 5 x 10^5 CFU attenuated STm or PBS for 7 days. Leukocytes were extracted from the liver by collagenase digestion and gradient centrifugation, and cells retrieved in the leukocyte fraction were examined by FACS for podoplanin expression. A) The gating strategy classified cells according to expression of CD11c and F4/80. B) Representative FACS plots of PBS-infected and STm-infected mice are shown. Absolute numbers of podoplanin$^+$ C) CD11c$^+$ F4/80$^-$ cells; D) CD11c$^-$ F4/80$^+$ cells; and E) CD11c$^+$ F4/80$^+$ cells are indicated above the proportion of cells in these populations F) CD11c$^+$ F4/80$^-$ cells G) CD11c$^-$ F4/80$^+$ cells H) CD11c$^+$ F4/80$^+$ cells; which express podoplanin. Data are taken from one experiment where n = 3 (PBS) and n = 7 (STm-infected), (however, the experiment has been repeated multiple times and results shown are representative). *p≤0.05 **p≤0.01 ***p≤0.001.

However, the frequency of these cells remains similar after infection (Fig 5.30 H). This detection of podoplanin in non-infected livers supports our histological data.

To further dissect which cells express podoplanin, each population was further phenotyped using Ly6C expression, which is up-regulated on monocyte populations on entering the liver (Tacke, 2012, Karlmark et al., 2009). The gating strategy is shown in Figure 5.31 A-C. The numbers of $CD11c^{+}$ $F4/80^{-}$ cells and $CD11c^{-}$ $F4/80^{+}$ cells expressing podoplanin are low in non-infected mice, regardless of Ly6C expression (Fig 5.31 D-F and J-K). The majority of $CD11c^{+}$ $F4/80^{+}$ cells which express podoplanin are $Ly6C^{lo}$ (Fig 5.31 N-P).

After infection, the highest proportion of $CD11c^{+}$ $F4/80^{-}$ $podoplanin^{+}$ cells are $Ly6C^{lo}$, although there are comparable numbers of $podoplanin^{+}$ cells in all three $CD11c^{+}$ $F4/80^{-}$ populations ($Ly6C^{hi}$ $Ly6C^{lo}$ and $Ly6C^{-}$) (Fig 5.31 D-I). $CD11c^{-}$ $F4/80^{+}$ cells were further gated into $Ly6C^{+}$ and $Ly6C^{-}$ cells. After infection, a slightly lower proportion of $CD11c^{-}$ $F4/80^{+}$ $Ly6C^{+}$ cells express podoplanin relative to $CD11c^{-}$ $F4/80^{+}$ $Ly6C^{-}$ cells, although cell numbers in each population are similar (Fig 5.31 J-M). The $F4/80^{+}$ $CD11c^{+}$ cells were further gated into three populations based on Ly6C expression. There is a greater proportion of $F4/80^{+}$ $CD11c^{+}$ cells expressing podoplanin when these cells are $Ly6C^{lo}$ or $Ly6C^{-}$ (compared to $Ly6C^{hi}$) (Fig 5.31 Q-S). Absolute numbers of $CD11c^{+}$ $F4/80^{+}$ cells expressing podoplanin increase significantly following infection, regardless of Ly6C expression (Fig 5.31 N-P).

Figure 5.31

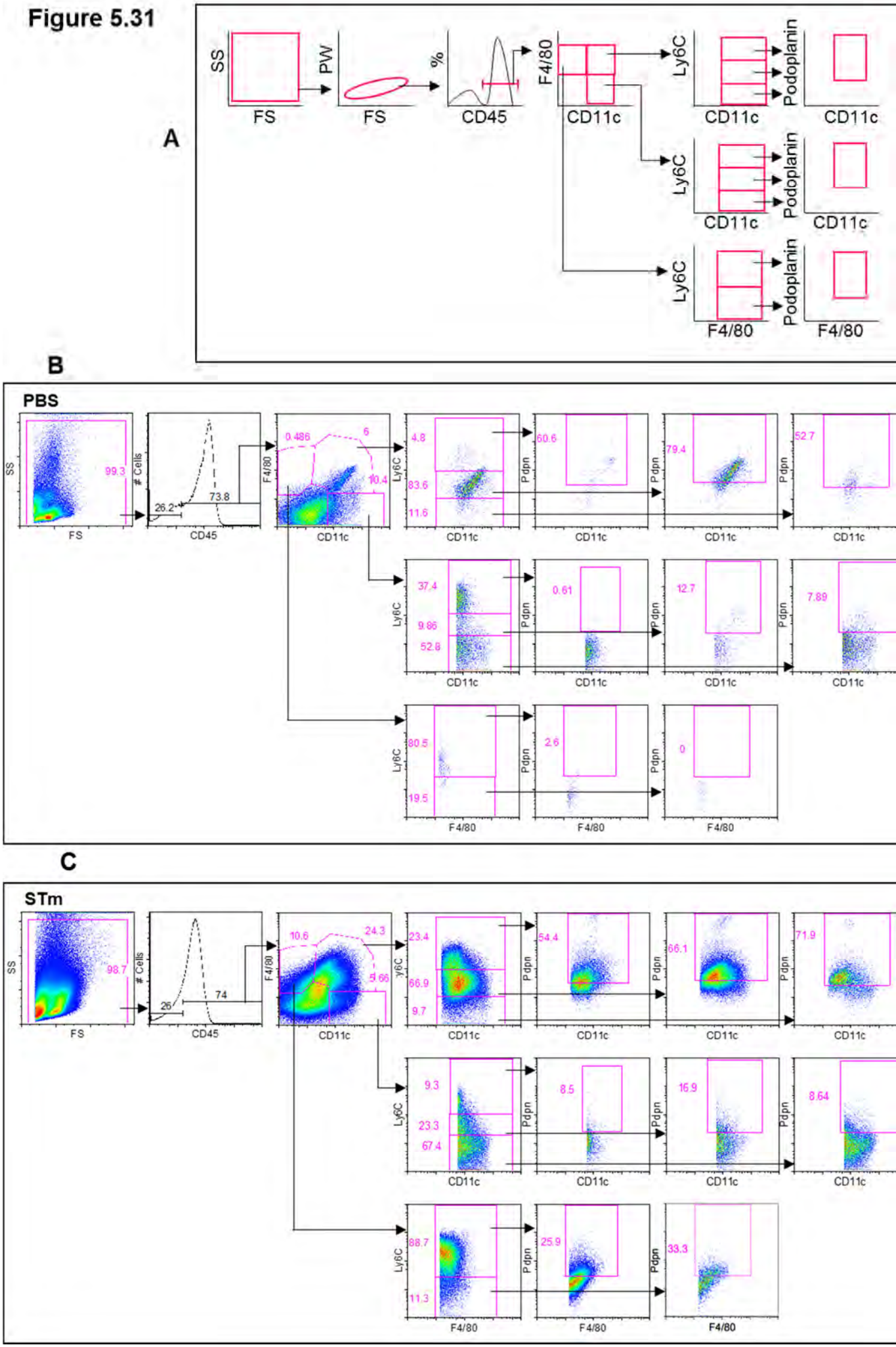
A
SS
FS
PW
FS
%
CD45
F4/80
CD11c
Ly6C
CD11c
Podoplanin
CD11c
Ly6C
CD11c
Podoplanin
CD11c
Ly6C
F4/80
Podoplanin
F4/80
B
PBS
SS
FS
99.3
Cells
CD45
26.2
73.8
F4/80
CD11c
0.486
6
10.4
Ly6C
CD11c
4.8
83.6
11.6
Pdpn
CD11c
60.6
Pdpn
CD11c
79.4
Pdpn
CD11c
52.7
Ly6C
37.4
9.86
52.8
Pdpn
CD11c
0.61
Pdpn
CD11c
12.7
Pdpn
CD11c
7.89
Ly6C
80.5
19.5
F4/80
Pdpn
F4/80
2.6
Pdpn
F4/80
0
C
STm
SS
FS
98.7
Cells
CD45
25
74
F4/80
CD11c
10.6
24.3
5.66
Ly6C
CD11c
23.4
66.9
9.7
Pdpn
CD11c
54.4
Pdpn
CD11c
66.1
Pdpn
CD11c
71.9
Ly6C
9.3
23.3
67.4
Pdpn
CD11c
8.5
Pdpn
CD11c
16.9
Pdpn
CD11c
8.64
Ly6C
88.7
11.3
F4/80
Pdpn
F4/80
25.9
Pdpn
F4/80
33.3

Figure 5.31 continued

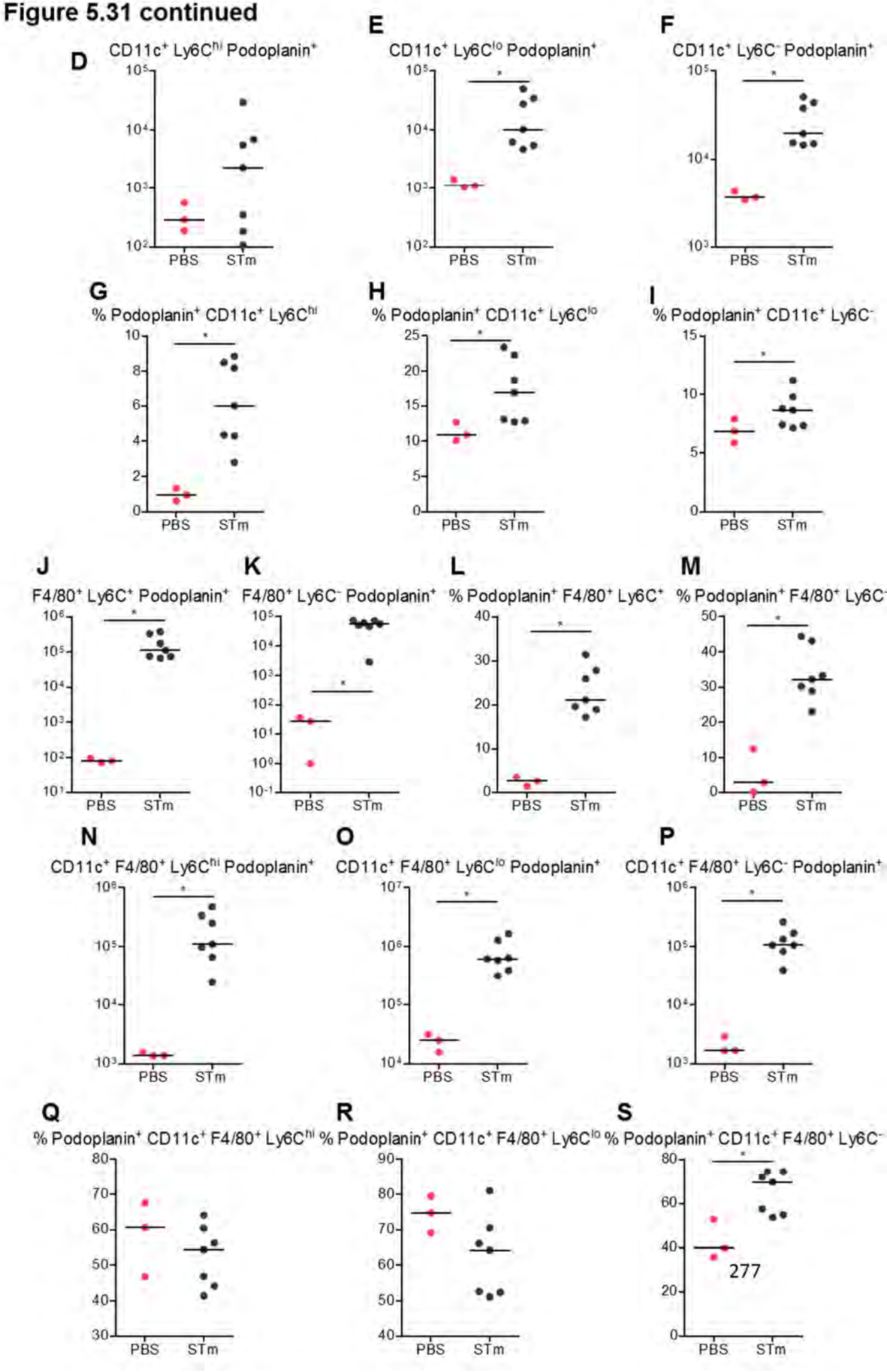

In summary, in the absence of infection, most podoplanin$^+$ cells are CD11c$^+$ F4/80$^+$ Ly6C^{lo} cells. After infection, the greatest numbers of podoplanin$^+$ cells are CD11c$^-$ F4/80$^+$ and CD11c$^+$ F4/80$^+$. In these populations, numbers of Ly6C$^+$ podoplanin$^+$ cells and Ly6C$^-$ podoplanin$^+$ cells are increased following infection, demonstrating that both Ly6C^{hi} (more monocyte lineage) and Ly6C^{lo} (both Kupffer cell and newly infiltrated macrophage populations) can express podoplanin (Tacke et al., 2009).

5.9.2.3 Podoplanin expression is highest on CD11c$^+$ F4/80$^+$ cells

To explore the level to which these cells express podoplanin, the MFI was investigated. As mentioned above, because the MFI of an indicated population is inclusive of all events acquired, the relative MFI between populations in a sample provides the most reliable interpretation.

Podoplanin MFI (gated on total cells) is increased at day 7 post-infection, relative to in non-infected mice, where the MFI is comparable to isotype (Fig 5.32 A-D). In CD45$^-$ cells, podoplanin MFI was not obtained due to the bimodal distribution of fluorescent intensity (Fig 5.32 B-D). In non-infected mice, podoplanin expression in CD11c$^+$ F4/80$^-$ cells, is marginally higher than isotype and this increases negligibly after infection (Fig 5.32 E). In CD11c$^-$ F4/80$^+$ cells, podoplanin MFI is equivalent to isotype in non-infected mice and increases 3-4 fold after infection (Fig 5.32 F). However, in CD11c$^+$ F4/80$^+$ cells from non-infected livers, the MFI of podoplanin is considerably above isotype and is approximately 10-fold higher than that measured on either CD11c$^+$ F4/80$^-$ cells or CD11c$^-$ F4/80$^+$ cells. This decreases slightly upon infection, but is still at least twice that recorded in any other population (Fig 5.32 E-G). These data are represented in histogram form (Fig 5.32 H-I).

Figure 5.32

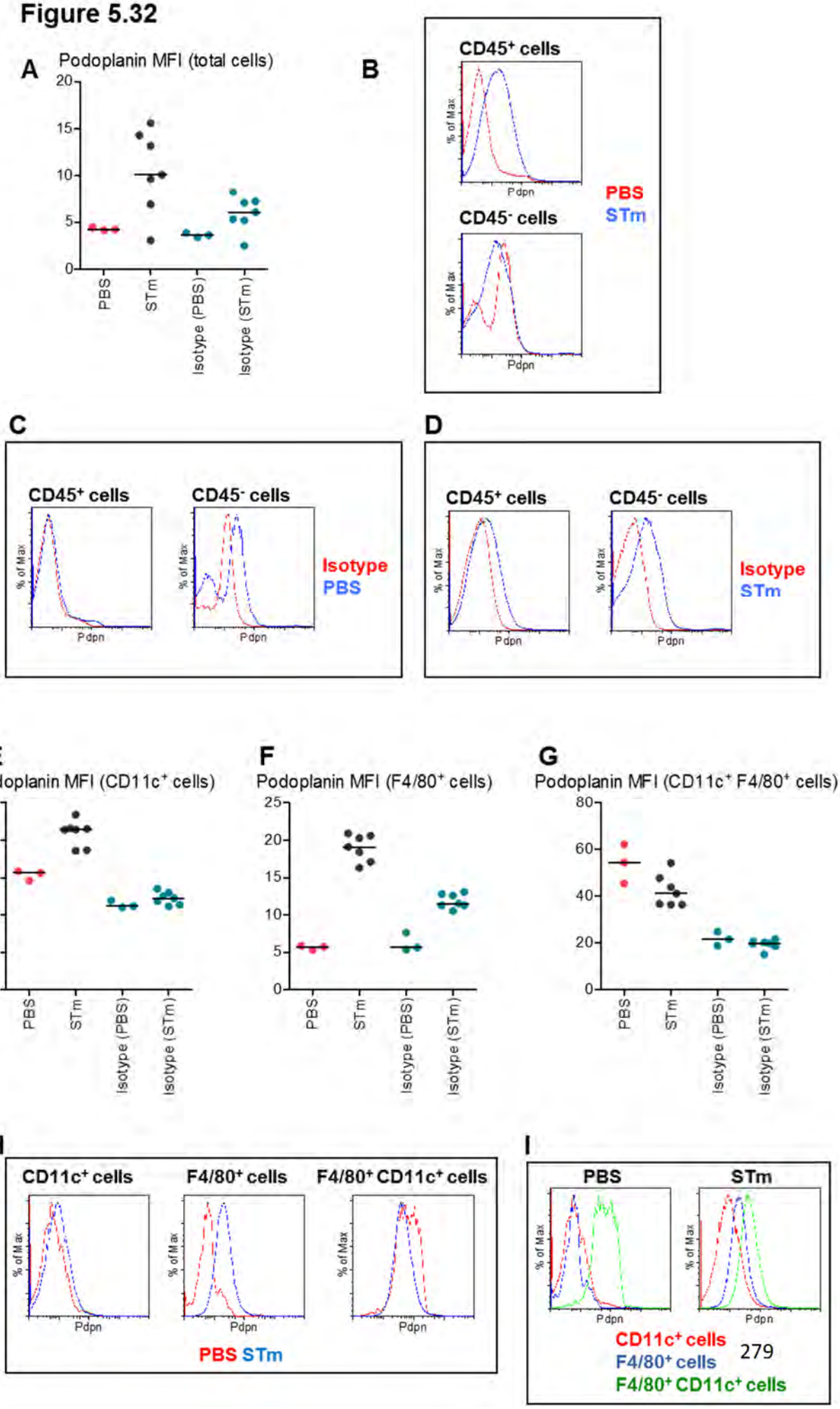
A
Podoplanin MFI (total cells)
20
15
10
5
0
PBS
STm
Isotype (PBS)
Isotype (STm)
B
CD45+ cells
% of Max
Pdpn
PBS
STm
CD45- cells
% of Max
Pdpn
C
CD45+ cells
% of Max
Pdpn
CD45- cells
% of Max
Pdpn
Isotype
PBS
D
CD45+ cells
% of Max
Pdpn
CD45- cells
% of Max
Pdpn
Isotype
STm
E
Podoplanin MFI (CD11c+ cells)
10
8
6
4
2
0
PBS
STm
Isotype (PBS)
Isotype (STm)
F
Podoplanin MFI (F4/80+ cells)
25
20
15
10
5
0
PBS
STm
Isotype (PBS)
Isotype (STm)
G
Podoplanin MFI (CD11c+ F4/80+ cells)
80
60
40
20
0
PBS
STm
Isotype (PBS)
Isotype (STm)
H
CD11c+ cells
% of Max
Pdpn
F4/80+ cells
% of Max
Pdpn
F4/80+ CD11c+ cells
% of Max
Pdpn
PBS STm
I
PBS
% of Max
Pdpn
STm
% of Max
Pdpn
CD11c+ cells
F4/80+ cells
F4/80+ CD11c+ cells

Figure 5.32 Podoplanin expression is highest on CD11c$^+$ F4/80$^+$ cells before and after infection

WT mice were infected (i.p.) with 5 x 10^5 CFU attenuated STm or PBS for 7 days. Leukocytes were extracted from the liver by collagenase digestion and gradient centrifugation. Cells retrieved in the leukocyte fraction were examined by FACS for podoplanin expression as was described above in Figure 5.30. A) The mean fluorescent intensity (MFI) of podoplanin expression was measured in total CD45$^+$ retrieved, relative to the relevant isotype controls (shown in blue).* B) Representative histograms showing podoplanin expression in CD45$^+$ cells (top panel) and CD45$^-$ cells (which were retained in the leukocyte fraction during gradient centrifugation) (bottom panel), 7 days after PBS (red) or STm (blue) infection. These histograms are shown relative to isotype control after C) PBS and D) STm infection. The MFI of podoplanin expression was measured in E) CD11c$^+$ F4/80$^-$ cells; F) CD11c$^-$ F4/80$^+$ cells and G) CD11c$^+$ F4/80$^+$ cells after PBS or STm infection. Relevant isotype controls are shown in blue. H) Representative histograms of podoplanin expression after PBS (red) or STm (blue) infection in CD11c$^+$ F4/80$^-$ cells (left panel); CD11c$^-$ F4/80$^+$ cells (middle panel); and CD11c$^+$ F4/80$^+$ cells (right panel). I) The histograms in H) are here presented in a manner which enables comparisons between populations where CD11c$^+$ F4/80$^-$ cells = red; CD11c$^-$ F4/80$^+$ cells = blue; and CD11c$^+$ F4/80$^+$ cells = green. Data are taken from one experiment (described in Figure 5.30) where n = 3 (PBS) and n = 7 (STm-infected), (however, the experiment has been repeated multiple times and results shown are representative).

*In this study, the MFI in an indicated population is inclusive of all events acquired, therefore, can seem lower than expected (particularly in comparison to levels detected histologically). Despite this, comparison of relative MFI between populations derived from the same sample can be extremely useful. However, in the non-leukocyte fraction of the Ficoll gradient, the majority of cells will be hepatocytes, thus will negatively skew interpretation of CD45$^-$ podoplanin expression.

These data support our histological observations that podoplanin is expressed by both $CD45^+$ and $CD45^-$ populations in the livers of non-infected mice and that after infection, podoplanin expression in the liver is increased. There are subtle differences in how podoplanin expression is altered by infection in different populations of cells.

5.9.3 Podoplanin expression increases within 24 hours of infection

We know that increased podoplanin expression in the liver during infection is due to increased numbers of podoplanin-expressing cells, and increased expression per cell. This is apparent by day 7, however, thrombi first appear by day 5 post-infection and so we hypothesised that podoplanin expression would already be increased by this time. To test this, podoplanin expression was assessed at early time-points post-infection in the liver by FACS and by IHC.

By histology, more $podoplanin^+$ cells are detected by 24 hours of infection, relative to in non-infected mice, and this is most apparent in cells adjacent to the vessels (Fig 5.33 A- B and H-I). Within 48 hours, $podoplanin^+$ cells are frequently in contact with other $podoplanin^+$ and $podoplanin^-$ cells in the parenchyma, and $podoplanin^+$ cells are seen beside vessels (Fig 5.33 C and J). By day 5, inflammatory lesions are established and many of the cells in lesions are $podoplanin^+$. Nearly all $podoplanin^+$ cells in the parenchyma also express F4/80 (Fig 5.33 D). Thrombi are formed by this time and $podoplanin^+$ (but largely $F4/80^-$) cells accumulate adjacent to vessels, especially in proximity to thrombi (Fig 5.33 K). At days 7 and 21, the podoplanin distribution is similar to that seen at day 5, but the number of $podoplanin^+$ cells are increased (and this is to a greater extent at day 21) (Fig 5.33 E-F and L-M). There are less $F4/80^+$ leukocytes in the liver by day 35, however, many of these are $podoplanin^+$ (Fig 5.33 G and N).

Figure 5.33

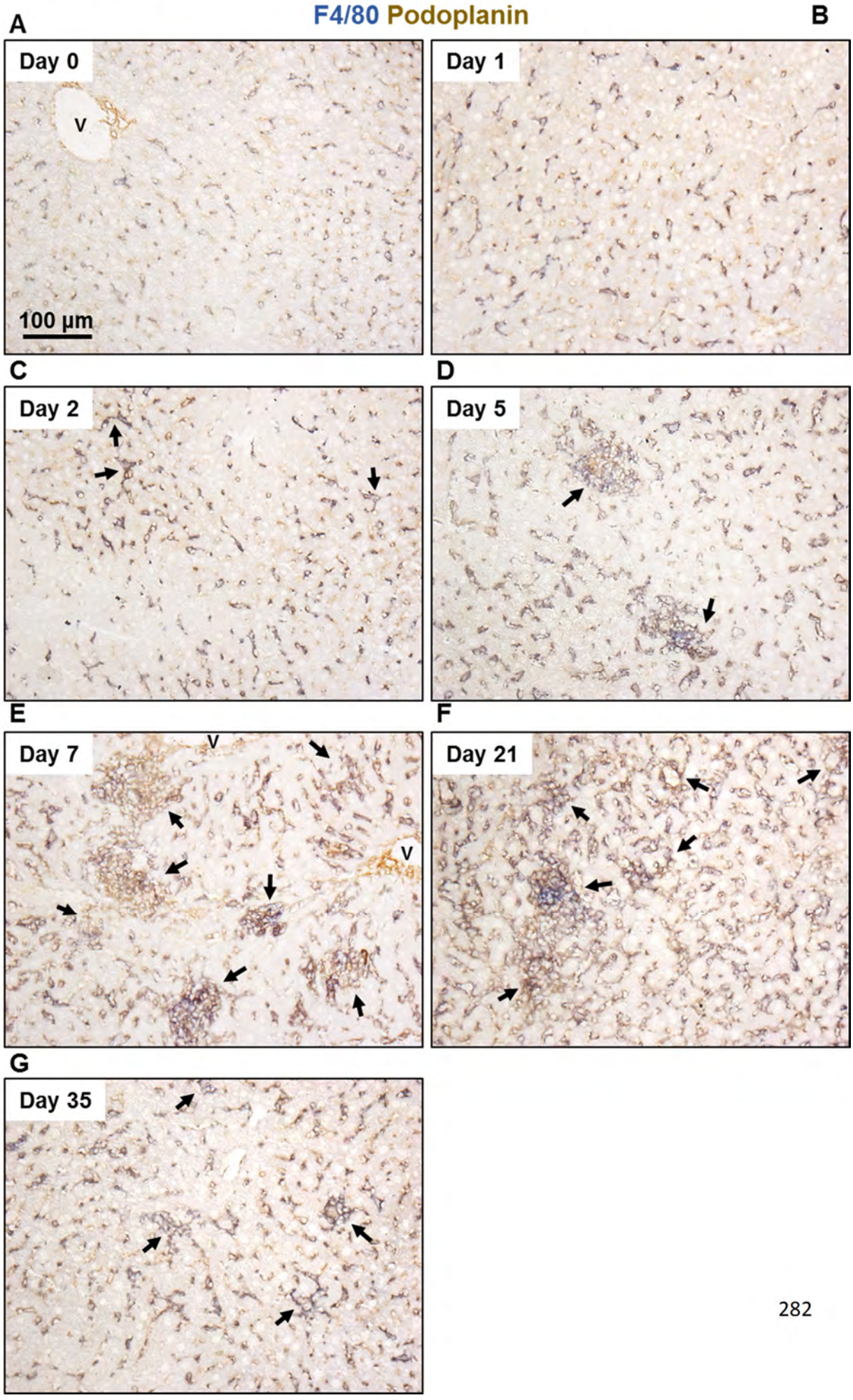
F4/80 Podoplanin
A
B
Day 0
V
100 µm
Day 1
C
D
Day 2
Day 5
E
F
Day 7
V
V
Day 21
G
Day 35

Figure 5.33 continued

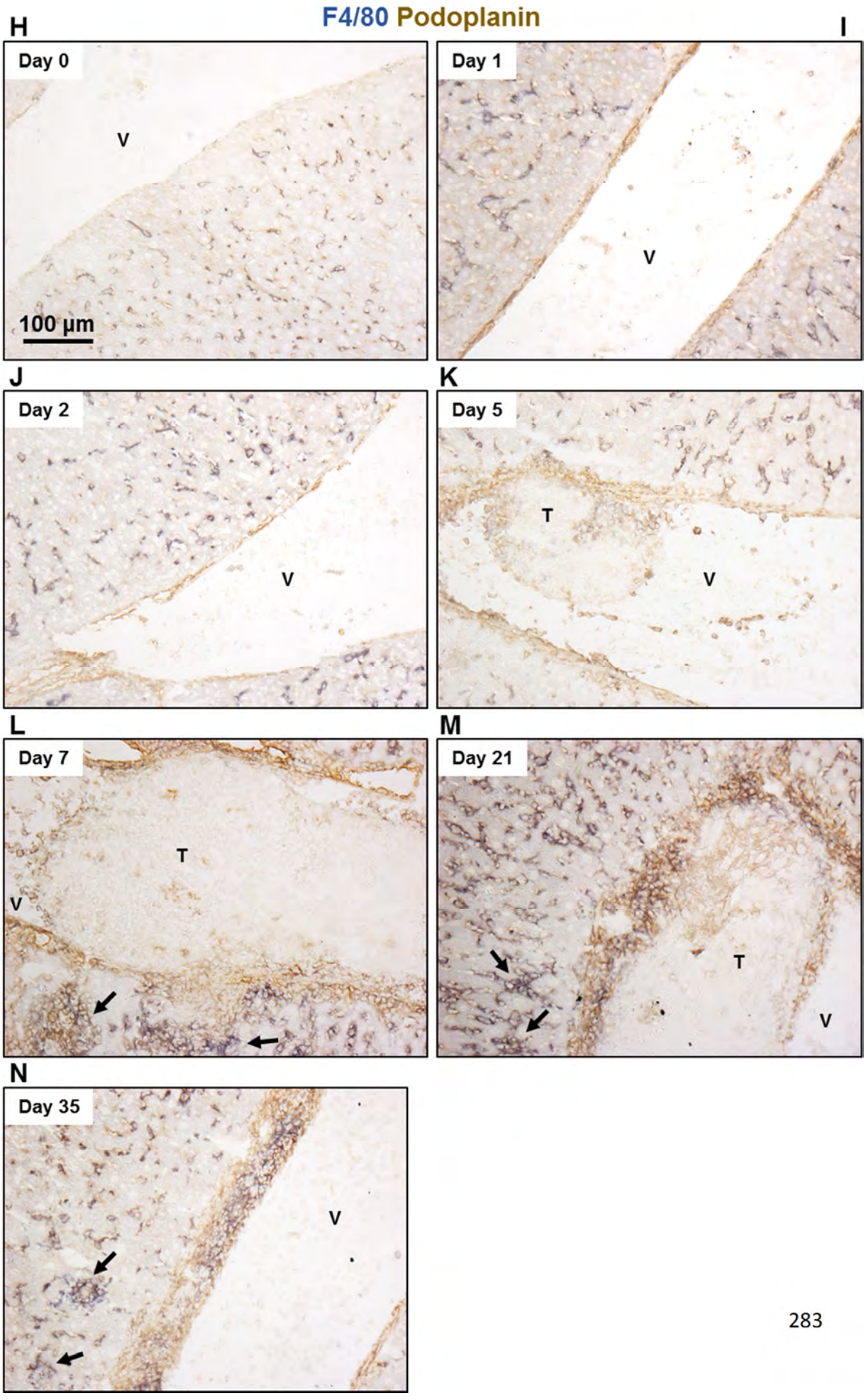

Figure 5.33 Increased podoplanin expression is detected within 24 hours of infection
WT mice were infected (i.p.) with 5 x 10^5 CFU attenuated STm. Mice were killed at the indicated time-points post-infection and podoplanin expression in the liver was assessed on frozen tissue sections by IHC. Podoplanin expression is shown in parenchymal areas at the time-points indicated (A to G), and in regions of proximity to vasculature (H to N). Podoplanin$^+$ cells = brown; F4/80$^+$ cells = blue; double positive podoplanin$^+$ F4/80$^+$ cells = black. V = vessel; T = thrombus; black arrows indicate inflammatory lesions. Images are representative from one experiment, where n = 4 at each time-point, (however, the experiment has been repeated multiple times and results shown are representative).

5.9.3.1 Podoplanin expression increases on F4/80$^+$ cells within 24 hours

Podoplanin was measured by FACS using the gating strategy outlined above (Fig 5.30), and illustrated by representative FACS plots in Figure 5.34 A. Absolute numbers of cells in all populations examined increase during the first week of infection (Fig 5.34 B-E). The proportion of CD11c$^+$ F4/80$^-$ cells expressing podoplanin increases from approximately 1% in non-infected livers to 2-3% within 24 hours, and this proportion is maintained at 72 hours (Fig 5.34 F). There is a 2-fold increase to approximately 6% by day 7. Absolute numbers of CD11c$^+$ F4/80$^-$ podoplanin$^+$ cells rise steadily during the first week, reaching approximately 5 x 10^5 cells per liver by day 7 (Fig 5.34 F and I). This pattern is similar yet more dynamic in CD11c$^-$ F4/80$^+$ cells. The initial proportion of podoplanin$^+$ cells doubles within 24 hours from approximately 10% to 20% of CD11c$^-$ F4/80$^+$ cells (Fig 5.34 G). At day 3, this proportion falls back to equivalent proportions as in non-infected mice. This drop is not reflected in absolute numbers; the 20-fold increase in CD11c$^-$ F4/80$^+$ podoplanin$^+$ cells within 24 hours is maintained at day 3 (Fig 5.34 J). By day 7, numbers are increased 10-20 fold, and the proportion of podoplanin$^+$ cells is similar to at 24 hours.

In contrast, podoplanin is expressed by 50-70% of CD11c$^+$ F4/80$^+$ cells in the liver in non-infected mice (Fig 5.34 H). This proportion of podoplanin$^+$ cells is greater than that of either the CD11c$^+$ F4/80$^-$ or CD11c$^-$ F4/80$^+$ populations at any point during infection. The proportion of CD11c$^+$ F4/80$^+$ cells which express podoplanin drops within 24 hours by approximately a third. This is recovered by day 7, and approximately 90% of CD11c$^+$ F4/80$^+$ cells express podoplanin at day 14. Numbers of podoplanin$^+$ CD11c$^+$ F4/80$^+$ cells increase steadily throughout the first few days of infection, increasing 100-fold by day 7 (Fig 5.34 K).

Figure 5.34

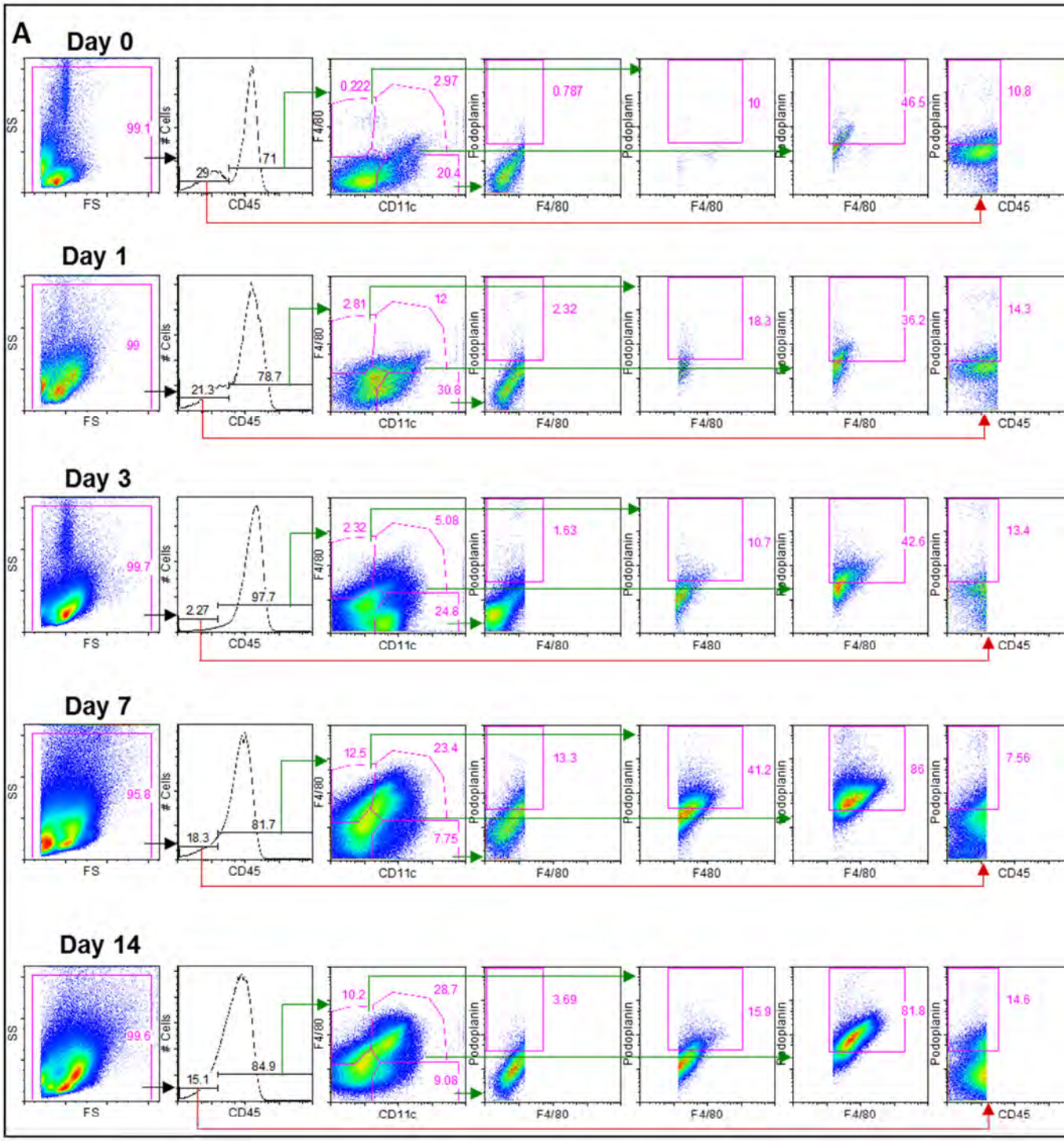

Figure 5.34 Increased podoplanin expression is detected within 24 hours of infection on myeloid populations by flow cytometry

WT mice were infected (i.p.) with 5 x 10^5 CFU attenuated STm. Mice were killed at the indicated time-points post-infection and leukocytes were extracted from the liver by collagenase digestion and gradient centrifugation. Cells retrieved in the leukocyte fraction of the gradient were examined by FACS for podoplanin expression. The gating strategy used is as described in Figure 5.30. A) Representative FACS plots are shown for each of the indicated time-points examined post-infection. Absolute numbers of B) $CD45^+$ cells, C) $CD11c^+$ $F4/80^-$ cells, D) $CD11c^-$ $F4/80^+$ cells, and E) $CD11c^+$ $F4/80^+$ cells are shown at the indicated time-points throughout infection. The proportion of F) $CD11c^+$ $F4/80^-$ cells, G) $CD11c^-$ $F4/80^+$ cells, and H) $CD11c^+$ $F4/80^+$ cells which express podoplanin are shown and absolute numbers of these $podoplanin^+$ cells are shown in I to K. L) The total number of $CD45^-$ cells retained in the leukocyte fraction of the gradient are shown at the indicated times post-infection. M) The proportion of these $CD45^-$ cells which express podoplanin is shown at the indicated time-points. N) The total number of $podoplanin^+$ $CD45^-$ cells (retained in the leukocyte fraction) at the indicated time-points during infection. Data are taken from one experiment where n = 3-6 at each time-point (with the exception of day 7, which includes data from two separate experiments). *p≤0.05 **p≤0.01 ***p≤0.001.

Figure 5.34 continued

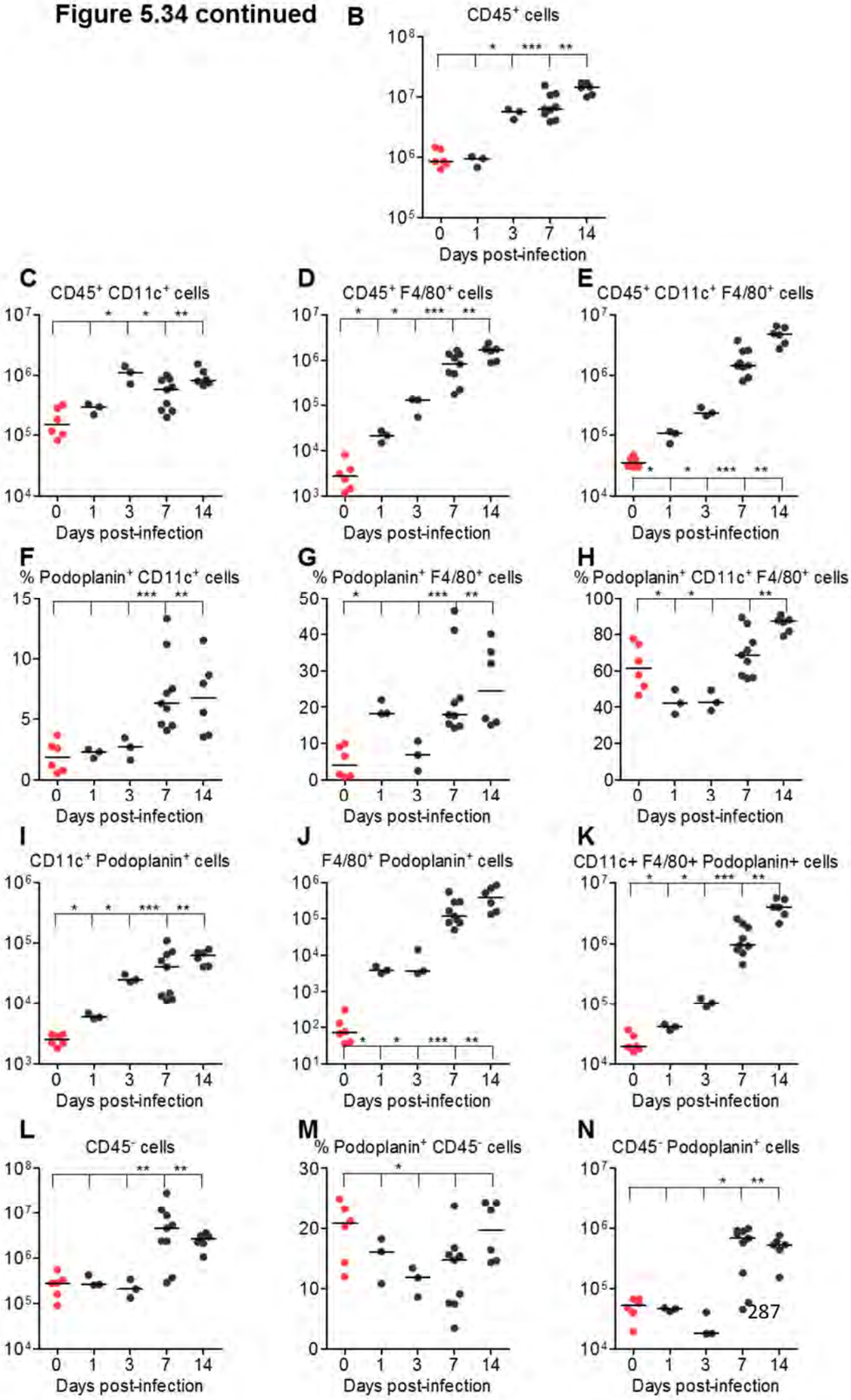

Numbers of CD45$^-$ cells (retained in the leukocyte fraction) increase between days 3 and 7, as do podoplanin$^+$ CD45$^-$ cells (Fig 5.34 L and N). The proportion of CD45$^-$ cells which are podoplanin$^+$ falls during the first 3 days, but recovers by day 14 (Fig 5.34 M).

Taken together, these data indicate increased podoplanin expression in the liver within 24 hours of infection, and this trend continues throughout the first week. During the first 24 hours, the largest increase in absolute number of podoplanin$^+$ cells occurs in CD11c$^-$ F4/80$^+$ cells, and it is also this population which increases the most by day 7 (approximate 1000-fold increase by day 7). However, numbers of CD11c$^+$ F4/80$^+$ podoplanin$^+$ cells also increase within the first 24 hours and although this increase is only 2-3 fold, this population constitutes the majority of podoplanin-expressing cells at any point throughout infection.

5.9.4 Podoplanin mean fluorescent intensity peaks at days 3 and 7 post-infection

infection

Podoplanin MFI in CD11c$^+$ F4/80$^+$ cells is greater than that in CD11c$^-$ F4/80$^+$ cells or CD11c$^+$ F4/80$^-$ cells at any time-point measured (Fig 5.35 A-D). While in this population, MFI remains constant until after 72 hours, there is a transient peak in podoplanin MFI at 24 hours in both CD11c$^-$ F4/80$^+$ and CD11c$^+$ F4/80$^-$ cells, which resolves by 72 hours and MFI increases in all three populations at day 7 (Fig 5.35 A-C). This dual peak also occurs in podoplanin MFI of total leukocytes isolated from the liver (Fig 5.35 E). Podoplanin MFI of CD45$^-$ cells decreases during infection from day 1 (Fig 5.35 F).

Figure 5.35

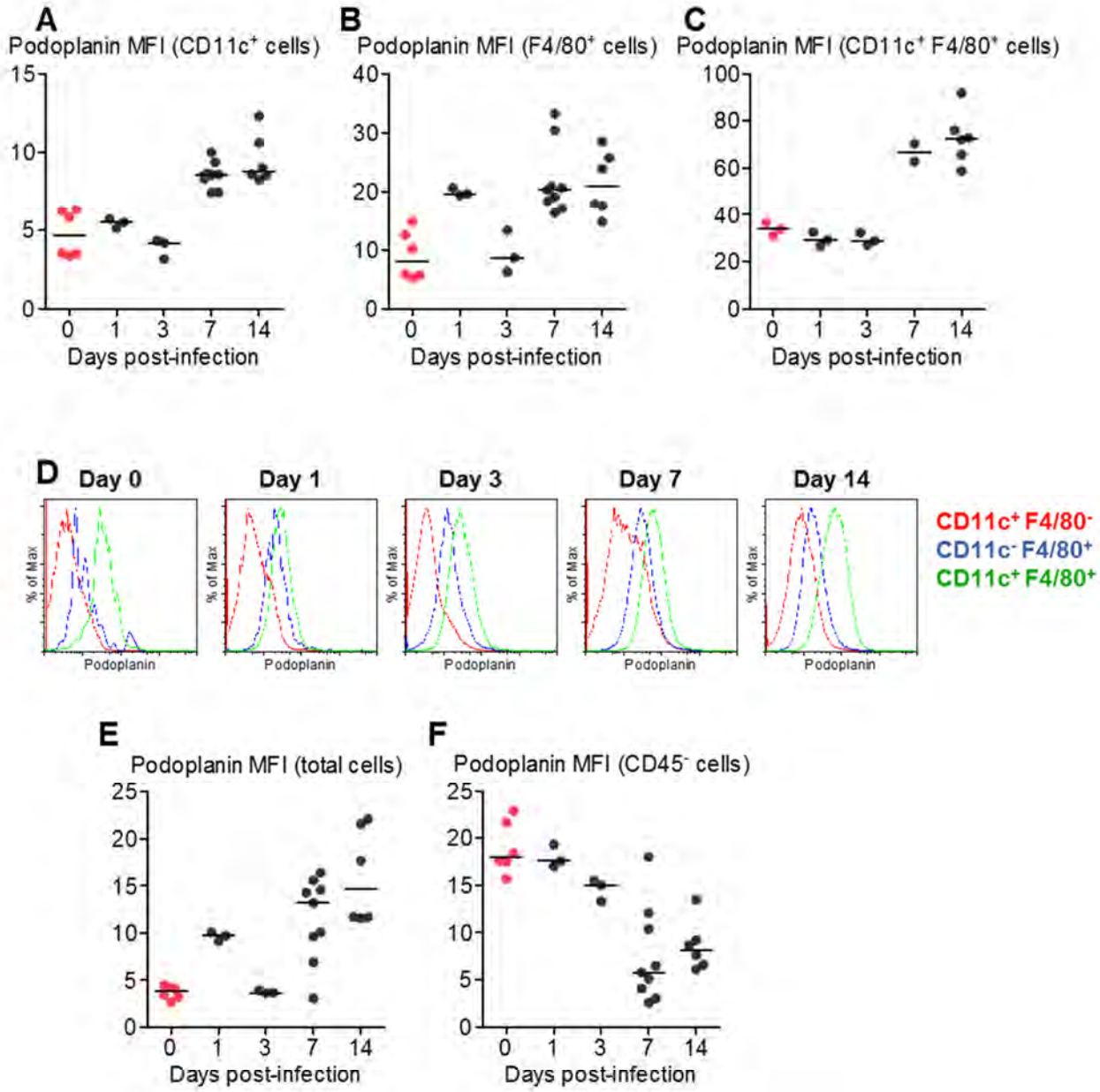

Figure 5.35 Podoplanin is most highly expressed on CD11c$^+$ F4/80$^+$ cells both before and after infection

This Figure is a continuation of Figure 5.34. WT mice were infected (i.p.) with 5 x 10^5 CFU attenuated STm and leukocytes were extracted from the liver at days 0, 1, 3, 7, and 14, as described in Figure 5.34. Cells retrieved in the leukocyte fraction of the gradient were examined by FACS for podoplanin expression. The MFI of podoplanin expression on A) CD11c$^+$ F4/80$^-$ cells, B) CD11c$^-$ F4/80$^+$ cells and C) CD11c$^+$ F4/80$^+$ cells, was measured at the indicated time-points post infection. (Podoplanin expression by cells stained with the relevant isotype control was negligible (data not shown)). D) Representative histograms illustrate relative podoplanin expression between CD11c$^+$ F4/80$^-$ cells (red), CD11c$^-$ F4/80$^+$ cells (blue), and CD11c$^+$ F4/80$^+$ cells (green). E) The MFI of podoplanin expression on total cells retrieved in the leukocyte fraction of the gradient is shown at the indicated time-points. F) The MFI of podoplanin of CD45$^-$ cells which were retained in the leukocyte fraction of the gradient is shown at the indicated times throughout infection. Data are taken from one experiment (that described in Figure 5.34) where n = 3-6 at each time-point (with the exception of day 7, which includes data from two separate experiments).

5.9.5 Podoplanin expression is comparable to WT in PF4.Cre.CLEC-2$^{fl/fl}$ mice

Podoplanin expression was quantified by FACS in WT and PF4.Cre.CLEC-2$^{fl/fl}$ mice. In the absence of infection, liver mass is equivalent and leukocyte cellularity is modestly increased in PF4.Cre.CLEC-2$^{fl/fl}$ mice, due to increased myeloid cells (Fig 5.36 A-H). Numbers of podoplanin^{+} cells are comparable or greater in PF4.Cre.CLEC-2$^{fl/fl}$ mice, although significantly lower proportions of CD11c^{-} F4/80^{+} and CD11c^{+} F4/80^{+} cells express podoplanin (Fig 5.36 I-N). Podoplanin MFI is marginally reduced in CD11c^{+} F4/80^{+} cells (Fig 5.36 O). Numbers of CD45^{-} cells retained in the leukocyte fraction are comparable in both strains, as are numbers and proportions of podoplanin^{+} cells (Fig 5.36 P-R).

Despite significantly less extensive hepatomegaly after infection, leukocyte cellularity is similar in PF4.Cre.CLEC-2$^{fl/fl}$ and WT mice (Fig 5.37 A-B). There are marginally fewer CD11c^{-} F4/80^{+} cells in PF4.Cre.CLEC-2$^{fl/fl}$ mice but other populations are similar to WT (Fig 5.37 C-H). Numbers and proportions of podoplanin^{+} cells are comparable, except for modestly reduced numbers of CD11c- F4/80^{+} podoplanin^{+} and CD11c^{+} F4/80^{+} podoplanin^{+} cells, relative to WT (Fig 5.37 I-N). Podoplanin MFI is comparable to WT in all CD45^{+} populations examined (Fig 5.37 O). Podoplanin^{+} CD45^{-} cells are comparable in both strains (Fig 5.37 P-R).

These data support our histological findings that podoplanin expression is elevated post-infection in PF4.Cre.CLEC-2$^{fl/fl}$ mice to a similar extent as in WT mice. Therefore the diminished thrombosis in PF4.Cre.CLEC-2$^{fl/fl}$ mice is likely not to be associated with differential podoplanin expression relative to WT mice.

Figure 5.36

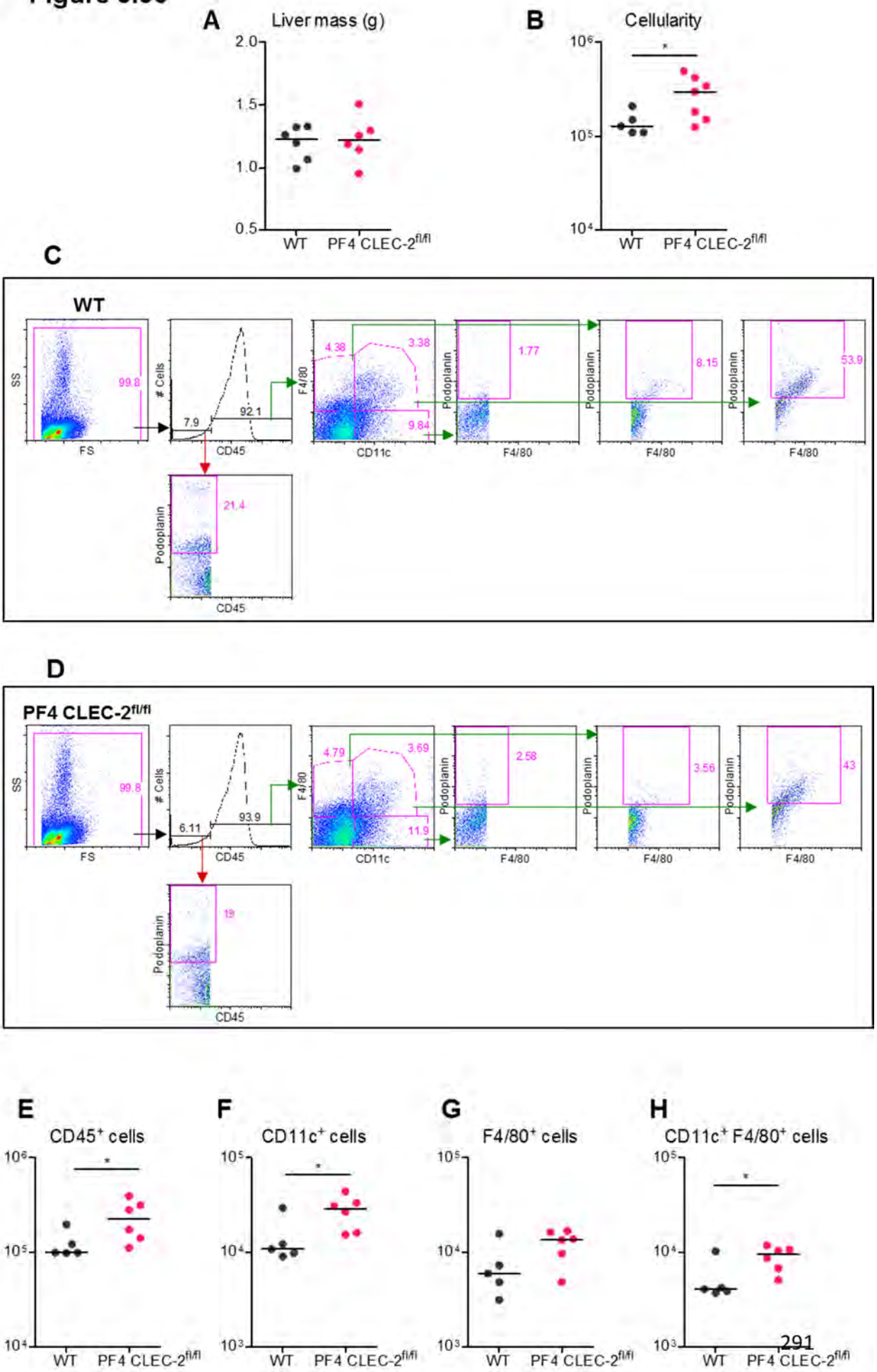
A
Liver mass (g)
2.0
1.5
1.0
0.5
WT
PF4 CLEC-2fl/fl
B
Cellularity
*
WT
PF4 CLEC-2fl/fl
C
WT
SS
FS
99.8
Cells
CD45
7.9
92.1
F4/80
CD11c
4.38
3.38
9.84
Podoplanin
1.77
8.15
53.9
21.4
D
PF4 CLEC-2fl/fl
99.8
6.11
93.9
4.79
3.69
11.9
2.58
3.56
43
19
E
CD45+ cells
F
CD11c+ cells
G
F4/80+ cells
H
CD11c+ F4/80+ cells

Figure 5.36 continued

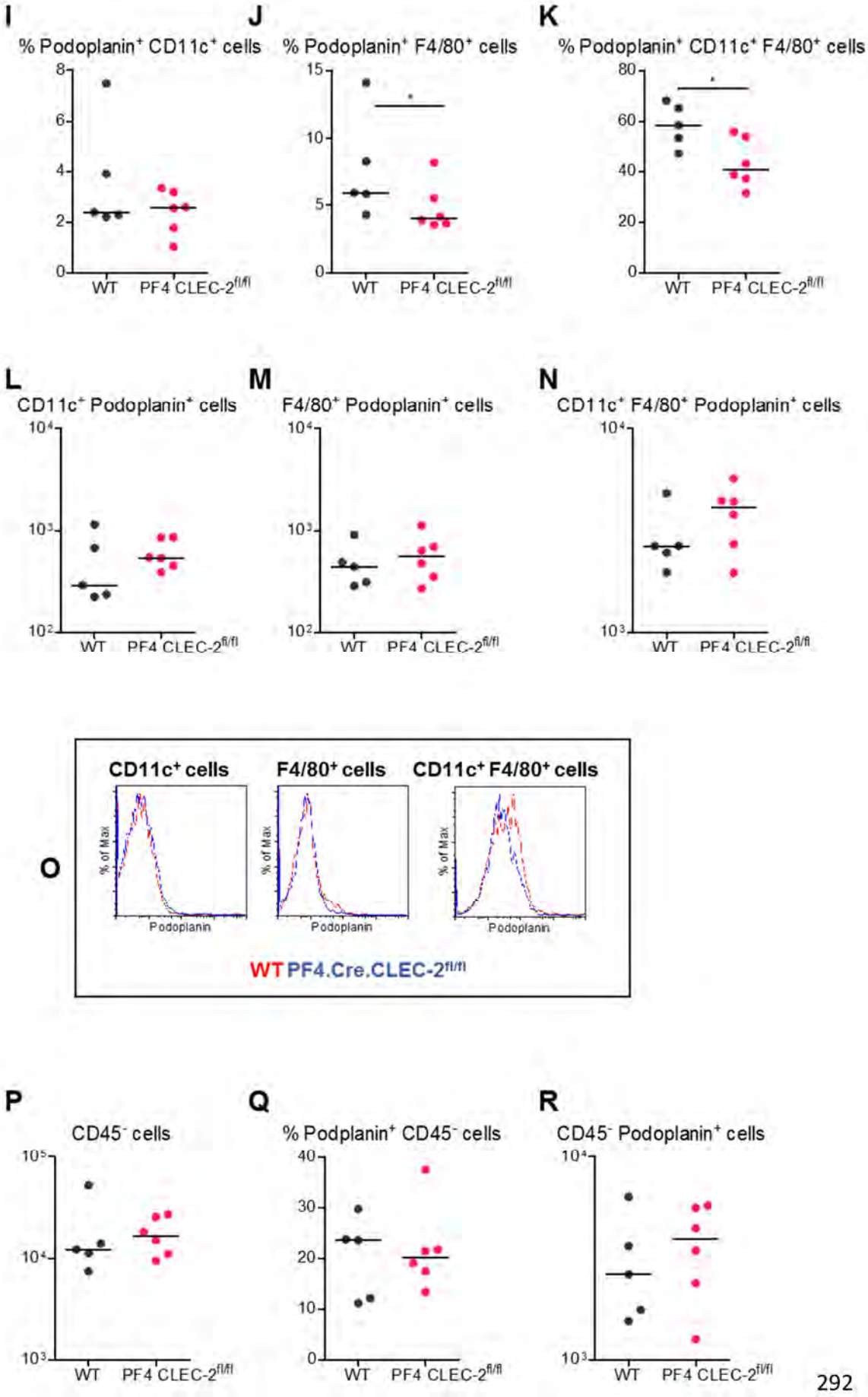

Figure 5.36 Podoplanin expression is comparable in non-infected WT and PF4.Cre.CLEC-2$^{fl/fl}$ mice

Leukocytes were extracted from the livers of non-infected WT and PF4.Cre.CLEC-2$^{fl/fl}$ mice (whereby CLEC-2 expression is absent in platelets and megakaryocytes) by collagenase digestion and gradient centrifugation. Cells retrieved in the leukocyte fraction of the gradient were examined by FACS for podoplanin expression. The gating strategy used is as described in Figure 5.30. A) Liver mass was measured in both strains of mice in the absence of infection. B) Leukocytes were extracted from the liver as described above and were quantified. Representative FACS plots from C) WT and D) PF4.Cre.CLEC-2$^{fl/fl}$ mice are shown. Absolute numbers of E) CD45$^+$ cells, F) CD11c$^+$ F4/80$^-$ cells, G) CD11c$^-$ F4/80$^+$ cells, and H) CD11c$^+$ F4/80$^+$ cells are shown. The proportion of I) CD11c$^+$ F4/80$^-$ cells, J) CD11c$^-$ F4/80$^+$ cells, and K) CD11c$^+$ F4/80$^+$ cells which express podoplanin are shown and absolute numbers of these podoplanin$^+$ cells are shown in L to N. O) Representative histograms illustrate the extent to which CD11c$^+$ F4/80$^-$ cells (left panel), CD11c$^-$ F4/80$^+$ cells (central panel), and CD11c$^+$ F4/80$^+$ cells (right panel) express podoplanin in PF4.Cre.CLEC-2$^{fl/fl}$ mice (blue) relative to WT mice (red). P) The total number of CD45$^-$ cells retained in the leukocyte fraction of the gradient are shown in WT and PF4.Cre.CLEC-2$^{fl/fl}$ mice. Q) The proportion of these CD45$^-$ cells which express podoplanin and R) the total number of podoplanin$^+$ CD45$^-$ cells (retained in the leukocyte fraction) is shown in both strains of mice. Data are taken from one experiment where n = 5-6 in each strain of mice. On histograms, PF4.Cre.CLEC-2$^{fl/fl}$ mice are written PF4 CLEC-2$^{fl/fl}$. *p≤0.05 **p≤0.01 ***p≤0.001.

Figure 5.37 Podoplanin expression is comparable in WT and PF4.Cre.CLEC-2$^{fl/fl}$ mice at day 7 post-infection

WT and PF4.Cre.CLEC-2$^{fl/fl}$ mice were infected (i.p.) with 5 x 10^5 CFU attenuated STm. Leukocytes were extracted from the livers by collagenase digestion and gradient centrifugation, and cells retrieved in the leukocyte fraction of the gradient were examined by FACS for podoplanin expression. The gating strategy used is as described in Figure 5.27. A) Liver mass was measured in both strains of mice at day 7 post-infection. B) Leukocytes were extracted from the liver as described above and were quantified. Representative FACS plots from C) WT and D) PF4.Cre.CLEC-2$^{fl/fl}$ mice are shown. Absolute numbers of E) CD45$^+$ cells, F) CD11c$^+$ F4/80$^-$ cells, G) CD11c$^-$ F4/80$^+$ cells, and H) CD11c$^+$ F4/80$^+$ cells are shown. The proportion of I) CD11c$^+$ F4/80$^-$ cells, J) CD11c$^-$ F4/80$^+$ cells, and K) CD11c$^+$ F4/80$^+$ cells which express podoplanin are shown and absolute numbers of these podoplanin$^+$ cells are shown in L to N. O) Representative histograms illustrate the extent to which CD11c$^+$ F4/80$^-$ cells (left panel), CD11c$^-$ F4/80$^+$ cells (central panel), and CD11c$^+$ F4/80$^+$ cells (right panel) express podoplanin in PF4.Cre.CLEC-2$^{fl/fl}$ mice (blue) relative to WT mice (red). P) The total number of CD45$^-$ cells retained in the leukocyte fraction of the gradient are shown in WT and PF4.Cre.CLEC-2$^{fl/fl}$ mice. Q) The proportion of these CD45$^-$ cells which express podoplanin and R) the total number of podoplanin$^+$ CD45$^-$ cells (retained in the leukocyte fraction) is shown in both strains of mice. Data are taken from one experiment where n = 9 (WT mice) and n = 5 (PF4.Cre.CLEC-2$^{fl/fl}$ mice), however, the experiment has been repeated multiple times and results shown are representative). On histograms, PF4.Cre.CLEC-2$^{fl/fl}$ mice are written PF4 CLEC-2$^{fl/fl}$. *p≤0.05 **p≤0.01 ***p≤0.001.

Figure 5.37

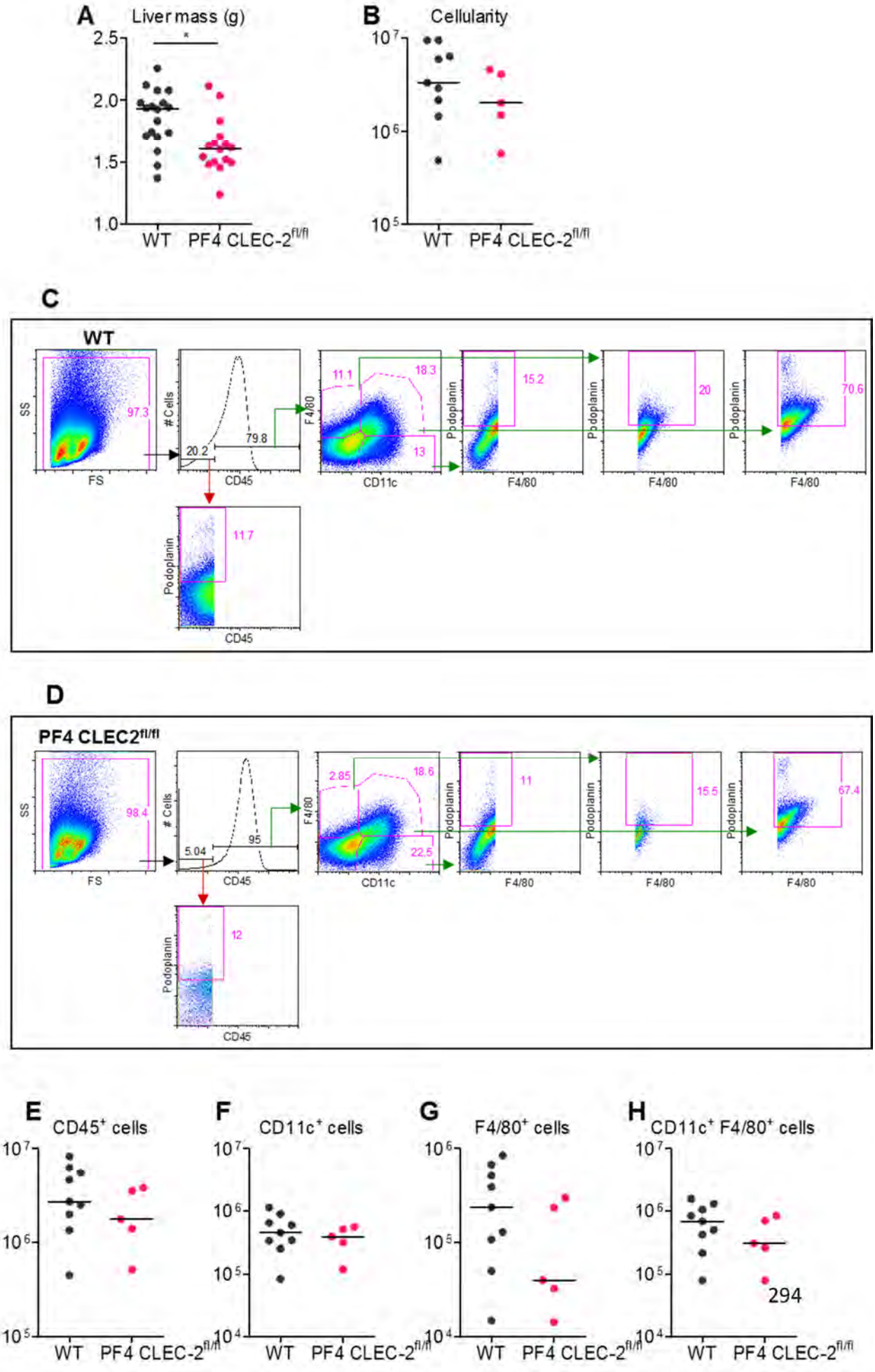
A
Liver mass (g)
2.5
2.0
1.5
1.0
*
WT
PF4 CLEC-2fl/fl
B
Cellularity
10^7
10^6
10^5
WT
PF4 CLEC-2fl/fl
C
WT
SS
FS
97.3
Cells
CD45
20.2
79.8
F4/80
CD11c
11.1
18.3
13
Podoplanin
F4/80
15.2
Podoplanin
F4/80
20
Podoplanin
F4/80
70.6
Podoplanin
CD45
11.7
D
PF4 CLEC2fl/fl
SS
FS
98.4
Cells
CD45
5.04
95
F4/80
CD11c
2.85
18.6
22.5
Podoplanin
F4/80
11
Podoplanin
F4/80
15.5
Podoplanin
F4/80
67.4
Podoplanin
CD45
12
E
CD45+ cells
10^7
10^6
10^5
WT
PF4 CLEC-2fl/fl
F
CD11c+ cells
10^7
10^6
10^5
10^4
WT
PF4 CLEC-2fl/fl
G
F4/80+ cells
10^6
10^5
10^4
WT
PF4 CLEC-2fl/fl
H
CD11c+ F4/80+ cells
10^7
10^6
10^5
10^4
294
WT
PF4 CLEC-2fl/fl

Figure 5.37 continued

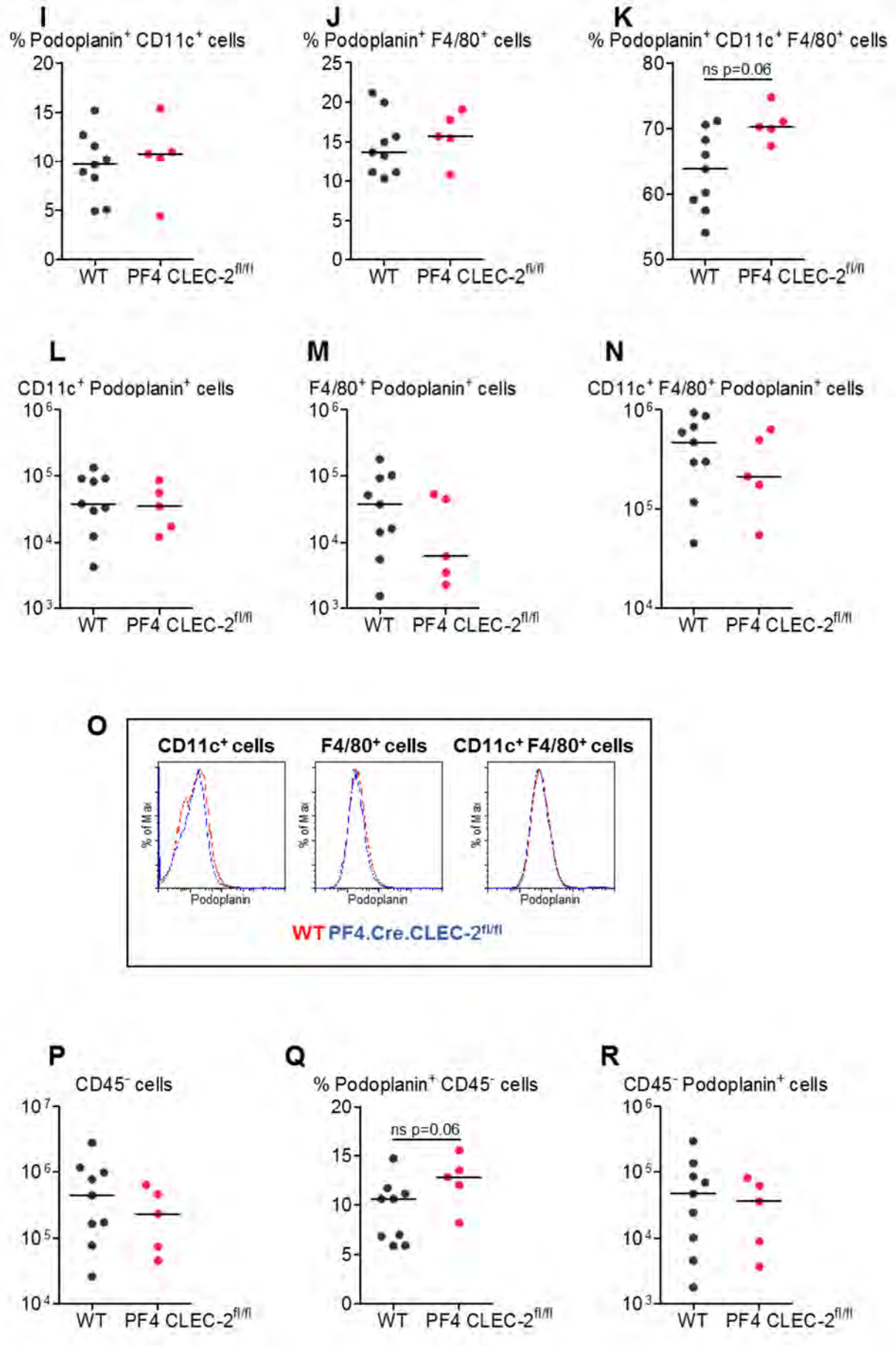

5.10 Clodronate-sensitive cells are required for thrombus development

Having demonstrated heterogeneous podoplanin expression in the liver during infection on both $CD45^+$ and $CD45^-$ populations, we wanted to determine if expression on any cell type in particular is important for thrombosis. To test this, mice were treated with clodronate-loaded liposomes, which have been shown to deplete macrophage populations, or control PBS-liposomes, 24 hours prior to *Salmonella* infection (Van Rooijen and Sanders, 1996, Flores-Langarica et al., 2011). Depletion was maintained throughout

infection by subsequent clodronate (or PBS) injections (Fig 5.38 A). Thrombosis and podoplanin expression were measured 7 days post-infection. Thrombosis is totally abrogated in the absence of clodronate-sensitive cells and thrombocytopenia is significantly less severe, although the MPV in these mice remains similar to that in PBS treated mice (Fig 5.38 B-F). These data demonstrate that clodronate-sensitive cells are important for thrombus development.

5.10.1 Podoplanin expression is reduced following clodronate treatment

To determine whether clodronate depletion alters podoplanin expression in livers post-infection, podoplanin expression was assessed by histology and FACS. Whilst podoplanin is still detected in the liver post-clodronate treatment, by histology there appears to be less expression in the parenchyma (Fig 5.39 A). Podoplanin expression is observed on $F4/80^-$ cells adjacent to the vessels both in PBS and clodronate-treated mice, albeit to a lower level (Fig 5.39 B). Staining for CD41 confirms the absence of platelet thrombi in clodronate-treated mice (Fig 5.39 C).

Figure 5.38

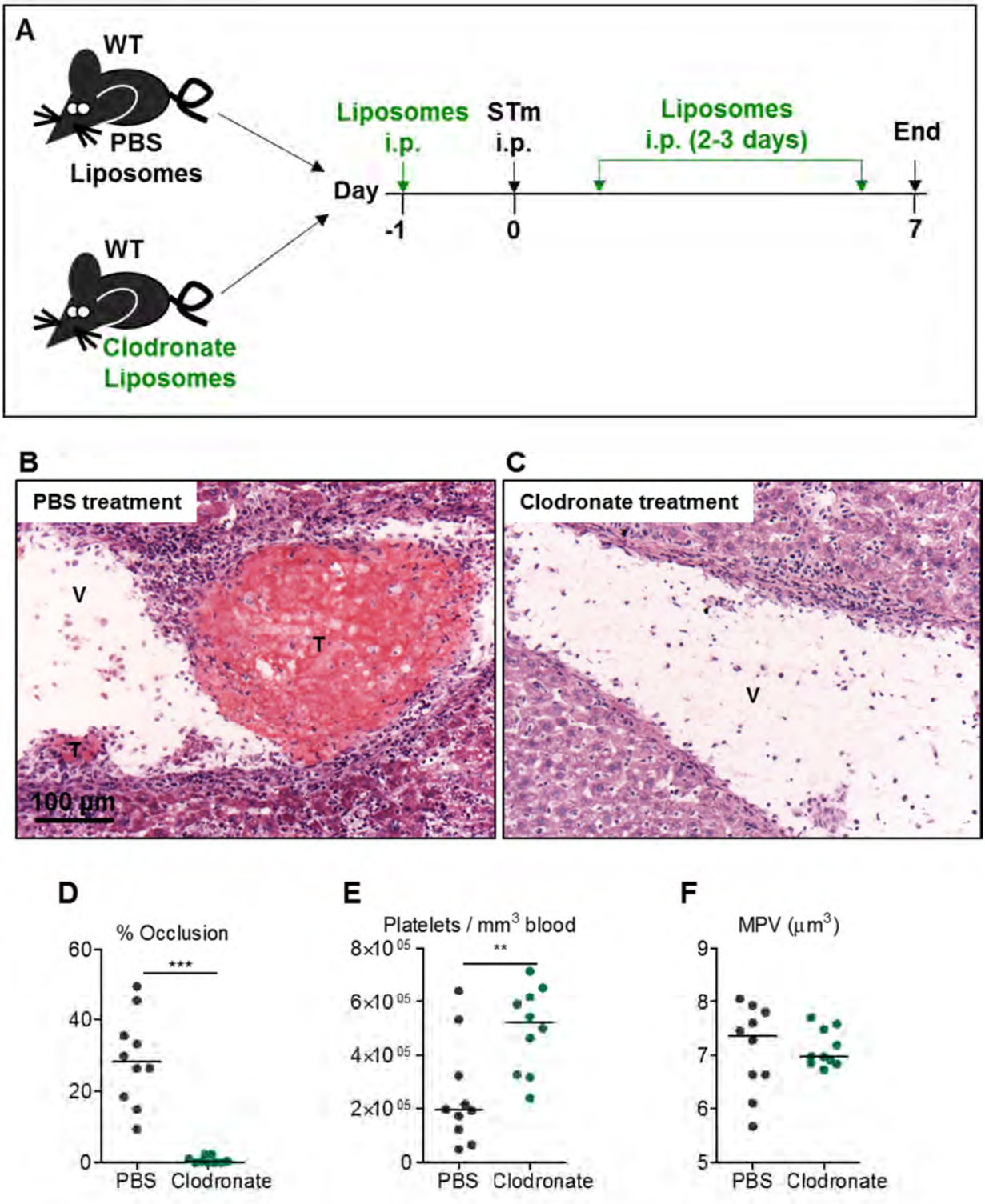

Figure 5.38 Thrombosis is severely abrogated in the absence of clodronate-sensitive cells
WT mice were treated (i.p.) with Clodronate or PBS liposomes 24 hours prior to infection (i.p.) with 5 x 10^5 CFU attenuated STm. Clodronate treatment was repeated every 2-3 days throughout infection to maintain the depletion. At day 7 post-infection, livers from B) PBS-treated mice and C) Clodronate-treated mice were examined for thrombosis by H&E of frozen tissue sections. V = vessel; T = thrombus. D) The extent of thrombosis was quantified by point counting the percentage of occlusion of all large vessels per tissue section (detailed in section 2.5.4.1), and counts are expressed as a percentage. At the time of sacrifice, blood was obtained from day 7-infected mice for assessment of E) platelet numbers and F) mean platelet volume. Images are representative and all data are taken from two experiments where n = 5 per treatment group in each experiment. *p≤0.05 **p≤0.01 ***p≤0.001.

Figure 5.39

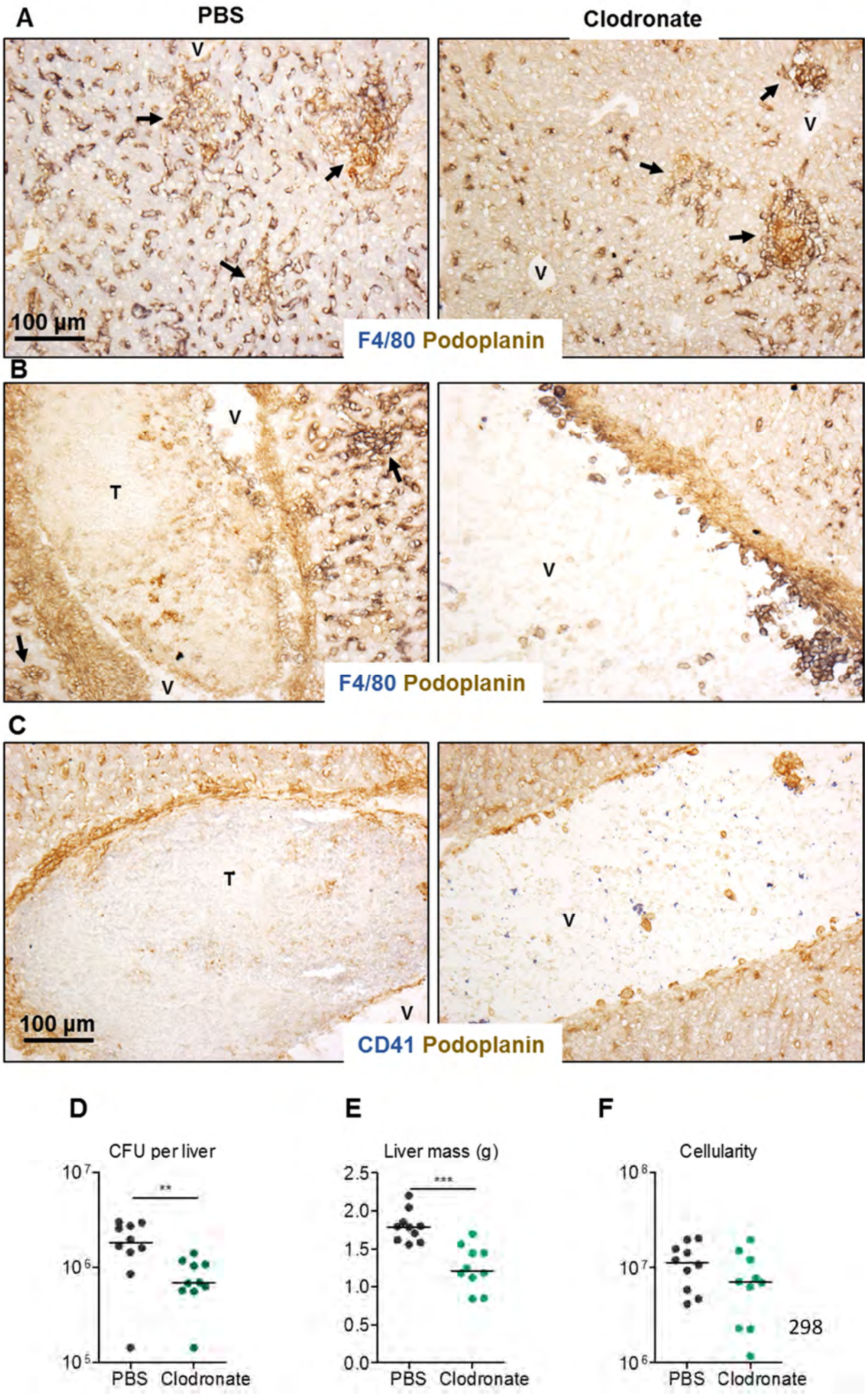
A
PBS
Clodronate
V
100 µm
F4/80 Podoplanin
B
T
F4/80 Podoplanin
C
CD41 Podoplanin
D
CFU per liver
**
PBS
Clodronate
E
Liver mass (g)
***
F
Cellularity
298

Figure 5.39 Podoplanin expression is decreased but is not absent in Clodronate-treated mice post-infection

WT mice were treated (i.p.) with Clodronate or PBS liposomes 24 hours prior to infection (i.p.) with 5 x 10^5 CFU attenuated STm. Clodronate treatment was repeated every 2-3 days throughout infection to maintain the depletion. Podoplanin expression in the liver was assessed in frozen tissue sections at day 7 post-infection in PBS-treated and Clodronate-treated mice. Podoplanin expression was reduced in A) parenchymal areas and B) in vascular regions post-infection in mice treated with Clodronate. Podoplanin$^+$ cells = brown; F4/80$^+$ cells = blue; double positive podoplanin$^+$ F4/80$^+$ cells = black. The absence of thrombi was further confirmed by staining for CD41$^+$ cells (blue) alongside podoplanin$^+$ cells (brown). V = vessel; T = thrombus; black arrows indicate inflammatory lesions. Images are representative of two experiments, where n = 5 per treatment group in each experiment. D) Bacterial load of the liver was determined and E) liver mass was measured for PBS-treated and Clodronate-treated mice at day 7 post-infection. F) Leukocytes were extracted from the livers by collagenase digestion and gradient centrifugation, and cells retrieved in the leukocyte fraction of the gradient were quantified at day 7 post-infection. All data are taken from two experiments where n = 5 per treatment group in each experiment. *p≤0.05 **p≤0.01 ***p≤0.001.

Following clodronate treatment, the liver bacterial burden is significantly lower, hepatomegaly is significantly less pronounced, and leukocyte numbers are modestly reduced (Fig 5.39 D-F). Representative FACS plots illustrate podoplanin expression (Fig 5.40 A-B). Numbers of total $CD45^+$ cells are not affected by clodronate treatment, however, there are significantly reduced $CD11c^-$ $F4/80^+$ and $CD11c^+$ $F4/80^+$ cells (Fig 5.40 C-F). Moreover, the proportion of cells which are $CD11c^+$ $F4/80^-$ is significantly increased and that of $CD11c^-$ $F4/80^+$ and $CD11c^+$ $F4/80^+$ cells are significantly reduced following clodronate depletion (Fig 5.40 G-J). Numbers of $podoplanin^+$ $CD11c^+$ $F4/80^-$ cells are not affected by clodronate treatment (Fig 5.40 K and N). However, numbers of $CD11c^-$ $F4/80^+$ $podoplanin^+$ and $CD11c^+$ $F4/80^+$ $podoplanin^+$ cells are significantly reduced, although the proportion of these cells which are $podoplanin^+$ is unchanged following treatment (Fig 5.40 L-M and O-P).

Numbers of $CD45^-$ cells recovered in the leukocyte fraction are significantly reduced following clodronate treatment, but remain a similar proportion of the total retrieved cells to that in PBS-treated mice (Fig 5.40 Q-R). Numbers of $CD45^-$ $podoplanin^+$ cells are unchanged, despite a significant increase in the proportion of these cells expressing podoplanin (Fig 5.40 S-T). Podoplanin MFI is similar in all $CD45^+$ populations examined following clodronate treatment, and is approximately doubled in $CD45^-$ cells (Fig 5.40 U-Z). Taken together, these data indicate a modest reduction in podoplanin expression following clodronate treatment, particularly in $CD11c^-$ $F4/80^+$ and $CD11c^+$ $F4/80^+$ cells. This supports our histological observations and suggests that reduced podoplanin following clodronate treatment could be associated with an absence of thrombus development.

Figure 5.40

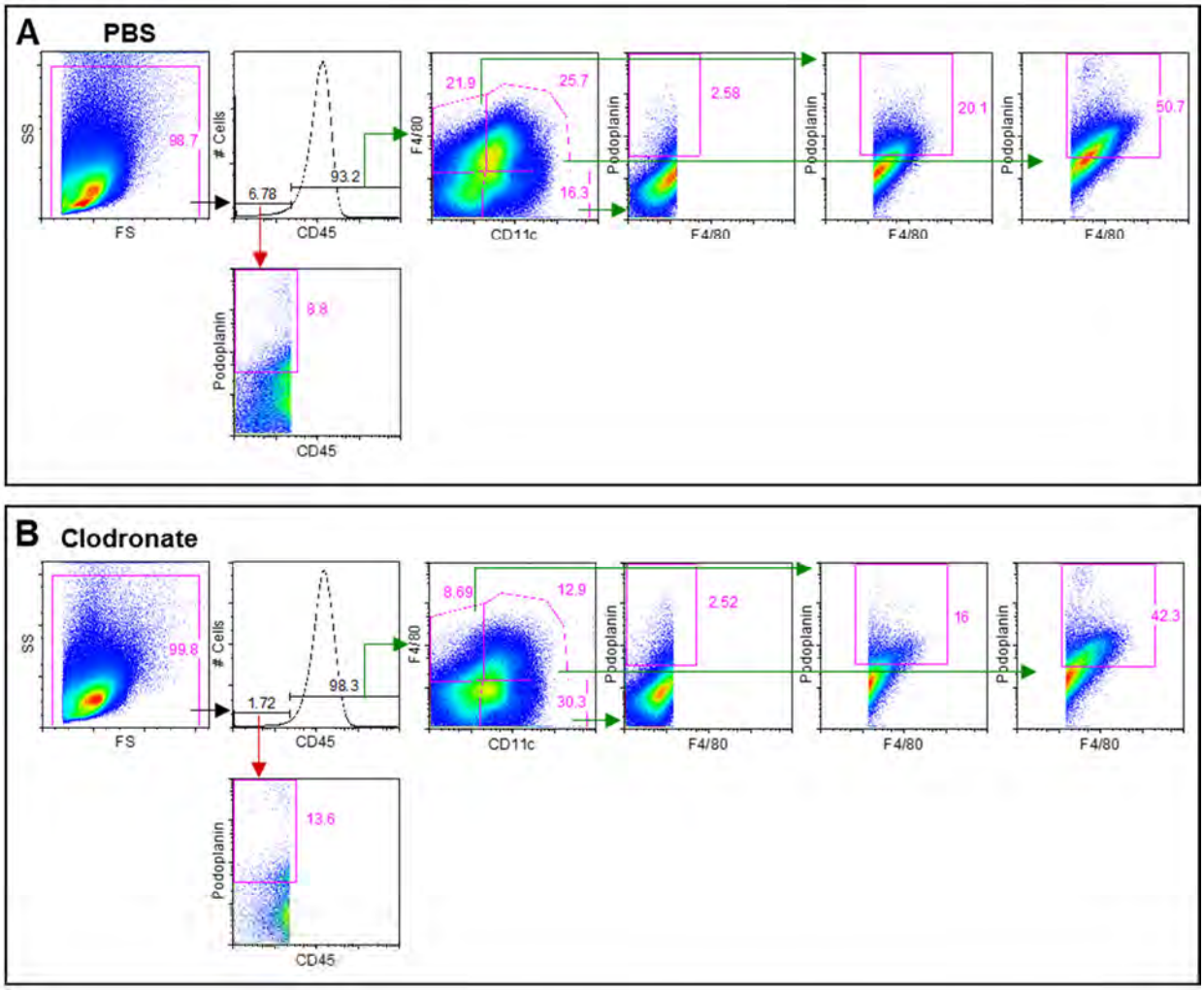

Figure 5.40 Podoplanin expression during infection is reduced following Clodronate treatment

WT mice were treated (i.p.) with Clodronate or PBS liposomes 24 hours prior to infection (i.p.) with 5 x 10^5 CFU attenuated STm. Clodronate treatment was repeated every 2-3 days throughout infection to maintain cell depletion. At day 7 post-infection, leukocytes were extracted from the livers by collagenase digestion and gradient centrifugation, and cells retrieved in the leukocyte fraction of the gradient were examined by FACS for podoplanin expression. The gating strategy used is as described in Figure 5.30. Representative FACS plots from A) PBS-treated and B) Clodronate-treated mice are shown. Absolute numbers of C) $CD45^+$ cells, D) $CD11c^+$ $F4/80^-$ cells, E) $CD11c^-$ $F4/80^+$ cells, and F) $CD11c^+$ $F4/80^+$ cells are shown. The proportion of each of these populations (out of total cells retrieved in the leukocyte fraction) are shown in G to J. The proportion of K) $CD11c^+$ $F4/80^-$ cells, L) $CD11c^-$ $F4/80^+$ cells, and M) $CD11c^+$ $F4/80^+$ cells which express podoplanin are shown and absolute numbers of these $podoplanin^+$ cells are shown in N to P. Q) The total number of $CD45^-$ cells retained in the leukocyte fraction of the gradient are shown and R) the proportion of total cells retrieved which were $CD45^-$ are indicated. S) The proportion of these $CD45^-$ cells which express podoplanin and T) the total number of $podoplanin^+$ $CD45^-$ cells (retained in the leukocyte fraction) is shown in both strains of mice. U) The MFI of podoplanin expression in total $CD45^+$ cells retrieved is shown relative to isotype controls. V) Representative histograms illustrate the extent to which $CD11c^+$ $F4/80^-$ cells (left panel), $CD11c^-$ $F4/80^+$ cells (central panel), and $CD11c^+$ $F4/80^+$ cells (right panel) express podoplanin in Clodronate-treated mice (blue) relative to PBS-treated mice (red). The MFI of podoplanin expression in W) $CD11c^+$ $F4/80^-$ cells, X) $CD11c^-$ $F4/80^+$ cells, Y) $CD11c^+$ $F4/80^+$ cells, and Z) $CD45^-$ cells (retained in the leukocyte fraction) are shown. All data are taken from two experiments where n = 5 per treatment group in each experiment. $^*p\leq0.05$ $^{**}p\leq0.01$ $^{***}p\leq0.001$.

Figure 5.40 continued

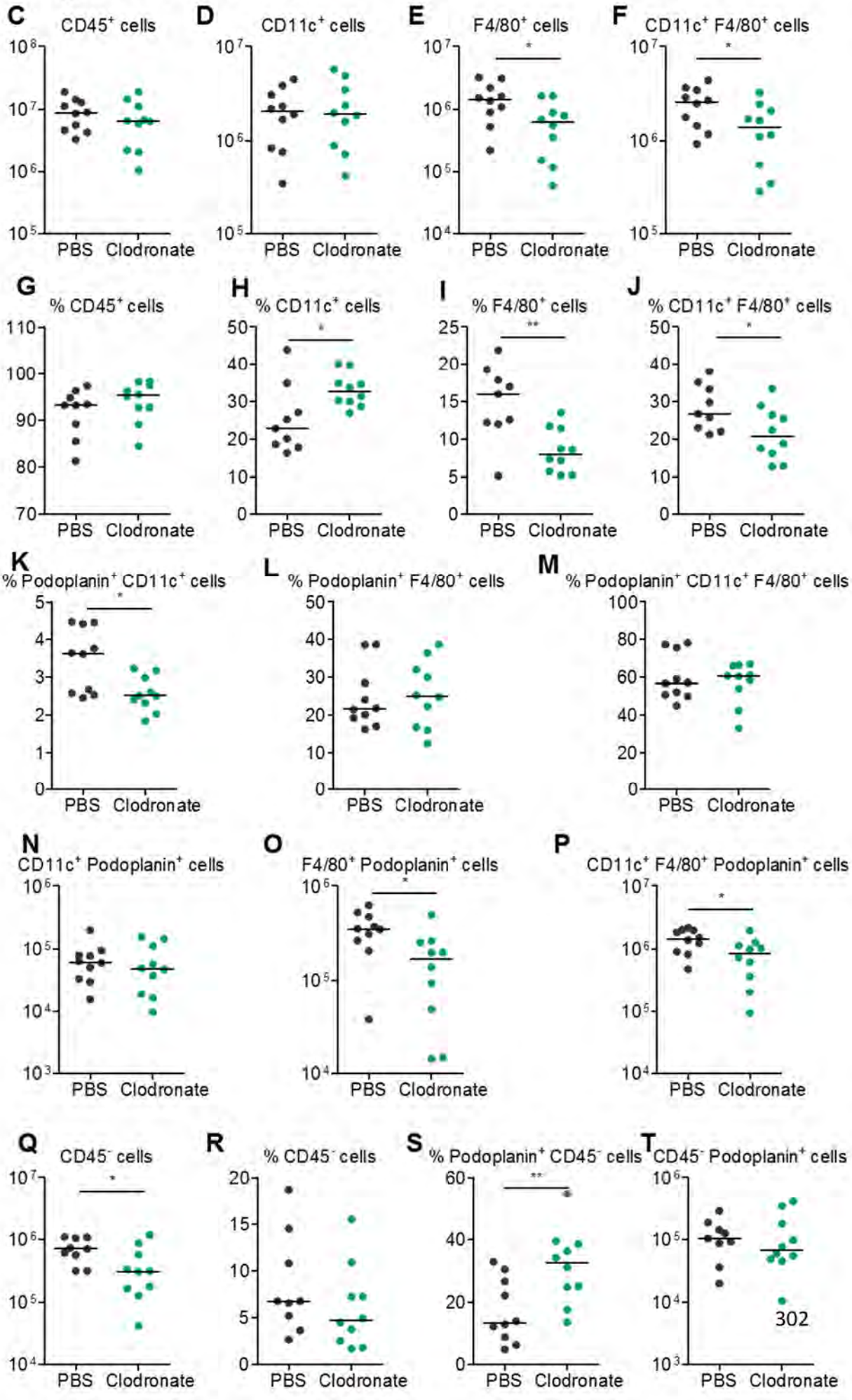

Figure 5.40 continued

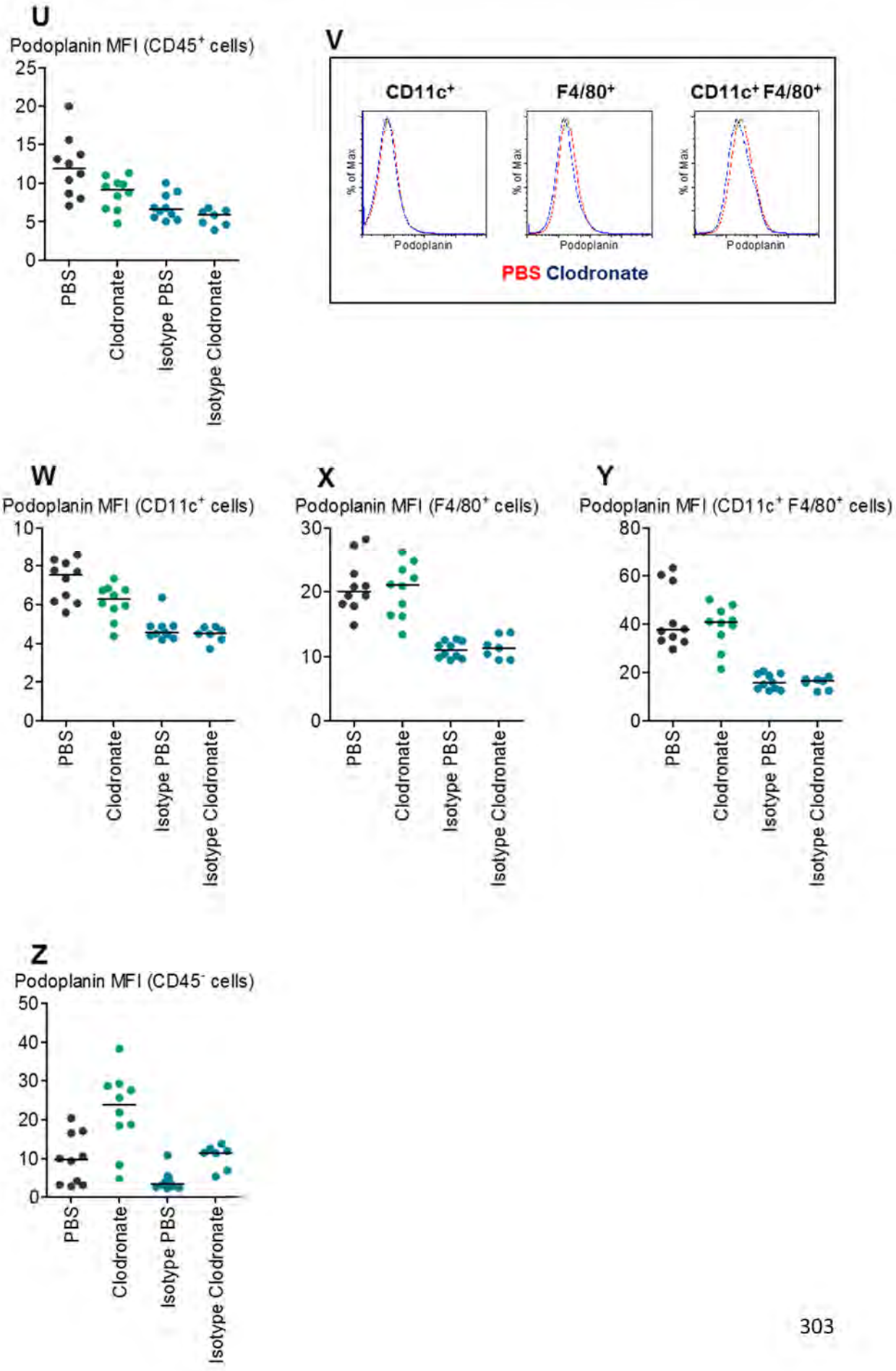

5.10.2 Multiple cell types are affected by clodronate treatment

To fully elucidate which cells are depleted by clodronate treatment, myeloid cells were characterised more rigorously by FACS. Representative FACS plots illustrate the gating strategy (Fig 5.41 A-B). Kupffer cells and infiltrating monocyte populations are derived from an initial F4/80^{+} Ly6G^{lo} gate (as described in Chapter 3). Total cells in this gate are modestly decreased following clodronate treatment although the proportion of cells in this gate (out of total cells retrieved) is similar (Fig 5.41 C-D). Kupffer cell numbers are variable following treatment, and the proportion of F4/80^{+} Ly6G^{lo} cells which are Kupffer cells remains the same (Fig 5.41 E-F). Further classification of cells in this "Kupffer cell gate" using CD11c and MHC II show that CD11c^{+} cells (likely to be activated Kupffer cells) tend to be reduced following treatment, regardless of MHC II expression (Fig 5.41 G-H and J-K). CD11c^{lo} MHC II^{hi} cells in this gate are increased upon treatment (Fig 5.41 I and L). These data suggest that F4/80^{+} Ly6G^{-} CD11b^{lo} Ly6C^{lo} CD11c^{+} cells are affected by clodronate treatment and that some of these cells have the capacity to present antigen via MHC II, and some do not.

Monocyte numbers (F4/80^{+} Ly6G^{lo} CD11b^{hi} Ly6C^{hi}) are variable, yet also tend to be reduced following clodronate treatment (Fig 5.41 M and P). Cells in this "monocyte gate" were further classified using CD11c and MHC II. All cells in this gate are CD11c^{lo}, however, only cells with low MHC II expression were affected by clodronate, although the proportion of monocytes which are MHC II^{lo} is negligible (Fig 5.41 N-O and Q-R). These data imply that MHC II^{lo} monocyte populations from the circulation are also affected by clodronate treatment.

Figure 5.41

A

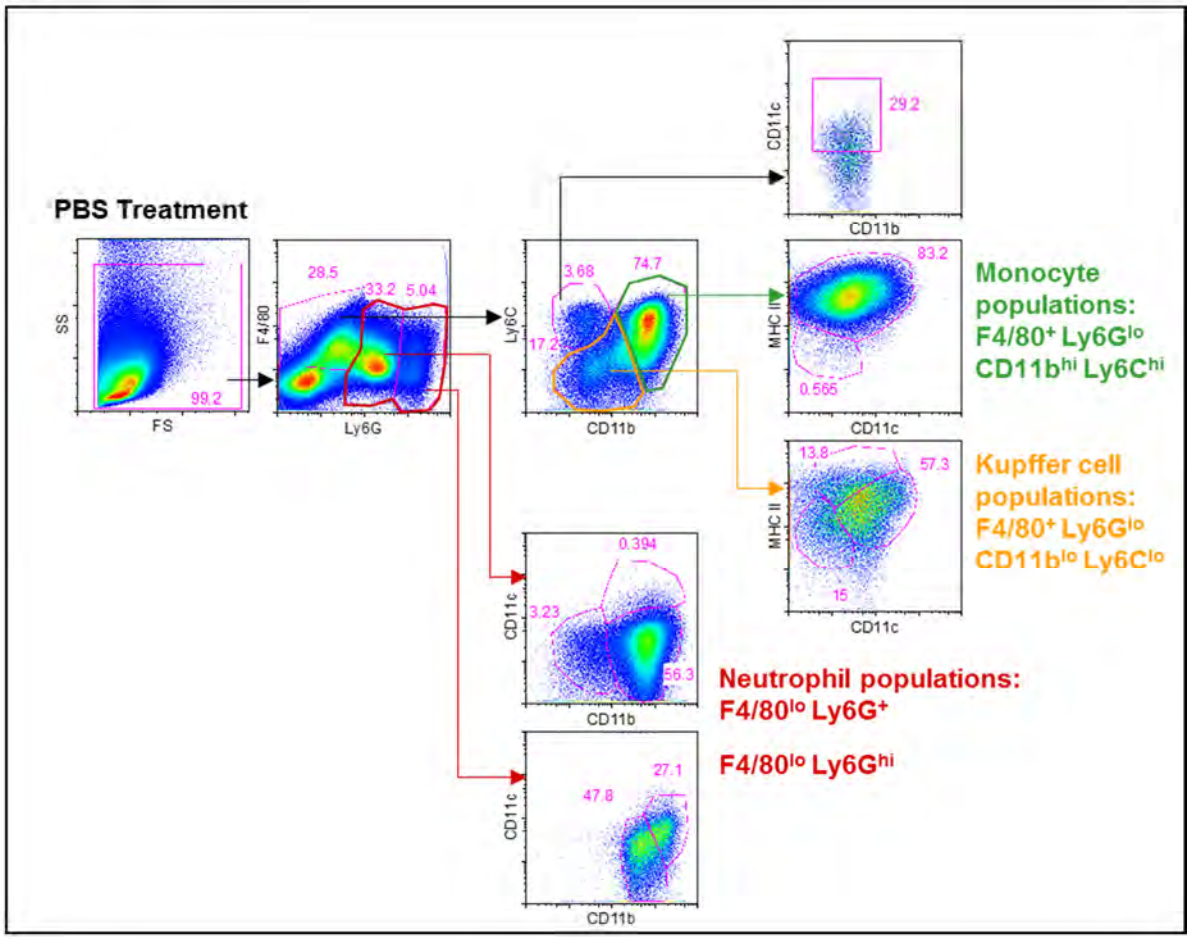

B

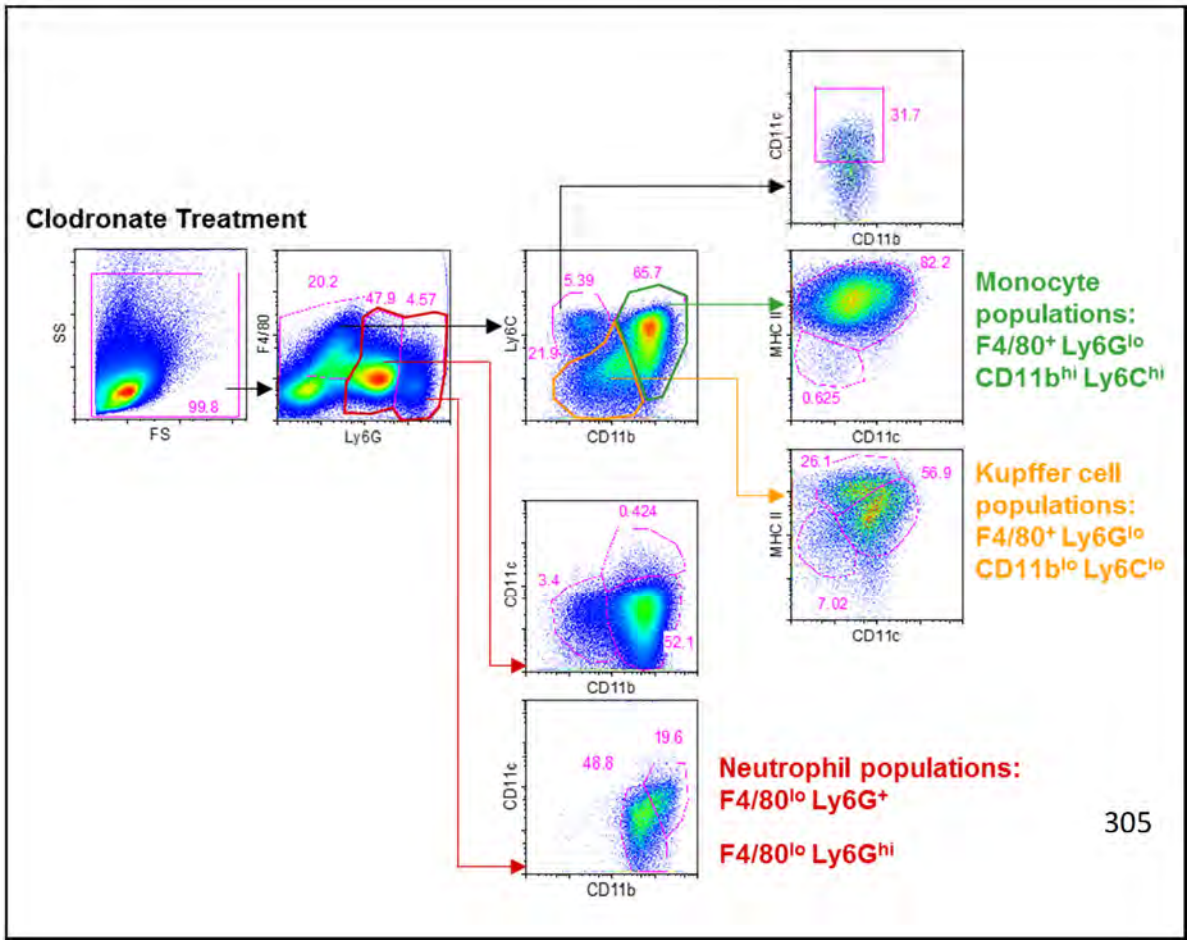

Figure 5.41 continued

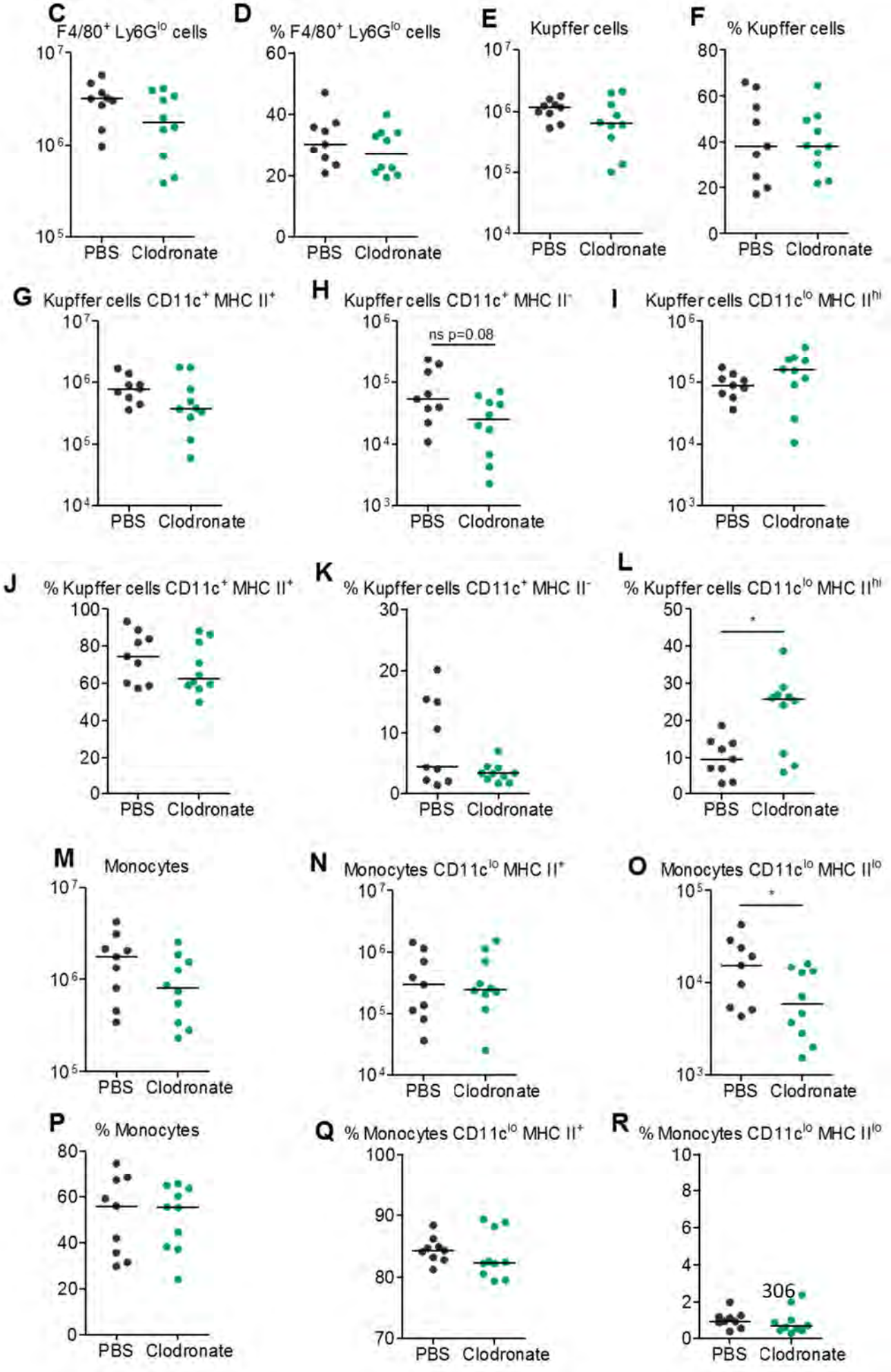

Figure 5.41 continued

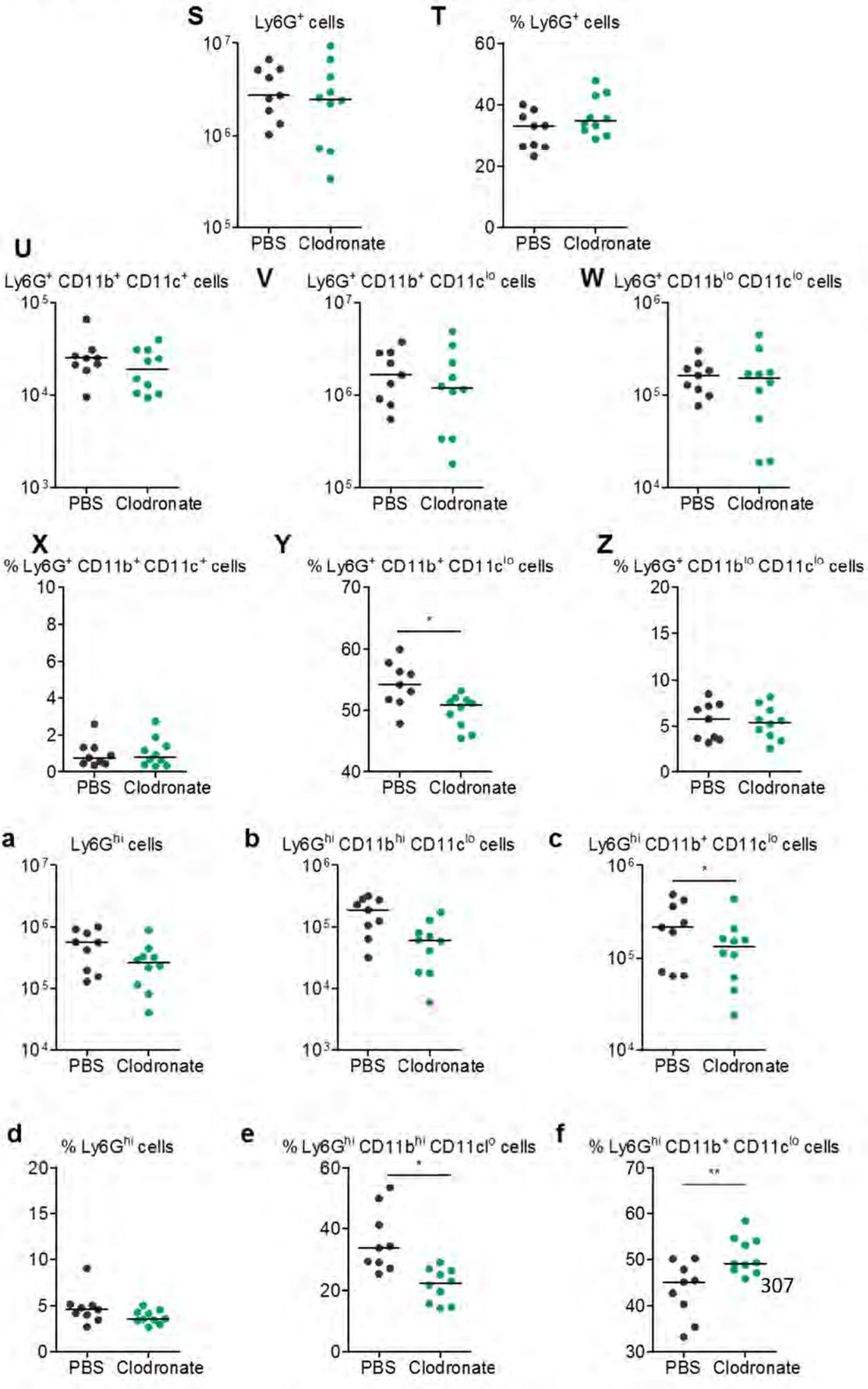

Figure 5.41 continued

Figure 5.41 Multiple cell types in the liver are affected by Clodronate treatment
WT mice were treated (i.p.) with Clodronate or PBS liposomes 24 hours prior to infection (i.p.) with 5 x 10^5 CFU attenuated STm. Clodronate treatment was repeated every 2-3 days throughout infection to maintain cell depletion. At day 7 post-infection, leukocytes were extracted from the liver by collagenase digestion and gradient centrifugation, and cells retrieved in the leukocyte fraction of the gradient were examined by FACS to identify which myeloid populations were affected by the treatment. Representative FACS plots from A) PBS-treated and B) Clodronate-treated mice are shown, illustrating the gating strategy used. C) Absolute numbers of F4/80$^+$ Ly6G^{lo} cells are shown alongside D) the percentage of these cells out of total cells retrieved. The absolute number of E) Kupffer cells, G) CD11c$^+$ MHC II$^+$ Kupffer cells, H) CD11c$^+$ MHC II$^-$ Kupffer cells, and I) CD11c^{lo} MHC II^{hi} Kupffer cells are shown. The proportion of F) Kupffer cells (out of total F4/80$^+$ Ly6G^{lo} cells) and J, K, L) associated sub-populations (out of total Kupffer cells) are indicated. The absolute number of M) monocytes, N) CD11c^{lo} MHC II$^+$ monocytes, and O) CD11c^{lo} MHC II^{lo} monocytes is shown above the proportion of P) monocytes (out of total F4/80$^+$ Ly6G^{lo} cells), Q and R) the associated sub-populations (out of total monocytes) of these cells. S) The absolute number and T) the proportion of total cells which are Ly6G$^+$ are shown. The absolute number of U) Ly6G$^+$ CD11b$^+$ CD11c$^+$ cells, V) Ly6G$^+$ CD11b$^+$ CD11c^{lo} cells, and W) Ly6G$^+$ CD11b^{lo} CD11c^{lo} cells is shown above the percentages of these cells out of total Ly6G$^+$ cells in X, Y and Z. a) The absolute number of Ly6G^{hi} cells and d) the percentage of these cells out of total cells retrieved are shown. The absolute numbers of b) Ly6G^{hi} CD11b^{hi} CD11c^{lo} cells and c) Ly6G^{hi} CD11b$^+$ CD11c^{lo} cells are shown above the percentage of these cells (out of total Ly6G^{hi} cells). All data are taken from two experiments where n = 5 per treatment group in each experiment. *p≤0.05 **p≤0.01 ***p≤0.001.

Whilst cells within the "Kupffer cell gate" and cells within the "monocyte gate" are referred to as Kupffer cells and monocytes respectively, these gates include multiple cells types which require further identification to be differentiated apart from Kupffer cells or monocytes. Thus these terms are used for ease of following the gating strategy.

Neutrophils were classified as F4/80^{lo}, Ly6G^{+} or Ly6G^{hi}, and were further phenotyped by CD11b and CD11c expression. Numbers and proportions of all Ly6G^{+} populations do not significantly change following treatment, with the exception of a reduced proportion of CD11b^{+} CD11c^{lo} cells (Fig 5.41 S-Z). Absolute numbers of Ly6G^{hi} cells are slightly lower following treatment, and this is apparent in both sub-populations but the proportion of total cells in this gate is unchanged (Fig 5.41 a-d). The proportion of Ly6G^{hi} cells which are CD11b^{hi} CD11c^{lo} significantly decreases upon treatment, and the proportion of CD11b^{+} CD11c^{lo} cells significantly increases (Fig 5.41 3-f). Taken together, these data show that multiple myeloid subsets are affected by clodronate treatment, including Kupffer cells, infiltrating monocyte populations, and neutrophil populations.

5.11 Discussion

In this chapter, we have demonstrated that thrombi develop in the liver during systemic *Salmonella* infection and that this host response (in addition to inflammatory foci formation) occurs independently of the adaptive immune response. Instead, thrombosis requires IFNγ-mediated inflammation and podoplanin up-regulation on myeloid populations, enabling platelet activation via CLEC-2. This is the first account of CLEC-2-mediated thrombus formation in an inflammatory environment. It is plausible that this interaction may be important in other aberrant physiological settings, such as cancer and trauma and so the implications from this study should be suitably considered in the future.

5.11.1 During *Salmonella* infection, thrombosis develops in the liver and is associated with thrombocytopenia

Here we describe the platelet-rich thrombi which develop in the hepatic venous system from day 5 post-infection. The severity of thrombosis peaks at day 21 and thrombi are largely resolved by day 35. Thus the development and resolution of thrombosis occurs in parallel with inflammatory lesion formation in the liver parenchyma. Furthermore, both phenotypes are most extensive at a time when the bacterial load of both the liver and the blood are under control. This suggested that both features are inflammatory responses which although initiated by the presence of bacteria, are exacerbated and persist due to the host immune system.

Additionally we show that thrombocytopenia occurs in parallel with thrombus development. In other words, thrombi, composed largely of $CD41^{+}$ platelets, form in the liver during the host inflammatory response, and at the same time, platelet numbers in the blood are severely reduced. As thrombosis resolves (which occurs alongside infiltrate dissolution in the liver), platelet numbers in the blood return to normal. Therefore this suggests that thrombocytopenia occurs due to platelet consumption in the liver. Other factors, including platelet synthesis and splenic haematopoiesis are likely to influence the dynamics of this relationship and are discussed further below (Jackson et al., 2010).

5.11.2 Interferon-γ is required for thrombus development and thrombocytopenia

In Chapter 4 we illustrated that IFNγ signalling is necessary for hepatic inflammation during *Salmonella* infection. Here, we demonstrate an abrogation of thrombus development in

the absence of IFNγ, thus inflammation mediated by IFNγ is required for infiltration of leukocytes in the liver, the formation of inflammatory foci and the development of thrombosis. Furthermore, in the absence of IFNγ, we detect no significant thrombocytopenia during infection. Diminished thrombocytopenia in IFNγ-deficient mice has been previously reported during endotoxin shock (Car et al., 1994). In our study, the absence of these inflammatory phenotypes occur despite the elevated bacterial burden measured in the liver, relative to WT mice. Thus both thrombosis and thrombocytopenia only occur in the presence of inflammatory IFNγ signalling, and based on their parallel occurrence, thrombocytopenia is likely to be a consequence of thrombosis, and platelet consumption in the liver.

5.11.3 Podoplanin expression is IFNγ-mediated

To identify the mechanism of thrombus development, we investigated potential inflammatory components which are known to play a role in platelet activation, including podoplanin (Astarita et al., 2012). In Chapter 3 we demonstrated the expression of podoplanin within the inflammatory lesions which develop in the liver parenchyma, thus we knew that podoplanin is up-regulated in the liver during infection. To demonstrate the inflammatory nature of this podoplanin up-regulation, we subsequently show here that podoplanin is not up-regulated in IFNγ-deficient mice during infection. Thus, inflammation driven by IFNγ is required for increased podoplanin expression. Of interest, *in vitro* culture of liver cells with IFNγ did not induce podoplanin expression (data not shown). Therefore, the activities of IFNγ are likely to be indirect, perhaps through the recruitment of other inflammatory cells or the activation of other cells and their promotion of podoplanin expression via other means (Honma et al., 2012, Ekwall et al., 2011). It is likely that

regulation of podoplanin expression may also differ between cell types (Astarita et al., 2012, Hong et al., 2002). Considering the known capacity of podoplanin to activate platelets via CLEC-2, we therefore investigated thrombus development in mice which lack CLEC-2 on platelets and so cannot become activated by podoplanin (Finney et al., 2012).

5.11.4 Thrombosis is mediated by CLEC-2 activation of platelets

Thrombosis development is severely abrogated during *Salmonella* infection when CLEC-2 expression on platelets and megakaryocytes is abolished. In these mice, inflammation is observed as in WT mice, with podoplanin expression abundant and inflammatory lesion formation intact, so lack of thrombosis is due to the absence of CLEC-2. Despite this, after infection, leukocyte cellularity is slightly below that of WT, as are numbers of podoplanin-expressing cells. These data may highlight a reduced ability of cells to respond to infection or to regulate inflammation (less extensive) in the absence of CLEC-2 on platelets.

In other studies, platelet CLEC-2 and GPVI expression are important for the maintenance of blood vessel integrity by the prevention of haemorrhage during induced inflammation (Boulaftali et al., 2013). When both these platelet receptors are absent, platelets are unable to contribute to vascular integrity. It is likely that our findings support these studies to some degree. Potentially, differential environmental factors, such as low shear in the portal vein, results in thrombosis in our system, which doesn't necessarily occur in other sites/vessel types (Hughes et al., 2010a).

Whilst thrombosis is severely abrogated in the absence of CLEC-2 expression on platelets, the phenotype is frequently not completely lost, suggesting that there could be low-level platelet activation by other mechanisms which is induced during *Salmonella* infection in WT mice. The close association between thrombi and the vascular endothelium raises the

possibility that thrombosis could additionally be mediated by activation of the collagen receptor GPVI, although studies on GPVI-deficient mice are required to test this. In this model, we hypothesise that damage to the endothelium caused by leukocyte infiltration may lead to exposure of collagen and platelet activation via platelet-expressed GPVI (Massberg et al., 2003). The necessity for both receptors could be tested using double transgenic mice whereby platelets lack expression of both CLEC-2 and GPVI (Boulaftali et al., 2013, Bender et al., 2013). We would expect thrombosis to be completely abrogated in these mice, as it is in IFNγ-deficient mice.

5.11.5 Adaptive lymphocytes are not required for thrombosis or thrombocytopenia

Considering the requirement for inflammatory podoplanin in platelet activation via CLEC-2, it was not surprising that thrombosis and thrombocytopenia occur in the absence of lymphocytes. Whilst podoplanin expression has been reported on Th17 cells, its expression is not detected on other T cell subsets or B cells, consistent with our own results in the liver (data not shown) (Peters et al., 2011, Miyamoto et al., 2013). Whilst T cells, and Th1 cells in particular, may play a role in the persistence of thrombosis (discussed below), lymphocytes are not required for initial thrombus development or the associated thrombocytopenia. Podoplanin is expressed on both $CD45^+$ and $CD45^-$ populations during *Salmonella* infection and we demonstrate that the haematopoietic source of podoplanin expression in the liver is largely myeloid cells.

5.11.6 CD45$^+$ podoplanin expression is primarily by CD11c$^+$ F4/80$^+$ cells and expression is induced on CD11c$^-$ F4/80$^+$ cells post-infection

We used FACS to investigate which myeloid populations express podoplanin during infection, based on their expression of CD11c and F4/80. Kupffer cells express F4/80 and can additionally express CD11c (Beattie et al., 2010). However, it is important to note that Kupffer cells are not a homogenous population. They can be both tolerogenic and inflammatory, and can be fully tissue-resident or can differentiate from newly released bone marrow-derived precursors (Klein et al., 2007). Classification of these cells based on surface markers alone is not sufficient and functional studies are required to properly segregate cells into discrete groups. Therefore, with the gating strategies used here, it is likely that multiple cell types will be present in each group (Klein et al., 2007, Tacke et al., 2009). For example, Kupffer cells are not the only F4/80$^+$ CD11c$^+$ cells found in the liver. Monocyte-derived dendritic cells are also positive for both markers and thus may contribute to the podoplanin-expressing milieu in this gate (Flores-Langarica et al., 2011, Segura and Amigorena, 2013).

Although the greatest number of podoplanin-expressing cells are CD11c$^+$ F4/80$^+$ (and this was the case at any time studied during infection), it is CD11c$^-$ F4/80$^+$ cells which are the most inducible expressers of podoplanin following infection. The number of CD11c$^-$ F4/80$^+$ podoplanin$^+$ cells increased approximately 80-fold in the first 24-hours of infection, to a total increase of 1000-fold by day 7. Although in total numbers, this is still less than CD11c$^+$ F4/80$^+$ podoplanin$^+$ cells, it is the largest fold change in any population studied. This is supported by histological observation that podoplanin is expressed by CD11c$^-$ F4/80$^+$ and CD11c$^+$ F4/80$^+$ cells. Thus our data comply with Kupffer cell (F4/80^{hi} CD11b^{lo}) and monocyte

(F4/80^{+} CD11b^{hi}) phenotypes described in the past, and demonstrate podoplanin expression by Kupffer cell populations, rather than by monocytes (Tacke et al., 2009). Other studies have shown increased podoplanin expression on macrophages *in vivo* during inflammation (Hou et al., 2010). Our data in the liver are in line with these observations, although we propose that both macrophages and other populations including MoDCs are at play. It will be important to further characterise podoplanin-expressing populations in the future.

5.11.7 Clodronate-sensitive cells are necessary for thrombosis induction

We show that clodronate treatment prior to *Salmonella* infection abolishes thrombus formation in the liver. Absolute numbers of CD11c^{-} F4/80^{+} podoplanin^{+} and CD11c^{+} F4/80^{+} podoplanin^{+} cells are reduced following treatment, thus clodronate depletes cells within both populations, either or both of which may be required for CLEC-2 activation. Whilst it is apparent that clodronate-sensitive cells are required for thrombosis, we do not have direct evidence that it is podoplanin expression by these cells which is required for thrombosis. Interestingly, in clodronate-treated mice, the bacterial burden of the liver is significantly less than in PBS-treated mice. However, it is unlikely that this is due to the absence of thrombosis because other mice which lack thrombi retain similar or greater bacterial loads compared to WT mice. Instead, the lower colonisation in clodronate-treated mice may be explained by loss of niche habitat for bacterial replication, and has been described elsewhere (Wijburg et al., 2000).

5.11.8 Podoplanin in inflammatory orchestration

Additionally, podoplanin is likely to be important in other aspects of the inflammatory response in addition to platelet activation. Podoplanin up-regulation in the liver is detected

within 24 hours, and in $CD11c^-$ $F4/80^+$ cells is up-regulated bimodally, whereby $CD11c^-$ $F4/80^+$ $podoplanin^+$ cells are elevated at both 24 hours and at day 7. This may reflect differing roles of podoplanin, including organising inflammation and activating platelets.

The importance of podoplanin in inflammatory orchestration is evident in the literature (Acton et al., 2012, Peters et al., 2011, Bekiaris et al., 2007, Boulaftali et al., 2013, Herzog et al., 2013). Of particular interest, podoplanin contributes to the recruitment of DCs from the periphery and to DC motility within lymph nodes, by interacting with DC-expressed CLEC-2 (Acton et al., 2012). Podoplanin expression in the spleen plays a significant role in the segregation of T and B cells regions, which is necessary for the induction of normal adaptive immune responses, and it is likely that podoplanin expression by non-haematopoietic cells is likely to be important in this organisation (Bekiaris et al., 2007, Withers et al., 2007). The up-regulation of podoplanin we detect on $CD45^-$ cells in this study suggests the likely importance of non-haematopoietic cells in our inflammation model. We also detect podoplanin up-regulation in the spleen despite the absence of thrombosis in this site. This further suggests podoplanin involvement in inflammation in a non-thrombus forming capacity, as is described elsewhere (Hou et al., 2010).

5.11.9 Inflammatory thrombosis: a role for TNFα

Thrombosis is absent in IFNγ-deficient mice due to lack of inflammation. Here we demonstrate the absence of thrombosis in TNFαR-deficient mice, despite the maintenance of inflammation and podoplanin up-regulation. This suggests that both inflammation and an independent TNFαR-mediated signal are necessary for thrombus development. Whilst there is evidence for TNFαR expression by platelets (Limb et al., 1999, Pignatelli et al., 2005), it is unlikely that this plays a role in the lack of thrombosis in these mice as there is

controversy regarding the functionality of platelet-expressed TNFαR (S. Watson, personal communication). Thus at this stage it is not apparent why mice lacking inflammatory TNFαR signalling lack thrombi whilst retaining leukocyte infiltrate and other aspects of hepatic inflammation. However, TNFαR$^{-/-}$ mice have a severe lack of inflammatory organisation in the spleen during *Salmonella* infection (data not shown). Further investigation of podoplanin expression in other inflammatory sites in these mice, together with determining the role of TNFαR signalling will be useful in future studies (Mastroeni et al., 1995).

5.11.10 Platelets: consumed or not produced

As mentioned above a general correlation between thrombosis and thrombocytopenia is observed during *Salmonella* infection. Both phenotypes are largely absent in IFNγ-deficient mice, yet thrombocytopenia is augmented when thrombosis is more severe, as in IL10-deficient mice, suggesting a common mechanism. This relationship is generally mirrored by MPV, whereby the more severe the thrombosis, the greater the thrombocytopenia and the larger the MPV. Considering elevated MPV can be associated with increased platelet production by megakaryocytes and can be indicative of consumptive thrombocytopenia (Tsakiris et al., 1999), we would expect the detected increase in MPV to reflect accelerated platelet production. The increased numbers of megakaryocytes detected in the spleen during infection supports this assumption, and has been described previously (Serefhanoglu et al., 2003, Brown et al., 2010).

During *Salmonella* infection, the bone marrow becomes colonised and haematopoiesis relocates in part to the spleen (Jackson et al., 2010, Kam et al., 1999, Hyland et al., 2005). Whether increased MPV is associated with increased platelet production in our model, or

whether it is a consequence of the shift to splenic platelet production remains to be seen. Additionally, sequestration of platelets in the spleen may contribute to loss of platelets in the blood; splenomegaly is a common feature of human and murine systemic *Salmonella* infection and splenic haematopoiesis is likely to account for this (Jackson et al., 2010). However, if newly formed platelets are unable to exit the spleen and thus pool in this site, this may explain both splenomegaly (to some extent) and thrombocytopenia (Aster, 1966). Our data suggest it is unlikely that thrombocytopenia is explained by a lack of platelet production, however future studies will include measurement of serum thrombopoeitin as an indication of the extent of platelet production. As an aside, splenic haematopoiesis and the associated increased megakaryocytes observed in the spleen, may disturb long-lived plasma cells in the bone marrow, which reside in unique micro-environmental niches in association with megakaryocytes (Winter et al., 2010).

5.11.12 Thrombosis and thrombocytopenia do not always occur together

We have described an association between thrombosis, thrombocytopenia and MPV. However, a marked reduction in thrombosis but not thrombocytopenia or MPV is seen during infection in mice which lack CLEC-2 expression on platelets. This demonstrates that the reduction in platelet count is not purely a consequence of platelet consumption during thrombosis in the liver. In their resting state, these mice can have slightly lower platelet numbers relative to littermate controls (Finney et al., 2012), although this alone cannot explain the extent of thrombocytopenia detected post-infection. Therefore, thrombosis in the liver cannot be the entire explanation behind thrombocytopenia, despite the relationship between these phenotypes in many of the mice we examined. To explain this, it is potentially possible that PF4.Cre.CLEC-$2^{fl/fl}$ mice may be thrombotic in other sites which

we have not yet detected. Alternatively, thrombosis and thrombocytopenia may be separately initiated in response to a common signal (such as IFNγ), but only thrombosis is CLEC-2/podoplanin mediated. It will be important to establish the mechanism of thrombocytopenia to further investigate this dissociation. Additionally, the shunt in haematopoiesis from the bone marrow to the spleen during *Salmonella* may contribute to thrombocytopenia.

5.11.13 Platelets as mediators of innate immunity

Aside from haemostasis, reduced platelet numbers in the blood may have other consequences in terms of host response to infection. Platelets have been implicated as innate mediators of inflammation, for example, platelets can release antimicrobial proteins from their granules upon activation (Fitzgerald et al., 2006a, Semple et al., 2011). Platelet consumption in the liver may have important systemic repercussions at other sites of colonisation. Although the anti-bacterial capacity of a platelet may be small in comparison to that of a neutrophil or a macrophage, their numbers and other actions (communication with other innate populations) may be vital (Engelmann and Massberg, 2013).

5.11.14 Thrombosis is an innate phenomenon, yet the adaptive system plays a role in its regulation

Although thrombi develop independently of adaptive immune cells (including T cells), we describe the increased severity of vascular occlusion in Tbet-deficient mice, in which $CD4^+$ Th1 cells are absent. This suggests there may be an inherent T cell mechanism of vascular protection, whereby thrombi are equivalent to those in WT mice in the absence of total T cells but vary in severity when specific T cell subsets are missing. Furthermore, thrombosis

tends to be less severe in the absence of IL4 (a Th2 effector cytokine), thus there may be a Th1 versus Th2 balance in thrombosis control, as there is in other aspects of immunity to *Salmonella* infection (Bobat et al., 2011). However, despite increased thrombosis in universally Tbet-deficient mice, thrombosis severity is equivalent to WT in mice whereby T cells are Tbet-deficient (data not shown). This may indicate that Tbet expression in a non-T cell population may play a regulatory role in thrombus development. In support of this, thrombosis is particularly fierce in B cell-deficient mice. Tbet in B cells plays a role in germinal centre responses (R. Coughlan, personal communication), thus Tbet in B cells may be important in restriction of thrombosis and that Th2 cells contribute to this regulation in some capacity via IL4 signalling. Nevertheless, the relationship between T cell subsets and thrombosis severity remains unclear.

5.11.15 Thrombosis is a liver-specific host response

One vital role of the liver is the sampling of and tolerogenicity towards non-pathogenic antigens, of which it is constantly exposed to because of its portal blood supply (Bilzer et al., 2006). Indeed the liver is the only organ which receives blood directly from the gut. The portal vein is likely to be the route of *Salmonella* entry into the liver in our i.p. infection model, although thrombosis is equivalent with i.v. infection. Thrombi develop in the portal vein, as identified by adjacency to the hepatic artery, bile duct and podoplanin^{+} lymphatic vessels. Whilst we cannot exclude additional thrombosis in the central venules, this phenotype is specifically venous, and is restricted to the liver.

Whether or not platelets in portal regions may be particularly prone to becoming activated in a CLEC-2-dependent manner is unknown. Platelets may be important in immune-surveillance, as was described recently in the context of ‘touch and go’ interactions with

Kupffer cells (Wong et al., 2013, Engelmann and Massberg, 2013). Potentially, a combination of antigen exposure, both in the portal circulation and directly via Kupffer cell interaction, in addition to a heightened predisposition to become activated due to "Kupffer cell kissing", may provide adequate stimulus for inflammatory podoplanin expression to activate platelets.

Although thrombosis has been described previously during murine *Salmonella* infections, evidence in the literature is limited (Mastroeni et al., 1995, Brown et al., 2010, Nakoneczna and Hsu, 1983) (R. Tsolis, personal communication). However, others have described thrombosis in multiple sites, including a DIC-like phenotype observed during chronic virulent *Salmonella* infection in Nramp non-susceptible mouse strains (Brown et al., 2010) (C. Detweiler, personal communication). Similarly, thrombi are also reported at other sites during virulent infection of Nramp-susceptible mouse strains (Mastroeni et al., 1995). In our study, thrombosis is a liver-specific phenotype and it is likely that discrepancy to previous reports may be accounted for by differing infection conditions.

5.11.16 Conclusion

The main implications of this chapter are that firstly, platelets are the main constituent of thrombi seen in the liver during *Salmonella* infection and in fact that the mechanism of thrombus development is driven by platelet activation. And secondly that this platelet activation is mediated by podoplanin up-regulation and its interaction with platelet-expressed CLEC-2. This is the first account of CLEC-2-mediated platelet thrombus formation in an inflammatory environment.

CHAPTER 6:

HAEMOSTASIS DURING *SALMONELLA* TYPHIMURIUM INFECTION

6.1 Introduction

In Chapter 5 we described the extensive thrombosis and thrombocytopenia which occur during systemic STm infection in mice and discussed the few references which have been made to these symptoms in human patients. Considering the striking phenotypes we observed, we were keen to explore additional haemostatic changes in our infection model, especially as there is a more profound awareness of such abnormalities in humans.

6.1.1 Evidence of human haemostatic abnormalities during NTS infections

In sub-Saharan Africa, severe anaemia is a common cause of illness and death in children due to loss of oxygen supply, yet the underlying cause of this anaemia is often unknown (Calis et al., 2008, Koram et al., 2000, Newton et al., 1997). In addition, anaemia is closely associated with NTS infections in sub-Saharan Africa (Graham et al., 2000a, Kurtzhals et al., 1997, Burgmann et al., 1996). A previous case-control study of children in Malawi reported that bacteraemia was “strongly associated with severe anaemia”, and in the areas studied, NTS was the most common cause of bacteraemia (Calis et al., 2008). Thus, anaemia is common in patients with systemic infection and is frequently observed in conjunction with NTS bacteraemia in children in sub-Saharan Africa (Graham et al., 2000a).

Anaemia of infection is a phrase used to describe the hypo-proliferative anaemia associated with low serum iron concentrations, which is frequently linked with chronic infection (Means, 2000). The anaemia associated with systemic infection can also commonly be caused by the destruction of red blood cells, as occurs during malaria. Malarial anaemia is characterised by haemolysis of erythrocytes by phagocytic cells in the spleen (Mabey et al., 1987). Haemolytic anaemia has been associated with reduced bactericidal activity in macrophages, which may explain the prevalence of NTS bacteraemia seen with malaria (Cunnington et al., 2012, Greenwood et al., 1978, Kaye et al., 1967, Warren and Weidanz, 1976, Graham et al., 2000a). Although the mechanisms as to how anaemia dampens the bactericidal capability of macrophages has not yet been fully described, it is likely that the accumulation of malarial pigment and the interference of erythrocyte components with reactive oxygen metabolism within macrophages may contribute (Mabey et al., 1987, Morpeth et al., 2009). Reduced bactericidal activity is likely to have a significant impact on the host's response to invasive *Salmonella* infection (Greenwood et al., 1978, Kaye et al., 1967, Warren and Weidanz, 1976, Graham et al., 2000a).

Another important mechanism which may contribute to anaemia is haemophagocytosis; the destruction of erythrocytes, (and leukocytes and platelets) by haemophagocytic macrophages in the bone marrow and spleen of infected individuals (Fisman, 2000, Fame et al., 1986). Haemophagocytosis has been a recognised clinical feature of typhoid fever for many years, whereby hyper-phagocytic macrophages have been referred to as *typhoidal cells* (Mallory, 1898). Nevertheless, although prognosis of systemic NTS infection is worse in individuals with anaemia, the condition has not been associated with cause of death (Calis et al., 2008, Graham et al., 2000a).

Altered peripheral leukocyte numbers have been previously reported in murine STm infections and this is primarily due to reduced lymphocyte numbers and neutrophil and monocyte populations decrease in the blood (Brown et al., 2010). There is far less data describing blood cell changes during human NTS infections. In typhoid fever, the white blood cell count is usually unchanged, however increased release of monocyte and granulocyte precursors from the bone marrow have been reported, which may indicate diminished peripheral mature leukocyte numbers (Mallouh and Sa'di, 1987, Pramoolsinsap and Viranuvatti, 1998, Udden et al., 1986). Therefore, whilst associations between systemic NTS infection and haematological abnormalities have been acknowledged, especially in reference to malarial anaemia and sickle cells disease, these have not been explored in detail. Furthermore, with the exception of reduced bacterial killing by macrophages during malarial anaemia, there is no indication in the literature as to how these complications may contribute to the overall host response to infection. Thus we were keen to characterise haemostatic complications during systemic NTS infection in mice with the view to understanding how these phenotypes may contribute to the host's ability to ultimately control the infection.

6.1.2 Aims of study

The link between the events observed in the liver and the vessels are likely to relate to the cellular nature of the blood. For ease of reference we have collated this information for all the events seen in the earlier results chapters into one chapter. Thus here we:

- Quantitatively describe the anaemia and leukopenias associated with our mouse model;

- Characterise these features in genetically altered mice to determine how the host immune system may contribute to these phenotypes.

RESULTS

6.2 Reference data for whole blood analysis

To investigate leukopenia and anaemia during infection, mice were infected i.p. with 5 x 10^5 attenuated bacteria as described in previous chapters, unless stated otherwise, and blood was analysed post-infection. For reference, normal values of haemostatic parameters in mice are provided in Table 6.1. As described in Chapters 3 and 5, bacterial colonisation of the liver peaks at day 7 post-infection, when bacterial numbers are approximately 10^6 CFU, and by day 50 the liver contains $<10^3$ bacteria. In the blood, bacterial numbers reach 10^2-10^3 by day 7 and are usually undetectable by day 14.

Parameter	Male	Female
White blood cells (per mm^3)	8.20 x10^3	6.55 x 10^3
Red blood cells (per mm^3)	8.97 x 10^6	9.56 x 10^6
Haemoglobin (g/dL)	13.10	14.30
Hematocrit (%)	41.50	45.65

Table 6.1. Median haematological parameters of C57BL/6J mice aged 3-7 months. Table is adapted from (Mazzaccara et al., 2008).

6.3 Leukopenia occurs during infection

In WT mice, total leukocyte numbers detected in the blood are diminished at day 7 post infection, and this diminution is exacerbated at day 21 (Fig 6.1 A). Leukopenia is resolving by day 28 and is near normal by day 50. This phenotype is primarily due to decreased lymphocytes; numbers drop by day 7 and this persists throughout infection, with numbers recovering only by day 50 (Fig 6.1 B). In contrast, the number of blood monocytes and neutrophils are generally the same or higher during infection, with monocyte numbers generally being elevated even at later times when tissue bacterial numbers are low (Fig 6.1 C-D). Eosinophil and basophil numbers are similar to pre-infection levels except for day 21 where they are consistently reduced (Fig 6.1 E-F). Taken together, these data indicate that when bacterial burdens are highest, blood lymphocyte numbers fall, and whilst blood monocytes increase, other myeloid cell numbers are generally more consistent. Despite this, leukopenia is observed which is resolved within 50 days.

6.4 Infection is associated with anaemia-linked blood abnormalities

Leukopenia is accompanied by a severe anaemia during infection. A decreased erythrocyte count is observed in the blood between days 7 and 21 post-infection, which is resolving by day 28 (Fig 6.2 A). As expected, haemoglobin concentration and haematocrit resemble the pattern of erythrocyte numbers in the blood (Fig 6.2 B-C). Red cell distribution width (RDW) (reflecting variability in red cell size) is increased from day 7, is particularly pronounced at day 21, and is still elevated by day 50 (Fig 6.2 D). The mean corpuscular volume is stable or lower throughout infection, indicating the anaemia is normocytic (Fig 6.2 E). The mean corpuscular haemoglobin (MCH) (or mass of haemoglobin per erythrocyte) decreases by day 7 and this persists throughout the 50 days measured (Fig 6.2 F).

Figure 6.1

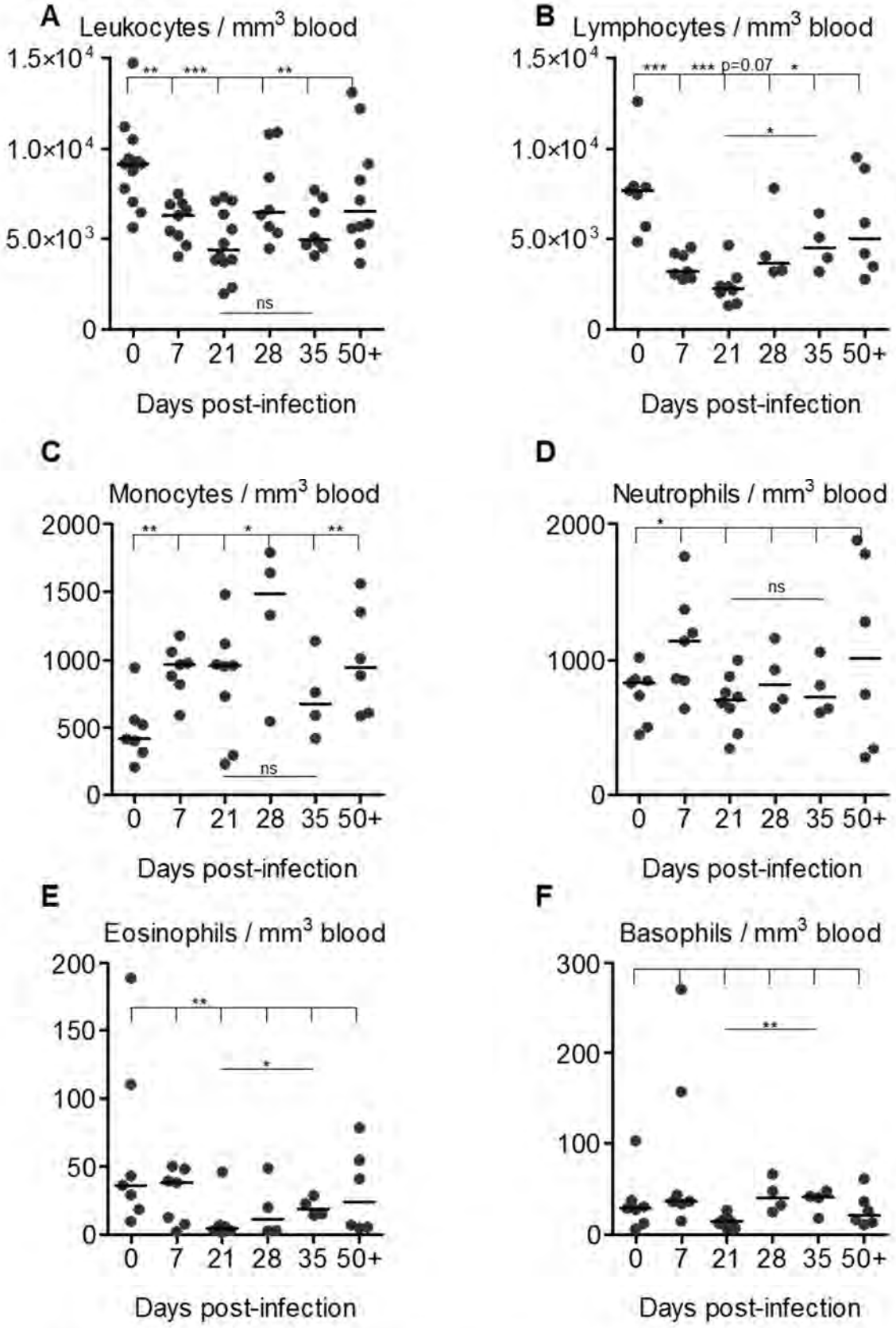

Figure 6.1 Leukopenia associated with decreased lymphocytes is detected during infection

WT mice were infected (i.p.) with 5 x 10^5 CFU attenuated STm and blood was obtained by cardiac puncture at the indicated time-points post-infection. Leukopenia was assessed in the blood by quantification of A) total leukocytes, B) lymphocytes, C) monocytes, D) neutrophils, E) eosinophils, and F) basophils using a whole blood counter. Data are taken from multiple experiments where n ≥ 3 at each time-point in each experiment. *p≤0.05 **p≤0.01 ***p≤0.001.

Figure 6.2

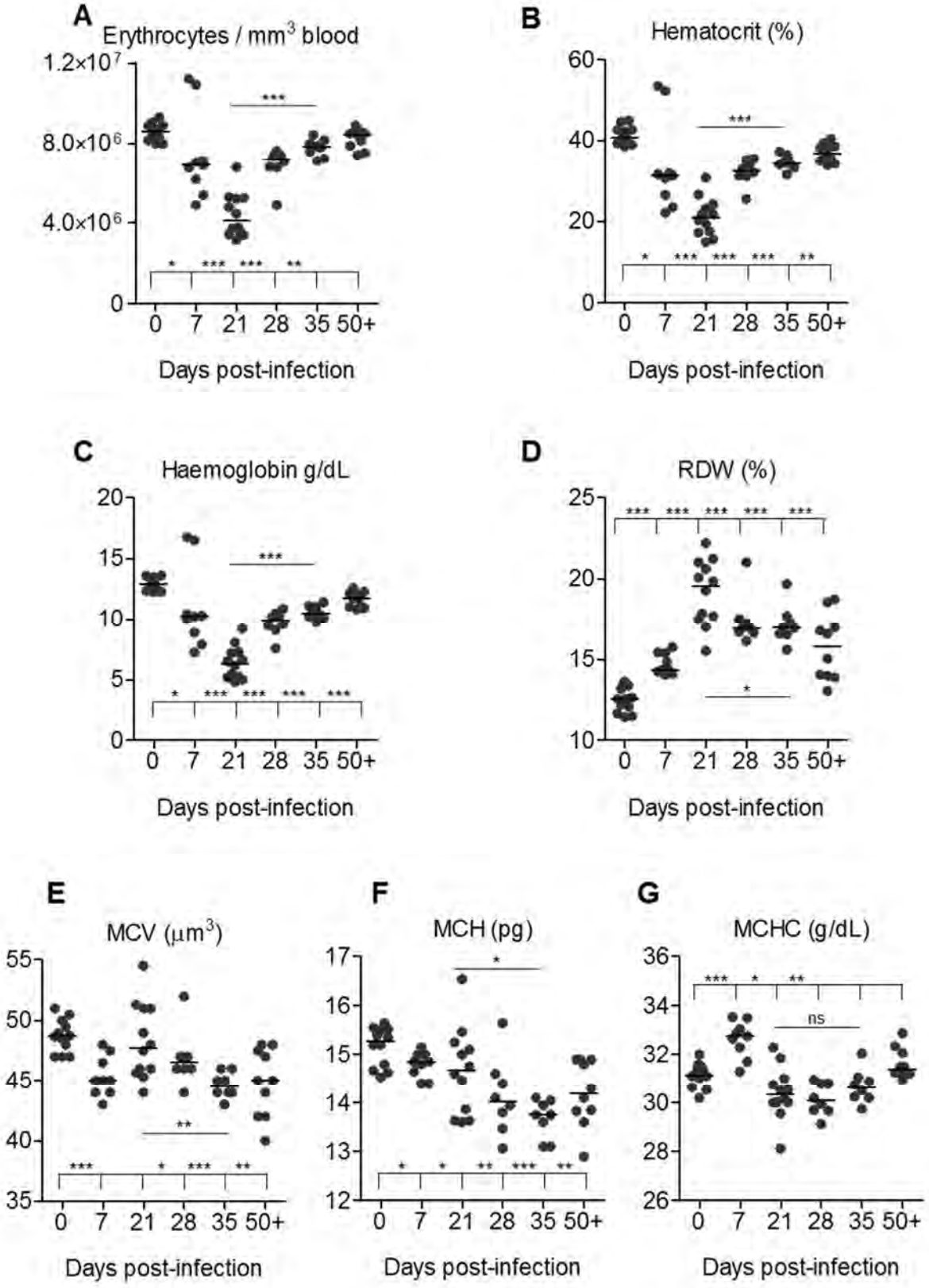

Figure 6.2 Normocytic anaemia is seen during infection
WT mice were infected (i.p.) with 5 x 10^5 CFU attenuated STm and blood was obtained by cardiac puncture at the indicated time-points post-infection. Anaemia was assessed in the blood by measurement of A) erythrocyte numbers, B) haematocrit, C) haemoglobin concentration, D) red cell distribution width (RDW), E) mean corpuscular volume (MCV), F) mean corpuscular haemoglobin (MCH), and G) mean corpuscular haemoglobin concentration (MCHC) using a whole blood counter. Data are taken from multiple experiments where n ≥ 3 at each time-point in each experiment. *p≤0.05 **p≤0.01 ***p≤0.001.

This indicates a lasting defect in red cells, despite normalising erythrocyte counts and universal haemoglobin concentrations. The mean corpuscular haemoglobin concentration (MCHC), which describes the mean haemoglobin concentration per set volume of erythrocytes, is increased at day 7 (Fig 6.2G). Taken together, these data describe a normocytic anaemia which peaks at day 21 post-infection and is not entirely resolved within 50 days.

6.5 Innate leukocytes accumulate in the absence of lymphocytes

Leukopenia and anaemia were measured in genetically modified mice which lack immune cells/molecules at day 7 post-infection. Reference values of all parameters examined for non-infected mice of each strain used are shown in Figure 6.3. Most parameters are comparable between strains, with the following exceptions. Mice deficient in Tbet and PF4.Cre.CLEC-2$^{fl/fl}$ mice have reduced monocyte numbers. Mice lacking B cells have elevated neutrophil counts while T cell-deficient mice have lower neutrophil numbers. Mice lacking IL6 or IL10 have reduced lymphocyte numbers but higher eosinophil numbers, and basophil numbers are increased in the absence of IFNγ and CD1d (Fig 6.3 A-J).

Interestingly, leukocyte numbers are similar between WT and Rag-1$^{-/-}$ mice, despite the absence of lymphocytes (Fig 6.4 A-B). This is due to significantly elevated monocyte numbers in the blood in Rag-1$^{-/-}$ mice and there is also a tendency for increased neutrophils and eosinophils (Fig 6.4 C-F). The anaemia in these mice occurs to a similar extent to that seen in WT mice (Fig 6.4 G-J). Despite their lack of B cells, IgHκ-deficient mice have less severe leukopenia than WT mice (Fig 6.5 A). They have a similar lymphocyte number to WT, which suggests some compensatory accumulation of T cells in the absence of B cells (Fig 6.5 B).

Figure 6.3

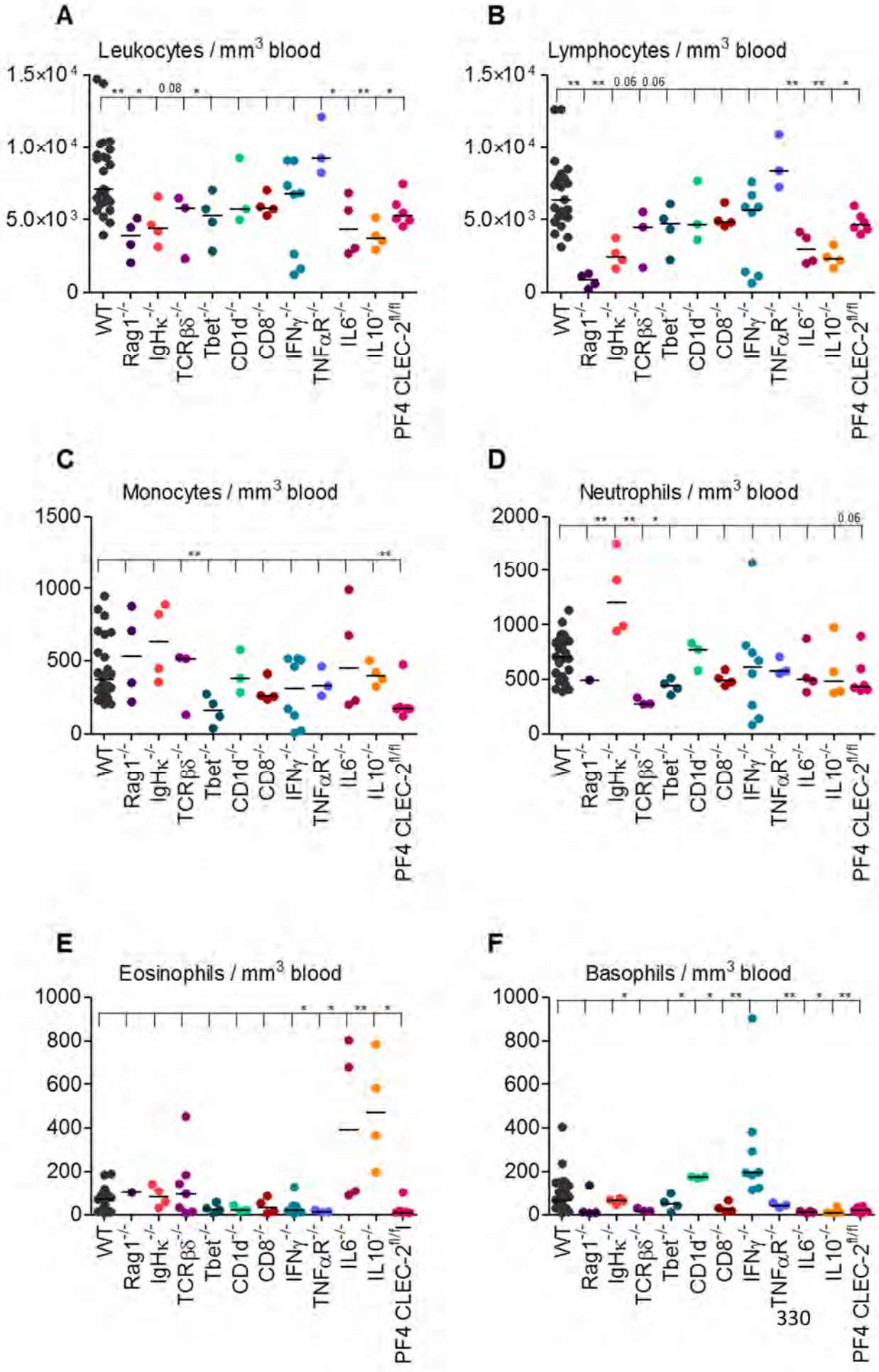
A
Leukocytes / mm3 blood
1.5×10^4
1.0×10^4
5.0×10^3
0
B
Lymphocytes / mm3 blood
C
Monocytes / mm3 blood
1500
1000
500
D
Neutrophils / mm3 blood
2000
E
Eosinophils / mm3 blood
F
Basophils / mm3 blood
800
600
400
200
WT
Rag1-/-
IgHκ-/-
TCRβδ-/-
Tbet-/-
CD1d-/-
CD8-/-
IFNγ-/-
TNFαR-/-
IL6-/-
IL10-/-
PF4 CLEC-2fl/fl

Figure 6.3 continued

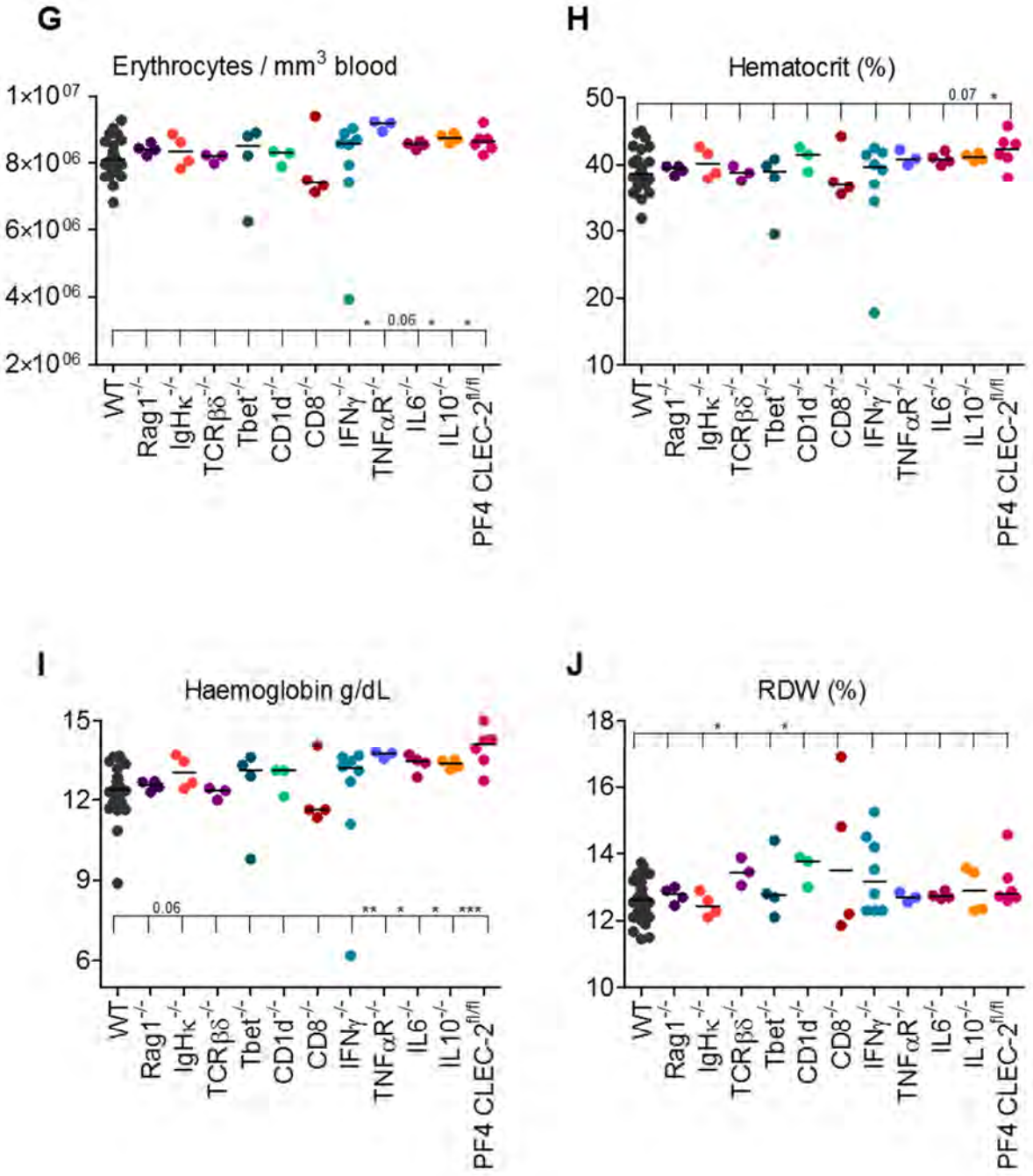

Figure 6.3 There is some variability in blood corpuscular constituency between genetically-altered mice strains

Blood was obtained by cardiac puncture from non-infected WT and genetically-altered mice (strains as indicated on Figure). The following parameters were quantified/measured in the blood of these mice, in the absence of infection: A) total leukocytes, B) lymphocytes, C) monocytes, D) neutrophils, E) eosinophils, F) basophils, G) erythrocytes, H) haematocrit, I) haemoglobin concentration, and J) red cell distribution width (RDW), using a whole blood counter. Data are taken from one (or multiple) experiment(s) per mouse strain where n ≥ 3 for each strain of mice. *p≤0.05 **p≤0.01 ***p≤0.001.

Figure 6.4

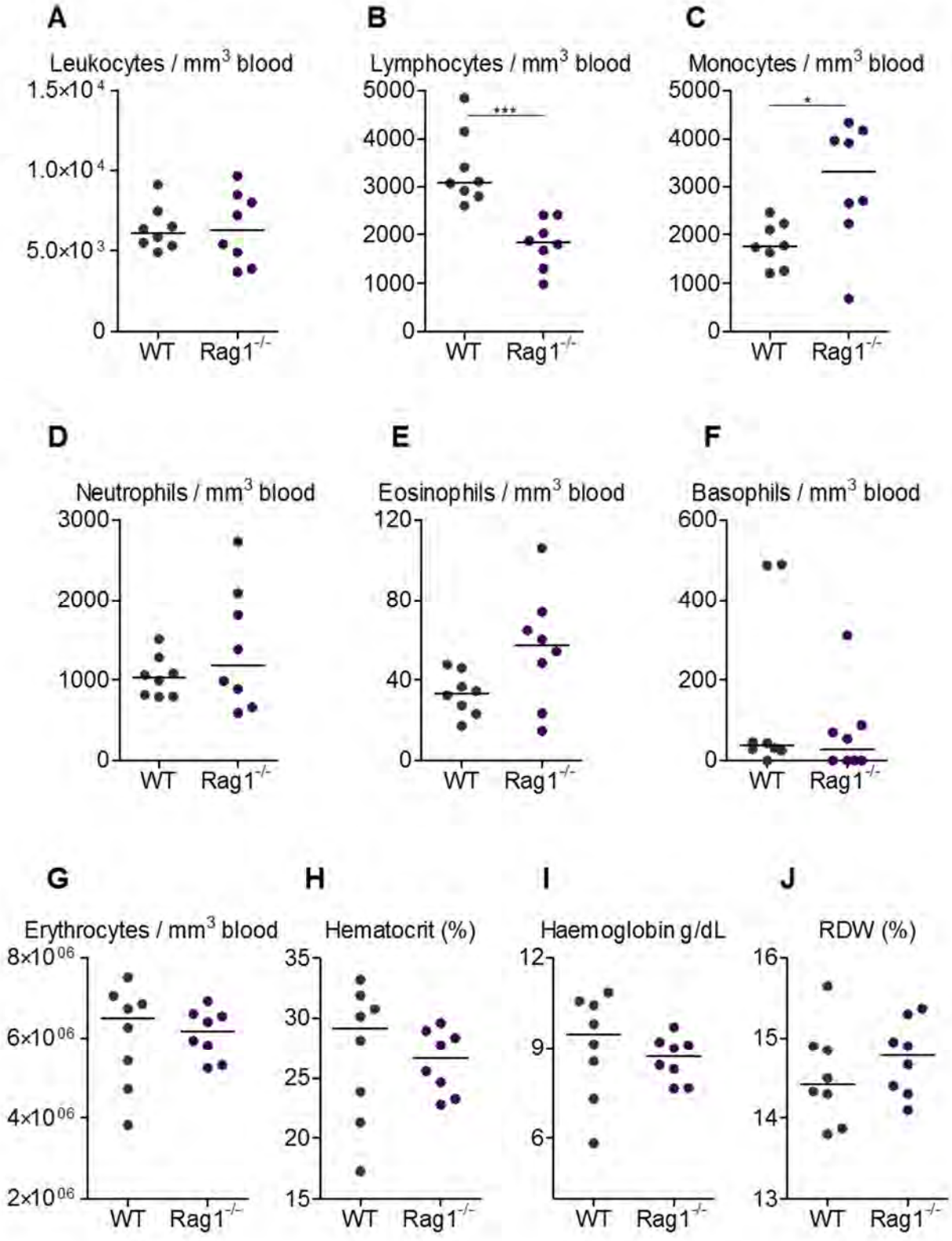

Figure 6.4 Blood monocytes are elevated in Rag-1-deficient mice
WT and Rag-1$^{-/-}$ mice were infected (i.p.) with 5 x 10^5 CFU attenuated STm and blood was obtained by cardiac puncture at day 7 post-infection. The following parameters were quantified/measured in the blood: A) total leukocytes, B) lymphocytes, C) monocytes, D) neutrophils, E) eosinophils, F) basophils, G) erythrocytes, H) haematocrit, I) haemoglobin concentration, and J) red cell distribution width (RDW), using a whole blood counter. Data are taken from two experiments where n = 4 in each experiment for each strain of mice. *p≤0.05 **p≤0.01 ***p≤0.001.

Figure 6.5

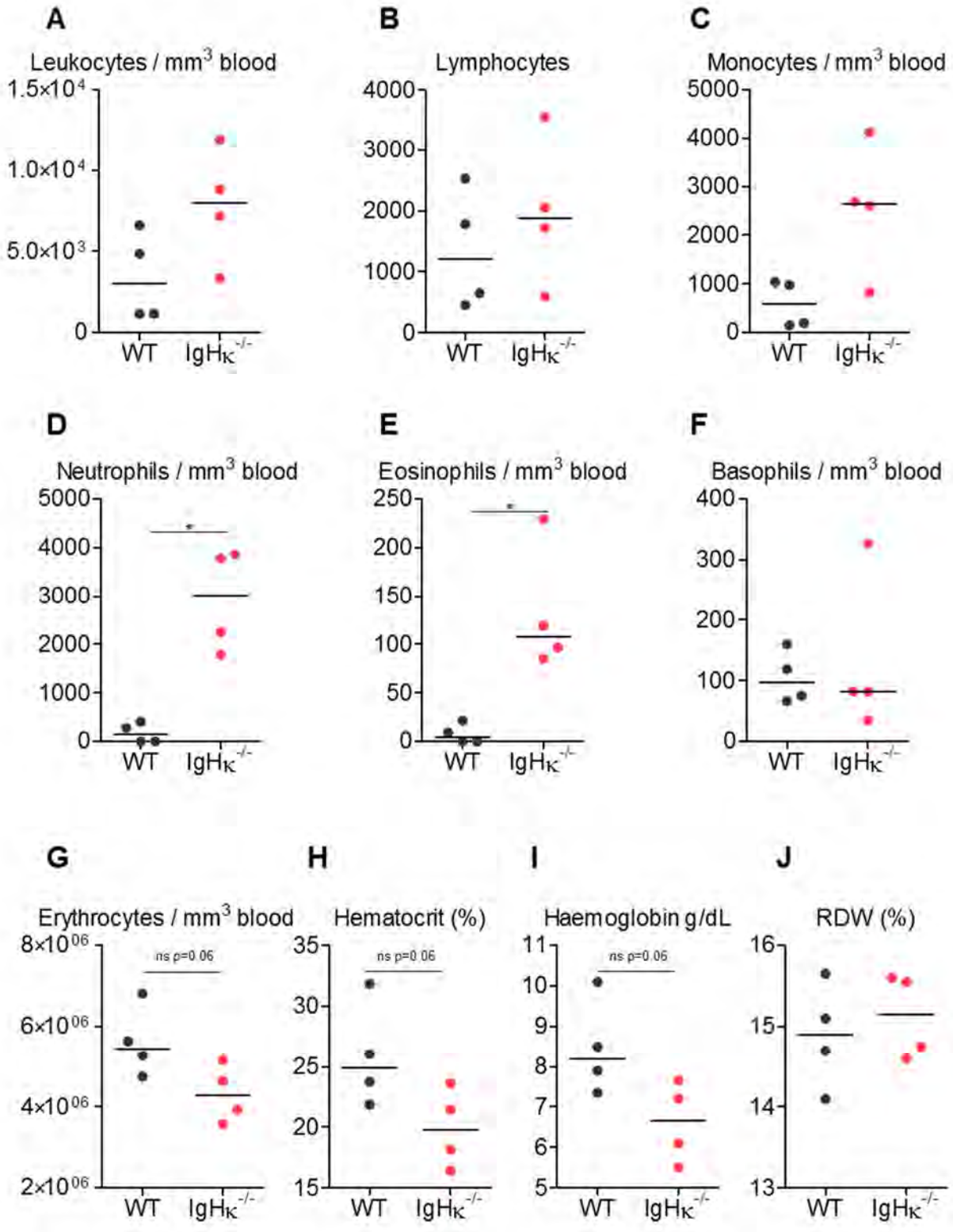

Figure 6.5 Myeloid cells and lymphocytes are elevated in IgHκ$^{-/-}$ mice and anaemia is heightened

WT and IgH$^{-/-}$κ$^{-/-}$ (IgHκ$^{-/-}$) mice were infected (i.p.) with 5 x 10^5 CFU attenuated STm and blood was obtained by cardiac puncture at day 7 post-infection. The following parameters were quantified/measured in the blood: A) total leukocytes, B) lymphocytes, C) monocytes, D) neutrophils, E) eosinophils, F) basophils, G) erythrocytes, H) haematocrit, I) haemoglobin concentration, and J) red cell distribution width (RDW), using a whole blood counter. Data are taken from one experiment where n = 4 for each strain of mice. *p≤0.05 **p≤0.01 ***p≤0.001.

Monocytes, neutrophils and eosinophils are all more prevalent in the blood relative to WT mice (Fig 6.5 C-F). Anaemia is heightened in B cell-deficient mice (Fig 6.5 G-J).

In mice which lack T cells, lymphocyte numbers are similar or higher than WT, suggesting increased B cells in the blood (Fig 6.6 A-B). Monocytes and neutrophils are also increased but there are fewer eosinophils and basophils (Fig 6.6 C-F). Whilst anaemia is detected in TCRβδ$^{-/-}$ mice, it is less pronounced; both erythrocyte numbers and haemoglobin concentration are significantly greater than in WT mice (Fig 6.6 G-J). These data indicate that in the absence of both B cells and T cells and also of each lymphocyte set individually, there is a more marked presence of particularly innate leukocytes in the blood, yet anaemia severity correlates with a lack of B cells.

6.6 Anaemia is associated with a lack of CD8 and CD1d but not Tbet or IL4

To determine if there was a relationship with T cells or T helper cell-associated molecules which could contribute to these phenotypes, leukopenia and anaemia were measured in mice lacking Tbet (required for CD4^{+} Th1 differentiation), IL4 (signature of CD4^{+} Th2 signalling), CD8, or CD1d (required for iNKT cell activation).

Tbet-deficient mice have significantly increased numbers of leukocytes in the blood, which is especially apparent in monocyte and neutrophil numbers, and a reduced anaemia compared to WT (Fig 6.7). Both IL4-deficient and IL4Rα-deficient mice have similar leukocyte numbers (in exception to modestly increased neutrophils) and extent of anaemia to WT mice, albeit with a RDW similar to naïve mice (Fig 6.8). Mice lacking CD8 have similar leukocyte numbers to WT but anaemia is accentuated in these mice (Fig 6.9).

Figure 6.6

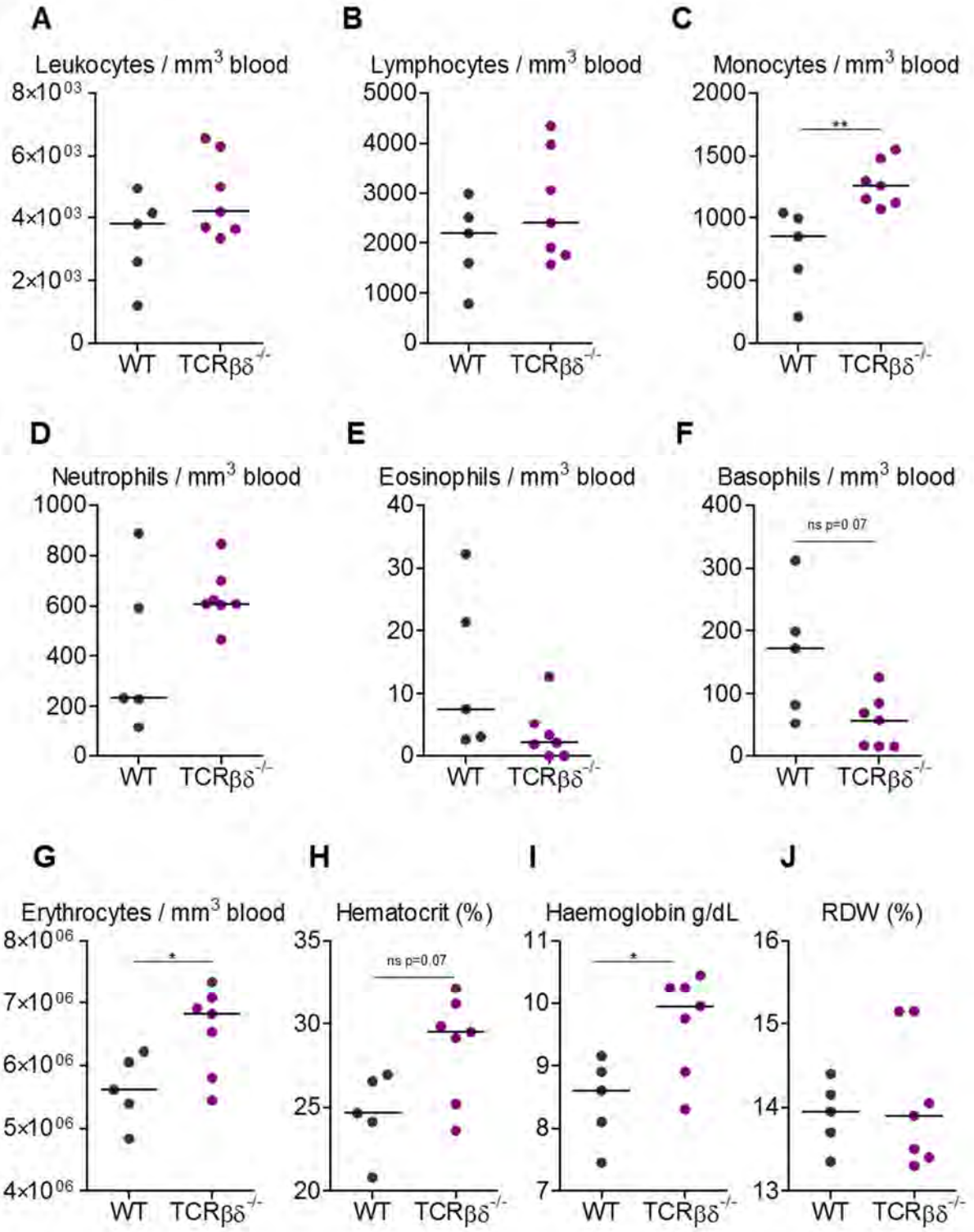

Figure 6.6 Blood monocytes, neutrophils and lymphocytes are elevated in TCRβδ$^{-/-}$ mice
WT and TCRβδ$^{-/-}$ mice were infected (i.p.) with 5 x 10^5 CFU attenuated STm and blood was obtained by cardiac puncture at day 7 post-infection. The following parameters were quantified/measured in the blood: A) total leukocytes, B) lymphocytes, C) monocytes, D) neutrophils, E) eosinophils, F) basophils, G) erythrocytes, H) haematocrit, I) haemoglobin concentration, and J) red cell distribution width (RDW), using a whole blood counter. Data are taken from two experiments where n = 3-5 for each strain of mice in each experiment. *p≤0.05 **p≤0.01 ***p≤0.001.

Figure 6.7

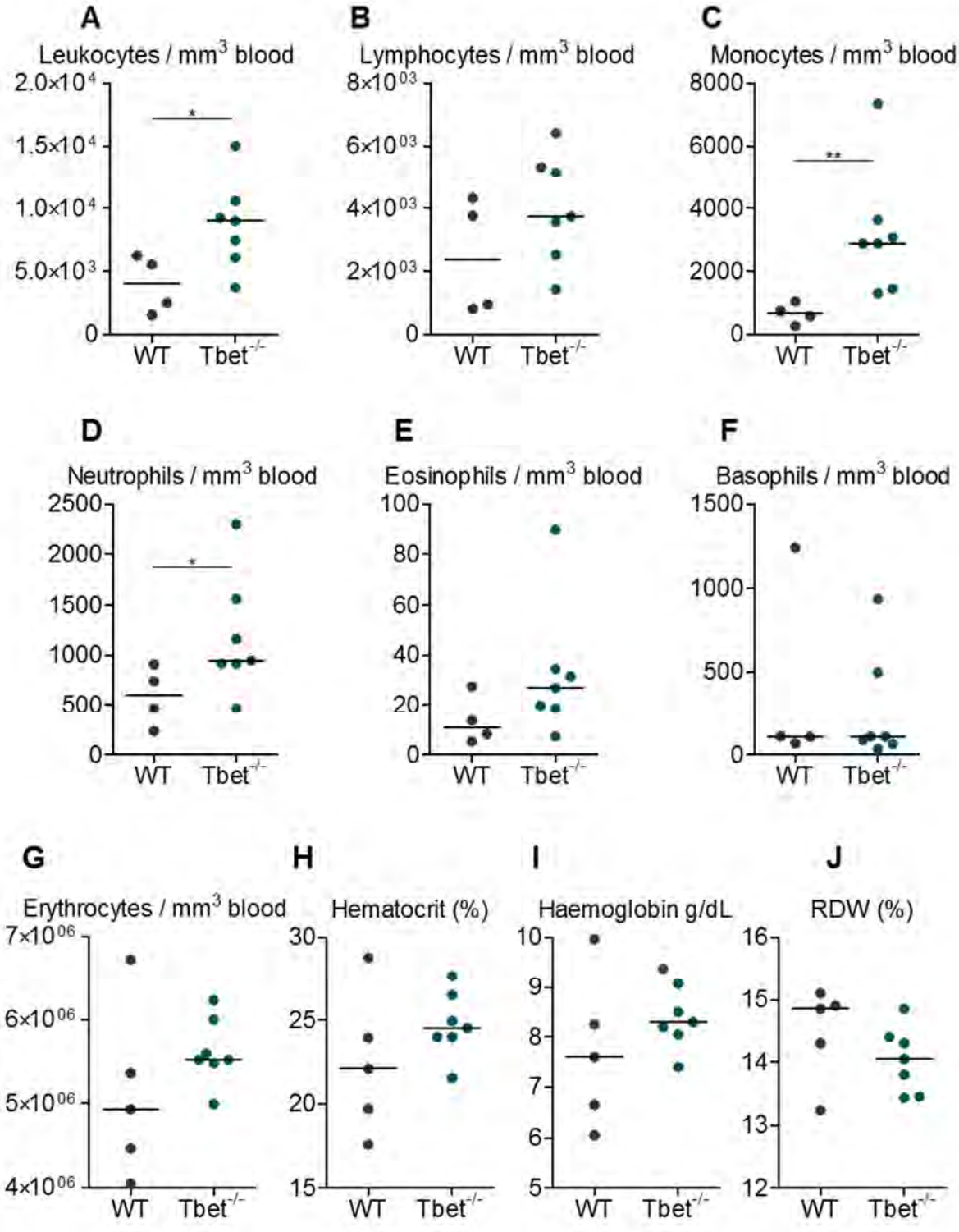

Figure 6.7 Blood leukocytes are elevated in Tbet$^{-/-}$ mice
WT and Tbet $^{-/-}$ mice were infected (i.p.) with 5 x 10^5 CFU attenuated STm and blood was obtained by cardiac puncture at day 7 post-infection. The following parameters were quantified/measured in the blood: A) total leukocytes, B) lymphocytes, C) monocytes, D) neutrophils, E) eosinophils, F) basophils, G) erythrocytes, H) haematocrit, I) haemoglobin concentration, and J) red cell distribution width (RDW), using a whole blood counter. Data are taken from two experiments where n = 3-5 for each strain of mice in each experiment. *p≤0.05 **p≤0.01 ***p≤0.001.

Figure 6.8

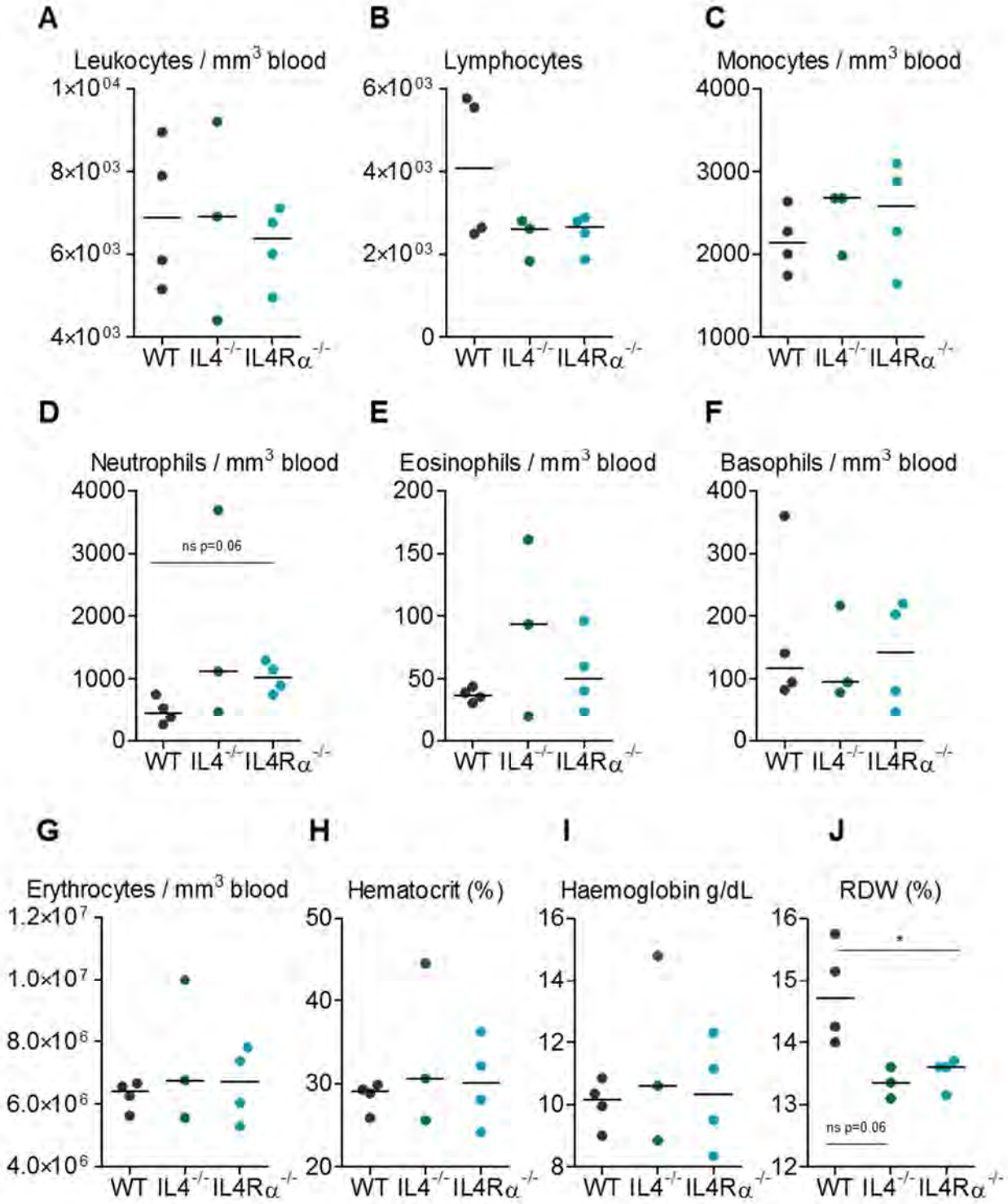

Figure 6.8 Absence of IL4 or IL4Rα has little impact on leukopenia or anaemia during infection

WT, IL4$^{-/-}$ and IL4Rα $^{-/-}$ mice were infected (i.p.) with 5 x 10^5 CFU attenuated STm and blood was obtained by cardiac puncture at day 7 post-infection. The following parameters were quantified/measured in the blood: A) total leukocytes, B) lymphocytes, C) monocytes, D) neutrophils, E) eosinophils, F) basophils, G) erythrocytes, H) haematocrit, I) haemoglobin concentration, and J) red cell distribution width (RDW), using a whole blood counter. Data are taken from one experiment where n = 3-4 for each strain of mice. *p≤0.05 **p≤0.01 ***p≤0.001.

Figure 6.9

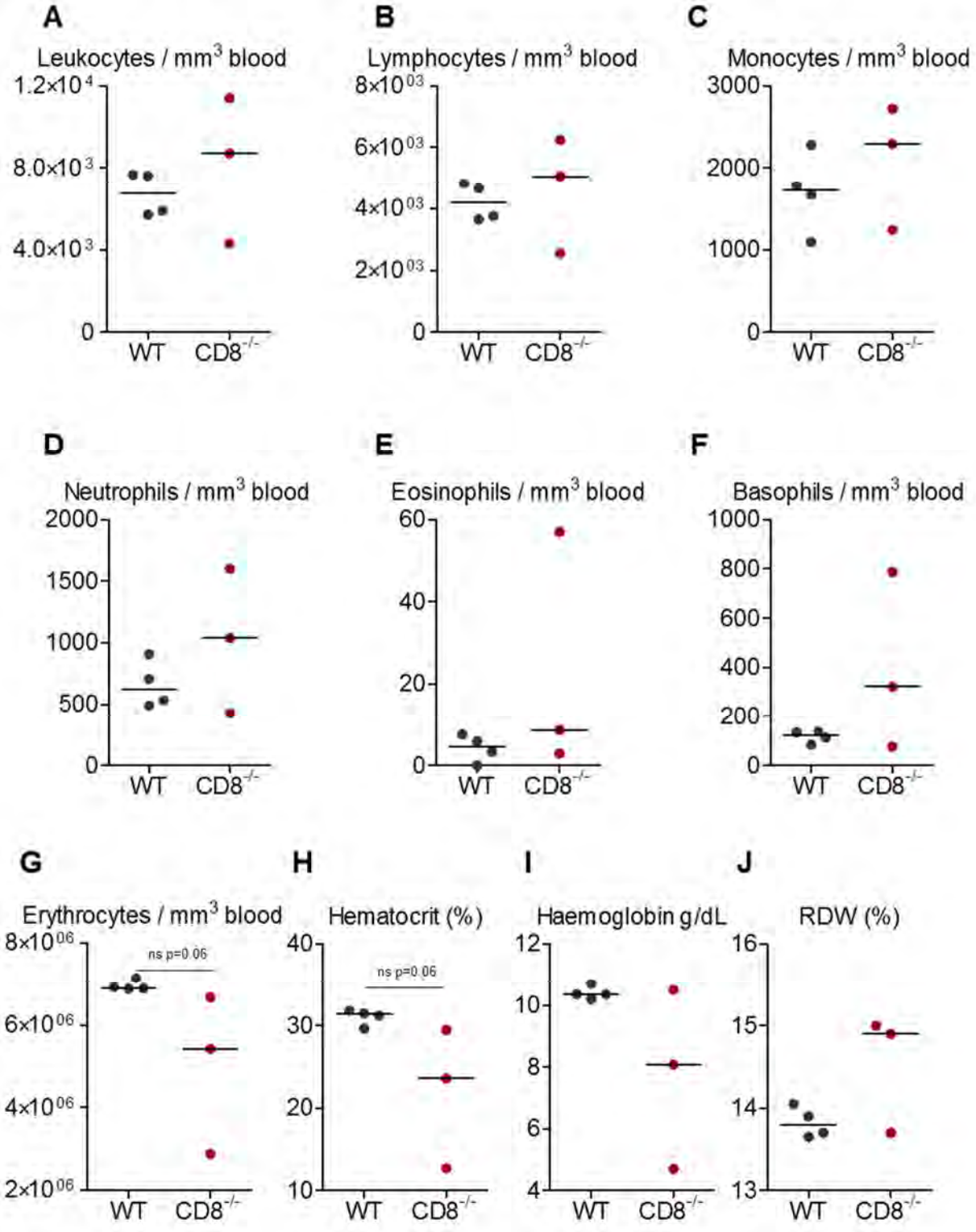

Figure 6.9 Anaemia is more pronounced during infection in the absence of CD8
WT and CD8 $^{-/-}$ mice were infected (i.p.) with 5 x 10^5 CFU attenuated STm and blood was obtained by cardiac puncture at day 7 post-infection. The following parameters were quantified/measured in the blood: A) total leukocytes, B) lymphocytes, C) monocytes, D) neutrophils, E) eosinophils, F) basophils, G) erythrocytes, H) haematocrit, I) haemoglobin concentration, and J) red cell distribution width (RDW), using a whole blood counter. Data are taken from one experiment where n = 4 (WT mice) and n= 3 (CD8 $^{-/-}$ mice). *p≤0.05 **p≤0.01 ***p≤0.001.

Finally, in CD1d-deficient mice, leukopenia is enhanced compared to WT (and this is detected in all cells except basophils), and anaemia is more pronounced, with a significantly increased RDW (Fig 6.10).

6.7 Leukopenia and anaemia are exacerbated by IFNγ and dampened by IL10

Blood cell parameters were assessed in mice lacking IFNγ, TNFαR, IL6 and IL10 to investigate how these inflammatory/anti-inflammatory mediators may affect leukopenia and anaemia. In IFNγ$^{-/-}$ mice, both leukopenia and anaemia are significantly less severe than in WT mice (Fig 6.11). In TNFαR-deficient mice leukocytes are generally similar or slightly elevated relative to WT, and anaemia is also comparable (Fig 6.12). With the exception of neutrophils, all leukocyte subsets in IL6-deficient mice are further decreased in the blood compared to WT, and anaemia is less severe (Fig 6.13). In the absence of anti-inflammatory IL10, neutrophils are increased in the blood, although other leukocyte numbers vary, and anaemia is more pronounced in these mice (Fig 6.14). It must be noted that IL10-deficient mice (and the corresponding WT control group) were infected with a lower dose of *Salmonella* (as these mice are less able to survive the normal dose of 5 x 10^5 organisms), hence WT parameters are not as extensive as they are with a normal bacterial dose.

Figure 6.10

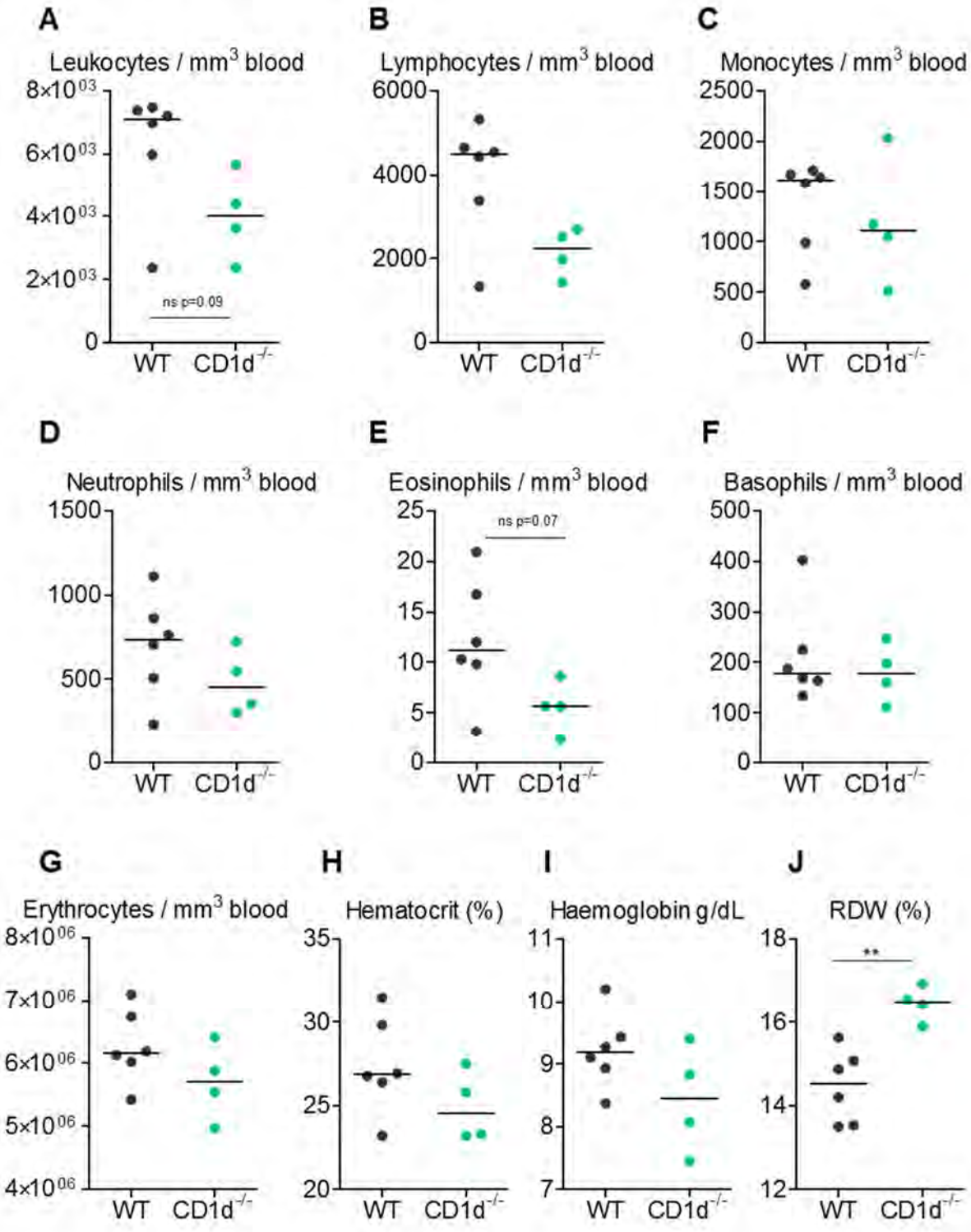

Figure 6.10 Leukopenia is enhanced and anaemia is more pronounced during infection in the absence of CD1d

WT and CD1d $^{-/-}$ mice were infected (i.p.) with 5 x 10^5 CFU attenuated STm and blood was obtained by cardiac puncture at day 7 post-infection. The following parameters were quantified/measured in the blood: A) total leukocytes, B) lymphocytes, C) monocytes, D) neutrophils, E) eosinophils, F) basophils, G) erythrocytes, H) haematocrit, I) haemoglobin concentration, and J) red cell distribution width (RDW), using a whole blood counter. Data are taken from one experiment where n = 6 (WT mice) and n= 4 (CD1d $^{-/-}$ mice). *p≤0.05 **p≤0.01 ***p≤0.001.

Figure 6.11

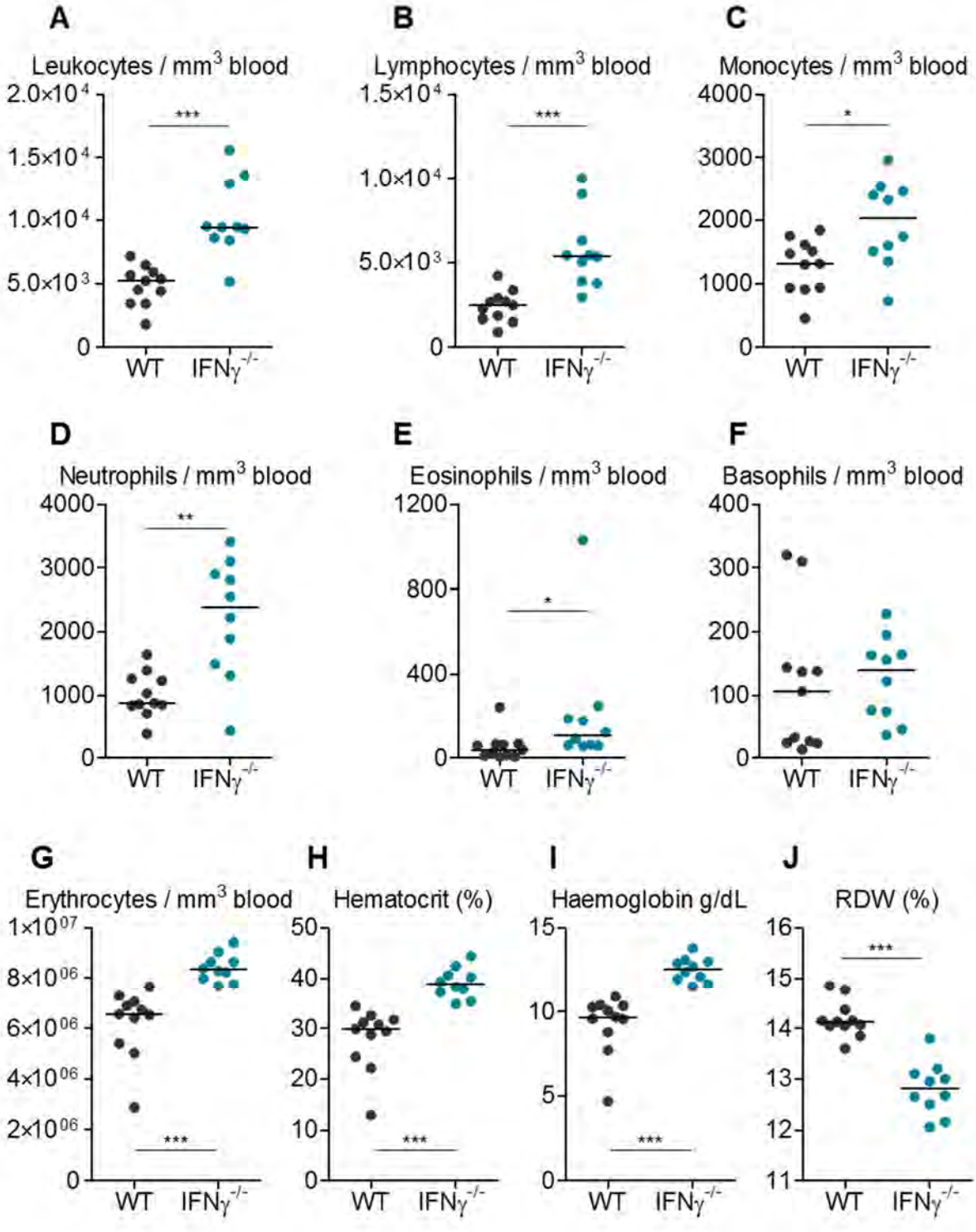

Figure 6.11 Leukopenia and anaemia are less severe during infection in the absence of IFNγ

WT and IFNγ $^{-/-}$ mice were infected (i.p.) with 5 x 10^5 CFU attenuated STm and blood was obtained by cardiac puncture at day 7 post-infection. The following parameters were quantified/measured in the blood: A) total leukocytes, B) lymphocytes, C) monocytes, D) neutrophils, E) eosinophils, F) basophils, G) erythrocytes, H) haematocrit, I) haemoglobin concentration, and J) red cell distribution width (RDW), using a whole blood counter. Data are taken from multiple experiments where n ≥ 3 per mouse strain in each experiment. *p≤0.05 **p≤0.01 ***p≤0.001.

Figure 6.12

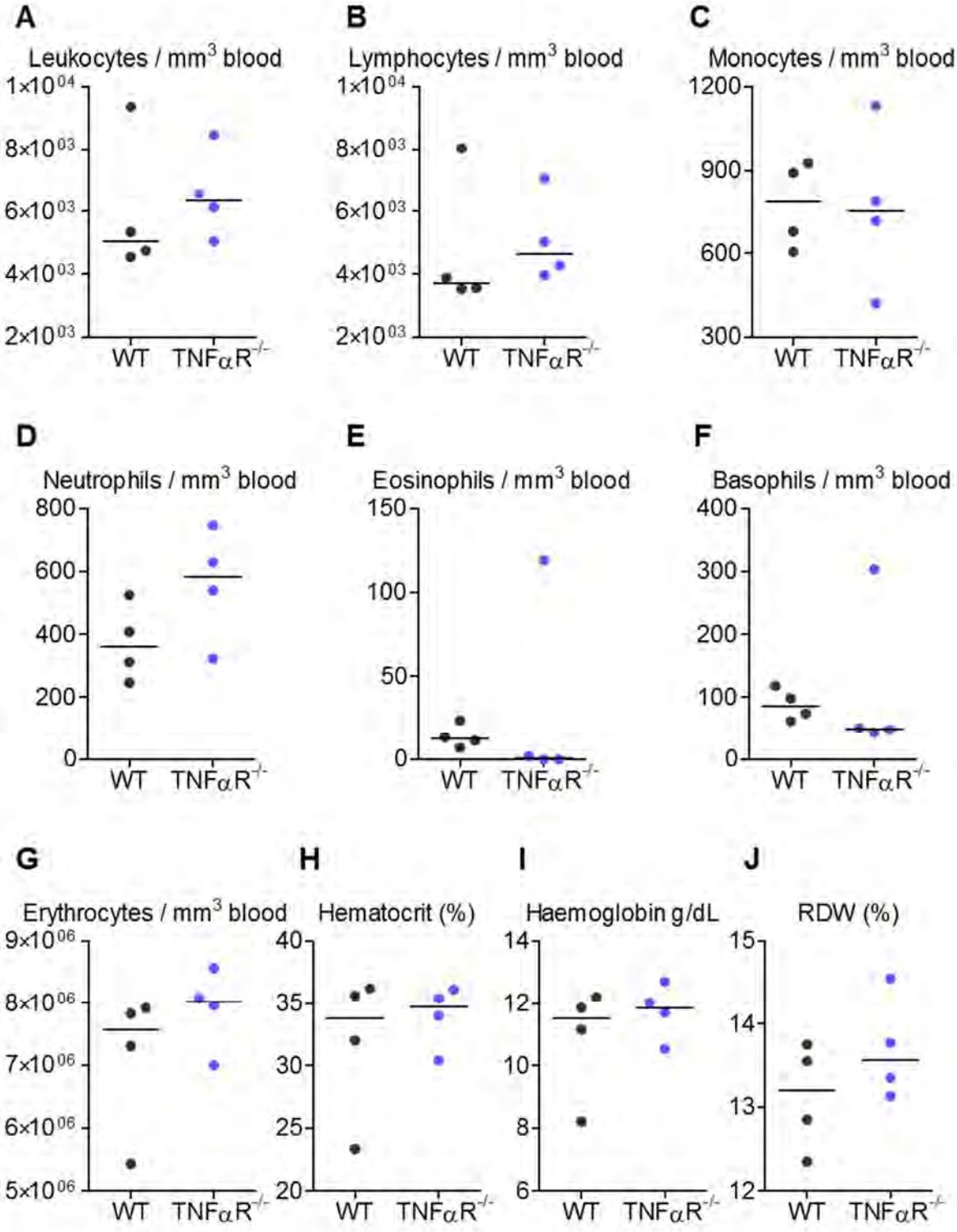

Figure 6.12 Loss of TNFα-Receptor signalling has little impact on leukopenia and anaemia

WT and TNFα $^{-/-}$ mice were infected (i.p.) with 5 x 10^5 CFU attenuated STm and blood was obtained by cardiac puncture at day 7 post-infection. The following parameters were quantified/measured in the blood: A) total leukocytes, B) lymphocytes, C) monocytes, D) neutrophils, E) eosinophils, F) basophils, G) erythrocytes, H) haematocrit, I) haemoglobin concentration, and J) red cell distribution width (RDW), using a whole blood counter. Data are taken from one experiment where n = 4 per mouse strain.

Figure 6.13

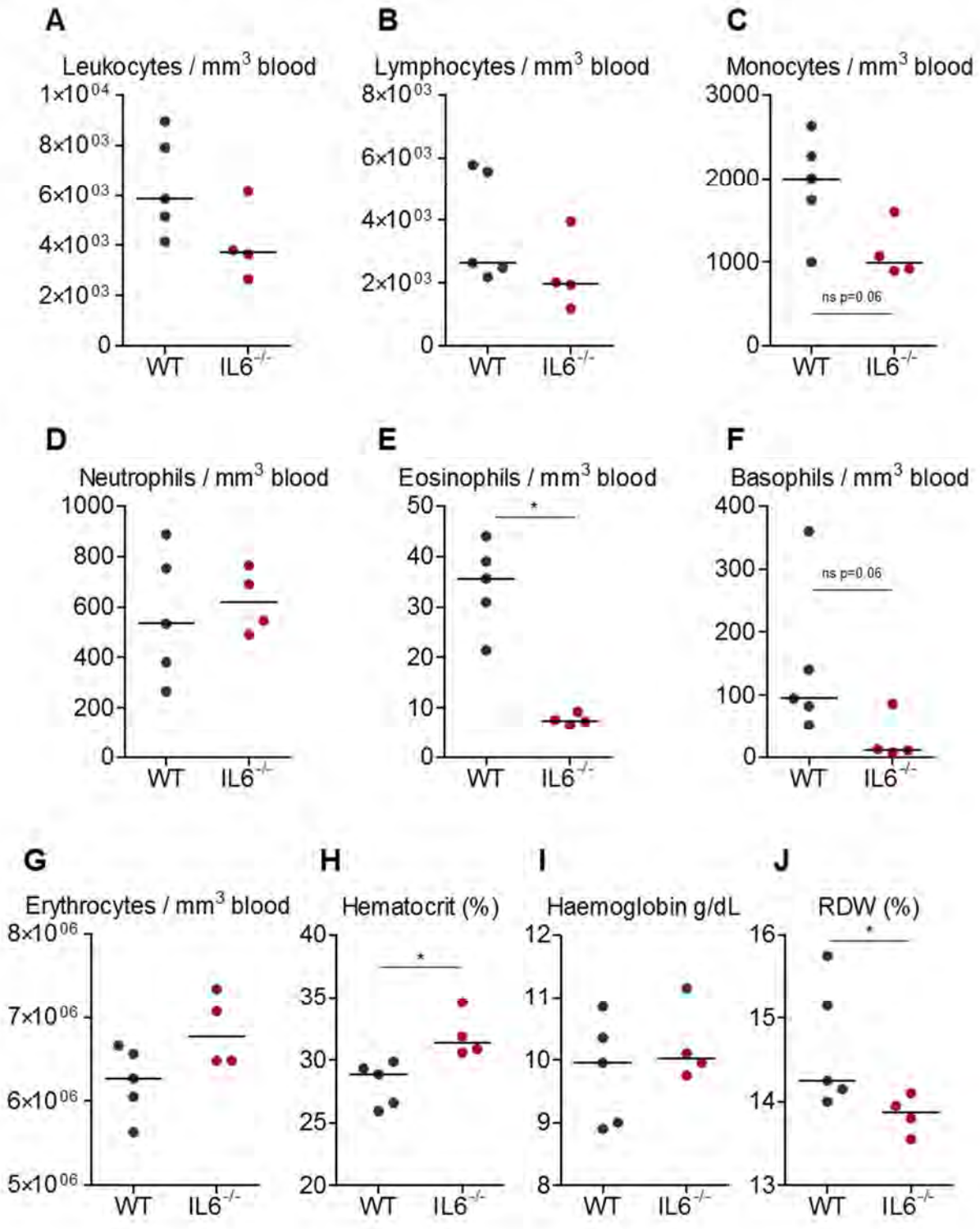

Figure 6.13 Leukopenia is generally more severe in the absence of IL6, whilst anaemia is less pronounced

WT and IL6 $^{-/-}$ mice were infected (i.p.) with 5 x 10^5 CFU attenuated STm and blood was obtained by cardiac puncture at day 7 post-infection. The following parameters were quantified/measured in the blood: A) total leukocytes, B) lymphocytes, C) monocytes, D) neutrophils, E) eosinophils, F) basophils, G) erythrocytes, H) haematocrit, I) haemoglobin concentration, and J) red cell distribution width (RDW), using a whole blood counter. Data are taken from one experiment where n = 4-5 per mouse strain. *p≤0.05 **p≤0.01 ***p≤0.001.

Figure 6.14

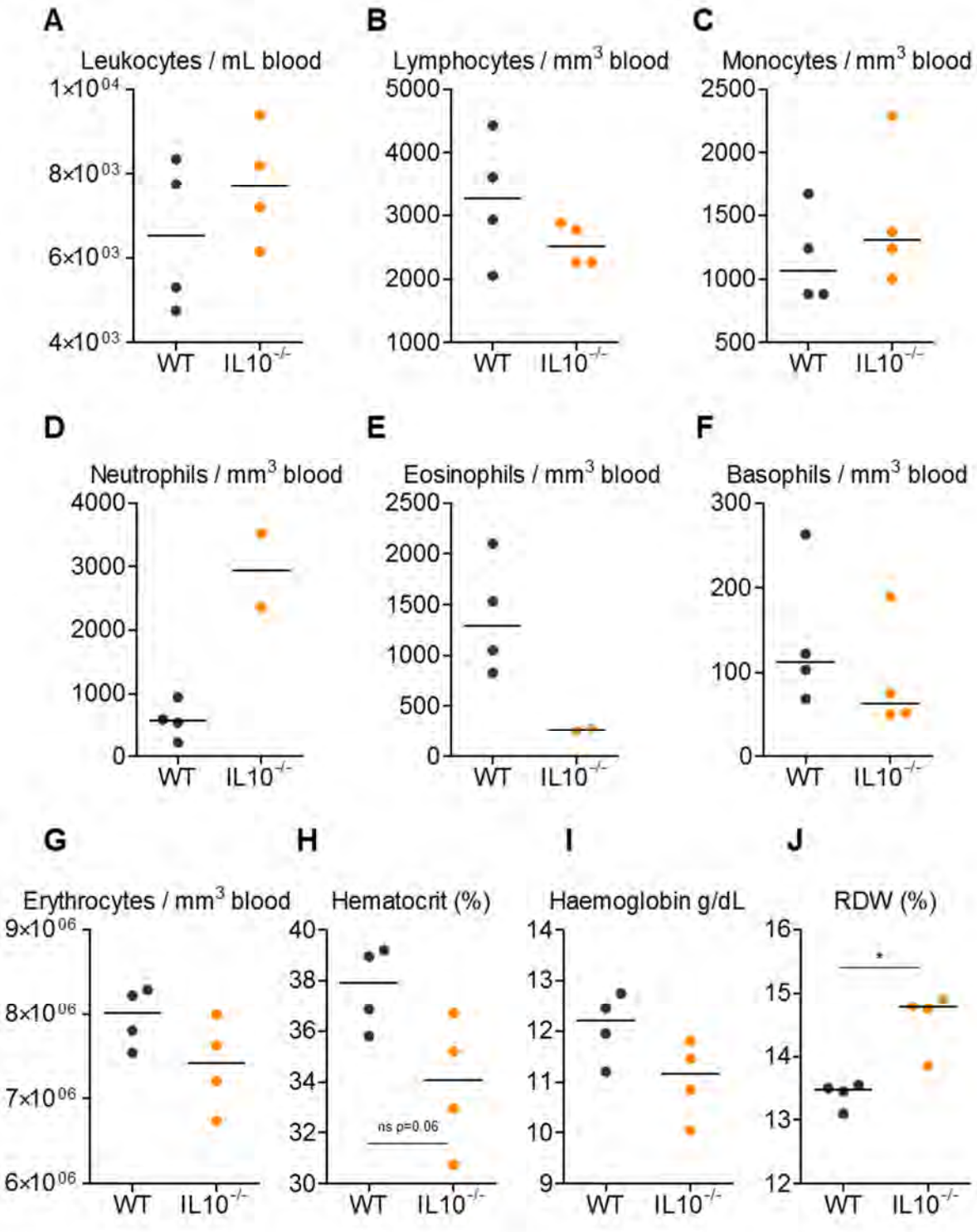

Figure 6.14 Neutrophils are elevated in the blood in the absence of IL10 and anaemia is more pronounced

WT and IL10 $^{-/-}$ mice were infected (i.p.) with 10^5 CFU attenuated STm (a lower than normal dose) and blood was obtained by cardiac puncture at day 7 post-infection. The following parameters were quantified/measured in the blood: A) total leukocytes, B) lymphocytes, C) monocytes, D) neutrophils, E) eosinophils, F) basophils, G) erythrocytes, H) haematocrit, I) haemoglobin concentration, and J) red cell distribution width (RDW), using a whole blood counter. Data are taken from one experiment where n = 4 per mouse strain. *p≤0.05 **p≤0.01 ***p≤0.001.

6.8 Loss of CLEC-2 and treatment with clodronate alter blood cell numbers

Finally, to determine whether there was a connection between leukopenia, anaemia and the inability to develop thrombi due to a lack of CLEC-2 on platelets or a depletion of podoplanin-expressing macrophage cells, we looked in the blood of these mice at day 7 post-infection. In PF4.Cre.CLEC-2$^{fl/fl}$ mice, leukopenia is not as severe as in WT mice (Fig 6.15 A-F). Lymphocyte, monocyte, neutrophil and eosinophil numbers are significantly greater than WT, however, these parameters can be altered in non-infected mice, given the blood-lymphatic mixing (Finney et al., 2012). Severity of anaemia is comparable to WT in these mice (Fig 6.15 G-J). Leukocyte numbers are less severely reduced in clodronate-treated mice relative to PBS-treated mice, and anaemia is generally absent in clodronate-treated mice (Fig 6.16).

Figure 6.15

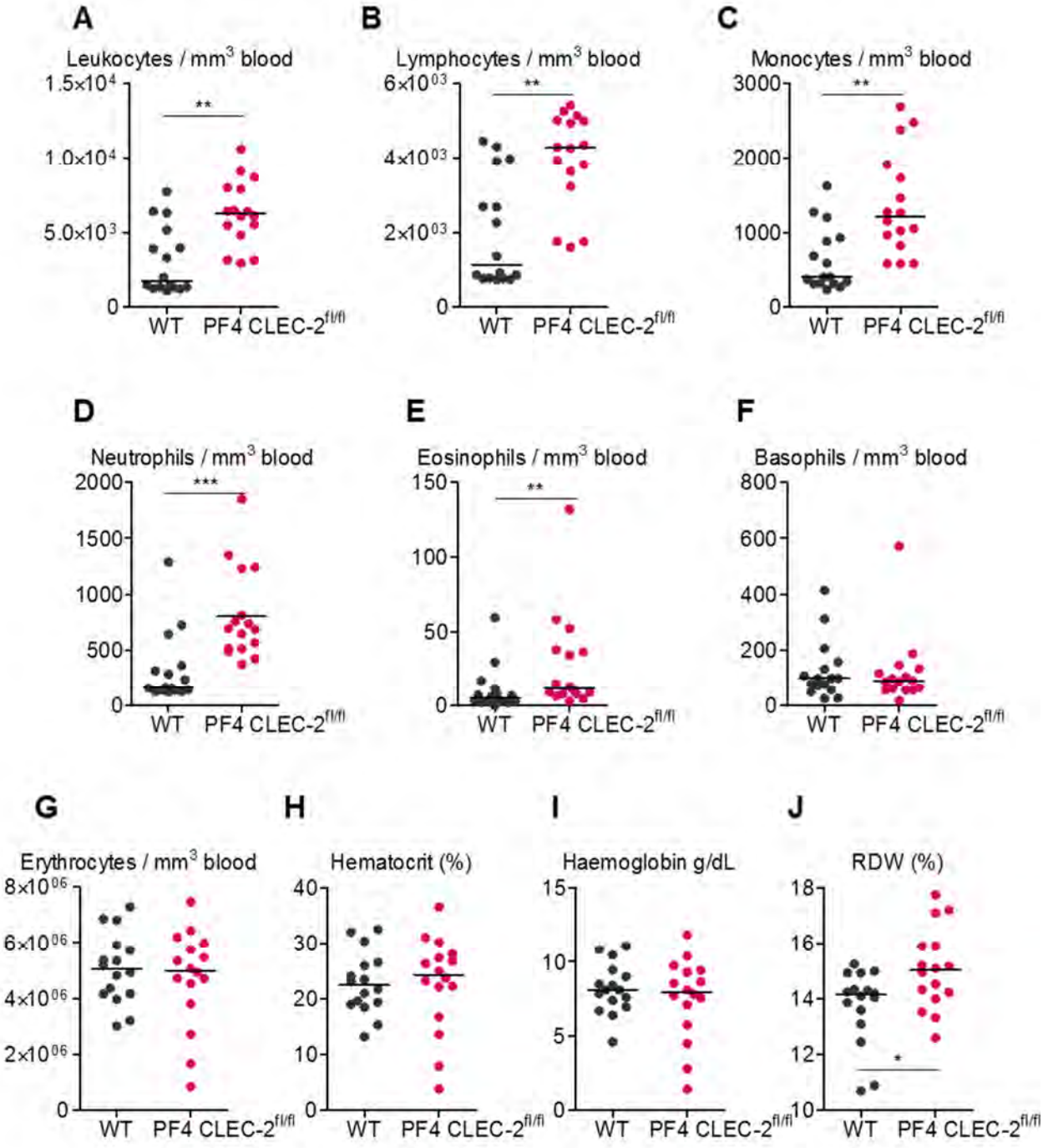

Figure 6.15 During infection, leukopenia is not as severe in PF4.Cre.CLEC-2$^{fl/fl}$ mice
WT and PF4.Cre.CLEC-2$^{fl/fl}$ mice were infected (i.p.) with 5 x 10^5 CFU attenuated STm and blood was obtained by cardiac puncture at day 7 post-infection. The following parameters were quantified/measured in the blood: A) total leukocytes, B) lymphocytes, C) monocytes, D) neutrophils, E) eosinophils, F) basophils, G) erythrocytes, H) haematocrit, I) haemoglobin concentration, and J) red cell distribution width (RDW), using a whole blood counter. Data are taken from multiple experiments where n ≥ 3 per mouse strain in each experiment. On histograms, PF4.Cre.CLEC-2$^{fl/fl}$ mice are written PF4 CLEC-2$^{fl/fl}$. *p≤0.05 **p≤0.01 ***p≤0.001.

Figure 6.16

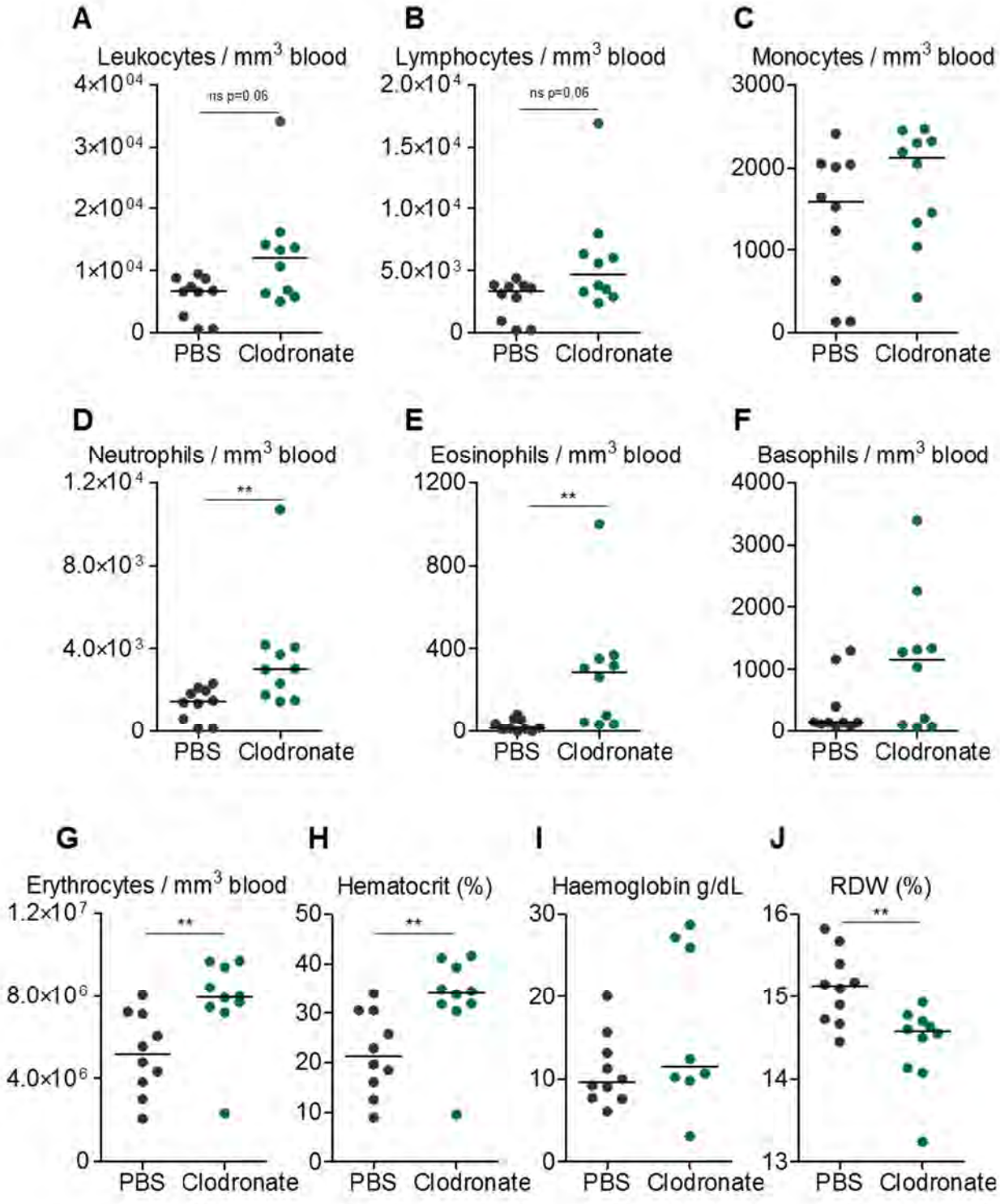

Figure 6.16 Anaemia is generally absent during infection in clodronate-treated mice
WT mice were treated (i.p.) with Clodronate or PBS liposomes 24 hours prior to infection (i.p.) with 5 x 10^5 CFU attenuated STm. Clodronate treatment was repeated every 2-3 days throughout infection to maintain cell depletion. At day 7 post-infection, blood was obtained by cardiac puncture and the following parameters were quantified/measured in the blood: A) total leukocytes, B) lymphocytes, C) monocytes, D) neutrophils, E) eosinophils, F) basophils, G) erythrocytes, H) haematocrit, I) haemoglobin concentration, and J) red cell distribution width (RDW), using a whole blood counter. Data are taken from two experiments where n = 5 per treatment group in each experiment. *p≤0.05 **p≤0.01 ***p≤0.001.

6.9 Discussion

Here we describe the leukopenia and anaemia detected in the blood during systemic STm infection.

6.9.1 Leukopenia is primarily due to reduction in circulating lymphocytes

Leukopenia is most pronounced at day 21 post-infection, and resolves during the following weeks, thus the most severe leukopenia corresponds with the most extensive leukocyte infiltration in the liver. Reduced lymphocyte numbers account for most of the detected leukopenia, whereas myeloid cells, especially monocytes can increase in the blood, especially early after infection. Bacteraemia is only transient in this infection and is absent by day 14. Increased innate cells in the blood early post-infection may reflect differential activities in the bone marrow (E. Ross, personal communication) or innate immune control of bacterial persistence in the blood (Gondwe et al., 2010). The reduced lymphocyte frequency in the blood during infection is likely to be explained by the redistribution of these cells to lymphoid organs and to effector sites including the liver, especially as this has been shown to occur rapidly after infection (Ross et al., 2012, Cunningham et al., 2007). In addition, whilst STm colonises primary lymphoid sites, previous studies have indicated that lymphocyte output of these tissues is not markedly diminished (Ross et al., 2012). Haematopoiesis in the spleen may further contribute to lymphocyte production (Jackson et al., 2010). Furthermore, the expansion of haematopoietic stem cells during infection has been recently described, although not in the context of *Salmonella* infection (Scumpia et al., 2010). Thus lymphopenia is probably more due to a redistribution of lymphocytes than a reduction in production, or in the destruction of these cells during infection.

6.9.2 Circulating myeloid cells accumulate in the absence of lymphocytes

Leukopenia differed between strains of genetically modified mice, indicating the influence of specific leukocyte subtypes/molecular mediators in individual features of leukopenia. Furthermore, the assays used in this chapter just looked at the cell type and did not subset cells further based on differential expression of phenotypic markers. In addition, our data provides no indication as to the extent of differentiation of individual cell types and therefore their ability to contribute to the host response. If a large proportion of leukocytes produced are actually immature blasts, it may influence their functionality (Ceredig et al., 2009, Cunnington et al., 2012). Despite a lack of lymphocytes in Rag-$1^{-/-}$ mice, total leukocyte numbers are equivalent to WT mice due to elevated numbers of innate cells in the blood of Rag-$1^{-/-}$ mice. These data could suggest lymphocytes play a role in regulating innate cell numbers in the blood, such as directing innate cells into tissues and thus preventing their accumulation in the circulation (Kaufmann, 1993).

When leukopenia was measured in mice lacking either B cells or T cells specifically, we detect an accumulation in the respective other type of lymphocyte (if B cells are absent we see elevated T lymphocytes in the blood, and vice versa). The enhanced numbers of myeloid cells in the circulation in both T cell-deficient and B cell-deficient mice suggests that production or mobility of myeloid cells may be altered when one or more lymphocyte subset is absent. In addition, leukopenia is increased in the absence of iNKT cells. Considering we also detect decreased leukocytes in the liver at day 7 in CD1$d^{-/-}$ mice, it suggests a distinct phenotype is induced in the absence of iNKT cells, which should be suitably explored in the future (Emoto and Emoto, 2009).

6.9.3 Leukopenia is absent in IFNγ-deficient but not TNFαR-deficient mice

We showed in Chapter 5 that mice lacking components of the IFNγ and TNFα inflammatory cytokine signalling pathways do not develop thrombosis in the liver and that thrombocytopenia is either totally absent or significantly reduced in these mice. Here we show an absence of leukopenia in IFNγ$^{-/-}$ mice relative to WT at day 7, whereby total leukocytes in the blood are more similar to those in non-infected mice. In IFNγ-deficient mice, there is very little inflammation in the liver post-infection, so it is not surprising that leukopenia in the blood is also absent. This observation supports the inflammatory role of IFNγ during infection.

However, in TNFαR$^{-/-}$ mice, the extent of leukopenia at day 7 is similar to that in infected WT mice. Hepatic inflammation is observed to a similar extent to WT mice by histology, although numbers of innate cells which accumulate in the liver are reduced relative to WT by flow analysis. Therefore, it is likely the leukopenia we detect in TNFαR$^{-/-}$ mice is associated with leukocyte infiltration into the liver and other sites at this time. However, in the absence of IL10, there are increased numbers of neutrophils in the blood. This may be explained by elevated IFNγ which is associated with these mice (Pie et al., 1997, Gazzinelli et al., 1996), and is likely to contribute to the extensive hepatic thrombosis and enhanced hepatic infiltration we observe. These data indicate that circulating leukocyte numbers do not always reflect the extent of tissue infiltration.

6.9.4 Anaemia

Multiple features of anaemia are observed during infection, including reduced erythrocyte count, haemoglobin concentration and haematocrit. These phenotypes peak in severity at day 21 and are generally resolved by day 50. This time-frame is significant as erythrocytes

survive for 3-4 months (Horky et al., 1978). Thus the kinetics of anaemia onset and resolution parallel those of leukopenia, thrombocytopenia, thrombosis and inflammatory lesion development. The red cell distribution width (RDW) provides a measure of the range in size of red cells produced in erythropoiesis and an increase in this parameter can indicate accelerated generation of new cells (Brown et al., 2010, Kurtzhals et al., 1997). Therefore our data suggest that red cell production is increased at days 7 and 21 and that this actually persists throughout the 50 days examined. However, altered RDW may also indicate variation in erythrocyte output due to the shunt of erythropoiesis to the spleen during infection (Jackson et al., 2010). Despite increased RDW, erythrocyte numbers are reduced in the blood, implying that production cannot always match utilisation/consumption. The maintenance of a heightened RDW throughout infection implicates a lasting effect of infection on erythrocytes.

Whilst mean corpuscular volume oscillates, it remains generally constant which indicates the anaemia is normocytic. Therefore, the reduced haematocrit and haemoglobin concentration is likely to not be a consequence of reduced capacity for erythrocytes to carry haemoglobin. Rather, (and as erythrocyte numbers indicate), the reduction in haematocrit and haemoglobin is probably caused by reduced cell counts. This suggests that the quality of erythrocytes produced is maintained: the generated cells are functional. These data all indicate either consumption/usage of erythrocytes which cannot be matched by the production of new cells. So what happens to erythrocytes during *Salmonella* infection? Erythropoiesis occurs in the spleen during STm infection, and potentially, erythrocytes may not leave the spleen efficiently following production, accounting for both reduced blood erythrocyte counts and splenomegaly (Jackson et al., 2010).

An alternative (or additional) explanation for reduced erythrocyte counts is the destruction of these cells during infection. Haemolytic anaemia is a common feature of malaria and could also explain the increased RDW detected when anaemia is most pronounced (Mabey et al., 1987). In addition, haemophagocytosis, the removal of erythrocytes (and other blood cells) by phagocytic cells, is well documented in typhoid fever (Mallouh and Sa'di, 1987, Mallory, 1898, Serefhanoglu et al., 2003, Fame et al., 1986, Veerakul et al., 2002). Either or both of these events could account for the observed phenotypes during STm infection (Nix et al., 2007). It is likely that bone marrow smears or further examination of the spleen will be required for detection of haemophagocytosis because these cells have been specifically reported in these sites in the past (Brown et al., 2010, Singh et al., 2005). Other groups have detected haemophagocytosis in the liver but we have not yet looked for this in our infection model (C. Detweiler, personal communication).

6.9.4.1 Differential regulation of anaemia by lymphocyte populations

Interestingly, despite an anaemia of equivalent extent to WT being measured in Rag-1-deficint mice, severity of anaemia differs when either T or B cells alone are absent. In mice lacking B cells, anaemia is more severe than WT, yet when T cells are absent, anaemia is less severe than WT. These data may indicate either a role for B cells in erythrocyte homeostasis, or the presence of T cells may promote development of anaemia. Considering the dampening in leukopenia and hepatic infiltration in the absence of T cells, it seems likely that anaemia is less pronounced in these mice in correlation with reduced inflammation. This would suggest the extent of anaemia parallels T cell-driven inflammation. Interestingly, on examination of anaemia in mice deficient in specific T cell subsets, we identified that in fact anaemia in Tbet mice is less extensive than WT and in

IL4$^{-/-}$ and IL4Rα$^{-/-}$ mice is equivalent to WT. Thus the dampened anaemia detected in total T cell-deficient mice is accountable to lack of Tbet. The absence of anaemia in IFNγ$^{-/-}$ mice indicates the necessity for inflammation in anaemia, which is supported by the accentuated anaemic features of IL10-deficient mice.

6.9.4.2 A role for clodronate-susceptible cells in erythrocyte phagocytosis?

The absence of anaemia in clodronate-treated mice would suggest that the inflammatory cells removed during treatment are required for anaemia development. Therefore this may indicate that these phagocytic cells play a role in erythrocyte destruction, probably due to their phagocytic capabilities. This is a really important observation as it identifies a potential haemophagocytosis phenotype in our infection model which is in line with previous reports both in mice and humans (Brown et al., 2010, Mallory, 1898). Thus our data would suggest that T cells drive expansion and accumulation of innate inflammatory cells which phagocytose erythrocytes during infection, resulting in anaemia. Whilst erythrocyte production shunts to the spleen, this is largely unable to prevent anaemia.

Haemophagocytosis has been reported in both mouse and human NTS infections, and is a known clinical feature of typhoid fever (Mallory, 1898, Brown et al., 2010, Nix et al., 2007). Moreover, murine typhoid fever has been described as a model of hemophagocytic lymphiohistocytosis (HLH), an inflammatory syndrome which occurs in response to infection, characterised by over-activation of macrophages and T cells (Brown et al., 2010). Murine studies into haemophagocytosis during STm infection have been largely performed in mice strains which are not Nramp-susceptible (Brown et al., 2010). However, murine studies resembling human systemic NTS infections are largely undertaken in Nramp-susceptible strains because of the likeness to the human infection (Monack et al., 2004a).

It is unclear in the literature the extent to which haemophagocytosis occurs in these mouse strains; the increased inflammation and cell death seen in Nramp-susceptible strains may camouflage haemophagocytosis (Nix et al., 2007). Therefore, it will be important to visualise these cells in future studies to confirm our observation histologically; bone marrow smears may be informative (C. Detweiler, personal communication).

6.9.5 Outlook: towards human NTS infection

Whilst we have identified that inflammation and potentially haemophagocytosis contribute to anaemia development during STm infection in mice, it is likely that these phenotypes will be complicated further in human NTS infections in sub-Saharan Africa. In the natural environment, additional co-infections such as malaria and fundamental problems including malnourishment are likely to play a role in host haemostasis, even in the absence of NTS infection (Graham et al., 2000b). Thus whilst we observe anaemia as a consequence of infection, in humans, anaemia is likely to be an underlying condition prevalent in malnourished children and frequently associated with malaria (Graham et al., 2000a, Cunnington et al., 2012). In addition, whilst anaemia is common in systemic NTS infections in children in tropical Africa, and this can worsen the prognosis of bacterial infection, the condition has not been associated with cause of death (Graham et al., 2000a, Calis et al., 2008).

CHAPTER 7:

FINAL DISCUSSION

7.1 Host response to systemic infection involves multiple systems

Systemic bacterial infections such as those caused by NTS require rapid and coordinated host responses to able to efficient control of bacterial replication and ultimately clear infection (Jones and Falkow, 1996, Mittrucker and Kaufmann, 2000). Whilst innate and adaptive immune mechanisms are essential in both pathogen recognition and active pathogen removal, they are not the only host systems at play. Inflammation and the directed infiltration of leukocytes into tissues is a prominent feature during immune responses to pathogen invasion. This system facilitates the proliferation of appropriate cells and their recruitment to the site of injury (Tam et al., 2008, Johansson et al., 2006, Wick, 2007). Many of the mediators which enable a co-ordinated inflammatory response are also sensitive and responsive to other host defence systems, including the coagulation system (Esmon, 2005, Esmon, 2004, Levi et al., 2004).

Coagulation is one aspect of the haemostatic system, a tightly regulated host response which helps to prevent excessive blood loss at sites of injury, maintains blood vessel integrity, and recently has been shown to influence inflammation (Esmon, 2005). Platelets, the corpuscular cells which facilitate fibrin clot formation during vessel injury, are key to the interplay the coagulation and inflammation systems (Jenne et al., 2013, Fitzgerald et al., 2006a). Platelets are increasingly recognised as mediators of innate immunity for multiple reasons, including their expression of TLRs, their antimicrobial contents of α-granules and their ability to respond to inflammatory stimuli and influence the recruitment

and activity of innate immune cells (Semple et al., 2011, Kerrigan and Cox, 2010). However, in recent years, it has become apparent that platelets may also be vital in the facilitation of adaptive lymphocyte activation and the establishment of cell-mediated host responses, in line with other cells of the innate system (Yeaman, 2010). A particularly exciting example of this, especially in relation to the work discussed here, is the interaction between platelets and Kupffer cells in the liver described by the group of Paul Kubes (Wong et al., 2013). This, and the evident contribution of platelets in a variety of host responses, including that against cancer, make these cells particularly exciting mediators of host responses, and in particular in regard to communication between the components of these multiple host systems (Boulaftali et al., 2013, Honn et al., 1992, Lowe et al., 2012).

7.2 Inflammation drives lesion development and thrombosis in the liver

Here we have demonstrated the bacterial colonisation of the liver during *Salmonella* infection and have characterised leukocyte infiltration and formation of inflammatory lesions in the hepatic parenchymal tissue. We have extensively explored the thrombosis phenotype which has been previously observed during *Salmonella* infections, but has not been directly attributed to the host response against infection (Mastroeni et al., 1995). By determining the mechanism of thrombus development and identifying the molecular components required for this phenotype, we have been able to describe this inflammatory feature as an active host response to infection. Therefore, the most significant outcome of this study is the recognition that the development of inflammatory lesions and thrombosis in the liver are both part of the host inflammatory response to infection and thus share regulation. These findings are briefly summarised in Figures 7.1 and 7.2 below.

Figure 7.1

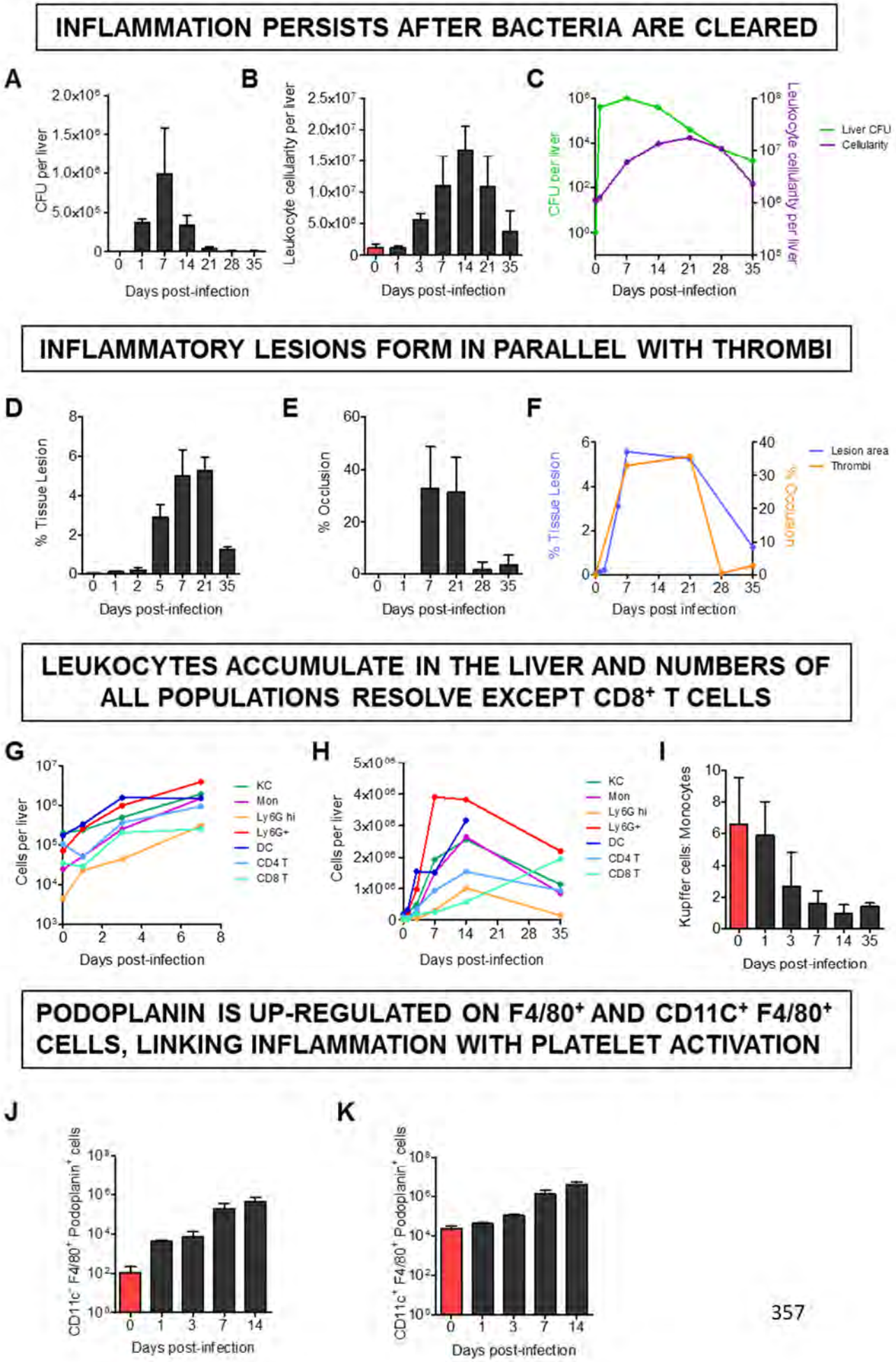
INFLAMMATION PERSISTS AFTER BACTERIA ARE CLEARED
A
CFU per liver
Days post-infection
B
Leukocyte cellularity per liver
Days post-infection
C
CFU per liver
Leukocyte cellularity per liver
Liver CFU
Cellularity
Days post-infection
INFLAMMATORY LESIONS FORM IN PARALLEL WITH THROMBI
D
% Tissue Lesion
Days post-infection
E
% Occlusion
Days post-infection
F
% Tissue Lesion
% Occlusion
Lesion area
Thrombi
Days post infection
LEUKOCYTES ACCUMULATE IN THE LIVER AND NUMBERS OF ALL POPULATIONS RESOLVE EXCEPT CD8+ T CELLS
G
Cells per liver
KC
Mon
Ly6G hi
Ly6G+
DC
CD4 T
CD8 T
Days post-infection
H
Cells per liver
KC
Mon
Ly6G hi
Ly6G+
DC
CD4 T
CD8 T
Days post-infection
I
Kupffer cells: Monocytes
Days post-infection
PODOPLANIN IS UP-REGULATED ON F4/80+ AND CD11C+ F4/80+ CELLS, LINKING INFLAMMATION WITH PLATELET ACTIVATION
J
CD11c- F4/80+ Podoplanin+ cells
Days post-infection
K
CD11c+ F4/80+ Podoplanin+ cells
Days post-infection

Figure 7.1 Key findings from this study regarding hepatic inflammation and its association with thrombosis

WT mice were infected (i.p.) with 5 x 10^5 CFU attenuated STm. A) Bacterial burden of the liver throughout infection. B) Leukocytes were isolated from the livers of non-infected and infected mice by collagenase digestion and gradient centrifugation. The total number of leukocytes retrieved from the liver was calculated at the indicated time-points post-infection. Data are taken from 3 experiments with similar results. C) The relationship between bacterial burden and leukocyte cellularity in the liver. D) The percentage of total liver area which is occupied by inflammatory lesions was measured using point counting. Counts were taken from one experiment where n = 3-4 at each time-point. E) At key time-points post-infection, thrombus formation was examined on frozen liver sections by H&E. The extent of thrombosis was quantified by point counting the percentage of occlusion of all large vessels per tissue section, and counts are expressed as a percentage. Data are taken from multiple experiments with similar results, where n > 4 at each time-point. F) The relationship between tissue area occupied by lesions and the percentage of vessel occlusion. G) Leukocytes isolated from the livers of infected mice were phenotyped by flow cytometry. All cell types studied increase in absolute number during days 0-7 of infection and H) this inflammation resolves during the following weeks with the exception of $CD8^+$ T cells. I) The ratio of Kupffer cells to monocytes during infection. Cells retrieved in the leukocyte fraction of the gradient which were I) $CD11c^-$ $F4/80^+$ or J) $CD11c^+$ $F4/80^+$ were further examined by flow cytometry for podoplanin expression. Absolute numbers of cells are shown. Data in G-J are taken from one experiment where n = 3-6 at each time-point (with the exception of day 7, which includes data from two separate experiments).

Figure 7.2 Inflammation in the liver during *Salmonella* Typhiumurium infection

A summary time-line of the events which occur in the liver following systemic i.p. infection with 5 x 10^5 CFU *Salmonella* Typhimurium. Histological observations are presented in blue, podoplanin expression is detailed in green, and the vasculature is referred to in red.

Figure 7.2

SALMONELLA TYPHIMURIUM INFECTION IN THE LIVER

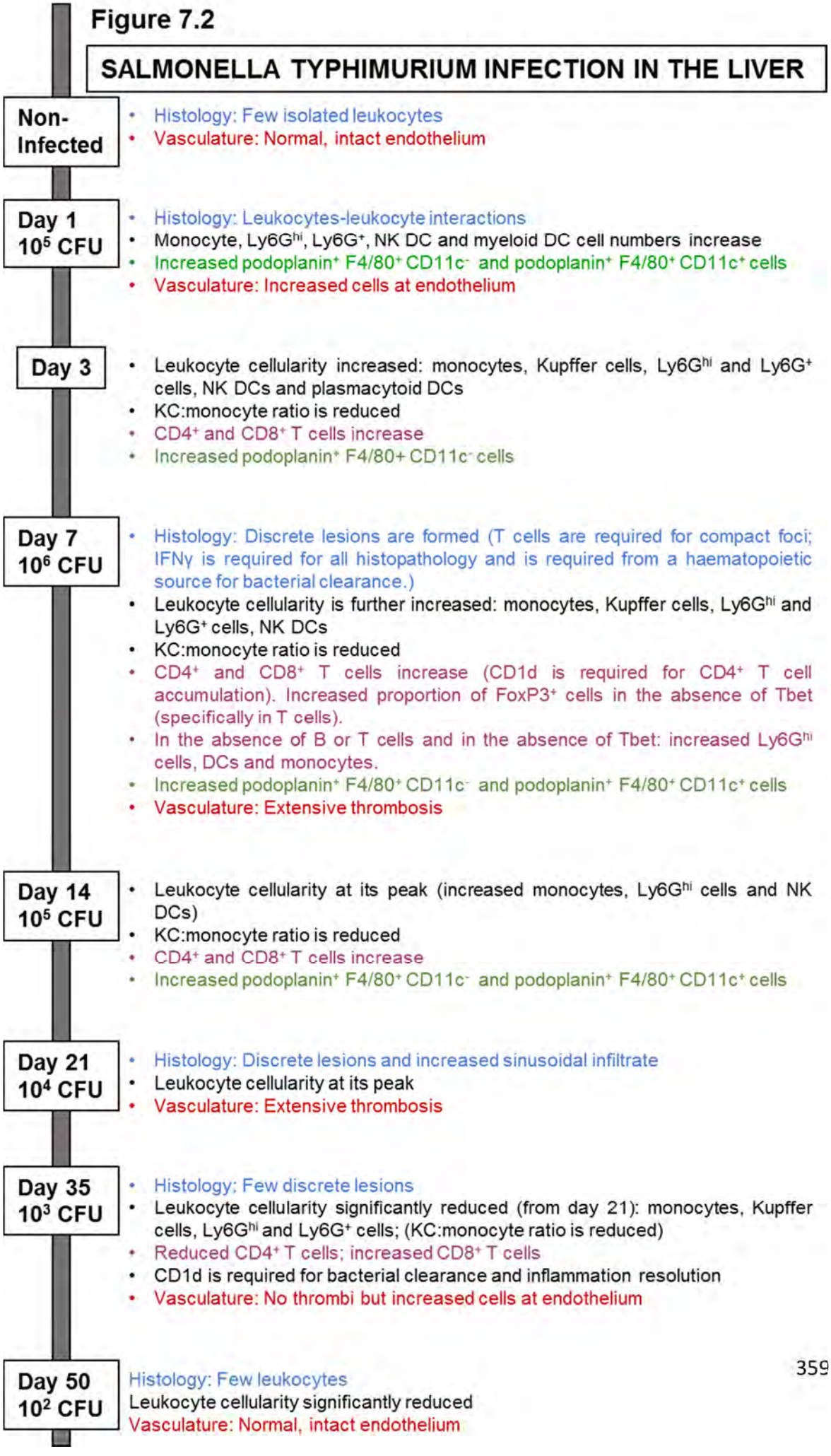

7.3 Inflammatory interferon-γ is required for podoplanin up-regulation during infection

Both leukocyte infiltration into the liver and the formation of thrombi in the liver vasculature require signalling by the inflammatory cytokine IFNγ. We have shown that IFNγ from both haematopoietic and non-haematopoietic sources is necessary in the recruitment of differential leukocyte populations into the liver and that haematopoietic IFNγ is required for the organised formation of lesions. One aspect of this infiltration which directly contributes to the formation of thrombi in the liver is the up-regulation of podoplanin expression, which is evident both on myeloid populations (in particular $CD11c^+$ $F4/80^+$ cells and $CD11c^-$ $F4/80^+$ cells) and on non-haematopoietic cells. Whilst podoplanin expression is necessary for platelet activation via platelet-expressed CLEC-2 (and our demonstration of this in thrombosis is novel), podoplanin likely also coordinates multiple aspects of cellular infiltrate organisation within the liver and in other sites (Astarita et al., 2012). Thus inflammatory podoplanin expression provides a shared molecular anchor between the immune response and platelet activation.

Whilst these inflammatory phenotypes are initiated by the presence of bacteria, which drives the initial inflammatory signals, both phenotypes persist once bacterial loads are resolving, indicating that maintenance of inflammation is not dependant on high bacterial numbers. Furthermore, the absence of any inflammatory phenotype in IFNγ-deficient mice, which harbour significantly higher bacterial loads in the liver relative to WT mice, further supports the inflammatory nature of these phenotypes.

7.4 Thrombocytopenia may be differentially regulated to thrombosis

In addition to hepatic inflammation and thrombus development, we observe severe thrombocytopenia, the extent of which parallels severity of liver thrombosis. Thus, it initially appeared that the relationship between these two platelet phenotypes is that thrombocytopenia is a consequence of thrombosis. This is demonstrated by the absence of thrombocytopenia in the absence of thrombosis (as seen in IFNγ-deficient mice) and the augmentation of thrombocytopenia when thrombosis is more severe (as in IL10-deficient mice).

However, liver thrombosis and thrombocytopenia do not always share this balance, suggesting that thrombocytopenia is not always a direct consequence of platelet consumption in the liver. Mice which lack CLEC-2 expression on platelets do not form thrombosis to nearly the same extent as is seen in WT mice. Yet these mice present a similar thrombocytopenia to that in CLEC-2-sufficient mice, so platelet loss is not directly explained by hepatic thrombosis. Furthermore, the absence of thrombi at other sites indicates that the thrombocytopenia is unrelated to the reduction in platelet count. This suggests that the thrombocytopenia, whilst initiated by a common signal with thrombosis, is driven by a different mechanism. We would suggest that platelet production is increased during infection, as illustrated by increased platelet size and increased numbers of megakaryocytes in the spleen, and thus it would appear not to be due to a reduction in platelet production (Brown et al., 2010, Tsakiris et al., 1999).

7.5 Outlook: human non-typhoidal bacteraemia

NTS infections place a significant clinical burden on young children and HIV-infected individuals in the developing world (Graham et al., 2000b, Graham and English, 2009). Essentially, the aim of this study was to identify potential mechanisms as to how infected individuals may die from these infections, which are associated with non-specific physiological symptoms (Graham et al., 2000c). Whilst, the co-existence between systemic NTS infections and anaemia is evident in the literature, and we support these findings here, anaemia is not thought to be the cause of death (Graham et al., 2000a). Evidence of liver pathology during human NTS bacteraemia is scarce, but is better described during typhoid and is associated with clinical complications in the outcome of infection (Pramoolsinsap and Viranuvatti, 1998). Thus, this provided a starting point for our work. The marked thrombosis in the liver provided a phenotype which could potentially explain the anecdotal "fading away during the night" observations that are frequently associated with death from NTS bacteraemia (C. MacLennan, personal communication). We hypothesise that if thrombosis such as we observe in the liver happens in other sites, this could explain how infected individuals die.

7.6 A role for immunothrombosis in host defence

An outstanding question is whether or not the thrombosis we observe is a protective inflammatory host mechanism against systemic *Salmonella*, or if it is an aberrant pathology associated with overt inflammation and platelet activation. Indeed, immunothrombosis, the formation of thrombi during inflammatory immune responses to invading pathogens, has been recently described and is becoming increasingly recognised (Engelmann and Massberg, 2013). It is believed that thrombosis contributes to host defence in a multitude

of ways, including the limiting of bacterial dissemination, and the recruitment and co-localisation of leukocytes with invading pathogens. Moreover, it appears that the many of the molecular mediators implicated in these thrombotic responses differ (or are dispensable) from those utilised during routine haemostasis, for example, the interplay between neutrophils, monocytes and platelets is integral to immunothrombosis, but not haemostasis (Engelmann and Massberg, 2013, von Bruhl et al., 2012). This poses immunothrombosis as an attractive therapeutic target, because many current antithrombotic agents are associated with increased risk of bleeding. Additional biological responses to bacterial invasion, including NETS, further contribute to the vascular response against pathogens, in a protective capacity (Clark et al., 2007). Our preliminary studies utilising anti-inflammatory or anti-coagulation agents have so far been inconclusive in determining the extent to which thrombosis is beneficial to the host, although these experiments are on-going.

Using genetically-modified mice, we show that those mice which present the most extensive clinical features during infection and thus struggle to control infection (as far as is humanely appropriate) are frequently those which lack IFNγ, Tbet or IL10 and those which are treated with clodronate. However, the reasons for this are likely to differ between these strains. We and others have demonstrated the heightened bacterial burden of IFNγ-deficient mice at day 7, and thus these mice succumb to infection due to uncontrolled bacterial replication in the absence of IFNγ (Ross et al. manuscript in preparation) (Mastroeni et al., 1992, Nauciel and Espinasse-Maes, 1992). In contrast, clodronate- treated mice have significantly reduced bacterial numbers in the liver relative to PBS-treated mice at day 7, yet present severe clinical signs of infection (Wijburg et al., 2000). However, the other two strains which present overt clinical signs are both

particularly susceptible to extensive thrombosis, more so than in WT mice. Thus these observations could suggest a putative association between thrombosis severity and clinical symptoms. Additionally, ascites, the build-up of fluid in the peritoneum, is common in these mice (data not shown). Therefore there may be a relationship between thrombus formation in the liver, extent of ascites and extent of clinical features of infection.

7.7 Relevance of our findings to therapeutic intervention

Our findings here may be of potential relevance to systemic human infections in the developing world due to our care to recapitulate the physiological conditions of the human infection (Santos et al., 2001). Human NTS infections are commonly treated with antimicrobials and so far, there is no available vaccine (MacLennan et al., 2008). NTS is the most common bacterial isolate recovered from bacteraemic children in sub-Saharan Africa (Graham et al., 2000b). The use of antibiotics can be delayed, due to inappropriate diagnosis, and the emergence of multi-drug resistant strains is an extremely serious problem (in the treatment of NTS and more globally in the treatment of bacterial infections)(Graham, 2002). Thus the extrapolation of scientific finding from studies such as ours will be vital in informing local clinicians and in the universal treatment of these infections.

Here we have demonstrated the general relationship between platelet count and thrombosis severity, which could be utilised by measuring platelet counts on patient arrival at clinic. This may provide a speedy indication as to the severity of the bacteraemia (de Jong et al. manuscript in preparation). However, our results also highlight that this association is more complex than purely platelet consumption during thrombosis and further work is required to determine the mechanism of thrombocytopenia. Despite this,

if we were to demonstrate that thrombosis either helps the host response against bacteraemia (or is damaging and could contribute to host death during bacteraemia), it is likely that regimes that increase or decrease platelet reactivity, respectively, may be useful in the treatment of bacteraemic individuals. A number of antiplatelet agents are already available clinically and cheaply, and appropriate use of these may intervene with the host thrombosis response whilst minimising the risk of associated bleeding (Engelmann and Massberg, 2013). By utilising the overlap between inflammation and platelet activation to our advantage, we may be able to preserve the time in which antimicrobials can be useful.

7.8 Future work

Whilst this study has provided a detailed characterisation of hepatic inflammation during systemic NTS infection and has identified much of the mechanism of platelet activation during the associated inflammatory thrombosis, it has also initiated multiple questions to be investigated in future work. These are briefly outlined below:

- One of the most fundamental questions regards the site of platelet activation. We have clearly shown that platelet-expressed CLEC-2 and podoplanin are required for thrombosis but we have not yet determined whether this podoplanin exposure occurs at sites of damaged vascular endothelium or elsewhere.
- Secondly, it is unclear exactly how TNFα contributes to thrombosis. We demonstrate that in the absence of signalling via the TNFα receptor, whilst inflammation and podoplanin expression remain intact, thrombosis is abolished. This finding therefore portrays a unique role of TNFα in the development of thrombosis which differs from the inflammatory signals provided by IFNγ.

- Thirdly, the thrombocytopenia which occurs in parallel to the thrombus development we observe in the liver vasculature must be driven by different means than purely the consumption of platelets during thrombosis. This is evidenced by the diminished blood platelet numbers in PF4.Cre.CLEC-$2^{fl/fl}$ mice despite the absence of thrombosis in these mice.
- Fourthly, future work should seek to identify whether neutrophil extracellular traps (NETS) play a role in thrombus production during NTS infection. Whilst all other leukocyte populations identified localise to the periphery of thrombi, neutrophils ($Ly6G^+$ cells) are found throughout the body of the thrombus, suggesting they are present as the structure develops. This could potentially indicate that NETS may be formed prior to or during thrombosis. However, this must be accurately determined using specific histological markers of NETs including neutrophil elastase and histones.

7.9 Conclusion

Cases describing clinical complications of a haemostatic nature during systemic infection have been available for many years (Huckstep 1962). Despite this, the overlap between the fields of coagulation and platelet haemostasis and infectious inflammation has been understated. The interplay between these systems is emerging quickly into a diverse, yet highly relevant field in today's society where the challenges of antimicrobial resistance drive us to explore alternative solutions for infection control.

This work aimed to investigate possible reasons why invasive NTS infections can be so devastating in a manner that does not focus on bacterial numbers. Although we concentrated on the liver for its role in host housekeeping and as a primary site of

colonisation, this was fortuitous as it allowed us to examine the role of infection on inflammation and haemostasis. The key finding is the close relationship between inflammation and thrombosis. Both these processes share a common platform of podoplanin and we have been able to show that thrombosis in this site requires CLEC-2. Therefore the study of one of these processes is likely to inform on the other and this provides a platform in which to study the multiple consequences of systemic infection on host function.

LIST OF REFERENCES

ACTON, S. E., ASTARITA, J. L., MALHOTRA, D., LUKACS-KORNEK, V., FRANZ, B., HESS, P. R., JAKUS, Z., KULIGOWSKI, M., FLETCHER, A. L., ELPEK, K. G., BELLEMARE-PELLETIER, A., SCEATS, L., REYNOSO, E. D., GONZALEZ, S. F., GRAHAM, D. B., CHANG, J., PETERS, A., WOODRUFF, M., KIM, Y. A., SWAT, W., MORITA, T., KUCHROO, V., CARROLL, M. C., KAHN, M. L., WUCHERPFENNIG, K. W. & TURLEY, S. J. 2012. Podoplanin-rich stromal networks induce dendritic cell motility via activation of the C-type lectin receptor CLEC-2. *Immunity,* 37**,** 276-89.

ADAMS, D. H. & EKSTEEN, B. 2006. Aberrant homing of mucosal T cells and extra-intestinal manifestations of inflammatory bowel disease. *Nat Rev Immunol,* 6**,** 244-51.

AMACHER, D. E. 2002. A toxicologist's guide to biomarkers of hepatic response. *Hum Exp Toxicol,* 21**,** 253-62.

AMITRANO, L., GUARDASCIONE, M. A., BRANCACCIO, V. & BALZANO, A. 2002. Coagulation disorders in liver disease. *Semin Liver Dis,* 22**,** 83-96.

ANGUS, D. C. & VAN DER POLL, T. 2013. Severe sepsis and septic shock. *N Engl J Med,* 369**,** 840-51.

ARENTOFT, H., SCHONHEYDER, H. & SCHONEMANN, N. K. 1993. Cerebral Salmonella typhimurium abscess in a patient with a stroke. *Infection,* 21**,** 251-3.

ARII, J., TANABE, Y., MIYAKE, M., NODA, M., TAKAHASHI, Y., HISHIKI, H. & KOHNO, Y. 2001. Acute encephalopathy associated with nontyphoidal salmonellosis. *J Child Neurol,* 16**,** 539-40.

ARORA, S., GUPTA, N., KUMAR, A. & KAUR, I. R. 2011. Salmonella enteritidis from a case of fever with thrombocytopenia. *Asian Pac J Trop Med,* 4**,** 328-9.

ASTARITA, J. L., ACTON, S. E. & TURLEY, S. J. 2012. Podoplanin: emerging functions in development, the immune system, and cancer. *Front Immunol,* 3**,** 283.

ASTER, R. H. 1966. Pooling of platelets in the spleen: role in the pathogenesis of "hypersplenic" thrombocytopenia. *J Clin Invest,* 45**,** 645-57.

BALARAM, P., KIEN, P. K. & ISMAIL, A. 2009. Toll-like receptors and cytokines in immune responses to persistent mycobacterial and Salmonella infections. *Int J Med Microbiol,* 299**,** 177-85.

BANCHEREAU, J. & STEINMAN, R. M. 1998. Dendritic cells and the control of immunity. *Nature,* 392**,** 245-52.

BARREIROS, A. P., SCHIRMACHER, P., LAUFENBERG-FELDMANN, R., MEYER ZUM BUSCHENFELDE, K. H. & SCHLAAK, J. F. 2000. The early immune response in the liver of BALB/c mice infected with S. typhimurium. *Scand J Immunol,* 51**,** 472-8.

BATTINELLI, E. M., HARTWIG, J. H. & ITALIANO, J. E., JR. 2007. Delivering new insight into the biology of megakaryopoiesis and thrombopoiesis. *Curr Opin Hematol,* 14**,** 419-26.

BEATTIE, L., PELTAN, A., MAROOF, A., KIRBY, A., BROWN, N., COLES, M., SMITH, D. F. & KAYE, P. M. 2010. Dynamic imaging of experimental Leishmania donovani-induced hepatic granulomas detects Kupffer cell-restricted antigen presentation to antigen-specific CD8 T cells. *PLoS Pathog,* 6**,** e1000805.

BEKIARIS, V., WITHERS, D., GLANVILLE, S. H., MCCONNELL, F. M., PARNELL, S. M., KIM, M. Y., GASPAL, F. M., JENKINSON, E., SWEET, C., ANDERSON, G. & LANE, P. J. 2007. Role of CD30 in B/T segregation in the spleen. *J Immunol,* 179**,** 7535-43.

BENDER, M., MAY, F., LORENZ, V., THIELMANN, I., HAGEDORN, I., FINNEY, B. A., VOGTLE, T., REMER, K., BRAUN, A., BOSL, M., WATSON, S. P. & NIESWANDT, B. 2013. Combined in vivo depletion of glycoprotein VI and C-type lectin-like receptor 2 severely compromises hemostasis and abrogates arterial thrombosis in mice. *Arterioscler Thromb Vasc Biol,* 33**,** 926-34.

BERGMEIER, W., CHAUHAN, A. K. & WAGNER, D. D. 2008. Glycoprotein Ibalpha and von Willebrand factor in primary platelet adhesion and thrombus formation: lessons from mutant mice. *Thromb Haemost,* 99**,** 264-70.

BERKLEY, J., MWARUMBA, S., BRAMHAM, K., LOWE, B. & MARSH, K. 1999. Bacteraemia complicating severe malaria in children. *Trans R Soc Trop Med Hyg,* 93**,** 283-6.

BERKOWITZ, F. E. 1992. Infections in children with severe protein-energy malnutrition. *Pediatr Infect Dis J,* 11**,** 750-9.

BIEMOND, B. J., LEVI, M., TEN CATE, H., SOULE, H. R., MORRIS, L. D., FOSTER, D. L., BOGOWITZ, C. A., VAN DER POLL, T., BULLER, H. R. & TEN CATE, J. W. 1995. Complete inhibition of endotoxin-induced coagulation activation in chimpanzees with a monoclonal Fab fragment against factor VII/VIIa. *Thromb Haemost,* 73**,** 223-30.

BILZER, M., ROGGEL, F. & GERBES, A. L. 2006. Role of Kupffer cells in host defense and liver disease. *Liver Int,* 26**,** 1175-86.

BITAR, R. & TARPLEY, J. 1985. Intestinal perforation in typhoid fever: a historical and state-of-the-art review. *Rev Infect Dis,* 7**,** 257-71.

BLANDEN, R. V., MACKANESS, G. B. & COLLINS, F. M. 1966. Mechanisms of acquired resistance in mouse typhoid. *J Exp Med,* 124**,** 585-600.

BOBAT, S., FLORES-LANGARICA, A., HITCHCOCK, J., MARSHALL, J. L., KINGSLEY, R. A., GOODALL, M., GIL-CRUZ, C., SERRE, K., LEYTON, D. L., LETRAN, S. E., GASPAL, F., CHESTER, R., CHAMBERLAIN, J. L., DOUGAN, G., LOPEZ-MACIAS, C., HENDERSON, I. R., ALEXANDER, J., MACLENNAN, I. C. & CUNNINGHAM, A. F. 2011. Soluble flagellin, FliC, induces an Ag-specific Th2 response, yet promotes T-bet-regulated Th1 clearance of Salmonella Typhimurium infection. *Eur J Immunol*.

BOKHARI, S. M., KIM, K. J., PINSON, D. M., SLUSSER, J., YEH, H. W. & PARMELY, M. J. 2008. NK cells and gamma interferon coordinate the formation and function of hepatic granulomas in mice infected with the Francisella tularensis live vaccine strain. *Infect Immun,* 76**,** 1379-89.

BOULAFTALI, Y., HESS, P. R., GETZ, T. M., CHOLKA, A., STOLLA, M., MACKMAN, N., OWENS, A. P., 3RD, WARE, J., KAHN, M. L. & BERGMEIER, W. 2013. Platelet ITAM signaling is critical for vascular integrity in inflammation. *J Clin Invest,* 123**,** 908-16.

BRENT, A. J., OUNDO, J. O., MWANGI, I., OCHOLA, L., LOWE, B. & BERKLEY, J. A. 2006. Salmonella bacteremia in Kenyan children. *Pediatr Infect Dis J,* 25**,** 230-6.

BRILL, A., FUCHS, T. A., CHAUHAN, A. K., YANG, J. J., DE MEYER, S. F., KOLLNBERGER, M., WAKEFIELD, T. W., LAMMLE, B., MASSBERG, S. & WAGNER, D. D. 2011. von Willebrand factor-mediated platelet adhesion is critical for deep vein thrombosis in mouse models. *Blood,* 117**,** 1400-7.

BRILL, A., FUCHS, T. A., SAVCHENKO, A. S., THOMAS, G. M., MARTINOD, K., DE MEYER, S. F., BHANDARI, A. A. & WAGNER, D. D. 2012. Neutrophil extracellular traps promote deep vein thrombosis in mice. *J Thromb Haemost,* 10**,** 136-44.

BRONZAN, R. N., TAYLOR, T. E., MWENECHANYA, J., TEMBO, M., KAYIRA, K., BWANAISA, L., NJOBVU, A., KONDOWE, W., CHALIRA, C., WALSH, A. L., PHIRI, A., WILSON, L. K., MOLYNEUX, M. E. & GRAHAM, S. M. 2007. Bacteremia in Malawian children with severe malaria: prevalence, etiology, HIV coinfection, and outcome. *J Infect Dis,* 195**,** 895-904.

BROWN, D. E., MCCOY, M. W., PILONIETA, M. C., NIX, R. N. & DETWEILER, C. S. 2010. Chronic murine typhoid fever is a natural model of secondary hemophagocytic lymphohistiocytosis. *PLoS One,* 5**,** e9441.

BROWN, S. P., CORNELL, S. J., SHEPPARD, M., GRANT, A. J., MASKELL, D. J., GRENFELL, B. T. & MASTROENI, P. 2006. Intracellular demography and the dynamics of Salmonella enterica infections. *PLoS Biol,* 4**,** e349.

BROZE, G. J., JR., WARREN, L. A., NOVOTNY, W. F., HIGUCHI, D. A., GIRARD, J. J. & MILETICH, J. P. 1988. The lipoprotein-associated coagulation inhibitor that inhibits the factor VII-tissue factor complex also inhibits factor Xa: insight into its possible mechanism of action. *Blood,* 71**,** 335-43.

BUITING, A. M. & VAN ROOIJEN, N. 1994. Liposome mediated depletion of macrophages: an approach for fundamental studies. *J Drug Target,* 2**,** 357-62.

BURGMANN, H., LOOAREESUWAN, S., KAPIOTIS, S., VIRAVAN, C., VANIJANONTA, S., HOLLENSTEIN, U., WIESINGER, E., PRESTERL, E., WINKLER, S. & GRANINGER, W. 1996. Serum levels of erythropoietin in acute Plasmodium falciparum malaria. *Am J Trop Med Hyg,* 54**,** 280-3.

BUTLER, T., BELL, W. R., LEVIN, J., LINH, N. N. & ARNOLD, K. 1978. Typhoid fever. Studies of blood coagulation, bacteremia, and endotoxemia. *Arch Intern Med,* 138**,** 407-10.

CABRERA, M., PEWE, L. L., HARTY, J. T. & FREVERT, U. 2013. In vivo CD8+ T cell dynamics in the liver of Plasmodium yoelii immunized and infected mice. *PLoS One,* 8**,** e70842.

CALIS, J. C., PHIRI, K. S., FARAGHER, E. B., BRABIN, B. J., BATES, I., CUEVAS, L. E., DE HAAN, R. J., PHIRI, A. I., MALANGE, P., KHOKA, M., HULSHOF, P. J., VAN LIESHOUT, L., BELD, M. G., TEO, Y. Y., ROCKETT, K. A., RICHARDSON, A., KWIATKOWSKI, D. P., MOLYNEUX, M. E. & VAN HENSBROEK, M. B. 2008. Severe anemia in Malawian children. *N Engl J Med,* 358**,** 888-99.

CAMERER, E., KOLSTO, A. B. & PRYDZ, H. 1996. Cell biology of tissue factor, the principal initiator of blood coagulation. *Thromb Res,* 81**,** 1-41.

CAR, B. D., ENG, V. M., SCHNYDER, B., OZMEN, L., HUANG, S., GALLAY, P., HEUMANN, D., AGUET, M. & RYFFEL, B. 1994. Interferon gamma receptor deficient mice are resistant to endotoxic shock. *J Exp Med,* 179**,** 1437-44.

CARTER, P. B. & COLLINS, F. M. 1974. The route of enteric infection in normal mice. *J Exp Med,* 139**,** 1189-203.

CARTER, P. B. & COLLINS, F. M. 1975. Peyer's patch responsiveness to Salmonella in mice. *J Reticuloendothel Soc,* 17**,** 38-46.

CASCALHO, M., MA, A., LEE, S., MASAT, L. & WABL, M. 1996. A quasi-monoclonal mouse. *Science,* 272**,** 1649-52.

CEREDIG, R., ROLINK, A. G. & BROWN, G. 2009. Models of haematopoiesis: seeing the wood for the trees. *Nat Rev Immunol,* 9**,** 293-300.

CHANG, C. J., CHANG, W. N., HUANG, L. T., CHANG, Y. C., HUANG, S. C., HUNG, P. L., HO, H. H., CHANG, C. S., WANG, K. W., CHENG, B. C., LUI, C. C., CHANG, H. W. & LU, C. H. 2003. Cerebral infarction in perinatal and childhood bacterial meningitis. *QJM,* 96**,** 755-62.

CHEESBROUGH, J. S., TAXMAN, B. C., GREEN, S. D., MEWA, F. I. & NUMBI, A. 1997. Clinical definition for invasive Salmonella infection in African children. *Pediatr Infect Dis J,* 16**,** 277-83.

CHEN, W., JIN, W., HARDEGEN, N., LEI, K. J., LI, L., MARINOS, N., MCGRADY, G. & WAHL, S. M. 2003. Conversion of peripheral CD4+CD25- naive T cells to CD4+CD25+ regulatory T cells by TGF-beta induction of transcription factor Foxp3. *J Exp Med,* 198**,** 1875-86.

CLARK, S. R., MA, A. C., TAVENER, S. A., MCDONALD, B., GOODARZI, Z., KELLY, M. M., PATEL, K. D., CHAKRABARTI, S., MCAVOY, E., SINCLAIR, G. D., KEYS, E. M., ALLEN-VERCOE, E., DEVINNEY, R., DOIG, C. J., GREEN, F. H. & KUBES, P. 2007. Platelet TLR4 activates neutrophil extracellular traps to ensnare bacteria in septic blood. *Nat Med,* 13**,** 463-9.

COHEN-SOLAL, J. F., CASSARD, L., FRIDMAN, W. H. & SAUTES-FRIDMAN, C. 2004. Fc gamma receptors. *Immunol Lett,* 92**,** 199-205.

CONLAN, J. W. 1996. Neutrophils prevent extracellular colonization of the liver microvasculature by Salmonella typhimurium. *Infect Immun,* 64**,** 1043-7.

CONLAN, J. W. & NORTH, R. J. 1992. Early pathogenesis of infection in the liver with the facultative intracellular bacteria Listeria monocytogenes, Francisella tularensis, and Salmonella typhimurium involves lysis of infected hepatocytes by leukocytes. *Infect Immun,* 60**,** 5164-71.

COOPER, A. M., DALTON, D. K., STEWART, T. A., GRIFFIN, J. P., RUSSELL, D. G. & ORME, I. M. 1993. Disseminated tuberculosis in interferon gamma gene-disrupted mice. *J Exp Med,* 178**,** 2243-7.

CORASH, L., LEVIN, J., MOK, Y., BAKER, G. & MCDOWELL, J. 1989. Measurement of megakaryocyte frequency and ploidy distribution in unfractionated murine bone marrow. *Exp Hematol,* 17**,** 278-86.

COREY, S. J., MINDEN, M. D., BARBER, D. L., KANTARJIAN, H., WANG, J. C. & SCHIMMER, A. D. 2007. Myelodysplastic syndromes: the complexity of stem-cell diseases. *Nat Rev Cancer,* 7**,** 118-29.

CORNET, A. D., BEISHUIZEN, A. & GROENEVELD, A. B. 2007. Activated protein C in sepsis: tightening pulmonary endothelial cells? *Crit Care Med,* 35**,** 2656-8.

CORRADO, E., RIZZO, M., TANTILLO, R., MURATORI, I., BONURA, F., VITALE, G. & NOVO, S. 2006. Markers of inflammation and infection influence the outcome of patients with baseline asymptomatic carotid lesions: a 5-year follow-up study. *Stroke,* 37**,** 482-6.

COX, D., KERRIGAN, S. W. & WATSON, S. P. 2011. Platelets and the innate immune system: mechanisms of bacterial-induced platelet activation. *J Thromb Haemost,* 9**,** 1097-107.

CRISPE, I. N. 2001. Isolation of mouse intrahepatic lymphocytes. *Curr Protoc Immunol,* Chapter 3**,** Unit 3 21.

CRISPE, I. N. 2003. Hepatic T cells and liver tolerance. *Nat Rev Immunol,* 3**,** 51-62.

CRISPE, I. N. 2009. The liver as a lymphoid organ. *Annu Rev Immunol,* 27**,** 147-63.

CRISPE, I. N. 2011. Liver antigen-presenting cells. *J Hepatol,* 54**,** 357-65.

CRUMP, J. A., LUBY, S. P. & MINTZ, E. D. 2004. The global burden of typhoid fever. *Bull World Health Organ,* 82**,** 346-53.

CUNNINGHAM, A. F., GASPAL, F., SERRE, K., MOHR, E., HENDERSON, I. R., SCOTT-TUCKER, A., KENNY, S. M., KHAN, M., TOELLNER, K. M., LANE, P. J. & MACLENNAN, I. C. 2007. Salmonella induces a switched antibody response without germinal centers that impedes the extracellular spread of infection. *J Immunol,* 178**,** 6200-7.

CUNNINGTON, A. J., DE SOUZA, J. B., WALTHER, M. & RILEY, E. M. 2012. Malaria impairs resistance to Salmonella through heme- and heme oxygenase-dependent dysfunctional granulocyte mobilization. *Nat Med,* 18**,** 120-7.

DALTON, D. K., PITTS-MEEK, S., KESHAV, S., FIGARI, I. S., BRADLEY, A. & STEWART, T. A. 1993. Multiple defects of immune cell function in mice with disrupted interferon-gamma genes. *Science,* 259**,** 1739-42.

DE BRITO, T., TRENCH VIEIRA, W. & D'AGOSTINO DIAS, M. 1977. Jaundice in typhoid hepatitis: a light and electron microscopy study based on liver biopsies. *Acta Hepatogastroenterol (Stuttg),* 24**,** 426-33.

DE LA FUENTE-AGUADO, J., BORDON, J., ESTEBAN, A. R., AGUILAR, A. & MORENO, J. A. 1999. Spontaneous non-typhoidal Salmonella peritonitis in patients with serious underlying disorders. *Infection,* 27**,** 224-7.

DEGEN, J. L., BUGGE, T. H. & GOGUEN, J. D. 2007. Fibrin and fibrinolysis in infection and host defense. *J Thromb Haemost,* 5 Suppl 1**,** 24-31.

DUGGAN, M. B. & BEYER, L. 1975. Enteric fever in young Yoruba children. *Arch Dis Child,* 50**,** 67-71.

EBONG, W. W. 1986. Acute osteomyelitis in Nigerians with sickle cell disease. *Ann Rheum Dis,* 45**,** 911-5.

EKWALL, A. K., EISLER, T., ANDERBERG, C., JIN, C., KARLSSON, N., BRISSLERT, M. & BOKAREWA, M. I. 2011. The tumour-associated glycoprotein podoplanin is expressed in fibroblast-like synoviocytes of the hyperplastic synovial lining layer in rheumatoid arthritis. *Arthritis Res Ther,* 13**,** R40.

ELKIND, M. S. & COLE, J. W. 2006. Do common infections cause stroke? *Semin Neurol,* 26**,** 88-99.

EMOTO, M. & EMOTO, Y. 2009. Intracellular bacterial infection and invariant NKT cells. *Yonsei Med J,* 50**,** 12-21.

ENGELMANN, B. & MASSBERG, S. 2013. Thrombosis as an intravascular effector of innate immunity. *Nat Rev Immunol,* 13**,** 34-45.

ESMON, C. T. 2004. Interactions between the innate immune and blood coagulation systems. *Trends Immunol,* 25**,** 536-42.

ESMON, C. T. 2005. The interactions between inflammation and coagulation. *Br J Haematol,* 131**,** 417-30.

EVEREST, P., ALLEN, J., PAPAKONSTANTINOPOULOU, A., MASTROENI, P., ROBERTS, M. & DOUGAN, G. 1997. Salmonella typhimurium infections in mice deficient in interleukin-4 production: role of IL-4 in infection-associated pathology. *J Immunol,* 159**,** 1820-7.

FAME, T. M., ENGELHARD, D. & RILEY, H. D., JR. 1986. Hemophagocytosis accompanying typhoid fever. *Pediatr Infect Dis,* 5**,** 367-9.

FARR, A. G., BERRY, M. L., KIM, A., NELSON, A. J., WELCH, M. P. & ARUFFO, A. 1992. Characterization and cloning of a novel glycoprotein expressed by stromal cells in T-dependent areas of peripheral lymphoid tissues. *J Exp Med,* 176**,** 1477-82.

FEHERVARI, Z. & SAKAGUCHI, S. 2004. Development and function of CD25+CD4+ regulatory T cells. *Curr Opin Immunol,* 16**,** 203-8.

FIELDS, P. I., SWANSON, R. V., HAIDARIS, C. G. & HEFFRON, F. 1986. Mutants of Salmonella typhimurium that cannot survive within the macrophage are avirulent. *Proc Natl Acad Sci U S A,* 83**,** 5189-93.

FINNEY, B. A., SCHWEIGHOFFER, E., NAVARRO-NUNEZ, L., BENEZECH, C., BARONE, F., HUGHES, C. E., LANGAN, S. A., LOWE, K. L., POLLITT, A. Y., MOURAO-SA, D., SHEARDOWN, S., NASH, G. B., SMITHERS, N., REIS E SOUSA, C., TYBULEWICZ, V. L. & WATSON, S. P. 2012. CLEC-2 and Syk in the megakaryocytic/platelet lineage are essential for development. *Blood,* 119**,** 1747-56.

FISMAN, D. N. 2000. Hemophagocytic syndromes and infection. *Emerg Infect Dis,* 6**,** 601-8.

FITZGERALD, J. R., FOSTER, T. J. & COX, D. 2006a. The interaction of bacterial pathogens with platelets. *Nat Rev Microbiol,* 4**,** 445-57.

FITZGERALD, J. R., LOUGHMAN, A., KEANE, F., BRENNAN, M., KNOBEL, M., HIGGINS, J., VISAI, L., SPEZIALE, P., COX, D. & FOSTER, T. J. 2006b. Fibronectin-binding proteins of Staphylococcus aureus mediate activation of human platelets via fibrinogen and fibronectin bridges to integrin GPIIb/IIIa and IgG binding to the FcgammaRIIa receptor. *Mol Microbiol,* 59**,** 212-30.

FLORES-LANGARICA, A., MARSHALL, J. L., BOBAT, S., MOHR, E., HITCHCOCK, J., ROSS, E. A., COUGHLAN, R. E., KHAN, M., VAN ROOIJEN, N., HENDERSON, I. R., MACLENNAN, I. C. & CUNNINGHAM, A. F. 2011. T-zone localized monocyte-derived dendritic cells promote Th1 priming to Salmonella. *Eur J Immunol,* 41**,** 2654-65.

FRANCHINI, M. & VENERI, D. 2004. Helicobacter pylori infection and immune thrombocytopenic purpura: an update. *Helicobacter,* 9**,** 342-6.

FUCHS, T. A., BRILL, A., DUERSCHMIED, D., SCHATZBERG, D., MONESTIER, M., MYERS, D. D., JR., WROBLESKI, S. K., WAKEFIELD, T. W., HARTWIG, J. H. & WAGNER, D. D. 2010. Extracellular DNA traps promote thrombosis. *Proc Natl Acad Sci U S A,* 107**,** 15880-5.

FUNG-LEUNG, W. P., KUNDIG, T. M., ZINKERNAGEL, R. M. & MAK, T. W. 1991. Immune response against lymphocytic choriomeningitis virus infection in mice without CD8 expression. *J Exp Med,* 174**,** 1425-9.

FURIE, B. & FURIE, B. C. 2005. Thrombus formation in vivo. *J Clin Invest,* 115**,** 3355-62.

FURIE, B. & FURIE, B. C. 2008. Mechanisms of thrombus formation. *N Engl J Med,* 359**,** 938-49.

GAO, B., JEONG, W. I. & TIAN, Z. 2008. Liver: An organ with predominant innate immunity. *Hepatology,* 47**,** 729-36.

GAZZINELLI, R. T., WYSOCKA, M., HIENY, S., SCHARTON-KERSTEN, T., CHEEVER, A., KUHN, R., MULLER, W., TRINCHIERI, G. & SHER, A. 1996. In the absence of endogenous IL-10, mice acutely infected with Toxoplasma gondii succumb to a lethal immune response dependent on CD4+ T cells and accompanied by overproduction of IL-12, IFN-gamma and TNF-alpha. *J Immunol,* 157**,** 798-805.

GIESEN, P. L., RAUCH, U., BOHRMANN, B., KLING, D., ROQUE, M., FALLON, J. T., BADIMON, J. J., HIMBER, J., RIEDERER, M. A. & NEMERSON, Y. 1999. Blood-borne tissue factor: another view of thrombosis. *Proc Natl Acad Sci U S A,* 96**,** 2311-5.

GONDWE, E. N., MOLYNEUX, M. E., GOODALL, M., GRAHAM, S. M., MASTROENI, P., DRAYSON, M. T. & MACLENNAN, C. A. 2010. Importance of antibody and complement for oxidative burst and killing of invasive nontyphoidal Salmonella by blood cells in Africans. *Proc Natl Acad Sci U S A,* 107**,** 3070-5.

GORDON, M. A. 2008. Salmonella infections in immunocompromised adults. *J Infect,* 56**,** 413-22.

GORDON, M. A., GRAHAM, S. M., WALSH, A. L., WILSON, L., PHIRI, A., MOLYNEUX, E., ZIJLSTRA, E. E., HEYDERMAN, R. S., HART, C. A. & MOLYNEUX, M. E. 2008. Epidemics of invasive Salmonella enterica serovar enteritidis and S. enterica Serovar typhimurium infection

associated with multidrug resistance among adults and children in Malawi. *Clin Infect Dis,* 46**,** 963-9.

GRAHAM, S. M. 2002. Salmonellosis in children in developing and developed countries and populations. *Curr Opin Infect Dis,* 15**,** 507-12.

GRAHAM, S. M. & ENGLISH, M. 2009. Non-typhoidal salmonellae: a management challenge for children with community-acquired invasive disease in tropical African countries. *Lancet,* 373**,** 267-9.

GRAHAM, S. M., HART, C. A., MOLYNEUX, E. M., WALSH, A. L. & MOLYNEUX, M. E. 2000a. Malaria and Salmonella infections: cause or coincidence? *Trans R Soc Trop Med Hyg,* 94**,** 227.

GRAHAM, S. M., MOLYNEUX, E. M., WALSH, A. L., CHEESBROUGH, J. S., MOLYNEUX, M. E. & HART, C. A. 2000b. Nontyphoidal Salmonella infections of children in tropical Africa. *Pediatr Infect Dis J,* 19**,** 1189-96.

GRAHAM, S. M., WALSH, A. L., MOLYNEUX, E. M., PHIRI, A. J. & MOLYNEUX, M. E. 2000c. Clinical presentation of non-typhoidal Salmonella bacteraemia in Malawian children. *Trans R Soc Trop Med Hyg,* 94**,** 310-4.

GRANT, A. J., FOSTER, G. L., MCKINLEY, T. J., BROWN, S. P., CLARE, S., MASKELL, D. J. & MASTROENI, P. 2009. Bacterial growth rate and host factors as determinants of intracellular bacterial distributions in systemic Salmonella enterica infections. *Infect Immun,* 77**,** 5608-11.

GRANT, A. J., LALOR, P. F., SALMI, M., JALKANEN, S. & ADAMS, D. H. 2002. Homing of mucosal lymphocytes to the liver in the pathogenesis of hepatic complications of inflammatory bowel disease. *Lancet,* 359**,** 150-7.

GREEN, S. D. & CHEESBROUGH, J. S. 1993. Salmonella bacteraemia among young children at a rural hospital in western Zaire. *Ann Trop Paediatr,* 13**,** 45-53.

GREENWOOD, B. M., BRADLEY-MOORE, A. M., BRYCESON, A. D. & PALIT, A. 1972. Immunosuppression in children with malaria. *Lancet,* 1**,** 169-72.

GREENWOOD, B. M., STRATTON, D., WILLIAMSON, W. A. & MOHAMMED, I. 1978. A study of the role of immunological factors in the pathogenesis of the anaemia of acute malaria. *Trans R Soc Trop Med Hyg,* 72**,** 378-85.

GREIG, H. B. & NAIDOO, P. D. 1981. A case of typhoid fever complicated by a severe bleeding syndrome due to deficiency of the prothrombin group of coagulation factors. *J Trop Med Hyg,* 84**,** 253-7.

GUILLOTEAU, L., BUZONI-GATEL, D., BLAISE, F., BERNARD, F. & PEPIN, M. 1991. Phenotypic analysis of splenic lymphocytes and immunohistochemical study of hepatic granulomas after a murine infection with Salmonella abortusovis. *Immunology,* 74**,** 630-7.

HANEL, R. A., ARAUJO, J. C., ANTONIUK, A., DA SILVA DITZEL, L. F., FLENIK MARTINS, L. T. & LINHARES, M. N. 2000. Multiple brain abscesses caused by Salmonella typhi: case report. *Surg Neurol,* 53**,** 86-90.

HARRISON, J. A., VILLARREAL-RAMOS, B., MASTROENI, P., DEMARCO DE HORMAECHE, R. & HORMAECHE, C. E. 1997. Correlates of protection induced by live Aro- Salmonella typhimurium vaccines in the murine typhoid model. *Immunology,* 90**,** 618-25.

HELAINE, S., CHEVERTON, A. M., WATSON, K. G., FAURE, L. M., MATTHEWS, S. A. & HOLDEN, D. W. 2014. Internalization of Salmonella by macrophages induces formation of nonreplicating persisters. *Science,* 343**,** 204-8.

HENSEL, M. 2000. Salmonella pathogenicity island 2. *Mol Microbiol,* 36**,** 1015-23.

HERKEL, J., SCHUCHMANN, M., TIEGS, G. & LOHSE, A. W. 2005. Immune-mediated liver injury. *J Hepatol,* 42**,** 920-3.

HERZOG, B. H., FU, J., WILSON, S. J., HESS, P. R., SEN, A., MCDANIEL, J. M., PAN, Y., SHENG, M., YAGO, T., SILASI-MANSAT, R., MCGEE, S., MAY, F., NIESWANDT, B., MORRIS, A. J., LUPU, F., COUGHLIN, S. R., MCEVER, R. P., CHEN, H., KAHN, M. L. & XIA, L. 2013. Podoplanin maintains high endothelial venule integrity by interacting with platelet CLEC-2. *Nature,* 502**,** 105-9.

HESPEL, C. & MOSER, M. 2012. Role of inflammatory dendritic cells in innate and adaptive immunity. *Eur J Immunol,* 42**,** 2535-43.

HESS, J., LADEL, C., MIKO, D. & KAUFMANN, S. H. 1996. Salmonella typhimurium aroA- infection in gene-targeted immunodeficient mice: major role of CD4+ TCR-alpha beta cells and IFN-gamma in bacterial clearance independent of intracellular location. *J Immunol,* 156**,** 3321-6.

HOGAN, K. A., WEILER, H. & LORD, S. T. 2002. Mouse models in coagulation. *Thromb Haemost,* 87**,** 563-74.

HOHMANN, E. L. 2001. Nontyphoidal salmonellosis. *Clin Infect Dis,* 32**,** 263-9.

HOISETH, S. K. & STOCKER, B. A. 1981. Aromatic-dependent Salmonella typhimurium are non-virulent and effective as live vaccines. *Nature,* 291**,** 238-9.

HONG, Y. K., HARVEY, N., NOH, Y. H., SCHACHT, V., HIRAKAWA, S., DETMAR, M. & OLIVER, G. 2002. Prox1 is a master control gene in the program specifying lymphatic endothelial cell fate. *Dev Dyn,* 225**,** 351-7.

HONMA, M., MINAMI-HORI, M., TAKAHASHI, H. & IIZUKA, H. 2012. Podoplanin expression in wound and hyperproliferative psoriatic epidermis: regulation by TGF-beta and STAT-3 activating cytokines, IFN-gamma, IL-6, and IL-22. *J Dermatol Sci,* 65**,** 134-40.

HONN, K. V., TANG, D. G. & CRISSMAN, J. D. 1992. Platelets and cancer metastasis: a causal relationship? *Cancer Metastasis Rev,* 11**,** 325-51.

HORKY, J., VACHA, J. & ZNOJIL, V. 1978. Comparison of life span of erythrocytes in some inbred strains of mouse using 14C-labelled glycine. *Physiol Bohemoslov,* 27**,** 209-17.

HOU, T. Z., BYSTROM, J., SHERLOCK, J. P., QURESHI, O., PARNELL, S. M., ANDERSON, G., GILROY, D. W. & BUCKLEY, C. D. 2010. A distinct subset of podoplanin (gp38) expressing F4/80+ macrophages mediate phagocytosis and are induced following zymosan peritonitis. *FEBS Lett,* 584**,** 3955-61.

HOUSE, D., BISHOP, A., PARRY, C., DOUGAN, G. & WAIN, J. 2001. Typhoid fever: pathogenesis and disease. *Curr Opin Infect Dis,* 14**,** 573-8.

HSU, H. S. 1989. Pathogenesis and immunity in murine salmonellosis. *Microbiol Rev,* 53**,** 390-409.

HSU, W., SHU, S. A., GERSHWIN, E. & LIAN, Z. X. 2007. The current immune function of hepatic dendritic cells. *Cell Mol Immunol,* 4**,** 321-8.

HUANG, G. C., CHANG, C. M., KO, W. C., HUANG, Y. L. & CHUANG, Y. C. 2005. Typhoid fever complicated by multiple organ involvement: report of two cases. *J Infect,* 51**,** E57-60.

HUANG, L. T. 1996. Salmonella meningitis complicated by brain infarctions. *Clin Infect Dis,* 22**,** 194-5.

HUGHES, C. E., NAVARRO-NUNEZ, L., FINNEY, B. A., MOURAO-SA, D., POLLITT, A. Y. & WATSON, S. P. 2010a. CLEC-2 is not required for platelet aggregation at arteriolar shear. *J Thromb Haemost,* 8**,** 2328-32.

HUGHES, C. E., POLLITT, A. Y., MORI, J., EBLE, J. A., TOMLINSON, M. G., HARTWIG, J. H., O'CALLAGHAN, C. A., FUTTERER, K. & WATSON, S. P. 2010b. CLEC-2 activates Syk through dimerization. *Blood,* 115**,** 2947-55.

HUSAIN, E. H. 2011. Fulminant hepatitis in typhoid fever. *J Infect Public Health,* 4**,** 154-6.

HYLAND, L., VILLARREAL-RAMOS, B., CLARKE, B., BAATEN, B. & HOU, S. 2005. Bone marrow immunosuppression in Salmonella-infected mice is prolonged following influenza virus infection. *Exp Hematol,* 33**,** 1477-85.

JACKSON, A., NANTON, M. R., O'DONNELL, H., AKUE, A. D. & MCSORLEY, S. J. 2010. Innate immune activation during Salmonella infection initiates extramedullary erythropoiesis and splenomegaly. *J Immunol,* 185**,** 6198-204.

JANEWAY, C. A., JR. & MEDZHITOV, R. 2002. Innate immune recognition. *Annu Rev Immunol,* 20**,** 197-216.

JANKA, G. E. 2007. Hemophagocytic syndromes. *Blood Rev,* 21**,** 245-53.

JELLEY-GIBBS, D. M., STRUTT, T. M., MCKINSTRY, K. K. & SWAIN, S. L. 2008. Influencing the fates of CD4 T cells on the path to memory: lessons from influenza. *Immunol Cell Biol,* 86**,** 343-52.

JENNE, C. N., URRUTIA, R. & KUBES, P. 2013. Platelets: bridging hemostasis, inflammation, and immunity. *Int J Lab Hematol,* 35**,** 254-61.

JOHANSSON, C., INGMAN, M. & JO WICK, M. 2006. Elevated neutrophil, macrophage and dendritic cell numbers characterize immune cell populations in mice chronically infected with Salmonella. *Microb Pathog,* 41**,** 49-58.

JOMANTAITE, I., DIKOPOULOS, N., KROGER, A., LEITHAUSER, F., HAUSER, H., SCHIRMBECK, R. & REIMANN, J. 2004. Hepatic dendritic cell subsets in the mouse. *Eur J Immunol,* 34**,** 355-65.

JONES, B. D. & FALKOW, S. 1996. Salmonellosis: host immune responses and bacterial virulence determinants. *Annu Rev Immunol,* 14**,** 533-61.

KAM, H. Y., OU, L. C., THRON, C. D., SMITH, R. P. & LEITER, J. C. 1999. Role of the spleen in the exaggerated polycythemic response to hypoxia in chronic mountain sickness in rats. *J Appl Physiol (1985),* 87**,** 1901-8.

KARIMA, R., MATSUMOTO, S., HIGASHI, H. & MATSUSHIMA, K. 1999. The molecular pathogenesis of endotoxic shock and organ failure. *Mol Med Today,* 5**,** 123-32.

KARIUKI, S., REVATHI, G., KARIUKI, N., KIIRU, J., MWITURIA, J. & HART, C. A. 2006. Characterisation of community acquired non-typhoidal Salmonella from bacteraemia and diarrhoeal infections in children admitted to hospital in Nairobi, Kenya. *BMC Microbiol,* 6**,** 101.

KARLMARK, K. R., WEISKIRCHEN, R., ZIMMERMANN, H. W., GASSLER, N., GINHOUX, F., WEBER, C., MERAD, M., LUEDDE, T., TRAUTWEIN, C. & TACKE, F. 2009. Hepatic recruitment of the inflammatory Gr1+ monocyte subset upon liver injury promotes hepatic fibrosis. *Hepatology,* 50**,** 261-74.

KAUFMANN, S. H. 1993. Immunity to intracellular bacteria. *Annu Rev Immunol,* 11**,** 129-63.

KAYE, D., GILL, F. A. & HOOK, E. W. 1967. Factors influencing host resistance to Salmonella infections: the effects of hemolysis and erythrophagocytosis. *Am J Med Sci,* 254**,** 205-15.

KAYE, D. & HOOK, E. W. 1963. The Influence of Hemolysis on Susceptibility to Salmonella Infection: Additional Observations. *J Immunol,* 91**,** 518-27.

KELLER, T. T., MAIRUHU, A. T., DE KRUIF, M. D., KLEIN, S. K., GERDES, V. E., TEN CATE, H., BRANDJES, D. P., LEVI, M. & VAN GORP, E. C. 2003. Infections and endothelial cells. *Cardiovasc Res,* 60**,** 40-8.

KERRIGAN, A. M., DENNEHY, K. M., MOURAO-SA, D., FARO-TRINDADE, I., WILLMENT, J. A., TAYLOR, P. R., EBLE, J. A., REIS E SOUSA, C. & BROWN, G. D. 2009. CLEC-2 is a phagocytic activation receptor expressed on murine peripheral blood neutrophils. *J Immunol,* 182**,** 4150-7.

KERRIGAN, A. M., NAVARRO-NUNEZ, L., PYZ, E., FINNEY, B. A., WILLMENT, J. A., WATSON, S. P. & BROWN, G. D. 2012. Podoplanin-expressing inflammatory macrophages activate murine platelets via CLEC-2. *J Thromb Haemost,* 10**,** 484-6.

KERRIGAN, S. W. & COX, D. 2010. Platelet-bacterial interactions. *Cell Mol Life Sci,* 67**,** 513-23.

KERRIGAN, S. W., DOUGLAS, I., WRAY, A., HEATH, J., BYRNE, M. F., FITZGERALD, D. & COX, D. 2002. A role for glycoprotein Ib in Streptococcus sanguis-induced platelet aggregation. *Blood,* 100**,** 509-16.

KHOSLA, S. N., SINGH, R., SINGH, G. P. & TREHAN, V. K. 1988. The spectrum of hepatic injury in enteric fever. *Am J Gastroenterol,* 83**,** 413-6.

KIM, H., JEOUNG, J. Y., HAM, S. Y. & KIM, S. R. 1999. Non-typhoid Salmonella meningitis complicated by a infarction of basal ganglia. *J Korean Med Sci,* 14**,** 342-4.

KINOSHITA, M., UCHIDA, T., SATO, A., NAKASHIMA, M., NAKASHIMA, H., SHONO, S., HABU, Y., MIYAZAKI, H., HIROI, S. & SEKI, S. 2010. Characterization of two F4/80-positive Kupffer cell subsets by their function and phenotype in mice. *J Hepatol,* 53**,** 903-10.

KITCHENS, C. S. 2009. Thrombocytopenia and thrombosis in disseminated intravascular coagulation (DIC). *Hematology Am Soc Hematol Educ Program***,** 240-6.

KLEIN, I., CORNEJO, J. C., POLAKOS, N. K., JOHN, B., WUENSCH, S. A., TOPHAM, D. J., PIERCE, R. H. & CRISPE, I. N. 2007. Kupffer cell heterogeneity: functional properties of bone marrow derived and sessile hepatic macrophages. *Blood,* 110**,** 4077-85.

KOCH, M. A., TUCKER-HEARD, G., PERDUE, N. R., KILLEBREW, J. R., URDAHL, K. B. & CAMPBELL, D. J. 2009. The transcription factor T-bet controls regulatory T cell homeostasis and function during type 1 inflammation. *Nat Immunol,* 10**,** 595-602.

KONDO, M., WEISSMAN, I. L. & AKASHI, K. 1997. Identification of clonogenic common lymphoid progenitors in mouse bone marrow. *Cell,* 91**,** 661-72.

KOPF, M., BAUMANN, H., FREER, G., FREUDENBERG, M., LAMERS, M., KISHIMOTO, T., ZINKERNAGEL, R., BLUETHMANN, H. & KOHLER, G. 1994. Impaired immune and acute-phase responses in interleukin-6-deficient mice. *Nature,* 368**,** 339-42.

KORAM, K. A., OWUSU-AGYEI, S., UTZ, G., BINKA, F. N., BAIRD, J. K., HOFFMAN, S. L. & NKRUMAH, F. K. 2000. Severe anemia in young children after high and low malaria transmission seasons in the Kassena-Nankana district of northern Ghana. *Am J Trop Med Hyg,* 62**,** 670-4.

KUCKLEBURG, C. J., YATES, C. M., KALIA, N., ZHAO, Y., NASH, G. B., WATSON, S. P. & RAINGER, G. E. 2011. Endothelial cell-borne platelet bridges selectively recruit monocytes in human and mouse models of vascular inflammation. *Cardiovasc Res,* 91**,** 134-41.

KUHN, R., LOHLER, J., RENNICK, D., RAJEWSKY, K. & MULLER, W. 1993. Interleukin-10-deficient mice develop chronic enterocolitis. *Cell,* 75**,** 263-74.

KUPZ, A., SCOTT, T. A., BELZ, G. T., ANDREWS, D. M., GREYER, M., LEW, A. M., BROOKS, A. G., SMYTH, M. J., CURTISS, R., 3RD, BEDOUI, S. & STRUGNELL, R. A. 2013. Contribution of Thy1+ NK cells to protective IFN-gamma production during Salmonella typhimurium infections. *Proc Natl Acad Sci U S A,* 110**,** 2252-7.

KURTZHALS, J. A., RODRIGUES, O., ADDAE, M., COMMEY, J. O., NKRUMAH, F. K. & HVIID, L. 1997. Reversible suppression of bone marrow response to erythropoietin in Plasmodium falciparum malaria. *Br J Haematol,* 97**,** 169-74.

LAING, R. B., WYNN, R. F., LEEN, C. L. & STANSFIELD, R. 1995. Spontaneous Salmonella peritonitis in HIV infection. *J Infect,* 30**,** 87-8.

LALOR, P. F. & ADAMS, D. H. 2002. The liver: a model of organ-specific lymphocyte recruitment. *Expert Rev Mol Med,* 4**,** 1-16.

LALOR, P. F., HERBERT, J., BICKNELL, R. & ADAMS, D. H. 2013. Hepatic sinusoidal endothelium avidly binds platelets in an integrin-dependent manner, leading to platelet and endothelial activation and leukocyte recruitment. *Am J Physiol Gastrointest Liver Physiol,* 304**,** G469-78.

LAVY, C. B., LAVY, V. R. & ANDERSON, I. 1995. Salmonella septic arthritis in Zambian children. *Trop Doct,* 25**,** 163-6.

LAX, S., HOU, T. Z., JENKINSON, E., SALMON, M., MACFADYEN, J. R., ISACKE, C. M., ANDERSON, G., CUNNINGHAM, A. F. & BUCKLEY, C. D. 2007. CD248/Endosialin is dynamically expressed on a subset of stromal cells during lymphoid tissue development, splenic remodeling and repair. *FEBS Lett,* 581**,** 3550-6.

LE POTTIER, L., DEVAUCHELLE, V., PERS, J. O., JAMIN, C. & YOUINOU, P. 2007. The mosaic of B-cell subsets (with special emphasis on primary Sjogren's syndrome). *Autoimmun Rev,* 6**,** 149-54.

LENTING, P. J., CASARI, C., CHRISTOPHE, O. D. & DENIS, C. V. 2012. von Willebrand factor: the old, the new and the unknown. *J Thromb Haemost,* 10**,** 2428-37.

LENTZ, B. R. 2003. Exposure of platelet membrane phosphatidylserine regulates blood coagulation. *Prog Lipid Res,* 42**,** 423-38.

LEPAGE, P., BOGAERTS, J., VAN GOETHEM, C., NTAHORUTABA, M., NSENGUMUREMYI, F., HITIMANA, D. G., VANDEPITTE, J., BUTZLER, J. P. & LEVY, J. 1987. Community-acquired bacteraemia in African children. *Lancet,* 1**,** 1458-61.

LEVI, M., DE JONGE, E., VAN DER POLL, T. & TEN CATE, H. 1999. Disseminated intravascular coagulation. *Thromb Haemost,* 82**,** 695-705.

LEVI, M., DE JONGE, E., VAN DER POLL, T. & TEN CATE, H. 2000. Novel approaches to the management of disseminated intravascular coagulation. *Crit Care Med,* 28**,** S20-4.

LEVI, M. & VAN DER POLL, T. 2005. Two-way interactions between inflammation and coagulation. *Trends Cardiovasc Med,* 15**,** 254-9.

LEVI, M., VAN DER POLL, T. & BULLER, H. R. 2004. Bidirectional relation between inflammation and coagulation. *Circulation,* 109**,** 2698-704.

LEVIN, J. & EBBE, S. 1994. Why are recently published platelet counts in normal mice so low? *Blood,* 83**,** 3829-31.

LEVINE, W. C., BUEHLER, J. W., BEAN, N. H. & TAUXE, R. V. 1991. Epidemiology of nontyphoidal Salmonella bacteremia during the human immunodeficiency virus epidemic. *J Infect Dis,* 164**,** 81-7.

LEWIS, D. H., CHAN, D. L., PINHEIRO, D., ARMITAGE-CHAN, E. & GARDEN, O. A. 2012. The immunopathology of sepsis: pathogen recognition, systemic inflammation, the compensatory anti-inflammatory response, and regulatory T cells. *J Vet Intern Med,* 26**,** 457-82.

LI, P. Z., LI, J. Z., LI, M., GONG, J. P. & HE, K. 2013. An efficient method to isolate and culture mouse Kupffer cells. *Immunol Lett,* 158**,** 52-56.

LIASKOU, E., WILSON, D. V. & OO, Y. H. 2012. Innate immune cells in liver inflammation. *Mediators Inflamm,* 2012**,** 949157.

LIMB, G. A., WEBSTER, L., SOOMRO, H., JANIKOUN, S. & SHILLING, J. 1999. Platelet expression of tumour necrosis factor-alpha (TNF-alpha), TNF receptors and intercellular adhesion molecule-1 (ICAM-1) in patients with proliferative diabetic retinopathy. *Clin Exp Immunol,* 118**,** 213-8.

LIN, F. R., WANG, X. M., HSU, H. S., MUMAW, V. R. & NAKONECZNA, I. 1987. Electron microscopic studies on the location of bacterial proliferation in the liver in murine salmonellosis. *Br J Exp Pathol,* 68**,** 539-50.

LINDGREN, S. W., STOJILJKOVIC, I. & HEFFRON, F. 1996. Macrophage killing is an essential virulence mechanism of Salmonella typhimurium. *Proc Natl Acad Sci U S A,* 93**,** 4197-201.

LOWE, K. L., NAVARRO-NUNEZ, L. & WATSON, S. P. 2012. Platelet CLEC-2 and podoplanin in cancer metastasis. *Thromb Res,* 129 Suppl 1**,** S30-7.

LUGO-VILLARINO, G., MALDONADO-LOPEZ, R., POSSEMATO, R., PENARANDA, C. & GLIMCHER, L. H. 2003. T-bet is required for optimal production of IFN-gamma and antigen-specific T cell activation by dendritic cells. *Proc Natl Acad Sci U S A,* 100**,** 7749-54.

MABEY, D. C., BROWN, A. & GREENWOOD, B. M. 1987. Plasmodium falciparum malaria and Salmonella infections in Gambian children. *J Infect Dis,* 155**,** 1319-21.

MACKENZIE, G., CEESAY, S. J., HILL, P. C., WALTHER, M., BOJANG, K. A., SATOGUINA, J., ENWERE, G., D'ALESSANDRO, U., SAHA, D., IKUMAPAYI, U. N., O'DEMPSEY, T., MABEY, D. C., CORRAH, T., CONWAY, D. J., ADEGBOLA, R. A. & GREENWOOD, B. M. 2010. A decline in the incidence of invasive non-typhoidal Salmonella infection in The Gambia temporally associated with a decline in malaria infection. *PLoS One,* 5**,** e10568.

MACLENNAN, C. A., GILCHRIST, J. J., GORDON, M. A., CUNNINGHAM, A. F., COBBOLD, M., GOODALL, M., KINGSLEY, R. A., VAN OOSTERHOUT, J. J., MSEFULA, C. L., MANDALA, W. L., LEYTON, D. L., MARSHALL, J. L., GONDWE, E. N., BOBAT, S., LOPEZ-MACIAS, C., DOFFINGER, R., HENDERSON, I. R., ZIJLSTRA, E. E., DOUGAN, G., DRAYSON, M. T., MACLENNAN, I. C. & MOLYNEUX, M. E. 2010. Dysregulated humoral immunity to nontyphoidal Salmonella in HIV-infected African adults. *Science,* 328**,** 508-12.

MACLENNAN, C. A., GONDWE, E. N., MSEFULA, C. L., KINGSLEY, R. A., THOMSON, N. R., WHITE, S. A., GOODALL, M., PICKARD, D. J., GRAHAM, S. M., DOUGAN, G., HART, C. A., MOLYNEUX, M. E. & DRAYSON, M. T. 2008. The neglected role of antibody in protection against bacteremia caused by nontyphoidal strains of Salmonella in African children. *J Clin Invest,* 118**,** 1553-62.

MAHTAB, E. A., WIJFFELS, M. C., VAN DEN AKKER, N. M., HAHURIJ, N. D., LIE-VENEMA, H., WISSE, L. J., DERUITER, M. C., UHRIN, P., ZAUJEC, J., BINDER, B. R., SCHALIJ, M. J., POELMANN, R. E. & GITTENBERGER-DE GROOT, A. C. 2008. Cardiac malformations and myocardial abnormalities in podoplanin knockout mouse embryos: Correlation with abnormal epicardial development. *Dev Dyn,* 237**,** 847-57.

MALIK, A. S. 2002. Complications of bacteriologically confirmed typhoid fever in children. *J Trop Pediatr,* 48**,** 102-8.

MALLORY, F. B. 1898. A Histological Study of Typhoid Fever. *J Exp Med,* 3**,** 611-38.

MALLOUH, A. A. & SA'DI, A. R. 1987. White blood cells and bone marrow in typhoid fever. *Pediatr Infect Dis J,* 6**,** 527-9.

MASSBERG, S., GAWAZ, M., GRUNER, S., SCHULTE, V., KONRAD, I., ZOHLNHOFER, D., HEINZMANN, U. & NIESWANDT, B. 2003. A crucial role of glycoprotein VI for platelet recruitment to the injured arterial wall in vivo. *J Exp Med,* 197**,** 41-9.

MASSBERG, S., GRAHL, L., VON BRUEHL, M. L., MANUKYAN, D., PFEILER, S., GOOSMANN, C., BRINKMANN, V., LORENZ, M., BIDZHEKOV, K., KHANDAGALE, A. B., KONRAD, I., KENNERKNECHT, E., REGES, K., HOLDENRIEDER, S., BRAUN, S., REINHARDT, C., SPANNAGL, M., PREISSNER, K. T. & ENGELMANN, B. 2010. Reciprocal coupling of coagulation and innate immunity via neutrophil serine proteases. *Nat Med,* 16**,** 887-96.

MASSON, P. L., HEREMANS, J. F. & SCHONNE, E. 1969. Lactoferrin, an iron-binding protein in neutrophilic leukocytes. *J Exp Med,* 130**,** 643-58.

MASTROENI, P. 2002. Immunity to systemic Salmonella infections. *Curr Mol Med,* 2**,** 393-406.

MASTROENI, P., ARENA, A., COSTA, G. B., LIBERTO, M. C., BONINA, L. & HORMAECHE, C. E. 1991. Serum TNF alpha in mouse typhoid and enhancement of a Salmonella infection by anti-TNF alpha antibodies. *Microb Pathog,* 11**,** 33-8.

MASTROENI, P., GRANT, A., RESTIF, O. & MASKELL, D. 2009. A dynamic view of the spread and intracellular distribution of Salmonella enterica. *Nat Rev Microbiol,* 7**,** 73-80.

MASTROENI, P., HARRISON, J. A., ROBINSON, J. H., CLARE, S., KHAN, S., MASKELL, D. J., DOUGAN, G. & HORMAECHE, C. E. 1998. Interleukin-12 is required for control of the growth of attenuated aromatic-compound-dependent salmonellae in BALB/c mice: role of gamma interferon and macrophage activation. *Infect Immun,* 66**,** 4767-76.

MASTROENI, P. & SHEPPARD, M. 2004. Salmonella infections in the mouse model: host resistance factors and in vivo dynamics of bacterial spread and distribution in the tissues. *Microbes Infect,* 6**,** 398-405.

MASTROENI, P., SKEPPER, J. N. & HORMAECHE, C. E. 1995. Effect of anti-tumor necrosis factor alpha antibodies on histopathology of primary Salmonella infections. *Infect Immun,* 63**,** 3674-82.

MASTROENI, P., VILLARREAL-RAMOS, B. & HORMAECHE, C. E. 1992. Role of T cells, TNF alpha and IFN gamma in recall of immunity to oral challenge with virulent salmonellae in mice vaccinated with live attenuated aro- Salmonella vaccines. *Microb Pathog,* 13**,** 477-91.

MAZZACCARA, C., LABRUNA, G., CITO, G., SCARFO, M., DE FELICE, M., PASTORE, L. & SACCHETTI, L. 2008. Age-Related Reference Intervals of the Main Biochemical and Hematological Parameters in C57BL/6J, 129SV/EV and C3H/HeJ Mouse Strains. *PLoS One,* 3**,** e3772.

MCKENZIE, S. E., TAYLOR, S. M., MALLADI, P., YUHAN, H., CASSEL, D. L., CHIEN, P., SCHWARTZ, E., SCHREIBER, A. D., SURREY, S. & REILLY, M. P. 1999. The role of the human Fc receptor Fc gamma RIIA in the immune clearance of platelets: a transgenic mouse model. *J Immunol,* 162**,** 4311-8.

MCSORLEY, S. J. & JENKINS, M. K. 2000. Antibody is required for protection against virulent but not attenuated Salmonella enterica serovar typhimurium. *Infect Immun,* 68**,** 3344-8.

MEANS, R. T., JR. 2000. The anaemia of infection. *Baillieres Best Pract Res Clin Haematol,* 13**,** 151-62.

MENDIRATTA, S. K., MARTIN, W. D., HONG, S., BOESTEANU, A., JOYCE, S. & VAN KAER, L. 1997. CD1d1 mutant mice are deficient in natural T cells that promptly produce IL-4. *Immunity,* 6**,** 469-77.

MILES, A. A., MISRA, S. S. & IRWIN, J. O. 1938. The estimation of the bactericidal power of the blood. *J Hyg (Lond),* 38**,** 732-49.

MIRZA, S. H. & HART, C. A. 1993. Plasmid encoded multi-drug resistance in Salmonella typhi from Pakistan. *Ann Trop Med Parasitol,* 87**,** 373-7.

MITTRUCKER, H. W. & KAUFMANN, S. H. 2000. Immune response to infection with Salmonella typhimurium in mice. *J Leukoc Biol,* 67**,** 457-63.

MITTRUCKER, H. W., KOHLER, A. & KAUFMANN, S. H. 2002. Characterization of the murine T-lymphocyte response to Salmonella enterica serovar Typhimurium infection. *Infect Immun,* 70**,** 199-203.

MITTRUCKER, H. W., KOHLER, A., MAK, T. W. & KAUFMANN, S. H. 1999. Critical role of CD28 in protective immunity against Salmonella typhimurium. *J Immunol,* 163**,** 6769-76.

MITTRUCKER, H. W., RAUPACH, B., KOHLER, A. & KAUFMANN, S. H. 2000. Cutting edge: role of B lymphocytes in protective immunity against Salmonella typhimurium infection. *J Immunol,* 164**,** 1648-52.

MIYAMOTO, Y., UGA, H., TANAKA, S., KADOWAKI, M., IKEDA, M., SAEGUSA, J., MORINOBU, A., KUMAGAI, S. & KURATA, H. 2013. Podoplanin is an inflammatory protein upregulated in Th17 cells in SKG arthritic joints. *Mol Immunol,* 54**,** 199-207.

MOHR, E., CUNNINGHAM, A. F., TOELLNER, K. M., BOBAT, S., COUGHLAN, R. E., BIRD, R. A., MACLENNAN, I. C. & SERRE, K. 2010. IFN-{gamma} produced by CD8 T cells induces T-bet-dependent and -independent class switching in B cells in responses to alum-precipitated protein vaccine. *Proc Natl Acad Sci U S A,* 107**,** 17292-7.

MOHRS, M., LEDERMANN, B., KOHLER, G., DORFMULLER, A., GESSNER, A. & BROMBACHER, F. 1999. Differences between IL-4- and IL-4 receptor alpha-deficient mice in chronic leishmaniasis reveal a protective role for IL-13 receptor signaling. *J Immunol,* 162**,** 7302-8.

MOLYNEUX, E. & FRENCH, G. 1982. Salmonella joint infection in Malawian children. *J Infect,* 4**,** 131-8.

MOLYNEUX, E., WALSH, A., PHIRI, A. & MOLYNEUX, M. 1998. Acute bacterial meningitis in children admitted to the Queen Elizabeth Central Hospital, Blantyre, Malawi in 1996-97. *Trop Med Int Health,* 3**,** 610-8.

MOLYNEUX, E. M., WALSH, A. L., MALENGA, G., ROGERSON, S. & MOLYNEUX, M. E. 2000. Salmonella meningitis in children in Blantyre, Malawi, 1996-1999. *Ann Trop Paediatr,* 20**,** 41-4.

MOMBAERTS, P., CLARKE, A. R., RUDNICKI, M. A., IACOMINI, J., ITOHARA, S., LAFAILLE, J. J., WANG, L., ICHIKAWA, Y., JAENISCH, R., HOOPER, M. L. & ET AL. 1992a. Mutations in T-cell antigen receptor genes alpha and beta block thymocyte development at different stages. *Nature,* 360**,** 225-31.

MOMBAERTS, P., IACOMINI, J., JOHNSON, R. S., HERRUP, K., TONEGAWA, S. & PAPAIOANNOU, V. E. 1992b. RAG-1-deficient mice have no mature B and T lymphocytes. *Cell,* 68**,** 869-77.

MONACK, D. M., BOULEY, D. M. & FALKOW, S. 2004a. Salmonella typhimurium persists within macrophages in the mesenteric lymph nodes of chronically infected Nramp1+/+ mice and can be reactivated by IFNgamma neutralization. *J Exp Med,* 199**,** 231-41.

MONACK, D. M., MUELLER, A. & FALKOW, S. 2004b. Persistent bacterial infections: the interface of the pathogen and the host immune system. *Nat Rev Microbiol,* 2**,** 747-65.

MORPETH, S. C., RAMADHANI, H. O. & CRUMP, J. A. 2009. Invasive non-Typhi Salmonella disease in Africa. *Clin Infect Dis,* 49**,** 606-11.

MOSMANN, T. R., CHERWINSKI, H., BOND, M. W., GIEDLIN, M. A. & COFFMAN, R. L. 1986. Two types of murine helper T cell clone. I. Definition according to profiles of lymphokine activities and secreted proteins. *J Immunol,* 136**,** 2348-57.

MOSMANN, T. R. & COFFMAN, R. L. 1989. TH1 and TH2 cells: different patterns of lymphokine secretion lead to different functional properties. *Annu Rev Immunol,* 7**,** 145-73.

MUYEMBE-TAMFUM, J. J., VEYI, J., KASWA, M., LUNGUYA, O., VERHAEGEN, J. & BOELAERT, M. 2009. An outbreak of peritonitis caused by multidrug-resistant Salmonella Typhi in Kinshasa, Democratic Republic of Congo. *Travel Med Infect Dis,* 7**,** 40-3.

NAKONECZNA, I. & HSU, H. S. 1980. The comparative histopathology of primary and secondary lesions in murine salmonellosis. *Br J Exp Pathol,* 61**,** 76-84.

NAKONECZNA, I. & HSU, H. S. 1983. Histopathological study of protective immunity against murine salmonellosis induced by killed vaccine. *Infect Immun,* 39**,** 423-30.

NAUCIEL, C. 1990. Role of CD4+ T cells and T-independent mechanisms in acquired resistance to Salmonella typhimurium infection. *J Immunol,* 145**,** 1265-9.

NAUCIEL, C. & ESPINASSE-MAES, F. 1992. Role of gamma interferon and tumor necrosis factor alpha in resistance to Salmonella typhimurium infection. *Infect Immun,* 60**,** 450-4.

NESBITT, A. & MIRZA, N. B. 1989. Salmonella septicaemias in Kenyan children. *J Trop Pediatr,* 35**,** 35-9.

NEWTON, C. R., WARN, P. A., WINSTANLEY, P. A., PESHU, N., SNOW, R. W., PASVOL, G. & MARSH, K. 1997. Severe anaemia in children living in a malaria endemic area of Kenya. *Trop Med Int Health,* 2**,** 165-78.

NGUYEN, T., HALL, M., HAN, Y., FIEDOR, M., HASSET, A., LOPEZ-PLAZA, I., WATSON, S., LUM, L. & CARCILLO, J. A. 2001. Microvascular thrombosis in pediatric multiple organ failure: Is it a therapeutic target? *Pediatr Crit Care Med,* 2**,** 187-196.

NGUYEN, T. C. & CARCILLO, J. A. 2006. Bench-to-bedside review: thrombocytopenia-associated multiple organ failure--a newly appreciated syndrome in the critically ill. *Crit Care,* 10**,** 235.

NIESWANDT, B., SCHULTE, V., BERGMEIER, W., MOKHTARI-NEJAD, R., RACKEBRANDT, K., CAZENAVE, J. P., OHLMANN, P., GACHET, C. & ZIRNGIBL, H. 2001. Long-term antithrombotic protection by in vivo depletion of platelet glycoprotein VI in mice. *J Exp Med,* 193**,** 459-69.

NIX, R. N., ALTSCHULER, S. E., HENSON, P. M. & DETWEILER, C. S. 2007. Hemophagocytic macrophages harbor Salmonella enterica during persistent infection. *PLoS Pathog,* 3**,** e193.

NNALUE, N. A., SHNYRA, A., HULTENBY, K. & LINDBERG, A. A. 1992. Salmonella choleraesuis and Salmonella typhimurium associated with liver cells after intravenous inoculation of rats are localized mainly in Kupffer cells and multiply intracellularly. *Infect Immun,* 60**,** 2758-68.

NOLAN, J. P. 1981. Endotoxin, reticuloendothelial function, and liver injury. *Hepatology,* 1**,** 458-65.

OHL, M. E. & MILLER, S. I. 2001. Salmonella: a model for bacterial pathogenesis. *Annu Rev Med,* 52**,** 259-74.

OLUBODUN, J. O., KUTI, J. A., ADEFUYE, B. O. & TALABI, A. O. 1994. Typhoid fever associated with severe hepatitis. *Cent Afr J Med,* 40**,** 262-4.

OPAL, S. M. 2003. Interactions between coagulation and inflammation. *Scand J Infect Dis,* 35**,** 545-54.

OZEN, H., SECMEER, G., KANRA, G., ECEVIT, Z., CEYHAN, M., DURSUN, A. & ANLAR, Y. 1995. Typhoid fever with very high transaminase levels. *Turk J Pediatr,* 37**,** 169-71.

PECK-RADOSAVLJEVIC, M. 2007. Review article: coagulation disorders in chronic liver disease. *Aliment Pharmacol Ther,* 26 Suppl 1**,** 21-8.

PESCHON, J. J., TORRANCE, D. S., STOCKING, K. L., GLACCUM, M. B., OTTEN, C., WILLIS, C. R., CHARRIER, K., MORRISSEY, P. J., WARE, C. B. & MOHLER, K. M. 1998. TNF receptor-deficient mice reveal divergent roles for p55 and p75 in several models of inflammation. *J Immunol,* 160**,** 943-52.

PETERS, A., PITCHER, L. A., SULLIVAN, J. M., MITSDOERFFER, M., ACTON, S. E., FRANZ, B., WUCHERPFENNIG, K., TURLEY, S., CARROLL, M. C., SOBEL, R. A., BETTELLI, E. & KUCHROO, V. K. 2011. Th17 cells induce ectopic lymphoid follicles in central nervous system tissue inflammation. *Immunity,* 35**,** 986-96.

PETERSEN, H. J., KEANE, C., JENKINSON, H. F., VICKERMAN, M. M., JESIONOWSKI, A., WATERHOUSE, J. C., COX, D. & KERRIGAN, S. W. 2010. Human platelets recognize a novel surface protein, PadA, on Streptococcus gordonii through a unique interaction involving fibrinogen receptor GPIIbIIIa. *Infect Immun,* 78**,** 413-22.

PEVERI, P., WALZ, A., DEWALD, B. & BAGGIOLINI, M. 1988. A novel neutrophil-activating factor produced by human mononuclear phagocytes. *J Exp Med,* 167**,** 1547-59.

PIE, S., MATSIOTA-BERNARD, P., TRUFFA-BACHI, P. & NAUCIEL, C. 1996. Gamma interferon and interleukin-10 gene expression in innately susceptible and resistant mice during the early phase of Salmonella typhimurium infection. *Infect Immun,* 64**,** 849-54.

PIE, S., TRUFFA-BACHI, P., PLA, M. & NAUCIEL, C. 1997. Th1 response in Salmonella typhimurium-infected mice with a high or low rate of bacterial clearance. *Infect Immun,* 65**,** 4509-14.

PIGNATELLI, P., DE BIASE, L., LENTI, L., TOCCI, G., BRUNELLI, A., CANGEMI, R., RIONDINO, S., GREGO, S., VOLPE, M. & VIOLI, F. 2005. Tumor necrosis factor-alpha as trigger of platelet activation in patients with heart failure. *Blood,* 106**,** 1992-4.

PRAMOOLSINSAP, C. & VIRANUVATTI, V. 1998. Salmonella hepatitis. *J Gastroenterol Hepatol,* 13**,** 745-50.

PROTZER, U., MAINI, M. K. & KNOLLE, P. A. 2012. Living in the liver: hepatic infections. *Nat Rev Immunol,* 12**,** 201-13.

PUNTENER, U., BOOTH, S. G., PERRY, V. H. & TEELING, J. L. 2012. Long-term impact of systemic bacterial infection on the cerebral vasculature and microglia. *J Neuroinflammation,* 9**,** 146.

RAJEKAR, H., WAI, C. T., LEE, K. H., WONG, S. Y. & TAN, K. C. 2008. Spontaneous bacterial peritonitis from Salmonella: an unusual bacterium with unusual presentation. *Hepatol Int,* 2**,** 388-9.

RAMACHANDRAN, S., GODFREY, J. J. & PERERA, M. V. 1974. Typhoid hepatitis. *JAMA,* 230**,** 236-40.

RAMAIAH, S. K. 2007. A toxicologist guide to the diagnostic interpretation of hepatic biochemical parameters. *Food Chem Toxicol,* 45**,** 1551-7.

RAMARATHINAM, L., NIESEL, D. W. & KLIMPEL, G. R. 1993. Salmonella typhimurium induces IFN-gamma production in murine splenocytes. Role of natural killer cells and macrophages. *J Immunol,* 150**,** 3973-81.

RAMARATHINAM, L., SHABAN, R. A., NIESEL, D. W. & KLIMPEL, G. R. 1991. Interferon gamma (IFN-gamma) production by gut-associated lymphoid tissue and spleen following oral Salmonella typhimurium challenge. *Microb Pathog,* 11**,** 347-56.

RAO, P. N., BHUSNURMATH, S. R. & NAIK, S. R. 1978. Typhoid fever manifesting with haematemesis, hepatitis and haemolysis. *J Trop Med Hyg,* 81**,** 146-50.

RAVINDRAN, R., FOLEY, J., STOKLASEK, T., GLIMCHER, L. H. & MCSORLEY, S. J. 2005. Expression of T-bet by CD4 T cells is essential for resistance to Salmonella infection. *J Immunol,* 175**,** 4603-10.

RAVINDRAN, R. & MCSORLEY, S. J. 2005. Tracking the dynamics of T-cell activation in response to Salmonella infection. *Immunology,* 114**,** 450-8.

RICHTER-DAHLFORS, A., BUCHAN, A. M. & FINLAY, B. B. 1997. Murine salmonellosis studied by confocal microscopy: Salmonella typhimurium resides intracellularly inside macrophages and exerts a cytotoxic effect on phagocytes in vivo. *J Exp Med,* 186**,** 569-80.

ROGER, V. L., GO, A. S., LLOYD-JONES, D. M., ADAMS, R. J., BERRY, J. D., BROWN, T. M., CARNETHON, M. R., DAI, S., DE SIMONE, G., FORD, E. S., FOX, C. S., FULLERTON, H. J., GILLESPIE, C., GREENLUND, K. J., HAILPERN, S. M., HEIT, J. A., HO, P. M., HOWARD, V. J., KISSELA, B. M., KITTNER, S. J., LACKLAND, D. T., LICHTMAN, J. H., LISABETH, L. D., MAKUC, D. M., MARCUS, G. M., MARELLI, A., MATCHAR, D. B., MCDERMOTT, M. M., MEIGS, J. B., MOY, C. S., MOZAFFARIAN, D., MUSSOLINO, M. E., NICHOL, G., PAYNTER, N. P., ROSAMOND, W. D., SORLIE, P. D., STAFFORD, R. S., TURAN, T. N., TURNER, M. B., WONG, N. D., WYLIE-ROSETT, J., AMERICAN HEART ASSOCIATION STATISTICS, C. & STROKE STATISTICS, S. 2011. Heart disease and stroke statistics--2011 update: a report from the American Heart Association. *Circulation,* 123**,** e18-e209.

ROSS, E. A., COUGHLAN, R. E., FLORES-LANGARICA, A., LAX, S., NICHOLSON, J., DESANTI, G. E., MARSHALL, J. L., BOBAT, S., HITCHCOCK, J., WHITE, A., JENKINSON, W. E., KHAN, M., HENDERSON, I. R., LAVERY, G. G., BUCKLEY, C. D., ANDERSON, G. & CUNNINGHAM, A. F. 2012. Thymic function is maintained during Salmonella-induced atrophy and recovery. *J Immunol,* 189**,** 4266-74.

ROY, M. F., LARIVIERE, L., WILKINSON, R., TAM, M., STEVENSON, M. M. & MALO, D. 2006. Incremental expression of Tlr4 correlates with mouse resistance to Salmonella infection and fine regulation of relevant immune genes. *Genes Immun,* 7**,** 372-83.

SAHA, M. R., SAHA, D., DUTTA, P., MITRA, U. & BHATTACHARYA, S. K. 2001. Isolation of Salmonella enterica serotypes from children with diarrhoea in Calcutta, India. *J Health Popul Nutr,* 19**,** 301-5.

SAKAGUCHI, S. 2004. Naturally arising CD4+ regulatory t cells for immunologic self-tolerance and negative control of immune responses. *Annu Rev Immunol,* 22**,** 531-62.

SAKAI, A., TANAKA, S. & KOUNTZ, S. L. 1978. Liver and immune responses. IV. Characteristics of the liver cell-lymphocyte interaction. *Transplantation,* 25**,** 110-4.

SALCEDO, S. P., NOURSADEGHI, M., COHEN, J. & HOLDEN, D. W. 2001. Intracellular replication of Salmonella typhimurium strains in specific subsets of splenic macrophages in vivo. *Cell Microbiol,* 3**,** 587-97.

SANTOS, R. L., ZHANG, S., TSOLIS, R. M., KINGSLEY, R. A., ADAMS, L. G. & BAUMLER, A. J. 2001. Animal models of Salmonella infections: enteritis versus typhoid fever. *Microbes Infect,* 3**,** 1335-44.

SARWEEN, N., CHODOS, A., RAYKUNDALIA, C., KHAN, M., ABBAS, A. K. & WALKER, L. S. 2004. CD4+CD25+ cells controlling a pathogenic CD4 response inhibit cytokine differentiation, CXCR-3 expression, and tissue invasion. *J Immunol,* 173**,** 2942-51.

SAUNDERS, B. M., BRISCOE, H. & BRITTON, W. J. 2004. T cell-derived tumour necrosis factor is essential, but not sufficient, for protection against Mycobacterium tuberculosis infection. *Clin Exp Immunol,* 137**,** 279-87.

SCHREIBER, H. A., HARDING, J. S., HUNT, O., ALTAMIRANO, C. J., HULSEBERG, P. D., STEWART, D., FABRY, Z. & SANDOR, M. 2011. Inflammatory dendritic cells migrate in and out of transplanted chronic mycobacterial granulomas in mice. *J Clin Invest,* 121**,** 3902-13.

SCUMPIA, P. O., KELLY-SCUMPIA, K. M., DELANO, M. J., WEINSTEIN, J. S., CUENCA, A. G., AL-QURAN, S., BOVIO, I., AKIRA, S., KUMAGAI, Y. & MOLDAWER, L. L. 2010. Cutting edge: bacterial infection induces hematopoietic stem and progenitor cell expansion in the absence of TLR signaling. *J Immunol,* 184**,** 2247-51.

SEGAL, A. W. 2005. How neutrophils kill microbes. *Annu Rev Immunol,* 23**,** 197-223.

SEGURA, E. & AMIGORENA, S. 2013. Inflammatory dendritic cells in mice and humans. *Trends Immunol,* 34**,** 440-5.

SEKI, S., HABU, Y., KAWAMURA, T., TAKEDA, K., DOBASHI, H., OHKAWA, T. & HIRAIDE, H. 2000. The liver as a crucial organ in the first line of host defense: the roles of Kupffer cells, natural killer (NK) cells and NK1.1 Ag+ T cells in T helper 1 immune responses. *Immunol Rev,* 174**,** 35-46.

SEKI, S., OSADA, S., ONO, S., AOSASA, S., HABU, Y., NISHIKAGE, T., MOCHIZUKI, H. & HIRAIDE, H. 1998. Role of liver NK cells and peritoneal macrophages in gamma interferon and interleukin-10 production in experimental bacterial peritonitis in mice. *Infect Immun,* 66**,** 5286-94.

SEMPLE, J. W., ITALIANO, J. E., JR. & FREEDMAN, J. 2011. Platelets and the immune continuum. *Nat Rev Immunol,* 11**,** 264-74.

SEREFHANOGLU, K., KAYA, E., SEVINC, A., AYDOGDU, I., KUKU, I. & ERSOY, Y. 2003. Isolated thrombocytopenia: the presenting finding of typhoid fever. *Clin Lab Haematol,* 25**,** 63-5.

SERRE, K., MOHR, E., TOELLNER, K. M., CUNNINGHAM, A. F., GRANJEAUD, S., BIRD, R. & MACLENNAN, I. C. 2008. Molecular differences between the divergent responses of ovalbumin-specific CD4 T cells to alum-precipitated ovalbumin compared to ovalbumin expressed by Salmonella. *Mol Immunol,* 45**,** 3558-66.

SHEPPARD, M., WEBB, C., HEATH, F., MALLOWS, V., EMILIANUS, R., MASKELL, D. & MASTROENI, P. 2003. Dynamics of bacterial growth and distribution within the liver during Salmonella infection. *Cell Microbiol,* 5**,** 593-600.

SILVA-HERZOG, E. & DETWEILER, C. S. 2008. Intracellular microbes and haemophagocytosis. *Cell Microbiol,* 10**,** 2151-8.

SILVA-HERZOG, E. & DETWEILER, C. S. 2010. Salmonella enterica replication in hemophagocytic macrophages requires two type three secretion systems. *Infect Immun,* 78**,** 3369-77.

SINGH, Z. N., RAKHEJA, D., YADAV, T. P. & SHOME, D. K. 2005. Infection-associated haemophagocytosis: the tropical spectrum. *Clin Lab Haematol,* 27**,** 312-5.

SINHA, A., SAZAWAL, S., KUMAR, R., SOOD, S., REDDAIAH, V. P., SINGH, B., RAO, M., NAFICY, A., CLEMENS, J. D. & BHAN, M. K. 1999. Typhoid fever in children aged less than 5 years. *Lancet,* 354**,** 734-7.

SOLTER, P. F. 2005. Clinical pathology approaches to hepatic injury. *Toxicol Pathol,* 33**,** 9-16.

SULLIVAN, B. M., JUEDES, A., SZABO, S. J., VON HERRATH, M. & GLIMCHER, L. H. 2003. Antigen-driven effector CD8 T cell function regulated by T-bet. *Proc Natl Acad Sci U S A,* 100**,** 15818-23.

SUN, H. 2006. The interaction between pathogens and the host coagulation system. *Physiology (Bethesda),* 21**,** 281-8.

SUZUKI-INOUE, K., FULLER, G. L., GARCIA, A., EBLE, J. A., POHLMANN, S., INOUE, O., GARTNER, T. K., HUGHAN, S. C., PEARCE, A. C., LAING, G. D., THEAKSTON, R. D., SCHWEIGHOFFER, E., ZITZMANN, N., MORITA, T., TYBULEWICZ, V. L., OZAKI, Y. & WATSON, S. P. 2006. A novel Syk-dependent mechanism of platelet activation by the C-type lectin receptor CLEC-2. *Blood,* 107**,** 542-9.

SUZUKI-INOUE, K., INOUE, O., DING, G., NISHIMURA, S., HOKAMURA, K., ETO, K., KASHIWAGI, H., TOMIYAMA, Y., YATOMI, Y., UMEMURA, K., SHIN, Y., HIRASHIMA, M. & OZAKI, Y. 2010. Essential in vivo roles of the C-type lectin receptor CLEC-2: embryonic/neonatal lethality of CLEC-2-deficient mice by blood/lymphatic misconnections and impaired thrombus formation of CLEC-2-deficient platelets. *J Biol Chem,* 285**,** 24494-507.

SWAIN, S. L., WEINBERG, A. D., ENGLISH, M. & HUSTON, G. 1990. IL-4 directs the development of Th2-like helper effectors. *J Immunol,* 145**,** 3796-806.

SZABO, S. J., KIM, S. T., COSTA, G. L., ZHANG, X., FATHMAN, C. G. & GLIMCHER, L. H. 2000. A novel transcription factor, T-bet, directs Th1 lineage commitment. *Cell,* 100**,** 655-69.

SZABO, S. J., SULLIVAN, B. M., STEMMANN, C., SATOSKAR, A. R., SLECKMAN, B. P. & GLIMCHER, L. H. 2002. Distinct effects of T-bet in TH1 lineage commitment and IFN-gamma production in CD4 and CD8 T cells. *Science,* 295**,** 338-42.

TACKE, F. 2012. Functional role of intrahepatic monocyte subsets for the progression of liver inflammation and liver fibrosis in vivo. *Fibrogenesis Tissue Repair,* 5 Suppl 1**,** S27.

TACKE, F., LUEDDE, T. & TRAUTWEIN, C. 2009. Inflammatory pathways in liver homeostasis and liver injury. *Clin Rev Allergy Immunol,* 36**,** 4-12.

TAM, M. A., RYDSTROM, A., SUNDQUIST, M. & WICK, M. J. 2008. Early cellular responses to Salmonella infection: dendritic cells, monocytes, and more. *Immunol Rev,* 225**,** 140-62.

TANIGUCHI, H., TOYOSHIMA, T., FUKAO, K. & NAKAUCHI, H. 1996. Presence of hematopoietic stem cells in the adult liver. *Nat Med,* 2**,** 198-203.

THOMSON, A. W. & KNOLLE, P. A. 2010. Antigen-presenting cell function in the tolerogenic liver environment. *Nat Rev Immunol,* 10**,** 753-66.

TIEDT, R., SCHOMBER, T., HAO-SHEN, H. & SKODA, R. C. 2007. Pf4-Cre transgenic mice allow the generation of lineage-restricted gene knockouts for studying megakaryocyte and platelet function in vivo. *Blood,* 109**,** 1503-6.

TILLEY, D. O., ARMAN, M., SMOLENSKI, A., COX, D., O'DONNELL, J. S., DOUGLAS, C. W., WATSON, S. P. & KERRIGAN, S. W. 2013. Glycoprotein Ibalpha and FcgammaRIIa play key roles in platelet activation by the colonizing bacterium, Streptococcus oralis. *J Thromb Haemost,* 11**,** 941-50.

TOYONAGA, T., HINO, O., SUGAI, S., WAKASUGI, S., ABE, K., SHICHIRI, M. & YAMAMURA, K. 1994. Chronic active hepatitis in transgenic mice expressing interferon-gamma in the liver. *Proc Natl Acad Sci U S A,* 91**,** 614-8.

TREYER, A. & MUSCH, A. 2013. Hepatocyte polarity. *Compr Physiol,* 3**,** 243-87.

TSAKIRIS, D. A., SCUDDER, L., HODIVALA-DILKE, K., HYNES, R. O. & COLLER, B. S. 1999. Hemostasis in the mouse (Mus musculus): a review. *Thromb Haemost,* 81**,** 177-88.

TSOLIS, R. M., XAVIER, M. N., SANTOS, R. L. & BAUMLER, A. J. 2011. How to become a top model: impact of animal experimentation on human Salmonella disease research. *Infect Immun,* 79**,** 1806-14.

UDDEN, M. M., BANEZ, E. & SEARS, D. A. 1986. Bone marrow histiocytic hyperplasia and hemophagocytosis with pancytopenia in typhoid fever. *Am J Med Sci,* 291**,** 396-400.

UHRIN, P., ZAUJEC, J., BREUSS, J. M., OLCAYDU, D., CHRENEK, P., STOCKINGER, H., FUERTBAUER, E., MOSER, M., HAIKO, P., FASSLER, R., ALITALO, K., BINDER, B. R. & KERJASCHKI, D. 2010. Novel function for blood platelets and podoplanin in developmental separation of blood and lymphatic circulation. *Blood,* 115**,** 3997-4005.

UMEZAWA, K., OHNISHI, N., TANAKA, K., KAMIYA, S., KOGA, Y., NAKAZAWA, H. & OZAWA, A. 1995. Granulation in livers of mice infected with Salmonella typhimurium is caused by superoxide released from host phagocytes. *Infect Immun,* 63**,** 4402-8.

VALLS SERON, M., HAIKO, J., PG, D. E. G., KORHONEN, T. K. & MEIJERS, J. C. 2010. Thrombin-activatable fibrinolysis inhibitor is degraded by Salmonella enterica and Yersinia pestis. *J Thromb Haemost,* 8**,** 2232-40.

VAN'T VEER, C. & VAN DER POLL, T. 2008. Keeping blood clots at bay in sepsis. *Nat Med,* 14**,** 606-8.

VAN BASTEN, J. P. & STOCKENBRUGGER, R. 1994. Typhoid perforation. A review of the literature since 1960. *Trop Geogr Med,* 46**,** 336-9.

VAN ROOIJEN, N. 1989. The liposome-mediated macrophage 'suicide' technique. *J Immunol Methods,* 124**,** 1-6.

VAN ROOIJEN, N. & SANDERS, A. 1996. Kupffer cell depletion by liposome-delivered drugs: comparative activity of intracellular clodronate, propamidine, and ethylenediaminetetraacetic acid. *Hepatology,* 23**,** 1239-43.

VAN SORGE, N. M., ZIALCITA, P. A., BROWNE, S. H., QUACH, D., GUINEY, D. G. & DORAN, K. S. 2011. Penetration and activation of brain endothelium by Salmonella enterica serovar Typhimurium. *J Infect Dis,* 203**,** 401-5.

VANCOTT, J. L., CHATFIELD, S. N., ROBERTS, M., HONE, D. M., HOHMANN, E. L., PASCUAL, D. W., YAMAMOTO, M., KIYONO, H. & MCGHEE, J. R. 1998. Regulation of host immune responses by modification of Salmonella virulence genes. *Nat Med,* 4**,** 1247-52.

VAZQUEZ-TORRES, A., JONES-CARSON, J., BAUMLER, A. J., FALKOW, S., VALDIVIA, R., BROWN, W., LE, M., BERGGREN, R., PARKS, W. T. & FANG, F. C. 1999. Extraintestinal dissemination of Salmonella by CD18-expressing phagocytes. *Nature,* 401**,** 804-8.

VAZQUEZ-TORRES, A., XU, Y., JONES-CARSON, J., HOLDEN, D. W., LUCIA, S. M., DINAUER, M. C., MASTROENI, P. & FANG, F. C. 2000. Salmonella pathogenicity island 2-dependent evasion of the phagocyte NADPH oxidase. *Science,* 287**,** 1655-8.

VEERAKUL, G., SANPAKIT, K., TANPHAICHITR, V. S., MAHASANDANA, C. & JIRARATTANASOPA, N. 2002. Secondary hemophagocytic lymphohistiocytosis in children: an analysis of etiology and outcome. *J Med Assoc Thai,* 85 Suppl 2**,** S530-41.

VERVLOET, M. G., THIJS, L. G. & HACK, C. E. 1998. Derangements of coagulation and fibrinolysis in critically ill patients with sepsis and septic shock. *Semin Thromb Hemost,* 24**,** 33-44.

VIDAL, S., TREMBLAY, M. L., GOVONI, G., GAUTHIER, S., SEBASTIANI, G., MALO, D., SKAMENE, E., OLIVIER, M., JOTHY, S. & GROS, P. 1995. The Ity/Lsh/Bcg locus: natural resistance to infection with intracellular parasites is abrogated by disruption of the Nramp1 gene. *J Exp Med,* 182**,** 655-66.

VIDAL, S. M., MALO, D., VOGAN, K., SKAMENE, E. & GROS, P. 1993. Natural resistance to infection with intracellular parasites: isolation of a candidate for Bcg. *Cell,* 73**,** 469-85.

VON BRUHL, M. L., STARK, K., STEINHART, A., CHANDRARATNE, S., KONRAD, I., LORENZ, M., KHANDOGA, A., TIRNICERIU, A., COLETTI, R., KOLLNBERGER, M., BYRNE, R. A., LAITINEN, I., WALCH, A., BRILL, A., PFEILER, S., MANUKYAN, D., BRAUN, S., LANGE, P., RIEGGER, J., WARE, J., ECKART, A., HAIDARI, S., RUDELIUS, M., SCHULZ, C., ECHTLER, K., BRINKMANN, V., SCHWAIGER, M., PREISSNER, K. T., WAGNER, D. D., MACKMAN, N., ENGELMANN, B. & MASSBERG, S. 2012. Monocytes, neutrophils, and platelets cooperate to initiate and propagate venous thrombosis in mice in vivo. *J Exp Med,* 209**,** 819-35.

WADA, H., USUI, M. & SAKURAGAWA, N. 2008. Hemostatic abnormalities and liver diseases. *Semin Thromb Hemost,* 34**,** 772-8.

WAHL, S. M., ALLEN, J. B., DOUGHERTY, S., EVEQUOZ, V., PLUZNIK, D. H., WILDER, R. L., HAND, A. R. & WAHL, L. M. 1986. T lymphocyte-dependent evolution of bacterial cell wall-induced hepatic granulomas. *J Immunol,* 137**,** 2199-209.

WALSH, A. L., PHIRI, A. J., GRAHAM, S. M., MOLYNEUX, E. M. & MOLYNEUX, M. E. 2000. Bacteremia in febrile Malawian children: clinical and microbiologic features. *Pediatr Infect Dis J,* 19**,** 312-8.

WARREN, H. S. & WEIDANZ, W. P. 1976. Malarial immunodepression in vitro: adherent spleen cells are functionally defective as accessory cells in the response to horse erythrocytes. *Eur J Immunol,* 6**,** 816-9.

WATSON, S. P., HERBERT, J. M. & POLLITT, A. Y. 2010. GPVI and CLEC-2 in hemostasis and vascular integrity. *J Thromb Haemost,* 8**,** 1456-67.

WETTERWALD, A., HOFFSTETTER, W., CECCHINI, M. G., LANSKE, B., WAGNER, C., FLEISCH, H. & ATKINSON, M. 1996. Characterization and cloning of the E11 antigen, a marker expressed by rat osteoblasts and osteocytes. *Bone,* 18**,** 125-32.

WICK, M. J. 2007. Monocyte and dendritic cell recruitment and activation during oral Salmonella infection. *Immunol Lett,* 112**,** 68-74.

WICKHAM, M. E., BROWN, N. F., PROVIAS, J., FINLAY, B. B. & COOMBES, B. K. 2007. Oral infection of mice with Salmonella enterica serovar Typhimurium causes meningitis and infection of the brain. *BMC Infect Dis,* 7**,** 65.

WIJBURG, O. L., SIMMONS, C. P., VAN ROOIJEN, N. & STRUGNELL, R. A. 2000. Dual role for macrophages in vivo in pathogenesis and control of murine Salmonella enterica var. Typhimurium infections. *Eur J Immunol,* 30**,** 944-53.

WINAU, F., HEGASY, G., WEISKIRCHEN, R., WEBER, S., CASSAN, C., SIELING, P. A., MODLIN, R. L., LIBLAU, R. S., GRESSNER, A. M. & KAUFMANN, S. H. 2007. Ito cells are liver-resident antigen-presenting cells for activating T cell responses. *Immunity,* 26**,** 117-29.

WINTER, O., MOSER, K., MOHR, E., ZOTOS, D., KAMINSKI, H., SZYSKA, M., ROTH, K., WONG, D. M., DAME, C., TARLINTON, D. M., SCHULZE, H., MACLENNAN, I. C. & MANZ, R. A. 2010. Megakaryocytes constitute a functional component of a plasma cell niche in the bone marrow. *Blood,* 116**,** 1867-75.

WITHERS, D. R., KIM, M. Y., BEKIARIS, V., ROSSI, S. W., JENKINSON, W. E., GASPAL, F., MCCONNELL, F., CAAMANO, J. H., ANDERSON, G. & LANE, P. J. 2007. The role of lymphoid tissue inducer cells in splenic white pulp development. *Eur J Immunol,* 37**,** 3240-5.

WONG, C. H., JENNE, C. N., PETRI, B., CHROBOK, N. L. & KUBES, P. 2013. Nucleation of platelets with blood-borne pathogens on Kupffer cells precedes other innate immunity and contributes to bacterial clearance. *Nat Immunol,* 14**,** 785-92.

YAGUCHI, A., LOBO, F. L., VINCENT, J. L. & PRADIER, O. 2004. Platelet function in sepsis. *J Thromb Haemost,* 2**,** 2096-102.

YAMAMOTO, T., SASHINAMI, H., TAKAYA, A., TOMOYASU, T., MATSUI, H., KIKUCHI, Y., HANAWA, T., KAMIYA, S. & NAKANE, A. 2001. Disruption of the genes for ClpXP protease in Salmonella enterica serovar Typhimurium results in persistent infection in mice, and development of persistence requires endogenous gamma interferon and tumor necrosis factor alpha. *Infect Immun,* 69**,** 3164-74.

YEAMAN, M. R. 2010. Platelets in defense against bacterial pathogens. *Cell Mol Life Sci,* 67**,** 525-44.

YEAMAN, M. R., BAYER, A. S., KOO, S. P., FOSS, W. & SULLAM, P. M. 1998. Platelet microbicidal proteins and neutrophil defensin disrupt the Staphylococcus aureus cytoplasmic membrane by distinct mechanisms of action. *J Clin Invest,* 101**,** 178-87.

YILDIRIM, I., CEYHAN, M., BAYRAKCI, B., UYSAL, M., KUSKONMAZ, B. & OZALTIN, F. 2010. A case report of thrombocytopenia-associated multiple organ failure secondary to Salmonella enterica serotype Typhi infection in a pediatric patient: successful treatment with plasma exchange. *Ther Apher Dial,* 14**,** 226-9.

YONEYAMA, H. & ICHIDA, T. 2005. Recruitment of dendritic cells to pathological niches in inflamed liver. *Med Mol Morphol,* 38**,** 136-41.

ZEERLEDER, S., HACK, C. E. & WUILLEMIN, W. A. 2005. Disseminated intravascular coagulation in sepsis. *Chest,* 128**,** 2864-75.

ZHANG, S., KINGSLEY, R. A., SANTOS, R. L., ANDREWS-POLYMENIS, H., RAFFATELLU, M., FIGUEIREDO, J., NUNES, J., TSOLIS, R. M., ADAMS, L. G. & BAUMLER, A. J. 2003. Molecular pathogenesis of Salmonella enterica serotype typhimurium-induced diarrhea. *Infect Immun,* 71**,** 1-12.

ZIMMERMANN, H. W., TRAUTWEIN, C. & TACKE, F. 2012. Functional role of monocytes and macrophages for the inflammatory response in acute liver injury. *Front Physiol,* 3**,** 56.

ZINSSER, H. H. & PRYDE, A. W. 1952. Experimental study of physical factors, including fibrin formation, influencing the spread of fluids and small particles within and from the peritoneal cavity of the dog. *Ann Surg,* 136**,** 818-27.